Robust multi-$\mathcal{H}_2$ output-feedback approach to aerial refuelling automation of large aircraft via linear matrix inequalities

by

Etienne H. Claase

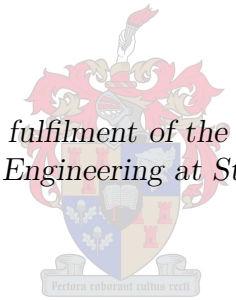

Thesis presented in partial fulfilment of the requirements for the degree Master of Science in Engineering at Stellenbosch University

Supervisor: Mr J.A.A. Engelbrecht
Department of Electrical & Electronic Engineering

March 2013

Declaration

By submitting this thesis electronically, I declare that the entirety of the work contained therein is my own, original work, that I am the sole author thereof (save to the extent explicitly otherwise stated), that reproduction and publication thereof by Stellenbosch University will not infringe any third party rights and that I have not previously in its entirety or in part submitted it for obtaining any qualification.

March 2013

Abstract

In recent years the aviation industry has shown an interest in the airborne refuelling of *large* transport aircraft to enable increased payload mass at take-off and to extend aircraft range. Due to the large volume of fuel to be transferred, a boom and receptacle refuelling system with a larger fuel transfer rate is employed. The refuelling operation is particularly difficult and strenuous for the pilot of the receiver aircraft, because the position of the receptacle relative to the tanker aircraft must be maintained within a narrow window for a relatively long period of time. The airborne refuelling of a large aircraft is typically much more difficult than that of a fighter aircraft, since the large aircraft is more sluggish, takes much longer to refuel, and has a relatively large distance between its refuelling receptacle and its centre of mass. These difficulties provide the motivation for developing flight control laws for Autonomous In-Flight Refuelling (AIFR) to alleviate the workload on the pilot.

The objective of the research is to design a flight control system that can regulate the receptacle of a receiver aircraft to remain within the boom envelope of a tanker aircraft in light and medium turbulence. The flight control system must be robust to uncertainties in the aircraft dynamic model, and must obey actuator deflection and slew rate limits.

Literature on AIFR shows a wide range of approaches, including Linear Quadratic Regulator (LQR), μ-synthesis and neural-network based adaptive control, none of which explicitly includes constraints on actuator amplitudes, actuator rates and regulation errors in the design/synthesis. A new approach to designing AIFR flight control laws is proposed, based on Linear Matrix Inequality (LMI) optimisation. The relatively new LMI technique enables optimised regulation of stochastic systems subject to time-varying uncertainties and coloured noise disturbance, while simultaneously constraining transient behaviour and multiple outputs and actuators to operate within their amplitude, saturation and slew rate limits. These constraints are achieved by directly formulating them as inequalities.

Samevatting

Die lugvaart industrie toon huidiglik 'n belangstelling in die brandstof oordrag tussen twee groot vervoervliegtuie gedurende vlug, met die doel om die maksimum opstyggewig kapasiteit sowel as die maksimum ononderbroke vlugafstand vermoë van die hervulde vliegtuig te vermeerder. 'n *Boom* hervulling-stelsel word geïmplementeer om die hoë spoed van brandstof oordrag te voorsien. Die verrigting van vluggebonde hervulling van 'n groot, trae vliegtuig is moeiliker en meer veeleisend as bv. van 'n vegvliegtuig, veral vir die vlieënier van die hervulde vliegtuig, wat sy *boom*-skakel moet reguleer binne 'n relatiewe klein *boom* bewegingsruimte vir 'n relatiewe lang tydperk. Die kinematika betrokke speel ook 'n groter rol in 'n *groot* hervulde vliegtuig a.g.v. die langer afstand tussen die *boom*-skakel en die massa middelpunt/draaipunt. Hierdie bied die motivering om 'n beheerstelsel te ontwikkel wat die taak outomaties uitvoer.

Die doel van die navorsing is om 'n beheerstelsel te ontwerp wat die *boom*-skakel van die hervulde vliegtuig outomaties reguleer binne die bewegingsruimte van die *boom*, gedurende ligte en matige turbulensie. Daar word van die beheerder vereis om robuust te wees teen onsekerhede in die vliegtuig se meganika, sowel as om die beheer oppervlaktes en turbines van die vliegtuig binne hul defleksie-, wringkrag- en sleurtempo-perke te hou.

Daar bestaan reeds 'n groot verskeidenheid van benaderings tot die outomatisering van luggebonde hervulling, onder andere LQR, μ-sintese en neurale-netwerk gebaseerde aanpasbare beheer, waarvan geeneen perke op aktueerders en regulasie foute direk in die ontwerp insluit nie. 'n Nuwe benadering word voorgestel wat gebaseer is op *Linear Matrix Inequality* (LMI) optimering. Die LMI tegniek is relatief nuut in die gebruik van beheerstelsel ontwerp. Dit stel die ontwerper in staat om 'n stogastiese stelsel, onderworpe aan tydvariante-stelsel-variasie *en* gekleurde ruis versteurings, optimaal te reguleer, *terwyl* aktueerders en stelsel gedrag direk beperk word.

Résumé

Ces dernières années, l'industrie aéronautique s'est intéressée au ravitaillement en vol de gros avions de transport afin de permettre une plus grande masse de charge utile au décollage et d'étendre la gamme d'avions. En raison de la grande quantité de carburant à transférer, un système de bras et de réceptacle de ravitaillement, doté d'un taux de transfert de carburant plus élevé, est utilisé. L'opération de ravitaillement est particulièrement difficile et pénible pour le pilote de l'avion récepteur car la position du réceptacle par rapport à l'avion ravitailleur doit être maintenue dans un espace restreint, et ce, pendant une période de temps relativement longue. Le ravitaillement en carburant d'un gros avion est en général beaucoup plus difficile que celui d'un avion de chasse étant donné que le gros avion est plus lent et que son temps de ravitaillement est beaucoup plus long et qu'il possède une distance relativement grande entre son réceptacle de ravitaillement et son centre de masse. Ces difficultés incitent à élaborer des lois relatives aux commandes de vol pour les Ravitaillements en vol d'appareils autonomes (AIFR) en vue d'alléger la charge de travail du pilote. L'objectif de la recherche est de concevoir un système de commande de vol pouvant stabiliser le réceptacle d'un avion récepteur afin qu'il reste dans le bras de ravitaillement d'un avion ravitailleur lorsque celui-ci traverse des turbulences légères et moyennes. Le système de commande de vol doit résister aux éléments d'incertitudes liés au modèle d'avion dynamique, et doit respecter les limites de débattement du vérin et de la vitesse d'asservissement. La documentation sur les AIFR montre des approches extrêmement diverses, relatives notamment au Régulateur quadratique linéaire (LQR), à la commande adaptative par réseaux de neurones et µ-synthèse, dont aucune n'inclut explicitement de restrictions sur les amplitudes du vérin, les cadences du vérin et les erreurs de stabilisation dans la conception / la synthèse. Une nouvelle approche sur l'élaboration de lois relatives aux commandes de vol pour les AIFR est proposée ; celle-ci est basée sur l'optimisation de l'inégalité matricielle linéaire (LMI). La technique relativement nouvelle de LMI permet de réguler de manière optimisée les systèmes stochastiques soumis aux incertitudes variables dans le temps et aux nuisances sonores de couleur, tout en restreignant simultanément les comportements transitoires et les multiples sorties et vérins à fonctionner dans leurs limites d'amplitude, de saturation et de vitesse d'asservissement. Ces restrictions sont obtenues en les formulant directement d'inégalités.

Contents

List of Figures

List of Tables

Listings

Nomenclature

Abbreviations

AIFR Autonomous In-Flight Refueling

AOV Average Output Variance

BMI(s) Bilinear Matrix Inequality(ies)

DC Direct Current

DCM Direction Cosine Matrix

DE(s) Differential Equation(s)

DM Delay Margin

DOF Degrees Of Freedom

EOM Equations Of Motion

ESL Electronic Systems Laboratory

FM Filter Margin

IEP(s) Instantaneous Eigenvalue Plot(s)

IFR In-Flight Refueling

IOC Instantaneous Output Covariance

L.H.S. Left Hand Side

LFT Linear Fractional Transform

LMI(s) Linear Matrix Inequality(ies)

LPF(s) Low-Pass Filter(s)

LPV Linear Parameter-Varying

LQG Linear Quadratic Gaussian

LTI Linear Time-Invariant

LTV Linear Time-Variant

MRTT Multi-Role Tanker Transport

NACoE National Aerospace Centre of Excellence

NLTV Non-Linear Time-Varying

PDS Power Density Spectrum

R.H.S. Right Hand Side

Control theory symbols

$\mathfrak{a}$ exponential decay rate

$\mathfrak{c}$ robust eigenvalue region cone half-angle

$\mathfrak{q}$ robust eigenvalue region disk centre

$\mathfrak{r}$ robust eigenvalue region disk radius

Atmospheric flight mechanics symbols

$\cdot_R$ relating to the receiver aircraft

$\cdot_T$ relating to the tanker aircraft

χ boom roll angle

δ control surface deflection or thrust

λ boom length

ψ, θ, ϕ Euler 3-2-1 aircraft orientation angles yaw, pitch and roll

σ boom pitch angle.

εx perturbation of flight mechanics variable x, i.e. $\varepsilon x \coloneqq x - x_r$

ϱ_d dynamic pressure

b wingspan

cg aircraft centre of gravity

h aircraft altitude

l aerodynamic chord

m aircraft mass

p, q, r aircraft roll, pitch and yaw angular velocities in aircraft axes

s wing surface

u, v, w aircraft axial, lateral and normal linear velocities in aircraft axes

x_r trim of flight mechanics variable x

Mathematical symbols and operators

$\cdot$ Product, used to indicate the product of the R.H.S. with the rightmost element of the previous line at an equation line break, i.e.

$$\begin{aligned} AB &= A \\ &\quad \cdot B \end{aligned}$$

.

$:$ *subject to* i.e. the L.H.S. is subject to the R.H.S.

$:=$ *defined as* i.e. the L.H.S. is defined to be equal to the R.H.S.

$\exists$ *there exists one or more* e.g. $\exists x \in \mathbb{R}^1 : 0 = ax^2 + b$, $\{a, b\} \subset \mathbb{R}^1$ reads, there exists at least one real scalar x such that $0 = ax^2 + b$ is satisfied, where a and b are real scalars.

$\forall$ *for all* e.g. $x > 0 \, \forall t$ reads, $x > 0$ is satisfied for all time.

$\gg$ *sufficiently greater than*, i.e. the addition or subtraction of the terms involved may be replaced by the larger term $(A \gg B) \iff (A - B \approx A)$

$\in$ *is an element in the set* i.e. the L.H.S. is an element in the R.H.S.

$\iff$ The R.H.S. or below is equivalent to the L.H.S. or above, i.e. the L.H.S. or above is a necessary and sufficient condition for the R.H.S. or below.

$\longrightarrow$ The R.H.S. or below follows from the L.H.S. or above. Informally used for reference purposes.

$\Longrightarrow$ The R.H.S. or below is deduced from the L.H.S. or above, i.e. the L.H.S. or above is a sufficient condition for the R.H.S. or below.

$\mapsto$ *maps to*, e.g. $\mathbf{f} := \{\mathbf{f} : \mathbb{R}^{n_x \times 1} \mapsto \mathbb{R}^{n_f \times 1}, \, \|\mathbf{f}(\mathbf{x})\|_2 < 1\}$ defines $\mathbf{f}$ as all the maps from $\mathbb{R}^{n_x \times 1}$ to $\mathbb{R}^{n_f \times 1}$ such that the Euclidean-norm of its corresponding output is smaller than one.

$\mathbb{C}^1, \mathbb{C}^{k \times 1}$ Set of all complex scalars, complex k-dim. column vectors.

$\mathbb{E}$ Expected value operator.

$\mathbb{P}$ Probability of an outcome.

$\mathbb{R}^1$, $\mathbb{R}^{k \times 1}$, $\mathbb{R}^{n \times m}$ Set of all real scalars, real k-dim. column vectors, real $n \times m$ matrices.

$\mathbb{Z}^1$ Set of all integer scalars.

$\mathbf{v}^*$, $\Re(\mathbf{v})$, $\Im(\mathbf{v})$ The complex conjugate, real part and imaginary part of $\mathbf{v} \in \mathbb{C}^{k \times 1}$, e.g. $\frac{1}{2}(\mathbf{v} + \mathbf{v}^*) = \Re(\mathbf{v}) \in \mathbb{R}^{k \times 1}$ and $\frac{1}{2}(\mathbf{v} - \mathbf{v}^*) = \Im(\mathbf{v}) \in \mathbb{R}^{k \times 1}$.

$\notin$ *is not an element in the set*, i.e. the L.H.S. is *not* an element in the R.H.S.

$\simeq$ *assumed to be equal.*

$\star$ Completes the symmetric matrix, i.e.

$$\begin{bmatrix} M_{11} & M_{12} & M_{13} \\ \star & M_{22} & M_{23} \\ \star & \star & M_{33} \end{bmatrix} := \begin{bmatrix} M_{11} & M_{12} & M_{13} \\ M_{12}^T & M_{22} & M_{23} \\ M_{13}^T & M_{23}^T & M_{33} \end{bmatrix}$$

where $M_{11} = M_{11}^T$, $M_{22} = M_{22}^T$ and $M_{33} = M_{33}^T$.

$\subset$ *is a subset of the set* i.e. the L.H.S. is a set whose elements are all contained in the R.H.S.

blkdiag Block-diagonalisation of matrices, i.e.

$$\text{blkdiag}\left(M_1, M_2, M_3, \ldots, M_n\right) \coloneqq \begin{bmatrix} M_1 & 0 & 0 & \cdots & 0 \\ 0 & M_2 & 0 & \cdots & 0 \\ 0 & 0 & M_3 & & \vdots \\ \vdots & \vdots & & \ddots & 0 \\ 0 & 0 & \cdots & 0 & M_n \end{bmatrix}$$

chol Cholesky factorisation of a positive definite matrix, e.g. $M = \text{chol}\left(M\right)^T \text{chol}\left(M\right)$ where $M > 0$.

diag Diagonal of a square matrix in column vector form, or the diagonalisation of a column vector, e.g. $\text{diag}\left(M\right) \in \mathbb{R}^{n\times 1}$ where $M \in \mathbb{R}^{n\times n}$, $\text{diag}\left(\mathbf{v}\right) \in \mathbb{R}^{k\times k}$ where $\mathbf{v} \in \mathbb{R}^{k\times 1}$, $\mathbf{v} = \text{diag}\left(\text{diag}\left(\mathbf{v}\right)\right)$.

eig Eigenvalues of a square matrix, e.g. $\text{eig}\left(M\right) \in \mathbb{C}^{n\times 1}$ where $M \in \mathbb{R}^{n\times n}$.

inf Infimum, i.e. the lower-bound of a scalar.

msv Maximum singular value operator of a real matrix, also known as the induced 2-norm, i.e. $\text{msv}\left(M\right) = \|M\|_{i2}$.

rand Uniformly distributed random element in a set, e.g. $\text{rand}\left(\{a : a^2 < 1\}\right)$ is a random number uniformly distributed between -1 and 1.

sup Supremum, i.e. the upper-bound of a scalar.

tr, trace Trace of a square matrix, i.e. the sum of the diagonal elements, e.g. $\text{tr}\left(M\right) \in \mathbb{R}^1$ where $M \in \mathbb{R}^{n\times n}$.

$\times$ Vector product.

$M > 0$ M is symmetric positive definite, i.e. $\mathbf{v}^T M \mathbf{v} > 0 \, \forall \mathbf{v} \neq \mathbf{0}$, where $M \in \mathbb{R}^{n\times n}$ and $\mathbf{v} \in \mathbb{R}^{n\times 1}$.

$M > N \iff M - N > 0$.

M^T Transpose of matrix M.

State-space notation

$\boldsymbol{\Delta}$ Uncertainty set.

Δ Uncertainty matrix.

$\dot{\mathbf{x}}$ State time-derivative, i.e. $\dot{\mathbf{x}} \coloneqq \frac{d\mathbf{x}}{dt}$.

$\mathbf{u}$ Control input.

$\mathbf{v}$ Estimator performance output.

$\mathbf{w}$ Unit intensity white noise input.

$\mathbf{x}$ State vector.

$\mathbf{y}$ Measurement output.

$\mathbf{z}$ Performance output.

$\mathcal{A}$, A Closed-loop and open-loop state matrix.

$\mathcal{B}$, B Closed-loop and open-loop input to state derivative gain.

$\mathcal{C}$, C Closed-loop and open-loop state to output gain.

$\mathcal{D}$, D Closed-loop and open-loop input to output feedthrough gain.

$\mathcal{G}$, G Closed-loop and open-loop model gain

$$\mathcal{G} \coloneqq \begin{bmatrix} \mathcal{A} & \mathcal{B} \\ \mathcal{C} & \mathcal{D} \end{bmatrix}, G \coloneqq \begin{bmatrix} A & B \\ C & D \end{bmatrix}$$

$\mathfrak{D}$ Variable domain.

$\mathfrak{S}$ Set defining uncertainty structure.

$\overline{P}$ Time-invariant observability matrix upper-bound, i.e. $\overline{P} > P(t_1, t)\ \forall t$.

$\overline{Q}_x$ Time-invariant state-covariance upper-bound, i.e. $\overline{Q}_x > Q_x(t)\ \forall t$.

$P(t_1, t)$ Observability matrix.

$Q_x(t)$ State-covariance/controllability matrix, i.e. $Q_x(t) = \mathbb{E}\left\{\mathbf{x}(t)\,\mathbf{x}^T(t)\right\}$.

Acknowledgements

I would like to extend my sincere gratitude to the following people and organisations who have contributed to the research reported in this thesis.

- Japie Engelbrecht for encouraging me to experiment with new methods.
- The Electronic Systems Laboratory (ESL), Airbus and the NACoE for funding the project.
- Johan Löfberg for providing the YALMIP software, which greatly reduced development time.
- K.C. Toh, M.J. Todd, and R.H. Tutuncu for providing the SDPT3 software.
- Friends and engineers in the ESL for their support, stimulating discussions and laughs.
- My mother, brothers and friends for their patients, belief and support.

Chapter 1

Introduction

1.1 Background

Aerial refuelling, also called in-flight refuelling (IFR) or airborne refuelling, is the practice of transferring fuel from one aircraft to another during flight. This allows the receiving aircraft, called the *receiver*, to remain airborne longer, and enables a take-off with either a greater payload or a shorter/safer take-off. Usually, the aircraft providing the fuel, called the *tanker*, is specially designed for the task. There exist two kinds of IFR systems, which are the *probe and drogue* system, and the *boom and receptacle* system.

The *probe and drogue* system consists of a tanker dragging a hose ending with a drogue, also called a basket, and a receiver with a probe that is rigid. To connect to the tanker, the receiver must put its probe in the basket, and then maintain the position for the duration of fuel transfer. Most fighter aircraft use the basket system (see Figure 1.1), as do some military transportation aircraft such as the C-160 Transall, the C-130 Hercules, and the A400M.

The *boom* refuelling system consists of a tanker with an articulated boom that is controlled by a member of the tanker's crew called the "boomer". To connect to the boom, the receiver must position its receptacle (a hole in its fuselage to receive the fuel) in a zone called the "contact envelope", for the duration needed by the boomer to catch the receptacle with the boom. After the connection, the boom is not ever controlled by the boomer, but becomes passive to follow the evolution of the receiver in the limit of a box called the "disconnect envelope", for the duration of fuel transfer. If the receiver goes out of the disconnect envelope before the end of the refuelling, the boom disconnects automatically. Generally, this system is used by heavy and sluggish aircraft such as the KC-10 Extender, A310-MRTT, A330-MRTT, C-5 Galaxy, and the Boeing 747 Air Force One (see Figure 1.2). [36]

In recent years the aviation industry has shown an interest in the airborne refuelling of *large* transport aircraft to enable increased payload mass at take-off and to extend aircraft range (see [5, 78] for the fuel saving capability of IFR for transport aircraft).

Airbus started collaborating with the Electronic Systems Laboratory (ESL) at Stellenbosch University on airborne refuelling automation in 2008. The goal of the

Figure 1.1: F-18 autopilot lines up the aircraft's refuelling probe with a Boeing 707 paradrogue basket.

research is to determine the feasibility of autonomous airborne refuelling between two Airbus A330-MRTT's during medium turbulence, as described by the Dryden model for atmospheric turbulence, over a large flight envelope and various flight tracks.

Piloted airborne refuelling of a large aircraft, such as the A330, is typically much more difficult than that of a fighter aircraft, since the large aircraft is more sluggish, takes much longer to refuel, and has a relatively large distance between its refuelling receptacle and its centre of mass. This difficulty provides the motivation for developing flight control laws to perform IFR.

The flight control laws generate actuator commands using feedback from noisy sensor measurements, such that the receiver refuelling receptacle is maintained within the boom envelope for the duration of 25 min in the presence of medium turbulence, while none of the control surfaces or thrusters operate outside specified ranges. It is also required that the task be achieved during various flight tracks, *i.e.* tanker bank-angle, climb-rate and ground-speed, specified by the tanker pilot on-line. No explicit structure is defined for the control laws. The control laws are confirmed via non-linear simulation using A330 aerodynamic-coefficients and moment of inertia data provided by Airbus.

Figure 1.2: KC-135 Boomer catching the receptacle of a C-17 Globemaster.

1.2 History

Airborne refuelling has a rich history, spanning almost a century to date.

On June 27, 1923, two aircraft became linked by hose 500 ft above ground, and one aircraft refuelled the other. The event was the first aerial refuelling in history (see Figure 1.3). Flying De Havilland 4B bi-planes over Rockwell Field, San Diego, the U.S. pilots succeeded in transferring 75 gal [1] of fuel from the leading to the trailing aircraft using a 50 ft rubber hose. Their success led to numerous experiments in range extension, flying non-stop from Canada to Mexico that same year, with two aerial refuellings in between, quadrupling the normal aircraft range. November 18, the same year, the first fatal crash resulting from an in-flight refuelling demonstration occurred at an air-show in Texas. In the 1930's, a series of aerial refuelling experiments were conducted at Farnborough, England, to investigate aerial refuelling capability to increase the maximum payload capacity of bombers by reducing the fuel-load at take-off. [71]

However, the development of next generation long-range aircraft, such as the Douglas DC-1, DC-2 and the Boeing B-29 Superfortress, postponed deployment of aerial refuelling until the Korean War in the 1950's. Three U.S. squadrons [2] of F-84 Thunderjets were deployed to Japan to assist South Korea in the war, using aerial refuelling to make the trans-Pacific flight possible. It was not until the 1950's that

1. 75 gal ≈ 280 l, approximately one tenth of the aircraft weight.
2. The three squadrons had a total of approximately sixty aircraft.

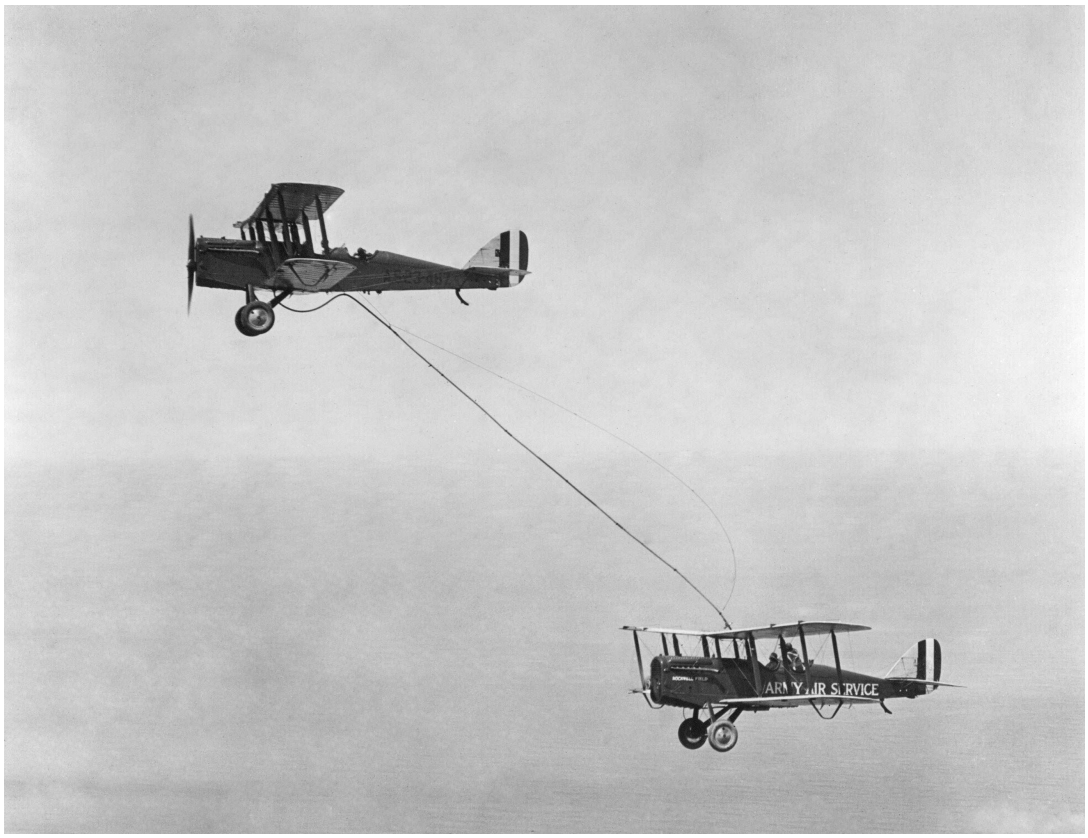

Figure 1.3: De Havilland DH-4B biplanes performing piloted aerial refuelling, using a 50 ft rubber hose and the so-called 'dangle-and-grab' refuelling system to transfer fuel from the top plane.

aerial refuelling became incorporated into military strategic planning. Consequently, in 1957, the U.S. Air Force succeeded in sending three B–52B's non-stop around the world, demonstrating global air-strike capability. [71]

On August 30, 2006, DARPA and NASA demonstrated the first hands-off autonomous aerial refuelling (see Figure 1.1). A Boeing 707 tanker and a modified F-18 receiver were fitted with differential Global Positioning System (GPS) and an optical tracker to perform the task. On January 21, 2011, DARPA, NASA and Northrop Grumman demonstrated the first high-altitude autonomous close-formation flight of two UAVs, the Grumman's Proteus test aircraft and NASA's Global Hawk, at an altitude of 45′000 ft and flying as close as 40 ft, in preparation for the first autonomous airborne refuelling between two UAVs, scheduled for December 2012. [22]

On May 17, 2011, Airbus Military demonstrated "buddy-buddy" in-flight refuelling between two A330-MRTT's, another first, enabling even longer range deployments (see Figure 1.4).

1.3 Project objectives

Airbus requirements for A330-MRTT (Multiple Role Tanker Transport) buddy-buddy IFR automation are given in [17] and are listed below.

Figure 1.4: A330-MRTT's demonstrating *buddy-buddy* refuelling.

Function requirements

FUNC 1: The function shall allow:

- To move from observation position to pre-contact position
- To move from pre-contact to contact position
- To maintain contact position within contact envelope until boom is connected
- To maintain position within disconnect envelope to support fuel dispersion
- To ensure disconnection and to move back to pre-contact position

Additional info 1: Observation position is defined as a position to the right or left behind the tanker (at approximately 0.5 Nm [3]) with a minimum of one receiver wingspan clearance between tanker and receiver.

Additional info 2: Pre-contact position is defined as approximately 50 ft behind and slightly below the boom nozzle where the receiver stabilises before being cleared to the contact position.

3. 0.5 Nm ≈ 926 m

FUNC 2: The function shall ensure a safe emergency breakaway in order to cover failure cases and/or exiting of the disconnect envelope.

Additional info: The emergency breakaway can be demanded either by the tanker or by the receiver in case of abnormal behaviour. The breakaway consists of moving backward quickly by reducing engine IDLE position and extending the full air-breaks of the receiver. The receiver should stay in visual contact with the tanker.

Performance requirements

PERF 1: The aircraft shall be able to stay within the contact envelope for at least 5 min during medium turbulence (see Section 2.2.3.2 for dimensions)

Additional info: 5 min is the duration required to connect the boom

PERF 2: The aircraft shall be able to stay within the disconnect envelope for at least 20 min during medium turbulence (see Section 2.2.3.2 for dimensions)

Additional info: 20 min is the duration required to transfer fuel

PERF 3: The aircraft shall be able to realise the task within the IFR mass & centre of mass envelope

Additional info: The A330-MRTT mass and cg envelope is defined in Figure 1.5 where the percentage of reference chord $l = 7.27\,\text{m}$ (%RC) is measured

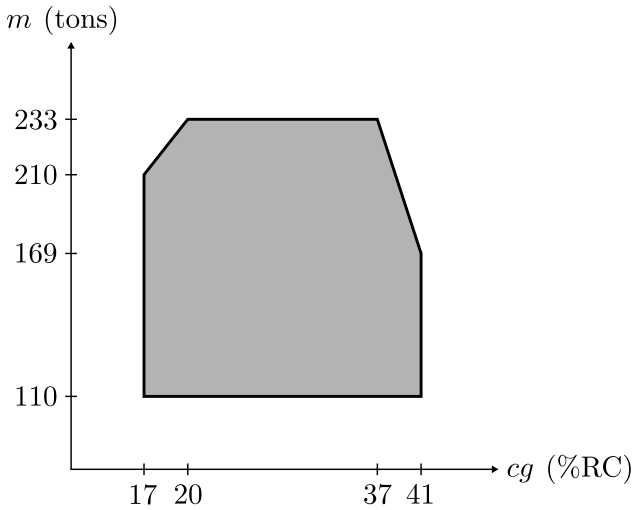

Figure 1.5: Mass and centre of gravity flight-envelope.

aft from the intersection of the wing leading edge and the fuselage.

PERF 4: The aircraft shall be able to realise the task within the IFR airspeed & altitude envelope

Additional info: A330-MRTT IFR calibrated airspeed and altitude envelope is defined in Figure 1.6

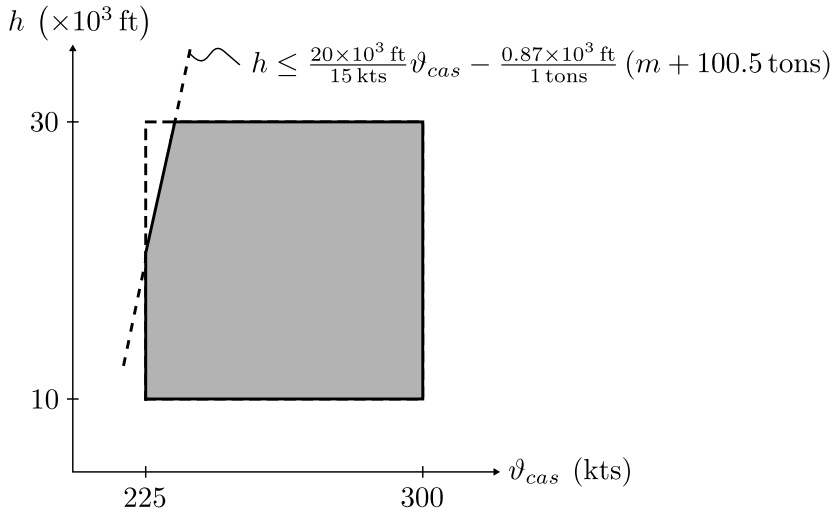

Figure 1.6: Calibrated airspeed and altitude flight-envelope.

PERF 5: The aircraft shall be able to realise the task in turn with a bank-angle up to 25°

PERF 6: The aircraft shall be able to realise the task during a toboggan manoeuvre

Additional info: A toboggan manoeuvre allows the tanker or receiver to maintain its speed by initiating a slow descent up to 500 ft/min

PERF 7: The aircraft shall be able to realise the task in still air, in light turbulence and in medium turbulence as defined by the Dryden model for atmospheric turbulence according to MIL-STD-1797 [2, pp.678-697]

Reliability requirements

REL 1: The robustness of the function shall be compatible with realistic sensor accuracies (see Section 4.2.1.6 for details)

REL 2: The robustness of the function shall be compatible with realistic sensor computation delays (see Section 4.2.1.6 for details)

1.4 Approach

Autonomous IFR (AIFR) is a rich regulation control problem, which requires high-performance in the presence of many different system components. It involves *tight-regulation* of a stochastic system with uncertainty, non-linearity, time-delays, normally distributed white noise disturbance[4], and actuator constraints. *Tight-regulation* designs achieve maximum regulation performance by assigning actuators to operate close to their amplitude and rate saturation limits. In such a design, it

4. Normally distributed white noise disturbance is inherent in the Dryden model for atmospheric turbulence.

is pertinent to specify the operating ranges of actuators and the system state, this being done by specifying σ-bounds, as variance is the measure of stochastic systems.

Theoretically, the actuators and state of a linearly controlled non-linear stochastic system, subject to normally distributed white noise disturbance, are unbounded. The system state and control input, constructed from the system state, have probability distributions that range to infinity, as does the normal distribution, unless there are non-linear constraints inherent in the system, such as actuator saturation. These unbounded distributions lead to the characterisation of amplitude in terms of stochastic variance, and the use of *variance-bounds*[5] rather than hard-bounds, which provides the probability of exceeding the hard-bounds, *i.e.* a risk criterion. The design task of meeting certain amplitude-bounds then translates to minimising the risk of exceedance.

It is well known that optimal variance control, *i.e.* Linear Quadratic Gaussian (LQG) control, also known as $\mathcal{H}_2$ control, of LTI systems, has no guaranteed stability margins, and usually results in instability when subjected to small gain or phase variations (see [26]). In the context of flight control, aerodynamic models are never exact, and the control has to perform under a certain level of model uncertainty. The inclusion of model uncertainty in the control design is called robust control. Robust control design dates back to the Bode plot in 1945 [10][6], where gain and phase margins were specified to accommodate model uncertainty. Modern robust control techniques allow the control to be optimally synthesised for a class of time-varying uncertain systems with respect to some performance index, such as the $\mathcal{H}_2$ index, to attain maximum robust performance.

Previous research on AIFR reveals a wide range of approaches, most of which rely on LQR/LQG control [23, 46, 14, 76]. Other approaches include pole-placement [36], μ-synthesis [15], quantitative feedback theory [62], and neural-network based adaptive control [81]. None of the previous AIFR approaches explicitly includes constraints on actuator amplitudes, actuator rates and regulation errors in the controller design/synthesis.

Several variance optimisation control techniques in the literature were considered in order to achieve tight regulation whilst incorporating the various system components of IFR. The only control techniques found that include multiple variance-constraints on system variables are the iterative LQG weight-adjustment techniques of [3, 57, 82] and the relatively new Linear Matrix Inequality (LMI) technique of Huang et al. [42], both of which synthesise an LTI controller for an LTI system. The LMI technique is found to be the most suitable, as LMIs are generally solvable and have the versatility to incorporate multiple criteria, *e.g.* multiple variance-constraints, regional eigenvalue-constraints, uncertainty, $\mathcal{H}_\infty$, *etc.*, into a single solvable problem. The Riccati equation-based LQG techniques require much less computing effort to solve than the LMI technique, but lack its versatility and global convergence. It is shown in Chapter 4 that a large LMI optimisation problem, *i.e.* the IFR automation

5. Gaussian/Normal distributions are completely described by their second-order moment/variance [64, pp.128].

6. Based on the work in [61, 6] (see [25] for a summary)

problem, with approximately 2200 scalar variables, is solved within a reasonable time-frame.

No single LMI formulation for controller optimisation/synthesis exists that readily incorporates all the system components of IFR. However, Scherer et al. [67] present a method for combining multiple LMIs into a single solvable problem, and the method is used to include the regional eigenvalue-constraints of Chilali and Gahinet [16] in the technique of Huang et al. [42]. Takaba and Katayama [75] present a method for generalising LMI formulations of LTI systems to include time-varying system uncertainty. Furthermore, the controller and estimator must be synthesised separately, because the only linear formulation of the output-feedback synthesis problem is based on the separation principle, in which the output-feedback controller is built by combining the solutions of two separate problems, a state-feedback problem and an output estimation problem, both solvable via LMI optimisation. The additional use of modelling techniques/tricks (see Section 4.2.1) completes the LMI formulation of IFR automation. A literature study on various LMI techniques considered for AIFR may be found in Appendix C.

The result is two separate LMI optimisation problems, of which the first is used to synthesise a state-feedback controller gain, and the second to synthesise an estimator feedback gain, both of which are combined post-synthesis into an estimator-based output feedback controller. Synthesis is based on the continuous-time LTI state-space system description with time-varying uncertainty, and includes regional eigenvalue-constraints and multiple variance-constraints.

Digital implementation is achieved via emulation, and regional eigenvalue constraints are used to separate the closed-loop eigenvalues from the *Nyquist frequency* to reduce the effect of aliasing. The software used to solve the LMI optimisation problems is the *sdpt3*.4 [7] solver and the YALMIP interface for MATLAB [8], both freely available.

1.5 Thesis outline

The thesis structure is illustrated by the following flow diagram

$$\text{Modelling} \rightarrow \text{LMI Control Theory} \rightarrow \text{IFR Control via LMIs} \rightarrow \text{Simulation}$$

The thesis covers the autopilot design from first principles up to non-linear simulation. In Chapter 2, a non-linear IFR model is developed. Chapter 3 provides the necessary LMI control theory to synthesise robust multi-$\mathcal{H}_2$ output feedback controllers. In Chapter 4, the IFR problem is cast into the LMI framework, which is used to synthesise IFR controllers. In Chapter 5, controller performance is evaluated by means of non-linear simulation.

7. Available at `http://www.math.nus.edu.sg/~mattohkc/sdpt3.html`
8. Available at `http://users.isy.liu.se/johanl/yalmip/`

Chapter 2

Model of aerial refuelling mechanics

2.1 Overview of model

In this chapter, a model of the aerial refuelling mechanics is developed to serve as the basis for the controller design and simulation.

The IFR mechanics developed consists of three components, which are: *individual aircraft mechanics*, *aircraft relative position kinematics,* and *atmospheric turbulence*. *Fuel transfer dynamics* and *aerodynamic coupling* are not included in our IFR model, but may be added at a later stage, to which end the controller design/synthesis approach developed in Chapter 4 will still be valid.

In Section 2.3, Six Degrees Of Freedom (6DOF) non-linear Equations Of Motion (EOM) are derived for a *rigid* aircraft, the motion variables of which are used to express the relative position kinematics of IFR in Section 2.4. In Section 2.5, the Dryden model for atmospheric turbulence is given and is extended by formulating the similarity of the turbulence at the tanker and at the receiver, resulting in a model better suited for IFR controller performance optimisation.

The transfer of fuel causes a change in the momentum and inertia of both tanker and receiver. Waishek [80] and Mao [53] derive EOM for the receiver that include the dynamic effects of fuel transfer, and show that the effects are considerable. The absence of *fuel transfer dynamics*, inherent in the *rigid body* assumption made in the flight mechanics derivations, limits the IFR controller presented in Chapters 4.3.5 to the pre-refuelling *contact-phase*, which is dedicated to connecting the boom nozzle to the receiver receptacle. The *contact-phase* has an estimate duration of 5 min and is considered the most difficult of the IFR phases, because it corresponds to the smallest boom envelope. Mao and Eke [54] summarise the research done in [9, 7, 8] on the *aerodynamic coupling* involved in IFR, specifically for a large receiver. A simple horseshoe vortex model was used for the tanker vortex field, for which the receiver exhibited diverging oscillations involving mainly bank and sideways displacement [9], as well as possible instability in vertical displacement [7]. The instability behaviour was also confirmed via wind tunnel tests [8].

The combination of the three components of IFR mechanics is illustrated by the block diagram in Figure 2.1, where $\mathbf{b}$ (boom) is the relative aircraft position, $\mathbf{m}_T$ and $\mathbf{m}_R$ are the respective motion of the tanker and receiver, $\boldsymbol{\delta}_T$ and $\boldsymbol{\delta}_R$ are the respective control surface deflections and thrust of the tanker and receiver, $\mathbf{g}_T$ and $\mathbf{g}_R$ are the turbulence (continuous gust) they experience, and $\boldsymbol{\eta}$ is white noise driving turbulence shaping filters, all formally defined in the following sections. *Individual aircraft dynamics* is derived

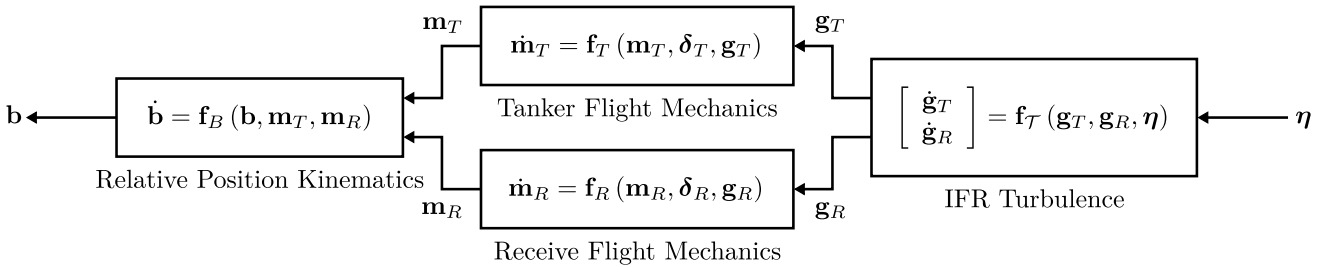

Figure 2.1: Components of IFR mechanics block diagram.

by applying Newton's Second Law and Euler's Law for a *rigid* aircraft. The commonly known form of the dynamics is obtained by changing the acceleration reference from the local geography to the aircraft itself with the Euler Transformation, and measuring all accelerations and velocities along the axes of the aircraft. *Individual aircraft mechanics* is completed by including the gimbal equations to govern the angles and angular rates used to describe the dynamics, and by including the climb-rate differential equation to govern the change in air density.

Relative position kinematics is derived simply by differentiating a vector triangle that describes the position of both ends of the boom with respect to the local geography. The final form of the kinematics is obtained by applying the Euler Transformation to transform the velocities of the boom ends to the variables used to describe the aircraft mechanics of the tanker and receiver, enabling trivial combination of the *individual aircraft mechanics* and *relative position kinematics*.

IFR turbulence is derived by extending the commonly used Dryden model for individual aircraft turbulence to include the similarity between the turbulence experienced by the tanker and receiver. The Gaussian distribution of the Dryden model allows the similarity to be described as covariance, whereas isotropy and homogeneity are used to describe the covariance.

The interested reader is referred to Appendix A.1 where the IFR mechanics is derived from first principles.

2.2 Frames, orientation and notation

This section introduces the frames, orientations and notation commonly used in aircraft mechanics modelling, as well as those unique to IFR.

2.2.1 Frames

In order to formulate the motion of an aircraft and the kinematics involved in IFR, a number of frames first need to be defined. Geographic, Body, Wind, Dryden, Refuelling, and Nozzle frames are defined as follows.

2.2.1.1 Geographical frame

An inertial frame is required if we are to apply *Newton's Second Law* and *Euler's Law* to describe the motion of an aircraft. For local subsonic atmospheric flight, the standard North-East-Down (NED) right-hand Cartesian frame G, shown in Figure 2.2, adequately approximates an inertial frame. The NED frame assumes a flat earth that is non-rotating. The origin of the frame, also known as its base point, is chosen to coincide with some convenient reference point G on the local geography [1] *e.g.* the starting position on a runway. From there, Cartesian component $\mathbf{g}_1$ (x-axis) points in the north direction, $\mathbf{g}_2$ (y-axis) points in the east direction and, together with $\mathbf{g}_1$, lies within a flat plane tangent to the earth's surface, and $\mathbf{g}_3$ (z-axis) completes the right-hand Cartesian base and points in the down direction.

Appendix A.1.2 is devoted to the localisation of *Newton's Second Law* and *Euler's Law* to the local geography. The localisation is used to investigates the error terms involved in approximating the inertial frame with the geographic frame, and concludes that the approximation is equivalent to assuming Galileo's hypothesis for falling bodies, valid for atmospheric flight with speeds less than Mach 5 [83, pp.81]. Appendix A.1.2 also considers the transglobal flight case, which may be included with the flat earth model with the use of geodetic measurements, equivalent to using a 2D world map, to account for the curvature of the earth.

2.2.1.2 Body frame

The body frame B, as shown in Figure 2.6, is fixed to the aircraft with its origin B chosen to coincide with the aircraft's centre of mass (cg). Cartesian component $\mathbf{b}_1$ lies in the aircraft plane of symmetry in the forward direction relative to the cockpit, and is parallel to the port side and starboard side thrust/propulsion vectors. $\mathbf{b}_3$ also lies in the aircraft plane of symmetry in the down direction relative to the cockpit and $\mathbf{b}_2$ completes the right-hand Cartesian base and points in the direction of the starboard wing (right wing).

1. Note that a frame is denoted by the same symbol as its base point.

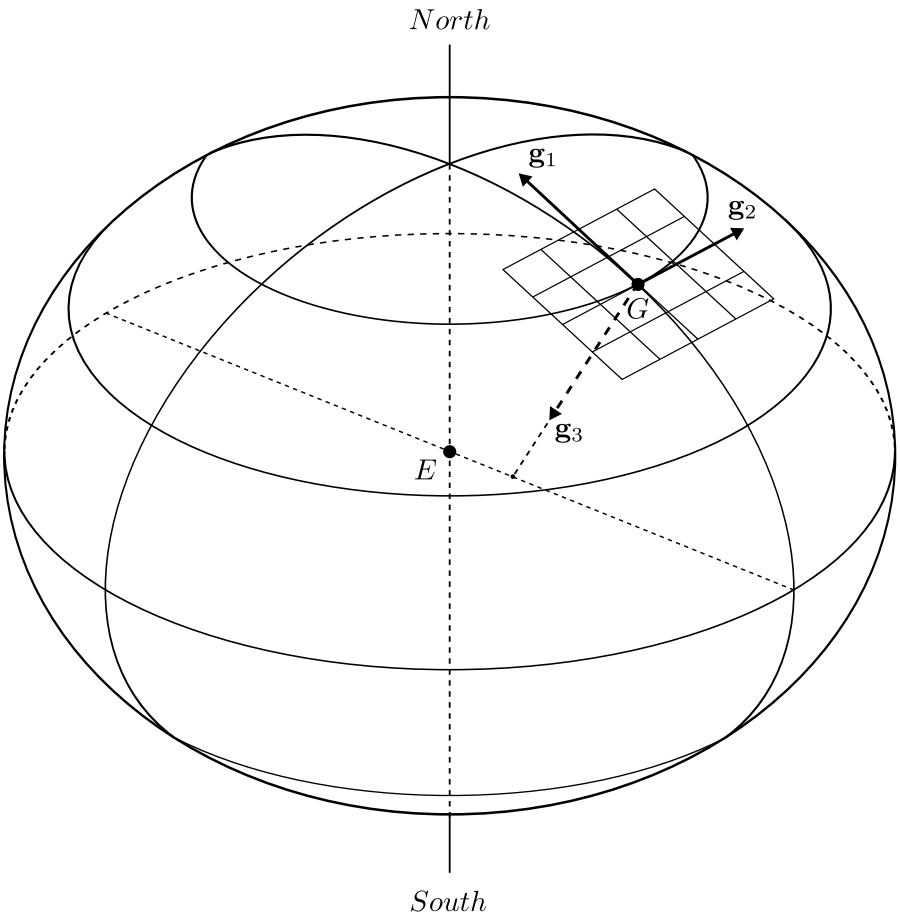

Figure 2.2: North-east-down runway frame.

2.2.1.3 Wind frame

The wind frame W, also known as the aerodynamic frame or the stability frame, is similar to the body frame in that its origin W coincides with the aircraft's centre of mass and thus moves with the aircraft. However, Cartesian component $\mathbf{w}_1$ points in the direction of the total velocity vector of point B with respect to the local surrounding atmosphere, *i.e.* in the direction of the wind relative to the aircraft, while $\mathbf{w}_3$ lies in the aircraft's plane of symmetry and points in the down direction relative to the cockpit. $\mathbf{w}_2$ completes the right-hand Cartesian base and points in the direction of the starboard wing for zero sideslip.

2.2.1.4 Dryden frame

The Dryden frame D, also referred to as the turbulence frame, is similar to the body frame in that its origin D coincides with the aircraft's centre of mass and thus moves with the aircraft. However, Cartesian component $\mathbf{d}_1$ points in the direction of the total velocity vector of the aircraft centre of mass B with respect to the surrounding *mean* atmosphere, *i.e.* with respect to surrounding atmosphere in the absence of the

turbulence, as seen in the aircraft body frame, while $\mathbf{d}_3$ lies in the aircraft's plane of symmetry and points in the down direction relative to the cockpit. $\mathbf{d}_2$ completes the right-hand Cartesian base and points in the direction of the starboard wing in straight and level flight. The Dryden frame coincides with the wind frame when the Dryden turbulence components are absent in the surrounding atmosphere, and the Dryden frame is used to include the Dryden turbulence components in the aircraft flight mechanics.

2.2.1.5 Refuelling frame

The refuelling frame J, also known as the boom joint frame, as shown in Figure 2.7, is fixed to the aircraft with its origin at the intersection of the aircraft and the boom, *i.e.* at the boom joint. Cartesian component $\mathbf{j}_1$ lies in the aircraft plane of symmetry and points in the backward direction, slightly upward relative to the cockpit, with an angle of $\kappa = \frac{3\pi}{180}$ rad relative to $-\mathbf{b}_1$. $\mathbf{j}_3$ also lies in the aircraft plane of symmetry in the up direction relative to the cockpit and $\mathbf{j}_2$ completes the right-hand Cartesian base and points in the direction of the starboard wing.

The refuelling frame is equivalent to the body frame, with a right-hand rotation of $(\pi - \kappa)$ rad about $\mathbf{b}_2$ and a linear translation to the boom joint.

2.2.1.6 Nozzle frame

The nozzle frame N, also known as the boom frame, as shown in Figure 2.7, is fixed to the variable length boom arm with its origin at the boom nozzle. Cartesian component $\mathbf{n}_1$ lies in the boom plane of symmetry and points away from the boom joint J, which is aligned with the length of the boom. $\mathbf{n}_3$ also lies in the boom plane of symmetry in the up direction relative to the cockpit when the boom is in its intermediate position, defined as being aligned with the length of the aircraft with $\mathbf{n}_1$ in the direction of $-\mathbf{b}_1$. $\mathbf{n}_2$ completes the right-hand Cartesian base and points in the direction of the starboard wing when the boom is in its intermediate position.

2.2.2 Orientations

The *Euler angles* system is one of two commonly used systems to describe the orientation of an aircraft, also known as aircraft attitude or rotation, because it is simple and intuitive to work with. The other is the *Quaternions* system, which is less intuitive and mathematically more complex.

The major drawback with Euler angles is that they experience a redundancy at two particular orientations whereas Quaternions avoid this singularity. However, for conventional flight, this redundancy (at $\pm\pi$ rad pitch angles) never comes into play, thus explaining the popularity of Euler angles. [63]

The Euler angles system describes the orientation of one frame to another with right-hand rotations about Cartesian base components in sequence. The three orientations

used in IFR mechanics modelling are given by: the rotation $\mathbf{R}^{BG}$ of the body frame B relative to the local geographic frame G; the rotation $\mathbf{R}^{BW}$ of the body frame B relative to the wind frame W; the rotation $\mathbf{R}^{NJ}$ of the nozzle frame N relative to the refuelling frame J. IFR rotations are defined as follows.

2.2.2.1 Aircraft orientation

$\mathbf{R}^{BG}$ is described through the sequence of rotations 3-2-1, denoted Euler 3-2-1 or yaw-pitch-roll. Two intermediate/synthetic frames X and Y are used to perform the rotations, and are illustrated in Figure 2.3 and given as

$$B \xleftarrow[\mathbf{y}_1]{\phi} Y \xleftarrow[\mathbf{x}_2]{\theta} X \xleftarrow[\mathbf{g}_3]{\psi} G \tag{2.1}$$

where ψ is the aircraft yaw angle, also known as its heading, θ is the aircraft pitch angle, and ϕ is the aircraft roll angle.

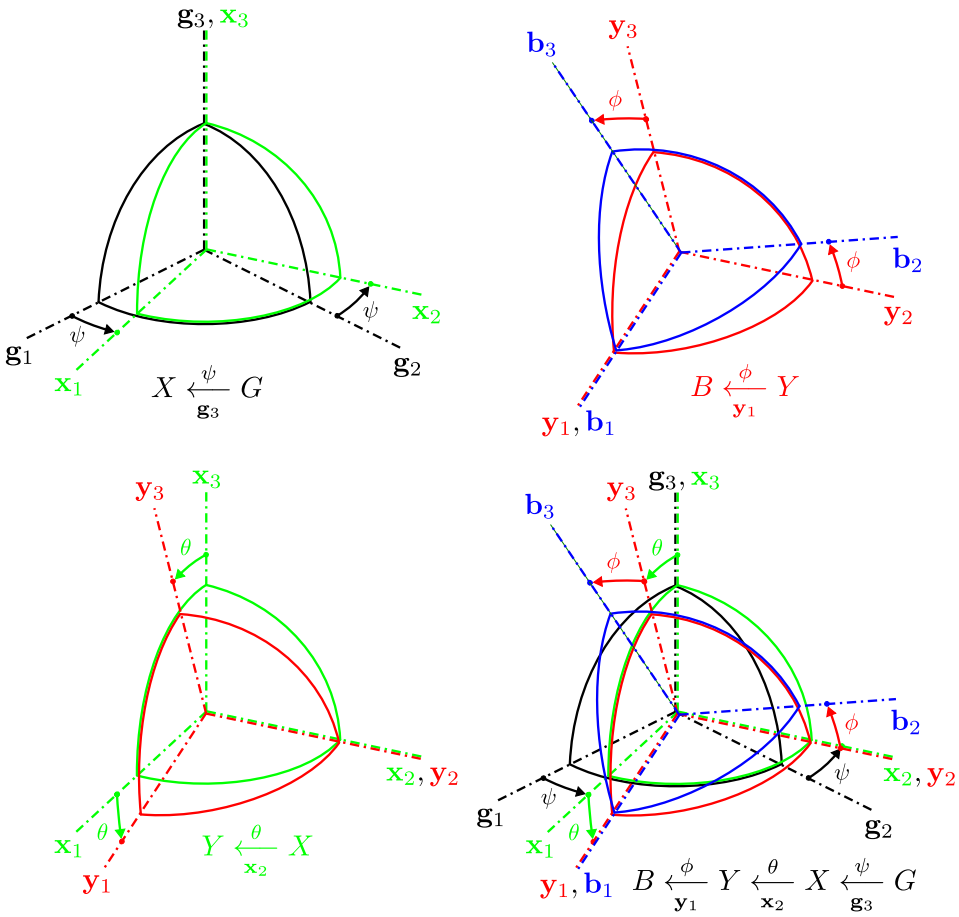

Figure 2.3: Euler 3-2-1 angle description of the rotation $\mathbf{R}^{BG}$ orange peel diagram.

$\mathbf{R}^{BW}$ is described through the sequence of rotations 3-2, denoted Euler 3-2. An intermediate/synthetic frame Z is used to perform the rotations, and is illustrated

in Figure 2.4 and given as

$$B \underset{\mathbf{z}_2}{\overset{\alpha}{\leftarrow}} Z \underset{\mathbf{s}_3}{\overset{-\beta}{\leftarrow}} W \tag{2.2}$$

where α is the angle of attack and β is the side-slip, the negative rotation of which is used as a matter of common convention.

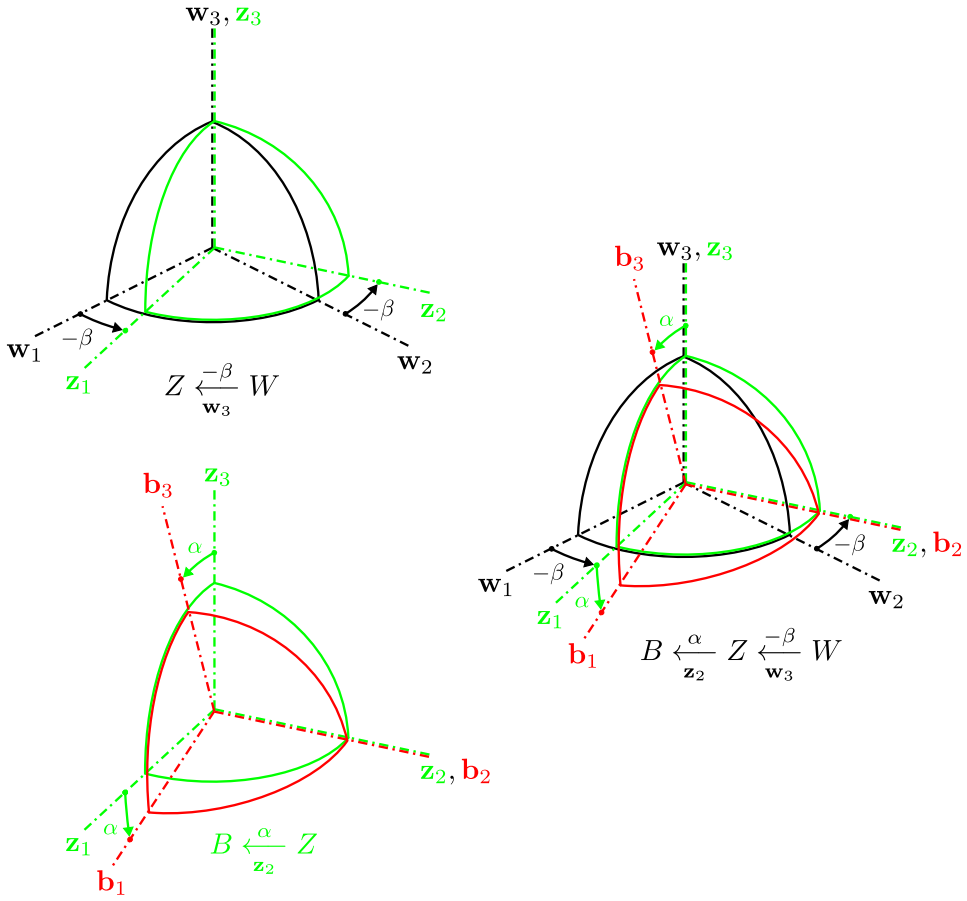

Figure 2.4: Euler 3-2 angle description of rotation $\mathbf{R}^{BS}$ orange peel diagram.

2.2.2.2 Boom orientation

$\mathbf{R}^{NJ}$ is described through the sequence of rotations 1-2, denoted Euler 1-2. An intermediate/synthetic frame U is used to perform the rotations, and is illustrated in Figure 2.5 and given as

$$N \underset{\mathbf{u}_2}{\overset{\sigma+\kappa}{\leftarrow}} U \underset{\mathbf{j}_1}{\overset{\chi}{\leftarrow}} J \tag{2.3}$$

where χ is the boom roll angle and $\sigma + \kappa$ is the boom pitch angle.

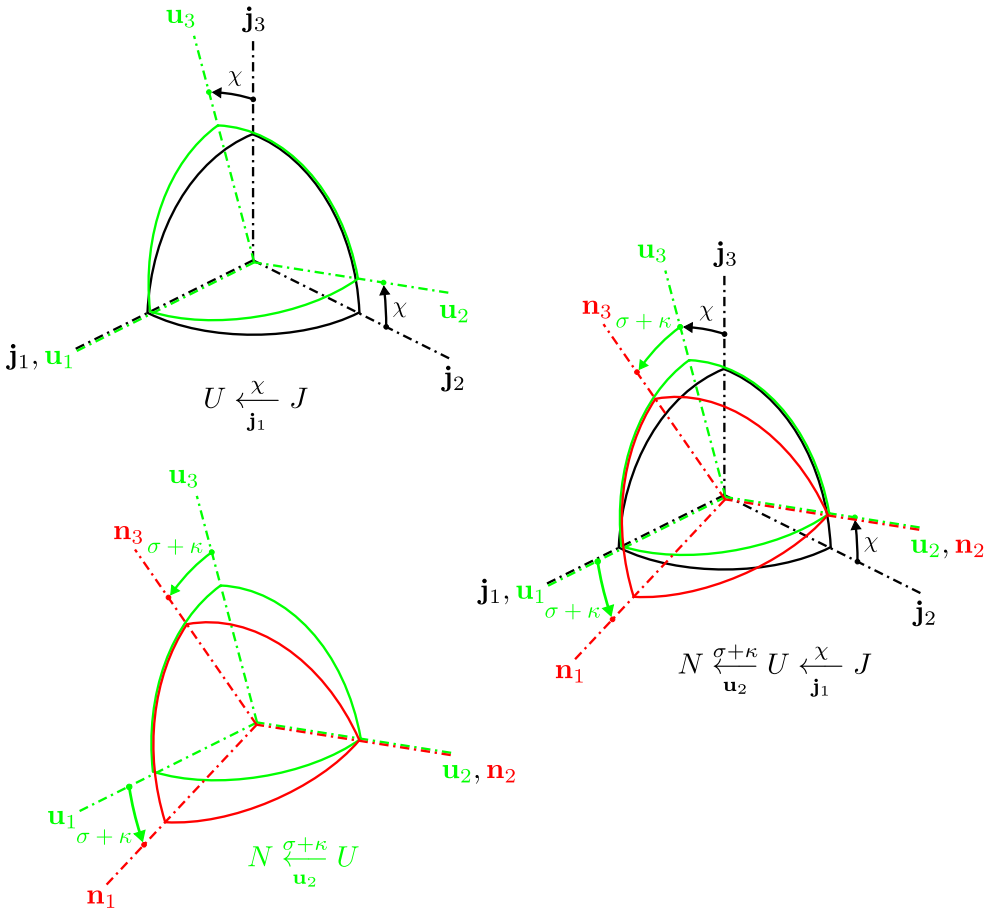

Figure 2.5: Euler 1-2 angle description of rotation $\mathbf{R}^{NJ}$ orange peel diagram.

2.2.3 Notations

2.2.3.1 Aircraft

Notations for an Airbus A330-MRTT are illustrated in Figure 2.6.

Aircraft motion variables are chosen as: the linear velocity

$$\left[D^G \mathbf{s}_{BG}\right]^B = \left[\mathbf{v}_B^G\right]^B = \begin{bmatrix} u \\ v \\ w \end{bmatrix} \tag{2.4}$$

of the aircraft *cg* with respect to the local geographic frame G, measured in body coordinates along its three base components; angular velocity

$$\left[\boldsymbol{\omega}^{BG}\right]^B = \begin{bmatrix} p \\ q \\ r \end{bmatrix} \tag{2.5}$$

of the body frame B with respect to the local geographic frame G, measured in body coordinates along its three base components; Euler angles ϕ, θ and ψ defined

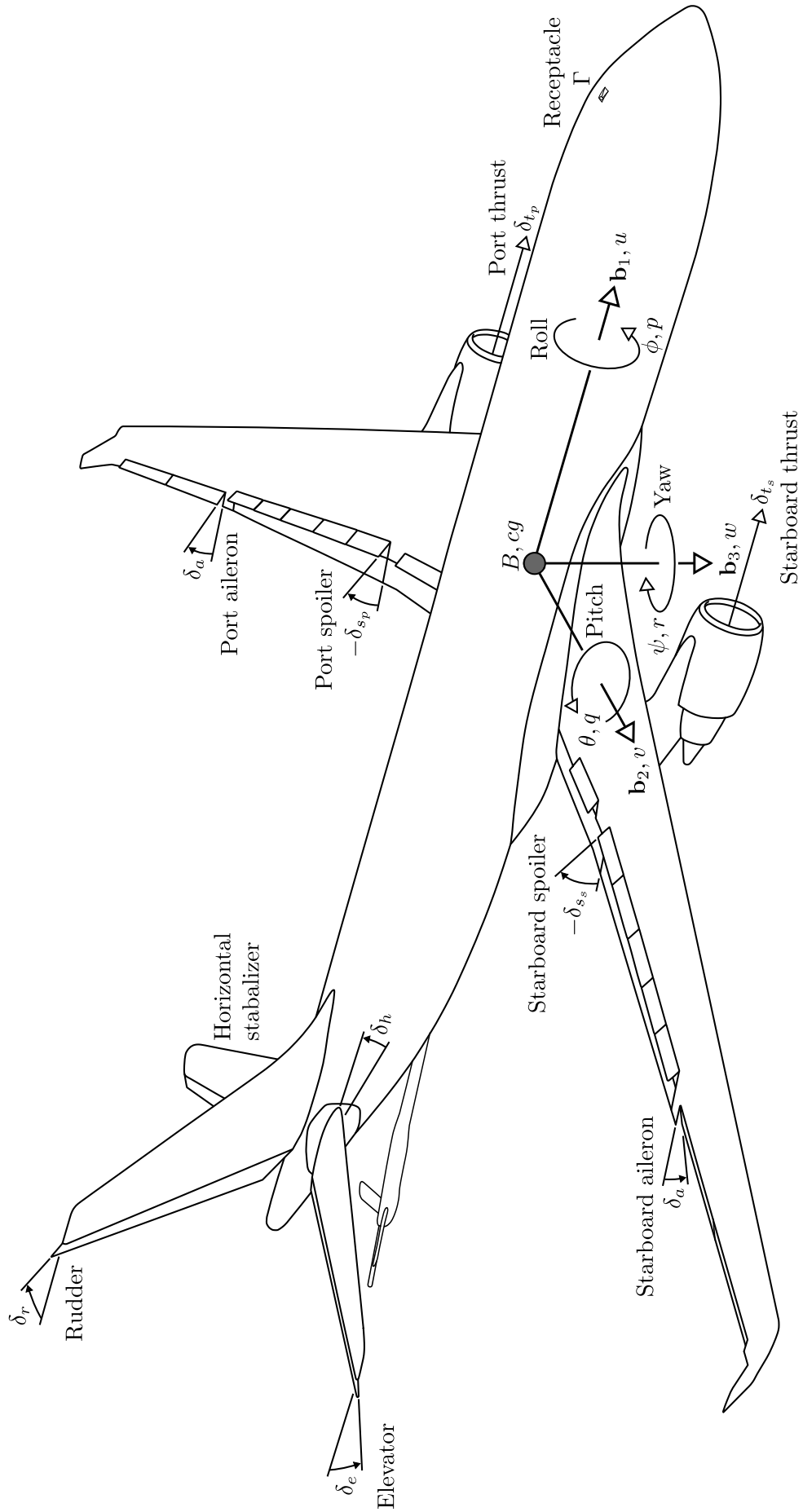

Figure 2.6: Aircraft notations.

above; altitude h. These motion variables arise naturally in the equations describing aircraft motion.

Aircraft control surfaces and thrust are: the deflections of ailerons δ_a; horizontal stabiliser δ_h; elevator δ_e; rudder δ_r; port and starboard spoilers δ_{s_p} and δ_{s_s}; port and starboard engine thrust/propulsion δ_{p_p} and δ_{p_s}. Aircraft spoilers and engines are used differentially.

The denotation of time dependencies of variables is omitted for convenience, *e.g.* u is used instead of $u(t)$. Aircraft motion variables, control surfaces and thrust are compactly written as

$$\mathbf{m} \coloneqq \begin{bmatrix} u \\ v \\ w \\ p \\ q \\ r \\ \phi \\ \theta \\ \psi \\ h \end{bmatrix}, \quad \boldsymbol{\delta} \coloneqq \begin{bmatrix} \delta_a \\ \delta_h \\ \delta_e \\ \delta_r \\ \delta_{s_p} \\ \delta_{s_s} \\ \delta_{t_p} \\ \delta_{t_s} \end{bmatrix} \tag{2.6}$$

The interested reader is referred to Appendix A.1.1 for the definition of basic tensor and projection notation used in (2.4) and (2.5).

2.2.3.2 Boom refuelling system

Notations for the boom refuelling system of the A330-MRTT are illustrated in Figure 2.7.

The boom refuelling system consists of a rigid boom with variable length λ, two control surfaces used to control its attitude,[2] a nozzle N connecting the boom to the receptacle of the receiver, and two gimbals connecting the boom to the aircraft at J, resulting in 3DOF.

The first gimbal is fixed to the aircraft, with freedom of rotation about $\mathbf{j}_1$ with positive right-hand rotation χ. The second gimbal is fixed to the first, with freedom of rotation about $\mathbf{u}_2$ with positive right-hand rotation $\sigma + \kappa$.

The maximum allowed perturbation of boom length $\varepsilon\lambda$ and gimbal angles $\varepsilon\sigma$ and $\varepsilon\chi$ define a boom envelope about its reference/centre, located at $\lambda_r = 15.73\,\text{m}$, $\sigma_r = \frac{30\pi}{180}\,\text{rad}$ and $\chi_r = 0$. Boom envelopes considered are the *contact envelope* and the *disconnect envelope*, the corresponding maximum perturbations of which are given in Table 2.1 and illustrated in Figure 2.8.

2. The control surfaces on the boom are used by the boom operator, who sits in the tail of the tanker facing the receiver, to connect and disconnect the boom to and from the receiver aircraft.

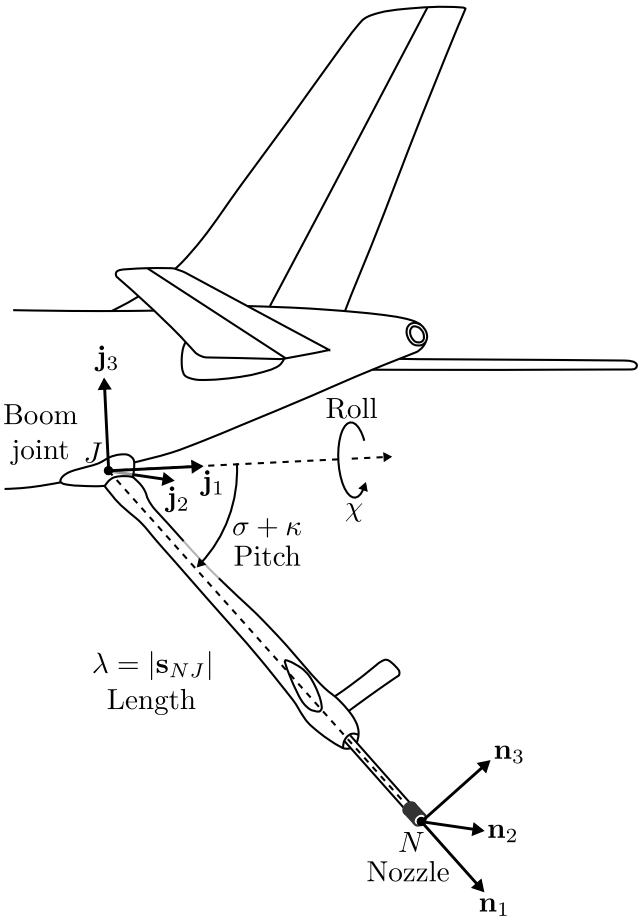

Figure 2.7: Refuelling system notations.

Boom perturbation component	Contact envelope	Disconnect envelope
$\varepsilon\lambda$	1.1 (0.3048) m [1]	6.1 (0.3048) m
$\varepsilon\sigma$	$\frac{4\pi}{180}$ rad	$\frac{10\pi}{180}$ rad
$\varepsilon\chi$	$\frac{10\pi}{180}$ rad	$\frac{20\pi}{180}$ rad

[1] 1 ft = 0.3048 m.

Table 2.1: Maximum boom perturbations defining boom envelopes.

2.3 Individual aircraft mechanics

The complete set of differential equations describing aircraft motion, known as the aircraft *Equations Of Motion* (EOM), is derived using the localised forms of *Newton's Second Law* for linear acceleration and of *Euler's Law* for angular acceleration (see Appendix A.1.2 for their localisation), and the *Euler transformation* (A.6). The aircraft mass distribution is assumed to be time-invariant, *i.e.* effects of fuel-transfer and shift in the centre of mass are omitted, which limits the EOM to the *contact phase*.

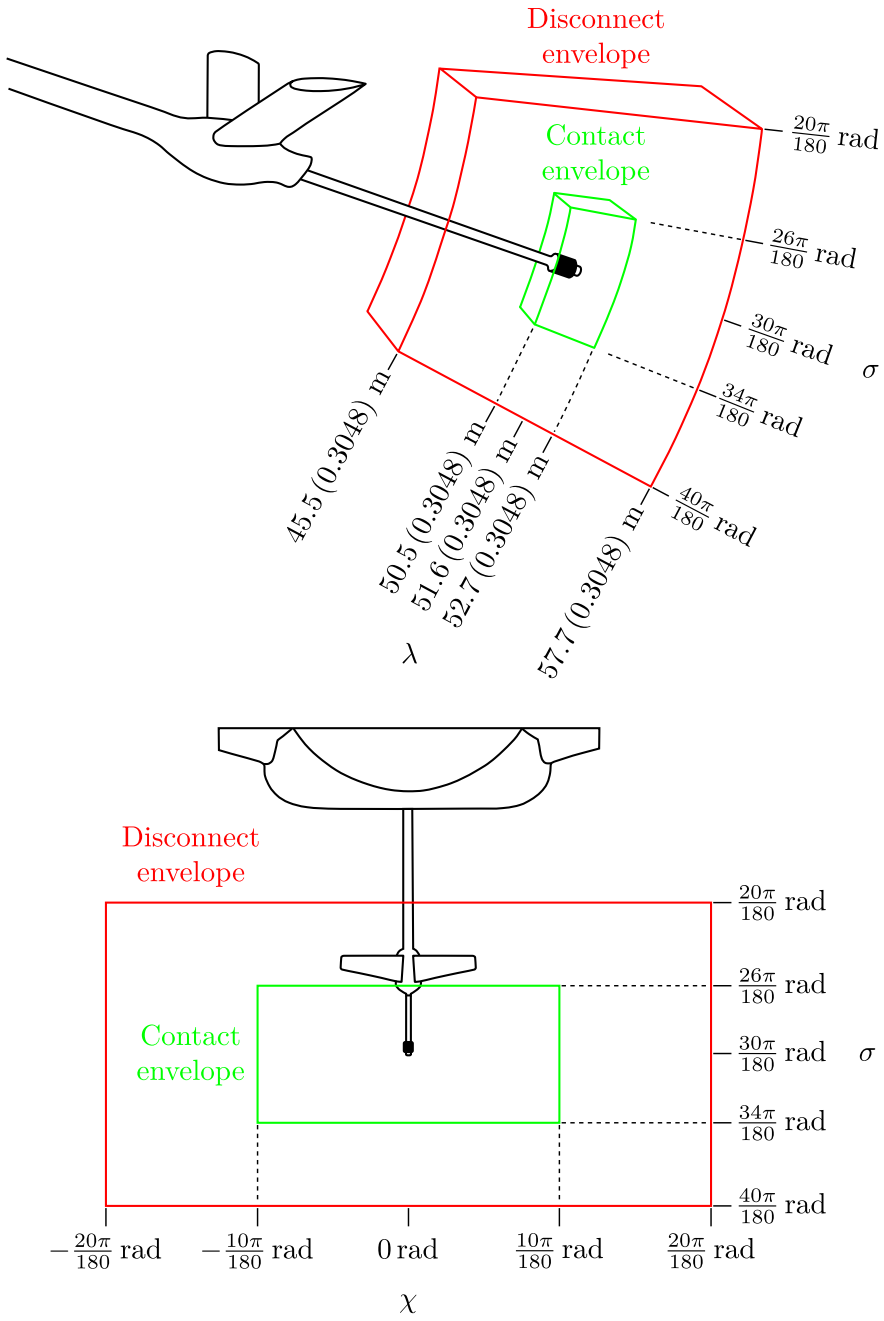

Figure 2.8: Boom envelopes. Views: L.H.S. of tanker (top); rear of tanker (bottom).

Aircraft linear acceleration is given in component form as

$$\begin{bmatrix} \dot{u} \\ \dot{v} \\ \dot{w} \end{bmatrix} \simeq - \begin{bmatrix} p \\ q \\ r \end{bmatrix} \times \begin{bmatrix} u \\ v \\ w \end{bmatrix} + [\mathbf{T}]^{BW} \left(\frac{\varrho_d s}{m_B} \begin{bmatrix} c_x \\ c_y \\ c_z \end{bmatrix} \right) + \frac{1}{m_B} \begin{bmatrix} \delta_{p_p} + \delta_{p_s} \\ 0 \\ 0 \end{bmatrix} + [\mathbf{T}]^{BG} \begin{bmatrix} 0 \\ 0 \\ g \end{bmatrix} \tag{2.7}$$

where $\times$ denotes the vector-product, a dot is used to denote the time-derivative, *e.g.* $\dot{u} \coloneqq \frac{du}{dt}$, ϱ_d is the dynamic pressure, s is the surface of the wing, m_B is the aircraft mass, c denotes an aerodynamic coefficient, $[\mathbf{T}]^{BW}$ is a Transformation matrix that converts measurement along the wind frame base vectors $\{\mathbf{w}_1, \mathbf{w}_2, \mathbf{w}_3\}$ to that of the body frame $\{\mathbf{b}_1, \mathbf{b}_2, \mathbf{b}_3\}$, $[\mathbf{T}]^{BG}$ is a Transformation matrix that converts measurement along the local geographic frame base vectors $\{\mathbf{g}_1, \mathbf{g}_2, \mathbf{g}_3\}$ to that of the body frame $\{\mathbf{b}_1, \mathbf{b}_2, \mathbf{b}_3\}$, and $g \simeq 9.81\,\mathrm{m/s^2}$ is the gravitational acceleration.

Aircraft angular acceleration is given in component form as

$$\begin{bmatrix} \dot{p} \\ \dot{q} \\ \dot{r} \end{bmatrix} \simeq \left(\left[\mathbf{I}_B^B \right]^B \right)^{-1} \left(- \begin{bmatrix} p \\ q \\ r \end{bmatrix} \times \left(\left[\mathbf{I}_B^B \right]^B \begin{bmatrix} p \\ q \\ r \end{bmatrix} \right) + [\mathbf{T}]^{BW} \left(\varrho_d s l \begin{bmatrix} c_l \\ c_m \\ c_n \end{bmatrix} \right) \right.$$
$$\left. + \left(\begin{bmatrix} \delta_{p_p} \\ 0 \\ 0 \end{bmatrix} \times \left[\mathbf{s}_{P_p B} \right]^B + \begin{bmatrix} \delta_{p_s} \\ 0 \\ 0 \end{bmatrix} \times \left[\mathbf{s}_{P_s B} \right]^B \right) \right) \tag{2.8}$$

where l is the reference cord length of the wing, P_p and P_s denote points on the portside and starboard engine thrust/propulsion vector respectively, *i.e.* the engine axes, and $\left[\mathbf{I}_B^B \right]^B$ is the aircraft moment of inertia about its centre of mass measured along the base components of the body frame B.

Transformation matrices are capable of interchanging between the measurements along the base components of any two frames. Consider the single axis yaw rotation shown in Figure 2.9 below. Given the coordinates of vector $\mathbf{v}$ measured along the

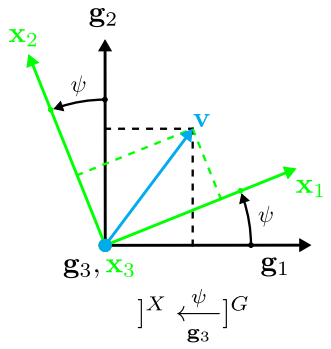

Figure 2.9: Single axes yaw rotation.

base components of the original frame G,

$$[\mathbf{v}]^G = \begin{bmatrix} v_1 \\ v_2 \\ v_3 \end{bmatrix} \tag{2.9}$$

then, through simple geometry it is straightforward to show that the coordinates of $\mathbf{v}$ in the rotated frame X are related to the coordinates of $\mathbf{v}$ in the original frame

through the transformation matrix below,

$$[\mathbf{T}]^{XG} = \begin{bmatrix} \cos\psi & \sin\psi & 0 \\ -\sin\psi & \cos\psi & 0 \\ 0 & 0 & 1 \end{bmatrix} \tag{2.10}$$

i.e.

$$[\mathbf{v}]^{X} = [\mathbf{T}]^{XG}\,[\mathbf{v}]^{G} \tag{2.11}$$

Similarly, the rotations through the pitch and roll angles, illustrated in Figure 2.3, yield their respective transformation matrices

$$[\mathbf{T}]^{YX} = \begin{bmatrix} \cos\theta & 0 & -\sin\theta \\ 0 & 1 & 0 \\ \sin\theta & 0 & \cos\theta \end{bmatrix} \tag{2.12}$$

and

$$[\mathbf{T}]^{BY} = \begin{bmatrix} 1 & 0 & 0 \\ 0 & \cos\phi & \sin\phi \\ 0 & -\sin\phi & \cos\phi \end{bmatrix} \tag{2.13}$$

(2.10), (2.12) and (2.13) can be multiplied together to relate the coordinates of vector $\mathbf{v}$ in original frame G to its coordinates in the frame which has been yawed, pitched and rolled,

$$\begin{aligned} [\mathbf{v}]^{B} &= [\mathbf{T}]^{BY}\,[\mathbf{v}]^{Y}, \quad [\mathbf{v}]^{Y} = [\mathbf{T}]^{YX}\,[\mathbf{v}]^{X}, \quad [\mathbf{v}]^{X} = [\mathbf{T}]^{XG}\,[\mathbf{v}]^{G} \\ [\mathbf{v}]^{B} &= [\mathbf{T}]^{BY}\,[\mathbf{T}]^{YX}\,[\mathbf{T}]^{XG}\,[\mathbf{v}]^{G} \\ &= [\mathbf{T}]^{BG}\,[\mathbf{v}]^{G} \end{aligned} \tag{2.14}$$

where

$$[\mathbf{T}]^{BG} = \begin{bmatrix} \cos\psi\cos\theta & \sin\psi\cos\theta & -\sin\theta \\ \cos\psi\sin\theta\sin\phi - \sin\psi\cos\phi & \sin\psi\sin\theta\sin\phi + \cos\psi\cos\phi & \cos\theta\sin\phi \\ \cos\psi\sin\theta\cos\phi + \sin\psi\sin\phi & \sin\psi\sin\theta\cos\phi - \cos\psi\sin\phi & \cos\theta\cos\phi \end{bmatrix} \tag{2.15}$$

(2.15) is commonly referred to as a Direction Cosine Matrix (DCM), and has the property of being orthonormal.

DCM $[\mathbf{T}]^{BW}$ may be similarly derived with the rotations defined in Figure 2.4 as

$$[\mathbf{T}]^{BW} = \begin{bmatrix} \cos\beta\cos\alpha & -\sin\beta\cos\alpha & -\sin\alpha \\ \sin\beta & \cos\beta & 0 \\ \cos\beta\sin\alpha & -\sin\beta\sin\alpha & \cos\alpha \end{bmatrix} \tag{2.16}$$

The aerodynamic coefficients are functions of the aircraft motion variables, wind components and control surface deflections, provided by Airbus in wind frame coordinates. $\varrho_d s$ and $\varrho_d sl$ are used to de-scale the aerodynamic coefficients to aerodynamic forces and moments respectively.

Euler 3-2-1 angles Differential Equation (DE), *i.e.* the time-rate of change of the Euler 3-2-1 angles, are included so that all the variables involved in (2.7) & (2.8) are governed. The Euler 3-2-1 angles DE, also known as the *gimbal equation*, is expressed in terms of body angular rates, and is given in [83, pp.121] as

$$\begin{bmatrix} \dot{\phi} \\ \dot{\theta} \\ \dot{\psi} \end{bmatrix} = \begin{bmatrix} 1 & \sin\phi\tan\theta & \cos\phi\tan\theta \\ 0 & \cos\phi & -\sin\phi \\ 0 & \sin\phi/\cos\theta & \cos\phi/\cos\theta \end{bmatrix} \begin{bmatrix} p \\ q \\ r \end{bmatrix}, \quad \theta \neq \frac{\pi}{2} + k\pi,\ k \in \mathbb{Z}^1 \tag{2.17}$$

Aircraft climb-rate is given as

$$\dot{h} = \begin{bmatrix} 0 & 0 & -1 \end{bmatrix} [\mathbf{T}]^{GB} \begin{bmatrix} u \\ v \\ w \end{bmatrix} \tag{2.18}$$

where $[\mathbf{T}]^{GB}$ is the transpose of $[\mathbf{T}]^{BG}$, and is included due to the dependency of aircraft linear and angular acceleration on altitude, inherent in the dynamic pressure ϱ_d and the aerodynamic coefficients.

The derivation of the aircraft 6DOF EOM from first principles is considered standard procedure, and can be found in Appendix A.1.3.

2.4 Aircraft relative position kinematics

The aircraft relative position kinematics is given in terms of the tanker and receiver aircraft motion variables, to enable its incorporation into tanker and receiver 6DOF EOM.

Refer to Figure 2.10. IFR regulation outputs λ, σ and χ are completely described by the relative position $\mathbf{s}_{\Gamma J}$ when measured along the base components of the tanker body frame,[3] which motivates the use of the tanker body frame to describe the aircraft relative position kinematics. The derivation is based on the time-derivative of vector triangle $\mathbf{s}_{\Gamma J} = \mathbf{s}_{\Gamma G} - \mathbf{s}_{JG}$ with respect to the local geographic frame G, which is then described with the tanker and receiver motion variables using the Euler transformation (A.6).

The DE describing aircraft relative position kinematics is derived in Appendix A.1.4 for time-invariant aircraft centre of mass, given in component form as

$$\begin{aligned} \begin{bmatrix} \dot{x}_b \\ \dot{y}_b \\ \dot{z}_b \end{bmatrix} = &- \begin{bmatrix} p_T \\ q_T \\ r_T \end{bmatrix} \times \begin{bmatrix} x_b \\ y_b \\ z_b \end{bmatrix} + [\mathbf{T}]^{TR} \left(\begin{bmatrix} p_R \\ q_R \\ r_R \end{bmatrix} \times [\mathbf{s}_{\Gamma R}]^R \right) \\ &+ [\mathbf{T}]^{TR} \begin{bmatrix} u_R \\ v_R \\ w_R \end{bmatrix} - \begin{bmatrix} p_T \\ q_T \\ r_T \end{bmatrix} \times [\mathbf{s}_{JT}]^T - \begin{bmatrix} u_T \\ v_T \\ w_T \end{bmatrix} \end{aligned} \tag{2.19}$$

3. As opposed to measuring $\mathbf{s}_{\Gamma J}$ along the base components of the receiver body frame, which requires additional relative attitude to describe λ, σ and χ.

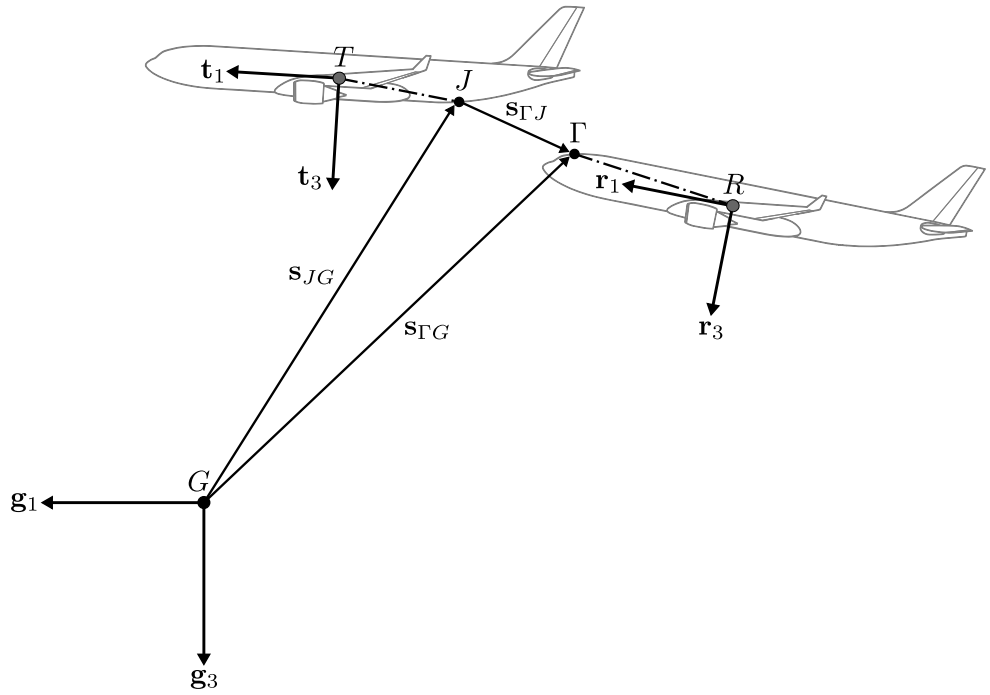

Figure 2.10: IFR kinematic coupling 2D vector diagram.

where

$$\begin{bmatrix} x_b \\ y_b \\ z_b \end{bmatrix} \coloneqq [\mathbf{s}_{\Gamma J}]^T \tag{2.20}$$

is the position of the receiver receptacle Γ relative to the tanker boom joint J measured along the base components of the tanker body frame, components with subscript T relate to the tanker, components with subscript R relate to the receiver, $[\mathbf{s}_{\Gamma R}]^R$ is the receiver receptacle position relative to its centre of mass measured along the base components of the receiver body frame and $[\mathbf{s}_{JT}]^T$ is the tanker boom joint position relative to its centre of mass measured along the base components of the tanker body frame. The aircraft relative position motion variables are compactly written as

$$\mathbf{b} \coloneqq \begin{bmatrix} x_b \\ y_b \\ z_b \end{bmatrix} \tag{2.21}$$

It is apparent that one of the 3DOF in relative position described by $\mathbf{b}$ is also described by relative altitude $h_T - h_R$. The relation between $h_T - h_R$ and $\mathbf{b}$ is derived in Appendix A.1.4 and given as

$$h_T - h_R = \begin{bmatrix} 0 & 0 & 1 \end{bmatrix} \left([\mathbf{T}]^{GR} [\mathbf{s}_{R\Gamma}]^R + [\mathbf{T}]^{GT} \begin{bmatrix} x_b \\ y_b \\ z_b \end{bmatrix} + [\mathbf{T}]^{GT} [\mathbf{s}_{JT}]^T \right) \tag{2.22}$$

Furthermore, assuming the nozzle is connected to the receiver receptacle, *i.e.* base point N and point Γ coincide, boom variables may be expressed in terms of relative

position components and are derived in Appendix A.1.4 as

$$\lambda = \sqrt{x_b^2 + y_b^2 + z_b^2}, \quad \lambda > 0 \tag{2.23}$$

$$\sigma = \cos^{-1}\left(\frac{-x_b \cos(\kappa) - z_b \sin(\kappa)}{\sqrt{x_b^2 + y_b^2 + z_b^2}}\right) - \kappa, \quad \lambda > 0,\ \sigma > 0 \tag{2.24}$$

and

$$\chi = \operatorname{sgn}(y_b) \cos^{-1}\left(\frac{-x_b \sin(\kappa) + z_b \cos(\kappa)}{\sqrt{y_b^2 + (-x_b \sin(\kappa) + z_b \cos(\kappa))^2}}\right), \quad \lambda > 0,\ -\pi < \chi < \pi \tag{2.25}$$

This concludes the IFR kinematics, and we proceed to the final model component of IFR.

2.5 Atmospheric turbulence

2.5.1 Dryden model

The Dryden model describes the atmospheric turbulence experienced by an aircraft with respect to the surrounding mean atmosphere, *i.e.* with respect to surrounding atmosphere in the absence of the turbulence. The model is presented as temporal linear shaping filters driven by zero-mean unit intensity Gaussian white noise, the bandwidths and gains of which are functions of altitude, mean airspeed and wingspan. The filter outputs, which contribute to the aircraft aerodynamic forces and moments, are added to the local mean atmosphere surrounding the aircraft.

The *Dryden*[4] turbulence model used is a very simple linear model, which characterises turbulence in terms of its spectral characteristics. Dryden turbulence is specified for an aircraft in MIL-F-8785C [1, pp.45-60] as *one-dimensional single-sided spatial spectrum functions* of *linear velocity* components

$$\phi_{u_g}(\Omega) = \sigma_{u_g}^2 \frac{2l_{u_g}}{\pi} \frac{1}{1 + (l_{u_g}\Omega)^2} \tag{2.26}$$

$$\phi_{v_g}(\Omega) = \sigma_{v_g}^2 \frac{l_{v_g}}{\pi} \frac{1 + 3(l_{v_g}\Omega)^2}{\left(1 + (l_{v_g}\Omega)^2\right)^2} \tag{2.27}$$

$$\phi_{w_g}(\Omega) = \sigma_{w_g}^2 \frac{l_{w_g}}{\pi} \frac{1 + 3(l_{w_g}\Omega)^2}{\left(1 + (l_{w_g}\Omega)^2\right)^2} \tag{2.28}$$

4. Named after Hugh L. Dryden (1898-1965), after whom the NASA Dryden Flight Research Centre was also named.

and of *angular velocity* components

$$\phi_{p_g}(\Omega) = 0.8\frac{\sigma_{w_g}^2}{l_{w_g}}\left(\frac{\pi l_{w_g}}{4b}\right)^{\frac{1}{3}}\frac{1}{1+\left(\frac{4b}{\pi}\Omega\right)^2} \tag{2.29}$$

$$\phi_{q_g}(\Omega) = \frac{\Omega^2}{1+\left(\frac{4b}{\pi}\Omega\right)^2}\phi_{w_g}(\Omega) \tag{2.30}$$

$$\phi_{r_g}(\Omega) = \frac{\Omega^2}{1+\left(\frac{3b}{\pi}\Omega\right)^2}\phi_{v_g}(\Omega) \tag{2.31}$$

where the spectra have Gaussian distributions, ϕ is measured in $(\mathrm{m}^3/\mathrm{s}^2)$, Ω $(\mathrm{rad}/\mathrm{m})$ is the spatial frequency, b (m) is the wingspan, l (m) is the turbulence scale length and σ $(\mathrm{m}/\mathrm{s}^2)$ is the turbulence standard deviation. u_g, v_g and w_g denote the components of turbulence linear velocity of the local atmosphere surrounding the aircraft with respect to its mean, measured along the base components $\mathbf{d}_1$, $\mathbf{d}_2$ and $\mathbf{d}_3$ of the Dryden frame respectively. p_g, q_g and r_g denote the components of turbulence angular velocity of the local atmosphere surrounding the aircraft with respect to its mean, measured along the base components $\mathbf{b}_1$, $\mathbf{b}_2$ and $\mathbf{b}_3$ of the body frame respectively. Furthermore, turbulence components u_g, v_g, w_g and p_g are considered mutually independent (uncorrelated).

The Dryden spectra are sufficiently accurate to use for controller optimisation at low frequencies and the cut-off region, although the fall-off is steeper than actual fall-off found in turbulence spectral analysis [60, 44, pp.953;2-117]. Depending on the aircraft, the steeper fall-off might fail to stimulate high-frequency aircraft modes [32, pp.538], resulting in poor turbulence rejection. Closed-loop turbulence rejection should be validated by including aircraft structural modes with the flight mechanics and using a turbulence model with a more accurate fall-off such as the *von Kármán* model, also specified in [1].

For engineering purposes, turbulence above $2'000\,(0.3048)$ m is adequately described as [32, pp.532,533,539]: *Gaussian*; *homogeneous* at constant altitude; *incompressible* in sub-sonic flight*; isotropic*. *Gaussian* processes have the advantage of being low-risk bounded in terms of their variance, *e.g.* 4σ-bound is maintained 99.994% of the time. *Gaussian homogeneous* turbulence at constant altitude permits the use of LTI spatial turbulence models in straight and level flight. *Incompressibility* amounts to [32, pp.538]

$$l_g \coloneqq l_{u_g} = l_{v_g} = l_{w_g} \tag{2.32}$$

The stochastic properties of *isotropic* turbulence are independent of orientation and amount to [32, pp.532]

$$\sigma_g^2 \coloneqq \sigma_{u_g}^2 = \sigma_{v_g}^2 = \sigma_{w_g}^2 \tag{2.33}$$

and are also useful for modelling cross-correlation between tanker and receiver turbulence components (see Section 2.5.2). The Dryden turbulence specified in MIL-STD-1797A [2, pp.678-697], as required by *Performance Specification no.7* in Section 1.3, has linear velocity *one-dimensional single-sided spatial spectrum functions* equal to those of MIL-F-8785C [1, pp.45-60] for medium/high altitude

($> 2'000\,(0.3048)$ ft), but does not assume incompressibility (2.32) and lacks angular velocity *one-dimensional single-sided spatial spectrum functions* present in the MIL-F-8785C description. We make the following assumption:

Assumption 1. The turbulence experienced in IFR admits incompressibility.

It follows that **we substitute the use of MIL-STD-1797A with MIL-F-8785C to describe Dryden turbulence**.

A number of transformations are performed on spatial functions (2.26)-(2.31), to obtain their respective temporal shaping-filters, driven by unit intensity Gaussian white noise, and can be found in Appendix A.1.7. The resulting shaping-filters assume that the aircraft speed relative to the local atmospheric mean is constant, and is given as

$$\mathcal{D}_{u_g}(j\omega) = \frac{\mathcal{U}_g(j\omega)}{\mathcal{N}_{u_g}(j\omega)} = \sigma_g \sqrt{\frac{2l_g}{\vartheta}} \frac{1}{1+\frac{l_g}{\vartheta}j\omega} \tag{2.34}$$

$$\mathcal{D}_{v_g}(j\omega) = \frac{\mathcal{V}_g(j\omega)}{\mathcal{N}_{v_g}(j\omega)} = \sigma_g \sqrt{\frac{l_g}{\vartheta}} \frac{1+\sqrt{3}\frac{l_g}{\vartheta}j\omega}{\left(1+\frac{l_g}{\vartheta}j\omega\right)^2} \tag{2.35}$$

$$\mathcal{D}_{w_g}(j\omega) = \frac{\mathcal{W}_g(j\omega)}{\mathcal{N}_{w_g}(j\omega)} = \sigma_g \sqrt{\frac{l_g}{\vartheta}} \frac{1+\sqrt{3}\frac{l_g}{\vartheta}j\omega}{\left(1+\frac{l_g}{\vartheta}j\omega\right)^2} \tag{2.36}$$

$$\mathcal{D}_{p_g}(j\omega) = \frac{\mathcal{P}_g(j\omega)}{\mathcal{N}_{p_g}(j\omega)} = \sigma_g \left(\frac{0.8\pi}{l_g\vartheta}\right)^{\frac{1}{2}} \left(\frac{\pi l_g}{4b}\right)^{\frac{1}{6}} \frac{1}{1+\frac{4b}{\pi\vartheta}j\omega} \tag{2.37}$$

$$\frac{\mathcal{D}_{q_g}(j\omega)}{\mathcal{D}_{w_g}(j\omega)} = \frac{\mathcal{Q}_g(j\omega)}{\mathcal{W}_g(j\omega)} = \frac{1}{\vartheta}\frac{j\omega}{1+\frac{4b}{\pi\vartheta}j\omega} \tag{2.38}$$

$$\frac{\mathcal{D}_{r_g}(j\omega)}{\mathcal{D}_{v_g}(j\omega)} = \frac{\mathcal{R}_g(j\omega)}{\mathcal{V}_g(j\omega)} = \frac{1}{\vartheta}\frac{j\omega}{1+\frac{3b}{\pi\vartheta}j\omega} \tag{2.39}$$

where ϑ is the aircraft speed relative to the surrounding atmospheric mean, $\mathcal{N}(j\omega)$ is the spectrum of the Gaussian/Normally distributed white noise filter input, and $\{\mathcal{U}_g(j\omega), \mathcal{V}_g(j\omega), \mathcal{W}_g(j\omega), \mathcal{P}_g(j\omega), \mathcal{Q}_g(j\omega), \mathcal{R}_g(j\omega)\}$ are conventional double-sided spectra of turbulence velocities components $\{u_g, v_g, w_g, p_g, q_g, r_g\}$.

MIL-F-8785C specifies the turbulence scale length above $2'000\,(0.3048)$ m as constant $l_g = 533.4$ m and the turbulence amplitude as

$$\sigma_g = \begin{cases} 3.048\iota, & 3'048 \le h < 3'475\,\text{m} \\ \left(3.048 - \left(\frac{3.048}{14630}\right)(h - 3'475)\right)\iota, & 3'475 \le h < 9'144\,\text{m} \end{cases} \quad (\text{m/s}) \tag{2.40}$$

where

$$\iota = \begin{cases} 0.5, & \text{for light turbulence} \\ 1, & \text{for medium turbulence} \\ 2, & \text{for severe turbulence} \end{cases} \quad (\text{rad}) \tag{2.41}$$

which decreases linearly above $11'400\,(0.3048)$ m.

A Bode-plot of the shaping-filters, with appropriate normalisations, is given in Figure 2.11, illustrating the turbulence spectrum involved in A330-MRTT atmospheric flight.

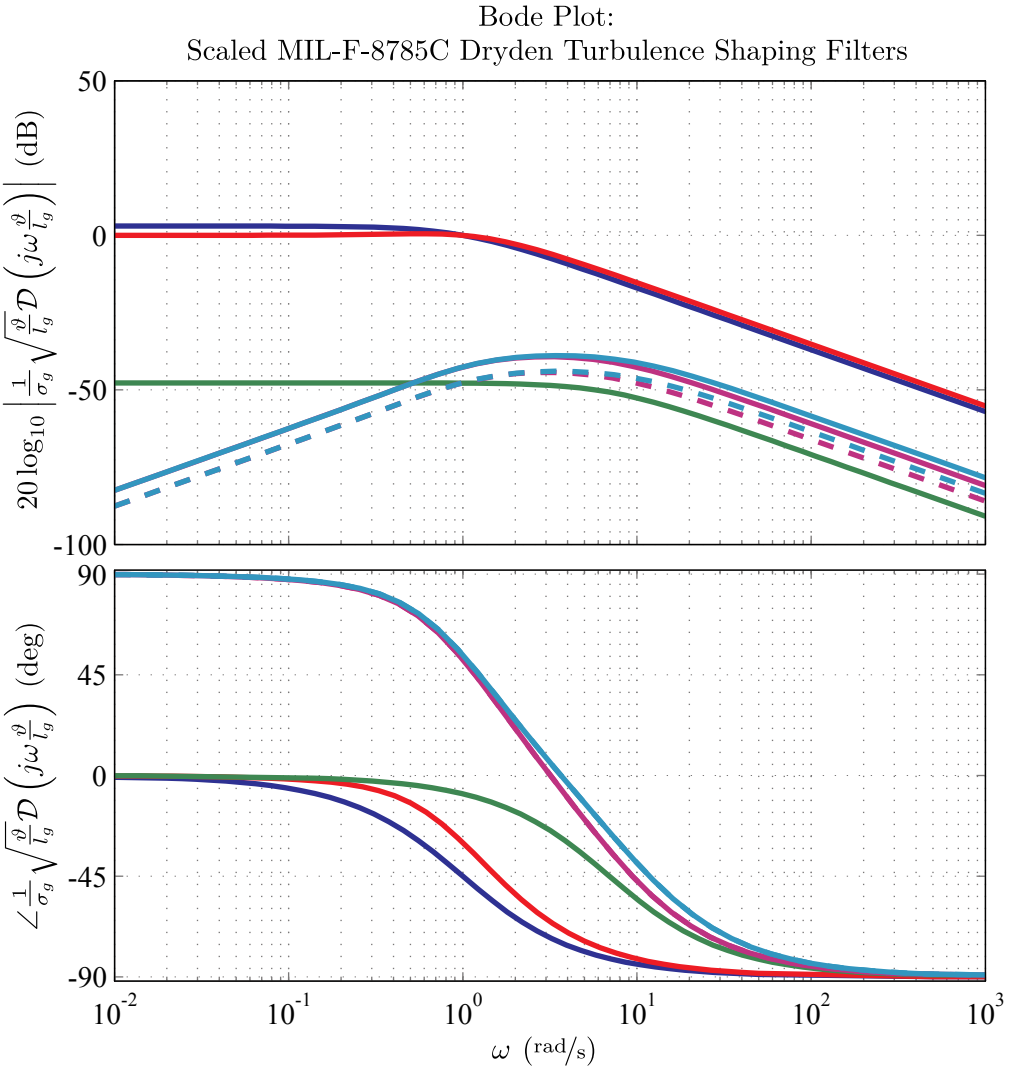

Figure 2.11: Bode plot of scaled MIL-F-8785C Dryden turbulence shaping filters for unit intensity white noise input. Multiplication factor for amplitude scaling is $\frac{1}{\sigma_g}\sqrt{\frac{\vartheta}{l_g}}$ ($\sqrt{\text{s}}/\text{m}$) and for frequency scaling $\frac{\vartheta}{l_g}$ (s). $b = 60.306\,\text{m}$, $l_g = 533.4\,\text{m}$, $\max\vartheta = 240\,\text{m/s}$, $\min\vartheta = 134\,\text{m/s}$. Turbulence components: u_g (blue); v_g and w_g (red); p_g (green); $\sup_\omega q_g$; (purple solid); $\inf_\omega q_g$ (purple dashed); $\sup_\omega r_g$ (cyan solid); $\inf_\omega r_g$ (cyan dashed).

The turbulence angular velocity components have bandwidths of approximately 1 decade higher than the linear velocity components, with only the amplitude of scaled turbulence components q_g and r_g varying over the flight-envelope with a range of

$$\begin{aligned} 20\log_{10}\left(\frac{\sup_\omega\left|\frac{1}{\sigma_g}\sqrt{\frac{\vartheta}{l_g}}\mathcal{D}_{q_g}\left(j\omega\frac{\vartheta}{l_g}\right)\right|}{\inf_\omega\left|\frac{1}{\sigma_g}\sqrt{\frac{\vartheta}{l_g}}\mathcal{D}_{q_g}\left(j\omega\frac{\vartheta}{l_g}\right)\right|}\right) &= 20\log\left(\frac{\max\vartheta}{\min\vartheta}\right) \\ &= 5.06\,\mathrm{dB} \\ &= 20\log_{10}\left(\frac{\sup_\omega\left|\frac{1}{\sigma_g}\sqrt{\frac{\vartheta}{l_g}}\mathcal{D}_{r_g}\left(j\omega\frac{\vartheta}{l_g}\right)\right|}{\inf_\omega\left|\frac{1}{\sigma_g}\sqrt{\frac{\vartheta}{l_g}}\mathcal{D}_{r_g}\left(j\omega\frac{\vartheta}{l_g}\right)\right|}\right) \end{aligned} \tag{2.42}$$

where

$$134 \leq \vartheta \leq 240\,\mathrm{m/s} \tag{2.43}$$

The Dryden turbulence model inputs and outputs are compactly written as

$$\boldsymbol{\eta} \coloneqq \begin{bmatrix} \eta_{u_g} & \eta_{v_g} & \eta_{w_g} & \eta_{p_g} \end{bmatrix}^T, \quad \mathbf{g} \coloneqq \begin{bmatrix} u_g & v_g & w_g & p_g & q_g & r_g \end{bmatrix}^T \tag{2.44}$$

where $\mathcal{N}(j\omega)|_{s=j\omega} = \mathcal{L}\{\eta(t)\}$,

$$\mathbb{E}\{\boldsymbol{\eta}(t)\} = \mathbf{0}, \quad \mathbb{E}\left\{\boldsymbol{\eta}(t)\,\boldsymbol{\eta}^T(t)\right\} = \uparrow(t)\,I \tag{2.45}$$

and $\uparrow(t)$ is the *Dirac delta* impulse function.

The turbulence velocity $\mathbf{g}$ is added to the local mean atmosphere surrounding the aircraft, with linear velocity components added along the base components of the Dryden frame and the angular velocity components added along the base components of the aircraft frame.

2.5.2 In-flight refuelling turbulence

During an aerial refuelling manoeuvre, the tanker and receiver aircraft experience similar turbulence. Our goal is to characterise the similarity and design a controller that, loosely speaking, corrects the difference in aircraft response to the turbulence, rather than rejecting all the turbulence.

Refer to Figure 2.12. Etkin [32, pp.532-534] formulates the spatial correlation of turbulence linear velocity components with the two fundamental spatial correlation functions $f(\xi)$ & $g(\xi)$. These correlations are derived for the Dryden model in Appendix A.1.7 as

$$R_{u_g}(\xi) \coloneqq \mathbb{E}\left\{u_g u_g'\right\} = \sigma_g^2 e^{-\frac{1}{l_g}|\xi|} = \sigma_g^2 f(\xi) \tag{2.46}$$

$$R_{w_g}(\xi) \coloneqq \mathbb{E}\left\{w_g w_g'\right\} = \sigma_g^2 e^{-\frac{1}{l_g}|\xi|}\left(1 - \frac{1}{2l_g}|\xi|\right) = \sigma_g^2 g(\xi) = R_{v_g}(\xi) \tag{2.47}$$

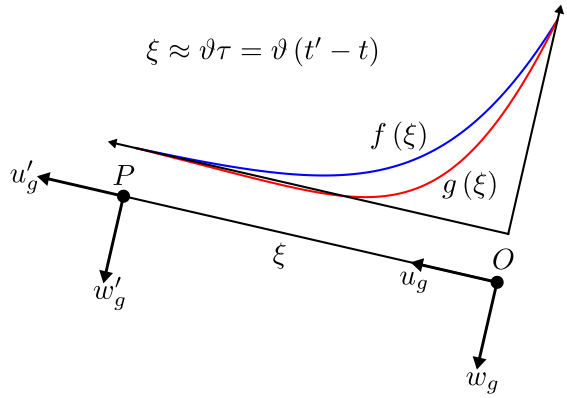

Figure 2.12: Dryden spatial correlation 2D vector diagram.

and

$$R_{u_g v_g}\,(\xi) = R_{u_g w_g}\,(\xi) = R_{v_g w_g}\,(\xi) = 0 \tag{2.48}$$

which describe the correlation between the turbulence linear velocities with respect to the local mean atmosphere at arbitrary points P and O, separated by a distance $\xi = |\mathbf{s}_{PO}|$ (m), measured in the directions u_g, v_g and w_g respectively. Section 2.5.1 considers the case in which the relative position vector $\mathbf{s}_{PO}$ is chosen parallel to $\mathbf{d}_1$ and uses the relation $\tau \approx \frac{\xi}{\vartheta}$, where ϑ is considered constant, to express the correlation between turbulence components at two instances in time as a function of time difference τ. The temporal correlation $R\,(\tau)$ is time-invariant for constant altitude due to the stationarity of the turbulence for constant altitude, and is converted to a temporal spectrum using the *Fourier transform*.

Refer to Figure 2.13. Isotropy is used in [32, pp.533] to formulate the *cross-*

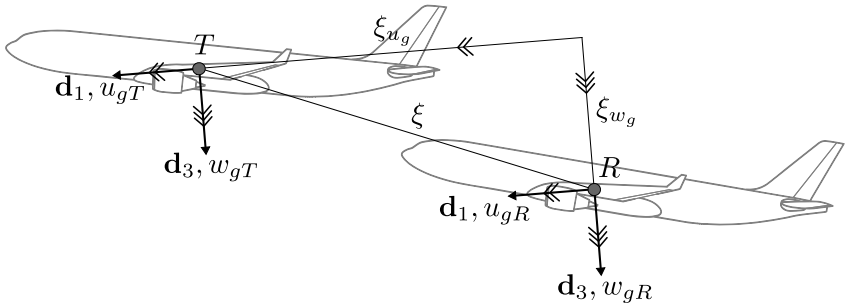

Figure 2.13: AAR turbulence correlation 2D vector diagram.

correlation between turbulence linear velocity components at tanker centre of mass T and receiver centre of mass R when u_g is not aligned with relative position vector $\mathbf{s}_{TR}$, given as

$$\frac{R_{i_T j_R}}{\sigma_g^2} = (f\,(\xi) - g\,(\xi))\,\frac{\xi_i \xi_j}{\xi^2} + g\,(\xi)\,\delta_{ij} \tag{2.49}$$

where

$$\{i,j\} \subset \{u_g, v_g, w_g\}, \quad \delta_{ij} = \begin{cases} 1 & i = j \\ 0 & i \neq j \end{cases} \tag{2.50}$$

Correlation between tanker and receiver angular velocity components q_g and r_g is inherent in the Dryden model with w_g and v_g as inputs to the shaping-filters of q_g and r_g respectively. The correlations involved in angular velocity component p_g are, however, not inherent in the Dryden model or described by (2.49). Assuming small angle between $\mathbf{d}_1$ and $\mathbf{b}_1$, the correlation of tanker and receiver roll turbulence $R_{p_{g,T}p_{g,R}}$ is approximated as vertical velocity correlation $R_{w_{g,T}w_{g,R}}$, while their cross-correlation with other components is assumed zero. [5]

The correlation of the tanker turbulence model output $\mathbf{g}_T$ and receiver turbulence model output $\mathbf{g}_R$ is achieved by correlating their white noise inputs, illustrated with the block diagram in Figure 2.14, where $V_{\mathcal{T}}\left([\mathbf{s}_{TR}]^D\right)$ is the intensity of the correlated

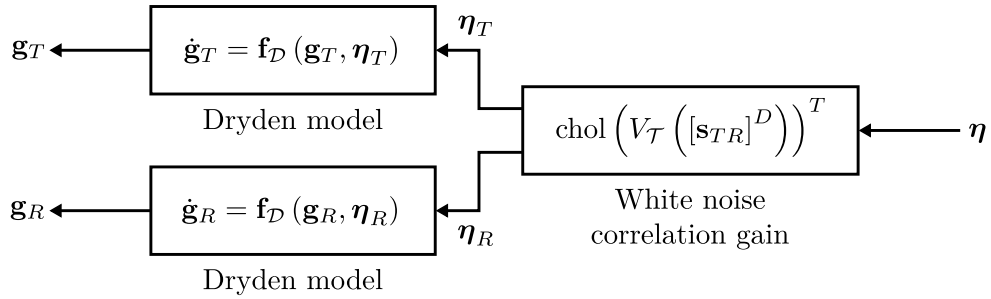

Figure 2.14: IFR turbulence block diagram.

white noise inputs as a function of the relative position $[\mathbf{s}_{TR}]^D$ of the tanker centre of mass relative to the receiver centre of mass measured along the base components of the Dryden frame, and is calculated with the state-space descriptions of the Dryden model in Section 4.2.1.5.

Now that models for the aerial refuelling mechanics and the turbulence have been derived, we can proceed to designing a suitable control system.

5. For a more accurate roll correlation, the derivation of roll spectrum in terms of linear velocity should be considered. See [27, 28]

Chapter 3

Theory of LMIs in control design

LMI Control Theory provides a method for designing optimal controllers and optimal estimators by formulating specifications and constraints in terms of linear matrix inequalities. Formulations exist to specify global stability, transient response, $\mathcal{H}_2$ and $\mathcal{H}_\infty$ norms, and uncertainty in terms of LMI constraints. The linear matrix inequalities can then be solved using efficient numerical methods to obtain the optimal control law or estimator.

3.1 Definition of an LMI and LMI problems

[13, pp.7] A Linear Matrix Inequality (LMI) has the form

$$M(\mathbf{v}) := M_0 + \sum_{i=1}^{m} v_i M_i > 0 \tag{3.1}$$

where $M_i = M_i^T \in \mathbb{R}^{n\times n}$, $i = 0, 1, \ldots, m$ are known symmetric matrices, the matrix inequality $M(\mathbf{v}) > 0$ has the scalar equivalent $\mathbf{s}^T M(\mathbf{v})\,\mathbf{s} > 0$ for all non-zero $\mathbf{s} \in \mathbb{R}^{n\times 1}$, and $\mathbf{v} = [v_1, v_2, \ldots, v_m]^T \in \mathbb{R}^{m\times 1}$ is the m-dimensional vector space constrained by $M(\mathbf{v}) > 0$, *i.e.* $\{\mathbf{v} \in \mathbb{R}^{m\times 1} : M(\mathbf{v}) > 0\}$.

Figure 3.1 illustrates the boundary of a simple 3D vector space constrained with an LMI, given as

$$\begin{aligned}
\mathbf{k} &= \left\{ \mathbf{v} = \begin{bmatrix} v_1 & v_2 & v_3 \end{bmatrix}^T \in \mathbb{R}^{3\times 1} : \begin{bmatrix} v_1 & v_2 \\ v_2 & v_3 \end{bmatrix} > 0 \right\} \\
&= \left\{ \mathbf{x} = \begin{bmatrix} v_1 & v_2 & v_3 \end{bmatrix}^T \in \mathbb{R}^{3\times 1} : (3.1),\ M_0 = \begin{bmatrix} 0 & 0 \\ 0 & 0 \end{bmatrix},\ M_1 = \begin{bmatrix} 1 & 0 \\ 0 & 0 \end{bmatrix} \right. \\
&\qquad \left. M_2 = \begin{bmatrix} 0 & 1 \\ 1 & 0 \end{bmatrix},\ M_3 = \begin{bmatrix} 0 & 0 \\ 0 & 1 \end{bmatrix} \right\}
\end{aligned} \tag{3.2}$$

where $\mathbf{k}$ is known as a positive definite cone which belongs to the interior of the hull.

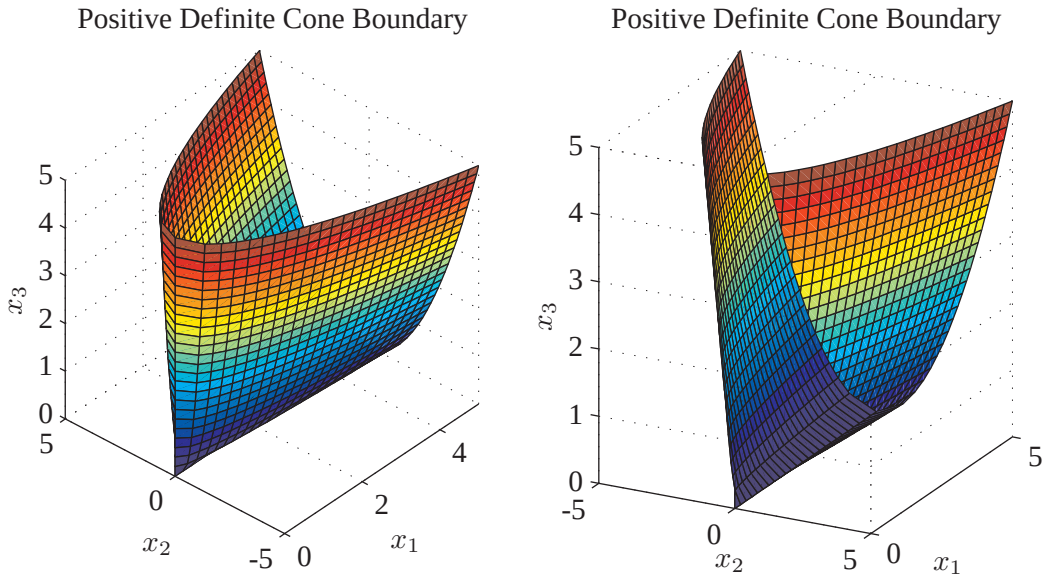

Figure 3.1: Two separate views of the 3D positive definite cone boundary.

LMIs are related to two numerical problems, the LMI *feasibility problem* and the LMI *minimisation problem*. The *feasibility problem*

$$\begin{aligned} &\text{feasibility} && \mathbf{v} \\ &\text{subject to} && (3.1) \end{aligned} \tag{3.3}$$

determines whether the vector space $\mathbf{v} \in \mathbb{R}^{m\times 1}$, constrained by (3.1), is feasible or empty/infeasible for a given set of matrices $\{M_0, M_1, \ldots, M_m\}$, and returns a single feasible point if the vector space is non-empty. The *minimisation problem*

$$\begin{aligned} &\text{minimise} && \mathbf{c}^T\mathbf{v} \\ &\text{subject to} && (3.1) \end{aligned} \tag{3.4}$$

determines the minimum of the linear scalar function $\mathbf{c}^T\mathbf{v}$ over the vector space $\mathbf{v} \in \mathbb{R}^{m\times 1}$, constrained by (3.1), for a given set of matrices $\{M_0, M_1, \ldots, M_m\}$ and the coefficient vector $\mathbf{c} \in \mathbb{R}^{m\times 1}$, and returns a single point corresponding to the minimum objective if the vector space is non-empty. The objective b describes the hyperplane in the vector space

$$\left\{\mathbf{v} \in \mathbb{R}^{m\times 1} : \mathbf{c}^T\mathbf{v} = b,\ b \in \mathbb{R}^1,\ \mathbf{c} \in \mathbb{R}^{m\times 1}\right\} \tag{3.5}$$

and is minimised in the direction $-\mathbf{c}$.

3.2 History of LMIs in control design

The history of LMIs in control design is summarised in [13, pp.2-4] as follows:

1890's LMIs are introduced to systems theory by the famous Russian mathematician Lyapunov. He formulates a general condition for system global stability by means of energy principles, and shows that the linear differential equation

$$\frac{d}{dt}\mathbf{x}(t) = \mathcal{A}\mathbf{x}(t), \quad \mathbf{x}(t) \in \mathbb{R}^{n_x \times 1} \tag{3.6}$$

is globally stable if, and only if, there exists a symmetric matrix L such that

$$L > 0, \quad \mathcal{A}^T L + L\mathcal{A} < 0 \tag{3.7}$$

1940's Lyapunov inequalities are applied by several control theory researchers in the former Soviet Union to some practical low order control engineering problems involving non-linearity. The LMIs are checked by hand.

Early 1960's The *Positive-Real Lemma* gives means to solve LMIs by graphical methods.

Early 1970's Certain LMI formulations relating to quadratic control can be solved by studying the symmetric solutions of an algebraic Riccati equation.

Early 1980's Many LMI problems can be reduced to a convex optimisation problem, which can be numerically solved by the ellipsoid algorithm.

Late 1980's Development of the robust and computationally efficient interior-point algorithm.

Research in the field continues, as LMI solvers provide convex, robust and computationally efficient solutions. The reader is referred to [13] for a more complete background on LMIs.

3.3 Advantages of LMIs for control applications

LMIs are attractive for control application for the following reasons [30, pp.3]:

1. *Efficient numerical solvers*: The LMI feasibility problem (3.3) and minimisation problem (3.4) are solvable via efficient interior-point methods with a polynomial time-complexity upper-bound. The solvers bring a numerical solution to problems when no analytical or closed-form solution is known. Thus, any problem that can be expressed in terms of (3.3) or (3.4) can readily be solved.
2. *Existing LMI formulations*: Since the introduction of LMIs to systems and control theory in the 1890's, many control problems have been reduced to their equivalent LMI forms. Some of these formulations can be found in [13, 30, 67] and include global stability, $\mathcal{H}_2$, $\mathcal{H}_\infty$, passivity, bounded output-peak, and regional pole constraints, among many others.

3. *Multiple criteria.* Multiple, possibly conflicting, specifications may be imposed on a vector space with LMI constraints, and are then cascade-able into a single solvable LMI, *e.g.* given the three specifications $F(\mathbf{v}) > 0$, $G(\mathbf{v}) > 0$ and $H(\mathbf{v}) > 0$, we may combine them as a single LMI

$$\text{blkdiag}\left(F(\mathbf{v}), G(\mathbf{v}), H(\mathbf{v})\right) = \begin{bmatrix} F(\mathbf{v}) & 0 & 0 \\ 0 & G(\mathbf{v}) & 0 \\ 0 & 0 & H(\mathbf{v}) \end{bmatrix} > 0 \tag{3.8}$$

This combining ability allows us to explore trade-offs and analyse limits of performance and feasibility. Scherer et al. [67] demonstrate this by using LMIs to design an optimal $\mathcal{H}_2$ controller for a floating platform with $\mathcal{H}_\infty$ and closed-loop pole constraints.

4. *Robustness against uncertainty.* LMIs are well suited for including uncertainty in M_i, which enables us to formulate an LMI that yields a robust solution.

3.4 LMI control design procedure

> "An important element of control design is the system *analysis*, which provides mathematical conditions for a given system to have certain properties. Such analysis results are directly useful for checking whether a designed controller satisfies a given set of (closed-loop) specifications. If an analysis result is 'nice' enough, then it may be useful for synthesis, *i.e.* for designing a controller based on the mathematical conditions characterising certain closed-loop properties." Iwasaki [43, pp.85]

Many LMI formulations for stability, performance and robustness analysis admit a *'nice' enough* form, such that it may be recast as an LMI controller synthesis problem, and solved via robust and computationally efficient algorithms.

The basic approach to LMI control design is summarised as follows:

1. Formulate a set of closed-loop system stability conditions and performance measures in terms of LMIs, *e.g.* Lyapunov stability, $\mathcal{H}_2$, $\mathcal{H}_\infty$, *etc.*
2. Introduce the controller as a variable(s) in the LMIs.
3. Apply the necessary substitutions, transformations, theorems, Lyapunov's shaping paradigm, *etc.* to remove the non-linearity introduced by the controller variable(s).
4. Specify a linear scalar objective function in LMI variables, where the minimum objective usually corresponds to the *best* closed-loop performance.
5. Use the appropriate algorithm to solve the controller variable(s) corresponding to the minimum objective.

The approach is demonstrated by the simple example of designing a state-feedback controller that guarantees the closed-loop stability of an LTI system.

3.4.1 Simple example

In the following example we give Lyapunov's global stability condition and show how it is formulated in terms of LMIs for the closed-loop LTI system (3.6). These LMIs are then recast as an LMI feasibility problem used to synthesise a stabilising state-feedback matrix.

Example 1. Given the closed-loop LTI system (3.6), where $\mathbf{x}(t)$ is the system state, we use the positive quadratic scalar function

$$V(\mathbf{x}(t)) = \mathbf{x}(t)^T L\mathbf{x}(t) > 0,\ L > 0,\ \frac{d}{dt}L = 0 \tag{3.9}$$

also referred to as the system energy function, to formulate the condition for stability, where

$$L = \begin{bmatrix} l_1 & l_2 & \cdots & l_{m-n_x+1} \\ l_2 & l_3 & \cdots & l_{m-n_x+2} \\ \vdots & \vdots & \ddots & \vdots \\ l_{m-n_x+1} & l_{m-n_x+2} & \cdots & l_m \end{bmatrix} \tag{3.10}$$

is an unknown symmetric matrix [1] containing the components of the vector space $\mathbf{l} = [l_1, l_2, \ldots, l_m]^T \in \mathbb{R}^{m\times 1}$. According to Lyapunov, the system is globally stable if the system energy

$$V(\mathbf{x}(t)) \begin{cases} > 0 & \mathbf{x}(t) \neq \mathbf{0} \\ = 0 & \mathbf{x}(t) = \mathbf{0} \end{cases} \tag{3.11}$$

is always reducing in size except at the zero energy state, *i.e.*

$$\frac{dV(\mathbf{x}(t))}{dt} < 0 \quad \forall V(\mathbf{x}(t)) \neq 0 \tag{3.12}$$

It follows from the substitution

$$\begin{aligned} \frac{dV(\mathbf{x}(t))}{dt} &= \frac{d}{dt}\left[\mathbf{x}(t)^T L\mathbf{x}(t)\right] \\ &= \dot{\mathbf{x}}(t)^T L\mathbf{x}(t) + \mathbf{x}(t)^T L\dot{\mathbf{x}}(t) \\ &= \mathbf{x}(t)^T \left(\mathcal{A}^T L + L\mathcal{A}\right)\mathbf{x}(t) \end{aligned} \tag{3.13}$$

and the scalar definition of an LMI, that the energy constraints $V(\mathbf{x}(t)) > 0$ and $\dot{V}(\mathbf{x}(t)) < 0$ may be imposed by (3.7). Now, given the open-loop form of (3.6)

$$\frac{d\mathbf{x}(t)}{dt} = A\mathbf{x}(t) + B_u\mathbf{u}(t) \tag{3.14}$$

where $\mathbf{u} \in \mathbb{R}^{n_u\times 1}$ is the control input which satisfies the state-feedback structure

$$\mathbf{u}(t) = K\mathbf{x}(t) \tag{3.15}$$

1. LMI formulations for control and estimation reside in a compact matrix variable form rather than in the scalar variable sum form (3.1).

and $B_u \in \mathbb{R}^{n_x \times n_u}$ is a known constant control input matrix, the unknown stabilising state-feedback gain K is introduced in the closed-loop system as

$$\mathcal{A} = A + B_u K \tag{3.16}$$

(3.7) is restated in terms of the controller variable as

$$L > 0, \quad (A + B_u K)^T L + L (A + B_u K) < 0 \tag{3.17}$$

which is non-linear in the matrix variables L and K. The non-linearity is removed by applying a non-singular congruent transformation with

$$Q \coloneqq L^{-1} \tag{3.18}$$

followed by the substitution

$$Y \coloneqq KQ \tag{3.19}$$

resulting in its equivalent LMI form

$$Q > 0, \quad AQ + B_u Y + QA^T + Y^T B_u < 0 \tag{3.20}$$

The preservation of an LMI under non-singular congruent transformations is apparent in the scalar definition of LMIs, shown step by step as

$$\begin{aligned}
&\left((A + B_u K)^T L + L (A + B_u K) < 0\right) \\
\iff \quad &\left(\mathbf{s}^T \left((A + B_u K)^T L + L (A + B_u K)\right) \mathbf{s} < 0 \; \forall \mathbf{s} \in \mathbb{R}^{n_x \times 1} \neq 0\right) \\
\iff \quad &\left(\begin{array}{c} \mathbf{r}^T \left((A + B_u K)^T L + L (A + B_u K)\right) \mathbf{r} < 0 \; \forall \mathbf{s} \in \mathbb{R}^{n_x \times 1} \neq 0, \\ \mathbf{r} = Q\mathbf{s}, \; \operatorname{rank}(Q) = n_x \end{array} \right) \\
\iff \quad &\left(\begin{array}{c} \mathbf{s}^T Q^T \left((A + B_u K)^T L + L (A + B_u K)\right) Q\mathbf{s} < 0 \; \forall \mathbf{s} \in \mathbb{R}^{n_x \times 1} \neq 0, \\ \operatorname{rank}(Q) = n_x \end{array} \right) \\
\iff \quad &\left(Q^T \left((A + B_u K)^T L + L (A + B_u K)\right) Q < 0, \; \operatorname{rank}(Q) = n_x\right) \\
\iff \quad &\left(Q (A + B_u K)^T + (A + B_u K) Q < 0, \; \operatorname{rank}(Q) = n_x, \; Q = L^{-1}\right)
\end{aligned} \tag{3.21}$$

where $\mathbf{s}$ represents by definition all the points in $\mathbb{R}^{n_x \times 1}$, as does $\mathbf{r} = Q\mathbf{s}$ if, and only if, Q is non-singular. The non-singularity of Q is inherent in $L > 0$. Thus, if a Q and Y can be found that satisfy (3.20), then $L = Q^{-1}$ and $K = YL$ will satisfy (3.17).

The LMI variables Q and Y are not directly related to desired system performance, and we omit the objective from the design, *i.e.* we are concerned with solving the LMI feasibility problem

$$\begin{aligned}
&\text{feasibility} \quad Q, \; Y \\
&\text{subject to} \quad Q > 0, \quad AQ + B_u Y + QA^T + Y^T B_u < 0
\end{aligned} \tag{3.22}$$

The solver used in the thesis is SDPT3-4.0, which implements the *infeasible primal-dual predictor-corrector path-following* interior-point method. The solver is used with the YALMIP interface for MATLAB, and solves the stabilising state-feedback problem for given $\mathtt{A} \coloneqq A$ and $\mathtt{Bu} \coloneqq B_u$ as follows

Listing 3.1: Lyapunov stability example.

```
[nx,nu]=size(Bu);
Q=sdpvar(nx,nx,'symmetric');
Y=sdpvar(nu,nx,'full');
LMI=[(Q>0),(A*Q+Bu*Y+(A*Q+Bu*Y)'<0)];
OBJ=[];
solvesdp(LMI,OBJ,sdpsettings('solver','sdpt3'));
K=double(Y)/double(Q);
```

The conditions for stability in terms of the energy function are intuitive, and it may be proven via eigenvalue decomposition that there exists a feasible L for a stabilisable LTI system and that L is empty for an unstabilisable LTI system. [2] The relation between the vector space and stability or performance becomes much more direct in the following sections, where the vector space describes the covariances of the system state.

See [13, 12, 30] for an elaborate theoretical background on LMIs and their application in the field of control theory.

The norm-bounded state-space system description is introduced next, which describes a more general class of systems than the LTI system (3.6) by allowing $\mathcal{A}$ to vary within specified norm-bounds.

3.5 Norm-bounded state-space model

The closed-loop norm-bounded state-space model is illustrated in Figure 3.2 and

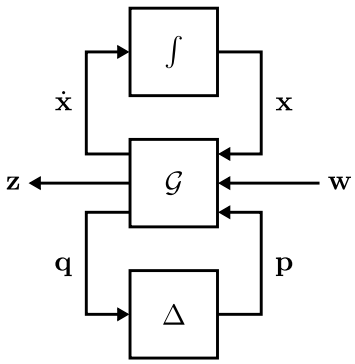

Figure 3.2: Closed-loop norm-bounded state-space model block diagram.

2. A system is stabilisable if there exists a control input $\mathbf{u}$ such that the system state $\mathbf{x}$ remains bounded, and is unstabilisable if no such control input exists.

defined in [74] as follows.

$$\begin{bmatrix} \dot{\mathbf{x}} \\ \mathbf{z} \\ \mathbf{q} \end{bmatrix} = \mathcal{G} \begin{bmatrix} \mathbf{x} \\ \mathbf{w} \\ \mathbf{p} \end{bmatrix} = \begin{bmatrix} \mathcal{A} & \mathcal{B}_w & \mathcal{B}_p \\ \mathcal{C}_z & \mathcal{D}_{zw} & \mathcal{D}_{zp} \\ \mathcal{C}_q & \mathcal{D}_{qw} & \mathcal{D}_{qp} \end{bmatrix} \begin{bmatrix} \mathbf{x} \\ \mathbf{w} \\ \mathbf{p} \end{bmatrix} \tag{3.23}$$
$$\mathbf{p} = \Delta \mathbf{q}, \quad \Delta \in \mathbf{\Delta}$$

where $\mathbf{x} \in \mathbb{R}^{n_x \times 1}$ is the system *state*, $\dot{\mathbf{x}} := \frac{d\mathbf{x}}{dt} \in \mathbb{R}^{n_x \times 1}$ the system *state derivative*, $\mathbf{w} \in \mathbb{R}^{n_w \times 1}$ the *exogenous input*, $\mathbf{z} \in \mathbb{R}^{n_z \times 1}$ the system *performance output*, $\mathbf{p} \in \mathbb{R}^{n_p \times 1}$ the *uncertainty output*, $\mathbf{q} \in \mathbb{R}^{n_p \times 1}$ the *uncertainty input*, $\mathcal{G} \in \mathbb{R}^{(n_x+n_z+n_q)\times(n_x+n_w+n_p)}$ the known constant *system matrix*[3] with sub-matrices $\mathcal{A}$, $\mathcal{B}_w$, *etc.*, and $\Delta \in \mathbf{\Delta}$ is structured NLTV model uncertainty. Δ is defined by the set of all structured norm-bounded expressions in $\boldsymbol{\rho}$

$$\mathbf{\Delta} := \left\{ F(\boldsymbol{\rho}) \,\middle|\, F : \mathbb{R}^{n_\rho \times 1} \mapsto \mathbb{R}^{n_p \times n_p},\ F(\boldsymbol{\rho}) \in \mathfrak{S},\ F(\boldsymbol{\rho})^T F(\boldsymbol{\rho}) < I, \text{ for every } \boldsymbol{\rho} \in \mathfrak{D}_\rho \right\} \tag{3.24}$$

where $\mathfrak{D}_\rho$ is the domain of the system dependency $\boldsymbol{\rho} = \begin{bmatrix} \rho_1 & \rho_1 & \cdots & \rho_{n_\rho} \end{bmatrix}^T$ and [4]

$$\mathfrak{S} := \left\{ S \in \mathbb{R}^{n_p \times n_p} \,\middle|\, S = \text{blkdiag}\left(\delta_1 I_{r_1}, \ldots, \delta_g I_{r_g}, \Delta_1, \ldots, \Delta_q\right), \right.$$
$$\left. \delta_i \in \mathbb{R}^{1\times 1},\ \Delta_k \in \mathbb{R}^{f_k \times f_k},\ i \in \{1, 2, \ldots, g\},\ k \in \{1, 2, \ldots, q\} \right\} \tag{3.25}$$

is the set defining the structure of $\mathbf{\Delta}$. For convenience, the notation is such that the time-dependency of the *vectors* is not shown, *e.g.* $\mathbf{x} := \mathbf{x}(t)$. In the following chapters, the invariance of Δ under some of the elements in $\boldsymbol{\rho}$ will be explicitly stated, *e.g.* $\frac{\partial \Delta}{\partial \rho_i} = 0 \; \forall \rho_i \neq t$ constrains Δ to be LTV or $\frac{\partial \Delta}{\partial x_i} = 0 \; \forall i = 1, 2, \ldots, n_x$ constrains Δ to be invariant under $\mathbf{x}$. Note that (3.23) includes as a special case the LTI model, when only $\mathcal{A}$ is non-zero.

(3.23) includes model variation/uncertainty with feedback through uncertainty Δ, and has the alternative form

$$\begin{aligned} \begin{bmatrix} \dot{\mathbf{x}} \\ \mathbf{z} \end{bmatrix} &= \mathcal{G}(\Delta) \begin{bmatrix} \mathbf{x} \\ \mathbf{w} \end{bmatrix} = \begin{bmatrix} \mathcal{A}(\Delta) & \mathcal{B}(\Delta) \\ \mathcal{C}(\Delta) & \mathcal{D}(\Delta) \end{bmatrix} \begin{bmatrix} \mathbf{x} \\ \mathbf{w} \end{bmatrix} \\ &= F_l(\mathcal{G}, \Delta) \\ &= \left(\begin{bmatrix} \mathcal{A} & \mathcal{B}_w \\ \mathcal{C}_z & \mathcal{D}_{zw} \end{bmatrix} + \begin{bmatrix} \mathcal{B}_p \\ \mathcal{D}_{zp} \end{bmatrix} \Delta \left(I - \mathcal{D}_{qp}\Delta\right)^{-1} \begin{bmatrix} \mathcal{C}_q & \mathcal{D}_{qw} \end{bmatrix} \right) \begin{bmatrix} \mathbf{x} \\ \mathbf{w} \end{bmatrix} \\ &= \begin{bmatrix} \mathcal{A} + \mathcal{B}_p\Delta\left(I - \mathcal{D}_{qp}\Delta\right)^{-1}\mathcal{C}_q & \mathcal{B}_w + \mathcal{B}_p\Delta\left(I - \mathcal{D}_{qp}\Delta\right)^{-1}\mathcal{D}_{qw} \\ \mathcal{C}_z + \mathcal{D}_{zp}\Delta\left(I - \mathcal{D}_{qp}\Delta\right)^{-1}\mathcal{C}_q & \mathcal{D}_{zw} + \mathcal{D}_{zp}\Delta\left(I - \mathcal{D}_{qp}\Delta\right)^{-1}\mathcal{D}_{qw} \end{bmatrix} \begin{bmatrix} \mathbf{x} \\ \mathbf{w} \end{bmatrix} \\ &\quad \Delta \in \mathbf{\Delta} \end{aligned} \tag{3.26}$$

3. The plural of *system matrix*, *i.e.* system matrices, refer to the sub-matrices of the system matrix, *e.g.* $\mathcal{A}$,$\mathcal{B}_w$, *etc.* of $\mathcal{G}$.

4. Note that the symbol δ may refer to actuators or uncertainty, and is distinguishable via its subscript.

where F_l is the *lower Linear Fractional Transform* (LFT) [70, pp.111].

Now, we proceed by deriving LMI formulations for robust stability and robust performance analysis in the following two sections, followed by the derivations of their controller synthesis equivalents. The stability and performance measures are derived for the norm-bounded state-space model, to ensure robustness in the presence of time-varying uncertainty.

3.6 Stability conditions

Robust global stability and *local stability in the presence of saturation* are the stability measures developed in the thesis. They serve to characterise the stability of a system subject to time-varying uncertainty and saturation.

3.6.1 Robust global stability

LMI formulation (3.7) of Lyapunov's stability condition, derived in Example 1, is reformulated here for the norm-bounded state-space model. The formulation relies on a theorem of Takaba [74] to remove the structured norm-bounded uncertainty Δ from the matrix inequalities. The resulting LMIs measure the global stability of an LTI system subject to NLTV uncertainty, and the resulting stability is referred to as robust global stability.

Lyapunov's condition for global stability is given as

$$\begin{aligned} & (\exists V(\mathbf{x}(t)) : (3.11), (3.12)) \\ \Longrightarrow \quad & \left(\lim_{t\to\infty} \mathbf{x}(t) = \mathbf{0} : \mathbf{x}(t_0) \in \mathbb{R}^{n_x \times 1} \right) \end{aligned} \tag{3.27}$$

where $\mathbf{x} \in \mathbb{R}^{n_x \times 1}$ is the state of the system.

Given the undisturbed NLTV model

$$\dot{\mathbf{x}} = \mathcal{A}(\Delta)\mathbf{x} = \left(\mathcal{A} + \mathcal{B}_p \Delta \left(I - \mathcal{D}_{qp}\Delta \right)^{-1} \mathcal{C}_q \right) \mathbf{x}, \quad \Delta \in \mathbf{\Delta} \tag{3.28}$$

we choose the energy function (3.9) [5] and, following the same procedure as in Example 1, the energy constraints in (3.27) may be imposed on NLTV model (3.28) as

$$\begin{aligned} & \left(\exists P > 0 : \mathcal{A}(\Delta)^T P + P\mathcal{A}(\Delta) < 0, \ \frac{d}{dt}P = 0 \right) \\ & \Longrightarrow \quad (\exists V(\mathbf{x}(t)) : (3.11), (3.12)) \end{aligned} \tag{3.29}$$

We may remove the variation Δ in (3.57) by applying the following theorem.

5. The more conventional LMI matrix variable P is used over L.

Theorem 1. *[74] Suppose there exist time-invariant matrices* $\{S, N\} \subset \mathbb{R}^{q\times q}$, $\{E, F\} \subset \mathbb{R}^{m\times q}$, $R = R^T \in \mathbb{R}^{m\times m}$, $J = J^T \in \mathbb{R}^{q\times q}$ *and matrix expressions* $\{\Omega(\boldsymbol{\varrho}), \Lambda(\boldsymbol{\varrho})\} \subset \left\{M(\boldsymbol{\varrho}) \middle| M : \mathbb{R}^{n_\rho} \mapsto \mathbb{R}^{q\times q}\right\}$ *satisfying*

$$\begin{aligned} \Lambda(\boldsymbol{\varrho})\Lambda(\boldsymbol{\varrho})^T < I, \quad \Lambda(\boldsymbol{\varrho})S = S\Lambda(\boldsymbol{\varrho}), \\ I + \Omega(\boldsymbol{\varrho})\Lambda(\boldsymbol{\varrho})N = \Omega(\boldsymbol{\varrho}) \end{aligned} \tag{3.30}$$

Then,

$$\begin{aligned} &\left(\begin{bmatrix} R + ETE^T & F + ETN^T \\ \left(F + ETN^T\right)^T & -T + NTN^T + J \end{bmatrix} < 0\right) \\ \Longrightarrow &\left(R + E\Omega(\boldsymbol{\varrho})\Lambda(\boldsymbol{\varrho})F^T + F\left(E\Omega(\boldsymbol{\varrho})\Lambda(\boldsymbol{\varrho})\right)^T + E\Omega(\boldsymbol{\varrho})\Lambda(\boldsymbol{\varrho})J\left(E\Omega(\boldsymbol{\varrho})\Lambda\right)^T < 0\right) \end{aligned} \tag{3.31}$$

where

$$T \coloneqq SS^T \tag{3.32}$$

Proof: See Appendix A.2.13.

To help match (3.29) with (3.31) according to (3.28), we present the following augmentation.

$$\begin{aligned} \Delta(I - \mathcal{D}_{qp}\Delta)^{-1} &= (I - \Delta\mathcal{D}_{qp})^{-1}(I - \Delta\mathcal{D}_{qp})\Delta(I - \mathcal{D}_{qp}\Delta)^{-1} \\ &= (I - \Delta\mathcal{D}_{qp})^{-1}\left(\Delta(I - \mathcal{D}_{qp}\Delta)^{-1} - \Delta\mathcal{D}_{qp}\Delta(I - \mathcal{D}_{qp}\Delta)^{-1}\right) \\ &= (I - \Delta\mathcal{D}_{qp})^{-1}\Delta(I - \mathcal{D}_{qp}\Delta)(I - \mathcal{D}_{qp}\Delta)^{-1} \\ &= (I - \Delta\mathcal{D}_{qp})^{-1}\Delta \end{aligned} \tag{3.33}$$

Given (3.28), (3.29) and (3.33), substituting $(R, E, \Omega(\boldsymbol{\varrho}), \Lambda(\boldsymbol{\varrho}), F, J, T, N)$ in Theorem 1 with

$$\left(\left(\mathcal{A}^TP + P\mathcal{A}\right), P\mathcal{B}_p, (I - \Delta\mathcal{D}_{qp})^{-1}, \Delta, \mathcal{C}_q^T, 0, W_L, \mathcal{D}_{qp}\right) \tag{3.34}$$

we obtain

$$\begin{aligned} &\left(\left[\begin{array}{c|c} \mathcal{A}^TP + P\mathcal{A} + P\mathcal{B}_pW_L\mathcal{B}_p^TP & \mathcal{C}_q^T + P\mathcal{B}_pW_L\mathcal{D}_{qp}^T \\ \hline \star & -W_L + \mathcal{D}_{qp}W_L\mathcal{D}_{qp}^T \end{array}\right] < 0 \right) \\ &\qquad W_L \in \mathfrak{C} \\ &\qquad\Longrightarrow \quad \left(\mathcal{A}(\Delta)^TP + P\mathcal{A}(\Delta) < 0\right) \end{aligned} \tag{3.35}$$

where $\star$ completes the symmetric matrix, *i.e.* $\star$ replaces $\left(\mathcal{C}_q^T + P\mathcal{B}_pW_L\mathcal{D}_{qp}^T\right)^T$, the horizontal and vertical lines are used as separators, and $\mathfrak{C}$ is the set of all positive

definite matrices that commute with all expressions in $\mathbf{\Delta}$, *i.e.* $W\Delta = \Delta W$ for all $\Delta \in \mathbf{\Delta}$ and $W \in \mathfrak{C}$, and is defined as

$$\mathfrak{C} := \left\{ W \in \mathbb{R}^{n_p \times n_p} \middle| W = W^T > 0,\ W = \text{blkdiag}\left(W_1, \ldots, W_g, w_1 I_{f_1}, \ldots, w_q I_{f_q}\right), \right.$$
$$\left. W_i \in \mathbb{R}^{r_i \times r_i},\ w_k \in \mathbb{R}^1,\ i \in \{1, 2, \ldots, g\},\ k \in \{1, 2, \ldots, q\} \right\} \tag{3.36}$$

Note that the structure $\mathfrak{C}$ may be imposed on W_L with the appropriate choice of matrices M_i in (3.1).

The non-linearity in (3.35), due to the multiplication of matrix variables P and W_L, is removed by applying a non-singular congruent transformation with

$$\begin{bmatrix} Q & 0 \\ 0 & I \end{bmatrix} := \begin{bmatrix} P^{-1} & 0 \\ 0 & I \end{bmatrix} \tag{3.37}$$

similar to that in Example 1, and results in its LMI equivalent

$$\left(\left[\begin{array}{c|c} \mathcal{A}^T P + P\mathcal{A} + P\mathcal{B}_p W_L \mathcal{B}_p^T P & \mathcal{C}_q^T + P\mathcal{B}_p W_L \mathcal{D}_{qp}^T \\ \hline \star & -W_L + \mathcal{D}_{qp} W_L \mathcal{D}_{qp}^T \end{array} \right] < 0 \right)$$
$$P > 0$$
$$\overset{P := Q^{-1}}{\Longleftrightarrow} \quad \left(\left[\begin{array}{c|c} Q\mathcal{A}^T + \mathcal{A}Q + \mathcal{B}_p W_L \mathcal{B}_p^T & Q\mathcal{C}_q^T + \mathcal{B}_p W_L \mathcal{D}_{qp}^T \\ \hline \star & -W_L + \mathcal{D}_{qp} W_L \mathcal{D}_{qp}^T \end{array} \right] < 0 \right) \tag{3.38}$$
$$Q > 0$$

Now, combining (3.27), (3.29), (3.35) and (3.38), we find the global stability condition $\lim_{t\to\infty} \mathbf{x}(t) = 0 : \mathbf{x}(t_0) \in \mathbb{R}^{n_x \times 1}$ of (3.28) in terms of LMI feasibility problem

$$\begin{aligned} &\text{feasibility} \quad W_L \in \mathfrak{C},\ Q > 0 \\ &\text{subject to} \quad \left[\begin{array}{c|c} Q\mathcal{A}^T + \mathcal{A}Q + \mathcal{B}_p W_L \mathcal{B}_p^T & Q\mathcal{C}_q^T + \mathcal{B}_p W_L \mathcal{D}_{qp}^T \\ \hline \star & -W_L + \mathcal{D}_{qp} W_L \mathcal{D}_{qp}^T \end{array} \right] < 0 \end{aligned} \tag{3.39}$$

3.6.2 Local stability in the presence of saturation

No known LMI formulation exists that directly includes saturation. The saturation is rather described with NLTV uncertainty for a specified system state domain. The system state is then constrained to reside within the specified domain to ensure that the NLTV uncertainty description remains valid. The derivation proceeds in a manner similar to Section 3.6.1, and the resulting LMIs measure the local stability of an LTI system subject to saturation.

A local stability condition is formulated for an undisturbed LTI model subject to saturation, defined as follows.

$$\begin{bmatrix} \dot{\mathbf{x}} \\ \acute{\mathbf{q}} \end{bmatrix} = \begin{bmatrix} \acute{\mathcal{A}} & \acute{\mathcal{B}}_p \\ \acute{\mathcal{C}}_q & 0 \end{bmatrix} \begin{bmatrix} \mathbf{x} \\ \acute{\mathbf{p}} \end{bmatrix} \tag{3.40}$$
$$\acute{\mathbf{p}} = \text{sat}\left(\acute{\mathbf{q}}\right)$$

where

$$\acute{\mathbf{q}} = \begin{bmatrix} \acute{q}_1 \\ \acute{q}_2 \\ \vdots \\ \acute{q}_{n_p} \end{bmatrix}, \quad \text{sat}\left(\acute{\mathbf{q}}\right) = \begin{bmatrix} \text{sat}\left(\acute{q}_1\right) \\ \text{sat}\left(\acute{q}_2\right) \\ \vdots \\ \text{sat}\left(\acute{q}_{n_{\acute{p}}}\right) \end{bmatrix}, \quad \text{sat}\left(\acute{q}_i\right) = \begin{cases} 1 & \acute{q}_i > 1 \\ \acute{q}_i & |\acute{q}_i| < 1 \\ -1 & \acute{q}_i < -1 \end{cases} \tag{3.41}$$

Boyd and Hindi [11] present a simple approach to include saturation in stability analysis. Refer to Figure 3.3. Their approach relies on the use of non-linear uncertainty

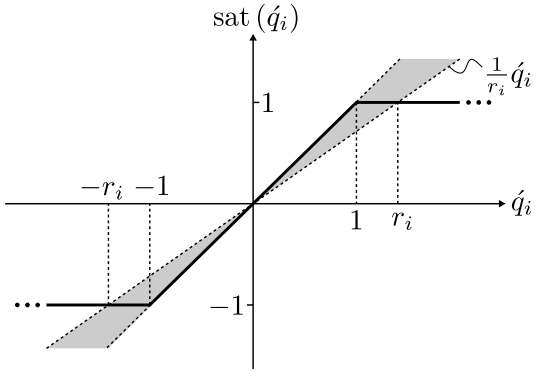

Figure 3.3: Saturation over a finite input domain.

to specify saturation for a *finite* input domain, defined as

$$\text{sat}\left(\acute{q}_i\right) = \left(\frac{r_i + 1}{2r_i} + \delta_i \frac{r_i - 1}{2r_i}\right) \acute{q}_i, \quad \acute{q}_i \in \left(-r_i, r_i\right), \quad \delta_i \in \mathbf{\Delta} \tag{3.42}$$

where $(r_i - 1)$ is the amount by which $\acute{q}_i$ may exceed the saturation level.

We replace the saturation operator in (3.40) with its local representation (3.42) and apply the lower linear fractional transform to obtain (3.28) where

$$\mathcal{A} = \acute{\mathcal{A}} + \acute{\mathcal{B}}_p R_L \acute{\mathcal{C}}_q, \quad \mathcal{B}_p = \acute{\mathcal{B}}_p, \quad \mathcal{C}_q = R_N \acute{\mathcal{C}}_q, \quad \mathcal{D}_{qp} = 0,$$
$$R_L \coloneqq \text{diag}\left(\frac{r_1 + 1}{2r_1}, \frac{r_2 + 1}{2r_2}, \ldots, \frac{r_{n_p} + 1}{2r_{n_p}}\right),$$
$$R_N \coloneqq \text{diag}\left(\frac{r_1 - 1}{2r_1}, \frac{r_2 - 1}{2r_2}, \ldots, \frac{r_{n_p} - 1}{2r_{n_p}}\right),$$
$$\Delta = \text{diag}\left(\delta_1, \delta_2, \ldots, \delta_{n_{\acute{p}}}\right) \in \mathbf{\Delta} \tag{3.43}$$

and

$$|\acute{q}_i| < r_i, \quad \acute{\mathbf{q}} = \acute{\mathcal{C}}_q \mathbf{x} \tag{3.44}$$

are the sufficient condition for (3.28) to include (3.40).

Lyapunov's condition for global stability (3.27) then reduces to the *local* stability conditions for (3.28)

$$\begin{aligned}(\exists V(\mathbf{x}(t)) : (3.11), (3.12),\ \mathbf{x}(t) \in \mathcal{R}\ \forall \mathbf{x}(t_0) \in \mathcal{R},\ |\acute{q}_i| < r_i\ \forall \mathbf{x}(t) \in \mathcal{R}) \\ \implies \left(\lim_{t\to\infty} \mathbf{x}(t) = \mathbf{0} : \mathbf{x}(t_0) \in \mathcal{R}\right)\end{aligned} \tag{3.45}$$

which guarantees the convergence of $\mathbf{x}(t)$ to $\mathbf{0}$ for any initial condition $\mathbf{x}(t_0)$ in local region $\mathcal{R}$, where the largest region $\mathcal{R}$ is referred to as the *region of attraction*. Sufficient conditions for local stability (3.45) are given in [11] as

$$\begin{aligned}\left(\exists Q_S > 0 : \acute{\mathcal{C}}_{q,i} Q_S \acute{\mathcal{C}}_{q,i}^T < r_i^2,\ \mathcal{A}(\Delta) Q_S + Q_S \mathcal{A}^T(\Delta) < 0,\ \frac{d}{dt} Q_S = 0\right) \\ \implies \left(\lim_{t\to\infty} \mathbf{x}(t) = \mathbf{0} : \mathbf{x}(t_0) \in \mathcal{R}\right)\end{aligned} \tag{3.46}$$

where $\mathcal{R}$ is defined as a hyper ellipsoid and $\acute{\mathcal{C}}_{q,i}$ is the i^{th} row of $\acute{\mathcal{C}}_q$.

The sufficient matrix inequality conditions in (3.46) are equivalent to those of global stability with the additional constraints

$$\acute{\mathcal{C}}_{q,i} Q_S \acute{\mathcal{C}}_{q,i}^T < r_i^2, \quad \mathcal{D}_{qp} = 0 \tag{3.47}$$

Thus, following (3.39) and (3.47), we find the region of attraction $\mathcal{R} = \left\{\mathbf{x} \in \mathbb{R}^{n_x \times 1} : \mathbf{x}^T Q_S^{-1} \mathbf{x} < 1\right\}$, such that (3.40) satisfies $\lim_{t\to\infty} \mathbf{x}(t) = 0 : \mathbf{x}(t_0) \in \mathcal{R}$, in terms of LMI optimisation problem

$$\begin{aligned}\text{minimise} \quad & -\operatorname{tr}(Q_S) \\ \text{subject to} \quad & \acute{\mathcal{C}}_{q,i} Q_S \acute{\mathcal{C}}_{q,i}^T < r_i^2 \\ & \left[\begin{array}{c|c} Q_S \mathcal{A}^T + \mathcal{A} Q_S + \mathcal{B}_p W_S \mathcal{B}_p^T & Q_S \mathcal{C}_q^T \\ \hline \mathcal{C}_q Q_S & -W_S \end{array}\right] < 0, \\ & W_S \in \mathfrak{C},\ Q_S > 0,\ (3.43)\end{aligned} \tag{3.48}$$

where the objective maximises the sum of the squares of the principle axes of hyper ellipsoid $\mathcal{R}$.

Note that LMI stability conditions may also be formulated for an undisturbed LTI model subject to saturation *and* NLTV uncertainty by including the NLTV uncertainty in (3.40) with $\acute{\Delta} \in \mathbf{\Delta}$, and carrying $\acute{\Delta}$ through the derivation.

3.7 Performance Measures

Robust Instantaneous Output Covariance (IOC), *robust Average Output Variance* (AOV) and *robust eigenvalue regions* are the performance measures developed in the thesis. They serve to characterise the error levels, bandwidth, transient behaviour and stability of a system subject to white noise disturbance and time-varying uncertainty. Two variance-type measures are used, *i.e.* robust IOC and robust AOV, due to their respective admittance to linear form when the controller is introduced as a variable.

3.7.1 Robust instantaneous output covariance

The IOC of an LTV system, with deterministic system matrices, is formulated by Kwakernaak and Sivan [48] in terms of a Riccati equation and applied here to the norm-bounded state-space description. The resulting Riccati equation is transformed to a matrix inequality by applying a theorem developed in Appendix A.2.14, after which we rely on the theorem of Takaba [74] to remove the structured norm-bounded uncertainty Δ from the matrix inequalities, similar to that in Section 3.6.1. The resulting LMIs measure an upper-bound of the IOC of an LTI system subject to LTV uncertainty, and the upper-bound is referred to as the robust IOC.

Given the LTV strictly-proper [6] model

$$\begin{aligned}\begin{bmatrix}\dot{\mathbf{x}}\\ \mathbf{z}\end{bmatrix} &= \begin{bmatrix}\mathcal{A}(\Delta) & \mathcal{B}(\Delta)\\ \mathcal{C}(\Delta) & 0\end{bmatrix}\begin{bmatrix}\mathbf{x}\\ \mathbf{w}\end{bmatrix}\\ &= \begin{bmatrix}\mathcal{A}+\mathcal{B}_p\Delta\left(I-\mathcal{D}_{qp}\Delta\right)^{-1}\mathcal{C}_q & \mathcal{B}_w+\mathcal{B}_p\Delta\left(I-\mathcal{D}_{qp}\Delta\right)^{-1}\mathcal{D}_{qw}\\ \mathcal{C}_z+\mathcal{D}_{zp}\Delta\left(I-\mathcal{D}_{qp}\Delta\right)^{-1}\mathcal{C}_q & 0\end{bmatrix}\begin{bmatrix}\mathbf{x}\\ \mathbf{w}\end{bmatrix}\\ \Delta\in\mathbf{\Delta},\ \frac{\partial\Delta}{\partial\rho_i} &= 0\ \forall\rho_i\neq t\end{aligned} \tag{3.49}$$

where the exogenous input $\mathbf{w}\in\mathbb{R}^{n_w\times 1}$ is specified as *white noise*, the robust IOC is given in [48] and derived in Appendix A.2.6 as

$$\mathbb{E}\left\{\mathbf{x}\mathbf{x}^T\right\} = Q_x(t) \tag{3.50}$$

where

$$\dot{Q}_x(t) = \mathcal{A}(\Delta)Q_x(t) + Q_x(t)\mathcal{A}^T(\Delta) + \mathcal{B}(\Delta)\mathcal{B}^T(\Delta) \tag{3.51}$$

and $\mathbf{w}$ is unit intensity white noise (see Appendix A.2.3 for white noise formulation).

The following theorem provides a means to transform a Riccati-type equation into two matrix inequalities, [7] and is used to transform the pair (3.50) and (3.51) into LMIs in a time-invariant upper-bound of the instantaneous state-covariance, *i.e.* $\overline{Q}_x > Q_x(t)$, which is independent of $\dot{Q}_x(t)$.

6. $\mathcal{D}(\Delta) = 0$ is a necessary condition for systems to have finite output variances/covariances.

7. The two resulting matrix inequalities may be combined with the block-diagonal operator, *e.g.* (3.8).

Theorem 2. *(Lyapunov variable upper bound) Suppose there exists a time-invariant matrix* $W > 0$ *and matrix expressions* $\{S(\boldsymbol{\varrho}), X(\boldsymbol{\varrho})\} \subset \left\{M(\boldsymbol{\varrho}) \middle| M : \mathbb{R}^{n_\varrho \times 1} \mapsto \mathbb{R}^{n \times n}, M(\boldsymbol{\varrho}) = M^T(\boldsymbol{\varrho})\right\}$, $R(\boldsymbol{\varrho}) \in \left\{M(\boldsymbol{\varrho}) \middle| M : \mathbb{R}^{n_\varrho \times 1} \mapsto \mathbb{R}^{n \times n}, M(\boldsymbol{\varrho}) > 0\right\}$ *and* $F(\boldsymbol{\varrho}) \in \left\{M(\boldsymbol{\varrho}) \middle| M : \mathbb{R}^{n_\varrho \times 1} \mapsto \mathbb{R}^{n \times n}\right\}$ *such that*

$$S(\boldsymbol{\varrho}) = F(\boldsymbol{\varrho}) X(\boldsymbol{\varrho}) + X(\boldsymbol{\varrho}) F^T(\boldsymbol{\varrho}) + R(\boldsymbol{\varrho}) \tag{3.52}$$

and

$$F(\boldsymbol{\varrho}) W + W F^T(\boldsymbol{\varrho}) + R(\boldsymbol{\varrho}) < 0 \tag{3.53}$$

Then

$$W > X(\boldsymbol{\varrho}) \tag{3.54}$$

Proof: See Appendix A.2.14.

Given (3.50) and (3.51), substituting $(S(\boldsymbol{\varrho}), F(\boldsymbol{\varrho}), X(\boldsymbol{\varrho}), R(\boldsymbol{\varrho}), W)$ in Theorem 2 with

$$\left(\dot{Q}_x(t), \mathcal{A}(\Delta), Q_x(t), \left(\mathcal{B}(\Delta)\mathcal{B}^T(\Delta)\right), \overline{Q}_x\right) \tag{3.55}$$

we obtain

$$\begin{aligned}&\left(\mathcal{A}(\Delta)\overline{Q}_x + \overline{Q}_x\mathcal{A}^T(\Delta) + \mathcal{B}(\Delta)\mathcal{B}^T(\Delta) < 0, \quad \overline{Q}_x > 0\right)\\ &\qquad \Longrightarrow \quad \left(\mathbb{E}\left\{\mathbf{x}\mathbf{x}^T\right\} < \overline{Q}_x\right)\end{aligned} \tag{3.56}$$

The robust IOC is formulated with (3.56) by applying a congruent transformation with $\mathcal{C}\left(\acute{\Delta}\right)$

$$\begin{aligned}&\left(\mathcal{A}(\Delta)\overline{Q}_x + \overline{Q}_x\mathcal{A}^T(\Delta) + \mathcal{B}(\Delta)\mathcal{B}^T(\Delta) < 0, \quad \overline{Q}_x > 0\right)\\ &\qquad \Longrightarrow \quad \mathbb{E}\left\{\mathbf{z}\mathbf{z}^T\right\} < \mathcal{C}\left(\acute{\Delta}\right)\overline{Q}_x\mathcal{C}^T\left(\acute{\Delta}\right), \quad \acute{\Delta} \in \boldsymbol{\Delta}\end{aligned} \tag{3.57}$$

where $\mathcal{C}\left(\acute{\Delta}\right)$ may be NLTV, however we constrain $\acute{\Delta}$ as $\frac{\partial \acute{\Delta}}{\partial \rho_i} = 0 \; \forall \rho_i \neq t$ to be coherent with $\overline{Q}_x$, and without loss of generality is included with Δ.

Given (3.57), substituting $(R, E, \Omega(\boldsymbol{\varrho}), \Lambda(\boldsymbol{\varrho}), F, J, T, N)$ in Theorem 1 with

$$\left(\begin{pmatrix} \mathcal{A}\overline{Q}_x + \overline{Q}_x\mathcal{A}^T \\ +\mathcal{B}_w\mathcal{B}_w^T \end{pmatrix}, \mathcal{B}_p, (I - \Delta\mathcal{D}_{qp})^{-1}, \Delta, \begin{pmatrix} \overline{Q}_x\mathcal{C}_q^T \\ +\mathcal{B}_w\mathcal{D}_{qw}^T \end{pmatrix}, \left(\mathcal{D}_{qw}\mathcal{D}_{qw}^T\right), W_Q, \mathcal{D}_{qp}\right) \tag{3.58}$$

and

$$\left(\left(-\overline{Q}_z + \mathcal{C}_z\overline{Q}_x\mathcal{C}_z^T\right), \mathcal{D}_{zp}, (I - \Delta\mathcal{D}_{qp})^{-1}, \Delta, \left(\mathcal{C}_z\overline{Q}_x\mathcal{C}_q^T\right), \left(\mathcal{C}_q\overline{Q}_x\mathcal{C}_q^T\right), W_C, \mathcal{D}_{qp}\right) \tag{3.59}$$

we obtain

$$\left(\begin{array}{c} \left[\begin{array}{c|c} \mathcal{A}\overline{Q}_x + \overline{Q}_x\mathcal{A}^T & \overline{Q}_x\mathcal{C}_q^T + \mathcal{B}_w\mathcal{D}_{qw}^T + \mathcal{B}_p W_Q \mathcal{D}_{qp}^T \\ +\mathcal{B}_w\mathcal{B}_w^T + \mathcal{B}_p W_Q \mathcal{B}_p^T & \\ \hline \star & -W_Q + \mathcal{D}_{qp} W_Q \mathcal{D}_{qp}^T + \mathcal{D}_{qw}\mathcal{D}_{qw}^T \end{array} \right] < 0 \\ W_Q \in \mathfrak{C} \end{array} \right) \\ \implies \quad \left(\mathcal{A}(\Delta)\overline{Q}_x + \overline{Q}_x\mathcal{A}^T(\Delta) + \mathcal{B}(\Delta)\mathcal{B}^T(\Delta) < 0 \right) \tag{3.60}$$

and

$$\left(\begin{array}{c} \left[\begin{array}{c|c} -\overline{Q}_z + \mathcal{C}_z\overline{Q}_x\mathcal{C}_z^T + \mathcal{D}_{zp} W_C \mathcal{D}_{zp}^T & \mathcal{C}_z\overline{Q}_x\mathcal{C}_q^T + \mathcal{D}_{zp} W_C \mathcal{D}_{qp}^T \\ \hline \star & -W_C + \mathcal{D}_{qp} W_C \mathcal{D}_{qp}^T + \mathcal{C}_q\overline{Q}_x\mathcal{C}_q^T \end{array} \right] < 0 \\ W_C \in \mathfrak{C} \\ \overline{Q}_z > 0 \end{array} \right) \\ \implies \quad \left(\mathcal{C}(\Delta)\overline{Q}_x\mathcal{C}^T(\Delta) < \overline{Q}_z \right) \tag{3.61}$$

respectively, where $\overline{Q}_z$ is included as a time-invariant upper-bound of $\mathcal{C}(\Delta)\overline{Q}_x\mathcal{C}^T(\Delta)$. Now, combining (3.50), (3.51), (3.57), (3.60) and (3.61), we find the robust IOC performance measure $\mathbb{E}\left\{\mathbf{z}\mathbf{z}^T\right\} < \overline{Q}_z$ of (3.49) in terms of LMI optimisation problem

$$\begin{array}{ll} \text{minimise} & \gamma \\ \text{subject to} & \mathcal{L}_C\left(\gamma, \overline{Q}_z, \overline{Q}_x, W_Q, W_C\right) \\ & \left[\begin{array}{c|c} \mathcal{A}\overline{Q}_x + \overline{Q}_x\mathcal{A}^T & \overline{Q}_x\mathcal{C}_q^T + \mathcal{B}_w\mathcal{D}_{qw}^T + \mathcal{B}_p W_Q \mathcal{D}_{qp}^T \\ +\mathcal{B}_w\mathcal{B}_w^T + \mathcal{B}_p W_Q \mathcal{B}_p^T & \\ \hline \star & -W_Q + \mathcal{D}_{qp} W_Q \mathcal{D}_{qp}^T + \mathcal{D}_{qw}\mathcal{D}_{qw}^T \end{array} \right] < 0 \\ & \left[\begin{array}{c|c} -\overline{Q}_z + \mathcal{C}_z\overline{Q}_x\mathcal{C}_z^T + \mathcal{D}_{zp} W_C \mathcal{D}_{zp}^T & \mathcal{C}_z\overline{Q}_x\mathcal{C}_q^T + \mathcal{D}_{zp} W_C \mathcal{D}_{qp}^T \\ \hline \star & -W_C + \mathcal{D}_{qp} W_C \mathcal{D}_{qp}^T + \mathcal{C}_q\overline{Q}_x\mathcal{C}_q^T \end{array} \right] < 0 \\ & \{W_Q, W_C\} \subset \mathfrak{C},\ \overline{Q}_x > 0,\ \overline{Q}_z > 0,\ \gamma \in \mathbb{R}^1 \end{array} \tag{3.62}$$

where $\overline{Q}_z$ is included as a variable, γ is included as an auxiliary scalar variable and additional LMIs are included with $\mathcal{L}_C$ to account for the objective, discussed in Section 3.9.

[74] shows that the feasibility of (3.62) implies robust stability formulated in Section 3.6.1. This is apparent when considering (3.35) and (3.60)

$$\begin{array}{l} \left(\mathcal{A}(\Delta)\overline{Q}_x + \overline{Q}_x\mathcal{A}^T(\Delta) + \mathcal{B}(\Delta)\mathcal{B}^T(\Delta) < 0,\ \overline{Q}_x > 0 \right) \\ \overset{P=\overline{Q}_x^{-1}}{\implies} \quad \left(\mathcal{A}(\Delta)^T P + P\mathcal{A}(\Delta) < 0,\ P > 0 \right) \end{array} \tag{3.63}$$

Thus, if (3.62) is included as one of the model performance measures, then (3.39) is readily included.

3.7.2 Robust average output variance

The AOV of an LTV system, with deterministic system matrices, is partly formulated by Kwakernaak and Sivan [48] and is completed in Appendix A.2.7. The formulation is derived in terms of a Riccati equation and applied here to the norm-bounded state-space description. The derivation proceeds in a similar manner to Section 3.7.1, and the resulting LMIs measure an upper-bound of the AOV of an LTI system subject to LTV uncertainty, and the upper-bound is referred to as the robust AOV.

The robust AOV for the LTV strictly-proper system (3.49) is partly given in [48] and derived in Appendix A.2.7 as

$$\lim_{t_1\to\infty}\frac{1}{t_1-t_0}\mathbb{E}\left\{\int_{t_0}^{t_1}\mathbf{z}^T(t)\,\mathbf{z}(t)\,dt\right\}=\lim_{t_1\to\infty}\frac{1}{t_1-t_0}\mathrm{tr}\left(\int_{t_0}^{t_1}\mathcal{B}^T(\Delta)\,P(t_1,t)\,\mathcal{B}(\Delta)\,dt\right) \tag{3.64}$$

where

$$-\frac{\partial P(t_1,t)}{\partial t}=\mathcal{A}^T(\Delta)\,P(t_1,t)+P(t_1,t)\,\mathcal{A}(\Delta)+\mathcal{C}^T(\Delta)\,\mathcal{C}(\Delta) \tag{3.65}$$

The derivation of robust AOV performance measure in terms of an LMI optimisation problem is similar to that of the robust IOC performance measure, and is summarised as follows.

Given (3.64) and (3.65), substituting $(S(\boldsymbol{\varrho}),F(\boldsymbol{\varrho}),X(\boldsymbol{\varrho}),R(\boldsymbol{\varrho}),W)$ in Theorem 2 with

$$\left(-\frac{\partial P(t_1,t)}{\partial t},\mathcal{A}^T(\Delta),P(t_1,t),\left(\mathcal{C}^T(\Delta)\,\mathcal{C}(\Delta)\right),\overline{P}\right) \tag{3.66}$$

we obtain

$$\begin{aligned}&\left(\mathcal{A}^T(\Delta)\,\overline{P}+\overline{P}\mathcal{A}(\Delta)+\mathcal{C}^T(\Delta)\,\mathcal{C}(\Delta)<0,\quad \overline{P}>0\right)\\ \Longrightarrow\quad &\left(\lim_{t_1\to\infty}\frac{1}{t_1-t_0}\mathbb{E}\left\{\int_{t_0}^{t_1}\mathbf{z}^T(t)\,\mathbf{z}(t)\,dt\right\}<\mathrm{tr}\left(\mathcal{B}^T(\Delta)\,\overline{P}\mathcal{B}(\Delta)\right)\right)\end{aligned} \tag{3.67}$$

Given (3.67), substituting $(R,E,\Omega(\boldsymbol{\varrho}),\Lambda(\boldsymbol{\varrho}),F,J,T,N)$ in Theorem 1 with

$$\left(\begin{pmatrix}\mathcal{A}^T\overline{P}+\overline{P}\mathcal{A}\\ +\mathcal{C}_z^T\mathcal{C}_z\end{pmatrix},\mathcal{C}_q^T,(I-\mathcal{D}_{qp}\Delta)^{-T},\Delta^T,\left(\overline{P}\mathcal{B}_p+\mathcal{C}_z^T\mathcal{D}_{zp}\right),\left(\mathcal{D}_{zp}^T\mathcal{D}_{zp}\right),W_P,\mathcal{D}_{qp}^T\right) \tag{3.68}$$

and

$$\left(\left(-V+\mathcal{B}_w^T\overline{P}\mathcal{B}_w\right),\mathcal{D}_{qw}^T,(I-\mathcal{D}_{qp}\Delta)^{-T},\Delta^T,\left(\mathcal{B}_w^T\overline{P}\mathcal{B}_p\right),\left(\mathcal{B}_p^T\overline{P}\mathcal{B}_p\right),W_V,\mathcal{D}_{qp}^T\right) \tag{3.69}$$

we obtain

$$\left(\begin{array}{c} \left[\begin{array}{c|c} \mathcal{A}^T\overline{P} + \overline{P}\mathcal{A} + \mathcal{C}_z^T\mathcal{C}_z + \mathcal{C}_q^T W_P \mathcal{C}_q & \overline{P}\mathcal{B}_p + \mathcal{C}_z^T\mathcal{D}_{zp} + \mathcal{C}_q^T W_P \mathcal{D}_{qp} \\ \hline \star & -W_P + \mathcal{D}_{qp}^T W_P \mathcal{D}_{qp} + \mathcal{D}_{zp}^T\mathcal{D}_{zp} \end{array}\right] < 0 \\ W_P \in \mathfrak{C} \end{array} \right)$$
$$\implies \quad \left(\mathcal{A}^T(\Delta)\overline{P} + \overline{P}\mathcal{A}(\Delta) + \mathcal{C}^T(\Delta)\mathcal{C}(\Delta) < 0\right) \tag{3.70}$$

and

$$\left(\begin{array}{c} \left[\begin{array}{c|c} -V + \mathcal{B}_w^T\overline{P}\mathcal{B}_w + \mathcal{D}_{qw}^T W_V \mathcal{D}_{qw} & \mathcal{B}_w^T\overline{P}\mathcal{B}_p + \mathcal{D}_{qw}^T W_V \mathcal{D}_{qp} \\ \hline \star & -W_V + \mathcal{D}_{qp}^T W_V \mathcal{D}_{qp} + \mathcal{B}_p^T\overline{P}\mathcal{B}_p \end{array}\right] < 0 \\ W_V \in \mathfrak{C} \\ V > 0 \end{array} \right)$$
$$\implies \quad \left(\mathcal{B}^T(\Delta)\overline{P}\mathcal{B}(\Delta) < V\right) \tag{3.71}$$

respectively, where V is included as a time-invariant upper-bound of $\mathcal{B}^T(\Delta)\overline{P}\mathcal{B}(\Delta)$.

Now, combining (3.64), (3.65), (3.67), (3.70) and (3.71), we find the robust AOV performance measure $\lim_{t_1\to\infty}\frac{1}{t_1-t_0}\mathbb{E}\left\{\int_{t_0}^{t_1}\mathbf{z}^T(t)\,\mathbf{z}(t)\,dt\right\} < \mathrm{tr}(V)$ of (3.49) in terms of LMI optimisation problem

$$\begin{array}{ll} \text{minimise} & \gamma \\ \text{subject to} & \mathcal{L}_V\left(\gamma, V, \overline{P}, W_P, W_V\right) \\ & \left[\begin{array}{c|c} \begin{array}{c}\mathcal{A}^T\overline{P} + \overline{P}\mathcal{A} \\ +\mathcal{C}_z^T\mathcal{C}_z + \mathcal{C}_q^T W_P\mathcal{C}_q\end{array} & \overline{P}\mathcal{B}_p + \mathcal{C}_z^T\mathcal{D}_{zp} + \mathcal{C}_q^T W_P\mathcal{D}_{qp} \\ \hline \star & -W_P + \mathcal{D}_{qp}^T W_P\mathcal{D}_{qp} + \mathcal{D}_{zp}^T\mathcal{D}_{zp} \end{array}\right] < 0 \\ & \left[\begin{array}{c|c} -V + \mathcal{B}_w^T\overline{P}\mathcal{B}_w + \mathcal{D}_{qw}^T W_V\mathcal{D}_{qw} & \mathcal{B}_w^T\overline{P}\mathcal{B}_p + \mathcal{D}_{qw}^T W_V\mathcal{D}_{qp} \\ \hline \star & -W_V + \mathcal{D}_{qp}^T W_V\mathcal{D}_{qp} + \mathcal{B}_p^T\overline{P}\mathcal{B}_p \end{array}\right] < 0 \\ & \{W_P, W_V\} \subset \mathfrak{C},\ \overline{P} > 0,\ V > 0,\ \gamma \in \mathbb{R}^1 \end{array} \tag{3.72}$$

where V is included as a variable, γ is included as an auxiliary scalar variable and additional LMIs are included with $\mathcal{L}_V$ to account for the objective, discussed in Section 3.9.

Even though (3.72) is derived for LTV systems, *i.e.* $\Delta \in \mathbf{\Delta}$, $\frac{\partial\Delta}{\partial\rho_i} = 0\,\forall\rho_i \neq t$, [30, Ch.7] shows that (3.72) also holds for *NLTV causal* variation if $\mathcal{D}_{qw} = 0$, $\mathcal{D}_{qp} = 0$ and $\mathcal{D}_{zp} = 0$, and is derived using *Itô calculus*, which is beyond the scope of this thesis. Furthermore, [30, Ch.7] forms the conjecture that (3.62) also holds for *NLTV causal* variation, where $\overline{Q}_z$ bounds the *average* output covariance.

Similar to (3.62), robust stability formulated in Section 3.6.1 is inherent in (3.72).

3.7.3 Robust eigenvalue regions

Convex eigenvalue regions of an LTI system are formulated by Chilali and Gahinet [16] in terms of LMIs and applied here to the norm-bounded state-space description. The derivation proceeds in a manner similar to that described in Section 3.6.1, and the resulting LMIs measure three eigenvalue regions, popular in the control literature, for an LTI system subject to NLTV uncertainty, referred to as robust eigenvalue regions.

The robust time-invariant eigenvalue region $\mathcal{R} \subset \mathbb{C}^1$ of NLTV matrix $\mathcal{A}(\Delta)$ in (3.28) is given as

$$\operatorname{eig}(\mathcal{A}(\Delta)) \subset \mathcal{R} \tag{3.73}$$

where the eigenvalue operator in the time-varying framework refers to the *set*, possibly continuous,[8] of all instantaneous eigenvalues, *i.e.*

$$\operatorname{eig}(\mathcal{A}(\Delta)) = \left\{ \operatorname{eig}\left(\mathcal{A}\left(\hat{\Delta}\right)\right) : \hat{\Delta} \in \mathbf{\Delta},\ \frac{d}{dt}\hat{\Delta} = 0 \right\} \tag{3.74}$$

[16] presents necessary and sufficient LMI conditions for the eigenvalues of a matrix to reside within a specified convex region. [16, Theorem 2.2] applies to a very general class of regions in the 1D complex domain $\mathbb{C}^1$, although we limit ourselves to the regions that we have found to admit linear form when the controller is introduced as a variable.

The following theorem provides LMI conditions for a robust maximum-real eigenvalue region, a robust disk eigenvalue region and a robust cone eigenvalue region, of which the combined region $\mathcal{R}$ is illustrated in Figure 3.4.

Theorem 3. *[16] (robust eigenvalue regions) Given the time-invariant scalars* $\{\mathfrak{a}, \mathfrak{r}, \mathfrak{q}, \mathfrak{c}\} \subset \mathbb{R}^1$ *and the NLTV matrix* $\mathcal{A}(\Delta)$ *in* (3.28)*, then*

$$\begin{aligned} &\left(\exists X_{\mathfrak{a}} > 0 : \mathcal{A}(\Delta) X_{\mathfrak{a}} + X_{\mathfrak{a}} \mathcal{A}(\Delta)^T + 2\mathfrak{a} X_{\mathfrak{a}} < 0,\ \frac{d}{dt} X_{\mathfrak{a}} = 0\right) \\ &\qquad \Longrightarrow \quad \left(eig(\mathcal{A}(\Delta)) \subset \left\{ z \in \mathbb{C}^1 : z < -\mathfrak{a} \right\}\right) \end{aligned} \tag{3.75}$$

$$\begin{aligned} &\left(\exists X_{\mathfrak{r}} > 0 : \begin{bmatrix} -\mathfrak{r} X_{\mathfrak{r}} & \mathfrak{q} X_{\mathfrak{r}} + \mathcal{A}(\Delta) X_{\mathfrak{r}} \\ \mathfrak{q} X_{\ominus} + X_{\mathfrak{r}} \mathcal{A}^T(\Delta) & -\mathfrak{r} X_{\mathfrak{r}} \end{bmatrix} < 0,\ \frac{d}{dt} X_{\mathfrak{r}} = 0\right) \\ &\qquad \Longrightarrow \quad \left(eig(\mathcal{A}(\Delta)) \subset \left\{ z \in \mathbb{C}^1 : (z + \mathfrak{q})^H (z + \mathfrak{q}) < \mathfrak{r}^2 \right\}\right) \end{aligned} \tag{3.76}$$

and

$$\begin{aligned} &\left(\begin{array}{c} \exists X_{\mathfrak{c}} > 0 : \\ \begin{bmatrix} \sin(\mathfrak{c}) \left(\mathcal{A}(\Delta) X_{\mathfrak{c}} + X_{\mathfrak{c}} \mathcal{A}^T(\Delta)\right) & \cos(\mathfrak{c}) \left(\mathcal{A}(\Delta) X_{\mathfrak{c}} - X_{\mathfrak{c}} \mathcal{A}^T(\Delta)\right) \\ \cos(\mathfrak{c}) \left(-\mathcal{A}(\Delta) X_{\mathfrak{c}} + X_{\mathfrak{c}} \mathcal{A}^T(\Delta)\right) & \sin(\mathfrak{c}) \left(\mathcal{A}(\Delta) X_{\mathfrak{c}} + X_{\mathfrak{c}} \mathcal{A}^T(\Delta)\right) \end{bmatrix} < 0, \\ \frac{d}{dt} X_{\mathfrak{c}} = 0 \end{array} \right) \\ &\qquad \Longrightarrow \quad \left(eig(\mathcal{A}(\Delta)) \subset \left\{ z \in \mathbb{C}^1 : \tan(\mathfrak{c}) < \frac{|\Im(z)|}{-\Re(z)} \right\}\right) \end{aligned} \tag{3.77}$$

8. The set is discrete when Δ is time-invariant or dependency $\boldsymbol{\rho}$ is discrete.

Proof: See [16].[9]

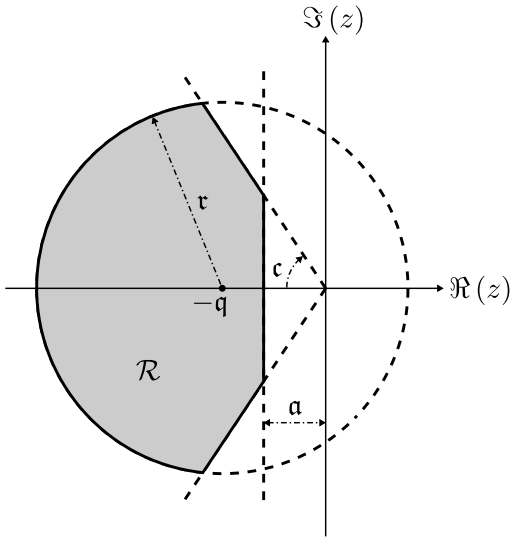

Figure 3.4: Robust eigenvalue region.

Given $\mathcal{A}(\Delta)$ in (3.28), (3.75), (3.76) and (3.77), substituting $(R, E, \Omega(\boldsymbol{\varrho}), \Lambda(\boldsymbol{\varrho}), F, J, T, N)$ in Theorem 2 with

$$\left(\left(\mathcal{A}X_{\mathfrak{a}} + X_{\mathfrak{a}}\mathcal{A}^T + 2\mathfrak{a}X_{\mathfrak{a}}\right), \mathcal{B}_p, (I - \Delta\mathcal{D}_{qp})^{-1}, \Delta, X_{\mathfrak{a}}\mathcal{C}_q^T, 0, W_{\mathfrak{a}}, \mathcal{D}_{qp}\right) \tag{3.78}$$

$$\left(\begin{pmatrix} (-\mathfrak{r}^2 + \mathfrak{q}^2) X_{\mathfrak{r}} \\ +\mathfrak{q}\mathcal{A}X_{\mathfrak{r}} \\ +\mathfrak{q}X_{\mathfrak{r}}\mathcal{A}^T \\ +\mathcal{A}X_{\mathfrak{r}}\mathcal{A}^T \end{pmatrix}, \mathcal{B}_p, (I - \Delta\mathcal{D}_{qp})^{-1}, \Delta, \begin{pmatrix} \mathfrak{q}X_{\mathfrak{r}}\mathcal{C}_q^T \\ +\mathcal{A}X_{\mathfrak{r}}\mathcal{C}_q^T \end{pmatrix}, \mathcal{C}_q X_{\mathfrak{r}}\mathcal{C}_q^T, W_{\mathfrak{r}}, \mathcal{D}_{qp}\right) \tag{3.79}$$

and

$$\begin{pmatrix} \left(\Theta \otimes \mathcal{A}X_{\mathfrak{c}} + (\Theta \otimes \mathcal{A}X_{\mathfrak{c}})^T\right), I_2 \otimes \mathcal{B}_p, I_2 \otimes (I - \Delta\mathcal{D}_{qp})^{-1}, \\ I_2 \otimes \Delta, (\Theta \otimes \mathcal{C}_q X_{\mathfrak{c}})^T, 0, W_{\mathfrak{c}}, I_2 \otimes \mathcal{D}_{qp} \end{pmatrix},$$

$$\Theta := \begin{bmatrix} \sin(\mathfrak{c}) & \cos(\mathfrak{c}) \\ -\cos(\mathfrak{c}) & \sin(\mathfrak{c}) \end{bmatrix} \tag{3.80}$$

9. Note that the lowercase Fraktur letters, *e.g.* $\mathfrak{a}$, $\mathfrak{r}$, $\mathfrak{q}$ and $\mathfrak{c}$, are not bolded and thus represent scalars.

we obtain

$$\left(\begin{array}{c} \left[\begin{array}{c|c} \mathcal{A}X_{\mathfrak{a}} + X_{\mathfrak{a}}\mathcal{A}^T + 2\mathfrak{a}X_{\mathfrak{a}} + \mathcal{B}_p W_{\mathfrak{a}} \mathcal{B}_p^T & X_{\mathfrak{a}}\mathcal{C}_q^T + \mathcal{B}_p W_{\mathfrak{a}} \mathcal{D}_{qp}^T \\ \hline \star & -W_{\mathfrak{a}} + \mathcal{D}_{qp} W_{\mathfrak{a}} \mathcal{D}_{qp}^T \end{array} \right] < 0 \\ W_{\mathfrak{a}} \in \mathfrak{C} \end{array} \right) \\ \Longrightarrow \quad \left(\mathcal{A}(\Delta) X_{\mathfrak{a}} + X_{\mathfrak{a}} \mathcal{A}^T(\Delta) + 2\mathfrak{a}X_{\mathfrak{a}} < 0 \right) \tag{3.81}$$

$$\left(\begin{array}{c} \left[\begin{array}{c|c} \begin{array}{c} (-\mathfrak{r}^2 + \mathfrak{q}^2) X_{\mathfrak{r}} + \mathfrak{q}\mathcal{A}X_{\mathfrak{r}} \\ +\mathfrak{q}X_{\mathfrak{r}}\mathcal{A}^T + \mathcal{A}X_{\mathfrak{r}}\mathcal{A}^T + \mathcal{B}_p W_{\mathfrak{r}} \mathcal{B}_p^T \end{array} & \mathfrak{q}X_{\mathfrak{r}}\mathcal{C}_q^T + \mathcal{A}X_{\mathfrak{r}}\mathcal{C}_q^T + \mathcal{B}_p W_{\mathfrak{r}} \mathcal{D}_{qp}^T \\ \hline \star & -W_{\mathfrak{r}} + \mathcal{D}_{qp} W_{\mathfrak{r}} \mathcal{D}_{qp}^T + \mathcal{C}_q X_{\mathfrak{r}} \mathcal{C}_q^T \end{array} \right] < 0 \\ W_{\mathfrak{r}} \in \mathfrak{C} \end{array} \right) \\ \Longrightarrow \quad \left(\left[\begin{array}{cc} -\mathfrak{r}X_{\mathfrak{r}} & \mathfrak{q}X_{\mathfrak{r}} + \mathcal{A}(\Delta) X_{\mathfrak{r}} \\ \mathfrak{q}X_{\mathfrak{r}} + X_{\mathfrak{r}}\mathcal{A}^T(\Delta) & -\mathfrak{r}X_{\mathfrak{r}} \end{array} \right] < 0 \right) \tag{3.82}$$

and

$$\left(\begin{array}{c} \left[\begin{array}{c|c} \begin{array}{c} \Theta \otimes \mathcal{A}X_{\mathfrak{c}} \\ + (\Theta \otimes \mathcal{A}X_{\mathfrak{c}})^T \\ + (I_2 \otimes \mathcal{B}_p) W_{\mathfrak{c}} (I_2 \otimes \mathcal{B}_p)^T \end{array} & \begin{array}{c} (\Theta \otimes \mathcal{C}_q X_{\mathfrak{c}})^T \\ + (I_2 \otimes \mathcal{B}_p) W_{\mathfrak{c}} (I_2 \otimes \mathcal{D}_{qp})^T \end{array} \\ \hline \star & \begin{array}{c} -W_{\mathfrak{c}} \\ + (I_2 \otimes \mathcal{D}_{qp}) W_{\mathfrak{c}} (I_2 \otimes \mathcal{D}_{qp})^T \end{array} \end{array} \right] < 0 \\ W_{\mathfrak{c}} = \left[\begin{array}{cc} W_{\mathfrak{c},1} & 0 \\ 0 & W_{\mathfrak{c},2} \end{array} \right], \{W_{\mathfrak{c},1}, W_{\mathfrak{c},2}\} \subset \mathfrak{C} \end{array} \right) \\ \Rightarrow \left(\left[\begin{array}{cc} \sin(\mathfrak{c}) \left(\mathcal{A}(\Delta) X_{\mathfrak{c}} + X_{\mathfrak{c}} \mathcal{A}^T(\Delta) \right) & \cos(\mathfrak{c}) \left(\mathcal{A}(\Delta) X_{\mathfrak{c}} - X_{\mathfrak{c}} \mathcal{A}^T(\Delta) \right) \\ \cos(\mathfrak{c}) \left(-\mathcal{A}(\Delta) X_{\mathfrak{c}} + X_{\mathfrak{c}} \mathcal{A}^T(\Delta) \right) & \sin(\mathfrak{c}) \left(\mathcal{A}(\Delta) X_{\mathfrak{c}} + X_{\mathfrak{c}} \mathcal{A}^T(\Delta) \right) \end{array} \right] < 0 \right) \tag{3.83}$$

respectively, where $\otimes$ is the *Kronecker product*[10] and is used for compactness, *e.g.*

$$\Theta \otimes \mathcal{A}X_{\mathfrak{c}} = \left[\begin{array}{cc} \sin(\mathfrak{c}) \mathcal{A}X_{\mathfrak{c}} & \cos(\mathfrak{c}) \mathcal{A}X_{\mathfrak{c}} \\ -\cos(\mathfrak{c}) \mathcal{A}X_{\mathfrak{c}} & \sin(\mathfrak{c}) \mathcal{A}X_{\mathfrak{c}} \end{array} \right] \tag{3.84}$$

and

$$I_2 = \left[\begin{array}{cc} 1 & 0 \\ 0 & 1 \end{array} \right] \tag{3.85}$$

10. Multiplication receives precedences over the *Kronecker product*.

Now, combining (3.75) and (3.81), we find the robust maximum-real eigenvalue region performance measure $\text{eig}\left(\mathcal{A}\left(\Delta\right)\right) \subset \left\{z \in \mathbb{C}^1 : z < -\mathfrak{a}\right\}$ of $\mathcal{A}\left(\Delta\right)$ in (3.28) in terms of LMI optimisation problem

$$\begin{aligned} &\text{minimise} && \gamma \\ &\text{subject to} && \mathcal{L}_{\mathfrak{a}}\left(\gamma, X_{\mathfrak{a}}, W_{\mathfrak{a}}\right) \\ & && \left[\begin{array}{c|c} \mathcal{A}X_{\mathfrak{a}} + X_{\mathfrak{a}}\mathcal{A}^T + 2\mathfrak{a}X_{\mathfrak{a}} + \mathcal{B}_p W_{\mathfrak{a}}\mathcal{B}_p^T & X_{\mathfrak{a}}\mathcal{C}_q^T + \mathcal{B}_p W_{\mathfrak{a}}\mathcal{D}_{qp}^T \\ \hline \star & -W_{\mathfrak{a}} + \mathcal{D}_{qp}W_{\mathfrak{a}}\mathcal{D}_{qp}^T \end{array}\right] < 0 \\ & && W_{\mathfrak{a}} \in \mathfrak{C},\ X_{\mathfrak{a}} > 0,\ \gamma \in \mathbb{R}^1 \end{aligned} \tag{3.86}$$

where $\mathfrak{a}$ is *not* included as a variable due to its multiplication with variable $X_{\mathfrak{a}}$, γ is included as an auxiliary scalar variable and additional LMIs are included with $\mathcal{L}_{\mathfrak{a}}$ to account for the objective, discussed in Section 3.9.

Similar to (3.62), robust stability formulated in Section 3.6.1 is inherent in (3.86) when $\mathfrak{a} > 0$.

Similarly, combining (3.76) and (3.82), we find the robust disk eigenvalue region performance measure $\text{eig}\left(\mathcal{A}\left(\Delta\right)\right) \subset \left\{z \in \mathbb{C}^1 : \left(z + \mathfrak{q}\right)^H \left(z + \mathfrak{q}\right) < \mathfrak{r}^2\right\}$ of $\mathcal{A}\left(\Delta\right)$ in (3.28) in terms of LMI optimisation problem

$$\begin{aligned} &\text{minimise} && \gamma \\ &\text{subject to} && \mathcal{L}_{\mathfrak{r}}\left(\gamma, X_{\mathfrak{r}}, W_{\mathfrak{r}}\right) \\ & && \left[\begin{array}{c|c} \begin{array}{c}\left(-\mathfrak{r}^2 + \mathfrak{q}^2\right) X_{\mathfrak{r}} + \mathfrak{q}\mathcal{A}X_{\mathfrak{r}} \\ +\mathfrak{q}X_{\mathfrak{r}}\mathcal{A}^T + \mathcal{A}X_{\mathfrak{r}}\mathcal{A}^T + \mathcal{B}_p W_{\mathfrak{r}}\mathcal{B}_p^T\end{array} & \begin{array}{c}\mathfrak{q}X_{\mathfrak{r}}\mathcal{C}_q^T + \mathcal{A}X_{\mathfrak{r}}\mathcal{C}_q^T \\ +\mathcal{B}_p W_{\mathfrak{r}}\mathcal{D}_{qp}^T\end{array} \\ \hline \star & \begin{array}{c}-W_{\mathfrak{r}} + \mathcal{D}_{qp}W_{\mathfrak{r}}\mathcal{D}_{qp}^T \\ +\mathcal{C}_q X_{\mathfrak{r}}\mathcal{C}_q^T\end{array} \end{array}\right] < 0 \\ & && W_{\mathfrak{r}} \in \mathfrak{C},\ X_{\mathfrak{r}} > 0,\ \gamma \in \mathbb{R}^1 \end{aligned} \tag{3.87}$$

where $\mathfrak{r}$ and $\mathfrak{q}$ are *not* included as variables due to their multiplication with variable $X_{\mathfrak{r}}$, γ is included as an auxiliary scalar variable and additional LMIs are included with $\mathcal{L}_{\mathfrak{r}}$ to account for the objective, discussed in Section 3.9.

Similarly, combining (3.77) and (3.83), we find the robust disk eigenvalue region performance measure $\text{eig}\left(\mathcal{A}\left(\Delta\right)\right) \subset \left\{z \in \mathbb{C}^1 : \tan\left(\mathfrak{c}\right) < \frac{|\Im(z)|}{-\Re(z)}\right\}$ of $\mathcal{A}\left(\Delta\right)$ in (3.28) in

terms of LMI optimisation problem

$$\begin{aligned}
&\text{minimise} \quad \gamma \\
&\text{subject to} \quad \mathcal{L}_{\mathfrak{c}}\left(\gamma, X_{\mathfrak{c}}, W_{\mathfrak{c}}\right) \\
&\left[\begin{array}{c|c}
\begin{array}{c}\Theta \otimes \mathcal{A}X_{\mathfrak{c}} \\ +\left(\Theta \otimes \mathcal{A}X_{\mathfrak{c}}\right)^T \\ +\left(I_2 \otimes \mathcal{B}_p\right) W_{\mathfrak{c}} \left(I_2 \otimes \mathcal{B}_p\right)^T\end{array} & \begin{array}{c}\left(\Theta \otimes \mathcal{C}_q X_{\mathfrak{c}}\right)^T \\ +\left(I_2 \otimes \mathcal{B}_p\right) W_{\mathfrak{c}} \left(I_2 \otimes \mathcal{D}_{qp}\right)^T\end{array} \\
\hline
\star & \begin{array}{c}-W_{\mathfrak{c}} \\ +\left(I_2 \otimes \mathcal{D}_{qp}\right) W_{\mathfrak{c}} \left(I_2 \otimes \mathcal{D}_{qp}\right)^T\end{array}
\end{array}\right] < 0 \\
&W_{\mathfrak{c}} = \left[\begin{array}{cc} W_{\mathfrak{c},1} & 0 \\ 0 & W_{\mathfrak{c},2}\end{array}\right], \; \{W_{\mathfrak{c},1}, W_{\mathfrak{c},2}\} \subset \mathfrak{C}, \; X_{\mathfrak{c}} > 0, \; \gamma \in \mathbb{R}^1
\end{aligned} \tag{3.88}$$

where $\mathfrak{c}$ is *not* included as a variable due to its multiplication with variable $X_{\mathfrak{c}}$, γ is included as an auxiliary scalar variable and additional LMIs are included with $\mathcal{L}_{\mathfrak{c}}$ to account for the objective, discussed in Section 3.9.

3.7.4 Performance in the presence of saturation

The only LMI approach to performance in the presence of saturation found in the literature describes saturation with non-linear uncertainty for a specified system state domain, similar to that of local stability in Section 3.6.2. The approach is used to formally support the problem discussed in Section 1.4, on the difficulty of including saturation when Gaussian distributed disturbances are involved. A probability index is presented that measures the probability of whether the norm-bounded uncertainty is a valid description of the saturation.

Refer to Section 3.6.2. The approach of Boyd and Hindi [11] to stability analysis in the presence of saturation is also applied to performance analysis. The *reachable sets with unit-energy inputs* property [13, pp.77-79] is used to ensure that $|q_i| < r_i$ when the model is subject to disturbance $\mathbf{w}$ with $\mathcal{L}_2$-norm bound

$$\|\mathbf{w}\|_{\mathcal{L}_2}^2 = \lim_{T\to\infty} \int_0^T \mathbf{w}^T(t)\,\mathbf{w}(t)\,dt < 1 \tag{3.89}$$

whilst minimising the $\mathcal{L}_2$-gain performance measure

$$\sup_{\|\mathbf{w}\|_{\mathcal{L}_2}\neq 0} \frac{\|\mathbf{z}\|_{\mathcal{L}_2}}{\|\mathbf{w}\|_{\mathcal{L}_2}} \tag{3.90}$$

where $\mathbf{z} \in \mathbb{R}^{n_z \times 1}$ is the system *performance output*.

$|q_i| < r_i$ cannot, however, be ensured for linearly controlled NLTV stochastic models subject to Gaussian white noise, due to the unbounded nature of the Gaussian

distribution. Probabilistic measures have to be used to characterise the *risk* of exceedance $(1 - \mathbb{P}\{|q_i| < r_i,\ i = 1, 2, \ldots, n_p\})$, rather than hard bounds. To this end, performance guarantees for the localisation of (3.40) involving $\lim_{t\to\infty}$ become invalid, due to the inevitability of $|q_i| > r_i$, while the remaining performance guarantees apply to (3.40) until the critical time t_c when one or more of the saturation inputs exceeds its allowed level r_i, after which nothing can be said about the performance of (3.40). Thus, the prolonging of t_c becomes of prime importance, which is indirectly achieved by minimising $(1 - \mathbb{P}\{|q_i| < r_i,\ i = 1, 2, \ldots, n_p\})$.

3.8 Controller synthesis

The controller structure considered for synthesis is *LTI output-feedback*. The LMI performance measures developed in the previous section are augmented by introducing the controller as a variable in the closed-loop system matrices, and applying necessary substitutions, transformations, theorems and Lyapunov's paradigm to remove the resulting non-linearity.

LMI global stability condition (3.39) is omitted for synthesis, due to its equivalence to (3.86) when $\alpha = 0$. Furthermore, only the approach to LMI local stability condition (3.48) is considered useful for our application, and is thus also omitted for synthesis, although it admits the same linear form as the LMI performance measures do when augmented for synthesis.

The open-loop form of norm-bounded state-space model (3.23) is used to introduce the controller variable, and is given as

$$\begin{bmatrix} \dot{\mathbf{x}} \\ \mathbf{z} \\ \mathbf{y} \\ \mathbf{q} \end{bmatrix} = G \begin{bmatrix} \mathbf{x} \\ \mathbf{w} \\ \mathbf{u} \\ \mathbf{p} \end{bmatrix} = \begin{bmatrix} A & B_w & B_u & B_p \\ C_z & D_{zw} & D_{zu} & D_{zp} \\ C_y & D_{yw} & D_{yu} & D_{yp} \\ C_q & D_{qw} & D_{qu} & D_{qp} \end{bmatrix} \begin{bmatrix} \mathbf{x} \\ \mathbf{w} \\ \mathbf{u} \\ \mathbf{p} \end{bmatrix} \tag{3.91}$$
$$\mathbf{p} = \Delta\mathbf{q}, \quad \Delta \in \mathbf{\Delta}$$

where $\mathbf{u} \in \mathbb{R}^{n_u \times 1}$ is the *control input* and $\mathbf{y} \in \mathbb{R}^{n_y \times 1}$ the *measurement output*. The block diagram of (3.91) is given for reference as Figure 3.5.

Given the open-loop form (3.91), where the control input satisfies the static output-feedback structure

$$\mathbf{u} = F\mathbf{y} \tag{3.92}$$

the unknown output-feedback gain F is introduced in closed-loop form (3.23) as

$$\begin{bmatrix} \dot{\mathbf{x}} \\ \mathbf{z} \\ \mathbf{q} \end{bmatrix} = \begin{bmatrix} A + B_u F_a C_y & B_w + B_u F_a D_{yw} & B_p + B_u F_a D_{yp} \\ C_z + D_{zu} F_a C_y & D_{zw} + D_{zu} F_a D_{yw} & D_{zp} + D_{zu} F_a D_{yp} \\ C_q + D_{qu} F_a C_y & D_{qw} + D_{qu} F_a D_{yw} & D_{qp} + D_{qu} F_a D_{yp} \end{bmatrix} \begin{bmatrix} \mathbf{x} \\ \mathbf{w} \\ \mathbf{p} \end{bmatrix} \tag{3.93}$$
$$\mathbf{p} = \Delta\mathbf{q}, \quad \Delta \in \mathbf{\Delta}, \quad F_a \coloneqq (I - FD_{yu})^{-1} F$$

The following theorem provides a means to remove non-linearity from a matrix inequality.

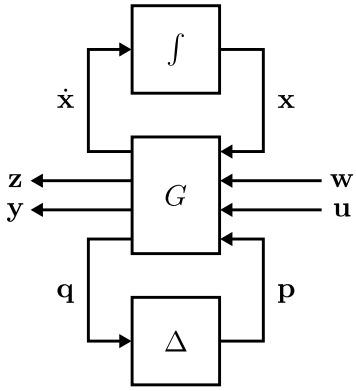

Figure 3.5: Open-loop norm-bounded state-space model block diagram.

Theorem 4. *[79] (Schur's complement) Given matrix* $S \in \mathbb{R}^{n\times m}$ *and symmetric matrices* $Q = Q^T \in \mathbb{R}^{n\times n}$ *and* $R = R^T \in \mathbb{R}^{m\times m}$ *, then*

$$\left(Q + SR^{-1}S^T < 0,\ R > 0\right) \iff \left(\begin{bmatrix} Q & S \\ S^T & -R \end{bmatrix} < 0\right) \tag{3.94}$$

Proof: See [79].

Given LMI robust IOC condition (3.62), substituting (Q, S, R) in Theorem 4 with

$$\left(\begin{bmatrix} \mathcal{A}\overline{Q}_x + \overline{Q}_x\mathcal{A}^T & \overline{Q}_x\mathcal{C}_q^T \\ \mathcal{C}_q\overline{Q}_x & -W_Q \end{bmatrix}, \begin{bmatrix} \mathcal{B}_pW_Q & \mathcal{B}_w \\ \mathcal{D}_{qp}W_Q & \mathcal{D}_{qw} \end{bmatrix}, \begin{bmatrix} W_Q & 0 \\ 0 & I \end{bmatrix}\right) \tag{3.95}$$

and

$$\left(\begin{bmatrix} -\overline{Q}_z & 0 \\ 0 & -W_C \end{bmatrix}, \begin{bmatrix} \mathcal{C}_z\overline{Q}_x & \mathcal{D}_{zp}W_C \\ \mathcal{C}_q\overline{Q}_x & \mathcal{D}_{qp}W_C \end{bmatrix}, \begin{bmatrix} \overline{Q}_x & 0 \\ 0 & W_C \end{bmatrix}\right) \tag{3.96}$$

and introducing the static output-feedback controller as a variable, as described by

the pair (3.23) and (3.93), we obtain

$$
\begin{aligned}
&\text{minimise} \quad \gamma \\
&\text{subject to} \quad \mathcal{L}_C\left(\gamma, \overline{Q}_z, \overline{Q}_x, W_Q, W_C\right) \\
&\left[\begin{array}{c|c|c|c}
\begin{array}{c} A\overline{Q}_x + \\ B_u F_a C_y \overline{Q}_x + \\ \overline{Q}_x A^T + \\ \overline{Q}_x \left(B_u F_a C_y\right)^T \end{array} & \begin{array}{c} \overline{Q}_x C_q^T + \\ \overline{Q}_x \left(D_{qu} F_a C_y\right)^T \end{array} & \begin{array}{c} B_p W_Q + \\ B_u F_a D_{yp} W_Q \end{array} & \begin{array}{c} B_w + \\ B_u F_a D_{yw} \end{array} \\
\hline
\star & -W_Q & \begin{array}{c} D_{qp} W_Q + \\ D_{qu} F_a D_{yp} W_Q \end{array} & \begin{array}{c} D_{qw} + \\ D_{qu} F_a D_{yw} \end{array} \\
\hline
\star & \star & -W_Q & 0 \\
\hline
\star & \star & \star & -I
\end{array}\right] < 0 \\
&\left[\begin{array}{c|c|c|c}
-\overline{Q}_z & 0 & \left(C_z + D_{zu} F_a C_y\right) \overline{Q}_x & \left(D_{zp} + D_{zu} F_a D_{yp}\right) W_C \\
\hline
\star & -W_C & \left(C_q + D_{qu} F_a C_y\right) \overline{Q}_x & \left(D_{qp} + D_{qu} F_a D_{yp}\right) W_C \\
\hline
\star & \star & -\overline{Q}_x & 0 \\
\hline
\star & \star & \star & -W_C
\end{array}\right] < 0 \\
&\{W_Q, W_C\} \subset \mathfrak{C},\ \overline{Q}_x > 0,\ \overline{Q}_z > 0,\ \gamma \in \mathbb{R}^1,\ F_a \in \mathbb{R}^{n_u \times n_y}
\end{aligned}
\tag{3.97}
$$

where the output-feedback controller is calculated post-synthesis as

$$F = F_a \left(I + D_{yu} F_a\right)^{-1} \tag{3.98}$$

although, the existence of $\left(I + D_{yu} F_a\right)^{-1}$ is not inherent in (3.97).

Schur's complement, given as Theorem 4, suffices to remove the quadratic terms involving two variables, which result from the introduction of controller variable F_a in (3.62), according to the pair (3.23) and (3.93), *e.g.* $\left(B_u F_a D_{yp}\right) W_Q \left(B_u F_a D_{yp}\right)^T$ where F_a and W_Q are the matrix variables, although bilinear terms remain, *e.g.* $B_u F_a C_y \overline{Q}_x$ is bilinear in the matrix variables F_a and $\overline{Q}_x$. The substitution

$$Y_C \coloneqq F_a C_y \overline{Q}_x \tag{3.99}$$

similar to (3.19), is generally not useful, because C_y is column-rank deficient in most control applications, in which case F_a cannot be obtained post-synthesis from Y_C, C_y and $\overline{Q}_x$. Similarly, Bilinear Matrix Inequalities (BMIs) also result when applying Schur's complement and introducing the static output-feedback gain as a variable in LMI performance measures (3.72), (3.86) and (3.87).

The LTI dynamic output-feedback case

$$\begin{bmatrix} \dot{\mathbf{x}}_f \\ \mathbf{u} \end{bmatrix} = \grave{F} \begin{bmatrix} \mathbf{x}_f \\ \mathbf{y} \end{bmatrix} = \begin{bmatrix} A_f & B_f \\ C_f & D_f \end{bmatrix} \begin{bmatrix} \mathbf{x}_f \\ \mathbf{y} \end{bmatrix} \tag{3.100}$$

where $\mathbf{x}_f \in \mathbb{R}^{n_{x_f} \times 1}$ is the *controller state*, also pertains to the form of (3.93) when system matrices are augmented as [31]

$$\begin{gathered}
\acute{A} = \begin{bmatrix} A & 0 \\ 0 & 0 \end{bmatrix}, \quad \acute{B}_u = \begin{bmatrix} 0 & B_u \\ I & 0 \end{bmatrix}, \quad \acute{C}_y = \begin{bmatrix} 0 & I \\ C_y & 0 \end{bmatrix}, \quad \acute{B}_p = \begin{bmatrix} B_p \\ 0 \end{bmatrix} \\
\acute{D}_{yp} = \begin{bmatrix} 0 \\ D_{yp} \end{bmatrix}, \quad \acute{B}_w = \begin{bmatrix} B_w \\ 0 \end{bmatrix}, \quad \acute{D}_{yw} = \begin{bmatrix} 0 \\ D_{yw} \end{bmatrix}, \quad \acute{C}_q = \begin{bmatrix} C_q & 0 \end{bmatrix} \\
\acute{D}_{qu} = \begin{bmatrix} 0 & D_{qu} \end{bmatrix}, \quad \acute{D}_{qp} = D_{qp}, \quad \acute{D}_{qw} = D_{qw} \\
\acute{C}_z = \begin{bmatrix} C_z & 0 \end{bmatrix}, \quad \acute{D}_{zu} = \begin{bmatrix} 0 & D_{zu} \end{bmatrix}, \quad \acute{D}_{zp} = D_{zp} \\
\acute{D}_{zw} = D_{zw}, \quad \acute{F}_a = \begin{bmatrix} A_f & 0 \\ 0 & 0 \end{bmatrix} + \begin{bmatrix} B_f & 0 \\ 0 & I \end{bmatrix} \begin{bmatrix} I & D_{yu} \\ D_f & I \end{bmatrix}^{-1} \begin{bmatrix} 0 & I \\ C_f & 0 \end{bmatrix}
\end{gathered} \tag{3.101}$$

Thus, LTI dynamic output-feedback also pertains to the bilinearity of static output-feedback synthesis.

Matrix inequality formulations of the output-feedback synthesis problem are generally *not linear*, and are known to result in either BMIs [30, Ch.14], or LMIs with a non-convex rank constraint [30, Ch.12-13], neither solvable via LMI optimisation nor any other known computationally efficient algorithm. [11] Many techniques have been proposed to deal with the bilinearity or the rank constraint using LMIs [20, 41, 29, 31, 30, 34, 59], but are only sub-optimal with no guarantee of convergence.

The only found linear formulation of the output-feedback synthesis problem is based on the separation principle, where the controller is built by combining the solutions of two separate problems, a state-feedback problem and an output estimation problem, both solvable via LMI optimisation. Two well-known examples of this approach are the LQG controller and the $\mathcal{H}_\infty$ output-feedback controller [30, Ch.8]. Thus, the LTI output-feedback structure considered for synthesis is limited to estimator-based state-feedback, in particular *predictor estimator-based state-feedback*, of which the block diagram is given in Figure 3.6.

3.8.1 State-feedback

Given the open-loop form (3.91), where $\mathbf{u} \in \mathbb{R}^{n_u \times 1}$ is the control input which satisfies the state-feedback structure

$$\mathbf{u} = K\mathbf{x} \tag{3.102}$$

the unknown state-feedback gain K is introduced in closed-loop system (3.23) as

$$\begin{gathered}
\begin{bmatrix} \dot{\mathbf{x}} \\ \mathbf{z} \\ \mathbf{q} \end{bmatrix} = \begin{bmatrix} A + B_u K & B_w & B_p \\ C_z + D_{zu} K & D_{zw} & D_{zp} \\ C_q + D_{qu} K & D_{qw} & D_{qp} \end{bmatrix} \begin{bmatrix} \mathbf{x} \\ \mathbf{w} \\ \mathbf{p} \end{bmatrix} \\
\mathbf{p} = \Delta \mathbf{q}, \quad \Delta \in \mathbf{\Delta}
\end{gathered} \tag{3.103}$$

11. Computationally inefficient algorithms refer to algorithms which find solutions in non-polynomial (NP) time.

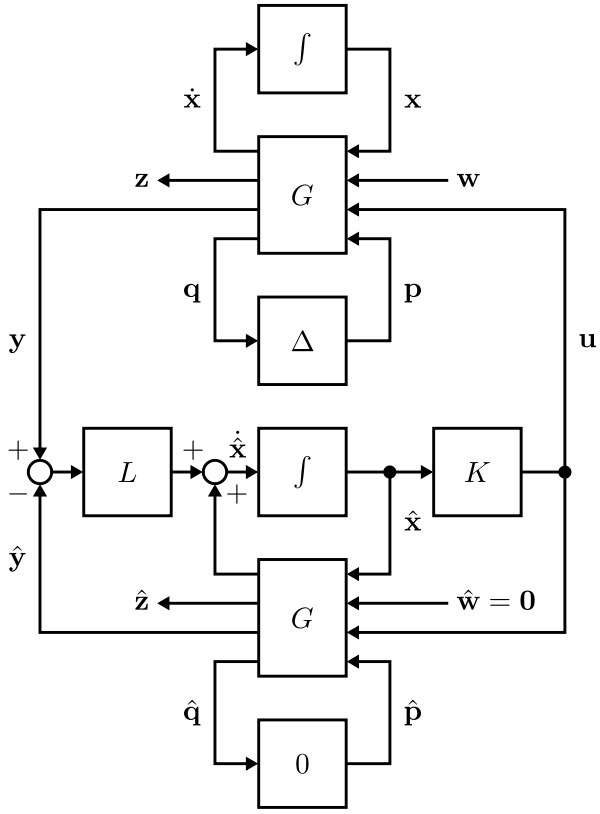

Figure 3.6: Predictor estimator-based state-feedback structure block diagram.

Given robust IOC LMI performance measure (3.62), substituting (Q, S, R) in Theorem 4 with

$$\left(\begin{bmatrix} \mathcal{A}\overline{Q}_x + \overline{Q}_x\mathcal{A}^T & \overline{Q}_x\mathcal{C}_q^T \\ \mathcal{C}_q\overline{Q}_x & -W_Q \end{bmatrix}, \begin{bmatrix} \mathcal{B}_pW_Q & \mathcal{B}_w \\ \mathcal{D}_{qp}W_Q & \mathcal{D}_{qw} \end{bmatrix}, \begin{bmatrix} W_Q & 0 \\ 0 & I \end{bmatrix} \right) \tag{3.104}$$

and

$$\left(\begin{bmatrix} -\overline{Q}_z & 0 \\ 0 & -W_C \end{bmatrix}, \begin{bmatrix} \mathcal{C}_z\overline{Q}_x & \mathcal{D}_{zp}W_C \\ \mathcal{C}_q\overline{Q}_x & \mathcal{D}_{qp}W_C \end{bmatrix}, \begin{bmatrix} \overline{Q}_x & 0 \\ 0 & W_C \end{bmatrix} \right) \tag{3.105}$$

respectively, followed by the introduction of the state-feedback gain as a variable according to (3.23) and (3.103), followed by the substitution

$$Y_C \coloneqq K\overline{Q}_x \tag{3.106}$$

we obtain the equivalent of (3.62) in terms of state-feedback synthesis LMI optimi-

sation problem

$$\begin{aligned} \text{minimise} \quad & \gamma \\ \text{subject to} \quad & \mathcal{L}_C\left(\gamma, \overline{Q}_z, \overline{Q}_x, W_Q, W_C, Y_C\right) \\ & \left[\begin{array}{c|c|c|c} A\overline{Q}_x + B_u Y_C + \left(A\overline{Q}_x + B_u Y_C\right)^T & \left(C_q\overline{Q}_x + D_{qu}Y_C\right)^T & B_p W_Q & B_w \\ \hline \star & -W_Q & D_{qp}W_Q & D_{qw} \\ \hline \star & \star & -W_Q & 0 \\ \hline \star & \star & \star & -I \end{array}\right] < 0 \\ & \left[\begin{array}{c|c|c|c} -\overline{Q}_z & 0 & \left(C_z\overline{Q}_x + D_{zu}Y_C\right) & D_{zp}W_C \\ \hline \star & -W_C & \left(C_q\overline{Q}_x + D_{qu}Y_C\right) & D_{qp}W_C \\ \hline \star & \star & -\overline{Q}_x & 0 \\ \hline \star & \star & \star & -W_C \end{array}\right] < 0 \\ & \{W_Q, W_C\} \subset \mathfrak{C},\ \overline{Q}_x > 0,\ \overline{Q}_z > 0,\ \gamma \in \mathbb{R}^1,\ Y_C \in \mathbb{R}^{n_u \times n_x} \end{aligned} \tag{3.107}$$

where Y_C is included in $\mathcal{L}_C$ for generality.

As mentioned at the start of Section 3.7, robust AOV LMI performance measure (3.72) does not admit to linear form for state-feedback synthesis.

Given robust maximum-real eigenvalue region LMI performance measure (3.86), substituting (Q, S, R) in Theorem 4 with

$$\left(\left[\begin{array}{cc} \left(\mathcal{A}X_{\mathfrak{a}} + X_{\mathfrak{a}}\mathcal{A}^T + 2\mathfrak{a}_K X_{\mathfrak{a}}\right) & X_{\mathfrak{a}}\mathcal{C}_q^T \\ \mathcal{C}_q X_{\mathfrak{a}} & -W_{\mathfrak{a}} \end{array}\right], \left[\begin{array}{c} \mathcal{B}_p W_{\mathfrak{a}} \\ \mathcal{D}_{qp} W_{\mathfrak{a}} \end{array}\right], W_{\mathfrak{a}}\right) \tag{3.108}$$

where $\mathfrak{a}_K$ is the minimum exponential decay rate of the closed-loop model with state-feedback control, followed by the introduction of the state-feedback gain as a variable according to (3.23) and (3.103), followed by the substitution

$$Y_{\mathfrak{a}} \coloneqq K X_{\mathfrak{a}} \tag{3.109}$$

we obtain the equivalent of (3.86) in terms of state-feedback synthesis LMI optimisation problem

$$\begin{aligned} \text{minimise} \quad & \gamma \\ \text{subject to} \quad & \mathcal{L}_{\mathfrak{a}}\left(\gamma, X_{\mathfrak{a}}, W_{\mathfrak{a}}, Y_{\mathfrak{a}}\right) \\ & \left[\begin{array}{c|c|c} AX_{\mathfrak{a}} + B_u Y_{\mathfrak{a}} + X_{\mathfrak{a}}A^T + Y_{\mathfrak{a}}^T B_u^T + 2\mathfrak{a}_K X_{\mathfrak{a}} & X_{\mathfrak{a}}C_q^T + Y_{\mathfrak{a}}^T D_{qu}^T & B_p W_{\mathfrak{a}} \\ \hline \star & -W_{\mathfrak{a}} & D_{qp}W_{\mathfrak{a}} \\ \hline \star & \star & -W_{\mathfrak{a}} \end{array}\right] < 0 \\ & W_{\mathfrak{a}} \in \mathfrak{C},\ X_{\mathfrak{a}} > 0,\ \gamma \in \mathbb{R}^1,\ Y_{\mathfrak{a}} \in \mathbb{R}^{n_u \times n_x} \end{aligned} \tag{3.110}$$

where $\mathfrak{a}_K$ is not included as a variable due to its multiplication with matrix variable $X_\mathfrak{a}$.

Given robust disk eigenvalue region LMI performance measure (3.87), substituting (Q, S, R) in Theorem 4 with

$$\left(\left[\begin{array}{c|c} \begin{array}{c}(-\mathfrak{r}_K^2+\mathfrak{q}_K^2)\,X_\mathfrak{r}\\ +\mathfrak{q}_K\mathcal{A}X_\mathfrak{r}\\ +\mathfrak{q}_K X_\mathfrak{r}\mathcal{A}^T\end{array} & \mathfrak{q}_K X_\mathfrak{r}\mathcal{C}_q^T \\ \hline \mathfrak{q}_K\mathcal{C}_q X_\mathfrak{r} & -W_\mathfrak{r}\end{array}\right], \left[\begin{array}{cc}\mathcal{A}X_\mathfrak{r} & \mathcal{B}_p W_\mathfrak{r}\\ \mathcal{C}_q X_\mathfrak{r} & \mathcal{D}_{qp}W_\mathfrak{r}\end{array}\right], \left[\begin{array}{cc}X_\mathfrak{r} & 0\\ 0 & W_\mathfrak{r}\end{array}\right]\right) \tag{3.111}$$

where $\mathfrak{r}_K$ and $\mathfrak{q}_K$ describe the robust disk eigenvalue region of the closed-loop model with state-feedback control, followed by the introduction of the state-feedback gain as a variable according to (3.23) and (3.103), followed by the substitution

$$Y_\mathfrak{r} \coloneqq KX_\mathfrak{r} \tag{3.112}$$

we obtain the equivalent of (3.87) in terms of state-feedback synthesis LMI optimisation problem

$$\begin{array}{ll}\text{minimise} & \gamma\\ \text{subject to} & \mathcal{L}_\mathfrak{r}(\gamma, X_\mathfrak{r}, W_\mathfrak{r}, Y_\mathfrak{r})\end{array}$$

$$\left[\begin{array}{c|c|c|c} \begin{array}{c}(-\mathfrak{r}_K^2+\mathfrak{q}_K^2)\,X_\mathfrak{r}\\ +\mathfrak{q}_K(AX_\mathfrak{r}+B_uY_\mathfrak{r})\\ +\mathfrak{q}_K(AX_\mathfrak{r}+B_uY_\mathfrak{r})^T\end{array} & \mathfrak{q}_K\begin{pmatrix}C_qX_\mathfrak{r}+\\ D_{qu}Y_\mathfrak{r}\end{pmatrix}^T & AX_\mathfrak{r}+B_uY_\mathfrak{r} & B_pW_\mathfrak{r}\\ \hline \star & -W_\mathfrak{r} & C_qX_\mathfrak{r}+D_{qu}Y_\mathfrak{r} & D_{qp}W_\mathfrak{r}\\ \hline \star & \star & -X_\mathfrak{r} & 0\\ \hline \star & \star & \star & -W_\mathfrak{r}\end{array}\right] < 0$$

$$W_\mathfrak{r}\in\mathfrak{C},\ X_\mathfrak{r}>0,\ \gamma\in\mathbb{R}^1,\ Y_\mathfrak{r}\in\mathbb{R}^{n_u\times n_x} \tag{3.113}$$

where $\mathfrak{r}_K$ and $\mathfrak{q}_K$ are not included as variables due to their multiplication with matrix variables $X_\mathfrak{r}$ and $Y_\mathfrak{r}$.

Given robust cone eigenvalue region LMI performance measure (3.88), substituting (Q, S, R) in Theorem 4 with

$$\left(\left[\begin{array}{c|c} \begin{array}{c}\Theta_K\otimes\mathcal{A}X_\mathfrak{c}\\ +(\Theta_K\otimes\mathcal{A}X_\mathfrak{c})^T\end{array} & (\Theta_K\otimes\mathcal{C}_qX_\mathfrak{c})^T\\ \hline \Theta_K\otimes\mathcal{C}_qX_\mathfrak{c} & -W_\mathfrak{c}\end{array}\right], \left[\begin{array}{c}(I_2\otimes\mathcal{B}_p)\,W_\mathfrak{c}\\ (I_2\otimes\mathcal{D}_{qp})\,W_\mathfrak{c}\end{array}\right], W_\mathfrak{c}\right) \tag{3.114}$$

where

$$\Theta_K \coloneqq \begin{bmatrix}\sin(\mathfrak{c}_K) & \cos(\mathfrak{c}_K)\\ -\cos(\mathfrak{c}_K) & \sin(\mathfrak{c}_K)\end{bmatrix} \tag{3.115}$$

and $\mathfrak{c}_K$ describe the robust cone eigenvalue region of the closed-loop model with state-feedback control, followed by the introduction of the state-feedback gain as a variable according to (3.23) and (3.103), followed by the substitution

$$Y_{\mathfrak{c}} \coloneqq K X_{\mathfrak{c}} \tag{3.116}$$

we obtain the equivalent of (3.88) in terms of state-feedback synthesis LMI optimisation problem

$$\begin{aligned}
&\text{minimise} && \gamma \\
&\text{subject to} && \mathcal{L}_{\mathfrak{c}}\left(\gamma, X_{\mathfrak{c}}, W_{\mathfrak{c}}\right) \\
& && \left[\begin{array}{c|c|c}
\begin{array}{c}\Theta_K \otimes A X_{\mathfrak{c}} \\ +\Theta_K \otimes B_u Y_{\mathfrak{c}} \\ +\left(\Theta_K \otimes A X_{\mathfrak{c}}\right)^T \\ +\left(\Theta_K \otimes B_u Y_{\mathfrak{c}}\right)^T\end{array} & \begin{array}{c}\\ \left(\Theta_K \otimes C_q X_{\mathfrak{c}}\right)^T \\ +\left(\Theta_K \otimes D_{qu} Y_{\mathfrak{c}}\right)^T\end{array} & \left(I_2 \otimes B_p\right) W_{\mathfrak{c}} \\
\hline
\star & -W_{\mathfrak{c}} & \left(I_2 \otimes D_{qp}\right) W_{\mathfrak{c}} \\
\hline
\star & \star & -W_{\mathfrak{c}}
\end{array}\right] < 0 \\
& && W_{\mathfrak{c}} \coloneqq \begin{bmatrix} W_{\mathfrak{c},1} & 0 \\ 0 & W_{\mathfrak{c},2} \end{bmatrix}, \; \{W_{\mathfrak{c},1}, W_{\mathfrak{c},2}\} \subset \mathfrak{C}, \\
& && X_{\mathfrak{c}} > 0, \; \gamma \in \mathbb{R}^1, \; Y_{\mathfrak{c}} \in \mathbb{R}^{n_u \times n_x}
\end{aligned} \tag{3.117}$$

where $\mathfrak{c}_K$ is not included as a variable due to its multiplication with matrix variables $X_{\mathfrak{c}}$ and $Y_{\mathfrak{c}}$.

State-feedback synthesis LMI optimisation problems (3.107), (3.110), (3.113) and (3.117) may be combined by applying *Lyapunov Shaping Paradigm* [67]

$$Q_K \coloneqq \overline{Q}_x = X_{\mathfrak{a}} = X_{\mathfrak{r}} = X_{\mathfrak{c}},\ Y_K \coloneqq Y_C = Y_{\mathfrak{a}} = Y_{\mathfrak{r}} = Y_{\mathfrak{c}} \tag{3.118}$$

which is a sufficient condition for K to be equal in all three LMI formulations.

We conclude the state-feedback synthesis by comparing state-feedback to state- and state-derivative-feedback in the norm-bounded state-space framework. The latter is formulated as

$$\mathbf{u} = K_P\mathbf{x} + K_D\dot{\mathbf{x}} \tag{3.119}$$

Given open-loop form (3.91), state- and state-derivative-feedback gains are introduced as variables in closed-loop form (3.23) as

$$\begin{bmatrix} \dot{\mathbf{x}} \\ \mathbf{z} \\ \mathbf{q} \end{bmatrix} = \begin{bmatrix} A + B_u\left(I - K_DB_u\right)^{-1}\left(K_P + K_DA\right) & B_w + B_u\left(I - K_DB_u\right)^{-1}K_DB_w & B_p + B_u\left(I - K_DB_u\right)^{-1}K_DB_p \\ C_z + D_{zu}\left(I - K_DB_u\right)^{-1}\left(K_P + K_DA\right) & D_{zw} + D_{zu}\left(I - K_DB_u\right)^{-1}K_DB_w & D_{zp} + D_{zu}\left(I - K_DB_u\right)^{-1}K_DB_p \\ C_q + D_{qu}\left(I - K_DB_u\right)^{-1}\left(K_P + K_DA\right) & D_{qw} + D_{qu}\left(I - K_DB_u\right)^{-1}K_DB_w & D_{qp} + D_{qu}\left(I - K_DB_u\right)^{-1}K_DB_p \end{bmatrix} \begin{bmatrix} \mathbf{x} \\ \mathbf{w} \\ \mathbf{p} \end{bmatrix} \tag{3.120}$$

$$\mathbf{p} = \Delta\mathbf{q}, \quad \Delta \in \boldsymbol{\Delta}$$

Excluding the state-derivative from feedback does not limit system closed-loop performance for LTI models, as $K_D\dot{\mathbf{x}}$ may exactly be reconstructed from the state and control input, where it is assumed that $K_DB_w = 0$, *i.e.* $\mathbf{u}$ is finite. When variation/uncertainty is introduced, however, the set of reachable closed-loop models is larger when K_D is included, as variation measured in $\dot{\mathbf{x}}$ as $\mathcal{B}_p\mathbf{p}$ is available for feedback, and we conclude that, unlike the LTI case, (3.119) is superior to state-feedback.

3.8.2 Estimator

The full-order predictor estimator illustrated in Figure 3.6 is given as

$$\begin{bmatrix} \dot{\widehat{\mathbf{x}}} \\ \widehat{\mathbf{y}} \end{bmatrix} = \begin{bmatrix} A & B_u \\ C_y & D_{yu} \end{bmatrix} \begin{bmatrix} \widehat{\mathbf{x}} \\ \mathbf{u} \end{bmatrix} + \begin{bmatrix} L \\ 0 \end{bmatrix} (\widehat{\mathbf{y}} - \mathbf{y}) \tag{3.121}$$

where a hat is used to denote estimator variables and $\mathbf{u}$ is exactly known.[12] (3.121) is a duplicate of the open-loop model (3.91) with zeroed disturbance input $\widehat{\mathbf{w}} = \mathbf{0}$, zeroed uncertainty $\widehat{\Delta} = 0$ and an additional feedback term $\begin{bmatrix} L^T & 0 \end{bmatrix}^T (\widehat{\mathbf{y}} - \mathbf{y})$, which uses the error in estimated output $(\widehat{\mathbf{y}} - \mathbf{y})$ to achieve convergence in estimator state error $\widehat{\mathbf{x}} - \mathbf{x}$, *i.e.* stability, as well as other estimator properties. Now, the state-feedback controller (3.102) may be transformed into an output-feedback controller by replacing the model state $\mathbf{x}$ in (3.102) with estimator state $\widehat{\mathbf{x}}$, *i.e.*

$$\mathbf{u} = K\widehat{\mathbf{x}} \tag{3.122}$$

The estimator properties we are concerned with are those of the estimation state error, also known as the estimator state perturbation,[13] defined as

$$\widetilde{\mathbf{x}} \coloneqq \widehat{\mathbf{x}} - \mathbf{x} \tag{3.123}$$

Estimator state error mechanics is derived with (3.91) and (3.121)-(3.123) as follows.

$$\begin{aligned} \dot{\widetilde{\mathbf{x}}} &= \dot{\widehat{\mathbf{x}}} - \dot{\mathbf{x}} \\ &= A\widehat{\mathbf{x}} + B_u\mathbf{u} + L\left((C_y\widehat{\mathbf{x}} + D_{yu}\mathbf{u}) - (C_y\mathbf{x} + D_{yw}\mathbf{w} + D_{yu}\mathbf{u} + D_{yp}\mathbf{p})\right) - \\ &\quad (A\mathbf{x} + B_w\mathbf{w} + B_u\mathbf{u} + B_p\mathbf{p}) \\ &= (A + LC_y)\,\widetilde{\mathbf{x}} - (B_w + LD_{yw})\,\mathbf{w} - (B_p + LD_{yp})\,\mathbf{p} \end{aligned} \tag{3.124}$$

where

$$\mathbf{p} = \Delta\mathbf{q} \tag{3.125}$$

and

$$\begin{aligned} \mathbf{q} &= C_q\mathbf{x} + D_{qw}\mathbf{w} + D_{qu}\mathbf{u} + D_{qp}\mathbf{p} \\ &= C_q\mathbf{x} + D_{qw}\mathbf{w} + D_{qu}K\widehat{\mathbf{x}} + D_{qp}\mathbf{p} \\ &= C_q\mathbf{x} + D_{qw}\mathbf{w} + D_{qu}K\left(\widetilde{\mathbf{x}} + \mathbf{x}\right) + D_{qp}\mathbf{p} \\ &= D_{qu}K\widetilde{\mathbf{x}} + \begin{bmatrix} D_{qw} & C_q + D_{qu}K \end{bmatrix} \begin{bmatrix} \mathbf{w} \\ \mathbf{x} \end{bmatrix} + D_{qp}\mathbf{p} \end{aligned} \tag{3.126}$$

12. $\mathbf{u}$ is generated by the control law.
13. The estimator state perturbation is defined with Zipfel notation in Appendix A.1.1 as $\widetilde{\mathbf{x}} := \varepsilon\widehat{\mathbf{x}} = \widehat{\mathbf{x}} - \widehat{\mathbf{x}}_r = \widehat{\mathbf{x}} - \mathbf{x}$

It follows that the state-feedback gain K is required for estimator synthesis. (3.124)-(3.126) are combined into the closed-loop estimator form

$$\begin{aligned}\begin{bmatrix}\dot{\widetilde{\mathbf{x}}}\\ \mathbf{v}\\ \mathbf{q}\end{bmatrix} &= \widetilde{\mathcal{G}}\begin{bmatrix}\widetilde{\mathbf{x}}\\ \begin{bmatrix}\mathbf{w}\\ \mathbf{x}\end{bmatrix}\\ \mathbf{p}\end{bmatrix}\\ &= \begin{bmatrix}\widetilde{\mathcal{A}} & \widetilde{\mathcal{B}}_w & \widetilde{\mathcal{B}}_p\\ \widetilde{\mathcal{C}}_z & \widetilde{\mathcal{D}}_{zw} & \widetilde{\mathcal{D}}_{zp}\\ \widetilde{\mathcal{C}}_q & \widetilde{\mathcal{D}}_{qw} & \widetilde{\mathcal{D}}_{qp}\end{bmatrix}\begin{bmatrix}\widetilde{\mathbf{x}}\\ \begin{bmatrix}\mathbf{w}\\ \mathbf{x}\end{bmatrix}\\ \mathbf{p}\end{bmatrix}\\ &= \begin{bmatrix}A+LC_y & \begin{bmatrix}-B_w-LD_{yw} & 0\end{bmatrix} & -B_p-LD_{yp}\\ \widetilde{C}_z & \widetilde{D}_{zw} & \widetilde{D}_{zp}\\ D_{qu}K & \begin{bmatrix}D_{qw} & C_q+D_{qu}K\end{bmatrix} & D_{qp}\end{bmatrix}\begin{bmatrix}\widetilde{\mathbf{x}}\\ \begin{bmatrix}\mathbf{w}\\ \mathbf{x}\end{bmatrix}\\ \mathbf{p}\end{bmatrix}\\ \mathbf{p} &= \Delta\mathbf{q}\end{aligned} \tag{3.127}$$

where $\mathbf{v} \in \mathbb{R}^{n_v \times 1}$ is included as the *estimator performance output* and the disturbance input consists of $\mathbf{w}$ and $\mathbf{x}$. Disturbance component $\mathbf{x}$ is either represented as white noise or omitted, depending on its spectral content. The most general closed-loop estimator that admits linearity for synthesis is given as

$$\begin{bmatrix}\dot{\widetilde{\mathbf{x}}}\\ \mathbf{v}\\ \mathbf{q}\end{bmatrix} = \begin{bmatrix}\widetilde{A}+L\widetilde{C}_y & \widetilde{B}_w+L\widetilde{D}_{yw} & \widetilde{B}_p+L\widetilde{D}_{yp}\\ \widetilde{C}_z & \widetilde{D}_{zw} & \widetilde{D}_{zp}\\ \widetilde{C}_q & \widetilde{D}_{qw} & \widetilde{D}_{qp}\end{bmatrix}\begin{bmatrix}\widetilde{\mathbf{x}}\\ \begin{bmatrix}\mathbf{w}\\ \mathbf{x}\end{bmatrix}\\ \mathbf{p}\end{bmatrix} \tag{3.128}$$

Now, given robust AOV LMI performance measure (3.72), substituting (Q, S, R) in Theorem 4 with

$$\left(\begin{bmatrix}\mathcal{A}^T\overline{P}+\overline{P}\mathcal{A} & \overline{P}\mathcal{B}_p\\ \mathcal{B}_p^T\overline{P} & -W_P\end{bmatrix}, \begin{bmatrix}\mathcal{C}_q^T W_P & \mathcal{C}_z^T\\ \mathcal{D}_{qp}^T W_P & \mathcal{D}_{zp}^T\end{bmatrix}, \begin{bmatrix}W_P & 0\\ 0 & I\end{bmatrix}\right) \tag{3.129}$$

and

$$\left(\begin{bmatrix}-V & 0\\ 0 & -W_V\end{bmatrix}, \begin{bmatrix}\mathcal{B}_w^T\overline{P} & \mathcal{D}_{qw}^T W_V\\ \mathcal{B}_p^T\overline{P} & \mathcal{D}_{qp}^T W_V\end{bmatrix}, \begin{bmatrix}\overline{P} & 0\\ 0 & W_V\end{bmatrix}\right) \tag{3.130}$$

respectively, followed by the introduction of the estimator feedback gain L as a variable according to the pair (3.127) and (3.128), followed by the substitution

$$Z_V \coloneqq \overline{P}L \tag{3.131}$$

we obtain the equivalent of (3.72) in terms of estimator synthesis LMI optimisation problem

$$
\begin{aligned}
\text{minimise} \quad & \gamma \\
\text{subject to} \quad & \mathcal{L}_V\left(\gamma, V, \overline{P}, W_P, W_V, Z_V\right) \\
& \left[\begin{array}{c|c|c|c}
\begin{array}{c}\left(\overline{P}\widetilde{A} + Z_V\widetilde{C}_y\right)^T \\ +\overline{P}\widetilde{A} + Z_V\widetilde{C}_y\end{array} & \overline{P}\widetilde{B}_p + Z_V\widetilde{D}_{yp} & \widetilde{C}_q^T W_P & \widetilde{C}_z^T \\ \hline
\star & -W_P & \widetilde{D}_{qp}^T W_P & \widetilde{D}_{zp}^T \\ \hline
\star & \star & -W_P & 0 \\ \hline
\star & \star & \star & -I
\end{array}\right] < 0 \\
& \left[\begin{array}{c|c|c|c}
-V & 0 & \left(\overline{P}\widetilde{B}_w + Z_V\widetilde{D}_{yw}\right)^T & \widetilde{D}_{qw}^T W_V \\ \hline
\star & -W_V & \left(\overline{P}\widetilde{B}_p + Z_V\widetilde{D}_{yp}\right)^T & \widetilde{D}_{qp}^T W_V \\ \hline
\star & \star & -\overline{P} & 0 \\ \hline
\star & \star & \star & -W_V
\end{array}\right] < 0 \\
& \{W_P, W_V\} \subset \mathfrak{C},\ \overline{P} > 0,\ V > 0,\ \gamma \in \mathbb{R}^1,\ Z_V \in \mathbb{R}^{n_x \times n_y}
\end{aligned}
\tag{3.132}
$$

As mentioned at the start of Section 3.7, robust IOC LMI performance measure (3.62) does not admit to linear form for estimator synthesis.

Given robust maximum-real eigenvalue region LMI performance measure (3.86), substituting (Q, S, R) in Theorem 4 with (3.108), followed by a non-singular congruent transformation with

$$
\begin{bmatrix} P_{\mathfrak{a}} & 0 & 0 \\ 0 & M_{\mathfrak{a}} & 0 \\ 0 & 0 & M_{\mathfrak{a}} \end{bmatrix} := \begin{bmatrix} X_{\mathfrak{a}}^{-1} & 0 & 0 \\ 0 & W_{\mathfrak{a}}^{-1} & 0 \\ 0 & 0 & W_{\mathfrak{a}}^{-1} \end{bmatrix} \tag{3.133}
$$

followed by the introduction of the estimator feedback gain L as a variable, according to the pair (3.127) and (3.128), followed by the substitution

$$
Z_{\mathfrak{a}} := P_{\mathfrak{a}} L \tag{3.134}
$$

we obtain the equivalent of (3.86) in terms of estimator synthesis LMI optimisation problem

$$
\begin{aligned}
\text{minimise} \quad & \gamma \\
\text{subject to} \quad & \mathcal{L}_{\mathfrak{a}}\left(\gamma, P_{\mathfrak{a}}, M_{\mathfrak{a}}, Z_{\mathfrak{a}}\right) \\
& \left[\begin{array}{c|c|c}
\begin{array}{c}\left(P_{\mathfrak{a}}\widetilde{A} + Z_{\mathfrak{a}}\widetilde{C}_y\right) \\ \left(P_{\mathfrak{a}}\widetilde{A} + Z_{\mathfrak{a}}\widetilde{C}_y\right)^T + 2\mathfrak{a}_L P_{\mathfrak{a}}\end{array} & \widetilde{C}_q^T M_{\mathfrak{a}} & P_{\mathfrak{a}}\widetilde{B}_p + Z_{\mathfrak{a}}\widetilde{D}_{yp} \\ \hline
\star & -M_{\mathfrak{a}} & M_{\mathfrak{a}}\widetilde{D}_{qp} \\ \hline
\star & \star & -M_{\mathfrak{a}}
\end{array}\right] < 0 \\
& M_{\mathfrak{a}} \in \mathfrak{C},\ P_{\mathfrak{a}} > 0,\ \gamma \in \mathbb{R}^1,\ Z_{\mathfrak{a}} \in \mathbb{R}^{n_x \times n_y}
\end{aligned}
\tag{3.135}
$$

where $\mathfrak{a}_L$ is the minimum exponential decay rate of the closed-loop estimator and is not included as a variable due to its multiplication with matrix variable $P_{\mathfrak{a}}$.

Given robust disk eigenvalue region LMI performance measure (3.87), substituting (Q, S, R) in Theorem 4 with (3.111), followed by a non-singular congruent transformation with

$$\begin{bmatrix} P_{\mathfrak{r}} & 0 & 0 & 0 \\ 0 & M_{\mathfrak{r}} & 0 & 0 \\ 0 & 0 & P_{\mathfrak{r}} & 0 \\ 0 & 0 & 0 & M_{\mathfrak{r}} \end{bmatrix} \coloneqq \begin{bmatrix} X_{\mathfrak{r}}^{-1} & 0 & 0 & 0 \\ 0 & W_{\mathfrak{r}}^{-1} & 0 & 0 \\ 0 & 0 & X_{\mathfrak{r}}^{-1} & 0 \\ 0 & 0 & 0 & W_{\mathfrak{r}}^{-1} \end{bmatrix} \tag{3.136}$$

followed by the introduction of the estimator feedback gain L as a variable according to the pair (3.127) and (3.128), followed by the substitution

$$Z_{\mathfrak{r}} \coloneqq P_{\mathfrak{r}} L \tag{3.137}$$

we obtain the equivalent of (3.87) in terms of estimator synthesis LMI optimisation problem

$$\begin{aligned} &\text{minimise} \quad \gamma \\ &\text{subject to} \quad \mathcal{L}_{\mathfrak{r}}\left(\gamma, P_{\mathfrak{r}}, M_{\mathfrak{r}}, Z_{\mathfrak{r}}\right) \\ &\left[\begin{array}{c|c|c|c} \begin{array}{c}\left(-\mathfrak{r}_L^2 + \mathfrak{q}_L^2\right) P_{\mathfrak{r}} \\ +\mathfrak{q}_L\left(P_{\mathfrak{r}}\widetilde{A} + Z_{\mathfrak{r}}\widetilde{C}_y\right) \\ +\mathfrak{q}_L\left(P_{\mathfrak{r}}\widetilde{A} + Z_{\mathfrak{r}}\widetilde{C}_y\right)^T\end{array} & \mathfrak{q}_L\widetilde{C}_q^T M_{\mathfrak{r}} & P_{\mathfrak{r}}\widetilde{A} + Z_{\mathfrak{r}}\widetilde{C}_y & P_{\mathfrak{r}}\widetilde{B}_p + Z_{\mathfrak{r}}\widetilde{D}_{yp} \\ \hline \star & -M_{\mathfrak{r}} & M_{\mathfrak{r}}\widetilde{C}_q & M_{\mathfrak{r}}\widetilde{D}_{qp} \\ \hline \star & \star & -P_{\mathfrak{r}} & 0 \\ \hline \star & \star & \star & -M_{\mathfrak{r}} \end{array}\right] < 0 \\ &M_{\mathfrak{r}} \in \mathfrak{C},\ P_{\mathfrak{r}} > 0,\ \gamma \in \mathbb{R}^1,\ Z_{\mathfrak{r}} \in \mathbb{R}^{n_x \times n_y} \end{aligned} \tag{3.138}$$

where $\mathfrak{r}_L$ and $\mathfrak{q}_L$ describe the robust disk eigenvalue region of the closed-loop estimator and are not included as variables due to their multiplication with matrix variables $P_{\mathfrak{r}}$, $M_{\mathfrak{r}}$ and $Z_{\mathfrak{r}}$.

Given robust maximum-real eigenvalue region LMI performance measure (3.86), substituting (Q, S, R) in Theorem 4 with (3.108), followed by a non-singular congruent transformation with

$$\begin{bmatrix} (I_2 \otimes P_{\mathfrak{c}}) & 0 & 0 \\ 0 & M_{\mathfrak{c}} & 0 \\ 0 & 0 & M_{\mathfrak{c}} \end{bmatrix} \coloneqq \begin{bmatrix} (I_2 \otimes X_{\mathfrak{c}}^{-1}) & 0 & 0 \\ 0 & W_{\mathfrak{c}}^{-1} & 0 \\ 0 & 0 & W_{\mathfrak{c}}^{-1} \end{bmatrix} \tag{3.139}$$

followed by the introduction of the estimator feedback gain L as a variable according to the pair (3.127) and (3.128), followed by the substitution

$$Z_{\mathfrak{c}} \coloneqq P_{\mathfrak{c}} L \tag{3.140}$$

we obtain the equivalent of (3.86) in terms of estimator synthesis LMI optimisation problem

$$
\begin{aligned}
\text{minimise} \quad & \gamma \\
\text{subject to} \quad & \mathcal{L}_{\mathfrak{c}}\left(\gamma, X_{\mathfrak{c}}, M_{\mathfrak{c}}\right) \\
& \left[\begin{array}{c|c|c}
\begin{array}{c}\Theta_L \otimes P_{\mathfrak{c}}\widetilde{A} \\ \Theta_L \otimes Z_{\mathfrak{c}}\widetilde{C}_y \\ +\left(\Theta_L \otimes P_{\mathfrak{c}}\widetilde{A}\right)^T \\ +\left(\Theta_L \otimes Z_{\mathfrak{c}}\widetilde{C}_y\right)^T\end{array} & \left(\Theta_L \otimes \widetilde{C}_q\right)^T M_{\mathfrak{c}} & \begin{array}{c} I_2 \otimes P_{\mathfrak{c}}\widetilde{B}_p \\ +I_2 \otimes Z_{\mathfrak{c}}\widetilde{D}_{yp}\end{array} \\
\hline
\star & -M_{\mathfrak{c}} & M_{\mathfrak{c}}\left(I_2 \otimes \widetilde{D}_{qp}\right) \\
\hline
\star & \star & -M_{\mathfrak{c}}
\end{array}\right] < 0 \\
& M_{\mathfrak{c}} \coloneqq \left[\begin{array}{cc} M_{\mathfrak{c},1} & 0 \\ 0 & M_{\mathfrak{c},2}\end{array}\right], \; \{M_{\mathfrak{c},1}, M_{\mathfrak{c},2}\} \subset \mathfrak{C}, \\
& P_{\mathfrak{c}} > 0, \; \gamma \in \mathbb{R}^1, \; Z_{\mathfrak{c}} \in \mathbb{R}^{n_x \times n_y}
\end{aligned} \tag{3.141}
$$

where

$$
\Theta_L \coloneqq \left[\begin{array}{cc} \sin\left(\mathfrak{c}_L\right) & \cos\left(\mathfrak{c}_L\right) \\ -\cos\left(\mathfrak{c}_L\right) & \sin\left(\mathfrak{c}_L\right)\end{array}\right] \tag{3.142}
$$

and $\mathfrak{c}_L$ describe the robust cone eigenvalue region of the closed-loop estimator and is not included as a variable due to its multiplication with matrix variable $P_{\mathfrak{c}}$.

Estimator synthesis LMI optimisation problems (3.132), (3.135) and (3.138) may be combined by applying *Lyapunov Shaping Paradigm* [67]

$$
P_L \coloneqq \overline{P} = P_{\mathfrak{a}} = P_{\mathfrak{r}} = P_{\mathfrak{c}}, \; Z_L \coloneqq Z_V = Z_{\mathfrak{a}} = Z_{\mathfrak{r}} = Z_{\mathfrak{c}} \tag{3.143}
$$

which is a sufficient condition for L to be equal in all three LMI formulations.

3.9 Design specifications and constraints

3.9.1 Multiple robust $\mathcal{H}_2$ bounds

Any LMI variable that serves as an output covariance upper-bound, such as the IOC upper-bound, can be used to include multiple $\mathcal{H}_2$ bounds simply by constraining each of its diagonal elements by the desired amount with a scalar inequality. Such a variable can also be used to include multiple covariance upper-bounds by applying a congruent transformation for each bound and bounding it by the desired amount with a matrix inequality.

Given robust IOC synthesis LMI optimisation problem (3.107), multiple robust IOC bounds may be included with $\mathcal{L}_C$ as

$$
\begin{aligned}
& \left(C_i \overline{Q}_z C_i^T < H_i\right) \\
\implies \quad & \left(\mathbb{E}\left\{C_i \mathbf{z} \left(C_i \mathbf{z}\right)^T\right\} < H_i\right)
\end{aligned} \tag{3.144}
$$

where i denotes the i^{th} constraint, $H_i = H_i^T \in \mathbb{R}^{n_{c_i} \times n_{c_i}}$ is a robust IOC bound and $C_i \in \mathbb{R}^{n_{c_i} \times n_z}$ selects the robust IOC to be bounded. Thus, by appropriately selecting $\mathbf{z}$ and including LMI constraints (3.144) for $i = 1, 2, \ldots$, (3.107) does not have to be duplicated to include a new robust IOC bound, resulting in an efficient method for including multiple robust IOC bounds. More generally, constraints may be included as

$$\left(\sum_j C_{ij} \overline{Q}_z C_{ij}^T < G_i \gamma + H_i \right)$$
$$\implies \quad \left(\sum_j \mathbb{E}\left\{ C_{ij} \mathbf{z} \left(C_{ij} \mathbf{z} \right)^T \right\} < G_i \gamma + H_i \right) \tag{3.145}$$

where i denotes the i^{th} constraint, $H_i = H_i^T \in \mathbb{R}^{n_{c_i} \times n_{c_i}}$ is a constant robust IOC bound, $\gamma \in \mathbb{R}^1$ is a variable scalar, $G_i \gamma = G_i^T \gamma \in \mathbb{R}^{n_{c_i} \times n_{c_i}}$ is a scalable robust IOC bound, $C_{ij} \in \mathbb{R}^{n_{c_i} \times n_z}$ selects a sum of robust IOCs to be bounded. Thus, multiple covariance-sums may be bounded, and scalar γ enables the bounds $G_i \gamma$ $i = 1, 2, \ldots$ to be minimised in proportion, whilst individually bounded by H_i. Each of the covariance-sums also includes as a special case the quadratic cost form of LQR/LQG.

Unfortunately, robust AOV synthesis LMI optimisation problem (3.132) does not allow multiple robust AOV bounds to be included with the above method, and requires duplicates to include new robust AOV bounds.

3.9.2 Robust amplitude bounds

Following the discussion in Section 1.4, an amplitude bound is not realisable in stochastic systems, subject to normally distributed white noise disturbance, unless the bound is inherent in the system, such as actuator saturation. Instead, a variance bound is used to characterise the risk of exceeding the amplitude bound, and is given for a 0.26% risk of exceedance as

$$\sigma_z^2 < \left(\frac{\overline{z}}{3} \right)^2 \tag{3.146}$$

where σ_z^2 is the variance of the variable $\mathbf{z}$ with amplitude bound $\overline{z} > \mathbf{z}^T \mathbf{z}$. Multiple variance bounds may be included in the method presented in the previous subsection.

The derivation of the variance bound is based on Appendix A.2.5, where it is shown that the state $\mathbf{x}$ of an LTV model (3.49), subject to zero mean *Gaussian* distributed white noise, is a zero mean Gaussian random process. It directly follows that the performance output $\mathbf{z}$ is also a zero mean Gaussian random process. Gaussian processes are strongly related to their amplitude, and are given in [64, pp.314] as

$$\mathbb{P}\left\{ \left\| \mathbf{z}\left(t\right) \right\|_2 \cap \left[0, 3\sigma_z\left(t\right) \right] \right\} = 0.9974 \tag{3.147}$$

where $\left\| \mathbf{z}\left(t\right) \right\|_2$ is the *Euclidean*-norm of $\mathbf{z}\left(t\right)$ and

$$\sigma_z^2\left(t\right) \coloneqq \mathbb{E}\left\{ \mathbf{z}^T\left(t\right) \mathbf{z}\left(t\right) \right\} \tag{3.148}$$

its variance.[14] Thus, an amplitude bound on performance output $\mathbf{z}$, given by

$$\|\mathbf{z}\|_2 < \overline{z} \quad \forall t \tag{3.149}$$

may be represented by the variance constraint

$$\sigma_z^2 < \left(\frac{\overline{z}}{3}\right)^2 \quad \forall t \tag{3.150}$$

which has a 0.26% risk of exceedance and is satisfied 99.74% of the time.

For the case in which the model inputs have arbitrary distributions and the model is NLTV, the reader is referred to the *central limit theorem* [64, 18].

3.9.3 Robust eigenvalue regions

The design specification of an eigenvalue region is based on its relation to system transient response. This relation is well-known for LTI model (3.6) (see Appendix A.2.9). However, the only relation for NLTV model (3.28) found in the literature is given in [13] as the minimum exponential decay-rate of its energy

$$\begin{aligned}\Big(\exists V(\mathbf{x}(t)) : (3.11),\ V(\mathbf{x}(t)) < V(\mathbf{x}(t_0))\, e^{-2\mathfrak{a}(t-t_0)}\ \forall \mathbf{x}(t_0) \in \mathbb{R}^{n_x \times 1} \neq \mathbf{0}\ \forall t > t_0\Big)\\ \iff \quad \Big(\mathrm{eig}(\mathcal{A}(\Delta)) \subset \left\{z \in \mathbb{C}^1 : z < -\mathfrak{a}\right\}\Big)\end{aligned} \tag{3.151}$$

with state-trajectory equivalent

$$\begin{aligned}\left(\exists P_{\mathfrak{a}} > 0 : \frac{\frac{d}{dt}\left(\|\mathrm{chol}(P_{\mathfrak{a}})\,\mathbf{x}(t)\|_2\right)}{\|\mathrm{chol}(P_{\mathfrak{a}})\,\mathbf{x}(t)\|_2} < -\mathfrak{a}\ \forall \mathbf{x}(t) \neq \mathbf{0}\right)\\ \iff \quad \Big(\mathrm{eig}(\mathcal{A}(\Delta)) \subset \left\{z \in \mathbb{C}^1 : z < -\mathfrak{a}\right\}\Big)\end{aligned} \tag{3.152}$$

We have succeeded in deriving a new robust spectral radius relation

$$\begin{aligned}\left(\exists X_{\mathfrak{r}} > 0 : \max_{\|\mathbf{x}\|_2 \neq 0} \frac{\|\mathrm{chol}(X_{\mathfrak{r}})\,\dot{\mathbf{x}}\|_2}{\|\mathrm{chol}(X_{\mathfrak{r}})\,\mathbf{x}\|_2} < \mathfrak{r}\right)\\ \iff \quad \Big(\mathrm{eig}(\mathcal{A}(\Delta)) \subset \left\{z \in \mathbb{C}^1 : z^H z < \mathfrak{r}^2\right\}\Big)\end{aligned} \tag{3.153}$$

where $\mathfrak{r}$ bounds the rate at which the state may change relative to its size. Furthermore, a formulation that relates the NLTV model state-trajectories to the robust cone eigenvalue region could *not* be found. However, we make the following conjecture.

Conjecture 1. *Suppose there exists an NLTV model* (3.28) *and real scalars* $\{\mathfrak{a}, \mathfrak{r}, \mathfrak{c}\} \in \mathbb{R}^1$ *satisfying*

$$eig(\mathcal{A}(\Delta)) \subset \left\{z \in \mathbb{C}^1 : \tan(\mathfrak{c}) < \frac{|\Im(z)|}{-\Re(z)}\right\},\ 0 < \mathfrak{c} < \frac{\pi}{2}\,\mathrm{rad},\ \mathfrak{r} > 0,\ \mathfrak{a} > 0 \tag{3.154}$$

14. *e.g.* the 3σ-bound for a zero mean Gaussian random variable with $\sigma_X^2 = 1$, given in Figure A.6, is $x = \pm 3$, where the area under the graph between $x = \pm 3$ is 99.74% of the total area.

Then, there exists a time-invariant symmetric matrix $X_{\mathfrak{c}} = X_{\mathfrak{c}}^T \in \mathbb{R}^{n_x \times n_x}$ *such that*

$$0 < \max_{\|\mathbf{x}\|_2 \neq 0} \frac{\|chol(X_{\mathfrak{c}})\,\dot{\mathbf{x}}\|_2}{-\frac{d}{dt}\left(\|chol(X_{\mathfrak{c}})\,\mathbf{x}\|_2\right)} < \sqrt{\tan^2(\mathfrak{c}) + 1},\ X_{\mathfrak{c}} > 0 \tag{3.155}$$

Conjecture 1 bounds the ratio of spectral radius $\mathfrak{r}$ in (3.153) to exponential decay-rate $\mathfrak{a}$ in (3.152) by $\sqrt{\tan^2(\mathfrak{c}) + 1}$, where $\mathfrak{c}$ describes the corresponding robust eigenvalue region in (3.154).

The minimum exponential decay-rate $\acute{\mathfrak{a}}$ is formulated by Boyd et al. [13] for undisturbed NLTV model (3.28) in terms of a Lyapunov energy function (3.11) as

$$\exists V(\mathbf{x}(t)) : (3.11),\ V(\mathbf{x}(t)) < V(\mathbf{x}(t_0))\, e^{-2\acute{\mathfrak{a}}(t-t_0)}\ \forall \mathbf{x}(t_0) \in \mathbb{R}^{n_x \times 1} \neq \mathbf{0}\ \forall t > t_0 \tag{3.156}$$

The energy function used in [13] is (3.9), and decay-rate lower bound (3.156) becomes

$$\begin{aligned}
&\left(\exists P_{\acute{\mathfrak{a}}} > 0 : \mathbf{x}^T(t)\, P_{\acute{\mathfrak{a}}} \mathbf{x}(t) < \left(e^{-\acute{\mathfrak{a}}(t-t_0)}\mathbf{x}(t_0)\right)^T P_{\acute{\mathfrak{a}}} \left(e^{-\acute{\mathfrak{a}}(t-t_0)}\mathbf{x}(t_0)\right), \quad \forall \mathbf{x}(t_0) \neq \mathbf{0}\right) \\
\iff &\left(\exists P_{\acute{\mathfrak{a}}} > 0 : \|\mathrm{chol}(P_{\acute{\mathfrak{a}}})\,\mathbf{x}(t)\|_2 < \|\mathrm{chol}(P_{\acute{\mathfrak{a}}})\,\mathbf{x}(t_0)\|_2\, e^{-\acute{\mathfrak{a}}(t-t_0)}, \quad \forall \mathbf{x}(t_0) \neq \mathbf{0}\right) \\
\iff &\left(\exists P_{\acute{\mathfrak{a}}} > 0 : \frac{\frac{d}{dt}\left(\|\mathrm{chol}(P_{\acute{\mathfrak{a}}})\,\mathbf{x}(t)\|_2\right)}{\|\mathrm{chol}(P_{\acute{\mathfrak{a}}})\,\mathbf{x}(t)\|_2} < -\acute{\mathfrak{a}}, \quad \forall \mathbf{x}(t) \neq \mathbf{0}\right)
\end{aligned} \tag{3.157}$$

LMI conditions equivalent to (3.157) are derived as

$$\begin{aligned}
&\left(\exists V(\mathbf{x}(t)) : V(\mathbf{x}(t)) < V(\mathbf{x}(t_0))\, e^{-2\acute{\mathfrak{a}}(t-t_0)}\ \forall \mathbf{x}(t_0) \neq \mathbf{0}\right) \\
\iff &\left(\exists V(\mathbf{x}(t)) : \frac{d}{dt}V(\mathbf{x}(t)) < -2\acute{\mathfrak{a}}V(\mathbf{x}(t))\ \forall \mathbf{x}(t) \neq \mathbf{0}\right) \\
&\overset{(3.28)}{\iff} \\
&\left(\exists P_{\acute{\mathfrak{a}}} > 0 : \mathbf{x}^T(t)\left(\mathcal{A}^T(\Delta)\, P_{\acute{\mathfrak{a}}} + P_{\acute{\mathfrak{a}}}\mathcal{A}(\Delta)\right)\mathbf{x}(t) < \mathbf{x}^T(t)\left(-2\acute{\mathfrak{a}}P_{\acute{\mathfrak{a}}}\right)\mathbf{x}(t)\ \forall \mathbf{x}(t) \neq \mathbf{0}\right) \\
\iff &\left(\exists P_{\acute{\mathfrak{a}}} > 0 : \mathcal{A}^T(\Delta)\, P_{\acute{\mathfrak{a}}} + P_{\acute{\mathfrak{a}}}\mathcal{A}(\Delta) + 2\acute{\mathfrak{a}}P_{\acute{\mathfrak{a}}} < 0\right) \\
\iff &\left(\exists X_{\acute{\mathfrak{a}}} > 0 : \mathcal{A}(\Delta)\, X_{\acute{\mathfrak{a}}} + X_{\acute{\mathfrak{a}}}\mathcal{A}^T(\Delta) + 2\acute{\mathfrak{a}}X_{\acute{\mathfrak{a}}} < 0\right)
\end{aligned} \tag{3.158}$$

which is equivalent to robust maximum-real eigenvalue region LMI performance measure (3.75), and we have $\acute{\mathfrak{a}} = \mathfrak{a}$. Thus, $\mathfrak{a}$ may be specified according to (3.156) or the second line in (3.158), referred to as the rate of convergence. The rate of convergence is useful for specifying instantaneous measures.

A similar relation to the radius of robust disk eigenvalue region (3.76) is developed for $\mathfrak{q} = 0$, using the *induced* 2-norm given in [70, pp.552-553] as

$$\|\mathcal{A}\|_{i2} \coloneqq \max_{\mathbf{b} \in \mathbb{R}^{n \times 1}, \|\mathbf{b}\|_2 \neq 0} \frac{\|\mathcal{A}\mathbf{b}\|_2}{\|\mathbf{b}\|_2} = \mathrm{msv}(\mathcal{A}) = \min_{\gamma \in \mathbb{R}^1} \sqrt{\gamma} : \mathcal{A}\mathcal{A}^T < \gamma I \tag{3.159}$$

where $\text{msv}(\mathcal{A})$ is the *maximum singular value* of $\mathcal{A}$. Given (3.76) and $\mathfrak{q} = 0$, the relation is presented as

$$\begin{gathered}
\left(\left[\begin{array}{cc} -\mathfrak{r}X_{\mathfrak{r}} & \mathcal{A}(\Delta)X_{\mathfrak{r}} \\ X_{\mathfrak{r}}\mathcal{A}^T(\Delta) & -\mathfrak{r}X_{\mathfrak{r}} \end{array}\right] < 0,\ X_{\mathfrak{r}} > 0\right) \\
\iff \quad \left(\mathcal{A}(\Delta)X_{\mathfrak{r}}\mathcal{A}^T(\Delta) < \mathfrak{r}^2 X_{\mathfrak{r}},\ X_{\mathfrak{r}} > 0\right) \\
\iff \quad \left(\text{chol}(X_{\mathfrak{r}})^{-T}\mathcal{A}(\Delta)X_{\mathfrak{r}}\mathcal{A}^T(\Delta)\,\text{chol}(X_{\mathfrak{r}})^{-1} < r^2 I,\ X_{\mathfrak{r}} > 0\right) \\
\iff \\
\left(\begin{array}{c} \text{msv}\left(\left(\text{chol}(X_{\mathfrak{r}})^{-T}\mathcal{A}(\Delta)\,\text{chol}(X_{\mathfrak{r}})^T\right)\text{chol}(X_{\mathfrak{r}})\mathcal{A}^T(\Delta)\,\text{chol}(X_{\mathfrak{r}})^{-1}\right) < \mathfrak{r}^2, \\ X_{\mathfrak{r}} > 0 \end{array}\right) \\
\iff \quad \left(\text{msv}\left(\text{chol}(X_{\mathfrak{r}})\mathcal{A}^T(\Delta)\,\text{chol}(X_{\mathfrak{r}})^{-1}\right)^2 < \mathfrak{r}^2,\ X_{\mathfrak{r}} > 0\right) \\
\iff \quad \left(\text{msv}\left(\text{chol}(X_{\mathfrak{r}})\mathcal{A}^T(\Delta)\,\text{chol}(X_{\mathfrak{r}})^{-1}\right) < \mathfrak{r},\ X_{\mathfrak{r}} > 0\right) \\
\iff \quad \left(\max_{\mathbf{b}\in\mathbb{R}^{n_x\times 1}, \|\mathbf{b}\|_2\neq 0} \frac{\left\|\text{chol}(X_{\mathfrak{r}})\mathcal{A}^T(\Delta)\,\text{chol}(X_{\mathfrak{r}})^{-1}\mathbf{b}\right\|_2}{\|\mathbf{b}\|_2} < \mathfrak{r},\ X_{\mathfrak{r}} > 0\right) \\
\iff \quad \left(\max_{\|\mathbf{x}\|_2\neq 0} \frac{\left\|\text{chol}(X_{\mathfrak{r}})\mathcal{A}^T(\Delta)\,\text{chol}(X_{\mathfrak{r}})^{-1}\,\text{chol}(X_{\mathfrak{r}})\mathbf{x}\right\|_2}{\|\text{chol}(X_{\mathfrak{r}})\mathbf{x}\|_2} < \mathfrak{r},\ X_{\mathfrak{r}} > 0\right) \\
\iff \quad \left(\max_{\|\mathbf{x}\|_2\neq 0} \frac{\|\text{chol}(X_{\mathfrak{r}})\dot{\mathbf{x}}\|_2}{\|\text{chol}(X_{\mathfrak{r}})\mathbf{x}\|_2} < \mathfrak{r},\ X_{\mathfrak{r}} > 0\right) \qquad (3.160)
\end{gathered}$$

where $\mathfrak{r}$ bounds the rate at which the state may change relative to its size. Thus, for $\mathfrak{q} = 0$, $\mathfrak{r}$ may be specified according to (3.153). (3.153) is analysed for pure exponential and sinusoidal trajectories as follows.

Given (3.76), $\mathfrak{q} = 0$, (3.153) and the exponential trajectory

$$\left(\mathbf{b} := \text{chol}(X_{\mathfrak{r}})\mathbf{x} = \mathbf{a}e^{\tau t} = \left[\begin{array}{c} a_1 \\ a_2 \\ \vdots \\ a_{n_x} \end{array}\right] e^{\tau t}\right) \quad \iff \quad \left(\dot{\mathbf{b}} = \tau \left[\begin{array}{c} a_1 \\ a_2 \\ \vdots \\ a_{n_x} \end{array}\right] e^{\tau t}\right) \qquad (3.161)$$

it follows that

$$\begin{gathered}
\left(\exists X_{\mathfrak{r}} > 0 : \left[\begin{array}{cc} -\mathfrak{r}X_{\mathfrak{r}} & \mathcal{A}(\Delta)X_{\mathfrak{r}} \\ X_{\mathfrak{r}}\mathcal{A}^T(\Delta) & -\mathfrak{r}X_{\mathfrak{r}} \end{array}\right] < 0,\ \frac{d}{dt}X_{\mathfrak{r}} = 0\right) \\
\overset{(3.160)}{\Longrightarrow} \quad \left(\max_{\|\mathbf{b}\|_2\neq 0} \frac{\dot{\mathbf{b}}^T\dot{\mathbf{b}}}{\mathbf{b}^T\mathbf{b}} < \mathfrak{r}^2\right) \\
\Longrightarrow \quad \left(\max_{\|\mathbf{b}\|_2\neq 0} \frac{\tau^2 e^{\tau t}\sum_i a_i^2}{e^{\tau t}\sum_i a_i^2} < \mathfrak{r}^2\right) \\
\Longrightarrow \quad (|\tau| < \mathfrak{r}) \qquad (3.162)
\end{gathered}$$

Thus, for $\mathfrak{q} = 0$, $\mathfrak{r}$ is an exponential decay-rate and growth-rate upper-bound for pure exponential trajectories. Given (3.76), $\mathfrak{q} = 0$, (3.160) and the sinusoidal trajectory

$$\left(\mathbf{d} \coloneqq \text{chol}\left(X_{\mathfrak{r}}\right) \mathbf{x} = \mathbf{c} \sin\left(\omega t + \boldsymbol{\phi}\right) = \begin{bmatrix} c_1 \sin\left(\omega t + \phi_1\right) \\ c_2 \sin\left(\omega t + \phi_2\right) \\ \vdots \\ c_{n_x} \sin\left(\omega t + \phi_{n_x}\right) \end{bmatrix} \right)$$
$$\iff \quad \left(\dot{\mathbf{d}} = \omega \mathbf{c} \cos\left(\omega t + \boldsymbol{\phi}\right) \right) \tag{3.163}$$

it follows that

$$\left(\exists X_{\mathfrak{r}} > 0 : \begin{bmatrix} -\mathfrak{r} X_{\mathfrak{r}} & \mathcal{A}\left(\Delta\right) X_{\mathfrak{r}} \\ X_{\mathfrak{r}} \mathcal{A}^T\left(\Delta\right) & -\mathfrak{r} X_{\mathfrak{r}} \end{bmatrix} < 0, \ \frac{d}{dt} X_{\mathfrak{r}} = 0 \right)$$
$$\overset{(3.160)}{\implies} \quad \left(\max_{\|\mathbf{b}\|_2 \neq 0} \frac{\dot{\mathbf{d}}^T \dot{\mathbf{d}}}{\mathbf{d}^T \mathbf{d}} < \mathfrak{r}^2 \right)$$
$$\implies \quad \left(\max_{\|\mathbf{d}\|_2 \neq 0} \frac{\omega^2 \sum_i c_i^2 \cos^2\left(\omega t + \phi_i\right)}{\sum_i c_i^2 \sin^2\left(\omega t + \phi_i\right)} < \mathfrak{r}^2 \right)$$
$$\implies \quad \left(\omega < \mathfrak{r} \right) \tag{3.164}$$

The final simplification in (3.164) is made by choosing $X_{\mathfrak{r}}$ such that the numerator and the denominator differ by the factor ω^2, *i.e.* their phase difference is removed. Thus, for $\mathfrak{q} = 0$, $\mathfrak{r}$ is a frequency upper-bound for pure sinusoidal trajectories. The pure trajectories, however, only serve to illustrate (3.160) for these special cases, as superposition does not hold for NLTV systems.

A similar formulation that relates the NLTV model trajectories to the robust cone eigenvalue region could *not* be found. However, in the LTI model framework, $\mathfrak{c}$ bounds the frequency at which the state-trajectory may oscillate relative to its decay-rate. Conjecture 1 is based on the geometric combination of spectral radius $\mathfrak{r}$ and minimum exponential decay-rate $\mathfrak{a}$ to achieve the ratio described by $\mathfrak{c}$, illustrated in Figure 3.7.

3.10 Solving LMIs

Many LMI solvers exist that implement the robust and computationally efficient interior-point algorithm. SDPT3, LMILAB, SEDUMI, SDPA and CSDP have been tested for our control application, of the scale of ±3300 scalar variables, and only SDPT3 and LMILAB are found to be robust enough to solve the large LMI optimisation problem.

SDPT3 is in the order of 5 times faster than LMILAB, and has proven to be a reliable LMI solver for our application when 64-bit true double calculations are used, *i.e.* when implemented on a 64-bit system.

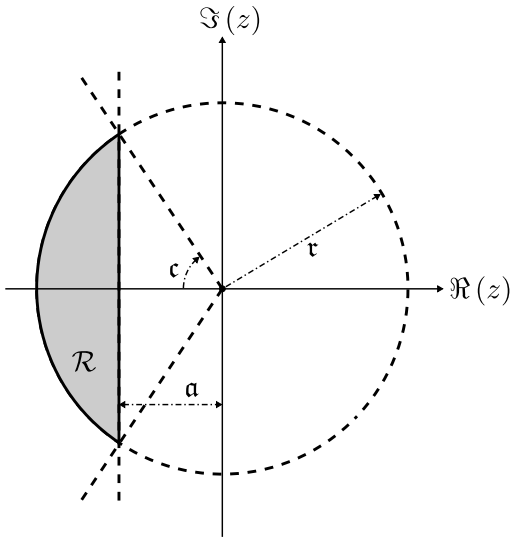

Figure 3.7: Robust cone eigenvalue region imposed by $\mathfrak{r}$ and $\mathfrak{a}$.

3.10.1 Sdpt3

SDPT3 is a MATLAB software package, found in the public domain, used to solve *large-scale* LMI optimisation problems. The algorithm implemented in SDPT3 is an *infeasible primal-dual path-following algorithm* which relies on interior-point methods to solve LMI problems robustly and efficiently. In the case of an infeasible LMI problem with a certificate of infeasibility, the algorithm may not find the certificate, otherwise approximate certificates of infeasibility are calculated. The algorithm tries to achieve feasibility and optimality of its iterates simultaneously. Initial iterates do not need to be feasible. See [77] for a user's guide.

3.10.2 Yalmip

YALMIP is a MATLAB software package, found in the public domain, used as a high-level interface with LMI solvers, and is compatible with most of the popular LMI solvers. YALMIP implements a large number of modelling tricks, allowing the user to create LMIs with a syntax similar that of (3.138), while YALMIP translates them to an efficient and numerically sound low-level form, which greatly reduces development time. [15]

3.10.3 LMI well-posedness

An optimisation problem is ill-posed if it lacks variable bounds, *i.e.* the optimisation problem is solved within the limit as one or more of its variables goes to infinity. In the LMI framework, variables may be bounded in a straightforward manner.

15. Take care when using YALMIP with LMILAB, as the former may reduce the computational speed of LMILAB by a factor of 10.

Positive definite matrix variables are bounded with their trace, while the remaining variables are bounded by the square of their *Frobenius*-norm, defined as

$$\|N\|_F^2 \coloneqq \operatorname{tr}\left(N^T N\right) \tag{3.165}$$

and bounded via LMIs by using LMIs' preservation under the trace operator and applying Schur's complement (Theorem 4), given as

$$\begin{aligned} & \left(\|N\|_F^2 < \operatorname{tr}(R) : N^T N < R,\ R > 0\right) \\ \iff \quad & \left(\|N\|_F^2 < \operatorname{tr}(R) : \begin{bmatrix} -R & N^T \\ N & -I \end{bmatrix} < 0,\ R > 0\right) \end{aligned} \tag{3.166}$$

Furthermore, finite numerical accuracy may cause some of the inequalities to be close to the boundary of strictness, [16] even though SDPT3 is suited for strict inequalities, causing inaccurate matrix inversions that are required post-synthesis. This is remedied by applying a positive *shift* of ϵ in the LMIs, defined as

$$(M > \epsilon I,\ \epsilon > 0) \quad \Longrightarrow \quad (M + \nabla > 0) \tag{3.167}$$

where ∇ represents the numerical inaccuracy and ϵ is dependent on both M and ∇, usually chosen in the order of the maximum numerical inaccuracy.

16. A strict inequality $>$ excludes equality, whereas a non-strict inequality $\geq$ includes the equality.

Chapter 4

Application of LMI control design to in-flight refuelling

In this chapter, we apply the robust multi-$\mathcal{H}_2$ estimator-based state-feedback control design technique, developed in the previous chapter, to IFR. The application serves to highlight some of the important aspects of the LMI technique, such as the representation of a system with the norm-bounded state-space model, performance specification, involved conservatism and implementation considerations. The controller architecture is discussed and formulated in Section 4.1. Section 4.2 provides the norm-bounded state-space representation of the IFR model, developed in Chapter 2, and IFR design specifications. Then, the IFR controller synthesis and implementation is provided in Sections 4.3 and 4.4 respectively.

4.1 Control architecture

A *predictor estimator-based state-feedback* controller structure was chosen for IFR automation, due to its admittance to LMI synthesis form developed in Section 3.8, and is illustrated in Figure 3.6.

State-feedback requires the system state corresponding to the model used for synthesis. The A330 avionics provides all aircraft-state estimates, as well as relative position state estimates, but excludes that of the turbulence. A radio-link provides a means for the tanker and receiver to share estimates. The turbulence state is uncontrollable, thus zeroing its corresponding elements in the state-feedback gain does not affect the eigenvalues of the closed-loop IFR model, although it may cause a degradation in variance performance. This fact is obvious when the model is considered in *controllability canonical form* and is shown as follows.

Open-loop norm-bounded state-space model (3.91) in *controllability canonical form*

is given as

$$\left[\begin{bmatrix}\dot{\mathbf{x}}_C\\ \dot{\mathbf{x}}_U\end{bmatrix}\right] = \left[\begin{bmatrix}A_C & A_{CU}\\ 0 & A_U\end{bmatrix} \begin{bmatrix}B_{Cu}\\ 0\end{bmatrix} \begin{bmatrix}B_{Cp}\\ B_{Up}\end{bmatrix}\right] \left[\begin{bmatrix}\mathbf{x}_C\\ \mathbf{x}_U\end{bmatrix}\right] \tag{4.1}$$
$$\left[\begin{bmatrix} C_{qC} & C_{qU}\end{bmatrix} D_{qu} \quad D_{qp}\right] \left[\begin{bmatrix}\mathbf{u}\\ \mathbf{p}\end{bmatrix}\right]$$
$$\mathbf{p} = \Delta\mathbf{q}, \quad \Delta \in \mathbf{\Delta}$$

where the performance output is omitted for the illustration, subscripts C and U are associated with the controllable and uncontrollable state respectively and, by definition, $A_{UC} = 0$ and $B_{Uu} = 0$. Applying the lower LFT to remove uncertainty input and output we obtain

$$\begin{bmatrix}\dot{\mathbf{x}}_C\\ \dot{\mathbf{x}}_U\end{bmatrix} = \begin{bmatrix}(A_C + B_{Cp}\Psi C_{qC}) & (A_{CU} + B_{Cp}\Psi C_{qU})\\ 0 & (A_U + B_{Up}\Psi C_{qU})\end{bmatrix} \begin{bmatrix}\mathbf{x}_C\\ \mathbf{x}_U\end{bmatrix} + \begin{bmatrix}(B_{Cu} + B_{Cp}\Psi D_{qu})\\ 0\end{bmatrix}\mathbf{u} \tag{4.2}$$
$$\Psi := (I - \Delta D_{qp})^{-1}\Delta, \ \Delta \in \mathbf{\Delta}$$

where $B_{Up}\Psi C_{qC} = 0$ and $B_{Up}\Psi D_{qu} = 0$ by definition. Given state-feedback structure $\mathbf{u} = \begin{bmatrix} K_C & K_U\end{bmatrix}\begin{bmatrix}\mathbf{x}_C\\ \mathbf{x}_U\end{bmatrix}$, the closed-loop form is given as

$$\begin{bmatrix}\dot{\mathbf{x}}_C\\ \dot{\mathbf{x}}_U\end{bmatrix} = \begin{bmatrix}\begin{pmatrix}A_C + B_{Cp}\Psi C_{qC} + \\ (B_{Cu} + B_{Cp}\Psi D_{qu})K_C\end{pmatrix} & \begin{pmatrix}A_{CU} + B_{Cp}\Psi C_{qU} + \\ (B_{Cu} + B_{Cp}\Psi D_{qu})K_U\end{pmatrix}\\ 0 & (A_U + B_{Up}\Psi C_{qU})\end{bmatrix}\begin{bmatrix}\mathbf{x}_C\\ \mathbf{x}_U\end{bmatrix} \tag{4.3}$$
$$\Psi := (I - \Delta D_{qp})^{-1}\Delta, \ \Delta \in \mathbf{\Delta}$$

The closed-loop eigenvalues of (4.3) is given in [70, pp.534] as

$$\text{eig}\begin{pmatrix}A_C + B_{Cp}\Psi C_{qC} + \\ (B_{Cu} + B_{Cp}\Psi D_{qu})K_C\end{pmatrix} \text{ and } \text{eig}\,(A_U + B_{Up}\Psi C_{qU}) \tag{4.4}$$

Thus, K_U does not affect the closed-loop eigenvalues of the model, although it augments the gain from $\mathbf{x}_U$ to $\dot{\mathbf{x}}_C$, *i.e.* the turbulence influence on the aircraft state.

Estimator formulation (3.121)-(3.128) is versatile enough to allow the synthesis of an estimator for only part of the model, and is applied to the synthesis of a *turbulence estimator*, which is implemented alongside the existing aircraft and relative position estimators to provide an estimate of the system state corresponding to the IFR model used for state-feedback synthesis. To this end, state-feedback gain elements corresponding to the turbulence state are included to achieve an increase in AIFR variance performance, *i.e.* regulation performance. The turbulence estimator is developed in Section 4.3.3.

The IFR model used for state-feedback synthesis is calculated for a predefined flight-domain with the algorithm presented in Appendix B.1. The IFR flight-domain is specified in Section 1.3 with parameters

$$\mathbf{d} = \begin{bmatrix} \nu_{T_r} & \phi_{T_r} & h_{T_r} & \dot{h}_{T_r} & m_T & cg_T & m_R & cg_R \end{bmatrix}^T \tag{4.5}$$

where ν is the groundspeed and subscript T_r denotes the reference/trim of the tanker. A controller has been synthesised, with the method presented in this Chapter, for the IFR model defined for the *whole* flight-domain, and has been found to be infeasible, *i.e.* unstable. Thus, the model variation over the whole flight-domain is too large for the fixed controller to stabilise. A gain-scheduling scheme, based on linear interpolation over a simplicial complex, is presented in Appendix B.2 and is used to combine multiple controllers synthesised for sub-domains. Figure 4.1 illustrates the gain-scheduling scheme for a flight-domain equally divided into 9 overlapping sub-domains over ground-speed and altitude, with centres $\mathbf{d}_i$ $i = 1, 2, \ldots, 9$ and corresponding gains U_i synthesised for the respective sub-domain, where U represents the state-feedback and estimator gains. The gain-scheduling scheme selects a simplex in the flight-domain, with sub-domain centres as its corners, which encloses the present operating point $\mathbf{d}$. The simplex corners are linearly interpolated to $\mathbf{d}$, described as a linear function with calculated coefficients β_i $i = 1, 2, 3$. The coefficients are then used to linearly interpolate the gains U_i corresponding to the simplex corners in the same manner, to obtain a gain U which corresponds to the present operating point $\mathbf{d}$. The result is a parameter varying controller, extending over the

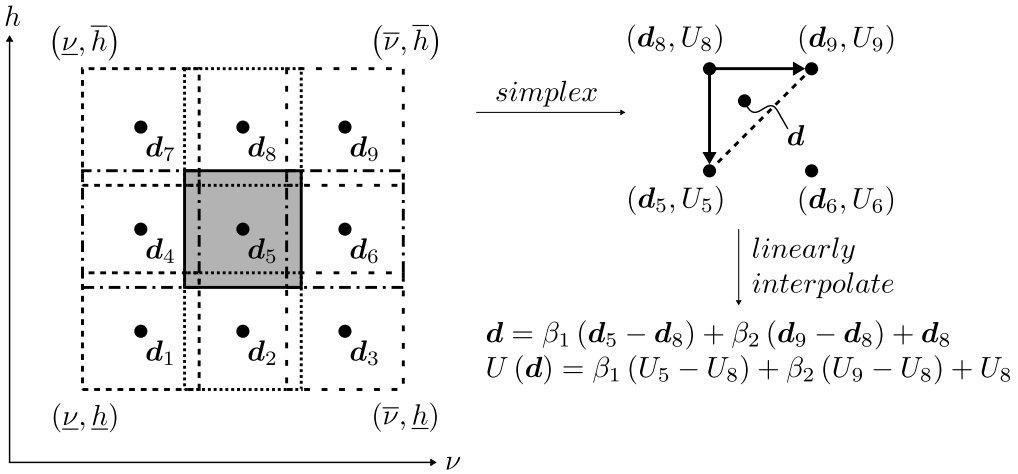

Figure 4.1: 2D illustration of simplicial complex based gain-scheduling.

whole flight-domain and, assuming the parameters vary sufficiently slow, the performance of each individual synthesised controller at their respective sub-domains is approximately attained. Gain-scheduling has the advantage over switched control of being continuous, whereas the discrete switched control causes unwanted transients. A comparison between gain-scheduling and switched control is not in the scope of this thesis. The size of IFR sub-domains used for synthesis depends on the attainable performance, and is experimentally determined.

Four aspects of controller architecture remain that are not limited by the synthesis formulations developed in Section 3.8, and are given as follows.

1. Responsibility for relative position regulation: This task is assigned to the pilot of the receiving aircraft when IFR is performed manually, while the tanker follows some flight path, such as a corkscrew. However, when IFR is performed autonomously, both tanker and receiver may actively regulate their relative position. By following the same logic of state- and state-derivative-feedback at the end of Section 3.8.1, it is obvious that a higher performance can be attained by assigning both aircraft to perform the regulation, as apposed to assigning the task to only one. A coupled controller architecture, which uses both aircraft to regulate the relative position, is included in the body of the thesis and is the focus of our analysis in Section 4.3.5 and Chapter 5. A partially decoupled control architecture is included as an extension in Appendix D, which only uses the receiver to regulate the relative position, while the tanker flies a specified flight track.
2. Absolute heading: The aircraft 6DOF EOM, described by (2.7), (2.8) and (2.17), are invariant under heading ψ. The boom kinematics (2.19), however, are expressed with tanker and receiver headings ψ_T and ψ_R, although the kinematics are invariant under absolute heading, *i.e.* the boom kinematics are invariant under any addition to both ψ_T and ψ_R, *e.g.* $\psi_T + \psi_{abs}$ and $\psi_R + \psi_{abs}$. Moreover, the IFR flight-path is defined by constant references for ground-speed ν_{T_r}, climb-rate $\dot{h}_{T_r}$ and bank-angle ϕ_{T_r}, resulting in a corkscrew flight-path with a constant heading time-derivative $\dot{\psi}_{T_r}$ unknown in size, due to the uncertainty in the aircraft aerodynamics. (see Appendix A.1.5). Thus, the perturbation/error $\varepsilon\psi_T := \psi_T - \psi_{T_r} = \psi_T - \int \dot{\psi}_{T_r}$ to be used in state-feedback, calculated with a constant error in $\dot{\psi}_{T_r}$, will have a ramp error as result. This is remedied by replacing absolute headings ψ_T and ψ_R with relative heading $\psi_{TR} := \psi_T - \psi_R$, *i.e.* setting $\psi_{abs} = -\psi_R$.
3. Removing system biases: It is common practise to remove estimator biases with *integrators*, as well as biases that arise from constant disturbances, such as tanker wake. Integrators may also be used to impose a unique trim, appropriately specified by the correct amount of references. In the case where a unique trim is not imposed, system variables may drift (within the non-unique trim space), causing them to exit their well-defined domains. Conditions are derived in Appendix A.1.6 for specifying a unique trim, and are applied here to the placement of integrators to achieve a unique trim at steady-state.
   The unique IFR trim, defined in Appendix A.1.6, is specified by fixing expres-

sions

$$\acute{\mathbf{g}}\left(\mathbf{m}_{AIFR}\right) = \begin{bmatrix} \nu_T \\ v_T \\ \dot{h}_T \\ \phi_T \\ v_R \\ x_b \\ y_b \\ z_b \end{bmatrix} = \acute{\mathbf{c}},\ \dot{\mathbf{g}}\left(\mathbf{m}_{AIFR}\right) = \frac{d}{dt}\begin{bmatrix} \nu_T \\ v_T \\ \dot{h}_T \\ p_T \\ q_T \\ r_T \\ \phi_T \\ \theta_T \\ u_R \\ v_R \\ w_R \\ p_R \\ q_R \\ r_R \\ \phi_R \\ \theta_R \\ \psi_{TR} \\ x_b \\ y_b \\ z_b \end{bmatrix} = \mathbf{0} \tag{4.6}$$

and control input

$$\acute{\boldsymbol{\delta}} = \begin{bmatrix} \delta_{e,T} \\ \delta_{s_p,T} \\ \delta_{s_s,T} \\ \delta_{t_p,T} - \delta_{t_s,T} \\ \delta_{e,R} \\ \delta_{s_p,R} \\ \delta_{s_s,R} \\ \delta_{t_p,R} - \delta_{t_s,R} \end{bmatrix} = \begin{bmatrix} 0 \\ \text{centre}\left(\delta_{s_p,T}\right) \\ \text{centre}\left(\delta_{s_s,T}\right) \\ 0 \\ 0 \\ \text{centre}\left(\delta_{s_p,R}\right) \\ \text{centre}\left(\delta_{s_s,R}\right) \\ 0 \end{bmatrix} \tag{4.7}$$

where

$$\mathbf{m}_{AIFR} = \begin{bmatrix} \begin{bmatrix} I_8 & 0_{8\times 2} \end{bmatrix} & 0 & 0 \\ 0 & \begin{bmatrix} I_8 & 0_{8\times 2} \end{bmatrix} & 0 \\ \begin{bmatrix} 0_{1\times 8} & 1 & 0_{1\times 1} \end{bmatrix} & \begin{bmatrix} 0_{1\times 8} & -1 & 0_{1\times 1} \end{bmatrix} & 0 \\ 0 & 0 & I_3 \end{bmatrix} \begin{bmatrix} \mathbf{m}_T \\ \mathbf{m}_R \\ \mathbf{b} \end{bmatrix} \tag{4.8}$$

$\acute{\mathbf{g}}$ is a function expressing known constant trim values $\acute{\mathbf{c}}$ in terms of AIFR motion variables $\mathbf{m}_{AIFR}$, $\dot{\mathbf{g}}\left(\mathbf{m}_{AIFR}\right)$ expresses the time-derivative of trim values known to be constant and $\acute{\boldsymbol{\delta}}$ is a function of IFR actuators which are fixed at chosen values to achieve the unique trim. Now, if we pass each of their estimated perturbations through their own dedicated integrator, *i.e.*

$$\mathbf{i} = \int_0^t \begin{bmatrix} \left(\acute{\mathbf{g}}\left(\widehat{\mathbf{m}_{AIFR}}\right) - \acute{\mathbf{c}}\right) \\ \dot{\mathbf{g}}\left(\widehat{\mathbf{m}_{AIFR}}\right) \\ \widehat{\acute{\boldsymbol{\delta}}} - \text{centre}\left(\acute{\boldsymbol{\delta}}\right) \end{bmatrix} dt \tag{4.9}$$

and appropriately include the integrator output $\mathbf{i}$ in the feedback such that the closed-loop system is exponentially stable, the unique trim defined by (4.6) and (4.7) is attained at steady state. The imposition is due to the fact that integrator inputs are zero at steady-state for exponentially stable systems. It follows that, at steady-state, the system will posses the negative of the biases of the integrated estimates, while removing the biases of all other estimates used for feedback.

Furthermore, $\dot{\mathbf{g}}\left(\mathbf{m}_{AIFR}\right)$ is such that $\begin{bmatrix} I & 0 \\ 0 & I \end{bmatrix}$

$$\left(\dot{\mathbf{m}}_{AIFR} = \mathbf{0}\right) \quad \Longrightarrow \quad \left(\dot{\mathbf{g}}\left(\mathbf{m}_{AIFR}\right) = \mathbf{0}\right) \tag{4.10}$$

and $\dot{\mathbf{m}}_{AIFR}$ is inherently passed through $\frac{1}{s}I$ to describe system dynamics, thus (4.9) may be reduced to

$$\mathbf{i}_{AIFR} = \int_0^t \begin{bmatrix} \left(\acute{\mathbf{g}}\left(\widehat{\mathbf{m}_{AIFR}}\right) - \acute{\mathbf{c}}\right) \\ \hat{\acute{\boldsymbol{\delta}}} - \text{centre}\left(\acute{\boldsymbol{\delta}}\right) \end{bmatrix} dt \tag{4.11}$$

which still imposes the unique trim, but does not require estimates of $\dot{\mathbf{g}}\left(\mathbf{m}_{AIFR}\right)$, thus excluding their biases from the closed-loop system.

The uniqueness of actuator dynamics are inherited in their diagonal structure, *i.e.* the actuator dynamics output $\boldsymbol{\delta}$ trim is unique due to (4.11), which corresponds to a unique actuator input due to the diagonal structure. By centring $\acute{\boldsymbol{\delta}}$ at trim, a maximum range is available for regulation, although a conventional trim of zero is chosen for elevators.

An example where variables drift outside their well defined-domains, are when spoiler deflections are not integrated, which may cause the remaining integrators to inappropriately assign spoilers, thrust and horizontal tail plane to maintain climb-rate and groundspeed, while aircraft pitch increases towards stalling point.

4. AIFR on-line reference input: The AIFR on-line reference is specified as a discrete vector value in real-time by the tanker and receiver pilots, and implemented by passing the reference through a Low-Pass Filter (LPF) with a sufficiently low bandwidth, and subtracting the filter output from the respective references in $\acute{\mathbf{c}}$. The reference specified for AIFR on-line is given as

$$\begin{bmatrix} \nu_{T_r} \\ \dot{h}_{T_r} \\ \phi_{T_r} \\ x_{b,r} \\ y_{b,r} \\ z_{b,r} \end{bmatrix} \tag{4.12}$$

where the first three elements are the inputs of the tanker pilot and the remainder is the inputs of the receiver pilot. By including relative position as an on-line reference, transition between receiver observation, pre-contact and contact position, defined in Section 1.4, can be achieved. [1]

1. A state machine may also be implemented to automate the tasks of the tanker and receiver pilots, by specifying the references according to a flight plan and the various phases of IFR.

A simple block diagram of the AIFR controller architecture is illustrated in Figure 4.2. A detailed block diagram of the AIFR controller structure can be found in Figure 4.11.

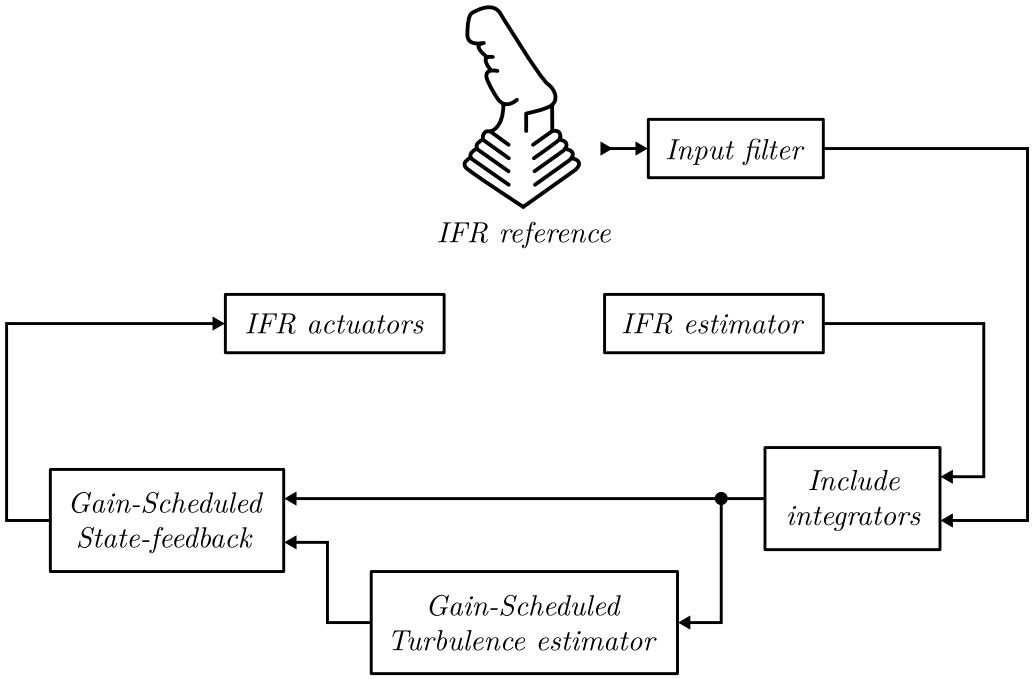

Figure 4.2: AIFR controller architecture.

4.2 LMI formulation

The IFR problem is cast into the LMI framework, developed in Chapter 3, by representing the IFR model with a norm-bounded state-space model and translating IFR specifications to LMI constraints.

4.2.1 Continuous-time norm-bounded state-space description

The representation of a system with a norm-bounded state-space model is generalised, and applied to each of the IFR components developed in Chapter 2, after which all the model components are combined into a single norm-bounded state-space model.

4.2.1.1 General Form

Refer to (3.91) and Figure 3.5. Given any open-loop finite-gain [2] strictly-proper NLTV, possibly uncertain, system

$$\begin{bmatrix} \dot{\mathbf{x}}_\rho \\ \mathbf{z}_\rho \\ \mathbf{y}_\rho \end{bmatrix} = S(\boldsymbol{\rho}) \begin{bmatrix} \mathbf{x}_\rho \\ \mathbf{w}_\rho \\ \mathbf{u}_\rho \end{bmatrix}, \quad \boldsymbol{\rho} \in \mathfrak{D}_\rho \tag{4.13}$$

where subscript ρ denotes the I/O variables of the system, we define its NLTV norm-bounded state-space description as (3.91) such that

$$\left(\mathbf{x}(t_0) = \mathbf{x}_\rho(t_0),\ \mathbf{w} = \mathbf{w}_\rho,\ \mathbf{u} = \mathbf{u}_\rho\right) \implies \left(\begin{bmatrix} \mathbf{x} \\ \dot{\mathbf{x}} \\ \mathbf{z} \\ \mathbf{y} \end{bmatrix} = \begin{bmatrix} \mathbf{x}_\rho \\ \dot{\mathbf{x}}_\rho \\ \mathbf{z}_\rho \\ \mathbf{y}_\rho \end{bmatrix} \ \forall t \geq t_0 \right) \tag{4.14}$$

Due to the finite-gain representation, I/O variables of the system is defined as the perturbation about its trim [13, pp.53-54][83, Ch.7][33, pp.260-261].

An algorithm is presented in Appendix B.1 that calculates a norm-bounded state-space description (3.91) using selected system I/O pairs.

4.2.1.2 Individual aircraft flight mechanics

The Airbus A330 perturbation *flight mechanics* is calculated as $G_{m,A}$ over variable domain $\mathfrak{D}_{m,A}$ in

$$\begin{bmatrix} \dot{\mathbf{x}} \\ \mathbf{z} \\ \mathbf{q} \end{bmatrix}_{m,A} = G_{m,A} \begin{bmatrix} \mathbf{x} \\ \mathbf{g} \\ \mathbf{u} \\ \mathbf{p} \end{bmatrix}_{m,A} = \begin{bmatrix} A & B_g & B_u & B_p \\ C_q & D_{qg} & D_{qu} & D_{qp} \end{bmatrix}_{m,A} \begin{bmatrix} \mathbf{x} \\ \mathbf{g} \\ \mathbf{u} \\ \mathbf{p} \end{bmatrix}_{m,A}$$

$$\mathbf{p}_{m,A} = \Delta_{m,A}\mathbf{q}_{m,A}, \quad \Delta_{m,A} \in \boldsymbol{\Delta}, \quad \begin{bmatrix} \mathbf{x} \\ \mathbf{g} \\ \mathbf{u} \end{bmatrix}_{m,A} \in \mathfrak{D}_{m,A}\ \forall t \tag{4.15}$$

where subscripts m and A denote the mechanics and aircraft (tanker T or receiver R) respectively, $\mathbf{x}_{m,A} \in \mathbb{R}^{10\times 1}$ is chosen as the perturbation ε of the motion variables defined by (2.6), and is given as

$$\mathbf{x}_{m,A} \coloneqq \varepsilon\mathbf{m} = \mathbf{m} - \mathbf{m}_r = \begin{bmatrix} \varepsilon u & \varepsilon v & \varepsilon w & \varepsilon p & \varepsilon q & \varepsilon r & \varepsilon\phi & \varepsilon\theta & \varepsilon\psi & \varepsilon h \end{bmatrix}^T \tag{4.16}$$

to which end the motion variables may be obtained as $\mathbf{m} = \mathbf{m}_r + \mathbf{x}_{m,A}$. $\mathbf{u}_{m,A} \in \mathbb{R}^{8\times 1}$ is chosen as the perturbation ε of the control surfaces and thrust defined by (2.6), and is given as

$$\mathbf{u}_{m,A} \coloneqq \varepsilon\boldsymbol{\delta} = \boldsymbol{\delta} - \boldsymbol{\delta}_r = \begin{bmatrix} \varepsilon\delta_a & \varepsilon\delta_h & \varepsilon\delta_e & \varepsilon\delta_r & \varepsilon\delta_{s_p} & \varepsilon\delta_{s_s} & \varepsilon\delta_{t_p} & \varepsilon\delta_{t_s} \end{bmatrix}^T \tag{4.17}$$

2. *Finite-gain* systems have zero output for zero input, which exclude backlash, stiction, *etc.* (see Section A.2.10)

$\mathbf{g}_{m,A}$ is the turbulence along the base components of the turbulence frame, $\mathbf{z}_{m,A}$ is included as performance output and $\mathfrak{D}_{m,A}$ defines the domain of input variables perturbation $\left[\begin{array}{ccc}\mathbf{x} & \mathbf{g} & \mathbf{u}\end{array}\right]^T_{m,A}$.

$G_{m,A}$ is dependent on $\mathfrak{D}_{m,A}$, and is valid for $\left[\begin{array}{ccc}\mathbf{x}^T & \mathbf{g}^T & \mathbf{u}^T\end{array}\right]^T_{m,A} \in \mathfrak{D}_{m,A}$. A case where $G_{m,A}$ becomes invalid as $\left[\begin{array}{ccc}\mathbf{x}^T & \mathbf{g}^T & \mathbf{u}^T\end{array}\right]^T_{m,A} \notin \mathfrak{D}_{m,A}$ can be observed in Figure 3.3 as a decrease in lower sector-bound $\frac{1}{r_i}\acute{q}_i$, when r_i is increased. It follows that we need to constrain the input variables $\left[\begin{array}{ccc}\mathbf{x}^T & \mathbf{g}^T & \mathbf{u}^T\end{array}\right]^T_{m,A}$ to the domain $\mathfrak{D}_A$ in order for the model to remain a valid description of the system, and is achieved by constraining the performance output, defined as

$$\mathbf{z}_{m,A} \coloneqq \mathbf{x}_{m,A} \tag{4.18}$$

where we require

$$\mathbf{z}_{m,A} \in \mathfrak{D}_{z_{m,A}} \tag{4.19}$$

$\mathbf{g}_{m,A}$ is uncontrollable and the domain of $\mathbf{u}_{m,A}$ is specified in the actuators and, as a result, is not included in $\mathbf{z}_{m,A}$.

The aircraft 6DOF EOM (2.7)-(2.18) incorporate aerodynamic coefficient and moment of inertia data provided by Airbus, with 10% and 0% uncertainty in the data respectively, and are used by the algorithm presented in Appendix B.1 to calculate $G_{m,A}$ over the domain listed in Table 4.1.

	Variable domain
symbol	maximum perturbation
εu	$10\,\mathrm{m/s}$
εv	$10\,\mathrm{m/s}$
εw	$10\,\mathrm{m/s}$
εp	$5\frac{\pi}{180}\,\mathrm{rad/s}$
εq	$5\frac{\pi}{180}\,\mathrm{rad/s}$
εr	$5\frac{\pi}{180}\,\mathrm{rad/s}$
$\varepsilon \phi$	$5\frac{\pi}{180}\,\mathrm{rad}$
$\varepsilon \theta$	$5\frac{\pi}{180}\,\mathrm{rad}$
$\varepsilon \psi$	$5\frac{\pi}{180}\,\mathrm{rad}$
εh	$10\,\mathrm{m}$
$\varepsilon \boldsymbol{\delta}$	$\min\left(\max_{\boldsymbol{\delta}}\left(\boldsymbol{\delta}-\boldsymbol{\delta}_r\right), \min_{\boldsymbol{\delta}}\left(\boldsymbol{\delta}_r-\boldsymbol{\delta}\right)\right)$ (see Table 4.3)
$\mathbf{g}_A$	$3\boldsymbol{\sigma}_g = 3\left[\sigma_{u_g}, \sigma_{v_g}, \ldots, \sigma_{r_g}\right]^T$ (see (2.40) and (2.34)-(2.39))

Table 4.1: A330 variable domain.

A numeric $G_{m,A}$ is given in Appendix E for a straight and level flight case, and, following the robust eigenvalue theory presented in Chapters 3.7.3 and 3.9.3, is used here to motivate the unconventional inclusion of altitude as a motion variable.

Instantaneous eigenvalues of a time-varying norm-bounded state-space model is given as

$$\sigma \pm j\omega \coloneqq \operatorname{eig}\left(A + B_p\Delta\left(I - D_{qp}\Delta\right)^{-1}C_q\right), \quad \Delta \in \mathfrak{S} \tag{4.20}$$

and is related to NLTV transient behaviour in Section 3.9.3 using $\max(\sigma)$ and $\omega_n \coloneqq \sqrt{\sigma^2 + \omega^2}$. Instantaneous eigenvalue plots are given in Figures 4.3 and 4.4 for the open-loop A330 with fixed actuators, generated using 1000 randomly generated Δ's, whose random components $\check{\delta}_i$ and $\check{\Delta}_k$ in $\mathfrak{S}$ is calculated as

$$\begin{aligned}
\check{\delta}_i &= \operatorname{rand}\left(\left\{a : a^2 < 1\right\}\right) \\
\check{\Delta}_k &= \frac{\operatorname{rand}\left(\left\{a : a^2 < 1\right\}\right)}{\operatorname{msv}\left(D_k\right)} D_k \\
D_k &\coloneqq \operatorname{rand}\left(\left\{\begin{bmatrix} m_{11} & m_{12} & \cdots & m_{1f_k} \\ m_{21} & m_{22} & \cdots & m_{2f_k} \\ \vdots & \vdots & \ddots & \vdots \\ m_{f_k1} & m_{f_k2} & \cdots & m_{f_kf_k} \end{bmatrix} : m_{ij}^2 < 1\right\}\right)
\end{aligned} \tag{4.21}$$

where $\operatorname{rand}(\mathbb{X})$ is a uniformly distributed random element in $\mathbb{X}$ and $\operatorname{msv}(X)$ is the maximum singular value of X, at the flight case defined by

$$\left(h_r, \vartheta_{cas,r}, m_A, cg_A, \phi_r, \dot{h}_r\right) = (20'000\,\text{ft}, 265\,\text{kts}, 171.5\,\text{tons}, 29\,\%\text{RC}, 0, 0) \tag{4.22}$$

and documented in Appendix E. Five of the A330 modes are identifiable in Figures 4.3 and 4.4 for the case where altitude is included as a variable, by analysing its corresponding instantaneous eigenvectors, and are listed in Table 4.2, with $\bullet$ denoting an ill-defined bound. (see [33] for aircraft modes). The calculated norm-bounded

mode	σ	ω	ω_n	$\cos\left(\arctan\left(\frlvert\omega\frrvert / -\sigma\right)\right)$
Phugoid	$\bullet$	$[\bullet, 0.199]$	$\bullet$	$[-1, 1]$
Short-period	$[-0.582, \bullet]$	$[\bullet, 1.19]$	$[\bullet, 1.32]$	$[0.421, \bullet]$
Altitude	$[\bullet, 0.350]$	$\bullet$	$\bullet$	$[-1, \bullet]$
Roll	$[-1.95, -1.92]$	0	$[1.92, 1.95]$	1
Dutch-Roll	$[-0.143, -0.106]$	$[1.12, 1.22]$	$[1.13, 1.23]$	$[0.0926, 0.124]$

Table 4.2: A330 mode summary.

state-space model is exponentially unstable in its Phugoid motion and in its altitude mode, and shows relatively small variation in its lateral roll modes compared to the remainder. Figures 4.3 and 4.4 also give the instantaneous eigenvalue plots for the case where altitude is fixed, *i.e.* $\varepsilon h = 0\,\forall t$. There is a notable difference in both the *Phugoid* and *Short-period* modes when $\varepsilon h = 0$, as well as an absent exponentially unstable *altitude mode*. Thus, if altitude is omitted from the A330 motion variables, its state-space representation will fail to include the faster exponentially unstable behaviour. Note that maximum robust exponential decay-rates and minimum robust disk eigenvalue bounds, calculated with LMI performance measures in Section

3.7.3 by iteratively increasing $\mathfrak{a}$ and reducing $\mathfrak{r}$ respectively, are also included in the instantaneous eigenvalue plots.

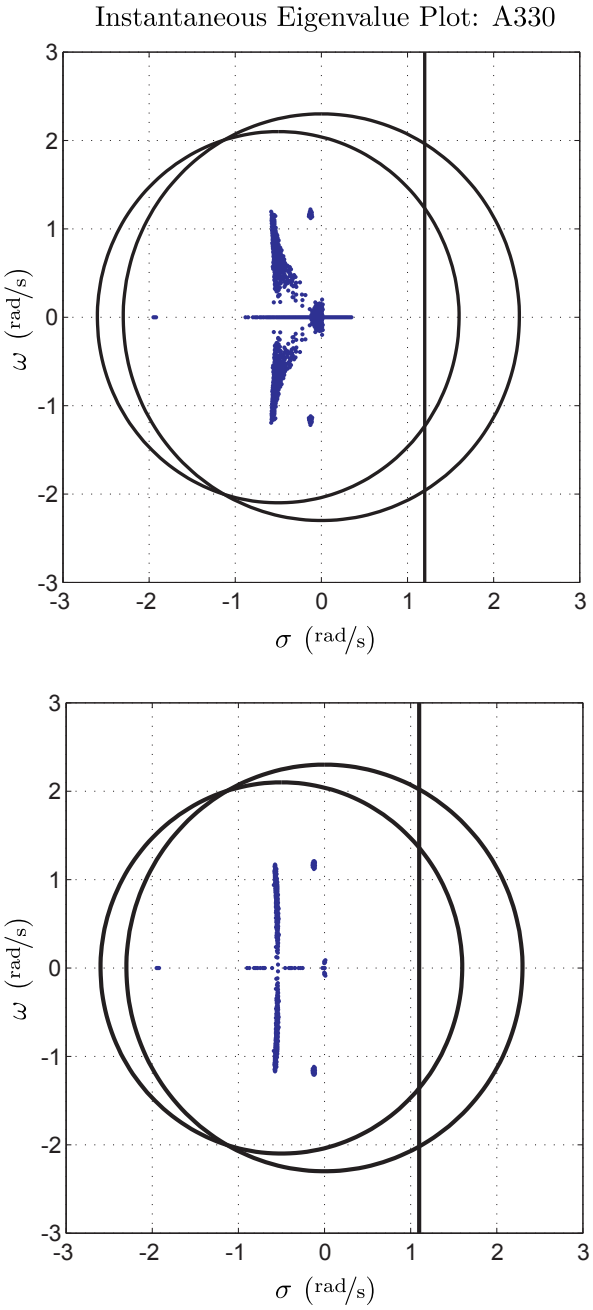

Figure 4.3: A330 open-loop instantaneous eigenvalue plot with regional eigenvalue constraints. Model: variable altitude with $\omega_n < 2.3$, $\sigma < 1.2$ and $\sqrt{(\sigma + 0.50)^2 + \omega^2} < 2.1$ (top); fixed altitude with $\omega_n < 2.3$, $\sigma < 1.1$ and $\sqrt{(\sigma + 0.50)^2 + \omega^2} < 2.1$ (bottom).

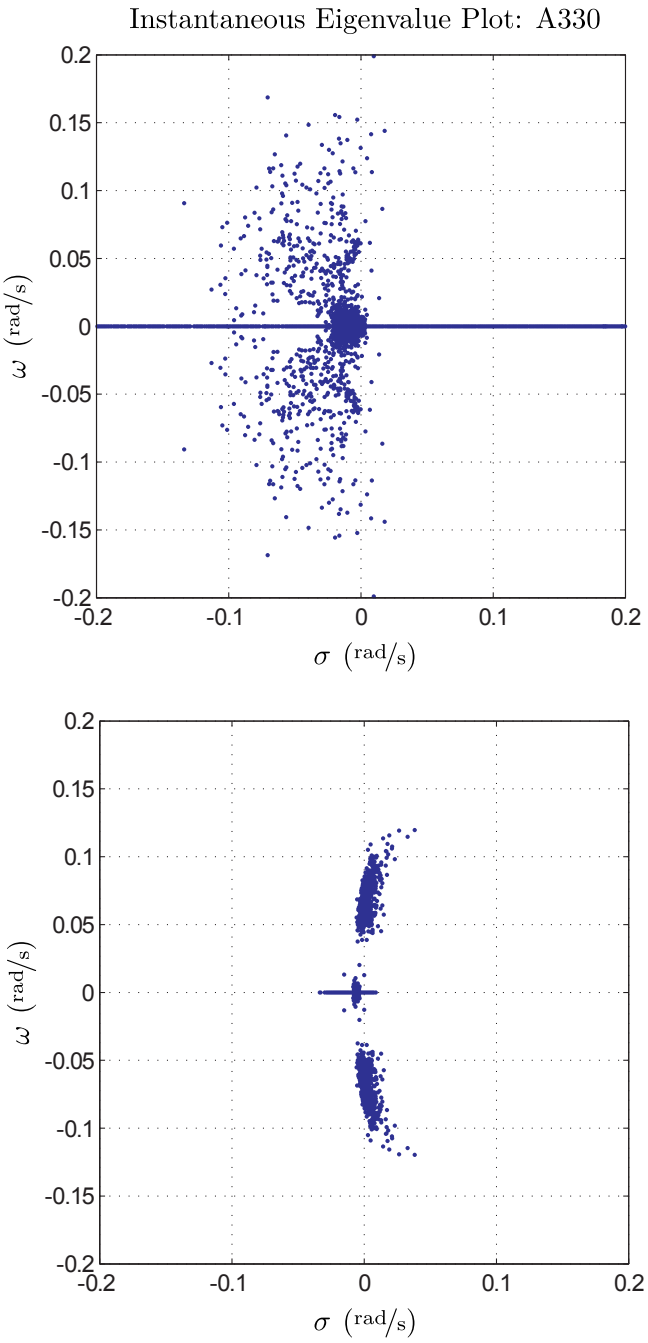

Figure 4.4: A330 open-loop instantaneous eigenvalue plot of Phugoid mode. Model: variable altitude top); fixed altitude (bottom).

4.2.1.3 Actuators

A330 actuator operating ranges and nominal mechanical properties are given in Table 4.3. A330 actuators possess uncertainty in both their bandwidths and their steady-state gains, and are specified as 5% for control surface actuators and 10%

$\boldsymbol{\delta}$	range	slew-rate ς	time-constant τ
δ_a	$[-0.368, 0.299]rad$	$0.698\,^{\text{rad}}/_{\text{s}}$	$0.07\,\text{s}$
δ_h	$[-0.240, 3.23\times10^{-2}]rad$	$5.24\times10^{-3}\,^{\text{rad}}/_{\text{s}}$	$0.1\,\text{s}$
δ_e	$[-0.524, 0.262]rad$	$0.524\,^{\text{rad}}/_{\text{s}}$	$0.07\,\text{s}$
δ_r	$[-0.134, 0.134]rad$	$0.524\,^{\text{rad}}/_{\text{s}}$	$0.025\,\text{s}$
δ_s	$[-0.595, 0]rad$	$0.698\,^{\text{rad}}/_{\text{s}}$	$0.05\,\text{s}$
δ_t	$[0, 0.153]/\text{N}kg.m.s^{-2}$	∞	$1.5\,\text{s}$

Table 4.3: A330 control surface and thrust operating ranges and nominal mechanical properties.

for thrusters. A norm-bounded state-space descriptions of the control surface actuators and thrusters are developed, which describes the dynamics associated with the uncertain bandwidths and steady state-gains.

A first-order actuator with an NLTV uncertain bandwidth and input gain is given as

$$\dot{x}_\kappa = \begin{bmatrix} -\beta(\boldsymbol{\rho}) & \beta(\boldsymbol{\rho})\,\mu(\boldsymbol{\rho}) \end{bmatrix} \begin{bmatrix} x_\kappa \\ u_\kappa \end{bmatrix}, \quad \boldsymbol{\rho} \in \mathfrak{D}_\rho \tag{4.23}$$

where $x_\kappa \in \mathbb{R}^1$ is the *actuator state* and *actuator output*, $u_\kappa \in \mathbb{R}^1$ the *actuator input*, $\beta : \mathbb{R}^{n_\rho} \mapsto \mathbb{R}^1$ the NLTV uncertain bandwidth with $\beta(\boldsymbol{\rho}) \in \left(\underline{\beta}, \overline{\beta}\right)$ for every $\boldsymbol{\rho} \in \mathfrak{D}_\rho$ and $\mu : \mathbb{R}^{n_\rho} \mapsto \mathbb{R}^1$ the NLTV uncertain input gain with $\mu(\boldsymbol{\rho}) \in \left(\underline{\mu}, \overline{\mu}\right)$ for every $\boldsymbol{\rho} \in \mathfrak{D}_\rho$. The norm-bounded state-space description of (4.23) is given as

$$\dot{x}_h = \begin{bmatrix} -\check{\beta}(1+f_\beta\delta_1) & \check{\beta}\check{\mu}(1+f_\beta\delta_1)(1+f_\mu\delta_2) \end{bmatrix} \begin{bmatrix} x_h \\ u_h \end{bmatrix} \tag{4.24}$$
$$\{\delta_1, \delta_2\} \subset \boldsymbol{\Delta}$$

where

$$\check{\beta} := \frac{\overline{\beta}+\underline{\beta}}{2}, \quad f_\beta := 1 - \frac{2\underline{\beta}}{\overline{\beta}+\underline{\beta}}, \quad \check{\mu} := \frac{\overline{\mu}+\underline{\mu}}{2}, \quad f_\mu := 1 - \frac{2\underline{\mu}}{\overline{\mu}+\underline{\mu}} \tag{4.25}$$

By expanding (4.24) as

$$\begin{aligned} \dot{x}_h &= -\check{\beta}(1+f_\beta\delta_1)\,x_h + \check{\beta}\check{\mu}(1+f_\beta\delta_1)(1+f_\mu\delta_2)\,u_h \\ &= -\check{\beta}x_h + \check{\beta}\check{\mu}u_h - \check{\beta}f_\beta\delta_1 x_h + \check{\beta}\check{\mu}(f_\mu\delta_2 + f_\beta\delta_1 + f_\beta f_\mu\delta_1\delta_2)\,u_h \\ &= -\check{\beta}x_h + \check{\beta}\check{\mu}u_h + \delta_1\check{\beta}f_\beta(-x_h + \check{\mu}u_h + \check{\mu}f_\mu\delta_2 u_h) + \check{\beta}\check{\mu}f_\mu\delta_2 u_h \end{aligned} \tag{4.26}$$

we may find its standard form via inspection as

$$\begin{bmatrix} \dot{x}_h \\ \mathbf{q}_h \end{bmatrix} = \left[\begin{array}{ccc} -\check{\beta} & \check{\beta}\check{\mu} & \begin{bmatrix} \check{\beta}f_\beta & \check{\beta}\check{\mu} \end{bmatrix} \\ \begin{bmatrix} -1 \\ 0 \end{bmatrix} & \begin{bmatrix} \check{\mu} \\ f_\mu \end{bmatrix} & \begin{bmatrix} 0 & \check{\mu} \\ 0 & 0 \end{bmatrix} \end{array}\right] \begin{bmatrix} x_h \\ u_h \\ \mathbf{p}_h \end{bmatrix} \tag{4.27}$$
$$\mathbf{p}_h = \begin{bmatrix} \delta_1 & 0 \\ 0 & \delta_2 \end{bmatrix}_h \mathbf{q}_h, \quad \begin{bmatrix} \delta_1 & 0 \\ 0 & \delta_2 \end{bmatrix}_h \in \boldsymbol{\Delta}$$

Furthermore, we may combine multiple such first-order models into a single norm-bounded state-space model, and is given as

$$\begin{bmatrix} \dot{\mathbf{x}}_h \\ \mathbf{q}_h \end{bmatrix} = \begin{bmatrix} -\mathrm{diag}\left(\check{\boldsymbol{\beta}}\right) & \mathrm{diag}\left(\check{\boldsymbol{\beta}}\right)\mathrm{diag}\left(\check{\boldsymbol{\mu}}\right) & \mathrm{diag}\left(\check{\boldsymbol{\beta}}\right)\begin{bmatrix} \mathrm{diag}\left(\mathbf{f}_\beta\right) & \mathrm{diag}\left(\check{\boldsymbol{\mu}}\right) \end{bmatrix} \\ \begin{bmatrix} -I \\ 0 \end{bmatrix} & \begin{bmatrix} \mathrm{diag}\left(\check{\boldsymbol{\mu}}\right) \\ \mathrm{diag}\left(\mathbf{f}_\mu\right) \end{bmatrix} & \begin{bmatrix} 0 & \mathrm{diag}\left(\check{\boldsymbol{\mu}}\right) \\ 0 & 0 \end{bmatrix} \end{bmatrix} \begin{bmatrix} \mathbf{x}_h \\ \mathbf{u}_h \\ \mathbf{p}_h \end{bmatrix}$$
$$\mathbf{p}_h = \Delta_h \mathbf{q}_h, \quad \Delta_h \in \boldsymbol{\Delta} \tag{4.28}$$

where Δ_h is diagonal and $\mathbf{z}_h$ may be included in (4.28) as the performance output

$$\mathbf{z}_h \coloneqq \begin{bmatrix} \mathbf{x}_h \\ \dot{\mathbf{x}}_h \end{bmatrix} \in \mathfrak{D}_{z_h} \tag{4.29}$$

where $\dot{\mathbf{x}}_h$ is readily available as a combination of the inputs, *i.e.*

$$\dot{\mathbf{x}}_h = -\mathrm{diag}\left(\check{\boldsymbol{\beta}}\right)\mathbf{x}_h + \mathrm{diag}\left(\check{\boldsymbol{\beta}}\right)\mathrm{diag}\left(\check{\boldsymbol{\mu}}\right)\mathbf{u}_h + \mathrm{diag}\left(\check{\boldsymbol{\beta}}\right)\begin{bmatrix} \mathrm{diag}\left(\mathbf{f}_\beta\right) & \mathrm{diag}\left(\check{\boldsymbol{\mu}}\right) \end{bmatrix}\mathbf{p}_h \tag{4.30}$$

It follows that the A330 actuators may be included with (4.28) and (4.29) as

$$\begin{bmatrix} \dot{\mathbf{x}} \\ \mathbf{z} \\ \mathbf{q} \end{bmatrix}_{a,A} = G_{a,A}\begin{bmatrix} \mathbf{x} \\ \mathbf{u} \\ \mathbf{p} \end{bmatrix}_{a,A} = \begin{bmatrix} A & B_u & B_p \\ C_z & D_{zu} & D_{zp} \\ C_q & D_{qu} & D_{qp} \end{bmatrix}_{a,A}\begin{bmatrix} \mathbf{x} \\ \mathbf{u} \\ \mathbf{p} \end{bmatrix}_{a,A} \tag{4.31}$$
$$\mathbf{p}_{a,A} = \Delta_{a,A}\mathbf{q}_{a,A}, \quad \Delta_{a,A} \in \boldsymbol{\Delta}$$
$$\mathbf{z}_{a,A} \in \mathfrak{D}_{z_a}$$

where subscript a, A denotes the actuators of aircraft A,

$$\mathbf{x}_{a,A} \coloneqq \mathbf{x}_h, \quad \mathbf{z}_{a,A} \coloneqq \mathbf{z}_h, \quad \mathbf{q}_{a,A} \coloneqq \mathbf{q}_h, \quad \mathbf{u}_{a,A} \coloneqq \mathbf{u}_h,$$
$$\mathbf{p}_{a,A} \coloneqq \mathbf{p}_h, \quad \Delta_{a,A} \coloneqq \Delta_h, \quad \mathfrak{D}_{z_a} \coloneqq \mathfrak{D}_{z_h} \tag{4.32}$$

and parameters are given as

$$\check{\boldsymbol{\beta}} = \begin{bmatrix} \frac{1}{\tau_a} & \frac{1}{\tau_h} & \cdots & \frac{1}{\tau_{ts}} \end{bmatrix}^T, \ \check{\boldsymbol{\mu}} = \mathbf{1}_{8\times 1}, \ \mathbf{f}_\beta = \mathbf{f}_\mu = \begin{bmatrix} f_c\mathbf{1}_{6\times 1} \\ f_t\mathbf{1}_{2\times 1} \end{bmatrix}, \ f_c = 0.05, \ f_t = 0.1 \tag{4.33}$$

Actuator performance output amplitude and slew-rate operating ranges may be specified with $\mathfrak{D}_{z_{a,A}}$ in (4.29) as described in Table 4.3.

4.2.1.4 Aircraft relative position kinematics

The norm-bounded state-space description of the aircraft relative position kinematics is similar to that of the individual aircraft flight mechanics. However, the relative position performance output $\mathbf{z}_{k,B}$ is used to specify an ellipsoid that fits inside the

considered boom envelope, due to the awkward shape of the boom envelope. Ellipsoidal variable regions are inherent in the LMI framework when quadratic measures are used, such as variance, which is apparent in the approach to local stability in Section 3.6.2.

The aircraft relative position kinematics is calculated as $\mathcal{G}_{k,B}$ over variable domain $\mathfrak{D}_{k,B}$ in

$$\begin{bmatrix} \dot{\mathbf{x}}_{k,B} \\ \mathbf{z}_{k,B} \\ \varepsilon h_R \\ \mathbf{q}_{k,B} \end{bmatrix} = \mathcal{G}_{k,B} \begin{bmatrix} \mathbf{x}_{k,B} \\ \mathbf{x}_T \\ \mathbf{x}_R \\ \mathbf{p}_{k,B} \end{bmatrix}$$

$$\mathbf{p}_{k,B} = \Delta_{k,B}\mathbf{q}_{k,B}, \quad \Delta_{k,B} \in \mathbf{\Delta}, \quad \begin{bmatrix} \mathbf{x}_{k,B} \\ \mathbf{x}_T \\ \mathbf{x}_R \end{bmatrix} \in \mathfrak{D}_{k,B}\, \forall t \tag{4.34}$$

where subscripts k and B denote relative position kinematics and the boom respectively, $\mathbf{x}_{k,B} \in \mathbb{R}^{3\times 1}$ is chosen as the perturbation ε of the motion variables defined by (2.21), and is given as

$$\mathbf{x}_{k,B} \coloneqq \varepsilon\mathbf{b} = \mathbf{b} - \mathbf{b}_r = \begin{bmatrix} \varepsilon x_b \\ \varepsilon y_b \\ \varepsilon z_b \end{bmatrix} \tag{4.35}$$

$\mathbf{x}_{T/R} \in \mathbb{R}^{10\times 1}$ is the state of the tanker/receiver defined by (4.16) and $\mathbf{z}_{k,B}$ is included as a performance output.

The aircraft relative kinematic equations (2.19) and (2.22) are used by the algorithm presented in Appendix B.1 to calculate $\mathcal{G}_{k,B}$ over the domain listed in Table 4.1 and the disconnect envelope listed in Table 2.1.

Similar to the aircraft mechanics, we need to constrain the input variables

$$\begin{bmatrix} \mathbf{x}_T^T & \mathbf{x}_R^T & \mathbf{x}_{k,B}^T \end{bmatrix}^T \tag{4.36}$$

to the domain $\mathfrak{D}_{k,B}$ in order for the model to remain a valid description of the system and that aircraft relative position regulation is achieved according to the specifications in Section 1.3. The domain of $\mathbf{x}_T$ and $\mathbf{x}_R$ is equally defined by $\mathfrak{D}_{k,B}$ and $\mathfrak{D}_{m,A}$, thus is readily constrained with $\mathbf{z}_{m,A}$ in (4.19).

Due to the non-linear relationship between the boom variables $\begin{bmatrix} \lambda & \sigma & \chi \end{bmatrix}^T$ in Section 2.2.3.2 and the nozzle variables $\begin{bmatrix} x_b & y_b & z_b \end{bmatrix}^T$ in (2.19), the non-linear constraints on the nozzle variables, illustrated in Figure 2.7 as the boom envelope, is represented by an ellipsoidal constraint. An ellipsoidal constraint includes joint variation of nozzle variables, which is absent in a rectangular constraint. LMI optimisation is used to find the ellipsoid of maximum size that fits within the boom envelope, and is formulated as follows.

A filled ellipsoid with non-zero volume is defined as [13, pp.11-12]

$$\mathcal{E} \coloneqq \left\{ \mathbf{a} \in \mathbb{R}^{3\times 1} \,\middle|\, \mathbf{a} = C\mathbf{b} + \mathbf{a}_0,\ \mathbf{b}^T\mathbf{b} < 1,\ \{\mathbf{b}, \mathbf{a}_0\} \subset \mathbb{R}^{3\times 1},\ C^TC > 0,\ C \in \mathbb{R}^{3\times 3} \right\} \tag{4.37}$$

which expresses an ellipsoid as a scaled, rotated and then displaced unit sphere, and its volume is given by [13, pp.12]

$$\text{vol}\left(\mathcal{E}\right) = \det\left(CC^T\right)^{\frac{1}{2}}\gamma \tag{4.38}$$

where γ is the volume of the unit sphere, *i.e.* the volume is proportional to the squared product of the ellipsoid principal axes. The boom envelope exterior space is defined as $\mathcal{S} \in \mathbb{R}^{3\times 1}$. It follows that, for the ellipsoid to fit entirely inside the boom envelope

$$\mathcal{E} \cap \mathcal{S} = \emptyset \tag{4.39}$$

which we formulate as

$$\left(\mathbf{s} - \mathbf{a}_0\right)^T C^{-T} C^{-1} \left(\mathbf{s} - \mathbf{a}_0\right) > 1 \quad \forall \mathbf{s} \in \mathcal{S} \tag{4.40}$$

i.e. we transform the ellipsoid and all the points $(\mathbf{s} - \mathbf{a}_0)$ exterior to the centred boom envelope with C^{-1}, such that the ellipsoid is a unit sphere centred at the origin and require that $C^{-1}\left(\mathbf{s} - \mathbf{a}_0\right)$ be outside the unit sphere for all $\mathbf{s} \in \mathcal{S}$.

In order to formulate $\max\{\text{R.H.S. (4.38)}\}$ s.t. (4.40) as a numerically tractable convex optimisation problem, a finite set $\mathcal{J} = \{\mathbf{s}_1, \mathbf{s}_2, \ldots, \mathbf{s}_N\}$ has to be constructed to represent $\mathcal{S}$. Furthermore, we use the tanker body-frame T as the reference, choose $\mathbf{a}_0$ at the centre of the boom envelope, *i.e.* at the nozzle for $\varepsilon\lambda = 0$, $\varepsilon\sigma = 0$ and $\varepsilon\chi = 0$, and choose

$$C = \begin{bmatrix} \cos\sigma_r & 0 & \sin\sigma_r \\ 0 & 1 & 0 \\ -\sin\sigma_r & 0 & \cos\sigma_r \end{bmatrix} \text{diag}\left(\sigma_1, \sigma_2, \sigma_3\right) \tag{4.41}$$

which scales the sphere with σ_1, σ_2 and σ_3 along its axes into an ellipsoid and the rotates it by σ_r clockwise about $\mathbf{b}_2$ and its origin for a proposed fit.[3] By choosing the rotation of the ellipsoid principal axes, as is done in (4.41), and including samples of the centres of each of the 6 surfaces of the boom envelope in $\mathcal{J}$, C will not be such that the ellipsoid passes through the holes in the finite sample set towards infinity to maximise the volume. Finally, we make the substitution

$$\begin{aligned} R &\coloneqq C^{-T}C^{-1} \\ &= \begin{bmatrix} \cos\sigma_r & 0 & \sin\sigma_r \\ 0 & 1 & 0 \\ -\sin\sigma_r & 0 & \cos\sigma_r \end{bmatrix} \text{diag}\left(\frac{1}{\sigma_1^2}, \frac{1}{\sigma_2^2}, \frac{1}{\sigma_3^2}\right) \begin{bmatrix} \cos\sigma_r & 0 & \sin\sigma_r \\ 0 & 1 & 0 \\ -\sin\sigma_r & 0 & \cos\sigma_r \end{bmatrix}^T \\ &= \begin{bmatrix} \cos\sigma_r & 0 & \sin\sigma_r \\ 0 & 1 & 0 \\ -\sin\sigma_r & 0 & \cos\sigma_r \end{bmatrix} D \begin{bmatrix} \cos\sigma_r & 0 & \sin\sigma_r \\ 0 & 1 & 0 \\ -\sin\sigma_r & 0 & \cos\sigma_r \end{bmatrix}^T \end{aligned} \tag{4.42}$$

where

$$D \coloneqq \text{diag}\left(d_1, d_2, d_3\right) \tag{4.43}$$

3. It follows from Singular Value Decomposition (SVD) that $C = U\Sigma V^T$, where U and V^T are orthonormal matrices (rotation) and $\Sigma = \text{diag}\left(\sigma_1, \sigma_1, \ldots, \sigma_n\right)$, for C square, scales the components of its input [70, pp.537-540].

and formulate the problem of finding the maximum volume ellipsoid as LMI optimisation problem

$$\begin{aligned}
&\min_{D=\mathrm{diag}(d_1,d_2,d_3)>0} \mathrm{tr}\,(D) && \text{s.t.}\\
&(\mathbf{s}_1-\mathbf{a}_0)^T R\,(\mathbf{s}_1-\mathbf{a}_0) &> 1\\
&(\mathbf{s}_2-\mathbf{a}_0)^T R\,(\mathbf{s}_2-\mathbf{a}_0) &> 1\\
&\qquad\vdots\\
&(\mathbf{s}_N-\mathbf{a}_0)^T R\,(\mathbf{s}_N-\mathbf{a}_0) &> 1\\
&\begin{bmatrix} \cos\sigma_r & 0 & \sin\sigma_r \\ 0 & 1 & 0 \\ -\sin\sigma_r & 0 & \cos\sigma_r \end{bmatrix} D \begin{bmatrix} \cos\sigma_r & 0 & \sin\sigma_r \\ 0 & 1 & 0 \\ -\sin\sigma_r & 0 & \cos\sigma_r \end{bmatrix}^T &= R\\
&\mathbf{s}_i &\in \mathcal{J}
\end{aligned} \tag{4.44}$$

where the objective

$$\min\ \mathrm{tr}\,(D) \Longleftrightarrow \min\ \left(\frac{1}{\sigma_1^2}+\frac{1}{\sigma_2^2}+\frac{1}{\sigma_3^2}\right) \tag{4.45}$$

is used to indirectly achieve

$$\max\ \mathrm{vol}\,(\mathcal{E}) \Longleftrightarrow \max\ \det\left(CC^T\right)^{\frac{1}{2}}\gamma \Longleftrightarrow \max\ \left(\sigma_1^2\sigma_2^2\sigma_3^2\right)^{\frac{1}{2}}\gamma \Longleftrightarrow \max\ |\sigma_1\sigma_2\sigma_3| \tag{4.46}$$

It follows from the preservation of LMIs under diagonalisation [4] that the N LMIs in (4.44) may be replaced by

$$\mathrm{diag}\left(\mathrm{diag}\left(\left(\begin{bmatrix}\mathbf{s}_1 & \mathbf{s}_2 & \cdots & \mathbf{s}_N\end{bmatrix}-\mathbf{a}_0\right)^T R\left(\begin{bmatrix}\mathbf{s}_1 & \mathbf{s}_2 & \cdots & \mathbf{s}_N\end{bmatrix}-\mathbf{a}_0\right)\right)\right) > I \tag{4.47}$$

The calculated ellipsoid is illustrated in Figure 4.5, where $\mathcal{J}$ contains 200 randomly generated samples over the boom envelope surface, including the surface centres mentioned above. Following the synthesis of D in (4.44), the ellipsoid representation of the boom constraint is given by

$$\|\mathbf{z}_{k,B}\|_2^2 = \mathbf{z}_{k,B}^T\mathbf{z}_{k,B} < 1 \tag{4.48}$$

where

$$\mathbf{z}_{k,B} = \mathcal{C}_{z,k,B}\mathbf{x}_{k,B} = D^{\frac{1}{2}}\begin{bmatrix} \cos\sigma_r & 0 & \sin\sigma_r \\ 0 & 1 & 0 \\ -\sin\sigma_r & 0 & \cos\sigma_r \end{bmatrix}^T \mathbf{x}_{k,B} \tag{4.49}$$

i.e.

$$\mathbf{z}_{k,B} \in \mathfrak{D}_{z_{k,B}}, \quad \mathfrak{D}_{z_{k,B}} = \left\{\mathbf{x} : \mathbf{x}^T\mathbf{x} < 1\right\} \tag{4.50}$$

4. This property follows directly from the scalar definition of LMIs.

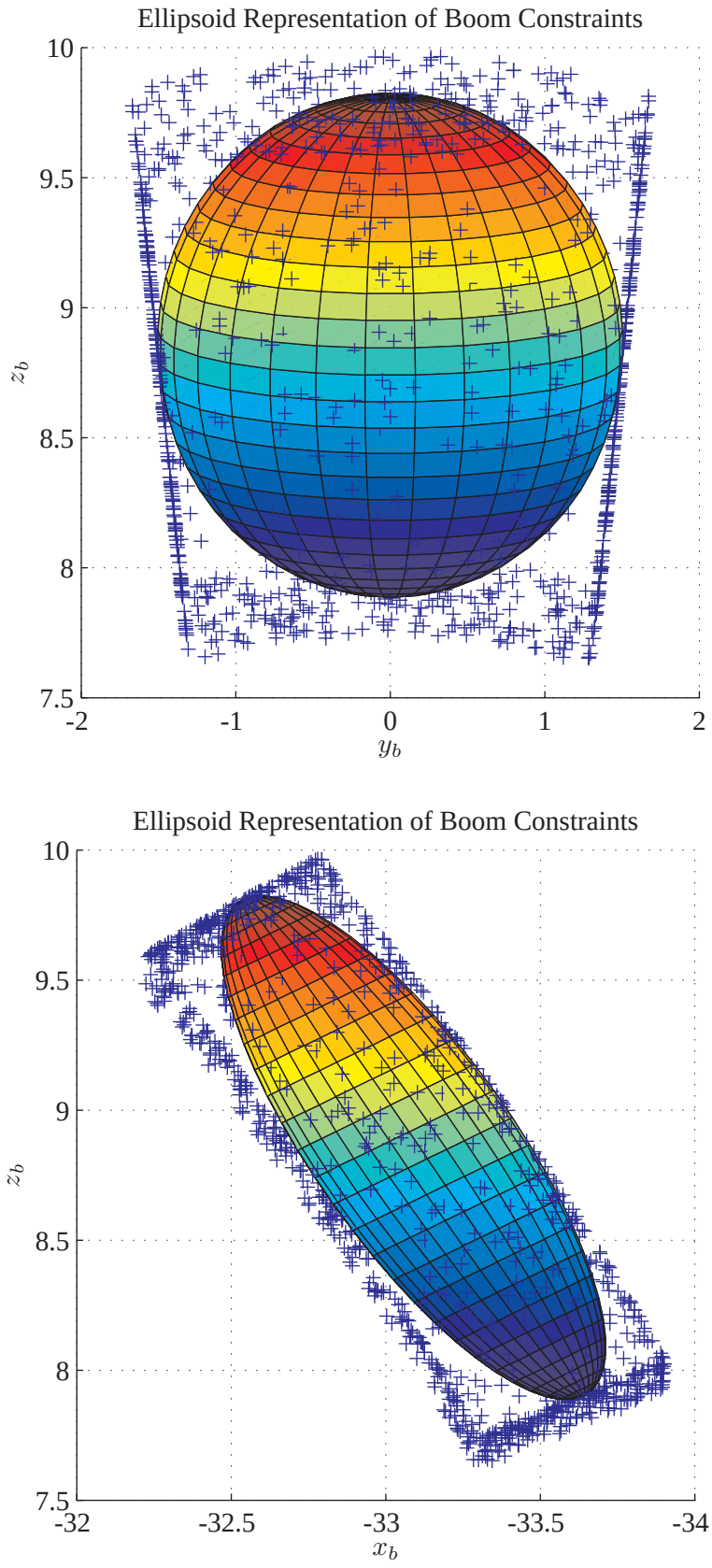

Figure 4.5: Two separate views of the ellipsoid representation of the boom constraints for the contact envelope.

4.2.1.5 Turbulence

The state-space representations of *Dryden* turbulence shaping-filters (2.34)-(2.39) may be derived with the inverse *Laplace* transform, and is given as

$$\dot{x}_{u_g} = -\frac{\vartheta}{l_g} x_{u_g} + \sigma_g \sqrt{\frac{2\vartheta}{l_g}} \eta_{u_g}, \tag{4.51}$$
$$u_g = x_{u_g}$$

$$\dot{\mathbf{x}}_{v,w_g} = \begin{bmatrix} 0 & 1 \\ -\left(\frac{\vartheta}{l_g}\right)^2 & -2\frac{\vartheta}{l_g} \end{bmatrix} \mathbf{x}_{v,w_g} + \begin{bmatrix} -\sigma_g \sqrt{\frac{l_g}{\vartheta}} \\ \sigma_g \sqrt{\frac{3\vartheta}{l_g}} \end{bmatrix} \eta_{v,w_g}, \tag{4.52}$$
$$v, w_g = \begin{bmatrix} 0 & 1 \end{bmatrix} \mathbf{x}_{v,w_g}$$

$$\dot{x}_{p_g} = -\frac{\pi\vartheta}{4b} x_{p_g} + \left(\frac{\sigma_g \pi}{4b} \left(\frac{0.8\pi\vartheta}{l_g} \right)^{\frac{1}{2}} \left(\frac{\pi l_g}{4b} \right)^{\frac{1}{6}} \right) \eta_{p_g}, \tag{4.53}$$
$$p_g = x_{p_g}$$

$$\dot{x}_{q_g} = -\frac{\pi\vartheta}{4b} x_{q_g} + \frac{\pi}{4b} w_g, \quad q_g = \dot{x}_{q_g} \tag{4.54}$$

$$\dot{x}_{r_g} = -\frac{\pi\vartheta}{3b} x_{r_g} + \frac{\pi}{3b} v_g, \quad r_g = \dot{x}_{r_g} \tag{4.55}$$

and, for fixed airspeed ϑ and fixed altitude, is compactly written as

$$\begin{bmatrix} \dot{\mathbf{x}} \\ \mathbf{g} \end{bmatrix}_{\mathcal{D},A} = \begin{bmatrix} \mathcal{A} & \mathcal{B}_w \\ \mathcal{C}_g & 0 \end{bmatrix}_{\mathcal{D},A} \begin{bmatrix} \mathbf{x} \\ \mathbf{w} \end{bmatrix}_{\mathcal{D},A} \tag{4.56}$$

where [5]

$$\mathbf{x}_{\mathcal{D},A} \coloneqq \begin{bmatrix} x_{u_g} & \mathbf{x}_{v_g}^T & x_{w_g} & x_{p_g} & x_{q_g} & x_{r_g} \end{bmatrix}_A^T, \quad \mathbf{w}_{\mathcal{D},A} \coloneqq \begin{bmatrix} \eta_{u_g} & \eta_{v_g} & \eta_{w_g} & \eta_{p_g} \end{bmatrix}^T \tag{4.57}$$

Furthermore, the Dryden turbulence state-space models for both tanker and receiver are concatenated into a single IFR Dryden turbulence model, given as

$$\begin{bmatrix} \dot{\mathbf{x}} \\ \mathbf{g} \end{bmatrix}_{\mathcal{T}} = \begin{bmatrix} \mathcal{A} & \mathcal{B}_w \\ \mathcal{C}_g & 0 \end{bmatrix}_{\mathcal{T}} \begin{bmatrix} \mathbf{x} \\ \mathbf{w} \end{bmatrix}_{\mathcal{T}} \tag{4.58}$$

where

$$\mathbf{x}_{\mathcal{T}} \coloneqq \begin{bmatrix} \mathbf{x}_{\mathcal{D},T} \\ \mathbf{x}_{\mathcal{D},R} \end{bmatrix}, \ \mathbf{g}_{\mathcal{T}} \coloneqq \begin{bmatrix} \mathbf{g}_{\mathcal{D},T} \\ \mathbf{g}_{\mathcal{D},R} \end{bmatrix},$$
$$\mathbf{w}_{\mathcal{T}} \coloneqq \mathrm{chol}\left(V_{\mathcal{T}}\right)^{-T} \begin{bmatrix} \mathbf{w}_{\mathcal{D},T} \\ \mathbf{w}_{\mathcal{D},R} \end{bmatrix}, \ \mathbb{E}\left\{\mathbf{w}_{\mathcal{T}} \mathbf{w}_{\mathcal{T}}^T\right\} = \uparrow(t)\, I \tag{4.59}$$

5. The more conventional $\mathbf{w}$ notation is used, rather than $\boldsymbol{\eta}$, to express state-space white noise input.

and

$$\mathcal{A}_{\mathcal{T}} = \begin{bmatrix} \mathcal{A}_{\mathcal{D}} & 0 \\ 0 & \mathcal{A}_{\mathcal{D}} \end{bmatrix}, \mathcal{B}_{w,\mathcal{T}} = \begin{bmatrix} \mathcal{B}_{\mathcal{D}} & 0 \\ 0 & \mathcal{B}_{\mathcal{D}} \end{bmatrix} \text{chol}\left(V_{\mathcal{T}}\right)^T = \widetilde{\mathcal{B}}_{\mathcal{T}} \text{chol}\left(V_{\mathcal{T}}\right)^T,$$
$$\mathcal{C}_{g,\mathcal{T}} = \begin{bmatrix} \mathcal{C}_{g,\mathcal{D}} & 0 \\ 0 & \mathcal{C}_{g,\mathcal{D}} \end{bmatrix} \tag{4.60}$$

T denotes the tanker, R denotes the receiver and $\text{chol}\left(V_{\mathcal{T}}\right)$ is the *Cholesky factorisation* of white noise intensity $V_{\mathcal{T}}$, *i.e.* $V_{\mathcal{T}} = \text{chol}\left(V_{\mathcal{T}}\right)^T \text{chol}\left(V_{\mathcal{T}}\right) > 0$. $V_{\mathcal{T}}$ is used to include the similarity/correlation between tanker and receiver turbulence, as formulated in Section 2.5.2. The intensity is calculated by solving the Riccati equation

$$\mathcal{A}_{\mathcal{T}} Q_{\mathcal{T}} + Q_{\mathcal{T}} \mathcal{A}_{\mathcal{T}}^T + \widetilde{\mathcal{B}}_{\mathcal{T}} V_{\mathcal{T}} \widetilde{\mathcal{B}}_{\mathcal{T}}^T = 0 \tag{4.61}$$

where some of the elements in $Q_{\mathcal{T}} = \mathbb{E}\left(\mathbf{x}_{\mathcal{T}} \mathbf{x}_{\mathcal{T}}^T\right)$ is fixed at known values. The Riccati equation is recast as an LMI optimisation problem, given by

$$\max_{V_{\mathcal{T}} \in \mathbb{S}^8_{++}, Q_{\mathcal{T}} \in \mathbb{S}^{16}_{++}} \lambda \quad \text{s.t.}$$
$$\lambda I < \mathcal{A}_{\mathcal{T}} Q_{\mathcal{T}} + Q_{\mathcal{T}} \mathcal{A}_{\mathcal{T}}^T + \widetilde{\mathcal{B}}_{\mathcal{T}} V_{\mathcal{T}} \widetilde{\mathcal{B}}_{\mathcal{T}}^T < 0$$
$$Q_{\mathcal{T}} > 0$$
$$\left(\begin{bmatrix} I_4 & 0_{4\times2} & 0_{4\times4} & 0_{4\times2} \\ 0_{4\times4} & 0_{4\times2} & I_4 & 0_{4\times2} \end{bmatrix} \mathcal{C}_{\mathcal{T}} \right) Q_{\mathcal{T}} \left(\begin{bmatrix} I_4 & 0_{4\times2} & 0_{4\times4} & 0_{4\times2} \\ 0_{4\times4} & 0_{4\times2} & I_4 & 0_{4\times2} \end{bmatrix} \mathcal{C}_{\mathcal{T}} \right)^T = R \tag{4.62}$$

where $R \in \mathbb{S}^8_{++}$ is fixed at a known value, used for variable elimination, and $\lambda_{sol} \approx 0$. The diagonal blocks in R is derived from (A.155) and (2.34)-(2.37) as

$$R_{11} = R_{22} = \sigma_g^2 \begin{bmatrix} I_3 & 0_{3\times1} \\ 0_{1\times3} & \left(\frac{\pi^7}{4000 b^4 l_g^2}\right)^{\frac{1}{3}} \end{bmatrix} \tag{4.63}$$

and cross-terms are given by (2.49). [6]

The turbulence spatial correlation functions in Appendix A.1.7 need to be studied further to directly include variation of ϑ and h in the model, due to the ill-defined Fourier-transform for variable ϑ and h. We indirectly include variation in (4.56) and (4.58) using multiple LTI models to represent the variation in the turbulence across a sub-domain, *i.e.* part of the flight-domain defined by Figure 1.6, and combining them into a single norm-bounded state-space model using the algorithm presented in Appendix B.1. Sub-domains are defined in Chapter 5 and the norm-bounded state-space representations of the Dryden turbulence model and the IFR turbulence model are given as

$$\begin{bmatrix} \dot{\mathbf{x}} \\ \mathbf{g} \\ \mathbf{q} \end{bmatrix}_{\mathcal{D},A} = \mathcal{G}_{\mathcal{D},A} \begin{bmatrix} \mathbf{x} \\ \mathbf{w} \\ \mathbf{p} \end{bmatrix}_{\mathcal{D},A} \tag{4.64}$$
$$\mathbf{q}_{\mathcal{D},A} = \Delta_{\mathcal{D},A} \mathbf{p}_{\mathcal{D},A}$$

6. The pitch and yaw components are inherent in R, due to their shaping-filter inputs (see (4.54) and (4.55)).

and

$$\begin{bmatrix} \dot{\mathbf{x}} \\ \mathbf{g} \\ \mathbf{q} \end{bmatrix}_{\mathcal{T}} = \mathcal{G}_{\mathcal{T}} \begin{bmatrix} \mathbf{x} \\ \mathbf{w} \\ \mathbf{p} \end{bmatrix}_{\mathcal{T}} \tag{4.65}$$
$$\mathbf{q}_{\mathcal{T}} = \Delta_{\mathcal{T}} \mathbf{p}_{\mathcal{T}}$$

This concludes the IFR Dryden turbulence state-space model.

4.2.1.6 Measurements

The A330 possesses avionics which accurately estimates selected aircraft variables, *i.e.* its motion variables, accelerations, control surface deflections and output thrust. We assume that the A330 is fitted with a radio-link, to be able to communicate its estimates to other aircraft, as well as relative position sensors and a relative position estimation algorithm, such as proposed in [66], to enable the aircraft to perform relative position regulation.

Estimates are assumed to have a bandwidth of $30\,{}^{\text{rad}}/_{\text{s}}$ and a sampling period of 10 ms, with arbitrary biases, 10% error in relative position and 1% error in aircraft variables relative to their maximum allowed perturbation. Given the integrator scheme presented in Section 4.1 to remove biases, estimation errors are represented as white noise filtered at $30\,{}^{\text{rad}}/_{\text{s}}$ with an output 3σ-bound equal to the error. The white noise intensity is calculated for a first-order LPF with bandwidth β as

$$V_{ii} = \left(\frac{2}{\omega_\beta}\right)\left(\frac{\text{error}_i}{3}\right)^2 \tag{4.66}$$

where V_{ii} is the i^{th} diagonal element of the white noise intensity matrix V, corresponding to the i^{th} error. Without loss of generality, the white noise intensity is absorbed into the noise input matrices using its Cholesky factorisation, as is done from (A.147) to (A.148) in Appendix A.2.6.

Mass and centre of mass estimation errors are assumed to be 10% of their range defined by Figure 1.5, and are represented as constant errors in the system, with no additional biases.

All estimates are available for feedback and are specified in Tables 4.4 and 4.5.

A330 estimator specifications: Parameters			
Symbols	Value	Unit	Description
ω_s	$\frac{2\pi}{10^{-3}}$	${}^{\text{rad}}/_{\text{s}}$	sample frequency
τ_d	10^{-2}	s	delay
ω_β	30	${}^{\text{rad}}/_{\text{s}}$	bandwidth

Table 4.4: A330 estimator parameter specifications.

A330 estimator specifications: Outputs				
Symbol		Error	Unit	Description
$\widehat{\mathbf{m}}$	$\widehat{u}$	10	$\times 10^{-2}\mathrm{m/s}$	linear velocity
	$\widehat{v}$	10		
	$\widehat{w}$	10		
	$\widehat{p}$	$5\frac{\pi}{180}$	$\times 10^{-2}\mathrm{rad/s}$	angular velocity
	$\widehat{q}$	$5\frac{\pi}{180}$		
	$\widehat{r}$	$5\frac{\pi}{180}$		
	$\widehat{\phi}$	$5\frac{\pi}{180}$	$\times 10^{-2}\mathrm{rad}$	orientation
	$\widehat{\theta}$	$5\frac{\pi}{180}$		
	$\widehat{\psi}$	$5\frac{\pi}{180}$		
	$\widehat{h}$	10	$\times 10^{-2}\,\mathrm{m}$	altitude
$\widehat{\boldsymbol{\delta}}$	$\widehat{\delta}_a$	0.299	$\times 10^{-2}\mathrm{rad}$	control surface deflection
	$\widehat{\delta}_h$	0.0603		
	$\widehat{\delta}_e$	0.262		
	$\widehat{\delta}_r$	0.134		
	$\widehat{\delta}_{s_p}$	0.298		
	$\widehat{\delta}_{s_s}$	0.298		
	$\widehat{\delta}_{t_p}$	0.0414	$\times 10^{-2}\mathrm{N/kg.m.s^{-2}}$	thrust
	$\widehat{\delta}_{t_s}$	0.0414		
	$\widehat{\nu}$	10	$\times 10^{-2}\mathrm{m/s}$	ground-speed
$\begin{bmatrix} I_6 \\ 0_{4\times 6} \end{bmatrix}^T \widehat{\dot{\mathbf{m}}}$	$\widehat{\dot{u}}$	0.400	$\times 10^{-2}\mathrm{m/s^2}$	linear acceleration
	$\widehat{\dot{v}}$	0.700		
	$\widehat{\dot{w}}$	4.00		
	$\widehat{\dot{p}}$	0.150	$\times 10^{-2}\mathrm{rad/s^2}$	angular acceleration
	$\widehat{\dot{q}}$	0.0500		
	$\widehat{\dot{r}}$	0.0300		
$\widehat{\mathbf{b}}$	$\widehat{x}_b$	1.26	$\times 10^{-1}\mathrm{m}$	relative position
	$\widehat{y}_b$	1.68		
	$\widehat{z}_b$	1.84		
	$\widehat{m}_B$	123	$\times 10^{-1}\mathrm{tons}$	mass
	$\widehat{cg}$	24	$\times 10^{-1}\%\mathrm{RC}$	centre of mass

Table 4.5: A330 estimator output specifications.

Estimates of IFR variables are denoted with a hat, and are related to their state-

space description as

$$\begin{aligned}
\widehat{\mathbf{m}} - \mathbf{m}_r - \mathbb{E}\left\{\widehat{\mathbf{m}} - \mathbf{m}\right\} &= \widehat{\mathbf{x}}_{m,A} = \mathbf{y}_m = e(s)\left(\mathbf{x}_{m,A} + D_{y_m\eta,A}\boldsymbol{\eta}_A\right) \\
\hat{\boldsymbol{\delta}} - \boldsymbol{\delta}_r - \mathbb{E}\left\{\hat{\boldsymbol{\delta}} - \boldsymbol{\delta}\right\} &= \widehat{\mathbf{u}}_{m,A} = \mathbf{y}_\delta = e(s)\left(\mathbf{u}_{m,A} + D_{y_\delta\eta,A}\boldsymbol{\eta}_A\right) \\
\widehat{\nu} - \nu_r - \mathbb{E}\left\{\widehat{\nu} - \nu\right\} &= \widehat{\varepsilon\nu} = y_\nu = e(s)\left(\varepsilon\nu + D_{y_\nu\eta,A}\boldsymbol{\eta}_A\right) \\
\begin{bmatrix} I_6 \\ 0_{4\times 6} \end{bmatrix}^T \left(\widehat{\dot{\mathbf{m}}} - \dot{\mathbf{m}}_r - \mathbb{E}\left\{\widehat{\dot{\mathbf{m}}} - \dot{\mathbf{m}}\right\}\right) &= \begin{bmatrix} I_6 \\ 0_{4\times 6} \end{bmatrix}^T \dot{\widehat{\mathbf{x}}}_{m,A} \\
&= \mathbf{y}_\alpha = e(s)\left(\begin{bmatrix} I_6 \\ 0_{4\times 6} \end{bmatrix}^T \dot{\mathbf{x}}_{m,A} + D_{y_\alpha\eta,A}\boldsymbol{\eta}_A\right) \\
\widehat{\mathbf{b}} - \mathbf{b}_r - \mathbb{E}\left\{\widehat{\mathbf{b}} - \mathbf{b}\right\} &= \widehat{\mathbf{x}}_{k,B} = \mathbf{y}_b = e(s)\left(\mathbf{x}_{k,B} + D_{y_b\eta,B}\boldsymbol{\eta}_B\right)
\end{aligned} \tag{4.67}$$

where $\boldsymbol{\eta}$ is a white noise vector with unknown off-diagonal elements in $\mathbb{E}\left\{\boldsymbol{\eta}\boldsymbol{\eta}^T\right\}$ and a unity diagonal, the *expected value* operator is used to include biases and $e(s)$ is the estimator transfer function with bandwidth $\omega_\beta = 30\,\text{rad/s}$ and delay $\tau_d = 10^{-2}\,\text{s}$. Note that $\mathbf{p}$ is not estimated,[7] and we set

$$\widehat{\mathbf{p}} = \mathbf{0} \tag{4.68}$$

The estimator dynamics $e(s)$ may be modelled as a first-order LPF and a Padé approximation of a time-delay (see Appendix A.2.11), although the corresponding state-space description will cause an increase in IFR model order/state-length of $53(1+n_p)$, where n_p is the order of the Padé approximation used and 53 is the total number IFR measurement outputs. The IFR sub-models in Chapters 4.2.1.2-4.2.1.5 have a total order of 55 corresponding to $\frac{n(n+1)}{2} = 1540$ scalar variables in each of the symmetric Lyapunov matrix variables Q_K and P_L in (3.118) and (3.143) respectively. Increasing the model order to 161 for $n_p = 1$, the scalar variables in Q_K and P_L increases significantly to 13041, which corresponds to an impractical solving time via SDPT3 (see Section 3.10.1). The robust eigenvalue design presented in Section 4.2.2.2 includes robustness against the influence of $e(s)$ on the remainder of the model, to which end $e(s)$ may be omitted from the model, *i.e.*

$$e(s) \approx 1 \tag{4.69}$$

Furthermore, the norm-bounded state-space description of the aircraft and relative position estimation noise is developed as follows.

The A330 aircraft estimator output is given as

$$\begin{aligned}
\mathbf{e}_A &= \mathbf{y}_{e,A} - \mathbf{e}_{A,r} \\
&= \begin{bmatrix} \mathbf{y}_m \\ \mathbf{y}_\delta \\ y_\nu \\ \mathbf{y}_\alpha \end{bmatrix}_A - \mathbf{e}_{A,r} = \begin{bmatrix} \mathbf{x}_{m,A} + D_{y_m\eta,A}\Delta_{w,A}\mathbf{w}_{e,A} \\ \mathbf{u}_{m,A} + D_{y_\delta\eta,A}\Delta_{w,A}\mathbf{w}_{e,A} \\ \varepsilon\nu + D_{y_\nu\eta,A}\Delta_{w,A}\mathbf{w}_{e,A} \\ \begin{bmatrix} I_6 & 0_{6\times 4} \end{bmatrix}\dot{\mathbf{x}}_{m,A} + D_{y_\alpha\eta,A}\Delta_{w,A}\mathbf{w}_{e,A} \end{bmatrix} - \mathbf{e}_{A,r}
\end{aligned} \tag{4.70}$$

7. The part of $\mathbf{p}_A$ representing exactly known non-linearity in the 6DoF EOM can be estimated, which will be the known non-linear function in estimated variables, *i.e.* $\left(\dot{\mathbf{p}}_A = \mathbf{f}\left(\mathbf{m}_A, \boldsymbol{\delta}_A\right)\right) \Longrightarrow \left(\dot{\widehat{\mathbf{p}}}_A = \mathbf{f}\left(\widehat{\mathbf{m}}_A, \widehat{\boldsymbol{\delta}}_A\right)\right)$, but falls outside the scope of this thesis.

where $\mathbf{w}_A$ is unit intensity white noise, Δ_w is used to include unknown off-diagonal elements in $\mathbb{E}\left\{\boldsymbol{\eta}\boldsymbol{\eta}^T\right\}$ and

$$D_{y_m\eta,A} = \begin{bmatrix} \operatorname{diag}\left(\sqrt{\frac{2}{\omega_\beta}}\frac{\max\left(\widehat{\mathbf{m}}-\mathbf{m}-\mathbb{E}\left\{\widehat{\mathbf{m}}-\mathbf{m}\right\}\right)}{3}\right) & 0_{10\times15} \\ 0_{15\times10} & 0_{15\times15} \end{bmatrix}$$

$$D_{y_\delta\eta,A} = \begin{bmatrix} 0_{10\times10} & 0_{10\times8} & 0_{10\times7} \\ 0_{8\times10} & \operatorname{diag}\left(\sqrt{\frac{2}{\omega_\beta}}\frac{\max\left(\widehat{\boldsymbol{\delta}}-\boldsymbol{\delta}-\mathbb{E}\left\{\widehat{\boldsymbol{\delta}}-\boldsymbol{\delta}\right\}\right)}{3}\right) & 0_{8\times7} \\ 0_{7\times10} & 0_{7\times8} & 0_{7\times7} \end{bmatrix}$$

$$D_{y_\nu\eta,A} = \begin{bmatrix} 0_{18\times18} & 0_{18\times1} & 0_{18\times6} \\ 0_{1\times18} & \operatorname{diag}\left(\sqrt{\frac{2}{\omega_\beta}}\frac{\max\left(\widehat{\nu}-\nu-\mathbb{E}\left\{\widehat{\nu}-\nu\right\}\right)}{3}\right) & 0_{1\times6} \\ 0_{6\times18} & 0_{6\times1} & 0_{6\times6} \end{bmatrix}$$

$$D_{y_\alpha\eta,A} = \begin{bmatrix} 0_{19\times19} & 0_{19\times6} \\ 0_{6\times19} & \operatorname{diag}\left(\sqrt{\frac{2}{\omega_\beta}}\frac{\max\left(\begin{bmatrix} I_6 & 0_{6\times4} \end{bmatrix}\left(\widehat{\mathbf{m}}-\dot{\mathbf{m}}-\mathbb{E}\left\{\widehat{\mathbf{m}}-\dot{\mathbf{m}}\right\}\right)\right)}{3}\right) \end{bmatrix}$$

Ground-speed perturbation is formulated as

$$\begin{aligned} \nu &= \sqrt{u^2+v^2+w^2} \\ \varepsilon\nu &= \sqrt{(u_r+\varepsilon u)^2+(v_r+\varepsilon v)^2+(w_r+\varepsilon w)^2}-\nu_r \end{aligned} \tag{4.71}$$

which is used to calculate a norm-bounded state-space description, similar to the flight mechanics in Section 4.2.1.2, using the algorithm presented in Appendix B.1, and is given as

$$\begin{bmatrix} \varepsilon\nu \\ \mathbf{q}_\nu \end{bmatrix} = \begin{bmatrix} C_\nu & B_{p,\nu} \\ C_{q,\nu} & D_{qp,\nu} \end{bmatrix}\begin{bmatrix} \begin{bmatrix} \varepsilon u \\ \varepsilon v \\ \varepsilon w \end{bmatrix} \\ \mathbf{p}_\nu \end{bmatrix} \tag{4.72}$$
$$\mathbf{p}_\nu = \Delta_\nu\mathbf{q}_\nu, \quad \Delta_\nu \in \boldsymbol{\Delta}$$

The norm-bounded state-space description of the unknown noise correlation is given as

$$\begin{bmatrix} \boldsymbol{\eta} \\ \mathbf{q}_w \end{bmatrix} = \begin{bmatrix} 0 & I \\ I & 0 \end{bmatrix}\begin{bmatrix} \mathbf{w} \\ \mathbf{p}_w \end{bmatrix} \tag{4.73}$$
$$\mathbf{p}_w = \Delta_w\mathbf{q}_w, \quad \Delta_w \in \boldsymbol{\Delta}$$

where Δ_w is a full matrix. (4.70), (4.72) and (4.73) is combined as the norm-bounded state-space description of the A330 aircraft estimator, and is given as

$$\begin{bmatrix} \mathbf{y} \\ \mathbf{q} \end{bmatrix}_{e,A} = \mathcal{G}_{e,A}\begin{bmatrix} \mathbf{x}_m \\ \dot{\mathbf{x}}_m \\ \mathbf{w}_e \\ \mathbf{u}_m \\ \mathbf{p}_e \end{bmatrix}_A \tag{4.74}$$
$$\mathbf{p}_{e,A} = \Delta_{e,A}\mathbf{q}_{e,A}, \quad \Delta_{e,A} \in \boldsymbol{\Delta}$$

where

$$\mathbf{q}_{e,A} = \begin{bmatrix} \mathbf{q}_\nu \\ \mathbf{q}_w \end{bmatrix}_A, \quad \mathbf{p}_{e,A} = \begin{bmatrix} \mathbf{p}_\nu \\ \mathbf{p}_w \end{bmatrix}_A,$$
$$\Delta_{e,A} = \text{blkdiag}\left(\Delta_{\nu,A}, \Delta_{w,A}\right) \tag{4.75}$$

The relative position estimator output is given as

$$\mathbf{e}_b = \mathbf{y}_b - \mathbf{e}_{b,r} = \mathbf{x}_{k,B} + D_{y_b\eta,B}\Delta_{w,B}\mathbf{w}_{e,B} - \mathbf{e}_{b,r} \tag{4.76}$$

and is combined with (4.73) as the norm-bounded state-space description of the relative position estimator, given as

$$\begin{bmatrix} \mathbf{y} \\ \mathbf{q} \end{bmatrix}_{e,B} = \mathcal{G}_{e,B} \begin{bmatrix} \mathbf{x}_{k,B} \\ \mathbf{w}_{e,B} \\ \mathbf{p}_{e,B} \end{bmatrix}$$
$$\mathbf{p}_{e,B} = \Delta_{e,B}\mathbf{q}_{e,B}, \quad \Delta_{e,B} \in \mathbf{\Delta} \tag{4.77}$$

where

$$\mathbf{y}_{e,B} = \mathbf{y}_b, \quad \mathbf{q}_{e,B} = \mathbf{q}_{w,B}, \quad \mathbf{p}_{e,B} = \mathbf{p}_{w,B}, \quad \Delta_{e,B} = \Delta_{w,B} \tag{4.78}$$

4.2.1.7 Comprehensive State-Space Model

IFR sub-models may be combined into a single model in a simple and straightforward manner when using the state-space description. The norm-bounded state-space description of the IFR model is given as follows.

A330 mechanics (4.15) is augmented with actuator mechanics (4.31) and estimator (4.74), resulting in the A330 norm-bounded state-space description given as

$$\begin{bmatrix} \begin{bmatrix} \dot{\mathbf{x}} \\ \mathbf{z} \\ \mathbf{q} \end{bmatrix}_{m,A} \\ \begin{bmatrix} \dot{\mathbf{x}} \\ \mathbf{z} \\ \mathbf{q} \end{bmatrix}_{a,A} \\ \begin{bmatrix} \mathbf{y} \\ \mathbf{q} \end{bmatrix}_{e,A} \end{bmatrix} = \text{blkdiag}\left(G_{m,A}, G_{a,A}, \mathcal{G}_{e,A}\right) \begin{bmatrix} \begin{bmatrix} \mathbf{x} \\ \mathbf{g} \\ \mathbf{u} \\ \mathbf{p} \end{bmatrix}_{m,A} \\ \begin{bmatrix} \mathbf{x} \\ \mathbf{u} \\ \mathbf{p} \end{bmatrix}_{a,A} \\ \begin{bmatrix} \mathbf{x}_m \\ \dot{\mathbf{x}}_m \\ \mathbf{w}_e \\ \mathbf{u}_m \\ \mathbf{p}_e \end{bmatrix}_A \end{bmatrix}$$
$$\begin{bmatrix} \mathbf{p}_{m,A} \\ \mathbf{p}_{a,A} \\ \mathbf{p}_{e,A} \end{bmatrix} = \text{blkdiag}\left(\Delta_{m,A}, \Delta_{a,A}, \Delta_{e,A}\right) \begin{bmatrix} \mathbf{q}_{m,A} \\ \mathbf{q}_{a,A} \\ \mathbf{q}_{e,A} \end{bmatrix}$$
$$\mathbf{u}_{m,A} = \mathbf{x}_{a,A}, \quad \mathbf{z}_{m,A} \in \mathfrak{D}_{z_{m,A}}, \quad \mathbf{z}_{a,A} \in \mathfrak{D}_{z_{a,A}} \tag{4.79}$$

and is compactly written as

$$\begin{bmatrix} \dot{\mathbf{x}} \\ \mathbf{z} \\ \mathbf{y} \\ \mathbf{q} \end{bmatrix}_A = G_A \begin{bmatrix} \mathbf{x} \\ \mathbf{g} \\ \mathbf{w} \\ \mathbf{u} \\ \mathbf{p} \end{bmatrix}_A = \begin{bmatrix} A & B_g & B_w & B_u & B_p \\ C_z & D_{zg} & D_{zw} & D_{zu} & D_{zp} \\ C_y & D_{yg} & D_{yw} & D_{yu} & D_{yp} \\ C_q & D_{qg} & D_{qw} & D_{qu} & D_{qp} \end{bmatrix}_A \begin{bmatrix} \mathbf{x} \\ \mathbf{g} \\ \mathbf{w} \\ \mathbf{u} \\ \mathbf{p} \end{bmatrix}_A$$
$$\mathbf{p}_A = \Delta_A \mathbf{q}_A, \quad \Delta_A \in \boldsymbol{\Delta}$$
$$\mathbf{z}_A \in \mathfrak{D}_{z_A} \tag{4.80}$$

where

$$\mathbf{x}_A \coloneqq \begin{bmatrix} \mathbf{x}_{m,A} \\ \mathbf{x}_{a,A} \end{bmatrix}, \quad \mathbf{z}_A \coloneqq \begin{bmatrix} \mathbf{z}_{m,A} \\ \mathbf{z}_{a,A} \end{bmatrix}, \quad \mathbf{y}_A \coloneqq \mathbf{y}_{e,A}, \quad \mathbf{q}_A \coloneqq \begin{bmatrix} \mathbf{q}_{m,A} \\ \mathbf{q}_{a,A} \\ \mathbf{q}_{e,A} \end{bmatrix},$$
$$\mathbf{g}_A = \mathbf{g}_{m,A}, \quad \mathbf{w}_A \coloneqq \mathbf{w}_{e,A}, \quad \mathbf{u}_A \coloneqq \mathbf{u}_{a,A}, \quad \mathbf{p}_A \coloneqq \begin{bmatrix} \mathbf{p}_{m,A} \\ \mathbf{p}_{a,A} \\ \mathbf{p}_{e,A} \end{bmatrix},$$
$$\Delta_A = \operatorname{blkdiag}\left(\Delta_{m,A}, \Delta_{a,A}, \Delta_{e,A}\right), \quad \mathfrak{D}_{z_A} = \left\{ \begin{bmatrix} \mathbf{x}_1 \\ \mathbf{x}_2 \end{bmatrix} : \mathbf{x}_1 \in \mathfrak{D}_{z_{m,A}}, \, \mathbf{x}_2 \in \mathfrak{D}_{z_{a,A}} \right\} \tag{4.81}$$

Similarly, the relative position kinematics (4.34) is augmented with the relative position estimator, given as

$$\begin{bmatrix} \begin{bmatrix} \dot{\mathbf{x}}_{k,B} \\ \mathbf{z}_{k,B} \\ \varepsilon h_R \\ \mathbf{q}_{k,B} \end{bmatrix} \\ \begin{bmatrix} \mathbf{y} \\ \mathbf{q} \end{bmatrix}_{e,B} \end{bmatrix} = \operatorname{blkdiag}\left(\mathcal{G}_{k,B}, \mathcal{G}_{e,B}\right) \begin{bmatrix} \begin{bmatrix} \mathbf{x}_{k,B} \\ \mathbf{x}_T \\ \mathbf{x}_R \\ \mathbf{p}_{k,B} \end{bmatrix} \\ \begin{bmatrix} \mathbf{x}_{k,B} \\ \mathbf{w}_{e,B} \\ \mathbf{p}_{e,B} \end{bmatrix} \end{bmatrix}$$
$$\begin{bmatrix} \mathbf{p}_{k,B} \\ \mathbf{p}_{e,B} \end{bmatrix} = \operatorname{blkdiag}\left(\Delta_{k,B}, \Delta_{e,B}\right) \begin{bmatrix} \mathbf{q}_{k,B} \\ \mathbf{q}_{e,B} \end{bmatrix}$$
$$\mathbf{z}_{k,B} \in \mathfrak{D}_{z_{k,B}} \tag{4.82}$$

The norm-bounded state-space description of the relative position kinematics in Section 2.4 is given by

$$\begin{bmatrix} \dot{\mathbf{x}}_B \\ \mathbf{z}_B \\ \varepsilon h_R \\ \mathbf{y}_B \\ \mathbf{q}_B \end{bmatrix} = \mathcal{G}_B \begin{bmatrix} \mathbf{x}_B \\ \mathbf{x}_T \\ \mathbf{x}_R \\ \mathbf{w}_B \\ \mathbf{p}_B \end{bmatrix}$$
$$\mathbf{p}_B = \Delta_B \mathbf{q}_B, \quad \Delta_B \in \boldsymbol{\Delta}$$
$$\mathbf{z}_B \in \mathfrak{D}_{z_B} \tag{4.83}$$

where

$$\mathbf{x}_B \coloneqq \mathbf{x}_{k,B}, \quad \mathbf{z}_B \coloneqq \mathbf{z}_{k,B}, \quad \mathbf{y}_B \coloneqq \mathbf{y}_{e,B}, \quad \mathbf{q}_B \coloneqq \begin{bmatrix} \mathbf{q}_{k,B} \\ \mathbf{q}_{e,B} \end{bmatrix},$$
$$\mathbf{w}_B \coloneqq \mathbf{w}_{e,B}, \quad \mathbf{p}_b \coloneqq \begin{bmatrix} \mathbf{p}_{k,B} \\ \mathbf{p}_{e,B} \end{bmatrix}, \quad \Delta_B = \mathrm{blkdiag}\left(\Delta_{k,B}, \Delta_{e,B}\right), \quad \mathfrak{D}_{z_B} = \mathfrak{D}_{z_{k,B}} \tag{4.84}$$

Now, the IFR state-space description may be obtained by combining the aircraft model (4.80), the relative position kinematics model (4.83) and the turbulence model (4.65), given as

$$\begin{bmatrix} \begin{bmatrix} \dot{\mathbf{x}} \\ \mathbf{z} \\ \mathbf{y} \\ \mathbf{q} \end{bmatrix}_T \\ \begin{bmatrix} \dot{\mathbf{x}} \\ \mathbf{z} \\ \mathbf{y} \\ \mathbf{q} \end{bmatrix}_R \\ \begin{bmatrix} \dot{\mathbf{x}}_B \\ \mathbf{z}_B \\ \varepsilon h_R \\ \mathbf{y}_B \\ \mathbf{q}_B \end{bmatrix} \\ \begin{bmatrix} \dot{\mathbf{x}}_\mathcal{T} \\ \mathbf{g}_T \\ \mathbf{g}_R \\ \mathbf{q}_\mathcal{T} \end{bmatrix} \end{bmatrix} = \mathrm{blkdiag}\left(G_T, G_R, \mathcal{G}_B, \mathcal{G}_\mathcal{T}\right) \begin{bmatrix} \begin{bmatrix} \mathbf{x} \\ \mathbf{g} \\ \mathbf{w} \\ \mathbf{u} \\ \mathbf{p} \end{bmatrix}_T \\ \begin{bmatrix} \mathbf{x} \\ \mathbf{g} \\ \mathbf{w} \\ \mathbf{u} \\ \mathbf{p} \end{bmatrix}_R \\ \begin{bmatrix} \mathbf{x}_B \\ \mathbf{x}_T \\ \mathbf{x}_R \\ \mathbf{w}_B \\ \mathbf{p}_B \end{bmatrix} \\ \begin{bmatrix} \mathbf{x}_\mathcal{T} \\ \mathbf{w}_\mathcal{T} \\ \mathbf{p}_\mathcal{T} \end{bmatrix} \end{bmatrix}$$
$$\begin{bmatrix} \mathbf{p}_T \\ \mathbf{p}_R \\ \mathbf{p}_B \\ \mathbf{p}_\mathcal{T} \end{bmatrix} = \mathrm{blkdiag}\left(\Delta_T, \Delta_R, \Delta_B, \Delta_\mathcal{T}\right) \begin{bmatrix} \mathbf{q}_T \\ \mathbf{q}_R \\ \mathbf{q}_B \\ \mathbf{q}_\mathcal{T} \end{bmatrix}$$
$$\begin{bmatrix} 0_{1\times 9} & 1_{1\times 1} & 0_{1\times 16} \end{bmatrix} \mathbf{x}_R = \varepsilon h_R, \quad \mathbf{z}_T \in \mathfrak{D}_{z_T}, \quad \mathbf{z}_R \in \mathfrak{D}_{z_R}, \quad \mathbf{z}_B \in \mathfrak{D}_{z_B} \tag{4.85}$$

and is compactly written as

$$\begin{bmatrix} \dot{\mathbf{x}} \\ \mathbf{z} \\ \mathbf{y} \\ \mathbf{q} \end{bmatrix}_{IFR} = G_{IFR} \begin{bmatrix} \mathbf{x} \\ \mathbf{w} \\ \mathbf{u} \\ \mathbf{p} \end{bmatrix}_{IFR} = \begin{bmatrix} A & B_g & B_w & B_u & B_p \\ C_z & D_{zg} & D_{zw} & D_{zu} & D_{zp} \\ C_y & D_{yg} & D_{yw} & D_{yu} & D_{yp} \\ C_q & D_{qg} & D_{qw} & D_{qu} & D_{qp} \end{bmatrix}_{IFR} \begin{bmatrix} \mathbf{x} \\ \mathbf{w} \\ \mathbf{u} \\ \mathbf{p} \end{bmatrix}_{IFR}$$
$$\mathbf{p}_{IFR} = \Delta_{IFR}\mathbf{q}_{IFR}, \quad \Delta_{IFR} \in \mathbf{\Delta}$$
$$\mathbf{z}_{IFR} \in \mathfrak{D}_{z_{IFR}} \tag{4.86}$$

where εh_R and other common input and output variables are remove via the linear fractional transform and

$$\mathbf{x}_{IFR} \coloneqq \begin{bmatrix} \text{blkdiag}\left(\begin{bmatrix} I_9 & 0_{9\times 1} \end{bmatrix}, I_{16}\right) \mathbf{x}_R \\ \mathbf{x}_B \\ \mathbf{x}_{\mathcal{T}} \end{bmatrix}, \; \mathbf{z}_{IFR} \coloneqq \begin{bmatrix} \mathbf{z}_T \\ \mathbf{z}_R \\ \mathbf{z}_B \end{bmatrix}, \; \mathbf{y}_{IFR} \coloneqq \begin{bmatrix} \mathbf{y}_T \\ \mathbf{y}_R \\ \mathbf{y}_B \end{bmatrix},$$

$$\mathbf{q}_{IFR} \coloneqq \begin{bmatrix} \mathbf{q}_T \\ \mathbf{q}_R \\ \mathbf{q}_B \\ \mathbf{q}_{\mathcal{T}} \end{bmatrix}, \; \mathbf{w}_{IFR} \coloneqq \begin{bmatrix} \mathbf{w}_T \\ \mathbf{w}_R \\ \mathbf{w}_B \\ \mathbf{w}_{\mathcal{T}} \end{bmatrix}, \; \mathbf{u}_{IFR} \coloneqq \begin{bmatrix} \mathbf{u}_T \\ \mathbf{u}_R \end{bmatrix}, \; \mathbf{p}_{IFR} \coloneqq \begin{bmatrix} \mathbf{p}_T \\ \mathbf{p}_R \\ \mathbf{p}_B \\ \mathbf{p}_{\mathcal{T}} \end{bmatrix},$$

$$\Delta_{IFR} = \text{blkdiag}\left(\Delta_T, \Delta_R, \Delta_B, \Delta_{\mathcal{T}}\right),$$

$$\mathfrak{D}_{z_{IFR}} = \left\{ \begin{bmatrix} \mathbf{z}_1 \\ \mathbf{z}_2 \\ \mathbf{z}_3 \end{bmatrix} : \mathbf{z}_1 \in \mathfrak{D}_{z_T}, \; \mathbf{z}_2 \in \mathfrak{D}_{z_R}, \; \mathbf{z}_3 \in \mathfrak{D}_{z_B} \right\} \tag{4.87}$$

Furthermore, the controller architecture, discussed in Section 4.1, is included in (4.86) as

$$\begin{bmatrix} \dot{\mathbf{x}} \\ \mathbf{z} \\ \mathbf{y} \\ \mathbf{q} \end{bmatrix}_\Theta = \begin{bmatrix} A & B_w & B_u & B_p \\ C_z & D_{zw} & D_{zu} & D_{zp} \\ C_y & D_{yw} & D_{yu} & D_{yp} \\ C_q & D_{qw} & D_{qu} & D_{qp} \end{bmatrix}_\Theta \begin{bmatrix} \mathbf{x} \\ \mathbf{w} \\ \mathbf{u} \\ \mathbf{p} \end{bmatrix}_\Theta \tag{4.88}$$

$$\mathbf{p}_\Theta = \Delta_\Theta \mathbf{q}_\Theta, \quad \Delta_\Theta \in \boldsymbol{\Delta}$$

$$\mathbf{z}_\Theta \in \mathfrak{D}_{z_\Theta}$$

and is obtained through the following augmentations:

1. Remove absolute-heading redundancy: Absolute-heading is removed by removing $\varepsilon\psi_T$ and replacing $\varepsilon\psi_R$ with $\varepsilon\psi_T - \varepsilon\psi_R$ in the state and performance- and measurement-outputs, and is achieved via the *ad hoc* singular transformation

$$\begin{bmatrix} \dot{\mathbf{x}} \\ \mathbf{z} \\ \mathbf{y} \\ \mathbf{q} \end{bmatrix}_X = \begin{bmatrix} T_{\dot{x}_\psi} & 0 & 0 & 0 \\ 0 & T_{z_\psi} & 0 & 0 \\ 0 & 0 & T_{y_\psi} & 0 \\ 0 & 0 & 0 & I \end{bmatrix} \begin{bmatrix} A & B_w & B_u & B_p \\ C_z & D_{zw} & D_{zu} & D_{zp} \\ C_y & D_{yw} & D_{yu} & D_{yp} \\ C_q & D_{qw} & D_{qu} & D_{qp} \end{bmatrix}_{IFR} \begin{bmatrix} T_{x_\psi} & 0 & 0 & 0 \\ 0 & I & 0 & 0 \\ 0 & 0 & I & 0 \\ 0 & 0 & 0 & I \end{bmatrix} \begin{bmatrix} \mathbf{x} \\ \mathbf{w} \\ \mathbf{u} \\ \mathbf{p} \end{bmatrix}_X$$

$$\mathbf{p}_X = \Delta_X \mathbf{q}_X, \quad \Delta_X \in \boldsymbol{\Delta}$$

$$\mathbf{z}_X \in \mathfrak{D}_{z_X} \tag{4.89}$$

where we use the intermediate state-space representation X and [8]

$$\Delta_X = \Delta_{IFR},\ \mathfrak{D}_{z_X} = \left\{ T_{\mathfrak{D}_\psi} \mathbf{z} : \mathbf{z} \in \mathfrak{D}_{z_{IFR}} \right\}$$

$$T_{\dot{x}_\psi} := \begin{bmatrix} I_8 & 0_{8\times 1} & 0_{8\times n_3} \\ 0_{n_3\times 8} & 0_{n_3\times 1} & I_{n_3} \end{bmatrix} \begin{bmatrix} I_8 & 0_{8\times 1} & 0_{8\times n_1} & 0_{8\times 1} & 0_{8\times n_2} \\ 0_{1\times 8} & 1 & 0_{1\times n_1} & 0_{1\times 1} & 0_{1\times n_2} \\ 0_{n_1\times 8} & 0_{n_1\times 1} & I_{n_1} & 0_{n_1\times 1} & 0_{n_1\times n_2} \\ 0_{1\times 8} & 1 & 0_{1\times n_1} & -1 & 0_{1\times n_2} \\ 0_{n_2\times 8} & 0_{n_2\times 1} & 0_{n_2\times n_1} & 0_{n_2\times 1} & I_{n_2} \end{bmatrix}$$

$$T_{x_\psi} := \begin{bmatrix} I_8 & 0_{8\times 1} & 0_{8\times n_1} & 0_{8\times 1} & 0_{8\times n_2} \\ 0_{1\times 8} & 1 & 0_{1\times n_1} & 0_{1\times 1} & 0_{1\times n_2} \\ 0_{n_1\times 8} & 0_{n_1\times 1} & I_{n_1} & 0_{n_1\times 1} & 0_{n_1\times n_2} \\ 0_{1\times 8} & 1 & 0_{1\times n_1} & -1 & 0_{1\times n_2} \\ 0_{n_2\times 8} & 0_{n_2\times 1} & 0_{n_2\times n_1} & 0_{n_2\times 1} & I_{n_2} \end{bmatrix} \begin{bmatrix} I_8 & 0_{8\times n_3} \\ 0_{1\times 8} & 0_{1\times n_3} \\ 0_{n_3\times 8} & I_{n_3} \end{bmatrix}$$

$$n_1 := 1 + n_{x_{a,T}} + 8, \quad n_2 := n_{x_{a,R}} + 3 + n_{x_T}, \quad n_3 := n_1 + 1 + n_2$$

$$T_{z_\psi} := \begin{bmatrix} I_8 & 0_{8\times 1} & 0_{8\times n_6} \\ 0_{n_6\times 8} & 0_{n_6\times 1} & I_{n_6} \end{bmatrix} \begin{bmatrix} I_8 & 0_{8\times 1} & 0_{8\times n_4} & 0_{8\times 1} & 0_{8\times n_5} \\ 0_{1\times 8} & 1 & 0_{1\times n_4} & 0_{1\times 1} & 0_{1\times n_5} \\ 0_{n_4\times 8} & 0_{n_4\times 1} & I_{n_4} & 0_{n_4\times 1} & 0_{n_4\times n_5} \\ 0_{1\times 8} & 1 & 0_{1\times n_4} & -1 & 0_{1\times n_5} \\ 0_{n_5\times 8} & 0_{n_5\times 1} & 0_{n_5\times n_4} & 0_{n_5\times 1} & I_{n_5} \end{bmatrix}$$

$$n_4 := 1 + n_{z_{a,T}} + 8, \quad n_5 := 1 + n_{z_{a,R}} + 3, \quad n_6 := n_4 + 1 + n_5$$

$$T_{y_\psi} := \begin{bmatrix} I_8 & 0_{8\times 1} & 0_{8\times 44} \\ 0_{44\times 8} & 0_{44\times 1} & I_{44} \end{bmatrix} \begin{bmatrix} I_8 & 0_{8\times 1} & 0_{8\times 24} & 0_{8\times 1} & 0_{8\times 19} \\ 0_{1\times 8} & 1 & 0_{1\times 24} & 0_{1\times 1} & 0_{1\times 19} \\ 0_{24\times 8} & 0_{24\times 1} & I_{24} & 0_{24\times 1} & 0_{24\times 19} \\ 0_{1\times 8} & 1 & 0_{1\times 24} & -1 & 0_{1\times 19} \\ 0_{19\times 8} & 0_{19\times 1} & 0_{19\times 24} & 0_{19\times 1} & I_{19} \end{bmatrix}$$

$$T_{\mathfrak{D}_\psi} := T_{z_\psi}$$

2. Include integrators: Integrators are included as the state $\mathbf{x}_i = \int \dot{\mathbf{x}}_i dt$ defined as

$$\dot{\mathbf{x}}_i := T_{x_i} \mathbf{y}_X \tag{4.90}$$

8. Note that each of the relative position transformation matrices are constructed from two matrices, of which one replaces $\varepsilon\psi$ with $\varepsilon\psi_T - \varepsilon\psi_R$, and the other removes the redundant absolute heading $\varepsilon\psi_T$.

where

$$T_{x_i} := \begin{bmatrix} \begin{bmatrix} 0_{1\times 17} & 1 & 0_{1\times 34} \end{bmatrix} \\ \begin{bmatrix} 0_{1\times 1} & 1 & 0_{1\times 50} \end{bmatrix} \\ \begin{bmatrix} 0_{1\times 6} & 1 & 0_{1\times 45} \end{bmatrix} \\ \begin{bmatrix} 0_{1\times 25} & 1 & 0_{1\times 26} \end{bmatrix} \\ \begin{bmatrix} 0_{3\times 49} & I_3 \end{bmatrix} \\ \begin{bmatrix} 0_{1\times 11} & 1 & 0_{1\times 40} \end{bmatrix} \\ \begin{bmatrix} 0_{2\times 13} & I_2 & 0_{2\times 37} \end{bmatrix} \\ \begin{bmatrix} 0_{1\times 15} & 1 & -1 & 0_{1\times 35} \end{bmatrix} \\ \begin{bmatrix} 0_{1\times 36} & 1 & 0_{1\times 15} \end{bmatrix} \\ \begin{bmatrix} 0_{2\times 38} & I_2 & 0_{2\times 12} \end{bmatrix} \\ \begin{bmatrix} 0_{1\times 40} & 1 & -1 & 0_{1\times 10} \end{bmatrix} \end{bmatrix} \tag{4.91}$$

$\varepsilon\dot{h}_T$ is excluded from $\dot{\mathbf{x}}_i$ as its integral εh_T is inherited in $\mathbf{x}_X$, and we find (4.88) where

$$\mathbf{x}_\Theta := \begin{bmatrix} \mathbf{x}_X \\ \mathbf{x}_i \end{bmatrix}, \begin{bmatrix} \mathbf{z} \\ \mathbf{q} \end{bmatrix}_\Theta := \begin{bmatrix} \mathbf{z} \\ \mathbf{q} \end{bmatrix}_X, \mathbf{y}_\Theta := \begin{bmatrix} \mathbf{y}_X \\ \mathbf{x}_i \end{bmatrix},$$
$$\begin{bmatrix} \mathbf{w} \\ \mathbf{u} \\ \mathbf{p} \end{bmatrix}_\Theta := \begin{bmatrix} \mathbf{w} \\ \mathbf{u} \\ \mathbf{p} \end{bmatrix}_X, \Delta_\Theta = \Delta_X, \mathfrak{D}_{z_\Theta} = \mathfrak{D}_{z_X}$$

This concludes the IFR norm-bounded state-space description.

4.2.2 Design specifications as LMI constraints

The LMI constraints developed in Section 3.9 are applied here to specify the robust stability [9] and robust performance requirements of IFR.

4.2.2.1 Multi-$\mathcal{H}_2$ design

The following assumption is required for the robust IOC and robust AOV performance measures, developed in Section 3.7, to be valid for the IFR system.

Assumption 2. The IFR system admits super-position, *i.e.* is linear time-varying.

Successfull AIFR is described as

$$\mathbf{z}_\Theta \in \mathfrak{D}_{z_\Theta} : (4.88) \tag{4.92}$$

where $\mathfrak{D}_{z_\Theta}$ describes hard-bounds on model variables. Following the discussion in Section 3.7.4 on the unbounded nature of model variables when subjected to

9. Note that stability is inherent in the performance LMIs (see Section 3.7.1).

Gaussian distributed inputs, $\mathbf{z}_\Theta \notin \mathfrak{D}_{z_\Theta}$ is an inevitable occurrence. We rely on minimising the risk of exceedance at each time instance, *i.e.*

$$\min \mathbb{P}\left\{\mathbf{z}_\Theta\left(t_i\right) \notin \mathfrak{D}_{z_\Theta}\right\} \tag{4.93}$$

related to variance for LTV models in Section 3.9.2, to indirectly prolong the critical time when one or more of the variables exceed their allowed level, after which a break-away law will steer the tanker and receiver clear of possible [10] collision, specified in Section 1.3.

Following the design specifications developed in Chapters 3.9.1 and 3.9.2, (4.93) is achieved via state-feedback by specifying $\mathcal{L}_C$ in (3.107) as

$$\mathcal{L}_C = \left(\begin{array}{c} \left[\begin{array}{c} \operatorname{diag}\left(\left[\begin{array}{cc} I_{51} & 0_{51\times 3} \end{array} \right] \overline{Q}_z \left[\begin{array}{c} I_{51} \\ 0_{3\times 51} \end{array} \right] \right) \\ \operatorname{trace}\left(\left[\begin{array}{cc} 0_{3\times 51} & I_3 \end{array} \right] \overline{Q}_z \left[\begin{array}{c} 0_{51\times 3} \\ I_3 \end{array} \right] \right) \end{array} \right] < \\ \gamma \left[\begin{array}{c} \left[\begin{array}{cc} I_8 & 0_{8\times 2} \end{array} \right] \min\left(\max\left(\varepsilon \mathbf{m}_T\right), -\min\left(\varepsilon \mathbf{m}_T\right)\right) \\ \min\left(\max\left(\varepsilon h_T\right), -\min\left(\varepsilon h_T\right)\right) \\ \min\left(\max\left(\varepsilon \boldsymbol{\delta}_T\right), -\min\left(\varepsilon \boldsymbol{\delta}_T\right)\right) \\ \min\left(\max\left(\varepsilon \dot{\boldsymbol{\delta}}_T\right), -\min\left(\varepsilon \dot{\boldsymbol{\delta}}_T\right)\right) \\ \left[\begin{array}{cc} I_8 & 0_{8\times 2} \end{array} \right] \min\left(\max\left(\varepsilon \mathbf{m}_R\right), -\min\left(\varepsilon \mathbf{m}_R\right)\right) \\ \min\left(\max\left(\varepsilon \psi_T - \varepsilon \psi_R\right), -\min\left(-\varepsilon \psi_T + \varepsilon \psi_R\right)\right) \\ \min\left(\max\left(\varepsilon h_R\right), -\min\left(\varepsilon h_R\right)\right) \\ \min\left(\max\left(\varepsilon \boldsymbol{\delta}_R\right), -\min\left(\varepsilon \boldsymbol{\delta}_R\right)\right) \\ \min\left(\max\left(\varepsilon \dot{\boldsymbol{\delta}}_R\right), -\min\left(\varepsilon \dot{\boldsymbol{\delta}}_R\right)\right) \\ 1 \end{array} \right]^{\mathbf{2}} \end{array} \right), \tag{4.94}$$

where γ is minimised, numerical values are listed in Table 4.1 and the contact envelope, specified in Table 2.1, is used in the calculation of $\mathcal{C}_{z,k,B}$ in (4.49). $\gamma = \frac{1}{9}$ corresponds to a 3σ-bound with a 0.26% risk of exceedance.

Furthermore, the influence of the estimator noise on (4.93) is indirectly minimised by specifying $\mathcal{L}_V$ in (3.132) as

$$\mathcal{L}_V = \left(\operatorname{tr}\left(V\right) < \gamma\right) \tag{4.95}$$

where γ is minimised and the performance output is specified as

$$\mathbf{v} = \operatorname{diag}\left(3\sqrt{\mathbb{E}\left\{\mathbf{x}\mathbf{x}^T\right\}}\right)^{-1} \widetilde{\mathbf{x}} \tag{4.96}$$

in (3.128) according to Table 4.1, *i.e.* we minimise the variance of the estimation error normalised with its corresponding state error 3σ-bound.

10. The model, and thus the performance guarantees, become invalid when $\mathbf{z}_\Theta \notin \mathfrak{D}_{z_\Theta}$, after which noting can be said about the stability or performance of the system.

4.2.2.2 Robust eigenvalue region design

Robust eigenvalue regions are designed for state-feedback and turbulence estimator synthesis to achieve desired AIFR transient/state-trajectory properties. A region is specified as the union of a half-space, a disk and a cone, all symmetric with respect to the real axis, and is related to transient properties in Section 3.9.3 by the *minimum exponential decay-rate* $\mathfrak{a}_{K/L}$, the *maximum spectral radius* $\mathfrak{r}_{K/L}$ for $\mathfrak{q}_{K/L} = 0$ and the *maximum imaginary-real ratio* $\tan\left(\mathfrak{c}_{K/L}\right)$, where subscript K/L denotes the robust eigenvalue region parameters of both the closed-loop model with state-feedback and the estimator. The resulting state-feedback region $\mathcal{R}_K$ constrains the transient behaviour of the plant model and the integrators, *i.e.* the flight- and actuator-mechanics of both aircraft, the boom kinematics, the turbulence and the integrators, while the estimator region $\mathcal{R}_L$ constrains the transient behaviour of the estimation error. The design technique is borrowed from linear systems theory and applied to the NLTV norm-bounded state-space description of the IFR system.

The design is based on constraining $\mathfrak{a}_{K/L}$, $\mathfrak{r}_{K/L}$ $\mathfrak{q}_{K/L}$ and $\mathfrak{c}_{K/L}$ for state-feedback and the estimator to achieve the following conflicting closed-loop objectives:

1. Maximum settling-time: $\mathfrak{a}$ is a direct measure of maximum settling-time and is related to a maximum 2% settling-time $t_{s,2\%} = \frac{-\ln(0.02)}{\mathfrak{a}}$ $\text{rad}/\text{rad.s}^{-1}$ in seconds. The maximum settling-time applies to the time required to converge to the zero state from a non-zero state, the time required to remove estimator biases via the integrators and the time required to converge to a step reference input. A lower-bound of $t_{s,2\%}$ is obtained by simply increasing $\mathfrak{a}$ in (3.110) and (3.135) until the synthesis becomes infeasible. Due to the uncontrollability of the turbulence state,
$$\mathfrak{a}_K < \min_i \left(\text{eig}_i \left(\mathcal{A}_{\mathcal{T}} \left(\Delta\right)\right)\right) \tag{4.97}$$
is a necessary condition for (3.110) to be feasible, *i.e.* the robust eigenvalue region must contain all uncontrollable states.[11] According to (4.51)-(4.55) we find an upper-bound
$$\min_i \left(\text{eig}_i \left(\mathcal{A}_{\mathcal{T}} \left(\boldsymbol{\rho}\right)\right)\right) \geq \frac{\vartheta}{l_g} \gtrsim 0.250\,\text{rad/s} \geq \mathfrak{a}_K \tag{4.98}$$
however, due to the conservatism involved in Theorem 1 the upper-bound to $\mathfrak{a}_K$ could be less.
2. Robust against aliasing: It is considered common practise to digitally implement a controller designed in the continuous time-domain by replacing integrators with forward numeric integrators [35, Ch.6-7]. Successful digital implementation requires sufficiently fast sampling [49, pp.12], where in the extreme case a forward numerical integrator is equal to a continuous integrator in the limit $\omega_s \to \infty$ (see Appendix A.2.1).
Maximum spectral radius $\mathfrak{r}$ is the measure of the maximum free oscillation frequency facilitated by an NLTV model (see Section 3.9.3), and **we form**

11. The turbulence estimator does not possess an uncontrollable state, and is thus not limited in this respect.

the conjecture that $\mathfrak{r}$ is equal to its bandwidth. Bandwidths are well-defined for LTI models, however we refer to the bandwidth of an NLTV model as the maximum frequency where cut-off occurs in the frequency content of the state-trajectories from any initial condition. Thus, we choose the maximum cut-off frequency $\mathfrak{r}_{K/L}$ for $\mathfrak{q}_{K/L} = 0$ to be sufficiently lower than the *Nyquist frequency* $\frac{\omega_s}{2} = 100\pi\,\text{rad/s}$, to minimise the effect of aliasing.

3. Turbulence rejection and estimation: The bandwidth of the closed-loop model with state-feedback and turbulence estimator is required to be greater than that of the turbulence, to facilitate the potential for good turbulence rejection and estimation respectively, *i.e.*

$$\mathfrak{r}_{K/L} > \max_i \left\| \text{eig}_i \left(\mathcal{A}_{\mathcal{T}} \left(\Delta \right) \right) \right\|_2, \quad \mathfrak{q}_{K/L} = 0 \tag{4.99}$$

Moreover, (4.99) is a necessary condition for (3.113) to be feasible. Similar to Objective 1 above, we find a lower-bound to the bandwidth of the closed-loop model with state-feedback as

$$\max_i \left\| \text{eig}_i \left(\mathcal{A}_{\mathcal{T}} \left(\boldsymbol{\rho} \right) \right) \right\|_2 \leq \frac{\pi \vartheta}{3b} \lesssim 4.18\,\text{rad/s} \leq \mathfrak{r}_K \tag{4.100}$$

4. Robust against delays: The on-board A330 estimator poses a 10 ms time-delay in its output (see Table 4.5), and an additional 10 ms communication delay exists in the transfer of data between aircrafts. Thus, the AIFR controller needs to be robust against $\tau_d = 30\,\text{ms}$, and we bound the phase margin required with $\mathfrak{r}_{K/L}$ as

$$\varphi_d = \tau_d \mathfrak{r}_{K/L} \tag{4.101}$$

where φ_d is the phase error caused by the delay at the bandwidth $\mathfrak{r}$.

5. Separation of state-feedback and estimator: It is well-known that for a given LTI model, the solution of the LQG output-feedback control problem is the same as the corresponding solution to the LQR problem except that in the control law the state is replaced by its estimate obtained from the solution of the corresponding LQE problem [48, pp.390][30, pp.166]. This result is known as the *separation principle*, [12] and is applied in [30, pp.166] to decoupled the robust $\mathcal{H}_2$/Popov output-feedback control problem into its corresponding state-feedback and state-estimation problems.
It is not proven that the combined solutions of the state-feedback and state-estimation problems derived in Section 3.8 is the solution to their corresponding output-feedback problem, however, by choosing $\mathfrak{a}_L$ sufficiently greater than $\mathfrak{r}_K$, the sub-models involved in state-feedback synthesis, *i.e.* the flight- and actuator mechanics of both aircraft, the boom kinematics, the turbulence and the integrators, is unaware of the faster error dynamics of the estimator. This approach is considered common practise and is discussed in [35, pp.304].

6. Robust against estimation filter: The AIFR controller needs to be robust against the fall-off and phase-lag of the $30\,\text{rad/s}$ low-pass filter at the input of

12. [30, pp.166] Any output feedback controller that stabilises an LTI model could be built by combining the solutions of a state feedback problem and an output estimation problem.

the A330 estimator (see Table 4.5). Similar to Objective 4 above, we bound the required gain- and phase-margin with $\mathfrak{r}_{K/L}$ as

$$\varphi_f = \tan^{-1}\left(\frac{\mathfrak{r}_{K/L}}{30}\right) \tag{4.102}$$

and

$$g_f = 1 - \frac{1}{\sqrt{1+\left(\frac{\mathfrak{r}_{K/L}}{30}\right)^2}} \tag{4.103}$$

where g_f is the gain error caused by the filter at the bandwidth $\mathfrak{r}$.

7. MIL-F-8785C [1, pp.13,22] damping ratio specification: MIL-F-8785C [1, pp.45-60] specifies the minimum allowed damping ratios for all the modes of a transport aircraft during aerial refuelling, and are specified for different levels of flying qualities, given in Table 4.6.

MIL-F-8785C damping ratio specifications for IFR	
Level of flying quality	$\cos\left(\mathfrak{c}_{K/L}\right)$
Adequate	0.35
Some degradation exists in mission effectiveness	0.25
IFR can be terminated safely	0.15

Table 4.6: IFR damping ratio specifications.

The constraints on the robust eigenvalue region parameters are summarised in Table 4.7, and used to design the robust closed-loop eigenvalue regions illustrated in Figure 4.6, where $(\mathfrak{r},\mathfrak{q})_K = (5\,{}^{\text{rad}}/_{\text{s}}, 0)$, $(\mathfrak{a},\mathfrak{r},\mathfrak{q},\mathfrak{c})_L = \left(10\,{}^{\text{rad}}/_{\text{s}}, 15\,{}^{\text{rad}}/_{\text{s}}, 0, \frac{\pi}{2}\,\text{rad}\right)$ and $(\mathfrak{a},\mathfrak{c})_K$ are experimentally determined.

ID	AIFR robust eigenvalue region design objective	value
1	settling-time	see Section 4.3.5
2	robust against aliasing	$\frac{\mathfrak{r}_{K/L}}{\left(\frac{\omega_s}{2}\right)} = \frac{15}{100\pi}\,\text{rad}$
3	turbulence rejection	$\mathfrak{r}_K = 5\,{}^{\text{rad}}/_{\text{s}}$
4	turbulence estimation	$\mathfrak{r}_L > 5\,{}^{\text{rad}}/_{\text{s}}$
5	robust against delays	$\varphi_d = 0.3\,\text{rad} = \frac{17.2\pi}{180}\,\text{rad}$
6	separation of state-feedback and estimator	$\frac{\mathfrak{a}_L}{\mathfrak{r}_K} = 2\,\text{rad}$
7	robust against estimator filter	$\varphi_f = \frac{26.6\pi}{180}\,\text{rad}$, $g_f = 0.106\,\text{rad}$
8	damping ratio specification [1, pp.13,22]	$\cos\left(\mathfrak{c}_{K/L}\right) > 0.35, 0.25, 0.15\,\text{rad}$

Table 4.7: AIFR robust eigenvalue region summary.

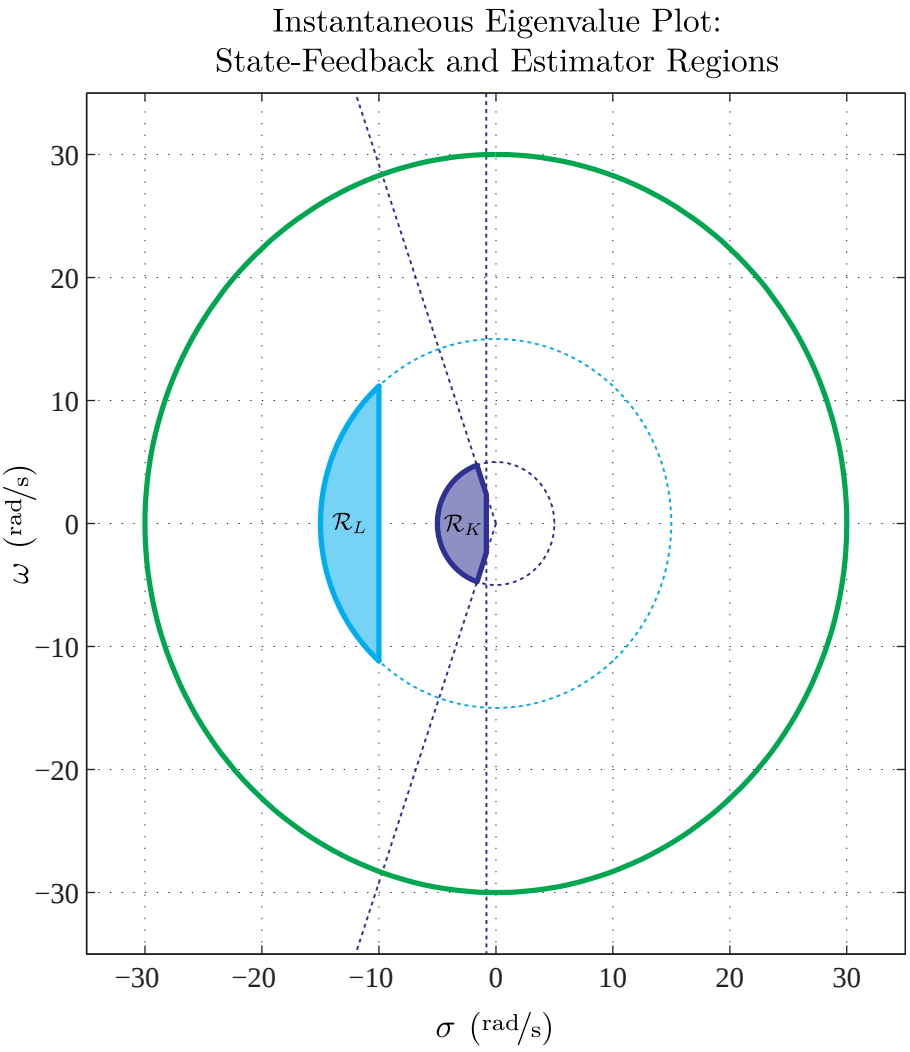

Figure 4.6: AIFR robust eigenvalue regions.

4.3 Controller synthesis

The IFR norm-bounded state-space model (4.88) is augmented for controller synthesis, after which the various LMI system measures developed in Section 3.8 for estimator-based state-feedback controller synthesis, are combined via Lyapunov's shaping paradigm and presented as the two separated LMI optimisation problems used for state-feedback synthesis and estimator synthesis. The estimator structure is augmented to isolate the part of the system state which have not already been estimated, to which end an estimator may be synthesised which estimates only the IFR turbulence state. An approach is presented to find appropriate synthesis parameters for the two LMI optimisation problems presented, and are used to synthesise and analyse numerous estimator-based state-feedback controllers for IFR, which are confirmed via non-linear simulation in Chapter 5.

Both coupled and partially decoupled AIFR are considered for synthesis, discussed

in controller architecture aspect no.1 in Section 4.1, where the latter does not form part of our main analysis and is included in Appendix D.

4.3.1 Model reduction

The norm-bounded state-space description of a system is known to be overconservative, in which case the model uncertainty Δ may be scaled as $\mathfrak{s}\Delta$. The model uncertainty scalar $\mathfrak{s} \in \mathbb{R}^1$ may equivalently be included for state-feedback synthesis by replacing the uncertainty input matrices B_p, D_{zp}, D_{yp} and D_{qp} with $\mathfrak{s}B_p$, $\mathfrak{s}D_{zp}$, $\mathfrak{s}D_{yp}$ and $\mathfrak{s}D_{qp}$ respectively.

State-estimates of the turbulence are required for state-feedback synthesis, when synthesised for IFR model (4.88). However, we have found the corresponding turbulence estimator, synthesised with the approach presented next in Section 4.3.3, to have poor noise performance, with $\max\left(\begin{bmatrix} 1 & 0 \end{bmatrix} \widehat{\mathbf{x}}_{v,w_g}\right) \approx 100 \max\left(\begin{bmatrix} 1 & 0 \end{bmatrix} \mathbf{x}_{v,w_g}\right)$ for both the tanker and receiver. The poor noise performance is possibly due to poor observability or the turbulence zeros, although we are not sure of its origin, and is remedied by replacing the turbulence components v_g and w_g in (4.52) by the first-order zeroless description [13]

$$\begin{aligned} \dot{x}_{v,w_g} &= -\frac{3}{2}\frac{\vartheta}{l_g} x_{u_g} + \sigma_g \sqrt{\frac{3\vartheta}{l_g}} \eta_{v,w_g}, \\ v, w_g &= x_{v,w_g} \end{aligned} \tag{4.104}$$

which maintains isotropy [14] and is illustrated in Figure 4.7. Furthermore, according to MIL-HDBK-1797A [2, pp.680], the angular turbulence components p_g, q_g and r_g are significant only if

$$\sqrt{\frac{b}{l_g}} \frac{\partial c_l}{\partial p} > \frac{\partial c_l}{\partial \beta} \tag{4.105}$$

$$\sqrt{\frac{\pi b}{8 l_g}} \frac{\partial c_m}{\partial q} > \frac{\partial c_m}{\partial \alpha} \tag{4.106}$$

and

$$\sqrt{\frac{\pi b}{6 l_g}} \frac{\partial c_n}{\partial r} > \frac{\partial c_n}{\partial \beta} \tag{4.107}$$

respectively, where α is the angle of attack and β is the side-slip angle. Only (4.105) is satisfied for the A330 aerodynamic coefficients, and we omit q_g and r_g for synthesis.

13. The bandwidth of the zeroless turbulence description is chosen such that its spectrum converges to the original turbulence description (4.52) as $\omega \to \infty$.

14. Isotropy is required for the IFR turbulence covariance calculation (4.62) to remain valid.

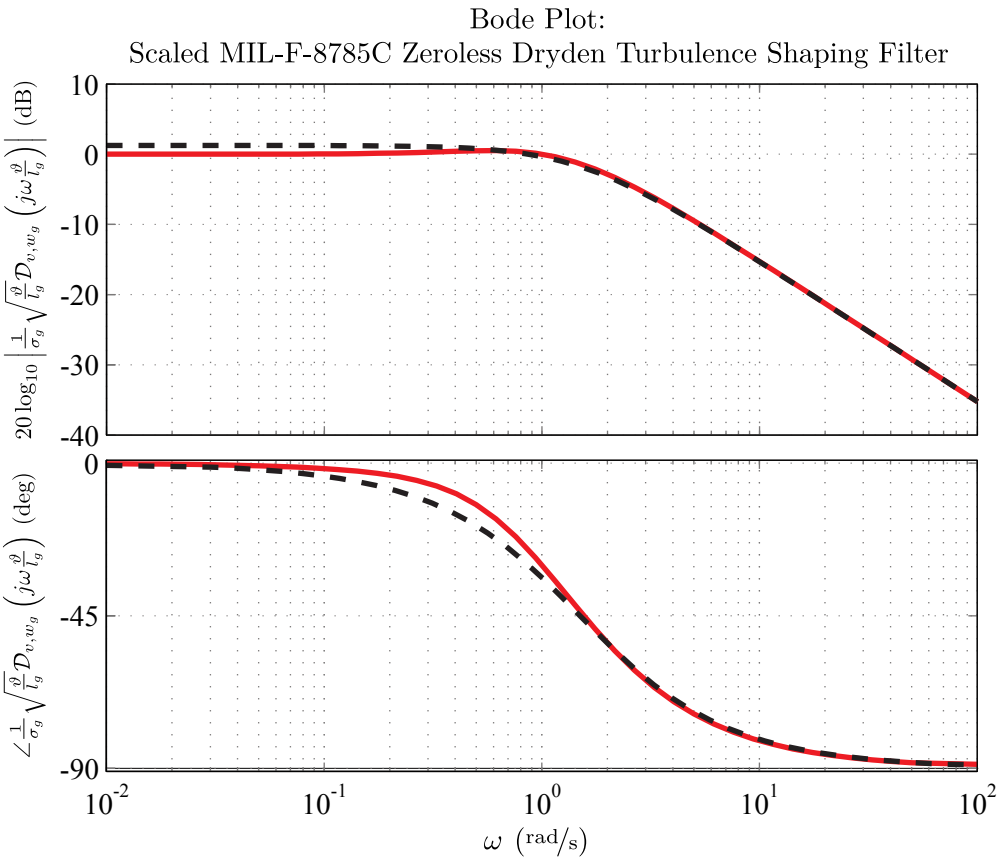

Figure 4.7: Bode plot of scaled MIL-F-8785C Zeroless Dryden turbulence shaping filter for unit intensity white noise input. Multiplication factor for amplitude scaling is $\frac{1}{\sigma_g}\sqrt{\frac{\vartheta}{l_g}}$ ($\sqrt{\text{s}}/\text{m}$) and for frequency scaling $\frac{\vartheta}{l_g}$ (s). Filters: v_g and w_g in (4.52) (red); zeroless v_g and w_g in (4.104) (black dashed).

The IFR model (4.88), augmented with the first-order zeroless turbulence description (4.104) and with the removal of q_g and r_g, is given by

$$\begin{bmatrix} \dot{\mathbf{x}} \\ \mathbf{z} \\ \mathbf{y} \\ \mathbf{q} \end{bmatrix}_C = \begin{bmatrix} A & B_w & B_u & B_p \\ C_z & D_{zw} & D_{zu} & D_{zp} \\ C_y & D_{yw} & D_{yu} & D_{yp} \\ C_q & D_{qw} & D_{qu} & D_{qp} \end{bmatrix}_C \begin{bmatrix} \mathbf{x} \\ \mathbf{w} \\ \mathbf{u} \\ \mathbf{p} \end{bmatrix}_C \tag{4.108}$$

$$\mathbf{p}_C = \Delta_C \mathbf{q}_C, \quad \Delta_C \in \mathbf{\Delta}$$

$$\mathbf{z}_C \in \mathfrak{D}_{z_C}$$

4.3.2 State-feedback formulation

The LMI optimisation problems developed in Section 3.8.1 for state-feedback synthesis are combined via Lyapunov's paradigm (3.118) and given as

minimise γ

subject to (4.94)

$$\left[\begin{array}{c|c|c|c} AQ_K + B_uY_K \\ +\left(AQ_K + B_uY_K\right)^T & \left(C_qQ_K + D_{qu}Y_K\right)^T & B_pW_Q & B_w \\ \hline \star & -W_Q & D_{qp}W_Q & D_{qw} \\ \hline \star & \star & -W_Q & 0 \\ \hline \star & \star & \star & -I \end{array}\right] < 0$$

$$\left[\begin{array}{c|c|c|c} -\overline{Q}_z & 0 & C_zQ_K + D_{zu}Y_K & D_{zp}W_C \\ \hline 0 & -W_C & C_qQ_K + D_{qu}Y_K & D_{qp}W_C \\ \hline \star & \star & -Q_K & 0 \\ \hline \star & \star & \star & -W_C \end{array}\right] < 0$$

$$\left[\begin{array}{c|c|c} AQ_K + B_uY_K + \\ Q_KA^T + Y_K^TB_u^T + 2\mathfrak{a}_KQ_K & Q_KC_q^T + Y_K^TD_{qu}^T & B_pW_{\mathfrak{a}} \\ \hline \star & -W_{\mathfrak{a}} & D_{qp}W_{\mathfrak{a}} \\ \hline \star & \star & -W_{\mathfrak{a}} \end{array}\right] < 0$$

$$\left[\begin{array}{c|c|c|c} \left(-\mathfrak{r}_K^2 + \mathfrak{q}_K^2\right)Q_K + \\ \mathfrak{q}_K\left(AQ_K + B_uY_K\right) + \\ \mathfrak{q}_K\left(AQ_K + B_uY_K\right)^T & \mathfrak{q}_K\begin{pmatrix} C_qQ_K + \\ D_{qu}Y_K \end{pmatrix}^T & AQ_K + B_uY_K & B_pW_{\mathfrak{r}} \\ \hline \star & -W_{\mathfrak{r}} & C_qQ_K + D_{qu}Y_K & D_{qp}W_{\mathfrak{r}} \\ \hline \star & \star & -Q_K & 0 \\ \hline \star & \star & \star & -W_{\mathfrak{r}} \end{array}\right] < 0$$

$$\left[\begin{array}{c|c|c} \Theta_K \otimes AQ_K \\ +\Theta_K \otimes B_uY_K \\ +\left(\Theta_K \otimes AQ_K\right)^T \\ +\left(\Theta_K \otimes B_uY_K\right)^T & \left(\Theta_K \otimes C_qQ_K\right)^T \\ +\left(\Theta_K \otimes D_{qu}Y_K\right)^T & \left(I_2 \otimes B_p\right)W_{\mathfrak{c}} \\ \hline \star & -W_{\mathfrak{c}} & \left(I_2 \otimes D_{qp}\right)W_{\mathfrak{c}} \\ \hline \star & \star & -W_{\mathfrak{c}} \end{array}\right] < 0$$

$$W_{\mathfrak{c}} \coloneqq \begin{bmatrix} W_{\mathfrak{c},1} & 0 \\ 0 & W_{\mathfrak{c},2} \end{bmatrix}, \{W_Q, W_C, W_{\mathfrak{a}}, W_{\mathfrak{r}}, W_{\mathfrak{c},1}, W_{\mathfrak{c},2}\} \subset \mathfrak{C},\ Q_K > 0,$$

$$\gamma \in \mathbb{R}^1,\ Y_K \in \mathbb{R}^{n_u \times n_x} \tag{4.109}$$

where the state-feedback gain is calculated post-synthesis as

$$K \coloneqq Y_K Q_K^{-1} \tag{4.110}$$

The coupled AIFR state-feedback gain is synthesised with LMI optimisation problem (4.109) and IFR model (4.108).

4.3.3 Turbulence estimator formulation

A turbulence estimator is synthesised and implemented, alongside the existing aircraft estimators, to provide the turbulence state estimate absent in the measurement output required for the state-feedback. Singular transformation matrices are used to isolate the estimated state in the IFR model from the remainder, used to formulate an estimator for only part of the model, which admits the form of the full state estimator developed in Section 3.8.2.

The observability matrix [70, pp.136]

$$\mathcal{O} = \begin{bmatrix} \mathcal{C} \\ \mathcal{C}\mathcal{A} \\ \mathcal{C}\mathcal{A}^2 \\ \vdots \\ \mathcal{C}\mathcal{A}^{(n_{\mathcal{A}}-1)} \end{bmatrix} \tag{4.111}$$

of the Dryden turbulence model (4.51)-(4.55) has a full column rank for the whole flight-envelope, confirmed with 8 linearly independent rows in the first 9 rows [15]

$$\begin{bmatrix} I_9 & 0 \end{bmatrix} \mathcal{O}_{\mathcal{D}} = \begin{bmatrix} 1 & 0 & 0 & 0 & 0 & 0 & 0 & 0 \\ 0 & 0 & 1 & 0 & 0 & 0 & 0 & 0 \\ 0 & 0 & 0 & 0 & 1 & 0 & 0 & 0 \\ 0 & 0 & 0 & 0 & 0 & 1 & 0 & 0 \\ 0 & 0 & 0 & 0 & \frac{\pi}{4b} & 0 & -\frac{\pi\vartheta}{4b} & 0 \\ 0 & 0 & \frac{\pi}{3b} & 0 & 0 & 0 & 0 & -\frac{\pi\vartheta}{3b} \\ -\frac{\vartheta}{l_g} & 0 & 0 & 0 & 0 & 0 & 0 & 0 \\ 0 & -\left(\frac{\vartheta}{l_g}\right)^2 & -2\frac{\vartheta}{l_g} & 0 & 0 & 0 & 0 & 0 \\ 0 & 0 & 0 & -\left(\frac{\vartheta}{l_g}\right)^2 & -2\frac{\vartheta}{l_g} & 0 & 0 & 0 \end{bmatrix} \tag{4.112}$$

Thus, the Dryden turbulence model is observable, and, if the Dryden model output is measureable, an estimator may be synthesised such that the estimation error $\tilde{\mathbf{x}}_{\mathcal{D}} \coloneqq \hat{\mathbf{x}}_{\mathcal{D}} - \mathbf{x}_{\mathcal{D}}$ is convergent. The Dryden model output is constructed from aircraft acceleration in (4.15), and is given as

$$\begin{aligned} &\left(\begin{bmatrix} I_6 & 0 \end{bmatrix} \dot{\mathbf{x}}_{m,A} = \begin{bmatrix} I_6 & 0 \end{bmatrix} \left(A_{m,A}\mathbf{x}_{m,A} + B_{g,m,A}\mathbf{g}_{m,A} + B_{u,m,A}\mathbf{u}_{m,A} + B_{p,m,A}\mathbf{p}_{m,A}\right)\right) \iff \\ &\left(\mathbf{g}_{m,A} = \left(\begin{bmatrix} I_6 \\ 0 \end{bmatrix} B_{g,m,A}\right)^{-1} \begin{bmatrix} I_6 \\ 0 \end{bmatrix} \left(\dot{\mathbf{x}}_{m,A} - \left(A_{m,A}\mathbf{x}_{m,A} + B_{u,m,A}\mathbf{u}_{m,A} + B_{p,m,A}\mathbf{p}_{m,A}\right)\right)\right) \end{aligned} \tag{4.113}$$

15. The linearly dependent row in (4.112) is indicated in red.

where $\begin{bmatrix} I_6 & 0 \end{bmatrix} B_{g,m,A}$ is invertible. It follows from the block diagonal structure (4.60) of the IFR turbulence model that its observability matrix also has full rank and is thus also observable, when accelerations of both the tanker and receiver is used.

Furthermore, estimator structure (3.121) is augmented to estimate only the part of the state abscent in the measurement output, given as follows.

Transformation matrices used for estimator augmentation are defined as

$$\mathbf{x} = \begin{bmatrix} T_{x_\mathcal{E}} & T_{x_r} \end{bmatrix} \begin{bmatrix} \mathbf{x}_\mathcal{E} \\ \mathbf{x}_r \end{bmatrix}, \; \mathbf{x}_\mathcal{E} = R_{x_\mathcal{E}}\mathbf{x}, \; \mathbf{x}_r = R_{x_r}\mathbf{x}$$
$$\widehat{\mathbf{x}}_r = N_{y_r}\mathbf{y}, \; \mathbf{y}_\mathcal{E} = R_{y_\mathcal{E}}\mathbf{y} \tag{4.114}$$

where $\mathbf{x}$ is the model state of the general norm-bounded state-space description (3.91), $\mathbf{x}_\mathcal{E}$ is the part of the state to be estimated and $\mathbf{x}_r$ the remainder, and $\mathbf{y}_\mathcal{E}$ is the part of the measurement used for estimation. Following the standard estimator structure (3.121), we isolate $\mathbf{x}_\mathcal{E}$ and $\mathbf{y}_\mathcal{E}$ as

$$\begin{bmatrix} \dot{\widehat{\mathbf{x}}}_\mathcal{E} \\ \widehat{\mathbf{y}}_\mathcal{E} \end{bmatrix} = \begin{bmatrix} R_{x_\mathcal{E}}\dot{\widehat{\mathbf{x}}} \\ R_{y_\mathcal{E}}\widehat{\mathbf{y}} \end{bmatrix} = \begin{bmatrix} R_{x_\mathcal{E}}A & R_{x_\mathcal{E}}B_u \\ R_{y_\mathcal{E}}C_y & R_{y_\mathcal{E}}D_{yu} \end{bmatrix} \begin{bmatrix} \widehat{\mathbf{x}} \\ \mathbf{u} \end{bmatrix} + \begin{bmatrix} L_\mathcal{E} \\ 0 \end{bmatrix} (R_{y_\mathcal{E}}\widehat{\mathbf{y}} - R_{y_\mathcal{E}}\mathbf{y}) \tag{4.115}$$

where we define the estimator gain as

$$L_\mathcal{E} \coloneqq R_{x_\mathcal{E}}L \tag{4.116}$$

Similar to (3.124) and (3.126), the estimator state error mechanics is derived as

$$\begin{aligned} \dot{\widetilde{\mathbf{x}}}_\mathcal{E} &= \left(R_{x_\mathcal{E}}A + L_\mathcal{E}R_{y_\mathcal{E}}C_y\right)T_{x_\mathcal{E}}\widetilde{\mathbf{x}}_\mathcal{E} + \left(R_{x_\mathcal{E}}A + L_\mathcal{E}R_{y_\mathcal{E}}C_y\right)T_{x_r}\widetilde{\mathbf{x}}_r \\ &\quad + \left(-R_{x_\mathcal{E}}B_w - L_\mathcal{E}R_{y_\mathcal{E}}D_{yw}\right)\mathbf{w} + \left(-R_{x_\mathcal{E}}B_p - L_\mathcal{E}R_{y_\mathcal{E}}D_{yp}\right)\mathbf{p} \end{aligned} \tag{4.117}$$

where

$$\mathbf{p} = \Delta\mathbf{q}, \quad \Delta \in \mathbf{\Delta} \tag{4.118}$$

and

$$\mathbf{q} = D_{qu}KT_{x_\mathcal{E}}\widetilde{\mathbf{x}}_\mathcal{E} + D_{qu}KT_{x_r}\widetilde{\mathbf{x}}_r + D_{qw}\mathbf{w} + \left(C_q + D_{qu}K\right)\mathbf{x} + D_{qp}\mathbf{p} \tag{4.119}$$

$\widetilde{\mathbf{x}}_r$ is expressed in terms of other input variables as

$$\begin{aligned} \widetilde{\mathbf{x}}_r &= N_{y_r}\mathbf{y} - \mathbf{x}_r \\ &= N_{y_r}\left(C_y\mathbf{x} + D_{yw}\mathbf{w} + D_{yu}\mathbf{u} + D_{yp}\mathbf{p}\right) - R_{x_r}\mathbf{x} \\ &= N_{y_r}\left(C_y\mathbf{x} + D_{yw}\mathbf{w} + D_{yu}K\widehat{\mathbf{x}} + D_{yp}\mathbf{p}\right) - R_{x_r}\mathbf{x} \\ &= N_{y_r}\left(C_y\mathbf{x} + D_{yw}\mathbf{w} + D_{yu}K\left(\widetilde{\mathbf{x}} + \mathbf{x}\right) + D_{yp}\mathbf{p}\right) - R_{x_r}\mathbf{x} \\ &= \left(N_{y_r}\left(C_y + D_{yu}K\right) - R_{x_r}\right)\mathbf{x} \\ &\quad + N_{y_r}\left(D_{yw}\mathbf{w} + D_{yu}KT_{x_\mathcal{E}}\widetilde{\mathbf{x}}_\mathcal{E} + D_{yu}KT_{x_r}\widetilde{\mathbf{x}}_r + D_{yp}\mathbf{p}\right) \\ &= \left(I - N_{y_r}D_{yu}KT_{x_r}\right)^{-1}\begin{pmatrix} \left(N_{y_r}\left(C_y + D_{yu}K\right) - R_{x_r}\right)\mathbf{x} \\ + N_{y_r}\left(D_{yw}\mathbf{w} + D_{yu}KT_{x_\mathcal{E}}\widetilde{\mathbf{x}}_\mathcal{E} + D_{yp}\mathbf{p}\right) \end{pmatrix} \end{aligned} \tag{4.120}$$

and is replace in (4.117) and (4.119) as

$$\begin{aligned}
\dot{\widetilde{\mathbf{x}}}_{\mathcal{E}} &= \left(R_{x_{\mathcal{E}}}A + L_{\mathcal{E}}R_{y_{\mathcal{E}}}C_y\right)T_{x_{\mathcal{E}}}\widetilde{\mathbf{x}}_{\mathcal{E}} \\
&\quad + \Upsilon_x\left(\left(N_{y_r}\left(C_y + D_{yu}K\right) - R_{x_r}\right)\mathbf{x} + N_{y_r}\left(D_{yw}\mathbf{w} + D_{yu}KT_{x_{\mathcal{E}}}\widetilde{\mathbf{x}}_{\mathcal{E}} + D_{yp}\mathbf{p}\right)\right) \\
&\quad + \left(-R_{x_{\mathcal{E}}}B_w - L_{\mathcal{E}}R_{y_{\mathcal{E}}}D_{yw}\right)\mathbf{w} + \left(-R_{x_{\mathcal{E}}}B_p - L_{\mathcal{E}}R_{y_{\mathcal{E}}}D_{yp}\right)\mathbf{p} \\
&= \left(R_{x_{\mathcal{E}}}A + L_{\mathcal{E}}R_{y_{\mathcal{E}}}C_y + \Upsilon_x N_{y_r}D_{yu}K\right)T_{x_{\mathcal{E}}}\widetilde{\mathbf{x}}_{\mathcal{E}} \\
&\quad + \left(-R_{x_{\mathcal{E}}}B_w - L_{\mathcal{E}}R_{y_{\mathcal{E}}}D_{yw} + \Upsilon_x N_{y_r}D_{yw}\right)\mathbf{w} \\
&\quad + \Upsilon_x\left(N_{y_r}\left(C_y + D_{yu}K\right) - R_{x_r}\right)\mathbf{x} \\
&\quad + \left(-R_{x_{\mathcal{E}}}B_p - L_{\mathcal{E}}R_{y_{\mathcal{E}}}D_{yp} + \Upsilon_x N_{y_r}D_{yp}\right)\mathbf{p}
\end{aligned} \tag{4.121}$$

and

$$\begin{aligned}
\mathbf{q} &= D_{qu}KT_{x_{\mathcal{E}}}\widetilde{\mathbf{x}}_{\mathcal{E}} \\
&\quad + \Upsilon_q\left(\left(N_{y_r}\left(C_y + D_{yu}K\right) - R_{x_r}\right)\mathbf{x} + N_{y_r}\left(D_{yw}\mathbf{w} + D_{yu}KT_{x_{\mathcal{E}}}\widetilde{\mathbf{x}}_{\mathcal{E}} + D_{yp}\mathbf{p}\right)\right) \\
&\quad + D_{qw}\mathbf{w} + \left(C_q + D_{qu}K\right)\mathbf{x} + D_{qp}\mathbf{p} \\
&= \left(D_{qu}K + \Upsilon_q N_{y_r}D_{yu}K\right)T_{x_{\mathcal{E}}}\widetilde{\mathbf{x}}_{\mathcal{E}} \\
&\quad + \left(D_{qw} + \Upsilon_q N_{y_r}D_{yw}\right)\mathbf{w} \\
&\quad + \left(C_q + D_{qu}K + \Upsilon_q\left(N_{y_r}\left(C_y + D_{yu}K\right) - R_{x_r}\right)\right)\mathbf{x} \\
&\quad + \left(D_{qp} + \Upsilon_q N_{y_r}D_{yp}\right)\mathbf{p}
\end{aligned} \tag{4.122}$$

respectively, where lengthy expressions are substituted for compactness, defined as

$$\begin{aligned}
\Upsilon_x &\coloneqq \left(R_{x_{\mathcal{E}}}A + L_{\mathcal{E}}R_{y_{\mathcal{E}}}C_y\right)T_{x_r}\left(I - N_{y_r}D_{yu}KT_{x_r}\right)^{-1} \\
\Phi_x &\coloneqq AT_{x_r}\left(I - N_{y_r}D_{yu}KT_{x_r}\right)^{-1} \\
\Psi_x &\coloneqq C_yT_{x_r}\left(I - N_{y_r}D_{yu}KT_{x_r}\right)^{-1} \\
\implies \Upsilon_x &= R_{x_{\mathcal{E}}}\Phi_x + L_{\mathcal{E}}R_{y_{\mathcal{E}}}\Psi_x
\end{aligned} \tag{4.123}$$

and

$$\Upsilon_q \coloneqq D_{qu}KT_{x_r}\left(I - N_{y_r}D_{yu}KT_{x_r}\right)^{-1} \tag{4.124}$$

Now, (4.121) and (4.122) are combined to find the equivalent open-loop estimator matrices used for synthesis corresponding to (3.128), given as

$$\begin{bmatrix} \widetilde{A} & \widetilde{B}_w & \widetilde{B}_u & \widetilde{B}_p \\ \widetilde{C}_z & \widetilde{D}_{zw} & \widetilde{D}_{zu} & \widetilde{D}_{zp} \\ \widetilde{C}_y & \widetilde{D}_{yw} & \widetilde{D}_{yu} & \widetilde{D}_{yp} \\ \widetilde{C}_q & \widetilde{D}_{qw} & \widetilde{D}_{qu} & \widetilde{D}_{qp} \end{bmatrix} =$$

$$\begin{bmatrix} R_{x_\mathcal{E}}\left(A+\Phi_x N_{y_r} D_{yu} K\right) T_{x_\mathcal{E}} & R_{x_\mathcal{E}}\left[\begin{array}{cc} \left(-B_w+\Phi_x N_{y_r} D_{yw}\right) & \Phi_x\left(N_{y_r}\left(C_y+D_{yu}K\right)-R_{x_r}\right) \end{array}\right] & I & R_{x_\mathcal{E}}\left(-B_p+\Phi_x N_{y_r} D_{yp}\right) \\ \widetilde{C}_z & \widetilde{D}_{zw} & 0 & \widetilde{D}_{zp} \\ R_{y_\mathcal{E}}\left(C_y+\Psi_x N_{y_r} D_{yu} K\right) T_{x_\mathcal{E}} & R_{y_\mathcal{E}}\left[\begin{array}{cc} \left(-I+\Psi_x N_{y_r}\right) D_{yw} & \Psi_x\left(N_{y_r}\left(C_y+D_{yu}K\right)-R_{x_r}\right) \end{array}\right] & 0 & R_{y_\mathcal{E}}\left(-I+\Psi_x N_{y_r}\right) D_{yp} \\ \left(D_{qu}K+\Upsilon_q N_{y_r} D_{yu} K\right) T_{x_\mathcal{E}} & \left[\begin{array}{cc} \left(D_{qw}+\Upsilon_q N_{y_r} D_{yw}\right) & \left(C_q+D_{qu}K+\Upsilon_q\left(N_{y_r}\left(C_y+D_{yu}K\right)-R_{x_r}\right)\right) \end{array}\right] & 0 & \left(D_{qp}+\Upsilon_q N_{y_r} D_{yp}\right) \end{bmatrix} \tag{4.125}$$

In the case of turbulence estimation, where the estimated state is uncontrollable, estimator structure (4.115) simplifies to its implementation form

$$\begin{bmatrix} \dot{\widehat{\mathbf{x}}}_\mathcal{E} \\ \widehat{\mathbf{y}}_\mathcal{E} \end{bmatrix} = \begin{bmatrix} R_{x_\mathcal{E}} A T_{x_\mathcal{E}} & 0 & 0 \\ R_{y_\mathcal{E}} C_y T_{x_\mathcal{E}} & R_{y_\mathcal{E}} C_y T_{x_r} N_{y_r} & R_{y_\mathcal{E}} D_{yu} \end{bmatrix} \begin{bmatrix} \widehat{\mathbf{x}}_\mathcal{E} \\ \mathbf{y} \\ \mathbf{u} \end{bmatrix} + \begin{bmatrix} L_\mathcal{E} \\ 0 \end{bmatrix} \left(\widehat{\mathbf{y}}_\mathcal{E} - R_{y_\mathcal{E}} \mathbf{y}\right) \tag{4.126}$$

and analysis form

$$\begin{bmatrix} \dot{\widehat{\mathbf{x}}}_\mathcal{E} \\ \mathbf{v} \\ \widehat{\mathbf{y}}_\mathcal{E} \end{bmatrix} = \begin{bmatrix} R_{x_\mathcal{E}} A T_{x_\mathcal{E}} & -L_\mathcal{E} R_{y_\mathcal{E}} & 0 & L_\mathcal{E} \\ \widetilde{C}_z & 0 & 0 & 0 \\ R_{y_\mathcal{E}} C_y T_{x_\mathcal{E}} & R_{y_\mathcal{E}} C_y T_{x_r} N_{y_r} & R_{y_\mathcal{E}} D_{yu} & 0 \end{bmatrix} \begin{bmatrix} \widehat{\mathbf{x}}_\mathcal{E} \\ \mathbf{y} \\ \mathbf{u} \\ \widehat{\mathbf{y}}_\mathcal{E} \end{bmatrix} \tag{4.127}$$

for

$$\widetilde{D}_{zw} = 0, \quad \widetilde{D}_{zp} = 0 \tag{4.128}$$

The LMI optimisation problems developed in Section 3.8.2 for estimator synthesis is combined via Lyapunov's paradigm (3.143) and given as

$$
\begin{aligned}
&\text{minimise} \quad \operatorname{tr}(V) \\
&\text{subject to} \\
&\left[\begin{array}{c|c|c|c}
\begin{array}{c}\left(P_L\widetilde{A}+Z_L\widetilde{C}_y\right)^T \\ +P_L\widetilde{A}+Z_L\widetilde{C}_y\end{array} & P_L\widetilde{B}_p+Z_L\widetilde{D}_{yp} & \widetilde{C}_q^T W_P & \widetilde{C}_z^T \\ \hline
\star & -W_P & \widetilde{D}_{qp}^T W_P & \widetilde{D}_{zp}^T \\ \hline
\star & \star & -W_P & 0 \\ \hline
\star & \star & \star & -I
\end{array}\right] < 0 \\
&\left[\begin{array}{c|c|c|c}
-V & 0 & \left(P_L\widetilde{B}_w+Z_L\widetilde{D}_{yw}\right)^T & \widetilde{D}_{qw}^T W_V \\ \hline
\star & -W_V & \left(P_L\widetilde{B}_p+Z_L\widetilde{D}_{yp}\right)^T & \widetilde{D}_{qp}^T W_V \\ \hline
\star & \star & -P_L & 0 \\ \hline
\star & \star & \star & -W_V
\end{array}\right] < 0 \\
&\left[\begin{array}{c|c|c}
\begin{array}{c}\left(P_L\widetilde{A}+Z_L\widetilde{C}_y\right) \\ \left(P_L\widetilde{A}+Z_L\widetilde{C}_y\right)^T+2\mathfrak{a}_L P_L\end{array} & \widetilde{C}_q^T M_{\mathfrak{a}} & P_L\widetilde{B}_p+Z_L\widetilde{D}_{yp} \\ \hline
\star & -M_{\mathfrak{a}} & M_{\mathfrak{a}}\widetilde{D}_{qp} \\ \hline
\star & \star & -M_{\mathfrak{a}}
\end{array}\right] < 0 \\
&\left[\begin{array}{c|c|c|c}
\begin{array}{c}\left(-\mathfrak{r}_L^2+\mathfrak{q}_L^2\right)P_L+ \\ \mathfrak{q}_L\left(P_L\widetilde{A}+Z_L\widetilde{C}_y\right)+ \\ \mathfrak{q}_L\left(P_L\widetilde{A}+Z_L\widetilde{C}_y\right)^T\end{array} & \mathfrak{q}_L\widetilde{C}_q^T M_{\mathfrak{r}} & P_L\widetilde{A}+Z_L\widetilde{C}_y & P_L\widetilde{B}_p+Z_L\widetilde{D}_{yp} \\ \hline
\star & -M_{\mathfrak{r}} & M_{\mathfrak{r}}\widetilde{C}_q & M_{\mathfrak{r}}\widetilde{D}_{qp} \\ \hline
\star & \star & -P_L & 0 \\ \hline
\star & \star & \star & -M_{\mathfrak{r}}
\end{array}\right] < 0 \\
&\left[\begin{array}{c|c|c}
\begin{array}{c}\Theta_L\otimes P_L\widetilde{A} \\ \Theta_L\otimes Z_L\widetilde{C}_y \\ +\left(\Theta_L\otimes P_L\widetilde{A}\right)^T \\ +\left(\Theta_L\otimes Z_L\widetilde{C}_y\right)^T\end{array} & \left(\Theta_L\otimes\widetilde{C}_q\right)^T M_{\mathfrak{c}} & \begin{array}{c}I_2\otimes P_L\widetilde{B}_p \\ +I_2\otimes Z_L\widetilde{D}_{yp}\end{array} \\ \hline
\star & -M_{\mathfrak{c}} & M_{\mathfrak{c}}\left(I_2\otimes\widetilde{D}_{qp}\right) \\ \hline
\star & \star & -M_{\mathfrak{c}}
\end{array}\right] < 0 \\
&M_{\mathfrak{c}} \coloneqq \begin{bmatrix} M_{\mathfrak{c},1} & 0 \\ 0 & M_{\mathfrak{c},2}\end{bmatrix},\ \{W_P, W_V, M_{\mathfrak{a}}, M_{\mathfrak{r}}, M_{\mathfrak{c},1}, M_{\mathfrak{c},2}\} \subset \mathfrak{C}, \\
&P_L > 0,\ \gamma \in \mathbb{R}^1,\ Z_L \in \mathbb{R}^{n_x\times n_y}
\end{aligned}
\tag{4.129}
$$

where the estimator gain is calculated post-synthesis as

$$L_{\mathcal{E}} \coloneqq P_L^{-1} Z_L \tag{4.130}$$

The AIFR robust eigenvalue design, given by Figure 4.6, constrains the closed-loop plant to be 2 times slower than the estimator error. Thus, white noise is not an accurate representation of the state disturbance $\mathbf{x}$ in the estimator. $\mathbf{x}$ is omitted from the estimator synthesis, *i.e.* $\mathbf{x} = \mathbf{0}$, resulting in a possibly larger presence of $\mathbf{x}$ in $\widetilde{\mathbf{x}}_{\mathcal{E}}$, but avoiding an over-conservative design.

The coupled AIFR turbulence estimator gain $L_{\mathcal{E},C}$ is synthesised with LMI optimisation problem (4.129), IFR model (4.108) and (4.125), where

$$\begin{aligned}
T_{x_{\mathcal{E},C}} &= \begin{bmatrix} 0_{37\times 8} \\ I_8 \\ 0_{15\times 8} \end{bmatrix} \\
T_{x_{r,C}} &= \begin{bmatrix} I_{37} & 0_{37\times 15} \\ 0_{6\times 37} & 0_{6\times 15} \\ 0_{15\times 37} & I_{15} \end{bmatrix} \\
R_{x_{\mathcal{E}}} &= \begin{bmatrix} 0_{6\times 37} & I_6 & 0_{6\times 15} \end{bmatrix} \\
N_{y_r} &= \text{blkdiag}\left(\begin{bmatrix} I_{17} & 0_{17\times 7} \end{bmatrix}, \begin{bmatrix} I_9 & 0_{9\times 1} \end{bmatrix}, \begin{bmatrix} I_8 & 0_{8\times 7} \end{bmatrix}, I_{18}\right) \\
R_{y_{\mathcal{E},C}} &= \text{blkdiag}\left(\begin{bmatrix} 0_{4\times 18} & I_4 & 0_{4\times 2} \end{bmatrix}, \begin{bmatrix} 0_{4\times 19} & I_4 & 0_{4\times 20} \end{bmatrix}\right)
\end{aligned} \tag{4.131}$$

in (4.114) and coupled state-feedback gain K, synthesised with IFR model (4.108) in Section 4.3.2, is used as K in (4.125).

4.3.4 Approach

The LMI optimisation problems (4.109) and (4.129), used for estimator-based state-feedback controller synthesis, are well-defined for fixed synthesis parameters. However, the relationship between the robust multi-$\mathcal{H}_2$ performance, settling-time, and damping are not apparent from the LMIs. We present an approach, based on the linear iteration of synthesis parameters and the use of relationship guidelines, to obtain a sub-optimal AIFR Linear Quadratic (LQ) cost in terms of multi-$\mathcal{H}_2$ performance, settling-time, and damping. Furthermore, the LMI optimisation problem (4.109) is **infeasible** when used to synthesise a robust multi-$\mathcal{H}_2$ state-feedback gain for IFR model (4.108) with the least constraining robust eigenvalue region chosen as $(\mathfrak{a}, \mathfrak{r}, \mathfrak{q}, \mathfrak{c})_K = (0.01\,\text{rad/s}, 5\,\text{rad/s}, 0, \frac{\pi}{2}\,\text{rad})$. [16] The infeasibility leads to the reduction of the model uncertainty, as discussed in Section 4.3.1, to which end uncertainty scaling $\mathfrak{s}_K$, where subscript K denotes the uncertainty scaling used for state-feedback synthesis, becomes part of the controller synthesis parameters. The approach proceeds as follows.

16. Note that for an infeasible state-feedback gain, the LMIs used to synthesise the estimator are ill-defined.

A predictor-estimator based state-feedback IFR controller is synthesised for the nominal flight-case with (4.109) and (4.129), of which the synthesis parameters are chosen to obtain a sub-optimal AIFR Linear Quadratic (LQ) cost in terms of the severity of turbulence the controller can reject, settling-time, and damping. The synthesis parameters, defined below, corresponding to the sub-optimal controller are then used to synthesise a controllers for a toboggan and a bank turn flight case, of which the resulting controllers are used to demonstrate the gain-scheduling scheme discussed in Section 4.1 and the on-line tanker bank reference, by executing a $0\,{}^{\mathrm{m}}/_{\mathrm{s}}$ to $500\,(0.00508)\ {}^{\mathrm{m}}/_{\mathrm{s}}$ toboggan manoeuvre and a $0\,\mathrm{rad}$ to $25\frac{\pi}{180}\,\mathrm{rad}$ bank manoeuvre. The approach used to obtain the sub-optimal cost, is based on linearly iterating the synthesis parameters until a local optimum is obtained according to the guidelines presented.

The robust multi-$\mathcal{H}_2$ performance of a controller, synthesised with (4.109) and (4.129) for a turbulence severity scaling factor $\iota = 1$ in (2.41), may be interpreted as the severity of turbulence the controller can reject while maintaining a 3σ-bound on all the constrained variables, if the turbulence is the dominant disturbance, which is the case for the noise levels given in Table 4.5. The severity of turbulence the controller can reject is calculated post-synthesis, by scaling the IOC matrix with ι^2, and is apparent from (3.56), (3.61), and the scalability property of LMIs (see Appendix A.2.12)

$$\begin{aligned}
&\left(\begin{array}{c} \mathcal{A}(\Delta)\,\overline{Q}_x + \overline{Q}_x\mathcal{A}^T(\Delta) + \mathcal{B}(\Delta)\,\mathcal{B}^T(\Delta) < 0 \\ \mathcal{C}_z(\Delta)\,\overline{Q}_x\mathcal{C}_z^T(\Delta) < \overline{Q}_z \end{array}\right) \\
\iff &\left(\begin{array}{c} \iota^2\left(\mathcal{A}(\Delta)\,\overline{Q}_x + \overline{Q}_x\mathcal{A}^T(\Delta) + \mathcal{B}(\Delta)\,\mathcal{B}^T(\Delta)\right) < 0 \\ \iota^2\mathcal{C}_z(\Delta)\,\overline{Q}_x\mathcal{C}_z^T(\Delta) < \iota^2\overline{Q}_z \end{array}\right) \\
\iff &\left(\begin{array}{c} \mathcal{A}(\Delta)\left(\iota^2\overline{Q}_x\right) + \left(\iota^2\overline{Q}_x\right)\mathcal{A}^T(\Delta) + (\iota\mathcal{B}(\Delta))\,(\iota\mathcal{B}(\Delta))^T < 0 \\ \mathcal{C}_z(\Delta)\left(\iota^2\overline{Q}_x\right)\mathcal{C}_z^T(\Delta) < \left(\iota^2\overline{Q}_z\right) \end{array}\right)
\end{aligned} \tag{4.132}$$

where $\iota\mathcal{B}(\Delta)$ is the new noise input matrix of the system and $\iota^2\overline{Q}_z$ its new IOC. Together with the robust multi-$\mathcal{H}_2$ proportional minimisation with γ in (4.94), the severity of turbulence the controller can reject, whilst maintaining a 3σ-bound on all the constrained variables, may be derived with (4.132), (4.94) and (3.146) as

$$\iota = \frac{1}{3\sqrt{\gamma}} \tag{4.133}$$

The LMI optimisation problem (4.109) is **infeasible** when used to synthesise a robust multi-$\mathcal{H}_2$ state-feedback gain for IFR model (4.108) with the least constraining robust eigenvalue region chosen as $(\mathfrak{a}, \mathfrak{r}, \mathfrak{q}, \mathfrak{c})_K = (0.01\,{}^{\mathrm{rad}}/_{\mathrm{s}}, 5\,{}^{\mathrm{rad}}/_{\mathrm{s}}, 0, \frac{\pi}{2}\,\mathrm{rad})$.[17] The infeasibility of (4.109) is due to either the infeasibility of static state-feedback controlled AIFR, or the conservatism involved in the norm-bounded state-space description, Lyapunov's shaping paradigm, and that of Theorems 1 and 2.

The conservatism involved in (4.109) is described as follows:

17. Note that for an infeasible state-feedback gain, the LMIs used to synthesise the estimator are ill-defined.

1. *Norm-bounded state-space description*: The conservatism involved in the norm-bounded state-space model is apparent in the description of non-linearity with norm-bounded uncertainty in Appendix A.2.10, whereby the set of all non-linearities, defined by the sector-bounds of the included non-linearity, is also included in the model.
2. *Lyapunov's shaping paradigm*: Popov [65, pp.24] has shown that the conservatism involved in Lyapunov's shaping paradigm can be significant, where he uses a multi-objective genetic algorithm to demonstrate, among others, its conservatism for mixed $\mathcal{H}_2/\mathcal{H}_\infty$ synthesis, where the $\mathcal{H}_2$ index is minimised and the $\mathcal{H}_\infty$ index is bounded. The synthesis is applied to a simple 2 cart mass-spring model (4^{th}-order model), for which the LMI approach, with the use of Lyapunov's shaping paradigm, obtains an $\mathcal{H}_2$ objective of 50% worse than that of the genetic algorithm.
3. *Theorems 1 and 2*: The conservatism involved in Theorems 1 and 2 are quantified in Appendices A.2.13 and A.2.14 respectively, although a means for their analysis is pending.

A post-synthesis LTI analysis criterion is used to remove the conservatism involved in (4.109), based on the LTI multi-$\mathcal{H}_2$ index and the LTI Multi-Input Multi-Output (MIMO) Delay Margin (DM) and Filter Margin (FM). LTI measures are used as the most superior measures of a system, which assumes that the expressions in $\mathbf{\Delta}$ that will result in superior performance to that of the LTI model are absent in the system. The LTI measures are used to determine when robust IFR performance specifications are *not* met. The criterion is not subject to the above mentioned conservatism,[18] but lacks guarantees on robust stability or robust performance. Instantaneous eigenvalue plots were considered for the criterion, but was found to be too dependent on the uncertainty sample set (4.21).[19]

The conservatism involved in (4.109) is reduced as follows:

1. *Reduce model uncertainty*: The conservatism involved in the norm-bounded state-space description is indirectly reduced by reducing the scale of the model uncertainty Δ according to Section 4.3.1. The model with reduced uncertainty, however, then fails to completely describe the system, thus the robust stability and performance measures are no longer valid. The reduced uncertainty model only serves as a means to make the synthesised controller robust against a portion of the system non-linearity, which may or may not be sufficient. Non-linear simulation is then used to determine the level of non-linearity the controller may be subjected to, by increasing turbulence severity, which in turn increases the involved non-linearity as system variables increase in amplitude and into their non-linear domains. The non-linear simulation measure is based on the *Taylor series expansion*, which holds that any finite-gain system approaches linearity for sufficiently small perturbations. The uncertainty scalar $\mathfrak{s}$, defined in Section 4.3.1, is used to scale the model uncertainty.

18. Lyapunov's shaping paradigm is not required for analysis.
19. Several large sample sets, each generated using 10000 randomly generated Δ's defined by (4.21), have shown that the shape of instantaneous eigenvalue plots is inclined to be maintained for different sets, but that its scale may vary significantly.

2. *LTI stability margins*: The LTI MIMO DM and FM are used to analyse the stability properties of controllers synthesised for reduced model uncertainty. The MIMO DM is defined as the *maximum* amount by which the measurement output vector, used for feedback, may be delayed, without destabilising the system. Similarly, the MIMO FM is the *minimum* first-order unity DC-gain LPF bandwidth by which the measurement output vector, used for feedback, may be filtered, without destabilising the system. The MIMO DM and FM, referred to as the stability margins, are measured independently, *i.e.* they do *not* measure the capability of simultaneous change in delay and filter bandwidth.
   These stability margins are chosen over the more conventional MIMO gain margin and phase margin, because they are more applicable to the dynamic characteristics of the on-board A330 estimators.
   The LTI MIMO DM serves as an *upper-bound* to the robust MIMO DM and the LTI MIMO FM serves as a *lower-bound* to the robust MIMO FM.
3. *LTI performance*: The LTI multi-$\mathcal{H}_2$ index is used as an lower-bound to system robust multi-$\mathcal{H}_2$ performance.

Furthermore, LMI optimisation problem (4.129) is **feasible** when used to synthesise a robust $\mathcal{H}_2$ estimator gain for the IFR model (4.108), with a robust eigenvalue region specified according to Section 4.2.2.2 as $(\mathfrak{a}, \mathfrak{r}, \mathfrak{q}, \mathfrak{c})_L = (10\,\text{rad/s}, 15\,\text{rad/s}, 0, \frac{\pi}{2}\,\text{rad})$, and a feasible state-feedback gain synthesised with reduced uncertainty. Thus, the conservatism involved in (4.129) is low enough such that the estimator may be synthesised for $\mathfrak{s} = 1$, where subscript L denotes the uncertainty scaling used for estimator synthesis, and its designed robust eigenvalue region, which are both used for every estimator synthesised.

The state-feedback synthesis parameters are defined as the uncertainty scaling $\mathfrak{s}_K$, the 2% settling-time $\frac{-\ln(0.02)}{\mathfrak{a}_K}$, and the damping $\cos(\mathfrak{c}_K)$. The flow diagram given in Figure 4.8 illustrates the linear iterative approach for determining IFR turbulence rejection and settling-time capabilities according to state-feedback synthesis parameters $\mathfrak{a}_K$ and $\mathfrak{s}_K$, of which the flow diagram may easily be extended to include damping. The flow diagram iterates through $\mathfrak{a}_K$ and $\mathfrak{s}_K$, where $\overline{\mathfrak{s}}_K$ is included as an upper-bound to $\mathfrak{s}_K$, which limits $\mathfrak{s}_K$ to uncertainty scales attaining $\iota_\Theta \geq 1.1$ for analysis with $\mathfrak{s}_\Theta = 0$, where ι_Θ is the severity of turbulence the estimator-based state-feedback controller can reject with the IFR model (4.88) and $\mathfrak{s}_\Theta$ is the corresponding model uncertainty scale. Bound $\overline{\mathfrak{s}}_K$ is used to avoid unnecessary grid points, whereas ϵ_Δ is a sufficiently small value used to include $\mathfrak{s}_K = 1 < 1 + \epsilon_\Delta$. The bound on ι_Θ for $\mathfrak{s}_\Theta = 0$ is chosen as 1.1 rather that 1, which includes a 10% margin for $\mathfrak{s}_\Theta \neq 0$, which is illustrated in Figure 4.9(a). The set of controllers resulting from the flow-diagram attaining $\iota_\Theta \geq 1.1$ for $\mathfrak{s}_\Theta = 0$, is further limited to controllers attaining $\text{DM}_\Theta \geq 30\,\text{ms}$ and $\text{FM}_\Theta \leq 30\,\text{rad/s}$ for $\mathfrak{s}_\Theta = 0$, required for robustness against the delays and bandwidths of the A330 estimators and the CCs, specified in Section 4.2.1.6. Together $\iota_\Theta \geq 1.1$, $\text{DM}_\Theta \geq 30\,\text{ms}$ and $\text{FM}_\Theta \leq 30\,\text{rad/s}$ for $\mathfrak{s}_\Theta = 0$ are referred to as the LTI criteria.

In addition to the linear iteration scheme presented above, guidelines are used to initiate state-feedback synthesis parameters for the linear iterations and to determine when a local optimum of AIFR LQ cost has been reached. The guidelines gives

approximate relationships between the performance measures and the state-feedback synthesis parameters, and are given in Figure 4.9. The guideline in Figure 4.9(a) is based on the results in [4, 59], which illustrates that the LTI turbulence rejection performance ι_Θ, for $\mathfrak{s}_\Theta = 0$, reduces as the uncertainty scale used for state-feedback synthesis increases, but that its performance is maintained over wider range of $\mathfrak{s}_\Theta$. The remaining guidelines are straight forward. Damping is not included in Figure 4.9, due to the use of $\mathfrak{q}_K \neq 0$ to indirectly include damping, and is motivated in Section 4.3.6. The convergence to zero or divergence to infinity present in the guides, are due to: $\mathfrak{a}_K = 0$, for which DM_Θ is approximately zero and FM_Θ is approximately infinite, where DM_Θ and FM_Θ are the respective MIMO DM and FM for IFR model (4.88); $\mathfrak{a}_K, \mathfrak{s}_K \gg$, which causes the LMI optimisation problem used for state-feedback synthesis to become infeasible. The calculation of the performance measures are presented in Section 4.3.5 with the results.

The two flight-cases considered for AIFR are defined as:

1. *Nominal flight-case*: The nominal flight-case is defined at the centre of the flight-envelope, and is given as

$$\begin{aligned}
\left(h_r, \vartheta_{cas,r}, \phi_r, \dot{h}_r\right) &= \left(20'000\,(0.3048)\ \mathrm{m}, 265\,(0.5144444)\ {}^{\mathrm{m}}/_{\mathrm{s}}, 0, 0\right) \\
(m_T, cg_T) &= \left((171.5 + 12.3\delta_{m_T}) \times 10^3\,\mathrm{kg}, (29 + 2.4\delta_{cg_T})\ \%\mathrm{RC}\right) \\
(m_R, cg_R) &= \left((171.5 + 12.3\delta_{m_R}) \times 10^3\,\mathrm{kg}, (29 + 2.4\delta_{cg_R})\ \%\mathrm{RC}\right)
\end{aligned} \tag{4.134}$$

   where $\boldsymbol{\delta}_n \coloneqq \{\delta_{m_T}, \delta_{cg_T}, \delta_{m_R}, \delta_{cg_R}\} \subset \boldsymbol{\Delta}$ and is included according to the mass and centre of mass measurement accuracies defined in Section 4.2.1.6. [20]

2. *Toboggan flight-case*: The toboggan flight-case is parted into three overlapping sub-domains over h, according to the gain-scheduling scheme, and is given as

$$\begin{aligned}
(h_r, \vartheta_{cas,r}) &= \left(0.3048\,(h_0 + 443\delta_{h_T})\ \mathrm{m}, 265\,(0.5144444)\ {}^{\mathrm{m}}/_{\mathrm{s}}\right) \\
\left(\phi_r, \dot{h}_r\right) &= \left(0, (-250 + 250\delta_{\dot{h}})\,0.00508\ {}^{\mathrm{m}}/_{\mathrm{s}}\right) \\
(m_T, cg_T) &= \left((220.7 + 12.3\delta_{m_T}) \times 10^3\,\mathrm{kg}, (19.4 + 2.4\delta_{cg_T})\ \%\mathrm{RC}\right) \\
(m_R, cg_R) &= \left((122.3 + 12.3\delta_{m_R}) \times 10^3\,\mathrm{kg}, (38.6 + 2.4\delta_{cg_R})\ \%\mathrm{RC}\right) \\
h_0 &\in \{29'557, 28'750, 27'943\}
\end{aligned} \tag{4.135}$$

   where $\boldsymbol{\delta}_n \coloneqq \{\delta_{m_T}, \delta_{cg_T}, \delta_{m_R}, \delta_{cg_R}, \delta_{h_T}, \delta_{\dot{h}}\} \subset \boldsymbol{\Delta}$, δ_{h_T} provides the altitude domain for the toboggan over 300 s, and $\delta_{\dot{h}}$ provides the climb-rate domain for the toboggan. [21] The toboggan flight-case describes the nominal speed and high altitude flight-case of a 0 to maximum toboggan, with tanker and receiver masses and centre of masses at opposite sides of the envelope.

20. $1\,\mathrm{ft} = 0.3048\,\mathrm{m}$ and $1\,\mathrm{kts} = 0.5144444\ {}^{\mathrm{m}}/_{\mathrm{s}}$.
21. $1\ {}^{\mathrm{ft}}/_{\mathrm{min}} = 0.00508\ {}^{\mathrm{m}}/_{\mathrm{s}}$.

3. *Bank flight-case*: The bank flight-case is parted into three overlapping sub-domains over ϕ, according to the gain-scheduling scheme, and is given as

$$\begin{aligned}(h_r, \vartheta_{cas,r}) &= (20'000\,(0.3048)\ \text{m}, 265\,(0.5144444)\ \text{m/s}) \\ \left(\phi_r, \dot{h}_r\right) &= \left((\phi_0 + 6\delta_\phi)\,\frac{\pi}{180}\,\text{rad}, 0\right) \\ (m_T, cg_T) &= \left((220.7 + 12.3\delta_{m_T}) \times 10^3\,\text{kg}, (19.4 + 2.4\delta_{cg_T})\ \%\text{RC}\right) \\ (m_R, cg_R) &= \left((122.3 + 12.3\delta_{m_R}) \times 10^3\,\text{kg}, (38.6 + 2.4\delta_{cg_R})\ \%\text{RC}\right) \\ \phi_0 &\in \{0, 9.5, 19\}\end{aligned} \tag{4.136}$$

where $\boldsymbol{\delta}_e \coloneqq \{\delta_{m_T}, \delta_{cg_T}, \delta_{m_R}, \delta_{cg_R}, \delta_\phi\} \subset \boldsymbol{\Delta}$ and δ_ϕ provides the bank domain for the bank turn over 300 s. The bank flight-case describes the nominal speed and nominal altitude flight-case of a zero to maximum bank turn, with tanker and receiver masses and centre of masses at opposite sides of the envelope.

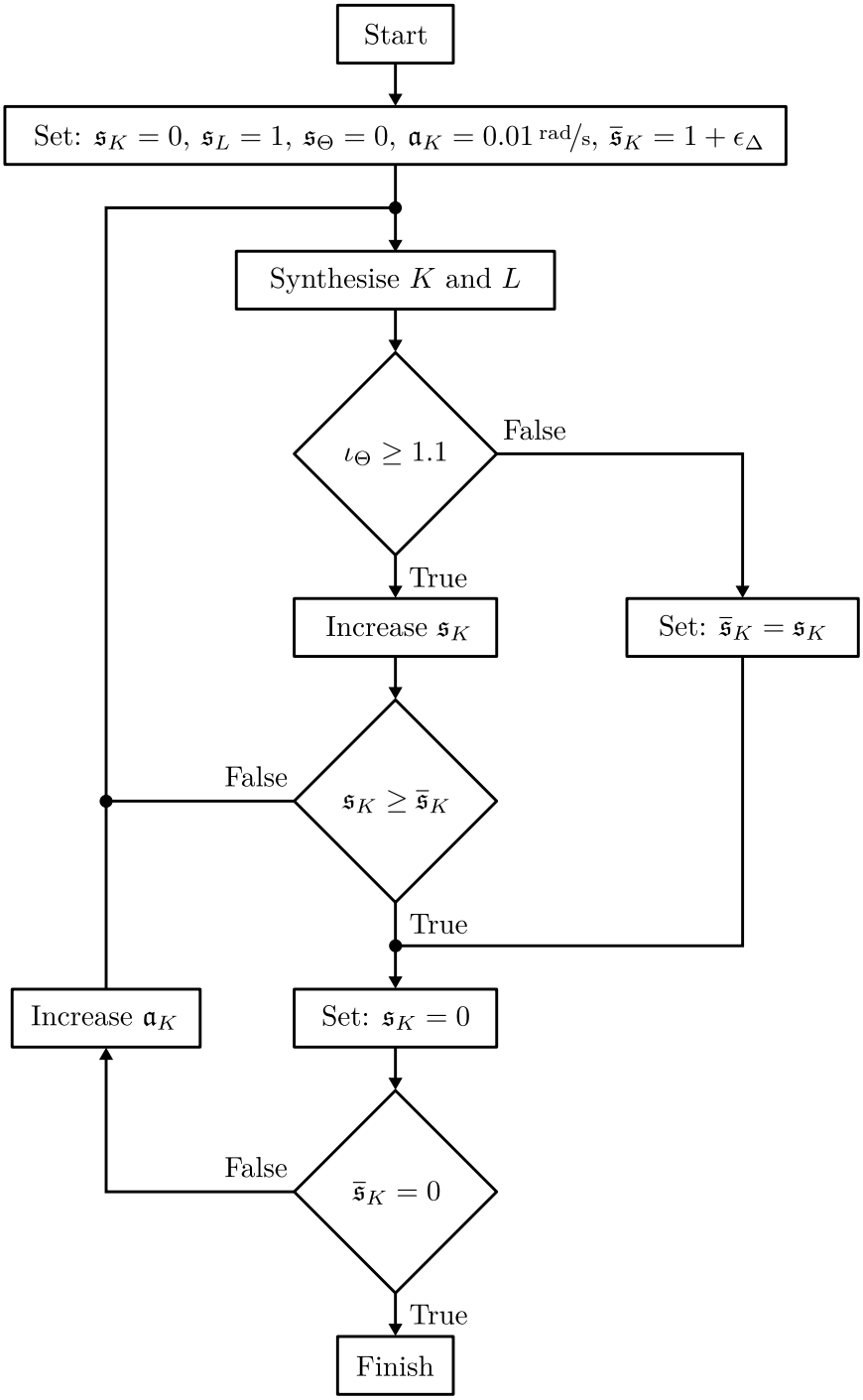

Figure 4.8: LTI multi-$\mathcal{H}_2$ and $\mathfrak{a}$ performance capability determination flow diagram.

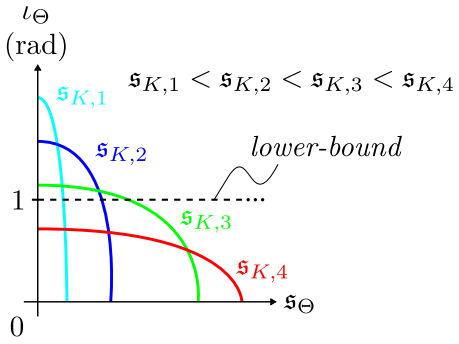

(a) Analysed turbulence rejection performance vs analysis uncertainty scale, for various synthesis uncertainty scales.

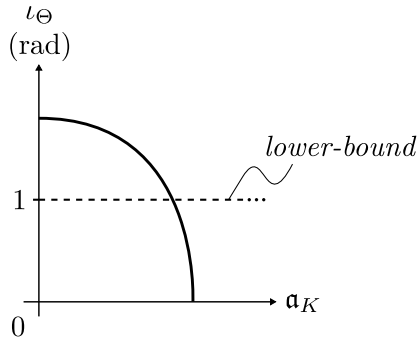

(b) Analysed turbulence rejection performance vs state-feedback synthesis exponential decay-rate.

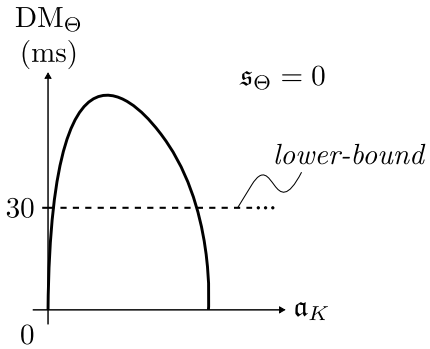

(c) Analysed DM vs state-feedback synthesis exponential decay-rate.

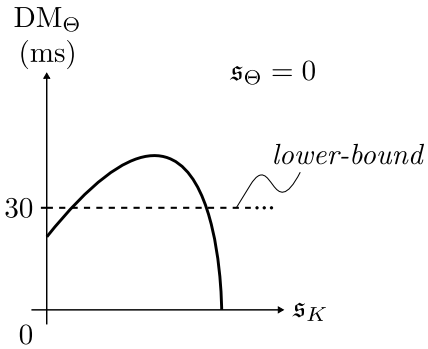

(d) Analysed DM vs state-feedback synthesis uncertainty scale.

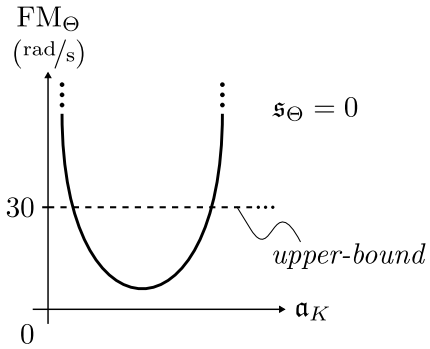

(e) Analysed FM vs synthesis exponential decay-rate.

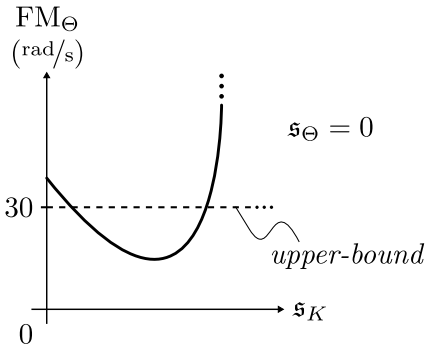

(f) Analysed FM vs state-feedback synthesis uncertainty scale.

Figure 4.9: Guidelines for IFR controller synthesis.

4.3.5 Results

Controller synthesis computation parameters and details are summarised in Table 4.8, with SDPT3 parameters unchanged from their default unless specified. Tests

Computation details		
Group	Description	Value(s)
Solver	YALMIP version	3
	MATLAB version	R2010a
	SDPT3 version	4.0
	SDPT3 accuracy	10^{-8}
	SDPT3 data scaling	Yes
	LMI shift	10^{-8}
	LMI variable bounds	$10^{8}\gamma$
Model	Norm-bounded state-space calculation parameters of Listing B.1	$(n_l, \epsilon_P, \epsilon_J, n_c, n_s, n_b) = (20, 0.01, 0.9, 10, 300, 300)$
Computer	CPU	64-bit Intel Core 2 Duo 3GHz
	RAM	1.9GiB
	OS	Ubuntu 10.04 LTS

Table 4.8: Controller synthesis computing details.

have demonstrated the superiority of the 64-bit true double precision calculations involved in SDPT3 over the 32-bit emulated double precision calculations, with factor differences of up 2 in obtained LMI objective γ, due to the change in LMI variable bounds to $10^4\gamma$ required by the 32-bit calculations.

State-feedback and estimator synthesis and analysis results for the nominal flight-case (4.134) are summarised in Tables 4.9, 4.10 and 4.11, with a variety of uncertainty scaling, and remaining state-feedback synthesis parameters corresponding to the sub-optimal AIFR LQ cost, determined according to Section 4.3.4 as

$$(\mathfrak{a}, \mathfrak{c})_K = \left(0.04\,\text{rad/s}, \cos^{-1}(0.177)\ \text{rad}\right) \tag{4.137}$$

A pure disk regional eigenvalue constraint is also included for state-feedback synthesis, which is such that the sub-optimal exponential decay-rate and damping are indirectly included, and the disk is given as

$$(\mathfrak{a}, \mathfrak{r}, \mathfrak{q}, \mathfrak{c})_K = \left(0, 2.48\,\text{rad/s}, 2.52\,\text{rad/s}, \frac{\pi}{2}\,\text{rad}\right) \tag{4.138}$$

and illustrated in Figure 4.10. The synthesis results are summarised with obtained LMI objective γ, solution accuracy $\max \nabla$, synthesis time t_{cpu}, rejectable turbulence severity ι_C and ι_Θ and stability margins DM_Θ and FM_Θ. The state-feedback LMI objective γ is given in terms of turbulence severity according to (4.133), which is a more intuitive measure and allows for comparison with the analysis results.[22]

22. The original state-feedback objective γ may be re-obtained as $\gamma = \frac{1}{9\iota^2}$.

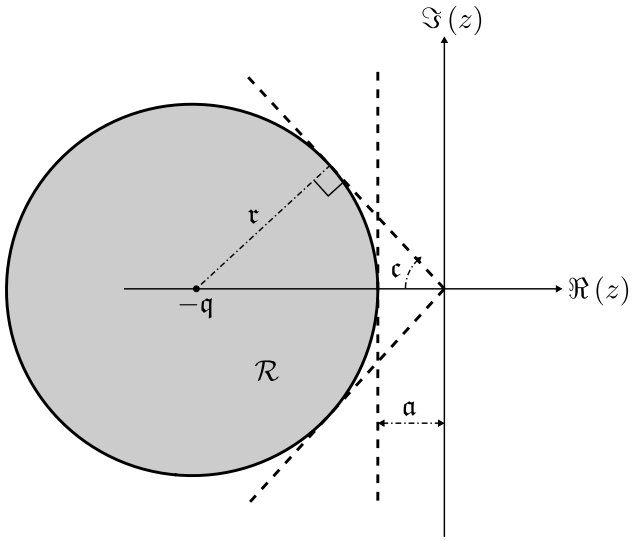

Figure 4.10: Indirect damping.

$\max \nabla$ is used by SDPT3 to determine when a sufficiently accurate solution has been obtained, defined in [77, pp.11] as

$$\max \nabla := \max \left(\text{relative gap, primal feasability measure, dual feasability measure}\right) \tag{4.139}$$

Indexes ι_C and ι_Θ are the severity of turbulence the estimator-based state-feedback controller can reject with respective IFR models (4.108) and (4.88), where the additional subscript SF denotes the use of pure state-feedback with the actual turbulence state. The various turbulence severity measures serve to bridge between the performance of the IFR model (4.88) and the reduced order IFR model (4.108) used for state-feedback synthesis. A turbulence severity measures is calculated for the corresponding closed-loop model according to (4.133) with either MATLAB *covar.m,* when $\mathfrak{s}_C, \mathfrak{s}_\Theta = 0$, or (3.62), when $\mathfrak{s}_C, \mathfrak{s}_\Theta \neq 0$, where *covar.m* has a calculation time of approximately 5 s. The DM_Θ and FM_Θ are calculated for the IFR model (4.88) with estimator-based state-feedback control. DM_Θ and FM_Θ are calculated with MATLAB *eig.m* for $\mathfrak{s}_\Theta = 0$ by including fourth-order Padé approximations and first-order unity DC gain LPFs, respectively, in the output used for feedback, and iterating the delay and bandwidth values until the real part of one or more of the eigenvalues is positive, where each iteration has a calculation time of approximately 1 s.

The estimator gain, synthesised with $\mathfrak{s}_L = 1$, results in a robust $\mathcal{H}_2$ performance that is equal for all the synthesised state-feedback gains in Table 4.9. The estimator synthesis and analysis results are summarised in Table 4.10, where γ_C and γ_Θ are the variances of the estimation error performance output of the respective IFR models (4.108) and (4.88). Additional estimator performance subscripts SF and $\mathbf{x} = 0$ denote the use of pure state-feedback with the actual turbulence state and the zeroing of the state's influence on the estimator, as is done for turbulence estimator optimisation in Section 4.3.3, respectively.

A robust analysis is summarised in Table 4.11 for estimator-based state-feedback controller no. 8 in Table 4.9, which corresponds to the largest state-feedback uncer-

tainty scaling $\mathfrak{s}_K = 0.05\,\text{rad}$ attaining $\iota_\Theta \geq 1.1$ for $\mathfrak{s}_\Theta = 0$, and also corresponds to the sub-optimal AIFR LQ cost. Only robust analysis measure $\gamma_{C,SF}|_{\mathbf{x}=\mathbf{0}}$ is included for the estimator, due to the infeasibility of LMI optimisation problem (3.62) when $\mathfrak{s}_C, \mathfrak{s}_\Theta = 1$.

Tables 4.12 and 4.13 summarise the controller synthesis and LTI analysis results for the toboggan flight-case (4.135) and bank turn flight-case (4.136) respectively, whose synthesis parameters are the same as the synthesis parameters of controller no.8 in Table 4.9.

Note that LMIs in (4.109) and (4.129) which are redundant in constraining the eigenvalue region of their respective models, is excluded from synthesis, *e.g.* if $\mathfrak{c}_K = \frac{\pi}{2}\,\text{rad}$ then the LMIs in (3.117) are excluded from (4.109). The removal of redundant LMIs removes its conservatism and variables from synthesis, resulting in superior performance and synthesis time.

An analysis of the following numeric results is presented in Section 4.3.6.

Table 4.9: IFR controller synthesis and LTI analysis results for the nominal flight-case (4.134).

	State-feedback synthesis								LTI analysis				
									$\mathfrak{s}_C, \mathfrak{s}_\Theta = 0$				
ID	$\mathfrak{s}_K$ (rad)	$\mathfrak{a}_K$ (rad/s)	$\mathfrak{r}_K$ (rad/s)	$\mathfrak{q}_K$ (rad/s)	$\cos(\mathfrak{c}_K)$ (rad)	$\iota_{C,SF}$ (rad)	∇ ($\times 10^{-6}$ rad)	t_{cpu} (s)	$\iota_{C,SF}$ (rad)	$\iota_{\Theta,SF}$ (rad)	ι_Θ (rad)	DM_Θ (ms)	FM_Θ (rad/s)
1	0	0	2.48	2.52	0	1.50	0.756	532	1.72	1.50	1.27	105	9
2	0	0.04	5	0	0.177	1.86	0.0983	725	1.93	1.68	1.44	92	11
3	1	0	2.48	2.52	0	0.942	23.8	7030	1.65	1.69	1.58	124	7
4[a]	1	0.04	5	0	0.177	0.273	1.07	6720	0.441	0.488	0.482	136	6
5	2	0	2.48	2.52	0	0.552	100	7780	1.45	1.51	1.39	135	7
6	3	0	2.48	2.52	0	0.380	71.7	7170	1.22	1.30	1.29	155	6
7	4	0	2.48	2.52	0	0.288	61.5	7440	1.10	1.18	1.17	166	6
8	5	0	2.48	2.52	0	0.231	76.7	7480	1.05	1.12	1.11	161	6
9[b]	5	0	2.48	2.52	0	0.160	69.9	8720	0.941	1.21	1.20	165	5

[a] Unstructured uncertainty removed, required for state-feedback synthesis feasibility.
[b] Thrust slew-rate of $\varsigma_t = 2 \times 10^{-3}$ rad/s included for state-feedback synthesis.

Table 4.10: IFR estimator synthesis and LTI analysis results for the controllers in Table 4.9.

Estimator synthesis			LTI analysis			
$(\mathfrak{a},\mathfrak{r},\mathfrak{q},\mathfrak{c})_L = (10\,\text{rad/s}, 15\,\text{rad/s}, 0, \frac{\pi}{2}\,\text{rad})$, $\mathfrak{s}_L = 1$			$\mathfrak{s}_C, \mathfrak{s}_\Theta = 0$			
$\gamma_{C,SF}\vert_{\mathbf{x}=\mathbf{0}}$ (rad)	∇ ($\times 10^{-6}$ rad)	t_{cpu} (s)	$\gamma_{C,SF}\vert_{\mathbf{x}=\mathbf{0}}$ (rad)	$\gamma_{C,SF}$ (rad)	$\gamma_{\Theta,SF}$ (rad)	γ_Θ (rad)
0.342	≤ 0.0834	≤ 240	0.0466	0.0548	0.0575	0.0575

Table 4.11: IFR controller robust analysis results for controller 8 in Table 4.9.

	Robust controller analysis			Robust estimator analysis
	$\mathfrak{s}_C, \mathfrak{s}_\Theta = 0.05$			$\mathfrak{s}_C = 1$
ID	$\iota_{C,SF}$ (rad)	$\iota_{\Theta,SF}$ (rad)	ι_Θ (rad)	$\gamma_{C,SF}\vert_{\mathbf{x}=\mathbf{0}}$ (rad)
8	0.303	0.343	0.310	0.0552

Table 4.12: IFR controller synthesis and LTI analysis results for toboggan flight-case (4.135) with synthesis parameters of controller 8 in Table 4.9.

	State-feedback synthesis				LTI analysis				
	$(\mathfrak{a},\mathfrak{r},\mathfrak{q},\mathfrak{c})_K = (0, 2.48\,\text{rad/s}, 2.52\,\text{rad/s}, \frac{\pi}{2}\,\text{rad})$ $\mathfrak{s}_K = 0.05\,\text{rad}$				$\mathfrak{s}_C, \mathfrak{s}_\Theta = 0$				
ID	h_0	$\iota_{C,SF}$ (rad)	∇ ($\times 10^{-6}$ rad)	t_{cpu} (s)	$\iota_{C,SF}$ (rad)	$\iota_{\Theta,SF}$ (rad)	ι_Θ (rad)	DM_Θ (ms)	FM_Θ (rad/s)
10	29′557	0.511	102	10600	1.42	1.58	1.36	141	7
11	28′750	0.531	84.7	8630	1.65	1.70	1.56	120	8
12	27′943	0.320	73.1	8890	1.20	1.31	1.28	118	8

Table 4.13: IFR controller synthesis and LTI analysis results for bank turn flight-case (4.136) with synthesis parameters of controller 8 in Table 4.9.

	State-feedback synthesis				LTI analysis				
	$(\mathfrak{a},\mathfrak{r},\mathfrak{q},\mathfrak{c})_K = (0, 2.48\,\text{rad/s}, 2.52\,\text{rad/s}, \frac{\pi}{2}\,\text{rad})$ $\mathfrak{s}_K = 0.05\,\text{rad}$				$\mathfrak{s}_C, \mathfrak{s}_\Theta = 0$				
ID	ϕ_0	$\iota_{C,SF}$ (rad)	∇ ($\times 10^{-6}$ rad)	t_{cpu} (s)	$\iota_{C,SF}$ (rad)	$\iota_{\Theta,SF}$ (rad)	ι_Θ (rad)	DM_Θ (ms)	FM_Θ (rad/s)
13	0	0.356	68.1	11200	1.24	1.22	1.22	133	8
14	9.5	0.339	173	11200	1.03	1.16	1.16	181	5
15	19	0.344	35.3	15000	1.06	1.12	1.12	140	7

4.3.6 Analysis

Estimator-based state-feedback controllers are synthesised and analysed for the IFR model developed in Chapter 2, of which the results are given in Section 4.3.5. The results are used here to analyse/quantify four aspects of the synthesis, which are the *effectiveness of the turbulence estimator*, *effectiveness of the model reduction*, *involved conservatism* and *numerical inaccuracy*. The analysis proceeds as follows:

1. *Effectiveness of the turbulence estimator*: The effectiveness of using the estimated turbulence state in the feedback loop, rather than the actual turbulence state, is determined by comparing the indices $\iota_{\Theta,SF}$ and ι_{Θ} in Tables 4.9 and 4.11, and is quantified as the reduction in turbulence rejection performance $\epsilon_{\iota,1} := \frac{\iota_{\Theta,SF}-\iota_{\Theta}}{\iota_{\Theta,SF}} \times 100\%$. The reduction in turbulence rejection performance has a range of $15.3 \geq \epsilon_{\iota,1} \geq 0.769\%$, of which the maximum reduction reduces to $\epsilon_{\iota,1} = 9.62\%$ when uncertainty is included for state-feedback synthesis.
   Furthermore, according to Table 4.10, the use of the estimated turbulence state in the feedback loop has no influence on the estimation error variance, *i.e.* $\epsilon_{\gamma,1} := \frac{\gamma_{\Theta}-\gamma_{\Theta,SF}}{\gamma_{\Theta,SF}} \times 100\% = 0\%$.
2. *Effectiveness of the model reduction*: Similar to analysis no.1 above, the effectiveness of the reduced-order turbulence model used for synthesis is determined by comparing $\iota_{C,SF}$ and $\iota_{\Theta,SF}$ in Tables 4.9 and 4.11, and is quantified as the reduction in turbulence rejection performance $\epsilon_{\iota,2} := \frac{\iota_{C,SF}-\iota_{\Theta,SF}}{\iota_{C,SF}} \times 100\%$. The reduction in turbulence rejection performance has a range of $13.0 \geq \epsilon_{\iota,2} \geq -28.9\%$, of which the maximum reduction reduces to $\epsilon_{\iota,2} = -2.42\%$ when uncertainty is included for state-feedback synthesis. Thus, the reduced order model, whose power is higher than the original model at lower frequencies (see Figure 4.7), is conservative when uncertainty is included for state-feedback synthesis.
   Furthermore, according to Table 4.10, the use of the reduced order turbulence model for synthesis has approximately no influence on the estimation error variance, *i.e.* $\epsilon_{\gamma,2} := \frac{\gamma_{\Theta,SF}-\gamma_{C,SF}}{\gamma_{C,SF}} \times 100\% \approx 0\%$.
   The zeroing of the state in the estimator synthesis formulation results in an optimistic estimation error variance, whose influence on estimation performance is quantified as the increase estimation error variance when the influence of the state on the estimator is included, and is calculated from Table 4.10 as $\epsilon_{\gamma,3} := \frac{\gamma_{C,SF}-\gamma_{C,SF}\big|_{\mathbf{x}=\mathbf{0}}}{\gamma_{C,SF}\big|_{\mathbf{x}=\mathbf{0}}} \times 100\% = 17.6\%$.
3. Involved conservatism:
   a) *Norm-bounded state-space description*: Due to the reduced uncertainty used for state-feedback synthesis, AIFR stability and performance are not guaranteed, which can only be measured via non-linear simulation. Non-linear simulation is used to determine the level of non-linearity the controller may be subjected to while maintaining adequate performance, by increasing turbulence severity from 0 upward, which in turn increases the involved non-linearity as system variables increase in amplitude and into their non-linear domains.

b) *Lyapunov's shaping paradigm*: By only considering $\iota_{C,SF}$ and $\gamma_{C,SF}|_{\mathbf{x}=\mathbf{0}}$, the effect of model reduction on the performance is eliminated. Also, considering only LTI synthesis and analysis, the conservatism involved in Theorems 1 and 2 is eliminated. Thus, the conservatism involved in Lyapunov's shaping paradigm may be measured by $\iota_{C,SF}$ with $\mathfrak{s}_K = 0$ for synthesis and $\mathfrak{s}_C = 0$ for analysis.
Considering $\iota_{C,SF}$ for LTI synthesis and analysis in Table 4.9, *i.e.* controllers no.1 and no.2, the conservatism involved in Lyapunov's shaping paradigm is measured as an increase of 14.7% in performance from the LTI synthesis to LTI analysis, which corresponds to controller no. 2. This conservatism measure does not, however, measure the amount by which the LTI analysis measure $\iota_{C,SF}$ will increase when Lyapunov's shaping paradigm is absent, it simply provides a means to quantify the conservatism, *i.e.* the analysis measure $\iota_{C,SF}$ may very well be the optimum.

c) *Simultaneous conservatism of Lyapunov's shaping paradigm and Theorems 1 and 2*: The conservatism involved in Theorems 1 and 2 cannot be measured directly, as it is not distinguishable from the conservatism involved in Lyapunov's shaping paradigm.
Theoretically, without conservatism, computation inaccuracies or the reduction of the model, an increase in uncertainty or/and a smaller eigenvalue region constraint results in either equal or poorer regulation performance. This fact is used to measure the level of synthesis performance increase which may be obtained when the conservatism involved in Lyapunov's paradigm *and* Theorems 1 and 2 is absent, by assuming that the influence of the numerical inaccuracy on the performance is sufficiently small.
Comparing controllers no.3 and no.4 in Table 4.9, of which the latter has a larger regional eigenvalue constraint and less uncertainty than the former, the simultaneous influence of Lyapunov's shaping paradigm and that of Theorems 1 and 2 is quantified as the increase of 245% in synthesised turbulence rejection performance from the least constraining controller no.4 to controller no.3. This large increase in turbulence rejection performance corresponds to omitted redundant LMIs in (3.110) and (3.113) from state-feedback synthesis, and provides the motivation for using a disk constraint with $\mathfrak{q}_K \neq 0$ to indirectly include damping and settling-time constraints.
Similar to analysis no.3b above, considering both $\iota_{C,SF}$ and $\gamma_{C,SF}|_{\mathbf{x}=\mathbf{0}}$ for robust synthesis and analysis in Tables 4.9, 4.10 and 4.11, the conservatism involved in Lyapunov's shaping paradigm and that of Theorems 1 and 2 is measured as an increase in turbulence rejection performance of 31.2% and a decrease in estimation error variance of 83.9% from the robust synthesis to robust analysis.

4. *Numerical inaccuracy*: The influence of numerical inaccuracy on performance cannot be separated from the above mentioned conservatism, and thus cannot be quantified independently. The numerical inaccuracy of the state-feedback controllers synthesised in Table 4.9 are bounded by $0.0983 \times 10^{-6} < \nabla < 100 \times$

10^{-6} (rad). The numerical inaccuracy of the synthesised estimator gains for the state-feedback gains in Table 4.9 are bounded by $\nabla < 0.0834 \times 10^{-6}$ (rad).

4.4 Implementation

The synthesised IFR controllers is implemented according to the controller architecture defined in Section 4.1, the estimator-based state-feedback structure defined in Section 3.8, and the A330 estimators defined in Section 4.2.1.6.

The synthesised IFR controllers, such as those listed in Table 4.9, are digitally implemented with the A330 avionics at $\omega_s = 200\pi$ rad/s, by replacing all continuous-time integrators in the controller with forward numerical integrators. Even though the synthesis is based on continuous-time models, the robust eigenvalue region design in Section 4.2.2.2 includes robustness against aliasing introduced by the digitisation. A block-diagram of the IFR control implementation is included as Figure 4.11, and explained as follows.

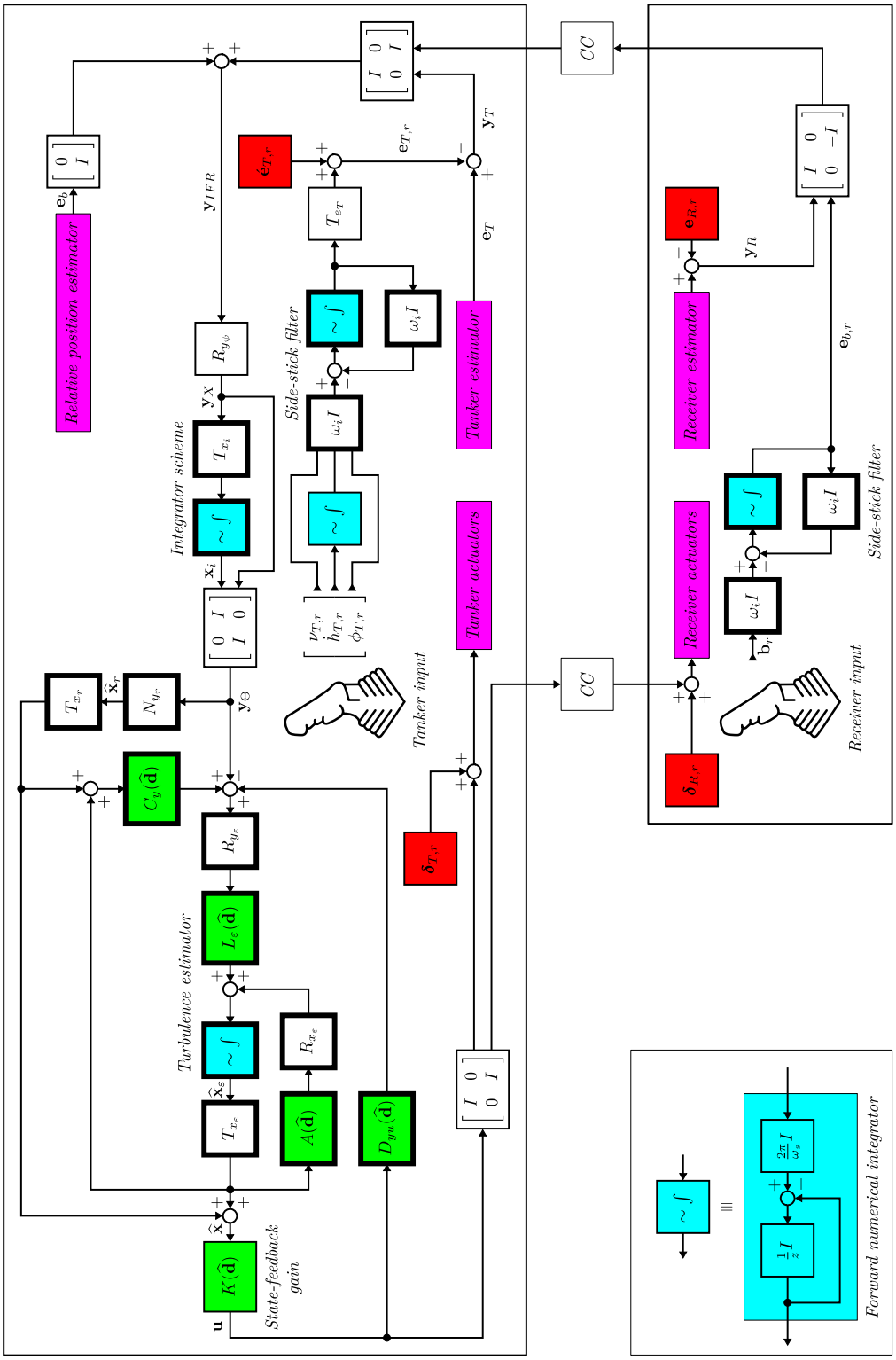

Figure 4.11: Coupled AIFR controller implementation.

The tanker and receiver are framed as separate systems, identifiable via their respective side-stick reference inputs, actuator inputs (magenta) and estimator outputs (magenta), connected by send and receive Communication Channels (CCs). For the fully coupled controller, the flight-control law is implemented with tanker avionics, while only a side-stick filter (bold) and reference (red) additions/subtractions are implemented with receiver avionics. [23] The reference (red) subtractions and additions are found at the estimator outputs and the actuator command inputs respectively, and serve to transform the IFR *system* into its finite gain form (4.13), to which control is applied. All references (red) but that of the side-sticks are fixed at system values when the autopilot is activated, after which the integrator scheme (bold), presented in Section 4.1, will correct any error/change in the system's trim/reference. The forward numerical integrators (cyan) of the turbulence estimator (bold) and the integrator scheme (bold) are initialised at zero, while that of the side-stick filters (bold) and climb-rate reference are initialised at system values when the autopilot is activated. Side-stick references are filtered at $\alpha = 0.01\,{}^{\text{rad}}/_{\text{s}}$ to avoid possible regulation overshoot, as the measures used for synthesis do not directly include reference transients. Even though it is preferred to have reference bandwidths lower than α, with the already slow response of the system, a smaller bandwidth would result in an impractically slow response time. Note that the references are feed-forward and do not affect the closed-loop eigenvalues of the system. Side-stick references should also be limited by slew-rate bounds to help prevent actuator saturation for large reference inputs, although the measures used for synthesis do not directly include these bounds and falls outside the scope of the thesis.

Furthermore, the transformation matrices used in the IFR model augmentations as well as estimator formulation are used in the implementation, along with the additional two transformation matrices

$$R_{y_\psi} \coloneqq \begin{bmatrix} I_8 & 0_{8\times1} & 0_{8\times24} & 0_{8\times1} & 0_{8\times16} \\ 0_{24\times8} & 0_{24\times1} & I_{24} & 0_{24\times1} & 0_{24\times16} \\ 0_{1\times8} & +1 & 0_{1\times24} & -1 & 0_{1\times16} \\ 0_{16\times8} & 0_{16\times1} & 0_{16\times24} & 0_{16\times1} & I_{16} \end{bmatrix}, \; \mathbf{y}_X = R_{y_\psi}\mathbf{y}_{IFR} \tag{4.140}$$

required to replace absolute heading with relative heading [24], and

$$T_{e_T} \coloneqq \begin{bmatrix} 0_{6\times3} \\ \begin{bmatrix} 0 & 0 & 1 \end{bmatrix} \\ 0_{2\times3} \\ \begin{bmatrix} 0 & 1 & 0 \end{bmatrix} \\ 0_{8\times3} \\ \begin{bmatrix} 1 & 0 & 0 \end{bmatrix} \\ 0_{6\times3} \end{bmatrix} \tag{4.141}$$

used with

$$\acute{\mathbf{e}}_{T,r} \coloneqq \text{blkdiag}\left(I_6, 0_{1\times1}, I_2, 0_{1\times1}, I_8, 0_{1\times1}, I_6\right)\mathbf{e}_{T,r} \tag{4.142}$$

23. Note that the flight-control law may be implemented with receiver avionics as well.
24. Note that $R_{y_\psi} \neq T_{y_\psi}$ due to the R.H.S. multiplication with T_{x_ψ}.

to include tanker side-stick reference inputs. The tanker and receiver absolute **heading estimates must support windup** to exclude discontinuities in the relative heading calculation. Gain-scheduled matrix gains (lime) are included as functions of flight-domain estimate $\widehat{\mathbf{d}}$ of (4.5), and are implemented with the simplicial-complex based linear-interpolation developed in Appendix B.2.

Refer to Chapter 5 for simulation results of the implemented IFR controller.

Chapter 5

Non-linear simulation

5.1 Overview of Simulation

MATLAB SIMULINK is used for non-linear simulation, with ODE3 set as its non-linear solver at a fixed sampling period of 1 ms.

The SIMULINK model of the A330 is provided by Airbus, which implements the standard aircraft 6DOF EOM given by (2.7)-(2.18), with additional: quaternion aircraft attitude description, to remove singularities in the simulation involved in the *gimbal equation* (2.17); A330 moment of inertia and aerodynamic coefficient data; velocity integrators to provide absolute position. The A330 model is duplicated to provide both tanker and receiver, whose relative position is inherent their absolute positions and attitudes. The MATLAB EMBEDDED FUNCTION is used to convert the relative position to boom variables λ, σ and χ according to (2.23)-(2.25). IFR turbulence is implemented with temporal LTI model (4.58), due to the absence of a time-varying spatial model. Estimates of the A330 and the relative position are included by adding white noise to the variables, which is passed through a $30\,{}^{\text{rad}}/_{\text{s}}$ LPF and delayed by 10 ms, as described by Table 4.5. The SIMULINK block diagram of the IFR model is not included, and is considered standard procedure. Since the IFR controller is designed to be implemented for the non-linear simulation model, we refer to the non-linear simulation model as the system.

The AIFR controller is implemented according to the block diagram given in Figure 4.11, where the CCs are included with 10 ms delays, and the implementation of scheduled gains (lime) is given in Figure B.1 and Appendix B.2.

A linear state-space model is included along-side the non-linear model, which implements the same controller and estimators, and is subjected to the same turbulence and measurement noise. [1]

Furthermore, all white noise sources are included with the BAND-LIMITED WHITE NOISE block with seed $\begin{bmatrix} 1 & 2 & \cdots & 61 \end{bmatrix}^T$, which corresponds to the white noise input vector $\mathbf{w}_\Theta$ of IFR model (4.88). The seed is reused in all simulations to

1. Note that the linear model does not include any saturation.

produce more comparable results.[2] The duration of each simulated AIFR is 300 s, which is the duration required to complete IFR contact.

The AIFR plots used to illustrate system trajectories is described as:

1. *Receptacle position plot*: The receptacle position plot illustrates the receiver receptacle position trajectory relative to the boom envelopes, which serves to show the relative position regulation performance of the controller.
2. *Receptacle time plot*: The receptacle time plot illustrates the receiver receptacle position trajectory relative to the boom envelopes over time, which serves to show the progression of the relative position regulation performance of the controller over time.
3. *Statistical plot*: The statistical plot illustrates the normalised 3σ-bounds, the normalised maximums and the normalised variances of the system variables. The statistics are plotted according to the indexes of the system variables, of which the indices corresponds to

$$\begin{bmatrix} \varepsilon\mathbf{m} \\ \varepsilon\boldsymbol{\delta} \\ \begin{bmatrix} I_6 & 0_{6\times 2} \end{bmatrix} \varepsilon\dot{\boldsymbol{\delta}} \end{bmatrix} \tag{5.1}$$

for both the tanker and receiver, which are normalised with their maximums according to the IFR multi-$\mathcal{H}_2$ performance specification (4.94), and corresponds to

$$\begin{bmatrix} \varepsilon\lambda \\ \varepsilon\sigma \\ \varepsilon\chi \\ \sqrt{\mathbf{z}_B^T\mathbf{z}_B} \\ \sqrt{\operatorname{diag}\left(\tilde{\mathbf{g}}_T\tilde{\mathbf{g}}_T^T\right)} \\ \sqrt{\operatorname{diag}\left(\tilde{\mathbf{g}}_R\tilde{\mathbf{g}}_R^T\right)} \end{bmatrix} \tag{5.2}$$

for receptacle regulation and the turbulence estimation errors, where $\varepsilon\lambda$, $\varepsilon\sigma$ and $\varepsilon\chi$ are normalised with the contact envelope maximums in Table 2.1, $\sqrt{\mathbf{z}_B^T\mathbf{z}_B}$ already has a maximum of 1 and is not normalised, and $\sqrt{\operatorname{diag}\left(\tilde{\mathbf{g}}_T\tilde{\mathbf{g}}_T^T\right)}$ and $\sqrt{\operatorname{diag}\left(\tilde{\mathbf{g}}_R\tilde{\mathbf{g}}_R^T\right)}$ are normalised component-wise with their corresponding standard deviations of the actual simulated turbulence components. Thus, the turbulence statistics illustrates the turbulence estimation error 3σ-bound relative to the actual turbulence 3σ-bound, while the remaining statistics illustrate the system perturbation relative to their constraints. The maximums serve to measure the hard-bounds of IFR, while the 3σ-bounds serve as the comparable measure used for synthesis.
4. *Maximum settling time plot*: The maximum settling-time plot illustrates the regional eigenvalue constraint $\mathfrak{a}$ on the AIFR trajectory according to the robust

2. Note that the Band-Limited White Noise block with the simulation sampling frequency of 2000π rad/s accurately approximates the infinite bandwidth of white noise when passed through a LPF a bandwidth of 30 rad/s or less.

trajectory interpretation (3.152), and is calculated with the discrete time-derivative

$$\frac{\frac{d}{dt}\left(\left\|\text{chol}\left(P_{\mathfrak{a}}\right)\mathbf{x}\left(t\right)\right\|_2\right)}{\left\|\text{chol}\left(P_{\mathfrak{a}}\right)\mathbf{x}\left(t\right)\right\|_2} \approx \frac{\left\|\text{chol}\left(P_{\mathfrak{a}}\right)\mathbf{x}\left(\left(k+1\right)T_s\right)\right\|_2 - \left\|\text{chol}\left(P_{\mathfrak{a}}\right)\mathbf{x}\left(kT_s\right)\right\|_2}{T_s\left\|\text{chol}\left(P_{\mathfrak{a}}\right)\mathbf{x}\left(kT_s\right)\right\|_2}, \quad k = 0, 1, 2, \ldots \tag{5.3}$$

where $T_s = 10^{-2}\,\text{s}$ is the sampling period of the trajectory data and the Lyapunov variable $P_{\mathfrak{a}} = X_{\mathfrak{a}}^{-1}$ from state-feedback synthesis is used.

5. *Spectral radius* plot: The spectral radius plot illustrates the regional eigenvalue constraint $\mathfrak{r}$ on the AIFR trajectory according to the robust trajectory interpretation (3.153), and is calculated with the discrete time-derivative

$$\frac{\left\|\text{chol}\left(X_{\mathfrak{r}}\right)\dot{\mathbf{x}}\right\|_2}{\left\|\text{chol}\left(X_{\mathfrak{r}}\right)\mathbf{x}\right\|_2} \approx \frac{\left\|\text{chol}\left(X_{\mathfrak{r}}\right)\frac{\mathbf{x}((k+1)T_s)-\mathbf{x}(kT_s)}{T_s}\right\|_2}{\left\|\text{chol}\left(X_{\mathfrak{r}}\right)\mathbf{x}\left(kT_s\right)\right\|_2}, \quad k = 0, 1, 2, \ldots \tag{5.4}$$

where $T_s = 10^{-2}\,\text{s}$ is the sampling period of the trajectory data and the Lyapunov variable $X_{\mathfrak{a}}$ from state-feedback synthesis is used.

6. *Turbulence estimation plots*: The turbulence estimation plot illustrates the accuracy of the turbulence estimator.
7. *Input plots:* The input plot illustrates the trajectories of references or included uncertainty over time.

5.2 Nominal flight-case

Controllers are synthesised for the nominal flight-case (4.134) and are summarised in Section 4.3.5. Controller no. 8 in Table 4.9 is used to determine the effectiveness of the LMI technique and measure the conservatism involved in the norm-bounded state-space description.

A ramp in turbulence severity with a gradient of $\frac{1}{300}\,\text{rad/s}$ is used to determine the turbulence rejection capability of the controller, of which the boom exits the contact envelope at a turbulence severity of $\iota = 1.42\,\text{rad}$, with no included uncertainty in actuators, weight, cg or aerodynamic coefficients. We choose a turbulence severity of $\iota = 1\,\text{rad}$ for non-linear simulation, *i.e.* medium turbulence, to analyse performance and robustness against uncertainty.

5.2.1 Steady-state performance without uncertainty

The receptacle position and time plot, as well as the statistical plot, the turbulence estimation plot and the turbulence estimation error plot is given in Figures 5.1, 5.2, 5.3, 5.4 and 5.5 respectively, for controller no.8, $\iota = 1\,\text{rad}$, and zero system uncertainty. Its AIFR success is calculated as 100% for the system, *i.e.* the receiver receptacle is maintained within the contact envelope 100% of the time, as well as

100% of the time for the linear model. The receptacle position plot shows that σ and χ is maintained within approximately 50% and 25% of the contact envelope bounds respectively, while λ is much closer to its bound at approximately 90% of the contact envelope bounds.

The 3σ regulation performance of the linear model, illustrated in the statistical plot, is used to evaluate performance degradation due to digitisation and the bandwidths and delays of the of estimators and CCs, which causes a maximum regulation performance degradation of

$$\frac{\max_i \left(\frac{3\sigma_{z_i}}{\overline{z}_i}\right) - \frac{1}{\iota_\Theta}\Big|_{\mathfrak{s}_\Theta=0}}{\frac{1}{\iota_\Theta}\Big|_{\mathfrak{s}_\Theta=0}} \times 100\% \quad \approx \quad 22.1\% \tag{5.5}$$

which corresponds to the rate of the horizontal stabiliser of the tanker and receiver, where $\frac{3\sigma_{z_i,sim}}{\overline{z}_i}$ is the i^{th} system constraint in Figure 5.3 and $\frac{1}{\iota_\Theta}\Big|_{\mathfrak{s}_\Theta=0}$ is the inverse of the LTI turbulence rejection performance of controller no.8 in Table 4.9. From the statistical plot, it is apparent that the system spoilers of both the tanker and receiver become saturated in amplitude, while their horizontal stabilisers saturate in rate, which are coherent with the poorer longitudinal relative position regulation seen in Figures 5.1 and 5.2. Even though these actuators saturate, the controller is robust enough to maintain system stability and relative position regulation. The saturation in the actuators is also apparent in the linear model, and we conclude that the cause of the actuator saturation is due to digitisation and the bandwidths and delays of the of estimators and CCs. The only other insufficient regulation that occurs is the roll-rate and roll-angle of the receiver, which is coherent with the saturation of the starboard side spoiler amplitudes of the receiver. The estimation errors of the turbulence are approximately equal for the linear and non-linear model, except for the axial turbulence components. The increase in axial turbulence estimation error, visible at approximately 15 s and 170 s in Figures 5.4 and 5.5, is possibly due to the non-linear drag induced by non-zero side-slip angle, of which the non-linear drag is compensated for by the negative axial turbulence estimate, although a means for determining its cause is pending.

Furthermore, controller no.1 in Table 4.9, which excludes uncertainty for state-feedback synthesis, attains similar regulation performance to controller no.8. The difference between controllers no.1 and no.8, however, becomes apparent when uncertainty is included in the system, which is analysed in Section 5.2.3.

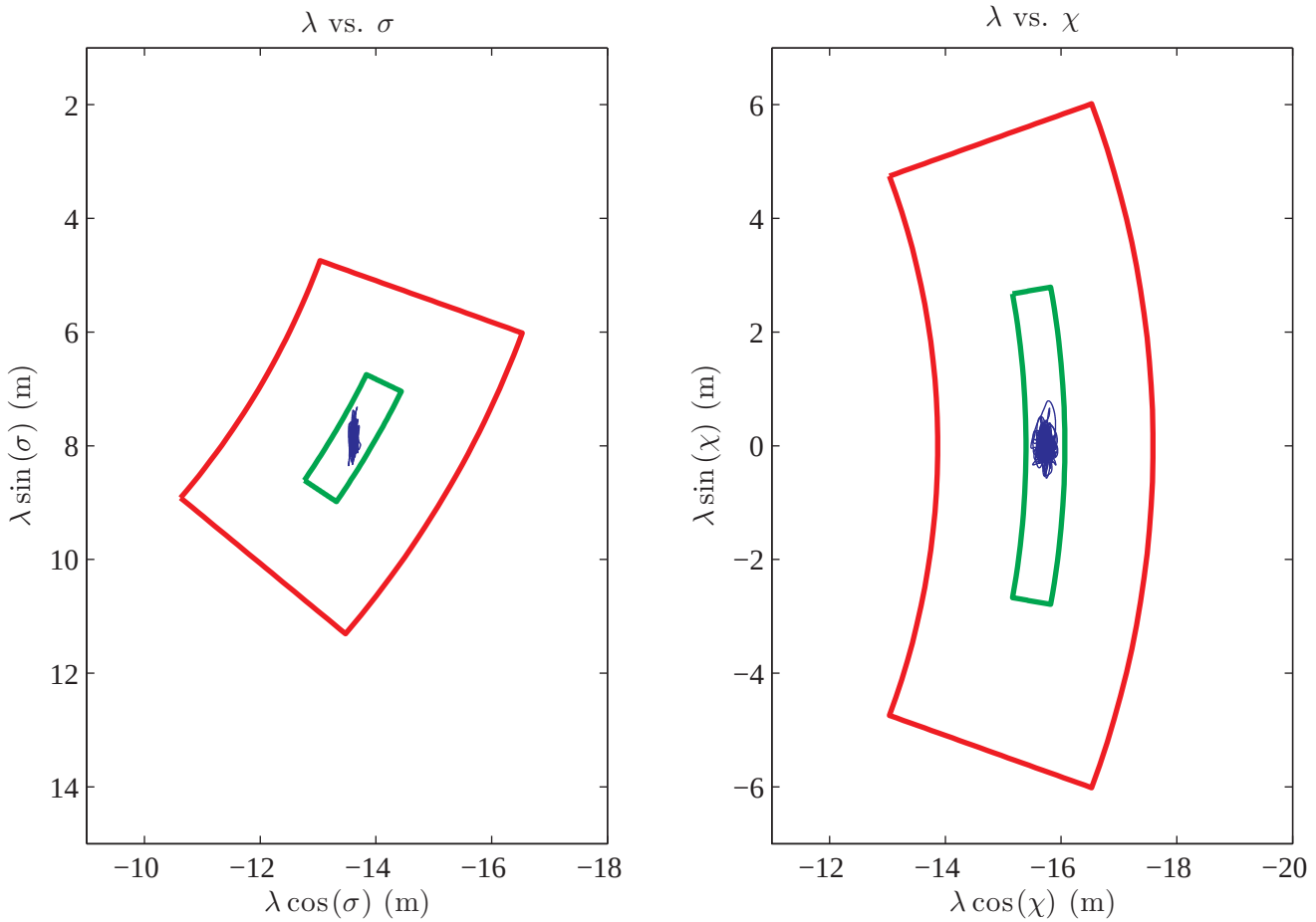

Figure 5.1: Receptacle position plot for the nominal flight-case (4.134), controller no.8 in Table 4.9, turbulence severity $\iota = 1\,\text{rad}$ (medium turbulence), and zero uncertainty. Legend: Contact envelope (green); Disconnect envelope (red); Non-linear model trajectory (blue).

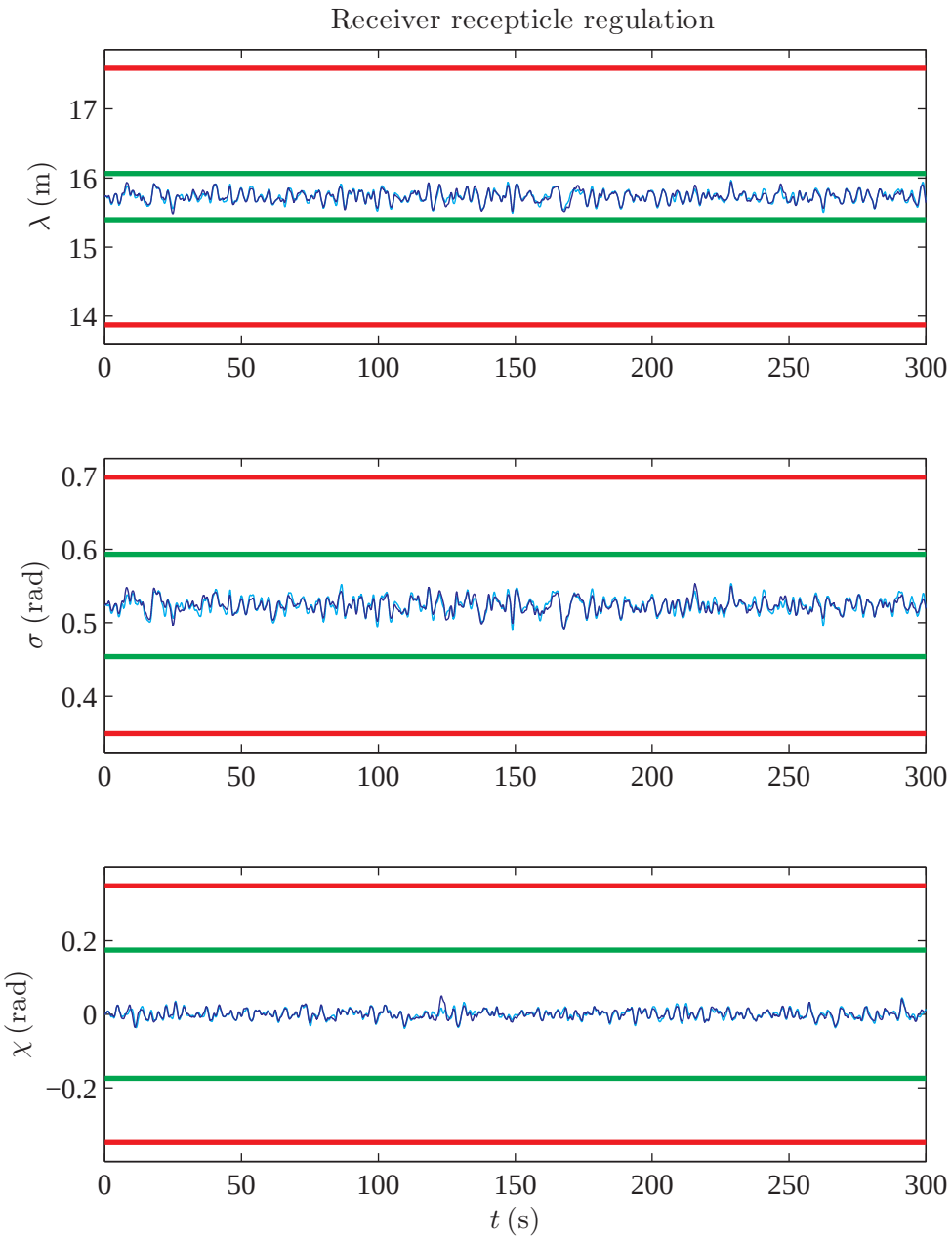

Figure 5.2: Receptacle time plot for the nominal flight-case (4.134), controller no.8 in Table 4.9, turbulence severity $\iota = 1$ rad (medium turbulence), and zero uncertainty. Legend: Contact envelope (green); Disconnect envelope (red); Linear model trajectory (cyan); Non-linear model trajectory (blue).

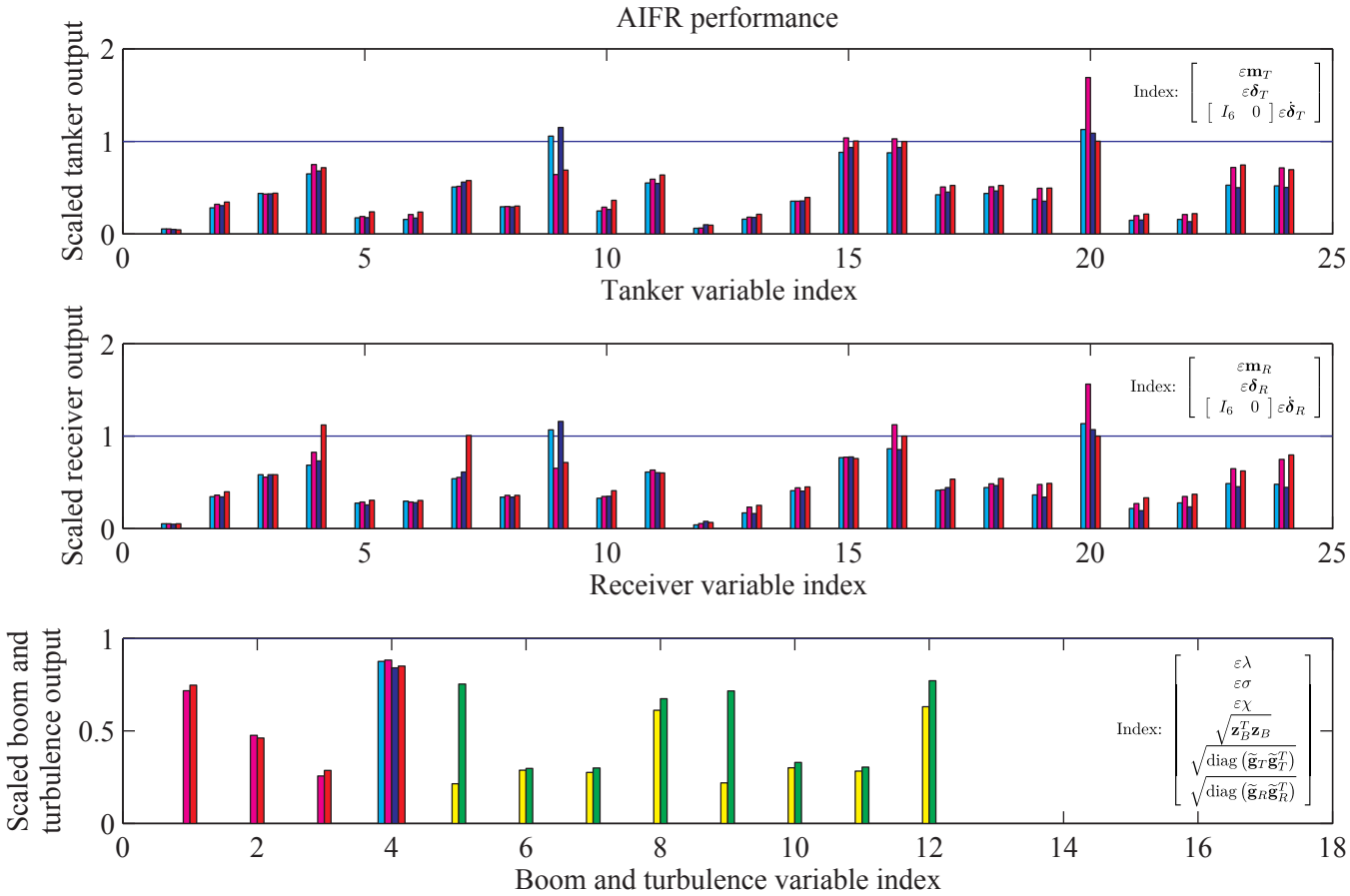

Figure 5.3: Statistical plot for the nominal flight-case (4.134), controller no.8 in Table 4.9, turbulence severity $\iota = 1\,\mathrm{rad}$ (medium turbulence), and zero uncertainty. Legend: Normalised 3σ-bounds of the linear model (cyan); Normalised maximums of the linear model (magenta); Normalised 3σ-bounds of the non-linear model (blue); Normalised maximums of the non-linear model (red); Normalised turbulence estimation error variances for the linear IFR model (yellow); Normalised turbulence estimation error variances for the non-linear IFR model (green).

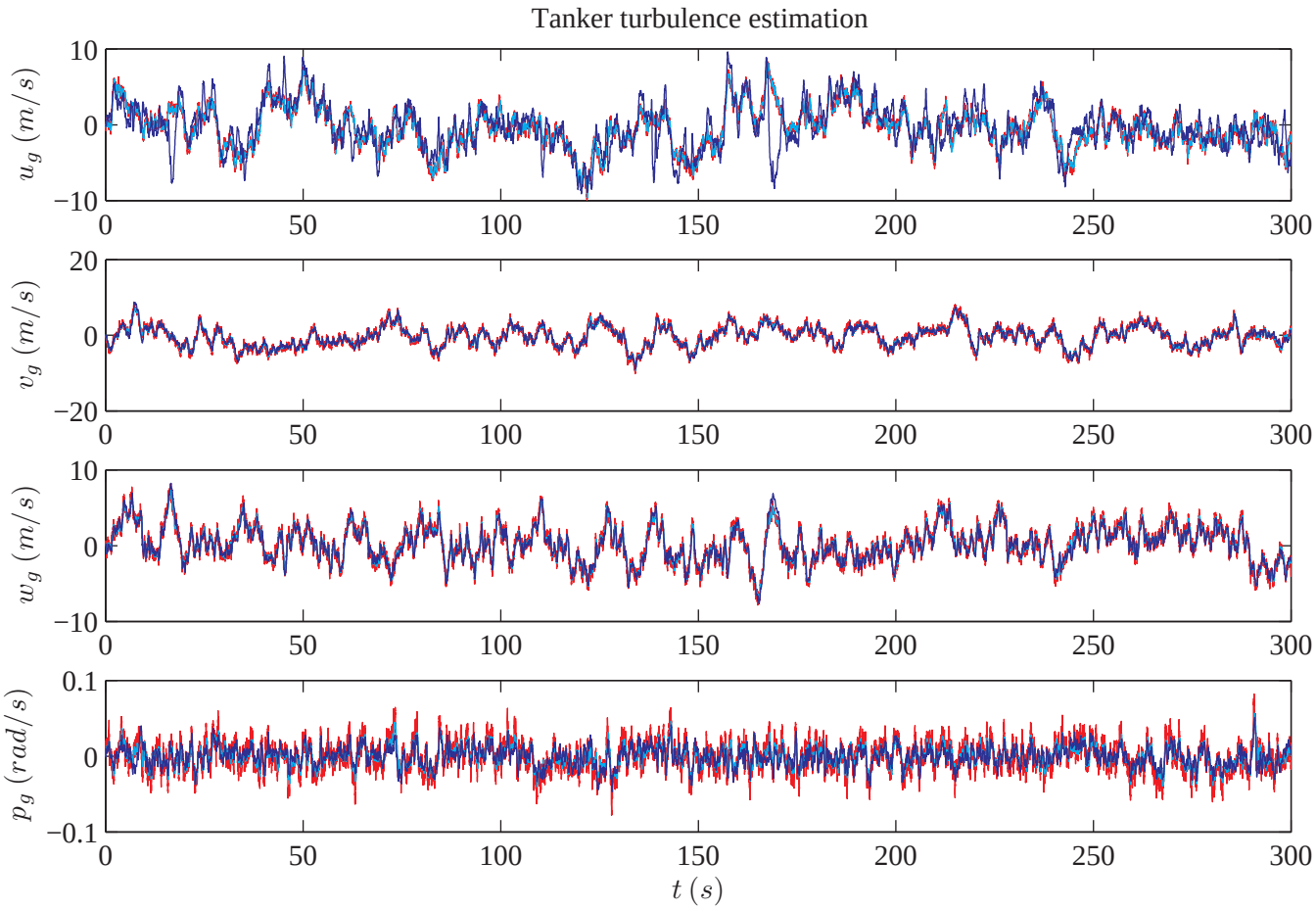

Figure 5.4: Tanker turbulence estimation plot for the nominal flight-case (4.134), controller no.8 in Table 4.9, turbulence severity $\iota = 1\,\text{rad}$ (medium turbulence), and zero uncertainty. Legend: Actual turbulence (red); Turbulence estimation for the non-linear model (blue); Turbulence estimation for the linear model (cyan).

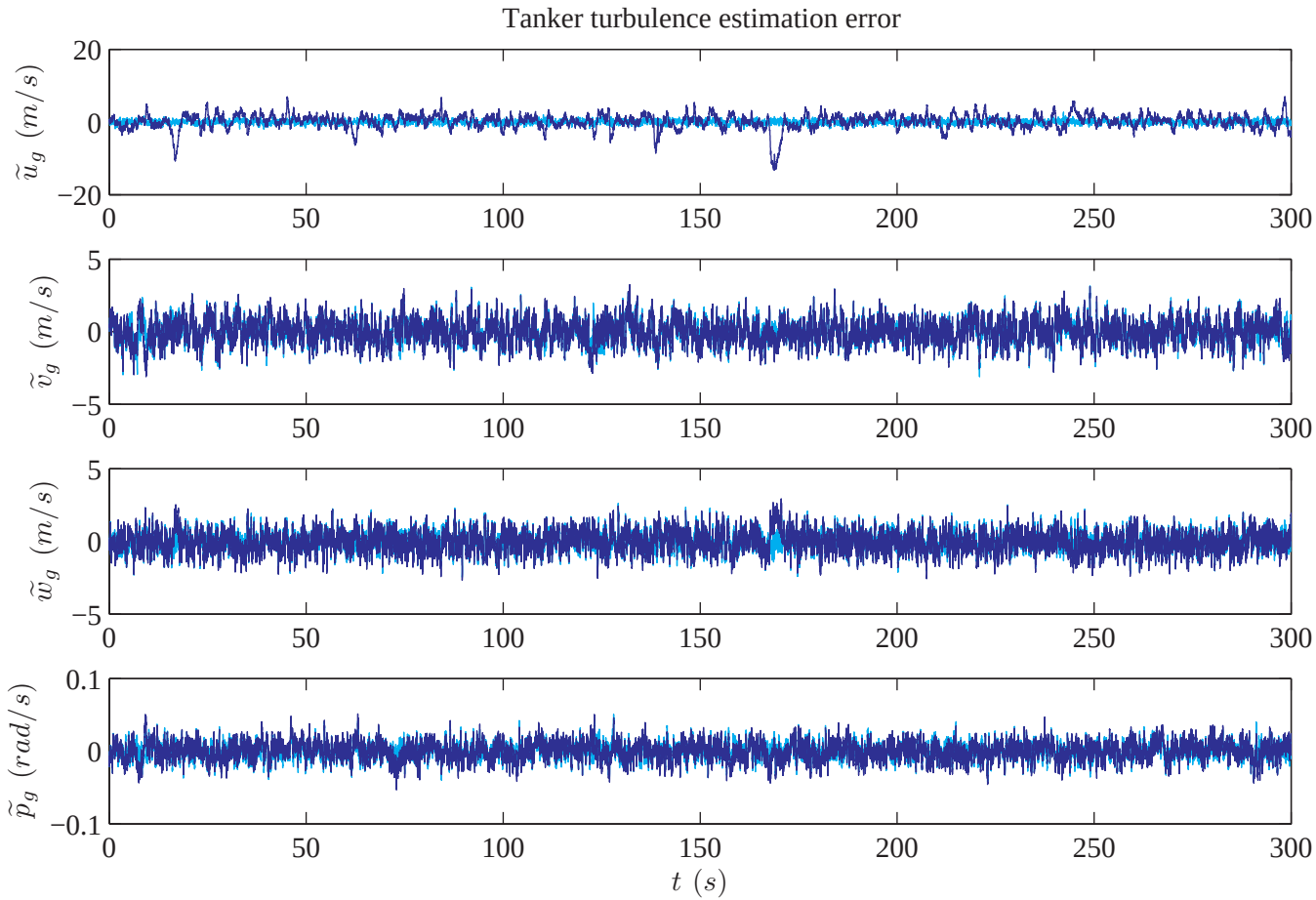

Figure 5.5: Tanker turbulence estimation error plot for the nominal flight-case (4.134), controller no.8 in Table 4.9, turbulence severity $\iota = 1\,\text{rad}$ (medium turbulence), and zero uncertainty. Legend: Turbulence estimation error for the non-linear model (blue); Turbulence estimation error for the linear model (cyan).

5.2.2 Transient response

The receptacle position and time plot, as well as the maximum settling-time and spectral radius plot is given in Figures 5.6, 5.7 and 5.8, for controller no.8, $\iota = 0$, zero system uncertainty, and a non-zero relative position initialisation of $\begin{bmatrix} \varepsilon x_b & \varepsilon y_b & \varepsilon z_b \end{bmatrix} = \begin{bmatrix} -2 & 2 & 2 \end{bmatrix}$ m. The receiver relative position is initialised in the direction $\begin{bmatrix} -1 & 1 & 1 \end{bmatrix}$, *i.e.* below, to the right and behind its trim, such that both longitudinal and lateral system modes are stimulated, and the amplitude of the relative position initialisation is chosen such that none of the actuators become saturated during the transition to the zero state/steady-state. The relative position transient is well behaved with the error converging to zero in approximately a straight line from the initial condition, apparent from Figure 5.6, and has an approximate 2% settling time of 7 s, apparent from Figure 5.7. The settling-time and spectral radius of the entire system state is illustrated with the maximum settling-time and spectral radius plot in Figure 5.8, both of which attains the synthesised constraints of $< -\mathfrak{a}$ and $< \mathfrak{r}$.

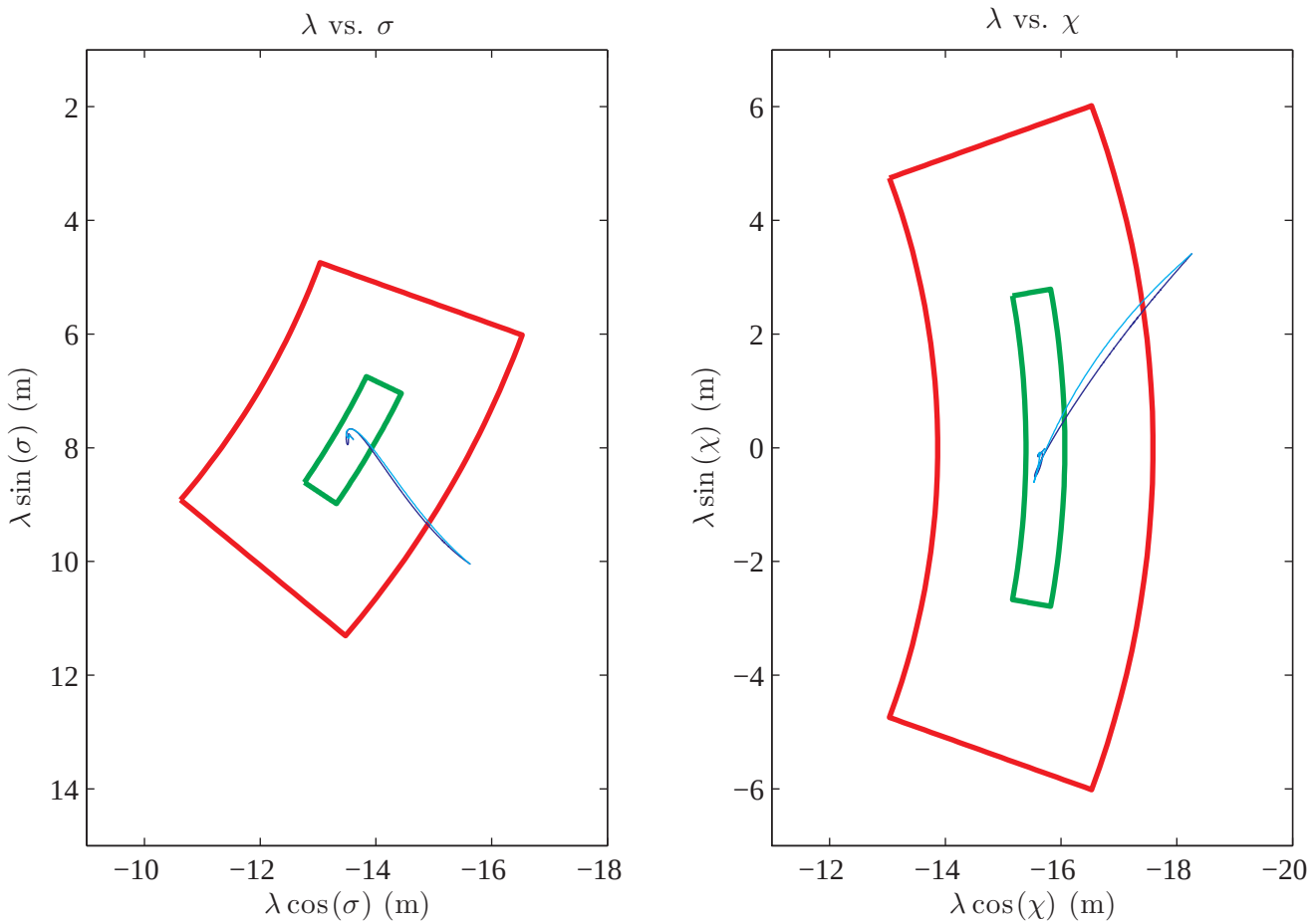

Figure 5.6: Receptacle time plot of initial offset in relative position for the nominal flight-case (4.134), controller no.8 in Table 4.9, turbulence severity $\iota = 0$, and zero uncertainty. Legend: Contact envelope (green); Disconnect envelope (red); Linear model trajectory (cyan); Non-linear model trajectory (blue)

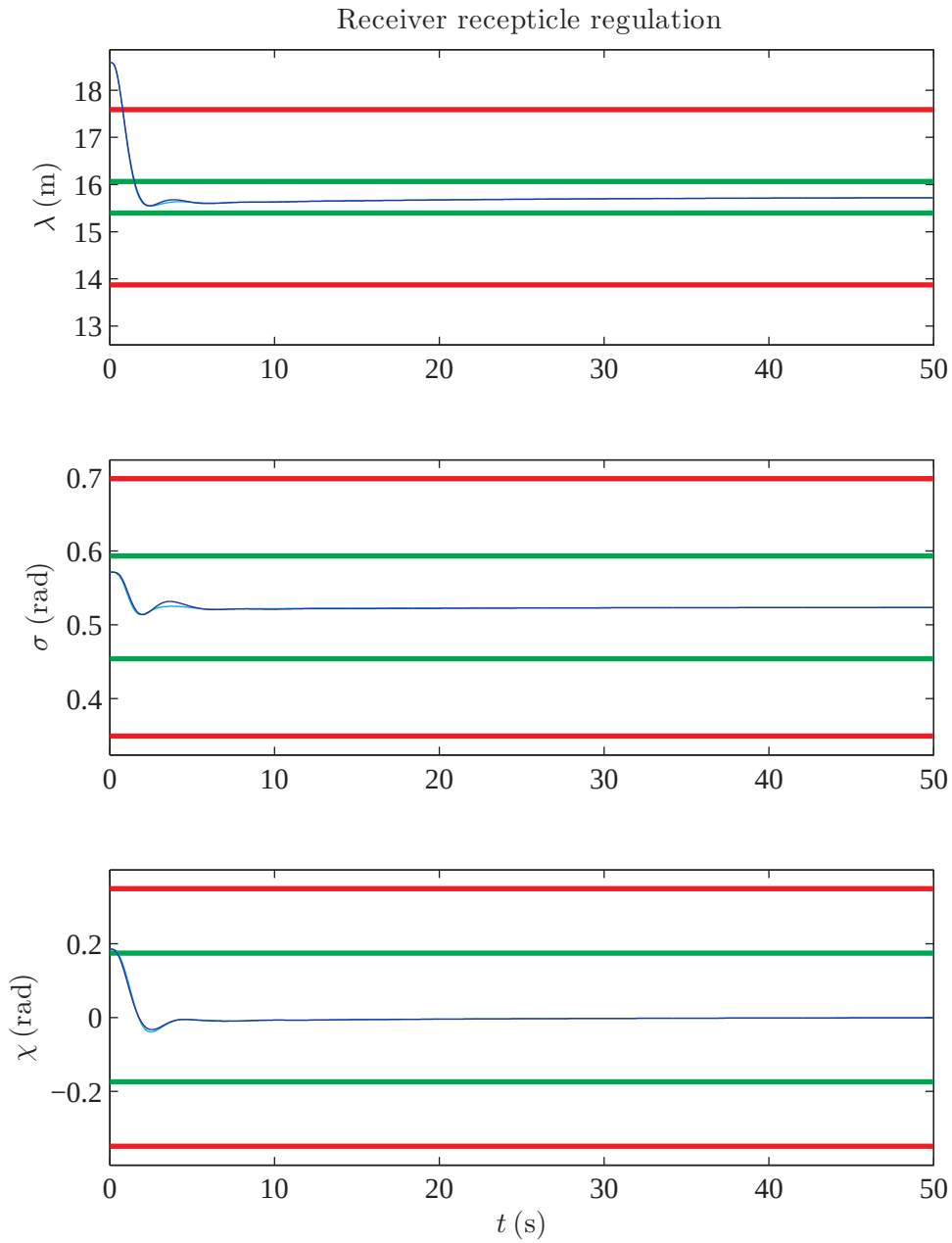

Figure 5.7: Receptacle time plot of initial offset in relative position for the nominal flight-case (4.134), controller no.8 in Table 4.9, zero turbulence, and zero uncertainty. Legend: Contact envelope (green); Disconnect envelope (red); Linear model trajectory (cyan); Non-linear model trajectory (blue)

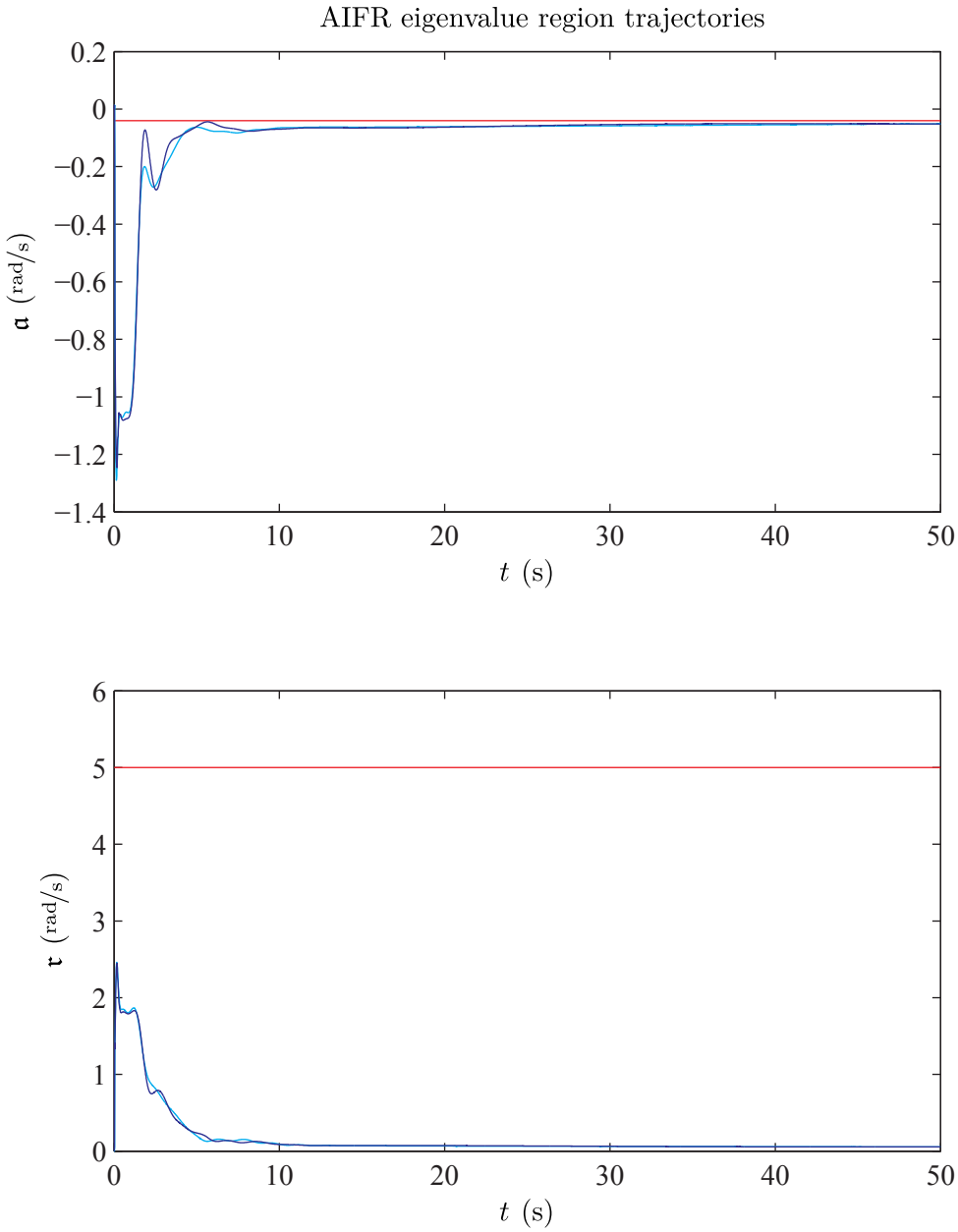

Figure 5.8: Maximum settling-time plot and the spectral radius plot of initial offset in relative position for the nominal flight-case (4.134), controller no.8 in Table 4.9, zero turbulence, zero measurement noise, and zero uncertainty. Legend: Contact envelope (green); Disconnect envelope (red); Linear model trajectory (cyan); Non-linear model trajectory (blue).

5.2.3 Robustness to uncertainty

Robustness of IFR controller no.8 against system uncertainty is evaluated by subjecting both aircraft to a case of system uncertainty, of which the uncertainty is particularly chosen in a destabilising direction. The aircraft uncertainty components, described in Section 4.2.1, are that of aerodynamic coefficients, actuator gains, actuator bandwidths, mass, and centre of mass, and all the components are chosen equally as $e_A(t)$ for aircraft A, with the exception of the centre of mass which is chosen as the negative of $e_A(t)$. Uncertainty $e_A(t)$ is LTV, and describes a more responsive aircraft for $e_A(t) > 0$ and a less responsive aircraft for $e_A(t) < 0$.

The receptacle time plot of the system uncertainty case for the nominal flight-case (4.134) and $\iota = 1\,\text{rad}$ is given in Figure 5.10, and the corresponding uncertainty trajectories $e_T(t)$ of the tanker and $e_R(t)$ of the receiver are given in Figure 5.9. The maximum uncertainty the controller may be subjected to while remaining stable is determined as 40% of the uncertainty described in Section 4.2.1, *e.g.* a maximum actuator bandwidth uncertainty of 2%, although the controller is subjected to 100% of the non-linearity involved in the IFR mechanics. Furthermore, controller no.1 in Table 4.9, which excludes uncertainty for state-feedback synthesis, remains stable for 30% of the uncertainty described in Section 4.2.1. Thus, the 5% uncertainty included for state-feedback synthesis of controller no.8, increases the robustness of the controller to uncertainty by 33%. We conclude from the non-linear simulation that the conservatism involved in the norm-bounded state-space representation of the system may be as high as $\frac{40\%}{5\%} \times 100\% = 800\%$.[3]

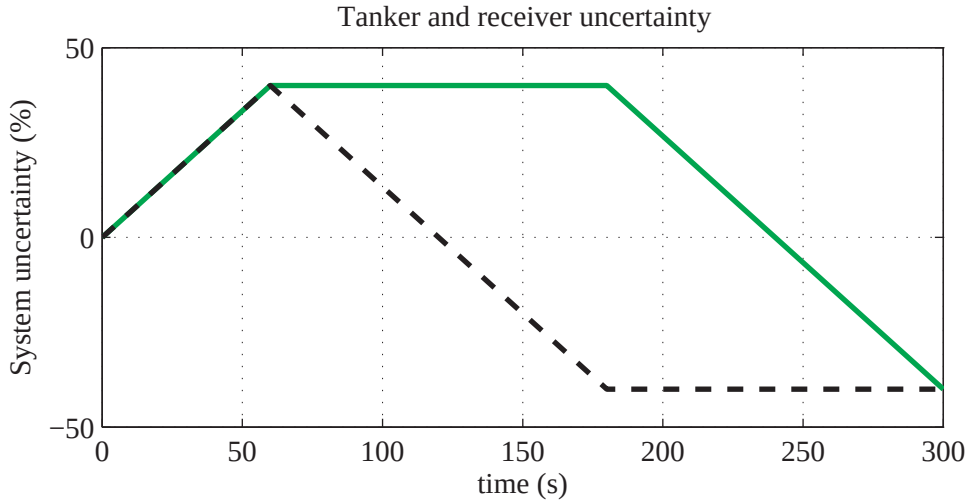

Figure 5.9: Uncertainty input plot of $e_T(t)$ and $e_R(t)$. Legend: $e_T(t)$ (black dashed); $e_R(t)$ (green).

3. It is not feasible to evaluate all the possible scenarios of system uncertainty via non-linear simulation, thus the conservatism involved in the norm-bounded state-space description serves as an upper-bound.

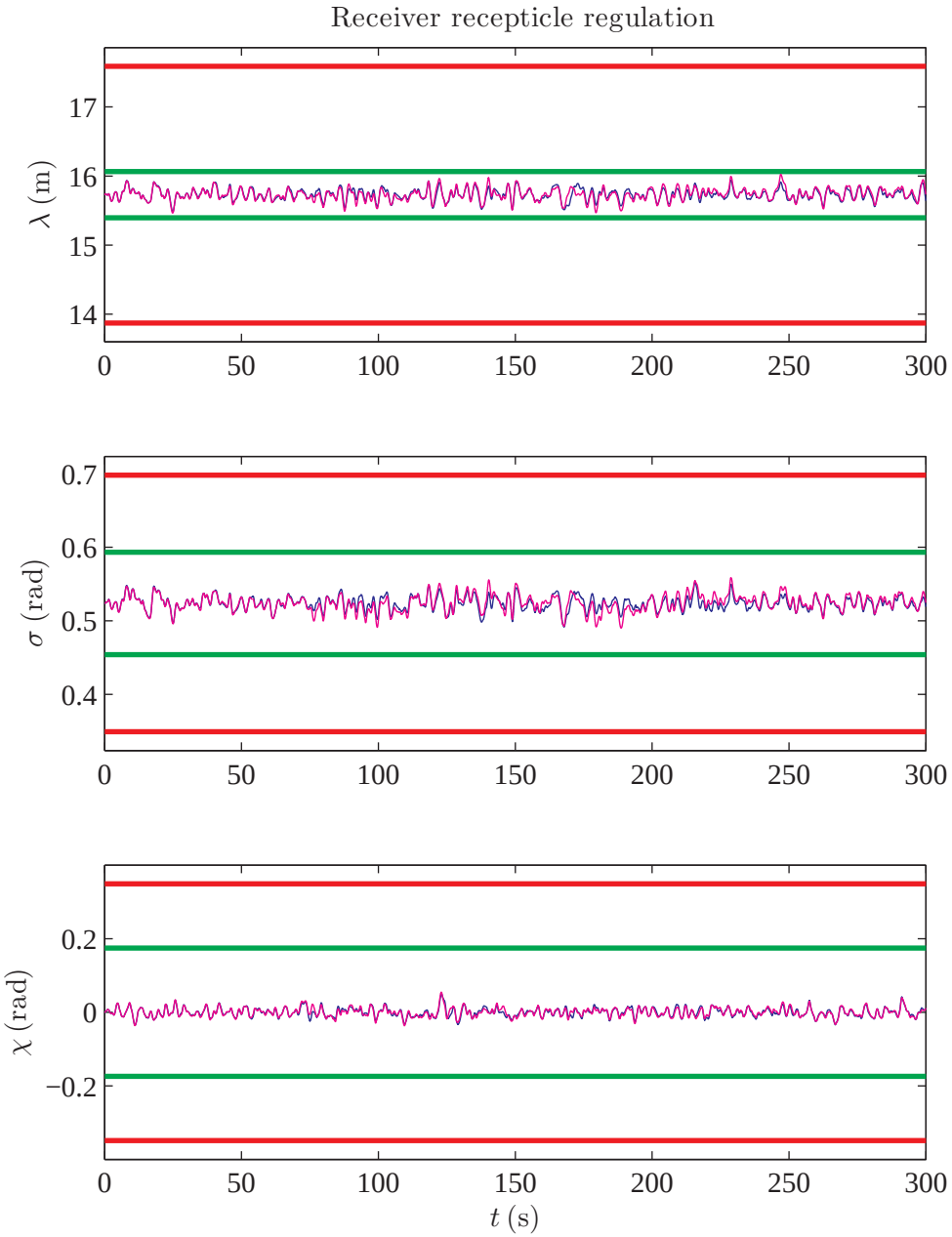

Figure 5.10: Receptacle time plot for the nominal flight-case (4.134), controller no.8 in Table 4.9, turbulence severity $\iota = 1\,\text{rad}$ (medium turbulence), and aircraft uncertainty in Figure 5.9. Legend: Contact envelope (green); Disconnect envelope (red); Non-linear model trajectory without uncertainty (blue); Non-linear model trajectory with uncertainty (magenta).

5.2.4 Robustness to thrust delay

The A330 thrusters are more accurately modelled by including a delay of 5 s from the thrust reference to the thrust output. This delay was excluded from the AIFR application of the LMI technique presented in Chapter 3, because the technique does not include system delays in the formulation, and would have unnecessarily complicated the analysis of the LMI technique itself.

A Padé approximation was originally used to include the thrust delays, accompanied by an estimator for each thruster used to estimate the state of the Padé approximation, and was found to result in instability. The instability is possibly due to poor observability of the Padé state or the zero found in the Padé approximation, although we are not sure of the origin. The instability is remedied by representing the thrust delay as a slew-rate at the thrust output, which indirectly assigns the thrusters to correct only low bandwidth state errors. IFR model (4.108) is augmented with an experimentally determined thrust slew-rate of $2\,{}^{\text{rad}}/_{\text{s}}$, used to synthesise controller no.9 in Table 4.9 with synthesis parameters equal to that of controller no.8. The receptacle position plot is given in Figure 5.11, for controller no.9, $\iota = 1\,\text{rad}$, zero system uncertainty, and thrust delays of 5 s. Its AIFR success is calculated as 99.7% for the system, of which only boom length exceeds the relative position constraints for the contact envelope, and occurs at approximately 20 s. Note that AIFR with controller no.8 is unstable when the thrust delays are included.

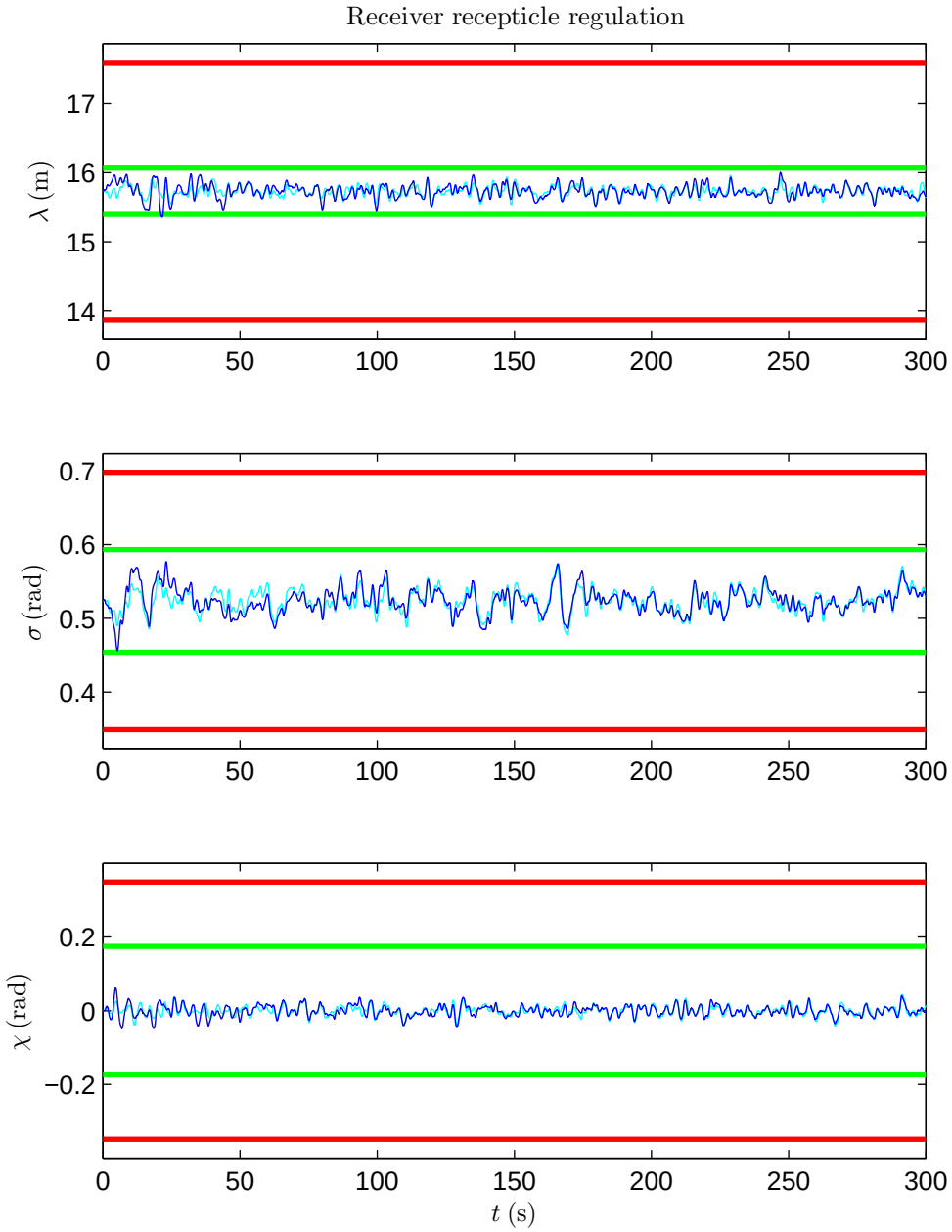

Figure 5.11: Receptacle time plot for the nominal flight-case (4.134), controller no.9 in Table 4.9, turbulence severity $\iota = 1\,\text{rad}$ (medium turbulence), and thrust delays of 5 s. Legend: Contact envelope (green); Disconnect envelope (red); Non-linear model trajectory (blue); Linear model trajectory (cyan).

5.3 Gain-scheduled control

5.3.1 Toboggan

The tanker toboggan input plot and the receptacle time plot is given in Figures 5.12 and 5.13 respectively, for the toboggan flight-case (4.135), the controllers in Table 4.12 implemented with gain-scheduling, turbulence severity $\iota = 1\,\text{rad}$, and zero uncertainty. Its AIFR success is calculated as 100% for both the system and the linear model. A slow reference LPF with a bandwidth of $0.01\,^{\text{rad}}/_{\text{s}}$ is used to avoid actuator saturation, of which the settling-time of the reference might be increased either by designing a higher order input filter or by including reference performance constraints as LMI constraints in the LMI optimisation problems used for synthesis, but falls outside the scope of this thesis. The simplicial complex based gain-scheduling scheme, developed in Appendix B.2, successfully combines the three controllers in Table 4.12 into a parameter varying controller, which approximately attains the turbulence rejection performance of each controller over the whole altitude domain of the toboggan.

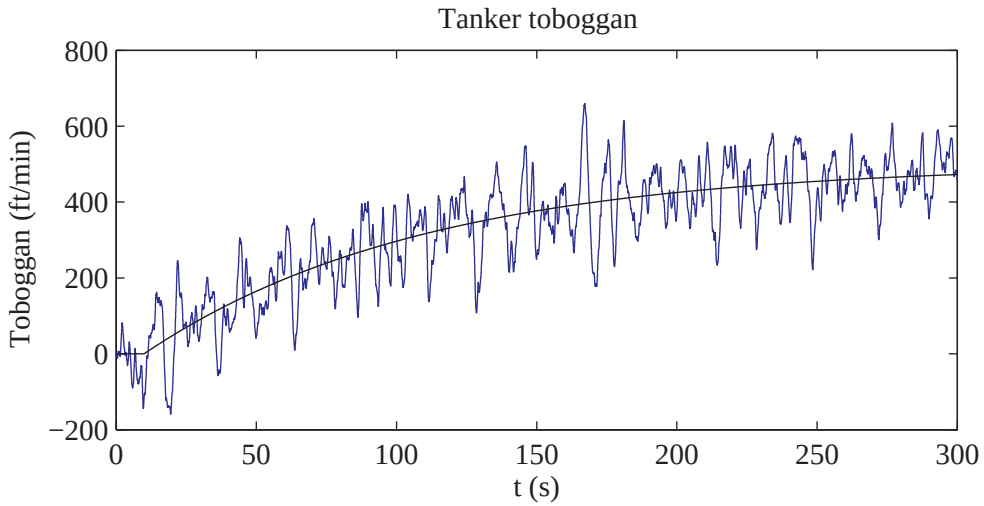

Figure 5.12: Input plot of toboggan reference and tanker toboggan. Legend: Toboggan reference (black); Tanker toboggan of the non-linear model (blue).

5.3.2 Bank turn

A bank turn is tested for the controllers in Table 4.13, which exhibits a large undershoot in tanker and receiver bank angle with a duration of approximately 50 s when a 0 to $25\frac{\pi}{180}\,\text{rad}$ bank step reference, filtered at $0.01\,^{\text{rad}}/_{\text{s}}$, is applied. The AIFR eventually becomes unstable when the reference is applied for $\iota = 0\,\text{rad}$, possibly due to the large error of the tanker roll integrator resulting from the undershoot, although a means for determining the cause of the system instability is pending. The large undershoot may be remedied by designing a higher order input filter, but falls outside the scope of this thesis.

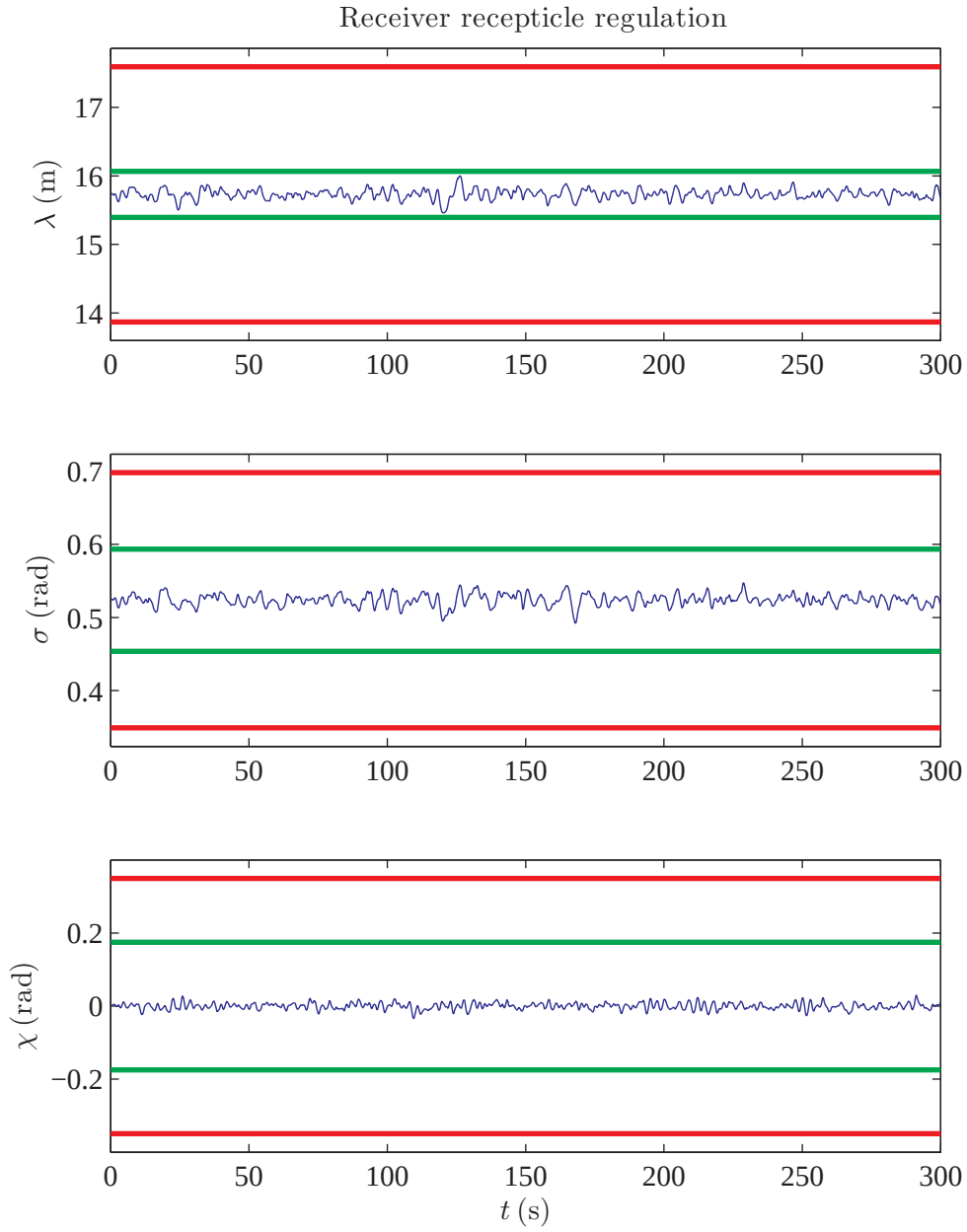

Figure 5.13: Receptacle time plot for the toboggan flight-case (4.135), the controllers in Table 4.12 implemented with gain-scheduling, turbulence severity $\iota = 1\,\text{rad}$ (medium turbulence), and zero uncertainty. Legend: Contact envelope (green); Disconnect envelope (red); Non-linear model trajectory (blue).

5.4 Nominal flight-case with partially decoupled controller

The receptacle time plot is given in Figure 5.14 for the nominal flight-case (4.134), decoupled controller no.16 in Table 5.14, turbulence severity $\iota = 1\,\text{rad}$, and zero uncertainty. Its AIFR success is calculated as 100% for both the system and the linear model. The decoupled controller, synthesised with the decoupled formulation in Appendix D, attains a turbulence rejection performance of approximately equal to that of coupled controller no.8 in Figure 5.2, where both controllers no.8 and no.16 have equal synthesis parameters.

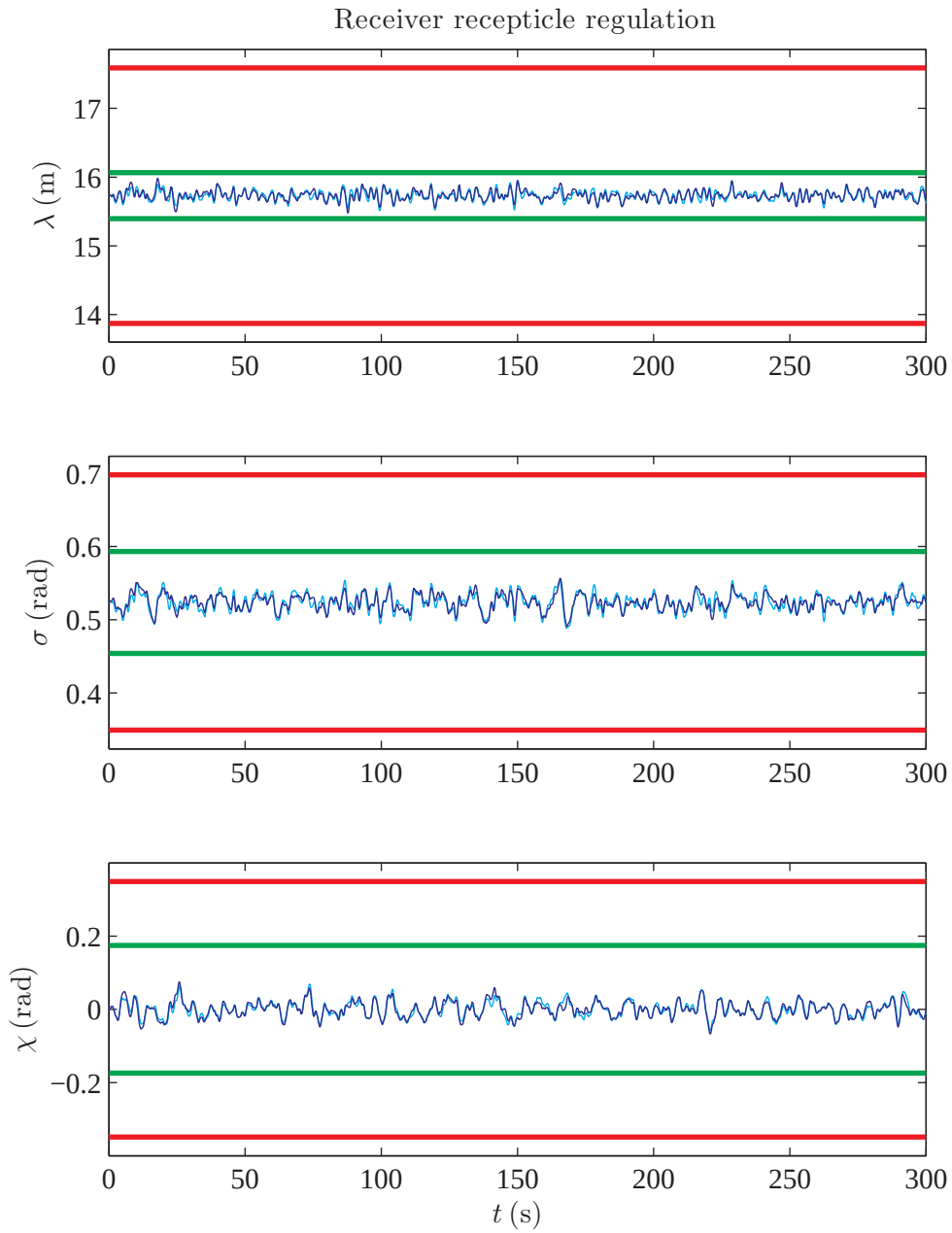

Figure 5.14: Receptacle time plot for the nominal flight-case (4.134), partially decoupled controller no.16 in Table D.1, turbulence severity $\iota = 1\,\text{rad}$ (medium turbulence), and zero uncertainty. Legend: Contact envelope (green); Disconnect envelope (red); Linear model trajectory (cyan); Non-linear model trajectory (blue).

Chapter 6

Conclusion and recommendations

6.1 Conclusion

This thesis has reported a technique to synthesise predictor-estimator-based state-feedback control laws for large uncertain stochastic systems with multiple constraints on system variables, based on the separation principle and generally solveable LMI optimisation. The LMI technique was applied to the automation of IFR between two A330 aircraft. A 60^{th} order norm-bounded state-space model for the IFR flight mechanics was developed, as well as a IFR Dryden turbulence model characterising the similarity between the turbulence experienced by the tanker and receiver. Several AIFR flight control laws were synthesised for the IFR model, with a controller architecture guaranteeing unique and zero-mean steady-state tracking. The synthesised flight control laws were validated via non-linear simulation for the IFR contact phase during medium turbulence, a case of system uncertainty and three common IFR flight tracks.

Guarantees on system robust performance inherent in the LMI technique become invalid when the norm-bounded model uncertainty is reduced, which is required to compensate for the large conservatism involved in the technique. To this end, the LMI technique reduces to an inexact design tool used to make the system robust against a portion of the involved uncertainty, which requires non-linear simulation for controller validation, as apposed to simply choosing the desired synthesis parameters and synthesising a controller with appropriate robust performance guarantees, which, strictly speaking, do not require validation.

Even though robust performance guarantees are abscent, the LMI technique presented has proven to be a usefull controller design tool.

6.2 Recommendation

A means for achieving robust performance guarantees with the LMI technique presented, is to remove non-linearity inherent in the system, to which end model uncertainty may be reduced whilst maintaining the guarantees. We propose the use of a fast adaptive neural-network inner-loop to linearise the system via state to state derivative NLTV gain inversion, to reduce the size of norm-bounded uncertainty required to completely describe the system.

Chapter 7

Future work

The following suggestions are aspects of the research that was not addressed, and could be the subject of follow-on research.

7.1 Average output covariance for NLTV variation

At the end of Section 3.7.1 we refer to [30, Ch.7], where it is proven that (3.72) also holds for LTI models with NLTV causal structured norm-bounded variation. [30, Ch.7] form the conjecture that (3.62) holds for LTI models with NLTV causal structured norm-bounded variation, where $\overline{Q}_{z_\Delta}$ bounds the *average* output covariance. Proving this conjecture will serve as a valuable addition to this thesis and [30].

Furthermore, [58] presents a parametrisation for LTI models with NLTI structured norm-bounded variation, with additional *slope restrictions*, that bounds the average output variance. These slope restrictions limits the class of systems represented by the variation, and serve to reduce conservatism in the variation. We propose a formulation for the average output *covariance* case, which will have the advantage of avoiding the duplication of LMIs required for each additional variance constraint in [58] (see motivation 1 in Section A.2.8).

7.2 Variance constraints via LQR/LQG

It is commonplace to design LQR/LQG controllers to meet multiple variance constrains on system input and output variables, even though LQR/LQG does not directly include variance constraints. Various techniques have been proposed to find appropriate LQR/LQG weights to meet multiple variance constraints [69, 35].

The solution to the stochastic linear optimal regulator problem, known as LQR control, finds a linear state-feedback controller $\mathbf{u} = K\mathbf{x}$ that minimises

$$J_{LQR} = \lim_{T\to\infty} \frac{1}{T}\mathbb{E}\left\{\int_0^T \mathbf{v}^T(t)\,\mathbf{v}(t)\,dt\right\} \tag{7.1}$$

for the LTI system

$$\begin{aligned} \dot{\mathbf{x}} &= A\mathbf{x} + B_w\mathbf{w} + B_u\mathbf{u} \\ \mathbf{v} &= C_v\mathbf{x} + D_{vu}\mathbf{u} \end{aligned} \tag{7.2}$$

where $\mathbf{w}$ is white noise with unit intensity [48, pp.220-221,253-255,259-260][13, pp.114-115]. The LQR controller may be found by solving min $\|T_{vw}\|_{\mathcal{H}_2}^2$ subject to $\mathbf{u} = K\mathbf{x}$ and any of (A.155), (A.156), (A.158)-(A.161). Variance constraints may trivially be introduces when using formulation (A.161), and is formulated for LQR synthesis in a similar manner to (3.107), given as

$$\begin{aligned} \text{minimise} \quad & \operatorname{tr}\left(\begin{bmatrix} C_v & D_{vu} \end{bmatrix} Z \begin{bmatrix} C_v & D_{vu} \end{bmatrix}^T\right) \\ \text{subject to} \quad & AQ + B_uY + QA^T + Y^TB_u^T + B_wB_w^T < 0 \\ & \left[\begin{array}{c|c} Z & \begin{bmatrix} I \\ 0 \end{bmatrix} Q + \begin{bmatrix} 0 \\ I \end{bmatrix} Y \\ \hline \star & Q \end{array}\right] > 0 \\ & Q > 0,\ Z > 0,\ Y \in \mathbb{R}^{n_u \times n_x} \end{aligned} \tag{7.3}$$

where

$$K = YQ^{-1},\ \lim_{T\to\infty} \frac{1}{T}\mathbb{E}\left\{\int_0^T \mathbf{v}(t)\,\mathbf{v}^T(t)\,dt\right\} < V \tag{7.4}$$

Variance constraints may be introduced in (7.3) as

$$\operatorname{tr}\left(\begin{bmatrix} C_{z,i} & D_{zu,i} \end{bmatrix} Z \begin{bmatrix} C_{z,i} & D_{zu,i} \end{bmatrix}^T\right) < 1 \tag{7.5}$$

where i denotes the i^{th} variance constraint. [12] It follows from convex theory that the feasible variable space Z is convex, with or without the variance constraints.

Based on the convexity of Z and the equivalence between the objective and 7.5, we form the following conjecture.

Conjecture 2. *(achieving VC with LQR) LMI optimisation problem* (7.3) *with additional variance constrains* (7.5) *may be solved without* (7.5)*, by augmenting* $\begin{bmatrix} C_v & D_{vu} \end{bmatrix}$.

If Conjecture 2 is true, then the variance-constrained LQR may be solved with conventional LQR. Moreover, with convex Z, someting may be said about the global convergence of weight adjustment techniques in [69, 35].

LQG controller synthesis is formulated as an LMI optimisation problem using (A.161) in [50], and is given as follows.

$$
\begin{aligned}
\min \quad & \operatorname{tr}\left(\begin{bmatrix} C_v & D_{vu} \end{bmatrix} Z \begin{bmatrix} C_v & D_{vu} \end{bmatrix}^T\right) \\
\text{subject to} \quad & \left[\begin{array}{c|c|c} AX + B_u\hat{C}_f + \left(AX + B_u\hat{C}_f\right)^T & \hat{A}_f^T + \left(A + B_u\hat{D}_f C_y\right) & B_w + B_u\hat{D}_f D_{yw} \\ \hline \star & A^TY + \hat{B}_f C_y + \left(A^TY + \hat{B}_f C_y\right)^T & YB_w + \hat{B}_f D_{yw} \\ \hline \star & \star & -I \end{array}\right] < 0 \\
& \left[\begin{array}{c|c|c} X & I & \left(\begin{bmatrix} I \\ 0 \end{bmatrix} X + \begin{bmatrix} 0 \\ I \end{bmatrix} \hat{C}_f\right)^T \\ \hline \star & Y & \left(\begin{bmatrix} I \\ 0 \end{bmatrix} + \begin{bmatrix} 0 \\ I \end{bmatrix} \hat{D}_f C_y\right)^T \\ \hline \star & \star & Z \end{array}\right] > 0 \\
& X \in \mathbb{S}^{n_x}_{++}, Y \in \mathbb{S}^{n_x}_{++}, Z \in \mathbb{S}^{(n_x+n_u)}_{++} \\
& \hat{A}_f \in \mathbb{R}^{n_x \times n_x},\ \hat{B}_f \in \mathbb{R}^{n_x \times n_y},\ \hat{C}_f \in \mathbb{R}^{n_u \times n_x},\ \hat{D}_f \in \mathbb{R}^{n_u \times n_y}
\end{aligned} \tag{7.6}
$$

where

$$D_{zw} + D_{zu}\hat{D}_f D_{yw} = 0 \tag{7.7}$$

and the LQG controller is calculated post-synthesis as

$$
\begin{aligned}
\begin{bmatrix} \dot{\mathbf{x}}_f \\ \mathbf{u} \end{bmatrix} &= \begin{bmatrix} A_f & B_f \\ C_f & D_f \end{bmatrix} \begin{bmatrix} \mathbf{x}_f \\ \mathbf{y} \end{bmatrix} \\
D_f &= \hat{D}_f \\
C_f &= \left(\hat{C}_f - D_f C_y X\right) M^{-T} \\
B_f &= N^{-1}\left(\hat{B}_f - YB_u D_f\right) \\
A_f &= N^{-1}\left(\hat{A}_f - NB_f C_y X - YB_u C_f M^T - Y\left(A + B_u D_f C_y\right) X\right) M^{-T} \\
NM^T &= I - YX
\end{aligned} \tag{7.8}
$$

Variance constraints may also be introduced in (7.6) with (7.5). Similar to (7.3), feasible variable space Z for LQG synthesis is also convex, with or without the variance constraints. It follows from the similarity between (7.6) and (7.3) that if Conjecture 2 is true, it will also hold for (7.6), *i.e.* LQG.

Unfortunately, $I - YX$ in (7.8) will be nearly singular if

$$\begin{bmatrix} X & I \\ I & Y \end{bmatrix} > 0 \tag{7.9}$$

is saturated at the optimum, which causes ill-conditioned inversions of M and N [67, pp.903]. This was found to be the case while experimenting with (7.6) for 8^{th} order mass-spring systems. Thus, even if Conjecture 2 is true, its practical implications may be questionable.

The theorem given below may possibly aid in proving Conjecture 2.

Theorem 5. *(using LQG to deduce infeasibility of a VC solution) If there exists a LQG cost function, for which substituting all the resulting LQG variances with their desired constraints results in a lower cost, then no linear controller exists that meets the desired variance constraints.*

Proof by deduction: The LQG problem is solved by finding the global minimum of a cost function for all linear controllers. If there exists a cost function, for which substituting the resulting LQG variances with the desired variance constraints results in a lower cost, the LQG problem is not solved by finding the global minimum of the cost function.

Furthermore, if the system noise is Gaussian, the LQG solution minimises the cost function for all linear *and* non-linear controllers [48, pp. 390]. Thus, if Conjecture 2 is true and the noise is Gaussian, then the solution to the convariance-constrained LQR/LQG formulated above for linear controllers, is also the solution for all non-linear controllers.

Appendix A

Math derivations, definitions and details

A.1 In-flight refuelling mechanics

A.1.1 Notation

Zipfel-notation [83, pp.218] is used exclusively to derive the *coordinate-independent* tensor mechanics of IFR, which we summarise as follows.

Bold lower-case symbols denote first-order tensors (vector with $3^1 = 3$ elements/-components), bold upper-case symbols denote second-order tensors (matrix with $3^2 = 9$ elements) and non-bold lower-case symbols denote zero-order tensors (scalars). Furthermore, superscripts denote frames/bodies and subscripts denote points.

First-order tensor variables used in the derivations are: position $\mathbf{s}$, *e.g.* $\mathbf{s}_{AB}$ is the position of point A with respect to point B, where points A and B are base points of frames A and B respectively; velocity $\mathbf{v}$, *e.g.* $\mathbf{v}_A^B = D^B\mathbf{s}_{AB}$ is the velocity of point A with respect to frame B , where D^B is the time-derivative operator taken with respect to frame B; linear momentum $\mathbf{p} \coloneqq m\mathbf{v}$, *e.g.* $\mathbf{p}_A^B = m^A\mathbf{v}_A^B$ is the linear momentum of point A with respect to frame B, where m^A is the mass of frame A; angular velocity $\boldsymbol{\omega}$, *e.g.* $\boldsymbol{\omega}^{AB}$ is the angular velocity of frame A with respect to frame B; angular momentum $\mathbf{l}$, *e.g.* $\mathbf{l}_A^{AB} = \mathbf{I}_A^A\boldsymbol{\omega}^{AB}$ is the angular momentum of frame A with respect to frame B, where $\mathbf{I}_A^A$ is the moment of inertia of frame A with respect to its base point A, a second-order tensor variable; linear force $\mathbf{f}$, *e.g.* $\mathbf{f}_B$ is the linear force acting on point B; moment $\mathbf{m}$, *e.g.* $\mathbf{m}_B$ is the moment acting on point B; right-handed Cartesian triad (orthonormal base vectors) $\{\mathbf{x}_1, \mathbf{x}_3, \mathbf{x}_3\}$ of some frame X, originating from base point X, and is used to represent frame orientation.

Second-order tensor variables used in the derivations are: rotation $\mathbf{R}$, *e.g.* $\mathbf{a}_i = \mathbf{R}^{AB}\mathbf{b}_i$, $i = 1, 2, 3$ expresses the orientation of the base vectors of frame A with respect to frame B; angular velocity $\boldsymbol{\Omega}$, *e.g.* $\boldsymbol{\Omega}^{AB} \coloneqq \left(D^B\mathbf{R}^{AB}\right)\mathbf{R}^{BA}$ is the angular velocity of frame A with respect to frame B, as is $\boldsymbol{\omega}^{AB}$, which inherits the function of the vector-product/cross-product, *i.e.* $\boldsymbol{\Omega}^{AB}\mathbf{s}_{AB} = \boldsymbol{\omega}^{AB} \times \mathbf{s}_{AB}$; moment of inertia

$\mathbf{I}$, *e.g.* $\mathbf{I}_B^A$ is the moment of inertia of frame A with respect to point B, *i.e.* the mass distribution of frame A with respect to point B.

Furthermore, the tensors may be projected onto Cartesian coordinate-systems, in order to be numerically evaluated. Projections are denoted by square brackets superscripted with the coordinate-system label, *e.g.* $[\mathbf{s}_{AB}]^C$ is $\mathbf{s}_{AB}$ projected onto Cartesian coordinate-system C, or $\left[\overline{\mathbf{b}_1}\right]^B = [\ 1 \quad 0 \quad 0\ ]\,\mathrm{m}$, where coordinate-system B and frame B have the same base vectors [1] and $\overline{\mathbf{b}_1}$ is the *transpose* of $\mathbf{b}_1$.[2] A more involved example is where $\mathbf{x} = 2\boldsymbol{\Omega}^{RI}\mathbf{v}_B^R + \boldsymbol{\Omega}^{RI}\boldsymbol{\Omega}^{RI}\mathbf{s}_{BR}$ is projected onto Cartesian coordinate-system C, where $\mathbf{x}$ is a first-order tensor describing *Coriolis* acceleration and centrifugal acceleration, which gives $[\mathbf{x}]^C = \left[2\boldsymbol{\Omega}^{RI}\mathbf{v}_B^R + \boldsymbol{\Omega}^{RI}\boldsymbol{\Omega}^{RI}\mathbf{s}_{BR}\right]^C = 2\left[\boldsymbol{\Omega}^{RI}\right]^C\left[\mathbf{v}_B^R\right]^C + \left[\boldsymbol{\Omega}^{RI}\right]^C\left[\boldsymbol{\Omega}^{RI}\right]^C[\mathbf{s}_{BR}]^C$. Projections may be interchanged using the orthonormal [3] transformation matrix $[\mathbf{T}]$, also known as the Direction Cosine Matrix (DCM). Transformation matrices are used differently for first- and second-order tensors *e.g.* $[\mathbf{x}]^A = [\mathbf{T}]^{AB}[\mathbf{x}]^B$ and $[\mathbf{X}]^A = [\mathbf{T}]^{AB}[\mathbf{X}]^B[\mathbf{T}]^{BA}$. The time-derivative operator may be replaced by the more conventional $\frac{d}{dt}$ if it is projected onto its own base vectors, *e.g.* $\left[D^B\mathbf{x}\right]^A = [\mathbf{T}]^{AB}\left[D^B\mathbf{x}\right]^B = [\mathbf{T}]^{AB}\left(\frac{d}{dt}[\mathbf{x}]^B\right)$.

Finally, perturbations are defined in terms of the *Component Perturbation Method* (CPM)[83, pp.218-219], given as

$$\varepsilon\mathbf{x} \coloneqq \mathbf{x} - \mathbf{R}^{DD_r}\mathbf{x}_r \tag{A.1}$$

where $\varepsilon\mathbf{x}$ is the perturbation, $\mathbf{x}_r$ is the reference, D is the observation frame and D_r is the observation frame at the reference. When the perturbation is projected onto Cartesian coordinate-system D, given as

$$[\varepsilon\mathbf{x}]^D = [\mathbf{x}]^D - \left[\mathbf{R}^{DD_r}\right]^D[\mathbf{x}_r]^D = [\mathbf{x}]^D - [\mathbf{T}]^{D_rD}[\mathbf{x}_r]^D = [\mathbf{x}]^D - [\mathbf{x}_r]^{D_r} \tag{A.2}$$

it has the quality of being practically implementable, *e.g.* the aircraft velocity perturbation $\left[\overline{\varepsilon\mathbf{v}_B^G}\right]^B = \left[\overline{\mathbf{v}_B^G}\right]^B - \left[\overline{\mathbf{v}_{B_r}^G}\right]^{B_r} = \begin{bmatrix} u_\varepsilon & v_\varepsilon & w_\varepsilon \end{bmatrix} = \begin{bmatrix} u & v & w \end{bmatrix} - \begin{bmatrix} u_r & v_r & w_r \end{bmatrix}$, where B is the aircraft body-frame, G is the local geographic frame, $\left[\overline{\mathbf{v}_B^G}\right]^B$ is the measurable instantaneous aircraft velocity and $\left[\overline{\mathbf{v}_{B_r}^G}\right]^{B_r}$ is a known/desired reference [4].

A.1.2 Newtonian mechanics, localisation and the flat earth model

Newton's second law and *Euler's law* deliver the fundamental equations of aerospace vehicle dynamics. For a *rigid* body B, with base point B at the centre of mass, *Newton's second law* postulates

$$D^I\mathbf{p}_B^I = \mathbf{f}_B \tag{A.3}$$

1. In our case, the Cartesian triad vector lengths of the frames are chosen as 1 m.
2. The Zipfel -notation for the transpose avoids ambiguity when the tanker body-frame T is used.
3. $([\mathbf{T}])^{-1} = \left[\overline{\mathbf{T}}\right]$
4. For aircraft, *reference* refers to trim.

The equation states that the time rate of change with respect to the inertial frame I of the linear momentum of a body B with respect to the inertial frame equals the force acting on the body. [83, pp.143-144]
For the same body, *Euler's law* postulates

$$D^I \mathbf{l}_B^{BI} = \mathbf{m}_B \tag{A.4}$$

The equation states that the time rate of change relative to the inertial frame of the angular momentum $\mathbf{l}_B^{BI}$ of a rigid body referred to its centre of mass is equal to the applied moment $\mathbf{m}_B$. [83, pp.183-185]

(A.3) and (A.4) describe the translational and attitude dynamics of a *rigid* body, respectively, with respect to the inertial frame. However, aircraft velocity, position and attitude sensor measurements are unrealisable when they are considered with respect to the inertial frame, which motivates the localisation of *Newton's second law* and *Euler's law* to the local geography. The localisation is achieved by assuming *Galileo's hypothesis for falling bodies*, and requires *Newton's law of universal gravitation* and the *Euler transformation* to derive.

Newton's law of universal gravitation postulates

$$\mathbf{f}_g = \mathfrak{g}\frac{m^B m^E}{(\overline{\mathbf{s}_{EB}}\mathbf{s}_{EB})^{\frac{3}{2}}}\mathbf{s}_{EB} \tag{A.5}$$

where $\mathbf{f}_g$ is the gravitational force on the body centre of mass B, E denotes the earth frame, with its base point at the earth's centre of mass, and $\mathfrak{g}$ is the gravitational constant. [55, pp.8]
The *Euler transformation* is given as

$$D^A\mathbf{x} = D^B\mathbf{x} + \mathbf{\Omega}^{BA}\mathbf{x} \tag{A.6}$$

where $\mathbf{x}$ represents any first order tensor and A and B represents any two frames. Thus, the transformation may be used to change the reference frame of the time-derivative operator D to any frame [83, pp.111-112]. Another important transformation results from (A.6) known as the *Coriolis transformation* and is derived as

$$\begin{aligned} D^I D^I \mathbf{s}_{BR} &= D^I\left(D^R\mathbf{s}_{BR} + \mathbf{\Omega}^{RI}\mathbf{s}_{BR}\right) \\ &= D^R\left(D^R\mathbf{s}_{BR} + \mathbf{\Omega}^{RI}\mathbf{s}_{BR}\right) + \mathbf{\Omega}^{RI}\left(D^R\mathbf{s}_{BR} + \mathbf{\Omega}^{RI}\mathbf{s}_{BR}\right) \\ &= \begin{cases} D^R D^R\mathbf{s}_{BR} + & \text{linear acceleration} \\ \left(D^R\mathbf{\Omega}^{RI}\right)\mathbf{s}_{BR} + & \text{angular acceleration} \\ 2\mathbf{\Omega}^{RI}\mathbf{v}_B^R + & \text{Coriolis acceleration} \\ \mathbf{\Omega}^{RI}\mathbf{\Omega}^{RI}\mathbf{s}_{BR} & \text{centrifugal acceleration} \end{cases} \end{aligned} \tag{A.7}$$

which also holds for all frames [83, pp.151-152].

Assumption 3. Galileo's hypothesis for falling bodies holds, *i.e.* all freely falling bodies accelerate at a constant rate with respect to the local geography.

For implementation purposes, *Galileo's hypothesis for falling bodies* is assumed when deriving the IFR dynamics and kinematics. The assumption serves to localise *Newton's Second Law* and *Euler's law* to an aircraft's surrounding geography, and in doing so, local geographic measurements may be used for feedback [5]. The hypothesis states that a freely falling body B accelerates at a constant rate with respect to the local geography, *i.e.*

$$D^G D^G \mathbf{s}_{BG} \backsimeq \mathbf{g} \tag{A.8}$$

where G denotes the local geographical frame, with a conventional North-East-Down (NED) orientated base $\left\{ \begin{array}{ccc} \mathbf{g}_1 & \mathbf{g}_2 & \mathbf{g}_3 \end{array} \right\}$ and its base point G fixed to the earth's surface, and $\mathbf{g}$ is the constant gravitational acceleration.

The motion of a freely falling body is described with *Newton's second law* and *Newton's law of universal gravitation*, and is given as

$$D^I D^I \mathbf{s}_{BI} = \mathfrak{g} \frac{m^E}{\left(\overline{\mathbf{s}_{EB}} \mathbf{s}_{EB}\right)^{\frac{3}{2}}} \mathbf{s}_{EB} \tag{A.9}$$

The underlying assumptions of (A.8) on the inertial motion of the geographical frame and on the locality of the body is revealed when compared to (A.9), *i.e.*

$$D^I D^I \mathbf{s}_{BI} \simeq D^G D^G \mathbf{s}_{BG}, \quad \mathfrak{g} \frac{m^E}{\left(\overline{\mathbf{s}_{EB}} \mathbf{s}_{EB}\right)^{\frac{3}{2}}} \mathbf{s}_{EB} \simeq \mathbf{g} \tag{A.10}$$

The underlying assumption on the inertial motion of the geographical frame is derived as

$$\begin{aligned} D^I D^I \mathbf{s}_{BI} &= D^I D^I \left(\mathbf{s}_{BG} + \mathbf{s}_{GI}\right) \\ &= D^G D^G \mathbf{s}_{BG} + \left(D^G \boldsymbol{\Omega}^{GI}\right) \mathbf{s}_{BG} + 2\boldsymbol{\Omega}^{GI} \mathbf{v}_B^G + \\ &\quad \boldsymbol{\Omega}^{GI} \boldsymbol{\Omega}^{GI} \mathbf{s}_{BG} + D^I D^I \mathbf{s}_{GI} \\ &\simeq D^G D^G \mathbf{s}_{BG}, \quad \forall \mathbf{s}_{BG} \in \mathcal{F}_{\mathbf{s}}, \forall \mathbf{v}_B^G \in \mathcal{F}_{\mathbf{v}} \end{aligned} \tag{A.11}$$

where $\mathcal{F}$ is a continuous set defining the aerospace vehicle flight domain, and $\mathcal{F}_{\mathbf{s}}$ and $\mathcal{F}_{\mathbf{v}}$ the continuous sets of possible body positions and velocities relative to the geographical frame respectively. By decoupling the terms involving the body from the remainder [6], $\mathbf{s}_{BG}$ and $\mathbf{v}_B^G$ are considered as variables, and the remainder as coefficients or constants, the final form of (A.11) must hold for all $\mathbf{s}_{BG} \in \mathcal{F}_{\mathbf{s}}$ and $\mathbf{v}_B^G \in \mathcal{F}_{\mathbf{v}}$. It follows that

$$\begin{aligned} &\left(D^I D^I \mathbf{s}_{GI} \simeq 0,\ D^G \boldsymbol{\Omega}^{GI} + \boldsymbol{\Omega}^{GI} \boldsymbol{\Omega}^{GI} \simeq 0,\ \boldsymbol{\Omega}^{GI} \simeq 0\right) \\ &\qquad \Longrightarrow \quad \left(D^I D^I \mathbf{s}_{GI} \simeq 0,\ \boldsymbol{\Omega}^{GI} \simeq 0\right) \end{aligned} \tag{A.12}$$

5. The assumption does not affect the use of inertial acceleration sensor measurements for feedback.

6. Respective terms may be decoupled if the body does not influence the motion of the geographical frame with respect to the inertial frame, *i.e.* $m^E \gg m^B$, which is true for aerospace vehicles.

Thus, the influence of the earth's rotation about the *sun*[7] and its own axis on aerospace vehicle dynamics and kinematics are assumed to be sufficiently small.

The underlying assumption on the locality of the body is derived by following the same logic as (A.12), given as

$$\begin{aligned} &\left(\mathfrak{g} \frac{m^E}{(\overline{\mathbf{s}_{EB}}\mathbf{s}_{EB})^{\frac{3}{2}}} \mathbf{s}_{EB} \simeq \mathbf{g}, \quad \forall \mathbf{s}_{BG} \in \mathcal{F}_{\mathbf{s}} \right) \\ \implies &\left(\frac{1}{(\overline{\mathbf{s}_{BE}}\mathbf{s}_{BE})} \simeq \frac{1}{(\overline{\mathbf{s}_{GE}}\mathbf{s}_{GE})}, \quad \forall \mathbf{s}_{BG} \in \mathcal{F}_{\mathbf{s}} \right) \end{aligned} \tag{A.13}$$

Thus, *Galileo's hypothesis* implies that $D^I D^I \mathbf{s}_{GI} \simeq 0$ and $\mathbf{\Omega}^{GI} \simeq 0$, *i.e.* all points fixed to the earth has no acceleration or angular velocity, and that $(\overline{\mathbf{s}_{BE}}\mathbf{s}_{BE}) \simeq (\overline{\mathbf{s}_{GE}}\mathbf{s}_{GE})$ for all $\mathbf{s}_{BG} \in \mathcal{F}_{\mathbf{s}}$.

It follows from (A.12), that by assuming terms involving $D^I D^I \mathbf{s}_{GI}$ and $\mathbf{\Omega}^{GI}$ are sufficiently small, *Newton's second law* may be localised as

$$(\text{A.11}) \longrightarrow \quad D^G \mathbf{p}_B^G \simeq \mathbf{f}_B \tag{A.14}$$

and *Euler's law* may be localised as

$$\begin{aligned} D^I \mathbf{l}_B^{BI} &= D^I \left(\mathbf{I}_B^B \boldsymbol{\omega}^{BI} \right) \\ &= D^G \left(\mathbf{I}_B^B \boldsymbol{\omega}^{BI} \right) + \mathbf{\Omega}^{GI} \left(\mathbf{I}_B^B \boldsymbol{\omega}^{BI} \right) \\ &= D^G \left(\mathbf{I}_B^B \left(\boldsymbol{\omega}^{BG} + \boldsymbol{\omega}^{GI} \right) \right) + \mathbf{\Omega}^{GI} \mathbf{I}_B^B \boldsymbol{\omega}^{BI} \\ &\simeq D^G \left(\mathbf{I}_B^B \boldsymbol{\omega}^{BG} \right) \\ \implies \quad D^G \mathbf{l}_B^{BG} &\simeq \mathbf{m}_B \end{aligned} \tag{A.15}$$

Next, the localisation is extended to transglobal flight by assuming a flat earth model. Figure A.1 depicts transglobal flight of aircraft B for an ellipsoid earth model, with earth-fixed geographical frame G, earth-mobile local geographical frame L, and the point of intersection D of the geodetic latitude line and the equatorial plane. The transglobal extension is achieved by introducing an additional frame L, whose base point moves with the aircraft on earth's ellipsoidal surface, in order for the aircraft to have a reference to determine its orientation with respect to the *local* geography. Frame L is defined by the conventional geodetic NED base vectors $\{\mathbf{l}_1, \mathbf{l}_2, \mathbf{l}_3\}$, where $\mathbf{l}_1$ and $\mathbf{l}_2$ are in the local horizontal plane, *i.e.* tangent to the ellipsoid, $\mathbf{l}_1$ points north and is parallel to the earth's lines of constant longitude, $\mathbf{l}_3$ completes the right-handed Cartesian base and is *not* necessarily parallel with $\mathbf{s}_{LE}$, and base point L is such that $\mathbf{s}_{LB} = (\overline{\mathbf{s}_{LB}}\mathbf{s}_{LB})^{\frac{1}{2}} \mathbf{l}_3$.

The localised form of *Newton's second law* is extended to the transglobal case by expressing the body's vertical acceleration with respect to frame L and expressing

7. The sun, *i.e.* the heliocentric frame [83, pp.58-59], experiences much less gravitational acceleration with respect to the inertial frame than the geographical frame, due to the large mass difference, and is thus much more stationary with respect to the inertial frame than the geographical frame.

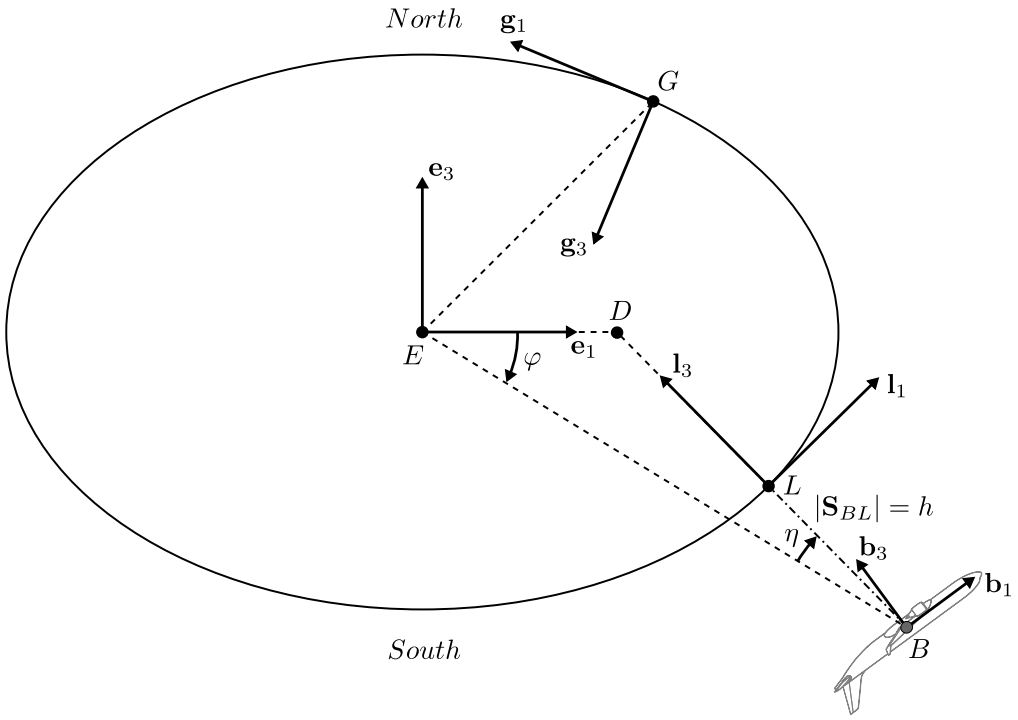

Figure A.1: Transglobal flight with geodetic orientation and localised frames 2D vector diagram.

the body's horizontal acceleration as the acceleration of frame L with respect to point D and frame E, and assuming, among others, that the translational acceleration due to the curvature of the earth is negligible. First, (A.14) is decomposed and referred to frame L via the *Coriolis transformation*

$$\begin{aligned} D^G D^G \mathbf{s}_{BG} &= D^G D^G \left(\mathbf{s}_{BL} + \mathbf{s}_{LD} + \mathbf{s}_{DG}\right) \\ &= D^L D^L \left(\mathbf{s}_{BL} + \mathbf{s}_{LD}\right) + \left(D^L \boldsymbol{\Omega}^{LG}\right) \left(\mathbf{s}_{BL} + \mathbf{s}_{LD}\right) + \\ &\quad 2\boldsymbol{\Omega}^{LG} \left(D^L \left(\mathbf{s}_{BL} + \mathbf{s}_{LD}\right)\right) + \boldsymbol{\Omega}^{LG}\boldsymbol{\Omega}^{LG} \left(\mathbf{s}_{BL} + \mathbf{s}_{LD}\right) + \\ &\quad D^G D^G \mathbf{s}_{DG} \end{aligned} \tag{A.16}$$

The assumptions made to simplify (A.16) are: the accelerating change of the ellipse radius is sufficiently smaller than the vertical acceleration of the body with respect to L, *i.e.* $D^L D^L \left(\mathbf{s}_{BL} + \mathbf{s}_{LD}\right) \simeq D^L D^L \mathbf{s}_{BL}$; the assumption in (A.13) on the locality of the body, *i.e.* $\mathbf{s}_{LD} \gg \mathbf{s}_{BL}$ and $\left(D^L \boldsymbol{\Omega}^{LG}\right) \left(\mathbf{s}_{BL} + \mathbf{s}_{LD}\right) \simeq \left(D^L \boldsymbol{\Omega}^{LG}\right) \mathbf{s}_{LD}$; the rate of change of the ellipse radius is sufficiently smaller than the vertical velocity of the body with respect to L, *i.e.* $\boldsymbol{\Omega}^{LG} \left(D^L \left(\mathbf{s}_{BL} + \mathbf{s}_{LD}\right)\right) \simeq \boldsymbol{\Omega}^{LG} \mathbf{v}_B^L$; the Coriolis acceleration and centrifugal acceleration caused by the curvature of the earth is negligible, i.e. $\boldsymbol{\Omega}^{LG} \mathbf{v}_B^L \simeq 0$ and $\boldsymbol{\Omega}^{LG}\boldsymbol{\Omega}^{LG} \mathbf{s}_{BD} \simeq 0$ respectively; the acceleration of the point of intersection of the geodetic latitude line and the equatorial plane with respect to the earth's centre of mass is negligible, i.e. $D^G D^G \mathbf{s}_{DG} \simeq 0$. It follows

that

$$D^G D^G \mathbf{s}_{BG} \simeq D^L D^L \mathbf{s}_{BL} + \left(D^L \boldsymbol{\Omega}^{LE}\right) \mathbf{s}_{LD}$$

$$\implies \quad m^B \left(D^L D^L \mathbf{s}_{BL} + \left(D^L \boldsymbol{\Omega}^{LE}\right) \mathbf{s}_{LD}\right) \simeq \mathbf{f}_B \tag{A.17}$$

where $D^L D^L \mathbf{s}_{BL}$ is the vertical acceleration component and $\left(D^L \boldsymbol{\Omega}^{LE}\right) \mathbf{s}_{LD}$ is the horizontal acceleration component. Note that the singularities in the orientation of frame L at both poles vanishes in (A.17), *i.e.* the components involved in the rotation of frame L about $\mathbf{l}_3$ vanishes at the poles as D coincides with E.

The localised form of *Euler's law* may be extended to the transglobal case by assuming the angular acceleration due to the earth's curvature is negligible, *i.e.*

$$\begin{aligned} D^G \left(\mathbf{I}_B^B \boldsymbol{\omega}^{BG}\right) &= D^G \left(\mathbf{I}_B^B \left(\boldsymbol{\omega}^{BL} + \boldsymbol{\omega}^{LG}\right)\right) \\ &= D^L \left(\mathbf{I}_B^B \left(\boldsymbol{\omega}^{BL} + \boldsymbol{\omega}^{LG}\right)\right) + \boldsymbol{\Omega}^{LG} \left(\mathbf{I}_B^B \left(\boldsymbol{\omega}^{BL} + \boldsymbol{\omega}^{LG}\right)\right) \\ &\simeq D^L \left(\mathbf{I}_B^B \boldsymbol{\omega}^{BL}\right) \\ \implies \quad D^L \mathbf{l}_B^{BL} &\simeq \mathbf{m}_B \end{aligned} \tag{A.18}$$

Note that there are singularities in the orientation of frame L present at the two earth poles, which may be remedied by locking onto the current line of longitude when frame L starts to rotates sufficiently fast about $\mathbf{l}_3$ with respect to the local geography due to the Geodetic orientation system and the pole, and adjusting the aircraft navigation accordingly. A smooth reset [8] of L to true Geodetic orientation will follow on exiting the singularity region.

Figure A.2 depicts the flight of aircraft B for a flat earth model, with geographical frame G and the local geographical frame L defined for the ellipsoid earth model. To tie (A.17) and (A.18) to the flat earth model, they are compared to localised acceleration derived for the flat earth model.

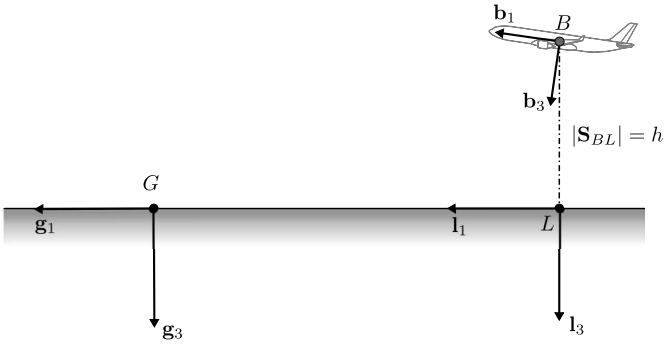

Figure A.2: Flat earth model and localised frames 2D vector diagram.

8. The smooth reset may be implemented with saturation limiters on the angular accelerations and rates.

The localised form of *Newton's second law* is extended to the flat earth model case by applying the *Coriolis transformation* to (A.10)

$$\begin{aligned} D^G D^G \mathbf{s}_{BG} &= D^G D^G \mathbf{s}_{BL} + D^G D^G \mathbf{s}_{LG} \\ (Coriolis) \longrightarrow \quad &= D^L D^L \mathbf{s}_{BL} + \left(D^L \boldsymbol{\Omega}^{LG}\right) \mathbf{s}_{BL} + \\ &\quad 2\boldsymbol{\Omega}^{LG} \mathbf{v}_B^L + \boldsymbol{\Omega}^{LG} \boldsymbol{\Omega}^{LG} \mathbf{s}_{BL} + \\ &\quad D^G D^G \mathbf{s}_{LG} \\ &= D^L D^L \mathbf{s}_{BL} + D^G D^G \mathbf{s}_{LG} \\ \Rightarrow m^B \left(D^L D^L \mathbf{s}_{BL} + D^G D^G \mathbf{s}_{LG}\right) &= \mathbf{f}_B \end{aligned} \tag{A.19}$$

which results in two terms describing the vertical and horizontal acceleration respectively, as in (A.17), with the horizontal term in a different form due to the earth's curvature in (A.17), *i.e.* $D^G D^G \mathbf{s}_{LG} \simeq \left(D^L \boldsymbol{\Omega}^{LE}\right) \mathbf{s}_{LD}$. Thus, the assumptions made to derive (A.17), serves to describe the translational motion of the aircraft for a flat earth model.

The localised form of *Euler's law* is extended to the flat earth model case, and results in (A.18), *i.e.*

$$D^L \mathbf{l}_B^{BL} \simeq \mathbf{m}_B \tag{A.20}$$

Thus, the assumptions made to derive (A.18), serves to describe the attitude motion of the aircraft for the flat earth model.

Finally, the direction of the gravity vector direction is simplified as

$$[\overline{\mathbf{g}}]^L \simeq \begin{bmatrix} 0 & 0 & g \end{bmatrix} \tag{A.21}$$

We conclude that localised forms of *Newton's second law* and *Euler's law*, *i.e.* (A.14) and (A.15) respectively, suffice to describe the translational and attitude motion of the aircraft for transglobal flight, if the aircraft does not fly over the earth's poles, which will result in singularity due to the geodetic orientation system. Localisations may be validated by testing that omitted terms are of order 100 less than the remainder, which robust feedback will comfortably correct.

This concludes the localisation of aerospace vehicle dynamics.

A.1.3 Aircraft equations of motion

The complete set of differential equations describing aircraft motion, known as the aircraft *Equations Of Motion* (EOM), is derived using the localised forms of *Newton's Second Law* for linear acceleration and *Euler's Law* for angular acceleration (see Appendix A.1.2), and the *Euler transformation* (A.6). The aircraft mass distribution is assumed to be time-invariant, *i.e.* effects of fuel-transfer and shift in the centre of mass are omitted, which limits the formulation to the *contact-phase* (see introduction of Section 2.1).

Newton's Second Law postulates [83, pp.143]

$$\begin{aligned} D^I \mathbf{p}_B^I &= \mathbf{f}_B \\ (\text{A.14}) \rightarrow \quad m^B D^G \mathbf{v}_B^G &\simeq \mathbf{f}_B \\ m^B \left(D^B \mathbf{v}_B^G + \Omega^{BG} \mathbf{v}_B^G \right) &\simeq \mathbf{f}_a + \mathbf{f}_p + \mathbf{f}_g \end{aligned} \tag{A.22}$$

where $\mathbf{f}_a$ is the aerodynamic force, $\mathbf{f}_p$ is the engine thrust and $\mathbf{f}_g$ is the gravitational force. (A.22) is projected to aircraft body coordinates $[\cdot]^B$ with aerodynamic forces transformed to *wind-axes W*

$$\begin{aligned} m^B \left[D^B \mathbf{v}_B^G \right]^B + m^B \left[\Omega^{BG} \right]^B \left[\mathbf{v}_B^G \right]^B &\simeq [\mathbf{f}_a]^B + [\mathbf{f}_p]^B + [\mathbf{f}_g]^B \\ m^B \left(\frac{d}{dt} \left[\mathbf{v}_B^G \right]^B \right) + m^B \left[\Omega^{BG} \right]^B \left[\mathbf{v}_B^G \right]^B &\simeq [\mathbf{T}]^{BW} [\mathbf{f}_a]^W + [\mathbf{f}_p]^B + [\mathbf{T}]^{BG} [\mathbf{f}_g]^G \end{aligned} \tag{A.23}$$

and, by replacing the projected tensors with aerodynamic coefficients and components defined in Section 2.2.3.1, the aircraft linear acceleration takes its final form

$$\begin{aligned} (\text{A.21}) \rightarrow \quad \begin{bmatrix} \dot{u} \\ \dot{v} \\ \dot{w} \end{bmatrix} \simeq & - \begin{bmatrix} p \\ q \\ r \end{bmatrix} \times \begin{bmatrix} u \\ v \\ w \end{bmatrix} + [\mathbf{T}]^{BW} \left(\frac{\varrho_d s}{\check{m}^B} \begin{bmatrix} c_x \\ c_y \\ c_z \end{bmatrix} \right) + \\ & \frac{1}{m^B} \begin{bmatrix} \delta_{p_p} + \delta_{p_s} \\ 0 \\ 0 \end{bmatrix} + [\mathbf{T}]^{BG} \begin{bmatrix} 0 \\ 0 \\ g \end{bmatrix} \end{aligned} \tag{A.24}$$

where $\times$ denotes the the vector-product, ϱ_d is the dynamic pressure, s is the surface of the wing [9] and c denotes an aerodynamic coefficient [10].

Euler's Law postulates [83, pp.181]

$$\begin{aligned} D^I \mathbf{l}_B^{BI} &= \mathbf{m}_B \\ (\text{A.15}) \rightarrow \quad D^G \left(\mathbf{I}_B^B \boldsymbol{\omega}^{BG} \right) &\simeq \mathbf{m}_B \\ D^B \left(\mathbf{I}_B^B \boldsymbol{\omega}^{BG} \right) + \boldsymbol{\Omega}^{BG} \left(\mathbf{I}_B^B \boldsymbol{\omega}^{BG} \right) &\simeq \mathbf{m}_a + \mathbf{m}_p \\ \mathbf{I}_B^B \left(D^B \boldsymbol{\omega}^{BG} \right) + \boldsymbol{\Omega}^{BG} \left(\mathbf{I}_B^B \boldsymbol{\omega}^{BG} \right) &\simeq \mathbf{m}_a + \mathbf{m}_p \end{aligned} \tag{A.25}$$

where $\mathbf{m}_a$ is the aerodynamic moment and $\mathbf{m}_p$ is the moment produced by engine thrust. (A.25) is projected to aircraft body coordinates $[\cdot]^B$ with aerodynamic forces transformed to the wind-*axes W*

$$\begin{aligned} \left[\mathbf{I}_B^B \right]^B \left[D^B \boldsymbol{\omega}^{BG} \right]^B + \left[\boldsymbol{\Omega}^{BG} \right]^B \left[\mathbf{I}_B^B \right]^B \left[\boldsymbol{\omega}^{BG} \right]^B &\simeq [\mathbf{m}_a]^B + [\mathbf{m}_p]^B \\ \left[\mathbf{I}_B^B \right]^B \left(\frac{d}{dt} \left[\boldsymbol{\omega}^{BG} \right]^B \right) + \left[\boldsymbol{\Omega}^{BG} \right]^B \left[\mathbf{I}_B^B \right]^B \left[\boldsymbol{\omega}^{BG} \right]^B &\simeq [\mathbf{T}]^{BW} [\mathbf{m}_a]^W + [\mathbf{m}_p]^B \end{aligned} \tag{A.26}$$

9. $\varrho_d s$ is used to de-scale the aerodynamic coefficients to aerodynamic derivatives.
10. The aerodynamic coefficients are given functions of the aircraft motion variables, provided by Airbus.

and, by replacing the projected tensors with components defined in Section 2.2.3.1, the aircraft angular acceleration takes its final form

$$\begin{bmatrix} \dot{p} \\ \dot{q} \\ \dot{r} \end{bmatrix} \simeq \left(\left[\mathbf{I}_B^B \right]^B \right)^{-1} \left(- \begin{bmatrix} p \\ q \\ r \end{bmatrix} \times \left(\left[\mathbf{I}_B^B \right]^B \begin{bmatrix} p \\ q \\ r \end{bmatrix} \right) + [\mathbf{T}]^{BS} \left(\varrho_d sl \begin{bmatrix} c_l \\ c_m \\ c_n \end{bmatrix} \right) + \left(\begin{bmatrix} \delta_{p_p} \\ 0 \\ 0 \end{bmatrix} \times \left[\mathbf{s}_{P_p B} \right]^B + \begin{bmatrix} \delta_{p_s} \\ 0 \\ 0 \end{bmatrix} \times \left[\mathbf{s}_{P_s B} \right]^B \right) \right) \tag{A.27}$$

where l is the reference cord length of the wing and P denotes a point on the engine thrust/propulsion vector, *i.e.* the engine axis.

Furthermore, Euler 3-2-1 angle Differential Equations (DEs), *i.e.* the time-rate of change of the Euler 3-2-1 angles, are included so that all the variables in (A.24) and (A.27) are governed. The Euler 3-2-1 angle DEs, also known as the *gimbal equations*, are expressed in terms of body angular rates, and is given in [83, pp.121] as

$$\begin{bmatrix} \dot{\phi} \\ \dot{\theta} \\ \dot{\psi} \end{bmatrix} = \begin{bmatrix} 1 & \sin\phi\tan\theta & \cos\phi\tan\theta \\ 0 & \cos\phi & -\sin\phi \\ 0 & \sin\phi/\cos\theta & \cos\phi/\cos\theta \end{bmatrix} \begin{bmatrix} p \\ q \\ r \end{bmatrix}, \quad \theta \neq \frac{\pi}{2} + k\pi,\ k \in \mathbb{Z}^1 \tag{A.28}$$

We conclude the aircraft EOM by formulating the aircraft climb-rate

$$\begin{aligned} \dot{h} &= \begin{bmatrix} 0 & 0 & -1 \end{bmatrix} \left[\overline{\mathbf{T}} \right]^{BG} \left[\mathbf{v}_B^G \right]^B \\ &= \begin{bmatrix} 0 & 0 & -1 \end{bmatrix} \left[\overline{\mathbf{T}} \right]^{BG} \begin{bmatrix} u \\ v \\ w \end{bmatrix} \end{aligned} \tag{A.29}$$

(A.24), (A.27), (A.28) & (A.29) completes the formulation of aircraft 6DOF EOM. The A330-MRTT model described in Section 1.3 implements aerodynamic coefficients with neural-networks in MATLAB mex-file format, from which a numerical perturbation model is obtained using the method described in Section B.1.

A.1.4 In-flight refuelling relative position kinematics

IFR relative position kinematics is derived in terms of tanker and receiver motion variables to enable easy trim calculation and incorporation into the IFR state-space model.

Refer to Dogan and Waishek [24, pp.586-589] and Figure 2.10. A kinematic equation, expressing the position of the receiver's receptacle relative to the tanker boom joint, in tanker coordinates, is developed by taking the time-derivative of its vector triangle with respect to the local geographic frame, given as

$$\begin{aligned} \mathbf{s}_{\Gamma J} &= \mathbf{s}_{\Gamma G} - \mathbf{s}_{JG} \\ D^G \mathbf{s}_{\Gamma J} &= D^G \mathbf{s}_{\Gamma G} - D^G \mathbf{s}_{JG} \end{aligned} \tag{A.30}$$

Terms involved in (A.30) are expanded as

$$D^G \mathbf{s}_{\Gamma J} = D^T \mathbf{s}_{\Gamma J} + \Omega^{TG} \mathbf{s}_{\Gamma J} \tag{A.31}$$

$$\begin{aligned} D^G \mathbf{s}_{\Gamma G} &= D^G \left(\mathbf{s}_{\Gamma R} + \mathbf{s}_{RG} \right) \\ &= D^G \mathbf{s}_{\Gamma R} + D^G \mathbf{s}_{RG} \\ &= D^R \mathbf{s}_{\Gamma R} + \Omega^{RG} \mathbf{s}_{\Gamma R} + \mathbf{v}_R^G \end{aligned} \tag{A.32}$$

$$\begin{aligned} D^G \mathbf{s}_{JG} &= D^G \left(\mathbf{s}_{JT} + \mathbf{s}_{TG} \right) \\ &= D^G \mathbf{s}_{JT} + D^G \mathbf{s}_{TG} \\ &= D^T \mathbf{s}_{JT} + \Omega^{TG} \mathbf{s}_{JT} + \mathbf{v}_T^G \end{aligned} \tag{A.33}$$

and combined as

$$\begin{aligned} \text{(A.30)-(A.33)} \rightarrow \quad D^T \mathbf{s}_{\Gamma J} + \Omega^{TG} \mathbf{s}_{\Gamma J} &= D^R \mathbf{s}_{\Gamma R} + \Omega^{RG} \mathbf{s}_{\Gamma R} + \mathbf{v}_R^G \\ &\quad - \left(D^T \mathbf{s}_{JT} + \Omega^{TG} \mathbf{s}_{JT} + \mathbf{v}_T^G \right) \end{aligned} \tag{A.34}$$

(A.34) is projected to tanker coordinates $[\cdot]^T$ to obtain its component form

$$\begin{aligned} \text{(A.34)} \rightarrow \quad \left[D^T \mathbf{s}_{\Gamma J} \right]^T + \left[\Omega^{TG} \right]^T \left[\mathbf{s}_{\Gamma J} \right]^T &= \left[D^R \mathbf{s}_{\Gamma R} \right]^T + \left[\Omega^{RG} \right]^T \left[\mathbf{s}_{\Gamma R} \right]^T + \left[\mathbf{v}_R^G \right]^T \\ &\quad - \left[D^T \mathbf{s}_{JT} \right]^T - \left[\Omega^{TG} \right]^T \left[\mathbf{s}_{JT} \right]^T - \left[\mathbf{v}_T^G \right]^T \end{aligned} \tag{A.35}$$

$$\begin{aligned} \text{(A.35)} \rightarrow \quad \frac{d}{dt} \left[\mathbf{s}_{\Gamma J} \right]^T &= - \left[\Omega^{TG} \right]^T \left[\mathbf{s}_{\Gamma J} \right]^T + \left[\mathbf{T} \right]^{TR} \frac{d}{dt} \left[\mathbf{s}_{\Gamma R} \right]^R + \left[\mathbf{T} \right]^{TR} \left[\Omega^{RG} \right]^R \left[\mathbf{s}_{\Gamma R} \right]^R \\ &\quad + \left[\mathbf{T} \right]^{TR} \left[\mathbf{v}_R^G \right]^R - \frac{d}{dt} \left[\mathbf{s}_{JT} \right]^T - \left[\Omega^{TG} \right]^T \left[\mathbf{s}_{JT} \right]^T - \left[\mathbf{v}_T^G \right]^T \end{aligned} \tag{A.36}$$

For *rigid bodies,* (A.36) simplifies to

$$\begin{aligned} \text{(A.35)} \rightarrow \quad \frac{d}{dt} \left[\mathbf{s}_{\Gamma J} \right]^T &= - \left[\Omega^{TG} \right]^T \left[\mathbf{s}_{\Gamma J} \right]^T + \left[\mathbf{T} \right]^{TR} \left[\Omega^{RG} \right]^R \left[\mathbf{s}_{\Gamma R} \right]^R + \\ &\quad \left[\mathbf{T} \right]^{TR} \left[\mathbf{v}_R^G \right]^R - \left[\Omega^{TG} \right]^T \left[\mathbf{s}_{JT} \right]^T - \left[\mathbf{v}_T^G \right]^T \end{aligned} \tag{A.37}$$

and, by replacing the projected tensors with components defined in Section 2.2.3.1, the kinematic coupling for a rigid tanker and receiver takes its final form

$$\begin{aligned} \text{(A.35)} \rightarrow \quad \begin{bmatrix} \dot{x}_b \\ \dot{y}_b \\ \dot{z}_b \end{bmatrix} &= - \begin{bmatrix} p_T \\ q_T \\ r_T \end{bmatrix} \times \begin{bmatrix} x_b \\ y_b \\ z_b \end{bmatrix} + \left[\mathbf{T} \right]^{TR} \left(\begin{bmatrix} p_R \\ q_R \\ r_R \end{bmatrix} \times \left[\mathbf{s}_{\Gamma R} \right]^R \right) + \\ &\quad \left[\mathbf{T} \right]^{TR} \begin{bmatrix} u_R \\ v_R \\ w_R \end{bmatrix} - \begin{bmatrix} p_T \\ q_T \\ r_T \end{bmatrix} \times \left[\mathbf{s}_{JT} \right]^T - \begin{bmatrix} u_T \\ v_T \\ w_T \end{bmatrix} \end{aligned} \tag{A.38}$$

where subscripts T and R denotes the tanker and receiver motion variables respectively, and $[\overline{\mathbf{s}_{\Gamma J}}]^T := \begin{bmatrix} x_b & y_b & z_b \end{bmatrix}$.

Receiver altitude h_R may be expressed in terms of boom motion variables and remaining tanker and receiver motion variables. A new vector triangle

$$\mathbf{s}_{RG} = \mathbf{s}_{RT} + \mathbf{s}_{TG} \tag{A.39}$$

is expanded as

$$\mathbf{s}_{RG} = \mathbf{s}_{R\Gamma} + \mathbf{s}_{\Gamma J} + \mathbf{s}_{JT} + \mathbf{s}_{TG} \tag{A.40}$$

and projected to geographic coordinates $[\cdot]^G$.

$$\begin{aligned} (\text{A.40}) \rightarrow \quad [\mathbf{s}_{RG}]^G &= [\mathbf{s}_{R\Gamma}]^G + [\mathbf{s}_{\Gamma J}]^G + [\mathbf{s}_{JT}]^G + [\mathbf{s}_{TG}]^G \\ &= [\mathbf{T}]^{GR}[\mathbf{s}_{R\Gamma}]^R + [\mathbf{T}]^{GT}[\mathbf{s}_{\Gamma J}]^T + [\mathbf{T}]^{GT}[\mathbf{s}_{JT}]^T + [\mathbf{s}_{TG}]^G \end{aligned} \tag{A.41}$$

Receiver altitude is isolated as

$$\begin{aligned} h_R &= -\begin{bmatrix} 0 & 0 & 1 \end{bmatrix}[\mathbf{s}_{RG}]^G \\ &= -\begin{bmatrix} 0 & 0 & 1 \end{bmatrix}\left([\mathbf{T}]^{GR}[\mathbf{s}_{R\Gamma}]^R + [\mathbf{T}]^{GT}[\mathbf{s}_{\Gamma J}]^T + [\mathbf{T}]^{GT}[\mathbf{s}_{JT}]^T + [\mathbf{s}_{TG}]^G\right) \\ &= -\begin{bmatrix} 0 & 0 & 1 \end{bmatrix}\left([\mathbf{T}]^{GR}[\mathbf{s}_{R\Gamma}]^R + [\mathbf{T}]^{GT}\begin{bmatrix} x_b \\ y_b \\ z_b \end{bmatrix} + [\mathbf{T}]^{GT}[\mathbf{s}_{JT}]^T\right) + h_T \end{aligned} \tag{A.42}$$

Furthermore, by assuming the nozzle N is connected to the receptacle Γ, boom variables λ, σ and χ, defined in Section 2.2.3.2, may be expressed with the relative position components x_b, y_b and z_b, by applying simple scalar- and vector-products, given as follows.

An angle φ between two first order tensors $\mathbf{x}$ and $\mathbf{y}$ is given in [83, pp.32] in terms of the scalar-product as

$$\varphi = \cos^{-1}\left(\frac{\overline{\mathbf{x}}\mathbf{y}}{|\mathbf{x}|\,|\mathbf{y}|}\right) \tag{A.43}$$

where $|\mathbf{x}|$ and $|\mathbf{y}|$ are the lengths of $\mathbf{x}$ and $\mathbf{y}$ respectively. The first order tensor $\mathbf{z}$ orthogonal to a surface passing through the origin described by $\mathbf{x}$ and $\mathbf{y}$ is given in [83, pp.33-34] in terms of the vector-product as

$$\mathbf{z} = \mathbf{X}\mathbf{y} \tag{A.44}$$

where $\mathbf{X}$ is the skew-symmetric of $\mathbf{x}$. It follows that the boom variables may be expressed with the relative position components as

$$|\lambda| = |\mathbf{s}_{\Gamma J}| \tag{A.45}$$

$$|\sigma| = \cos^{-1}\left(\frac{\overline{\mathbf{s}_{\Gamma J}}\mathbf{j}_1}{|\mathbf{s}_{\Gamma J}|\,|\mathbf{j}_1|}\right) - \kappa \tag{A.46}$$

and

$$|\chi| = \cos^{-1}\left(\frac{\overline{\mathbf{t}_2}\,(\mathbf{J}_1\mathbf{s}_{\Gamma J})}{|\mathbf{t}_2|\,|\mathbf{J}_1\mathbf{s}_{\Gamma J}|}\right) \tag{A.47}$$

where $\mathbf{j}_1$ is the boom roll-axes, $\mathbf{t}_2$ is the starboard-side base component of the tanker and the vector product is such that χ is zero in the boom-down position. (A.46) and (A.47) both possess the singularity inherent in $\cos^{-1}$ and is ill-defined as the boom length reaches zero. However, we do not require them to be non-singular as they are not used for feedback, but used to test regulation performance. Thus, for the region of interest, *i.e.* the *contact* and *disconnect* envelopes, $\lambda = |\lambda|$ and $\sigma = |\sigma|$, and we add a sign to χ as

$$\chi = \operatorname{sgn}(y_b)\,|\chi| \tag{A.48}$$

Boom variables expressions are projected to tanker coordinates $[\cdot]^T$ and result in their final forms

$$\lambda = \sqrt{x_b^2 + y_b^2 + z_b^2} \tag{A.49}$$

$$\begin{aligned}
\sigma &= \cos^{-1}\left(\frac{[\overline{\mathbf{s}_{\Gamma J}}]^T\,[\mathbf{j}_1]^T}{\left|[\mathbf{s}_{\Gamma J}]^T\right|\left|[\mathbf{j}_1]^T\right|}\right) - \kappa \\
&= \cos^{-1}\left(\frac{\begin{bmatrix} x_b & y_b & z_b \end{bmatrix}\begin{bmatrix} -\cos(\kappa) \\ 0 \\ -\sin(\kappa) \end{bmatrix}}{\sqrt{x_b^2 + y_b^2 + z_b^2}\left|[\mathbf{j}_1]^T\right|}\right) - \kappa \\
&= \cos^{-1}\left(\frac{-x_b\cos(\kappa) - z_b\sin(\kappa)}{\sqrt{x_b^2 + y_b^2 + z_b^2}}\right) - \kappa
\end{aligned} \tag{A.50}$$

and

$$\begin{aligned}
\chi &= \operatorname{sgn}(y_b)\cos^{-1}\left(\frac{\left[\overline{\mathbf{t}_2}\right]^T\left(\left[\mathbf{J}_1\right]^T\left[\mathbf{s}_{\Gamma J}\right]^T\right)}{\left|\left[\overline{\mathbf{t}_2}\right]^T\right|\left|\left[\mathbf{J}_1\right]^T\left[\mathbf{s}_{\Gamma J}\right]^T\right|}\right) \\
&= \operatorname{sgn}(y_b)\cos^{-1}\left(\frac{\begin{bmatrix}0 & 1 & 0\end{bmatrix}\left(\begin{bmatrix}0 & \sin(\kappa) & 0\\ -\sin(\kappa) & 0 & \cos(\kappa)\\ 0 & -\cos(\kappa) & 0\end{bmatrix}\begin{bmatrix}x_b\\ y_b\\ z_b\end{bmatrix}\right)}{\left\|\begin{bmatrix}0 & \sin(\kappa) & 0\\ -\sin(\kappa) & 0 & \cos(\kappa)\\ 0 & -\cos(\kappa) & 0\end{bmatrix}\begin{bmatrix}x_b\\ y_b\\ z_b\end{bmatrix}\right\|}\right) \\
&= \operatorname{sgn}(y_b)\cos^{-1}\left(\frac{-x_b\sin(\kappa)+z_b\cos(\kappa)}{\left\|\begin{bmatrix}y_b\sin(\kappa)\\ -x_b\sin(\kappa)+z_b\cos(\kappa)\\ -y_b\cos(\kappa)\end{bmatrix}\right\|}\right) \\
&= \operatorname{sgn}(y_b)\cos^{-1}\left(\frac{-x_b\sin(\kappa)+z_b\cos(\kappa)}{\sqrt{y_b^2+\left(-x_b\sin(\kappa)+z_b\cos(\kappa)\right)^2}}\right) \qquad \text{(A.51)}
\end{aligned}$$

This concludes the IFR kinematics coupling.

A.1.5 In-flight refuelling reference flight

Equations describing the reference flight of IFR is derived for trim calculation purposes. The tanker, leading the IFR manoeuvre, has a reference flight defined by fixed ground-speed

$$\begin{aligned}
\nu_{T_r} &= \left|\mathbf{v}_{T_r}^G\right| \\
&= \left\|\left[\mathbf{v}_{T_r}^G\right]^{T_r}\right\|_2 \\
&= \sqrt{u_{T,r}^2+v_{T,r}^2+w_{T,r}^2} \\
\dot{\nu}_{T_r} &= 0 \qquad \text{(A.52)}
\end{aligned}$$

fixed climb-rate

$$\begin{aligned}
\dot{h}_{T_r} &= \begin{bmatrix}0 & 0 & -1\end{bmatrix}\left[\overline{\mathbf{T}}\right]^{T_rG}\left[\mathbf{v}_{T_r}^G\right]^{T_r} \\
(??) \rightarrow &= u_{T_r}\sin\theta_{T_r}-v_{T_r}\cos\theta_{T_r}\sin\phi_{T_r}-w_{T_r}\cos\theta_{T_r}\cos\phi_{T_r} \\
\ddot{h}_{T_r} &= 0 \qquad \text{(A.53)}
\end{aligned}$$

and fixed bank-angle

$$\begin{aligned}
\phi_{T_r} &= \phi_{T_r} \\
\dot{\phi}_{T_r} &= 0 \qquad \text{(A.54)}
\end{aligned}$$

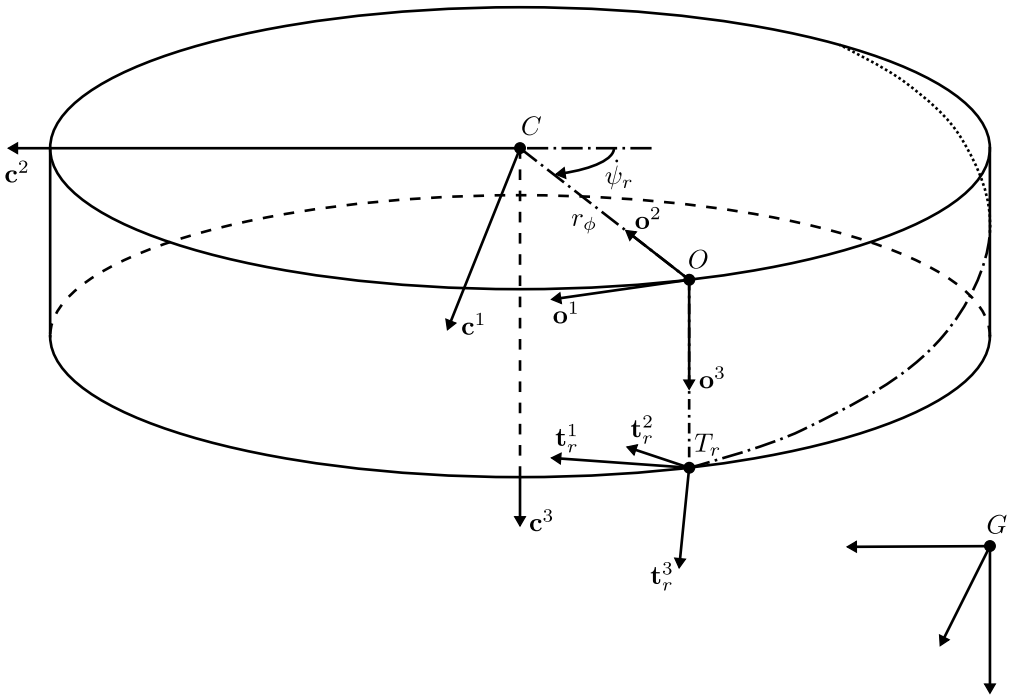

Figure A.3: Tanker reference flight vector diagram

which is specified by the tanker pilot. The anticipated resulting manoeuvre of the tanker is called a *corkscrew*, and is confirmed in Section A.1.6.

Refer to Figure A.3. Two artificial frames, C and O, additional to the local geographic frame G and tanker body reference frame T_r, are used to describe the *corkscrew* in terms of tanker motion variables. C and O are used to describe the circular reference flight produced by fixed ground-speed and bank angle, as well as a constant climb-rate. C is aligned with and fixed to the geographical frame, with $\mathbf{c}_3$ as the *corkscrew* centre. The *corkscrew* disk or cylinder is defined by frame C and tanker centre of mass T_r. O has zero climb-rate and is fixed to the horizontal plane, defined by $\mathbf{c}_1$ and $\mathbf{c}_2$, on the corkscrew radius, with $\mathbf{o}_3$ and $\mathbf{s}_{TO}$ parallel to $\mathbf{c}_3$, $\mathbf{o}_1$ tangent to the disk in the direction of the tanker horizontal velocity and $\mathbf{o}_2$ parallel to $\mathbf{s}_{CO}$. The resulting *corkscrew* frame properties are formulated as

$$\begin{aligned}
D^C\mathbf{s}_{CG} &= \mathbf{0} \\
\mathbf{R}^{CG} &= I \\
\boldsymbol{\Omega}^{CG} &= \mathbf{0} \\
D^O\mathbf{s}_{OC} &= \mathbf{0} \\
D^O\boldsymbol{\omega}^{OC} &= \mathbf{0} \\
D^O\mathbf{v}_{T_r}^O &= \mathbf{0} \\
\mathbf{s}_{T_rO} &= \left(\overline{\mathbf{o}^3}\mathbf{s}_{T_rO}\right)\mathbf{o}^3 \\
\boldsymbol{\omega}^{OC} &= \left(\overline{\mathbf{o}^3}\boldsymbol{\omega}^{OC}\right)\mathbf{o}^3 \\
\boldsymbol{\Omega}^{T_rO} &= \mathbf{0}
\end{aligned} \tag{A.55}$$

The corresponding time-derivatives of the aircraft motion variable are derived next, to achieve a trim, *i.e.* to maintain fixed ground-speed, climb-rate and bank-angle. Linear acceleration for a *corkscrew* is derived as

$$\begin{aligned}
D^{T_r}\mathbf{v}_{T_r}^{G} &= D^{T_r}D^{G}\mathbf{s}_{T_rG} \\
&= D^{T_r}\left(D^{C}\mathbf{s}_{T_rG} + \boldsymbol{\Omega}^{CG}\mathbf{s}_{T_rG}\right) \\
&= D^{T_r}\left(D^{C}\left(\mathbf{s}_{T_rC} + \mathbf{s}_{CG}\right) + \boldsymbol{\Omega}^{CG}\mathbf{s}_{T_rG}\right) \\
&= D^{T_r}\left(D^{C}\mathbf{s}_{T_rC} + D^{C}\mathbf{s}_{CG} + \boldsymbol{\Omega}^{CG}\mathbf{s}_{T_rG}\right) \\
\text{(A.55)} \rightarrow \quad &= D^{T_r}D^{C}\mathbf{s}_{T_rC} \\
&= D^{T_r}D^{C}\left(\mathbf{s}_{T_rO} + \mathbf{s}_{OC}\right) \\
&= D^{T_r}D^{C}\mathbf{s}_{T_rO} + D^{T_r}D^{C}\mathbf{s}_{OC} \\
&= D^{T_r}\left(D^{O}\mathbf{s}_{T_rO} + \boldsymbol{\Omega}^{OC}\mathbf{s}_{T_rO}\right) + D^{T_r}\left(D^{O}\mathbf{s}_{OC} + \boldsymbol{\Omega}^{OC}\mathbf{s}_{OC}\right) \\
\text{(A.55)} \rightarrow \quad &= D^{T_r}D^{O}\mathbf{s}_{T_rO} + D^{T_r}\left(\boldsymbol{\Omega}^{OC}\mathbf{s}_{OC}\right) \\
&= D^{O}D^{O}\mathbf{s}_{T_rO} + \boldsymbol{\Omega}^{OT_r}D^{O}\mathbf{s}_{T_rO} + D^{O}\left(\boldsymbol{\Omega}^{OC}\mathbf{s}_{OC}\right) + \boldsymbol{\Omega}^{OT_r}\boldsymbol{\Omega}^{OC}\mathbf{s}_{OC} \\
&= \mathbf{0}
\end{aligned} \tag{A.56}$$

Angular acceleration for a *corkscrew* is derived as

$$\begin{aligned}
D^{T_r}\boldsymbol{\omega}^{T_rG} &= D^{T_r}\left(\boldsymbol{\omega}^{T_rO} + \boldsymbol{\omega}^{OC} + \boldsymbol{\omega}^{CG}\right) \\
\text{(A.55)} \rightarrow \quad &= D^{T_r}\boldsymbol{\omega}^{OC} \\
&= D^{O}\boldsymbol{\omega}^{OC} + \boldsymbol{\Omega}^{OT_r}\boldsymbol{\omega}^{OC} \\
\text{(A.55)} \rightarrow \quad &= \mathbf{0}
\end{aligned} \tag{A.57}$$

Euler 3-2-1 angle time-derivatives for a *corkscrew* are derived as

$$\begin{aligned}
\text{(2.17)} \rightarrow \quad \begin{bmatrix} \dot{\phi}_{T_r} \\ \dot{\theta}_{T_r} \\ \dot{\psi}_{T_r} \end{bmatrix} &= \begin{bmatrix} 1 & \sin\phi_{T_r}\tan\theta_{T_r} & \cos\phi_{T_r}\tan\theta_{T_r} \\ 0 & \cos\phi_{T_r} & -\sin\phi_{T_r} \\ 0 & \sin\phi_{T_r}/\cos\theta_{T_r} & \cos\phi_{T_r}/\cos\theta_{T_r} \end{bmatrix} \left[\boldsymbol{\omega}^{T_rG}\right]^{T_r} \\
&= \begin{bmatrix} 1 & \sin\phi_{T_r}\tan\theta_{T_r} & \cos\phi_{T_r}\tan\theta_{T_r} \\ 0 & \cos\phi_{T_r} & -\sin\phi_{T_r} \\ 0 & \sin\phi_{T_r}/\cos\theta_{T_r} & \cos\phi_{T_r}/\cos\theta_{T_r} \end{bmatrix} \left[\boldsymbol{\omega}^{OC}\right]^{T_r} \\
&= \begin{bmatrix} 1 & \sin\phi_{T_r}\tan\theta_{T_r} & \cos\phi_{T_r}\tan\theta_{T_r} \\ 0 & \cos\phi_{T_r} & -\sin\phi_{T_r} \\ 0 & \sin\phi_{T_r}/\cos\theta_{T_r} & \cos\phi_{T_r}/\cos\theta_{T_r} \end{bmatrix} [\mathbf{T}]^{T_rO} \begin{bmatrix} 0 \\ 0 \\ \dot{\psi}_{T_r} \end{bmatrix} \\
&= \dot{\psi}_{T_r} \begin{bmatrix} 1 & \sin\phi_{T_r}\tan\theta_{T_r} & \cos\phi_{T_r}\tan\theta_{T_r} \\ 0 & \cos\phi_{T_r} & -\sin\phi_{T_r} \\ 0 & \sin\phi_{T_r}/\cos\theta_{T_r} & \cos\phi_{T_r}/\cos\theta_{T_r} \end{bmatrix} \begin{bmatrix} -\sin\theta_{T_r} \\ \cos\theta_{T_r}\sin\phi_{T_r} \\ \cos\theta_{T_r}\cos\phi_{T_r} \end{bmatrix} \\
&= \begin{bmatrix} 0 \\ 0 \\ \dot{\psi}_{T_r} \end{bmatrix}
\end{aligned} \tag{A.58}$$

where $\dot{\psi}_{T_r}$ is unknown and given by

$$\left[\boldsymbol{\omega}^{OC}\right]^{O} = \begin{bmatrix} 0 \\ 0 \\ \dot{\psi}_{T_r} \end{bmatrix} \tag{A.59}$$

which completes the tanker motion variable time-derivatives for a *corkscrew*.

Furthermore, the tanker and receiver relative position for reference flight is given in Section 2.2.3.2 as

$$\begin{aligned} \left[\mathbf{s}_{\Gamma J}\right]^{T_r} &= \begin{bmatrix} -\lambda_r \cos\sigma_r \\ 0 \\ \lambda_r \sin\sigma_r \end{bmatrix} \\ \left[D^{T_r}\mathbf{s}_{\Gamma J}\right]^{T_r} &= \mathbf{0} \end{aligned} \tag{A.60}$$

Finally, for a *corkscrew* tanker reference flight, the receiver reference flight will also be a *corkscrew* with fixed ground-speed, climb-rate and bank-angle, but unknown ground-speed and bank-angle due to a larger turn radius $r_{\phi_R} > r_{\phi_T}$ for $\phi_{T_r} \neq 0$, for which (A.56)-(A.58) will also hold.

This concludes the IFR reference flight kinematics. See Appendix A.1.6 for its application to IFR trim calculation.

A.1.6 Trim

We define *trim* as the *constant motion maintained* within a mechanical system.

Given the system governing equation

$$\dot{\mathbf{m}} = \mathbf{g}\left(\mathbf{m}, \boldsymbol{\delta}\right) \tag{A.61}$$

where $\mathbf{m} \in \mathbb{R}^{n_m \times 1}$ is the system motion variables, $\boldsymbol{\delta} \in \mathbb{R}^{n_\delta \times 1}$ is the system input and $\mathbf{g} : \mathbb{R}^{n_m \times 1} \times \mathbb{R}^{n_\delta \times 1} \mapsto \mathbb{R}^{n_m \times 1}$ is a nonlinear function that governs the change of the motion variables, constant motion may be defined as

$$\begin{aligned} \mathbf{c} &= \mathbf{h}\left(\mathbf{m}\right) \\ \frac{d^n}{dt^n}\begin{bmatrix} \mathbf{c} \\ \boldsymbol{\delta} \end{bmatrix} &= \mathbf{0}\ \forall n \in \mathbb{Z} \cap (0, \infty) \end{aligned} \tag{A.62}$$

where we limit $\boldsymbol{\delta}$ to be constant. We expand the first-order time-derivative of $\mathbf{c}$ as

$$\dot{\mathbf{c}} = \frac{d}{dt}\mathbf{h}\left(\mathbf{m}\right) = \mathbf{q}\left(\mathbf{m}, \dot{\mathbf{m}}\right) = \mathbf{q}\left(\mathbf{m}, \mathbf{g}\left(\mathbf{m}, \boldsymbol{\delta}\right)\right) = \mathbf{p}\left(\mathbf{m}, \boldsymbol{\delta}\right) = \mathbf{0} \tag{A.63}$$

and if we can express $\dot{\mathbf{c}}$ as a function of only $\mathbf{c}$ and $\boldsymbol{\delta}$, the time-derivatives in (A.62) of higher order than one may be omitted, *i.e.*

$$\begin{aligned} &\left(\dot{\mathbf{c}} = \mathbf{p}\left(\mathbf{m}, \boldsymbol{\delta}\right) = \mathbf{r}\left(\mathbf{c}, \boldsymbol{\delta}\right) = \mathbf{0},\ \frac{d^n}{dt^n}\boldsymbol{\delta} = \mathbf{0}\ \forall n \in \mathbb{Z} \cap (0, \infty)\right) \\ &\qquad \Longrightarrow \quad \left(\frac{d^n}{dt^n}\dot{\mathbf{c}} = \mathbf{0}\ \forall n \in \mathbb{Z} \cap (0, \infty)\right) \end{aligned} \tag{A.64}$$

Furthermore, by specifying part of $\mathbf{c}$ and assuming that $\mathbf{r}(\mathbf{c}, \boldsymbol{\delta})$ exists, we may use (A.62) and (A.64) to solve the system motion variables and input corresponding to the constant motion, defined as

$$\begin{bmatrix} \mathbf{m} \\ \boldsymbol{\delta} \end{bmatrix} : \begin{bmatrix} \acute{\mathbf{c}} \\ \mathbf{0} \end{bmatrix} = \begin{bmatrix} \acute{\mathbf{g}}(\mathbf{m}) \\ \mathbf{p}(\mathbf{m}, \boldsymbol{\delta}) \end{bmatrix} \tag{A.65}$$

where $\acute{\mathbf{c}}$ is the specified part in $\mathbf{c}$ with corresponding function $\acute{\mathbf{g}}(\mathbf{m})$, and is solvable via the Newton-Raphson iterative solver [37, pp.271-272]. Note that in the case that $\mathbf{m}$ is time-varying, the Newton-Raphson solver will find a solution to $\mathbf{m}$ for an arbitrary time instance, for which (A.65) will hold.

The Newton-Raphson solver is a common tool used to solve coupled non-linear equations, even though there is no guarantee of convergence, and is based on a calculation with the *Jacobian matrix*, *i.e.* the matrix containing the first order partial derivatives of the coupled non-linear equations in all directions, making it a linearising algorithm. The Newton-Raphson iterative solver is defined as follows.

Given the non-linear vector equation

$$\mathbf{y} = \mathbf{f}(\mathbf{x}) \tag{A.66}$$

$\mathbf{x}$ may be solved for a specified $\mathbf{y} = \mathbf{y}_{sol}$ with the iterative algorithm

$$\mathbf{x}_{i+1} = \mathbf{x}_i + J_i^{-1}(\mathbf{y}_{sol} - \mathbf{f}(\mathbf{x}_i)) \tag{A.67}$$

where i is used denote the progression of the algorithm and the Jacobian matrix is defined as

$$J_i := \left.\frac{\partial \mathbf{f}}{\partial \mathbf{x}}\right|_{\mathbf{x}=\mathbf{x}_i} = \begin{bmatrix} \frac{\partial f_1}{\partial x_1} & \frac{\partial f_1}{\partial x_2} & \cdots & \frac{\partial f_1}{\partial x_{n_x}} \\ \frac{\partial f_2}{\partial x_1} & \frac{\partial f_2}{\partial x_2} & \cdots & \frac{\partial f_2}{\partial x_{n_x}} \\ \vdots & \vdots & \ddots & \\ \frac{\partial f_{n_f}}{\partial x_1} & \frac{\partial f_{n_f}}{\partial x_2} & & \frac{\partial f_{n_f}}{\partial x_{n_x}} \end{bmatrix}_{\mathbf{x}=\mathbf{x}_i} \tag{A.68}$$

If $\mathbf{f}(\mathbf{x})$ is non-analytical, the partial derivatives in the Jacobian matrix is linearly approximated as

$$\frac{\partial f_j}{\partial x_l} \overset{lin}{\simeq} \frac{f_j(\mathbf{x}_i + \epsilon x_l \mathbf{e}_l) - f_j(\mathbf{x}_i)}{\epsilon x_l} \tag{A.69}$$

where ϵx_l is a sufficiently small finite number, $\mathbf{e}_l$ is the l^{th} column of the identity matrix of size n_x and it is assumed that there is a means to calculate $\mathbf{f}(\mathbf{x})$.

Following basic linear algebra, $\mathbf{x}_{sol}$ is unique if $n_x = n_f$ and J has full rank at the solution, *i.e.*

$$\begin{aligned} &\left(\mathbf{y} = \mathbf{f}(\mathbf{x}) \overset{lin}{\simeq} J_{sol}\mathbf{x}\ \forall \mathbf{x} \in [(\mathbf{x}_{sol} - \epsilon\mathbf{x}), (\mathbf{x}_{sol} + \epsilon\mathbf{x})]\right) \\ \implies &\left(\mathbf{x} \overset{lin}{\simeq} J_{sol}^{-1}\mathbf{y}\ \forall \mathbf{x} \in [(\mathbf{x}_{sol} - \epsilon\mathbf{x}), (\mathbf{x}_{sol} + \epsilon\mathbf{x})]\right) \end{aligned} \tag{A.70}$$

Thus, we may deduce that the trim of is unique if

Thus, we may deduce that, in order for the trim described by (A.65) to be unique in terms of the system motion variables and control input, it is required that

$$(n_{\acute{g}} + n_p) = (n_m + n_\delta) = \text{rank} \left(\frac{\partial \begin{bmatrix} \acute{\mathbf{g}}(\mathbf{m}) \\ \mathbf{p}(\mathbf{m}, \boldsymbol{\delta}) \end{bmatrix}}{\partial \begin{bmatrix} \mathbf{m} \\ \boldsymbol{\delta} \end{bmatrix}} \right) \Bigg|_{\substack{\mathbf{m} = \mathbf{m}_r \\ \boldsymbol{\delta} = \boldsymbol{\delta}_r}} \tag{A.71}$$

We demonstrate the above trim criteria by calculating the IFR motion variables and control input corresponding to a *corkscrew* trim (see Appendix A.1.5 for a definition of a corkscrew manoeuvre).

Both tanker and receiver have 10 motion variables and 8 control inputs, *i.e.* $n_{m_T} = n_{m_R} = 10$ and $n_{\delta_T} = n_{\delta_R} = 8$ as defined by (2.6), whereas the relative position is described by 3 motion variables, *i.e.* $n_b = 3$ as defined by (2.21). The IFR trim is independent of absolute heading, which causes one of ψ_T or ψ_R to be redundant, *i.e.* the corkscrew trim description is independent of absolute heading for which (A.71) will not be satisfied if absolute heading is included in $\mathbf{m}$, unless an instantaneous absolute heading is included in $\acute{\mathbf{c}}$. The redundancy is remedied by replacing the absolute headings ψ_T or ψ_R with relative heading $\psi_{TR} := \psi_T - \psi_R$. Furthermore, as noted in Section 2.4, there is a redundancy in receiver altitude h_R, which is replaced by its expression in terms of tanker altitude, tanker and receiver attitude and the relative position motion variables. Thus, there is a total of 37 IFR trim variables to be solved, and we require $(n_{\acute{g}} + n_p) = 37$ and the rank constraint for the trim to be unique. We select $\mathbf{c}$ with known ground-speed $\nu_{T,r}$, climb-rate $\dot{h}_{T,r}$, bank-angle $\phi_{T,r}$ and relative positions $x_{b,r}$, $y_{b,r}$ and $z_{b,r}$, and complete $\mathbf{c}$ with motion variables that are known to have a zero time-derivative.

The dependency of the aircraft motion on altitude inherent in the air density, however, causes the IFR trim corresponding to the known references to be more complex than anticipated in Section A.1.5. As the aircraft descends into denser air, the lift and drag increases for a constant airspeed vector, requiring the aircraft to pitch forward slightly and increase thrust to maintain the known references. Thus, neither $\boldsymbol{\delta}$ nor θ will be constant for IFR trim, however, the errors involved when assuming that they are constant, *i.e.* assuming the aircraft motion is invariant under altitude, will comfortably be corrected with robust feedback. Thus, we assume a corkscrew trim for IFR and fix h_T as a parameter at the initial altitude.

Now, the condition $\dot{\mathbf{c}} = \mathbf{r}(\mathbf{c}, \boldsymbol{\delta})$ is achieved by selecting $\mathbf{c}$ to be n_m non-equal equations in $\mathbf{m}_{AIFR}$, where

$$\mathbf{m}_{AIFR} = \begin{bmatrix} \begin{bmatrix} I_8 & 0_{8\times 2} \end{bmatrix} & 0 & 0 \\ 0 & \begin{bmatrix} I_8 & 0_{8\times 2} \end{bmatrix} & 0 \\ \begin{bmatrix} 0_{1\times 8} & 1 & 0_{1\times 1} \end{bmatrix} & \begin{bmatrix} 0_{1\times 8} & -1 & 0_{1\times 1} \end{bmatrix} & 0 \\ 0 & 0 & I_3 \end{bmatrix} \begin{bmatrix} \mathbf{m}_T \\ \mathbf{m}_R \\ \mathbf{b} \end{bmatrix} \tag{A.72}$$

i.e. $\mathbf{m}$ is non-linearly transformed to $\mathbf{c}$ with invertable $\mathbf{h}$, such that $\dot{\mathbf{c}} = \mathbf{p}(\mathbf{m}, \boldsymbol{\delta}) = \mathbf{p}(\mathbf{h}^{-1}(\mathbf{c}), \boldsymbol{\delta}) = \mathbf{r}(\mathbf{c}, \boldsymbol{\delta})$.

$$\mathbf{g}(\mathbf{m}) = \begin{bmatrix} \nu_T \\ v_T \\ \dot{h}_T \\ p_T \\ q_T \\ r_T \\ \phi_T \\ \theta_T \\ u_R \\ v_R \\ w_R \\ p_R \\ q_R \\ r_R \\ \phi_R \\ \theta_R \\ \psi_{TR} \\ x_b \\ y_b \\ z_b \end{bmatrix} \in \mathbb{R}^{20\times 1},\ \acute{\mathbf{g}}(\mathbf{m}) = \begin{bmatrix} \nu_T \\ v_T \\ \dot{h}_T \\ \phi_T \\ v_R \\ x_b \\ y_b \\ z_b \end{bmatrix} \in \mathbb{R}^{8\times 1},\ n_{\acute{h}} + n_p = 28 \tag{A.73}$$

where a zero sideslip is chosen for both tanker and receiver trim, *i.e.* $v_T = v_R = 0$. Following (A.71), the trim as described by (A.73) is not unique due to $n_{\acute{h}} + n_p \neq 36$. Uniqueness is imposed by fixing 8 of the inputs as

$$\acute{\boldsymbol{\delta}} = \begin{bmatrix} \delta_{e,T} \\ \delta_{s_p,T} \\ \delta_{s_s,T} \\ \delta_{t_p,T} - \delta_{t_s,T} \\ \delta_{e,R} \\ \delta_{s_p,R} \\ \delta_{s_s,R} \\ \delta_{t_p,R} - \delta_{t_s,R} \end{bmatrix} = \begin{bmatrix} 0 \\ \text{centre}\left(\delta_{s_p,T}\right) \\ \text{centre}\left(\delta_{s_s,T}\right) \\ 0 \\ 0 \\ \text{centre}\left(\delta_{s_p,R}\right) \\ \text{centre}\left(\delta_{s_s,R}\right) \\ 0 \end{bmatrix} \tag{A.74}$$

where

$$\text{centre}(\delta) := \frac{1}{2}\left(\max(\delta) + \min(\delta)\right) \tag{A.75}$$

as defined in Table 4.3 and $\acute{\boldsymbol{\delta}}$ denotes the fixed actuators with known values. Thus, pitch moment is set with δ_h, a conventional trim of zero is chosen for elevators, spoilers are set to their centres to provide maximum range for control and no differential thrust is used at trim. Now, (A.73) and (A.74) satisfies (A.64) and (A.71), thus a unique IFR trim is achieved.

A.1.7 Dryden turbulence model transformations

An effort is made here to avoid confusion due to the various forms the turbulence functions (2.26)-(2.31) may take.

The derivation process is given as

$$\phi(\Omega) \rightarrow \mathcal{P}(\Omega) \rightarrow R(\xi) \rightarrow R(\tau) \rightarrow \mathcal{P}(\omega) \rightarrow \mathcal{D}(j\omega) \tag{A.76}$$

where Ω ($^{\text{rad}}/_{\text{m}}$) and ξ (m) are *spatial* scalars and ω ($^{\text{rad}}/_{\text{s}}$) and τ (s) their *temporal* counterparts, ϕ is known as the *spectrum function*, $\mathcal{P}$ the *Power Density Spectrum* (PDS), R the correlation and $\mathcal{D}$ the white noise shaping-filter, all the functions are *one-dimensional* and all functions, except ϕ, are *double-sided*. Also, steps $\mathcal{P}(\Omega)$ to $\mathcal{P}(\omega)$ are not calculated, but included to show the change of variables.

(2.26)-(2.31) are transformed to $\mathcal{P}(\Omega)$, which is the preferred form for electrical engineering purposes and admits standard Fourier transform tables, by using their relationship to $R(\xi)$. The relation between $\mathcal{P}$ and ϕ is obtained by considering the standard Fourier transform [64, pp.225]

$$\begin{aligned} \mathcal{P}_{ij}(\omega) &= \int_{-\infty}^{\infty} R_{ij}(\tau)\, e^{-j\omega\tau} d\tau = \mathcal{F}\{R_{ij}(\tau)\} \\ \iff \mathcal{P}_{ij}(\Omega) &= \int_{-\infty}^{\infty} R_{ij}(\xi)\, e^{-j\Omega\xi} d\xi = \mathcal{F}\{R_{ij}(\xi)\} \end{aligned} \tag{A.77}$$

and the definition of spectral functions Etkin [32, pp.25]

$$\begin{aligned} \overleftrightarrow{\phi}_{ij}(\omega) &= \frac{1}{2\pi} \int_{-\infty}^{\infty} R_{ij}(\tau)\, e^{-j\omega\tau} d\tau \\ \iff \phi_{ij}(\omega) &= \frac{1}{\pi} \int_{-\infty}^{\infty} R_{ij}(\tau)\, e^{-j\omega\tau} d\tau \\ \iff \phi_{ij}(\Omega) &= \frac{1}{\pi} \int_{-\infty}^{\infty} R_{ij}(\xi)\, e^{-j\Omega\xi} d\xi \end{aligned} \tag{A.78}$$

where $\overleftrightarrow{\phi}_{ij}(\omega)$ denotes the *double-sided* version of $\phi_{ij}(\omega)$, as is related as

$$\mathcal{P}_{ij}(\Omega) = \pi \phi_{ij}(\Omega) \tag{A.79}$$

The PDSs of turbulence components (2.26)-(2.31) follows as

$$\mathcal{P}_{u_g}(\Omega) = 2\sigma_{u_g}^2 l_u \frac{1}{1 + (l_u\Omega)^2} \tag{A.80}$$

$$\mathcal{P}_{v_g}(\Omega) = \sigma_{v_g}^2 l_v \frac{1 + 3(l_v\Omega)^2}{\left(1 + (l_v\Omega)^2\right)^2} \tag{A.81}$$

$$\mathcal{P}_{w_g}(\Omega) = \sigma_{w_g}^2 l_w \frac{1 + 3(l_w\Omega)^2}{\left(1 + (l_w\Omega)^2\right)^2} \tag{A.82}$$

$$\mathcal{P}_{p_g}(\Omega) = 0.8\frac{\sigma_{w_g}^2\pi}{l_w}\left(\frac{\pi l_w}{4b}\right)^{\frac{1}{3}}\frac{1}{1+\left(\frac{4b}{\pi}\Omega\right)^2} \tag{A.83}$$

$$\mathcal{P}_{q_g}(\Omega) = \frac{\Omega^2}{1+\left(\frac{4b}{\pi}\Omega\right)^2}\mathcal{P}_{w_g}(\Omega) \tag{A.84}$$

$$\mathcal{P}_{r_g}(\Omega) = \frac{\Omega^2}{1+\left(\frac{3b}{\pi}\Omega\right)^2}\mathcal{P}_{v_g}(\Omega) \tag{A.85}$$

(A.80)-(A.85) are transformed to their temporal counterparts $\mathcal{P}(\omega)$ by using their correlation functions, the linear variable substitution $\xi = \vartheta\tau$, where airspeed ϑ is assumed to be constant, and Fourier transform identity given in [72, pp.192] as

$$\left(\mathcal{F}\{x(\xi)\} = X(\Omega)\right) \iff \left(\mathcal{F}\{x(\vartheta\tau)\} = \frac{1}{\vartheta}X(\Omega)\Big|_{\Omega=\frac{\omega}{\vartheta}}\right) \tag{A.86}$$

The relation between $\mathcal{P}(\Omega)$ and $\mathcal{P}(\omega)$ follows as

$$\begin{aligned}(\xi = \vartheta\tau) \longrightarrow \quad R_{ij}(\xi) &= R_{ij}(\vartheta\tau)\\ \iff \quad \mathcal{F}\{R_{ij}(\xi)\} &= \mathcal{F}\{R_{ij}(\vartheta\tau)\}\\ &= \frac{1}{\vartheta}\mathcal{P}(\Omega)\Big|_{\Omega=\frac{\omega}{\vartheta}}\end{aligned} \tag{A.87}$$

and the corresponding turbulence components as

$$\mathcal{P}_{u_g}(\omega) = \frac{2\sigma_{u_g}^2 l_u}{\vartheta}\frac{1}{1+\left(\frac{l_u}{\vartheta}\omega\right)^2} \tag{A.88}$$

$$\mathcal{P}_{v_g}(\omega) = \frac{\sigma_{v_g}^2 l_v}{\vartheta}\frac{1+3\left(\frac{l_v}{\vartheta}\omega\right)^2}{\left(1+\left(\frac{l_v}{\vartheta}\omega\right)^2\right)^2} \tag{A.89}$$

$$\mathcal{P}_{w_g}(\omega) = \frac{\sigma_{w_g}^2 l_w}{\vartheta}\frac{1+3\left(\frac{l_w}{\vartheta}\omega\right)^2}{\left(1+\left(\frac{l_w}{\vartheta}\omega\right)^2\right)^2} \tag{A.90}$$

$$\mathcal{P}_{p_g}(\omega) = 0.8\frac{\sigma_{w_g}^2\pi}{l_w\vartheta}\left(\frac{\pi l_w}{4b}\right)^{\frac{1}{3}}\frac{1}{1+\left(\frac{4b}{\pi\vartheta}\omega\right)^2} \tag{A.91}$$

$$\mathcal{P}_{q_g}(\omega) = \frac{1}{\vartheta^2}\frac{\omega^2}{1+\left(\frac{4b}{\pi\vartheta}\omega\right)^2}\mathcal{P}_{w_g}(\omega) \tag{A.92}$$

$$\mathcal{P}_{r_g}(\omega) = \frac{1}{\vartheta^2}\frac{\omega^2}{1+\left(\frac{3b}{\pi\vartheta}\omega\right)^2}\mathcal{P}_{v_g}(\omega) \tag{A.93}$$

$\mathcal{P}(\omega)$ is represented by shaping-filter $\mathcal{D}(j\omega)$, driven by Gaussian white noise, by using their relation $\mathcal{P}(\omega) = \mathcal{D}(j\omega)\mathcal{D}(-j\omega)$, and is given as

$$\mathcal{D}_{u_g}(j\omega) = \sigma_{u_g}\sqrt{\frac{2l_u}{\vartheta}}\frac{1}{1+\frac{l_u}{\vartheta}j\omega} \tag{A.94}$$

$$\mathcal{D}_{v_g}(j\omega) = \sigma_{v_g}\sqrt{\frac{l_v}{\vartheta}}\frac{1+\sqrt{3}\frac{l_v}{\vartheta}j\omega}{\left(1+\frac{l_v}{\vartheta}j\omega\right)^2} \tag{A.95}$$

$$\mathcal{D}_{w_g}(j\omega) = \sigma_{w_g}\sqrt{\frac{l_w}{\vartheta}}\frac{1+\sqrt{3}\frac{l_w}{\vartheta}j\omega}{\left(1+\frac{l_w}{\vartheta}j\omega\right)^2} \tag{A.96}$$

$$\mathcal{D}_{p_g}(j\omega) = \sigma_{w_g}\left(\frac{0.8\pi}{l_w\vartheta}\right)^{\frac{1}{2}}\left(\frac{\pi l_w}{4b}\right)^{\frac{1}{6}}\frac{1}{1+\frac{4b}{\pi\vartheta}j\omega} \tag{A.97}$$

$$\mathcal{D}_{q_g}(j\omega) = \frac{1}{\vartheta}\frac{j\omega}{1+\frac{4b}{\pi\vartheta}j\omega}\mathcal{D}_{w_g}(j\omega) \tag{A.98}$$

To conclude, thespatial correlation functions of (A.80)-(A.83) are derived by taking the inverse Fourier transforms of $\mathcal{P}(\omega)$ [64, pp.225]

$$R_{ij}(\tau) = \frac{1}{2\pi}\int_{-\infty}^{\infty}\mathcal{P}_{ij}(\omega)e^{j\omega\tau}d\omega \tag{A.99}$$

$$\iff \quad R_{ij}(\xi) = \frac{1}{2\pi}\int_{-\infty}^{\infty}\mathcal{P}_{ij}(\Omega)e^{j\Omega\xi}d\Omega \tag{A.100}$$

and are obtained as

$$R_{u_g}(\xi) = \sigma_{u_g}^2 e^{-\frac{1}{l_u}|\xi|} \tag{A.101}$$

$$R_{v_g}(\xi) = \sigma_{v_g}^2 e^{-\frac{1}{l_v}|\xi|}\left(1-\frac{1}{2l_v}|\xi|\right) \tag{A.102}$$

$$R_{w_g}(\xi) = \sigma_{w_g}^2 e^{-\frac{1}{l_w}|\xi|}\left(1-\frac{1}{2l_w}|\xi|\right) \tag{A.103}$$

$$R_{p_g}(\xi) = \sigma_{w_g}^2\left(\frac{0.1\pi^2}{bl_w}\right)\left(\frac{\pi}{4}\frac{l_w}{b}\right)^{\frac{1}{3}}e^{-\frac{\pi}{4b}|\xi|} \tag{A.104}$$

A.2 Control theory

A.2.1 Leibniz notation

Leibniz notation (see Stewart [73]) proves useful in stochastic analysis and derivations in Appendices A.2.3 and A.2.6. *Leibniz's* differentiation and integration limit pair is given by

$$\frac{df(x)}{dx} := \lim_{\Delta x \to 0} \frac{f(x+\Delta x) - f(x)}{\Delta x} \tag{A.105}$$

$$\int_a^b f(x)\,dx := \lim_{\substack{n\to\infty \\ \Delta x \to 0}} \sum_{i=0}^{n-1} f(x_i)\,\Delta x, \quad x_0 = a,\ x_n = b \tag{A.106}$$

where $f(x) \in \mathbb{R}^1$ is a function in $x \in \mathbb{R}^1$, *i.e.* $f\colon \mathbb{R}^1 \mapsto \mathbb{R}^1$.

A.2.2 Differentiation and integration rules

The following differentiation and integration rules prove useful in stochastic analysis and derivations in Appendices A.2.3 and A.2.6.

Theorem 6. *For the real functions $A\colon \mathbb{R}^1 \times \mathbb{R}^1 \mapsto \mathbb{R}^{p\times m}$ and $B\colon \mathbb{R}^1 \mapsto \mathbb{R}^{q\times p}$ and real scalars $\{t,\tau\} \subset \mathbb{R}^1$, the following differentiation, and integration rules hold.*

1. *Differentiating an integral:*

$$\frac{d}{dt}\left[\int_{t_0}^{t} A(t,\tau)\,d\tau\right] = \int_{t_0}^{t} \frac{\partial A(t,\tau)}{\partial t} d\tau + A(t,t) \tag{A.107}$$

2. *Interchanging order of integration:*

$$\int_{t_0}^{t_1}\int_{t_0}^{t} B(\tau)\,A(t,\tau)\,d\tau dt = \int_{t_0}^{t_1} B(\tau) \int_{\tau}^{t_1} A(t,\tau)\,dt d\tau \tag{A.108}$$

Proof of Rule 1: It follows from (A.105) *and* (A.106) *that*

$$\begin{aligned}
\{\textit{L.H.S.}\ (\text{A.107})\} &= \lim_{\Delta t\to 0} \frac{\int_{t_0}^{t+\Delta t} A(t+\Delta t,\tau)\,d\tau - \int_{t_0}^{t} A(t,\tau)\,d\tau}{\Delta t} \\
&= \lim_{\substack{n\to\infty \\ \Delta t,\Delta\tau\to 0}} \frac{\sum_{i=0}^{n} A(t+\Delta t,\tau_i)\,\Delta\tau - \sum_{i=0}^{n-1} A(t,\tau_i)\,\Delta\tau}{\Delta t}, \\
&\quad \tau_0 = t_0,\ \tau_{n-1} = t,\ \Delta\tau = \Delta t \\
&= \lim_{\substack{n\to\infty \\ \Delta t,\Delta\tau\to 0}} \left[\sum_{i=0}^{n-1} \frac{A(t+\Delta t,\tau_i) - A(t,\tau_i)}{\Delta t}\Delta\tau \right. \\
&\quad \left. + \frac{A(t+\Delta t,\tau_n)\,\Delta\tau}{\Delta t}\right] \\
&= \lim_{\substack{n\to\infty \\ \Delta t,\Delta\tau\to 0}} \left[\sum_{i=0}^{n-1} \frac{\partial A(t,\tau_i)}{\partial t}\Delta\tau + A(t+\Delta t, t+\Delta t)\right] \\
&= \int_{t_0}^{t} \frac{\partial A(t,\tau_i)}{\partial t} d\tau + A(t,t) \\
&= \{\textit{R.H.S.}\ (\text{A.107})\}
\end{aligned} \tag{A.109}$$

Proof of Rule 2: It follows from (A.105) *and* (A.106) *that*

$$
\begin{aligned}
\{\textit{L.H.S.}\ (\text{A.108})\} &= \lim_{\substack{n\to\infty \\ \Delta\tau\to 0}} \sum_{j=0}^{n-1} \left[\sum_{i=0}^{j} B(\tau_i)\, A(\tau_j, \tau_i)\, \Delta\tau \right] \Delta\tau, \\
&\quad \tau_0 = t_0,\ \tau_j = t,\ \tau_{n-1} = t_1 \\
(C_{ji} \coloneqq B(\tau_i)\, A(\tau_j, \tau_i)) \rightarrow \quad &= \lim_{\substack{n\to\infty \\ \Delta\tau\to 0}} \sum_{j=0}^{n-1} \left[\sum_{i=0}^{j} C_{ji}\Delta\tau \right] \Delta\tau, \\
&= \lim_{\substack{n\to\infty \\ \Delta\tau\to 0}} \left([C_{00}] + [C_{10} + C_{11}] \right. \\
&\quad + \ldots + [C_{k0} + C_{k1} + \ldots + C_{kk}] \\
&\quad + \ldots + \Big[C_{(n-1)0} + C_{(n-1)1} + \ldots + C_{(n-1)k} \\
&\quad \left. + \ldots + C_{(n-1)(n-1)} \Big] \right) \Delta\tau\Delta\tau, \\
&\quad 0 < k < n-1 \\
&= \lim_{\substack{n\to\infty \\ \Delta\tau\to 0}} \Big(\Big[C_{00} + C_{10} + \ldots + C_{k0} + \ldots + C_{(n-1)0} \Big] \\
&\quad + \Big[C_{11} + C_{21} + \ldots + C_{k1} + \ldots + C_{(n-1)1} \Big] \\
&\quad + \ldots + \Big[C_{kk} + C_{(k+1)k} + \ldots + C_{(n-1)k} \Big] \\
&\quad + \ldots + \Big[C_{(n-1)(n-1)} \Big] \Big) \Delta\tau\Delta\tau \\
&= \lim_{\substack{n\to\infty \\ \Delta\tau\to 0}} \sum_{i=0}^{n-1} \left[\sum_{j=i}^{n-1} C_{ji}\Delta\tau \right] \Delta\tau \\
&= \lim_{\substack{n\to\infty \\ \Delta\tau\to 0}} \sum_{i=0}^{n-1} \left[\sum_{j=i}^{n-1} B(\tau_i)\, A(\tau_j, \tau_i)\, \Delta\tau \right] \Delta\tau \\
&= \lim_{\substack{n\to\infty \\ \Delta\tau\to 0}} \sum_{i=0}^{n-1} \left[B(\tau_i) \sum_{j=i}^{n-1} A(\tau_j, \tau_i)\, \Delta\tau \right] \Delta\tau \\
&= \int_{t_0}^{t_1} B(\tau) \int_{\tau}^{t_1} A(t, \tau)\, dt d\tau \\
&= \{\textit{R.H.S.}\ (\text{A.108})\}
\end{aligned}
$$

A.2.3 White noise formulation

Kwakernaak and Sivan [48] gives a simple but rich interpretation and mathematical formulation of stochastic white noise processes. It is said that two samples, $\mathbf{w}(t_1) \in \mathbb{R}^{n_w \times 1}$ and $\mathbf{w}(t_2) \in \mathbb{R}^{n_w \times 1}$, of a white noise process are uncorrelated, even for small

$\triangle t = |t_2 - t_1|$, *i.e.*[11]

$$R_w(t_1, t_2) \coloneqq \mathbb{E}\left\{\mathbf{w}(t_1)\mathbf{w}^T(t_2)\right\} \backsimeq 0 \quad |t_1 - t_2| > \varepsilon \tag{A.110}$$

for arbitrarily small $\varepsilon > 0$. Furthermore, it is said that

$$R_w(t_1, t_2) = \uparrow (t_2 - t_1) V(t_1) \tag{A.111}$$

where $\uparrow (t)$ is the *Dirac delta* impulse function, which contains the property of uncorrelated samples and formulates white noise as a process of infinite power. Thus, white noise is not a real world process, but proves to be mathematically useful for stochastic system analysis and design (see Section 2.5).

To interpret (A.111), Kwakernaak and Sivan [48] defines white noise as the time derivative of a process $\mathbf{v}(t) \in \mathbb{R}^{n_v \times 1}$ with uncorrelated increments,

$$\mathbf{w}(t) = \lim_{\Delta t \to 0} \frac{\mathbf{v}(t + \Delta t) - \mathbf{v}(t)}{\Delta t} \tag{A.112}$$

where $\mathbf{v}(t)$ is defined as follows.

Definition 1. A stochastic process $\mathbf{v}(t) \in \mathbb{R}^{n_v \times 1}$ with uncorrelated increments is defined as follows.

For time instances $t_4 \geq t_3 \geq t_2 \geq t_1 \geq t_0$ and arbitrary $t_a, t_b \geq t_0$:

1. The measure of $\mathbf{v}(t)$ is initialised at t_0 as

$$\mathbf{v}(t_0) = 0 \tag{A.113}$$

2. $\mathbf{v}(t)$ has zero mean increments, *i.e.*

$$\mathbb{E}\{\mathbf{v}(t_2) - \mathbf{v}(t_1)\} = \mathbf{0}, \quad \mathbb{E}\{\mathbf{v}(t_4) - \mathbf{v}(t_3)\} = \mathbf{0} \tag{A.114}$$

3. $\mathbf{v}(t)$ has uncorrelated increments, *i.e.*

$$\mathbb{E}\{[\mathbf{v}(t_2) - \mathbf{v}(t_1)][\mathbf{v}(t_3) - \mathbf{v}(t_2)]\} = 0 \tag{A.115}$$

The autocorrelation of $\mathbf{v}(t)$ can be calculated using (A.113) & (A.115).

$$\begin{aligned}
R_v(t_a, t_b) &= \mathbb{E}\left\{\mathbf{v}(t_a)\mathbf{v}^T(t_b)\right\} \\
&= \mathbb{E}\left\{\lim_{n\to\infty}\sum_{i=1}^{n}[\mathbf{v}(\tau_i) - \mathbf{v}(\tau_{i-1})]\lim_{m\to\infty}\sum_{j=1}^{m}\left[\mathbf{v}^T(\tau_j) - \mathbf{v}^T(\tau_{j-1})\right]\right\}, \\
&\quad \tau_0 = t_0,\ \tau_n = t_a,\ \tau_m = t_b \\
&= \mathbb{E}\left\{\lim_{k\to\infty}\sum_{k=1}^{p}\left[(\mathbf{v}(\tau_k) - \mathbf{v}(\tau_{k-1}))(\mathbf{v}(\tau_k) - \mathbf{v}(\tau_{k-1}))^T\right]\right\}, \\
&\quad \tau_p = \min(t_a, t_b), \quad \tau_0 = t_0 \\
&= \int_{t_0}^{\min(t_a,t_b)} V(\tau)\, d\tau
\end{aligned} \tag{A.116}$$

11. Δt may be the smallest practically realisable sampling period, $w(t_1)$ and $w(t_2)$ would still be uncorrelated. This correlation property could be confirmed for a wide-sense stationary process by correlating an arbitrarily large sample set and normalising with the sample set length.

where $V(t)$ is the change in covariance of $\mathbf{v}(t)$, and is defined as

$$\begin{aligned} V(t) &:= \lim_{\Delta t \to 0} \frac{\mathbb{E}\left\{\mathbf{v}(t+\Delta t)\,\mathbf{v}^T(t+\Delta t) - \mathbf{v}(t)\,\mathbf{v}^T(t)\right\}}{\Delta t} \\ &= \lim_{\Delta t \to 0} \frac{\mathbb{E}\left\{[\mathbf{v}(t+\Delta t) - \mathbf{v}(t)]\,[\mathbf{v}(t+\Delta t) - \mathbf{v}(t)]^T\right\}}{\Delta t} \end{aligned} \tag{A.117}$$

and expressed i.t.o white noise as

$$\begin{aligned} V(t) &:= \lim_{\Delta t \to 0} \frac{\mathbb{E}\left\{[\mathbf{v}(t+\Delta t) - \mathbf{v}(t)]\,[\mathbf{v}(t+\Delta t) - \mathbf{v}(t)]^T\right\}}{\Delta t \Delta t}\Delta t \\ &= \lim_{\Delta t \to 0} \mathbb{E}\left\{\mathbf{w}(t)\,\mathbf{w}^T(t)\right\}\Delta t \end{aligned} \tag{A.118}$$

Furthermore, the autocorrelation $R_v(t_a, t_b)$ may be expressed in terms of the covariance $Q_v(t) := R_v(t,t)$ as

$$\begin{aligned} R_v(t_a, t_b) &= \begin{cases} Q_v(t_a) & t_b \geq t_a \\ Q_v(t_b) & t_a \geq t_b \end{cases} \\ &= u(t_b - t_a)\,Q_v(t_a) + u(t_a - t_b)\,Q_v(t_b) \end{aligned} \tag{A.119}$$

where $u(t) \in \mathbb{R}^1$ is the step function

$$u(t) := \begin{cases} 0 & t < 0 \\ 1 & t \geq 0 \end{cases} \tag{A.120}$$

and

$$Q_v(t) = \int_{t_0}^{t} V(\tau)\,d\tau \tag{A.121}$$

A realisation of $v(t) \in \mathbb{R}^1$, with constant $V(t) = 1$ and a Gaussian distribution, is illustrated in Figure A.4.

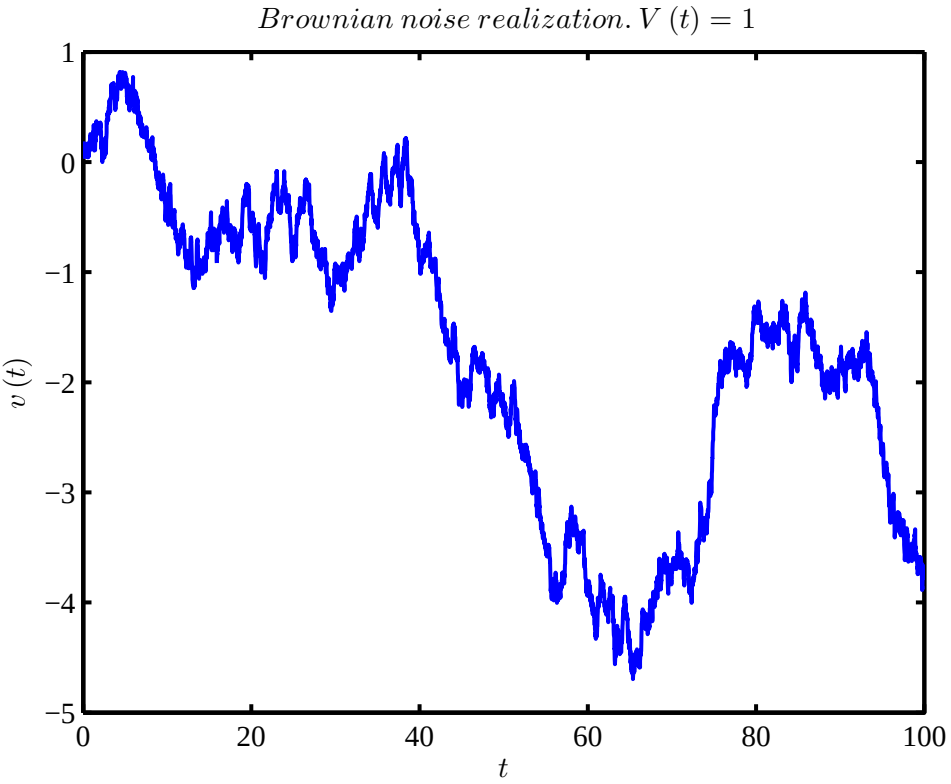

Figure A.4: Brownian motion realisation. Simulated in MATLAB *Simulink*.

To conclude the definition of a white noise process, it is shown that $\frac{dv(t)}{dt}$ has the same statistical properties as $w(t)$.

$$\begin{aligned}
R_{\dot{v}}(t_1,t_2) =& \mathbb{E}\left\{\dot{\mathbf{v}}(t_1)\,\dot{\mathbf{v}}^T(t_2)\right\} \\
=& \mathbb{E}\left\{\lim_{\Delta t\to 0}\left(\frac{\mathbf{v}(t_1+\Delta t)-\mathbf{v}(t_1)}{\Delta t}\right)\left(\frac{\mathbf{v}(t_2+\Delta t)-\mathbf{v}(t_2)}{\Delta t}\right)^T\right\} \\
=& \mathbb{E}\left\{\lim_{\Delta t\to 0}\frac{\mathbf{v}(t_1+\Delta t)\,\mathbf{v}^T(t_2+\Delta t)}{\Delta t\Delta t}\right\} - \mathbb{E}\left\{\lim_{\Delta t\to 0}\frac{\mathbf{v}(t_1+\Delta t)\,\mathbf{v}^T(t_2)}{\Delta t\Delta t}\right\} - \\
& \mathbb{E}\left\{\lim_{\Delta t\to 0}\frac{\mathbf{v}(t_1)\,\mathbf{v}^T(t_2+\Delta t)}{\Delta t\Delta t}\right\} + \mathbb{E}\left\{\lim_{\Delta t\to 0}\frac{\mathbf{v}(t_1)\,\mathbf{v}^T(t_2)}{\Delta t\Delta t}\right\} \\
=& \lim_{\Delta t\to 0}\left(\frac{\mathbb{E}\left\{\mathbf{v}(t_1+\Delta t)\,\mathbf{v}^T(t_2+\Delta t)\right\}}{\Delta t\Delta t} - \frac{\mathbb{E}\left\{\mathbf{v}(t_1+\Delta t)\,\mathbf{v}^T(t_2)\right\}}{\Delta t\Delta t} - \right. \\
& \left. \frac{\mathbb{E}\left\{\mathbf{v}(t_1)\,\mathbf{v}^T(t_2+\Delta t)\right\}}{\Delta t\Delta t} + \frac{\mathbb{E}\left\{\mathbf{v}(t_1)\,\mathbf{v}^T(t_2)\right\}}{\Delta t\Delta t}\right) \\
=& \lim_{\Delta t\to 0}\left(\frac{f(t_1+\Delta t,t_2)-f(t_1,t_2)}{\Delta t}\right), \quad \text{where} \\
& f(t_1,t_2) := \lim_{\Delta t\to 0}\left(\frac{\mathbb{E}\left\{\mathbf{v}(t_1)\,\mathbf{v}^T(t_2+\Delta t)\right\}}{\Delta t} - \frac{\mathbb{E}\left\{\mathbf{v}(t_1)\,\mathbf{v}^T(t_2)\right\}}{\Delta t}\right) \\
=& \frac{\partial}{\partial t_1}\left(\lim_{\Delta t\to 0}\left(\frac{\mathbb{E}\left\{\mathbf{v}(t_1)\,\mathbf{v}^T(t_2+\Delta t)\right\}}{\Delta t} - \frac{\mathbb{E}\left\{\mathbf{v}(t_1)\,\mathbf{v}^T(t_2)\right\}}{\Delta t}\right)\right) \\
=& \frac{\partial^2}{\partial t_1\partial t_2}\mathbb{E}\left\{\mathbf{v}(t_1)\,\mathbf{v}^T(t_2)\right\} \\
=& \frac{\partial^2}{\partial t_1\partial t_2}\left(u(t_2-t_1)\,Q_v(t_1)+u(t_1-t_2)\,Q_v(t_2)\right), \quad t_1,t_2\geq t_0 \\
=& \uparrow(t_2-t_1)\,V(t_1). \qquad \text{(A.122)}
\end{aligned}$$

The final three steps in (A.122) is illustrated in Figure A.5 for $\mathbf{v}(t)$ Wide Sense Stationary (WSS), *i.e.* $V(t)=V_0$. The following integration rules holds for white

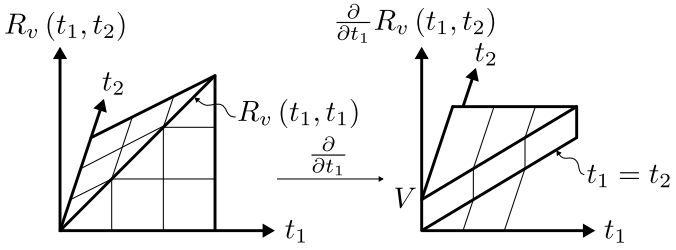

Figure A.5: Illustration of $\frac{\partial^2}{\partial t_1\partial t_2}\mathbb{E}\left\{\mathbf{v}(t_1)\,\mathbf{v}^T(t_2)\right\}$ for $\mathbf{v}(t)$ WSS.

noise as defined above.

Theorem 7. *[48, pp.98] Let* $\mathbf{w}(t)$ *be a vector valued white noise process with intensity* $V(t)$*. Also, let* $A_1(t)$*,* $A_2(t)$ *and* $A(t)$ *be given deterministic*[12] *time-varying matrices with compatible dimensions. Then*

1.
$$\mathbb{E}\left\{\int_{t_1}^{t_2} A(t)\,\mathbf{w}(t)\,dt\right\} = 0; \tag{A.123}$$

2.
$$\mathbb{E}\left\{\left[\int_{t_1}^{t_2} A_1(t)\,\mathbf{w}(t)\,dt\right]^T W \left[\int_{t_3}^{t_4} A_2(t)\,\mathbf{w}(t)\,dt\right]\right\} = \int_I \operatorname{tr}\left[V(t)\,A_1^T(t)\,W A_2(t)\right] dt \tag{A.124}$$

where I *is the intersection of* $[t_1, t_2]$ *and* $[t_3, t_4]$ *and* W *is any given weight matrix;*

3.
$$\mathbb{E}\left\{\left[\int_{t_1}^{t_2} A_1(t)\,\mathbf{w}(t)\,dt\right]\left[\int_{t_3}^{t_4} A_2(t)\,\mathbf{w}(t)\,dt\right]^T\right\} = \int_I A_1(t)\,V(t)\,A_2^T(t)\,dt \tag{A.125}$$

where I *is defined as before.*

Proof of Rule 1:

$$\begin{aligned}
\{\textit{L.H.S.}\ (\text{A.123})\} &= \lim_{\substack{n\to\infty \\ \Delta\tau\to 0}} \mathbb{E}\left\{\sum_{i=0}^{n-1} A(\tau_i)\,\mathbf{w}(\tau_i)\,\Delta\tau\right\}, \quad \tau_0 = t_1,\ \tau_{n-1} = t_2 \\
&= \lim_{\substack{n\to\infty \\ \Delta\tau\to 0}} \sum_{i=0}^{n-1} A(\tau_i)\,\mathbb{E}\{\mathbf{w}(\tau_i)\}\,\Delta\tau \\
(\text{A.110}) \to \quad &= 0 \\
&= \{\textit{R.H.S.}\ (\text{A.123})\}
\end{aligned} \tag{A.126}$$

Proof of Rule 2: the integration time-windows are assumed to be $t_4 \geq t_3$ *and* $t_2 \geq t_1$

12. Determinism is required to resolve the expected value operator without additional assumptions on $A_i(t)$.

to simplify the derivation, which may be enforced with the signs of $A_1(t)$ *and* $A_2(t)$.

{L.H.S. (A.124)*}*

$$
\begin{aligned}
&= tr\mathbb{E}\left\{\left[\int_{t_1}^{t_2} A_1(t)\,\mathbf{w}(t)\,dt\right]^T W\left[\int_{t_3}^{t_4} A_2(t)\,\mathbf{w}(t)\,dt\right]\right\}\\
&= \lim_{\substack{n,m\to\infty\\ \Delta\tau,\Delta\tau'\to 0}} tr\mathbb{E}\left\{\left[\sum_{i=0}^{n-1}\mathbf{w}^T(\tau_i)\,A_1^T(\tau_i)\,\Delta\tau\right] W\left[\sum_{j=k}^{m+k-1} A_2(\tau_j)\,\mathbf{w}(\tau_j)\,\Delta\tau\right]\right\},\\
&\quad \tau_0 = t_1,\ \tau_{n-1} = t_2,\ \tau_k = t_3,\ \tau_{m+k-1} = t_4\\
&= \lim_{\substack{n,m\to\infty\\ \Delta\tau,\Delta\tau'\to 0}} tr\mathbb{E}\left\{\sum_{i=l}^{p+l-1}\mathbf{w}(\tau_i)\,\mathbf{w}^T(\tau_i)\,A_1^T(\tau_i)\,WA_2(\tau_i)\,\Delta\tau\Delta\tau\right.\\
&\quad \left.+\sum_{i=0}^{n-1}\sum_{\substack{j=k\\ j\neq i}}^{m+k-1}\mathbf{w}(\tau_j)\,\mathbf{w}^T(\tau_i)\,A_1^T(\tau_i)\,WA_2(\tau_j)\,\Delta\tau\Delta\tau\right\},\\
&\quad \tau_l = \max(\tau_0,\tau_k),\ \tau_{p+l-1} = \max(\tau_l,\min(\tau_{n-1},\tau_{m+k-1}))\\
&= \lim_{\substack{n,m\to\infty\\ \Delta\tau,\Delta\tau'\to 0}} tr\left[\sum_{i=l}^{p+l-1}\mathbb{E}\left\{\mathbf{w}(\tau_i)\,\mathbf{w}^T(\tau_i)\,\Delta\tau\right\}A_1^T(\tau_i)\,WA_2(\tau_i)\,\Delta\tau\right.\\
&\quad \left.+\sum_{i=0}^{n-1}\sum_{\substack{j=k\\ j\neq i}}^{m+k-1}\mathbb{E}\left\{\mathbf{w}(\tau_j)\,\mathbf{w}^T(\tau_i)\right\}A_1^T(\tau_i)\,WA_2(\tau_j)\,\Delta\tau\Delta\tau\right]\\
\text{(A.110)\&(A.118)}\rightarrow\quad &= tr\int_I V(t)\,A_1^T(t)\,WA_2(t)\,dt\\
&= \{\textit{R.H.S.}\ (\text{A.124})\}
\end{aligned}
$$

Proof of Rule 3: similar to that of Rule 2.

A.2.4 State solution of an LTV system

The Linear Time-Varying (LTV) state-space model is given as

$$
\begin{aligned}
\dot{\mathbf{x}}(t) &= \mathcal{A}(t)\,\mathbf{x}(t) + \mathcal{B}_w(t)\,\mathbf{w}(t)\\
\mathbf{z}(t) &= \mathcal{C}_z(t)\,\mathbf{x}(t)
\end{aligned}
\tag{A.127}
$$

where $\mathbf{w}\in\mathbb{R}^{n_w\times 1}$ is white noise as defined in Appendix A.2.3 and $\mathbf{x}\in\mathbb{R}^{n_x\times 1}$ the state vector. The well-known solution to $\mathbf{x}(t)$ in (A.127) is given by [48, pp.12]

$$
\mathbf{x}(t) = \Phi(t,t_0)\,\mathbf{x}(t_0) + \int_{t_0}^{t}\Phi(t,\tau)\,\mathcal{B}_w(\tau)\,\mathbf{w}(\tau)\,d\tau,
\tag{A.128}
$$

where $\Phi\colon \mathbb{R}^1\times\mathbb{R}^1\mapsto\mathbb{R}^{n_x\times n_x}$ is the *State Transition Matrix* (STM) satisfying

$$
\frac{\partial\Phi(t,\tau)}{\partial t} = \mathcal{A}(t)\,\Phi(t,\tau)
\tag{A.129}
$$

$$\Phi(\tau,\tau) = I \tag{A.130}$$

Upon inspection of (A.128), it is obvious that the solution is based on superposition. The solution is confirmed by taking the time derivative of (A.128)

$$\begin{aligned}
\dot{\mathbf{x}}(t) &= \dot{\Phi}(t,t_0)\,\mathbf{x}(t_0) + \frac{d}{dt}\left[\int_{t_0}^{t} \Phi(t,\tau)\,\mathcal{B}_w(\tau)\,\mathbf{w}(\tau)\,d\tau\right] \\
\text{(A.107)} \rightarrow &= \dot{\Phi}(t,t_0)\,\mathbf{x}(t_0) + \int_{t_0}^{t} \frac{\partial\Phi(t,\tau)}{\partial t}\mathcal{B}_w(\tau)\,\mathbf{w}(\tau)\,d\tau + \Phi(t,t)\,\mathcal{B}_w(t)\,\mathbf{w}(t) \\
&= \mathcal{A}(t)\,\Phi(t,t_0)\,\mathbf{x}(t_0) + \int_{t_0}^{t} \mathcal{A}(t)\,\Phi(t,\tau)\,\mathcal{B}_w(\tau)\,\mathbf{w}(\tau)\,d\tau + \mathcal{B}_w(t)\,\mathbf{w}(t) \\
&= \mathcal{A}(t)\left(\Phi(t,t_0)\,\mathbf{x}(t_0) + \int_{t_0}^{t} \Phi(t,\tau)\,\mathcal{B}_w(\tau)\,\mathbf{w}(\tau)\,d\tau\right) + \mathcal{B}_w(t)\,\mathbf{w}(t) \\
&= \mathcal{A}(t)\,\mathbf{x}(t) + \mathcal{B}_w(t)\,\mathbf{w}(t)
\end{aligned} \tag{A.131}$$

A STM satisfying (A.129) & (A.130) exists for an LTV system if its system matrices are piecewise continuous, with a finite amount of discontinuities in any finite time interval [19, Chapter 11], and may be expressed in terms of $\mathcal{A}(t)$ using the *Peano-Baker* series.

Properties 1. [19] The STM of (A.128) has the following properties:

1. $$\Phi(t_1,t)\,\Phi(t,t_0) = \Phi(t_1,t_0) \tag{A.132}$$
   where t is not restricted to lie between t_0 and t_1
2. $\Phi(t,t_0)$ is non-singular, *i.e.*
   $$\operatorname{rank}(\Phi(t,t_0)) = n_x \tag{A.133}$$
3. $\Phi(t,t_0)$ is unique, *i.e.*
   $$\exists!\Phi\colon \mathbb{R}^1 \times \mathbb{R}^1 \mapsto \mathbb{R}^{n_x \times n_x} \tag{A.134}$$
4. $$\Phi^{-1}(t,t_0) = \Phi(t_0,t) \tag{A.135}$$
5. By definition
   $$\frac{\partial\Phi(t,\tau)}{\partial t} = \mathcal{A}(t)\,\Phi(t,\tau) \tag{A.136}$$
6. $$\frac{\partial\Phi(\tau,t)}{\partial t} = -\Phi(\tau,t)\,\mathcal{A}(t) \tag{A.137}$$
7. By definition
   $$\Phi(\tau,\tau) = I \tag{A.138}$$

A.2.5 Gaussian distributed state of an LTV system

The general Gaussian or normal density function is defined for random variable $X \in \mathbb{R}^1$ with realisation $x \in \mathbb{R}^1$ as [64, pp.313]

$$f_X(x) \coloneqq \frac{1}{\sqrt{2\pi\sigma_X^2}} e^{-\frac{(x-a_X)^2}{2\sigma_X^2}} \tag{A.139}$$

where

$$a_X \coloneqq \mathbb{E}[X], \quad \sigma_X^2 \coloneqq \mathbb{E}\left[(X-a_X)^2\right], \quad \int_{-\infty}^{\infty} f_X(x)\,dx = 1 \tag{A.140}$$

and is given in Figure A.6 for $a_X = 0$ and $\sigma_X^2 = 1$. Peebles [64, pp.102-105]

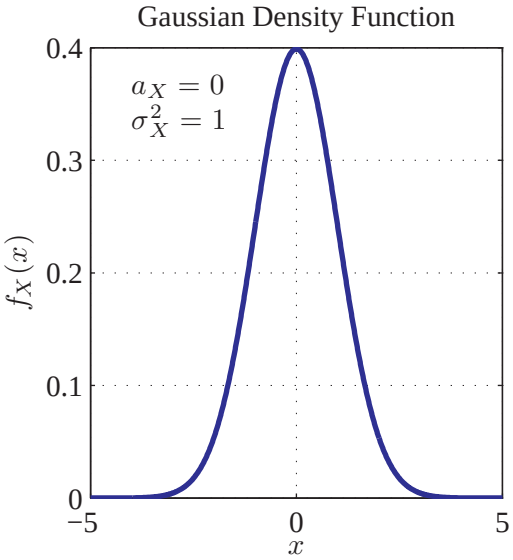

Figure A.6: Gaussian density function $f_X(x)$ for $a_X = 0$ and $\sigma_X^2 = 1$.

shows that the density function of a sum of *independent* random variables $S = X_1 + X_2 + \ldots + X_N$ is the $(N-1)$-fold convolution of the N individual density functions, *i.e.*

$$f_S(s) = f_{X_1}(x_1) \star f_{X_2}(x_2) \star \cdots \star f_{X_N}(x_N) \tag{A.141}$$

It follows that the density function of the sum of two zero mean independent Gaussian random variables$Y_i = Y_{i-1} + X_{i+1}$ is

$$\begin{aligned}
f_{Y_i}(y_i) &= f_{Y_{i-1}}(y_{i-1}) \star f_{X_{i+1}}(x_{i+1}) \\
&= \int_{-\infty}^{\infty} f_{Y_{i-1}}(y_{i-1}) f_{X_{i+1}}(y_i - y_{i-1})\, dy_{i-1} \\
&= \int_{-\infty}^{\infty} \left(\frac{1}{\sqrt{2\pi\sigma_{Y_{i-1}}^2}} e^{-\frac{y_{i-1}^2}{2\sigma_{Y_{i-1}}^2}} \frac{1}{\sqrt{2\pi\sigma_{X_{i+1}}^2}} e^{-\frac{(y_i - y_{i-1})^2}{2\sigma_{X_{i+1}}^2}} \right) dy_{i-1} \\
&= \frac{1}{\sqrt{2\pi\left(\sigma_{Y_{i-1}}^2 + \sigma_{X_{i+1}}^2\right)}} e^{-\frac{y_i^2}{2\left(\sigma_{Y_{i-1}}^2 + \sigma_{X_{i+1}}^2\right)}} \int_{-\infty}^{\infty} \frac{1}{\sqrt{2\pi\sigma_I^2}} e^{-\frac{\left(y_{i-1} - y_i \frac{\sigma_I^2}{\sigma_{X_{i+1}}^2}\right)^2}{2\sigma_I^2}} dy_{i-1}, \\
&\qquad \sigma_I^2 := \frac{\sigma_{Y_{i-1}}^2 \sigma_{X_{i+1}}^2}{\sigma_{Y_{i-1}}^2 + \sigma_{X_{i+1}}^2} \\
&= \frac{1}{\sqrt{2\pi\left(\sigma_{Y_{i-1}}^2 + \sigma_{X_{i+1}}^2\right)}} e^{-\frac{y_i^2}{2\left(\sigma_{Y_{i-1}}^2 + \sigma_{X_{i+1}}^2\right)}}
\end{aligned} \tag{A.142}$$

Thus, the sum of two zero mean independent Gaussian random variables is also a zero mean Gaussian random variable. It follows from the associative property of convolution, and choosing $Y_0 = X_1$, that

$$f_S(s) = \frac{1}{\sqrt{2\pi \sum_{i=1}^{N} \sigma_{X_1}^2}} e^{-\frac{s^2}{2\sum_{i=1}^{N} \sigma_{X_1}^2}} \tag{A.143}$$

Thus, the sum of N zero mean independent Gaussian random variables is also a zero mean Gaussian random variable.

Now, given the LTV system (A.127), where $\mathbf{w}^T(t) = [w_1(t), w_2(t), \ldots, w_{n_w}(t)]$ and $\mathbf{x}(t_0)$ are a zero mean independent Gaussian random process and variable respectively. Then, the system state $\mathbf{x}(t)$ is an infinite sum (continuous integration) of zero mean independent Gaussian random variables, given by (A.128)

$$\begin{aligned}
\mathbf{x}(t) &= \Phi(t, t_0)\mathbf{x}(t_0) + \int_{t_0}^{t} \Phi(t, \tau)\mathcal{B}_w(\tau)\mathbf{w}(\tau)\, d\tau \\
\text{(A.106)} \rightarrow \quad &= \Phi(t, t_0)\mathbf{x}(t_0) + \sum_{i=0}^{n} \Phi(t, \tau_i)\mathcal{B}_w(\tau_i)\mathbf{w}(\tau_i)\Delta\tau
\end{aligned} \tag{A.144}$$

and is thus also a zero mean Gaussian random variable for all time instances, *i.e.* a zero mean Gaussian random process. The case where $\mathbf{x}(t_0)$ is a known initial condition, $\mathbf{x}(t)$ still pertains a Gaussian distribution, but with mean $\mathbb{E}\{\mathbf{x}(t)\} = \Phi(t, t_0)\mathbf{x}(t_0)$, which converges to zero for an exponentially stable DE.

White noise, as defined in Appendix A.2.3, admits to the statistical properties of the input $\mathbf{w}(t)$ defined above, if it has a Gaussian distribution. Non-zero cross-correlation in $\mathbf{w}(t)$ may be included by augmenting $\mathcal{B}_w(t)$.

A.2.6 State covariance of an LTV system

In the stochastic setting, the linear time-varying system matrices of (A.127) are considered to be deterministic. The autocorrelation of the system state $x(t)$ is

derived with *Leibniz* notation as follows.

$$
\begin{aligned}
R_x(t_1,t_2) &= \mathbb{E}\left\{\mathbf{x}(t_1)\,\mathbf{x}^T(t_2)\right\},\\
(\text{A.128}) \rightarrow \quad &= \mathbb{E}\left\{\Phi(t_1,t_0)\,\mathbf{x}(t_0)\,\mathbf{x}^T(t_0)\,\Phi^T(t_2,t_0)\right\}+\\
&\quad \mathbb{E}\left\{\Phi(t_1,t_0)\,\mathbf{x}(t_0)\int_{t_0}^{t_2}\left(\Phi(t_2,t)\,\mathcal{B}_w(t)\,\mathbf{w}(t)\right)^T dt\right\}+\\
&\quad \mathbb{E}\left\{\int_{t_0}^{t_1}\Phi(t_1,t)\,\mathcal{B}_w(t)\,\mathbf{w}(t)\,dt\mathbf{x}^T(t_0)\,\Phi^T(t_2,t_0)\right\}+\\
&\quad \mathbb{E}\left\{\int_{t_0}^{t_1}\Phi(t_1,t)\,\mathcal{B}_w(t)\,\mathbf{w}(t)\,dt\int_{t_0}^{t_2}\left(\Phi(t_2,t)\,\mathcal{B}_w(t)\,\mathbf{w}(t)\right)^T dt\right\}\\
(\text{A.125}) \rightarrow \quad &= \mathbb{E}\left\{\Phi(t_1,t_0)\,\mathbf{x}(t_0)\,\mathbf{x}^T(t_0)\,\Phi^T(t_2,t_0)\right\}\\
&\quad +\mathbb{E}\left\{\Phi(t_1,t_0)\,\mathbf{x}(t_0)\lim_{\substack{m\to\infty\\ \Delta\tau\to 0}}\sum_{i=0}^{m-1}\left[\mathbf{w}^T(\tau_i)\,\mathcal{B}_w^T(\tau_i)\,\Phi^T(t_2,\tau_i)\,\Delta\tau\right]\right\}\\
&\quad +\mathbb{E}\left\{\lim_{\substack{n\to\infty\\ \Delta\tau\to 0}}\sum_{i=0}^{n-1}\left[\Phi(t_1,\tau_i)\,\mathcal{B}_w(\tau_i)\,\mathbf{w}(\tau_i)\,\Delta\tau\right]\mathbf{x}^T(t_0)\,\Phi^T(t_2,t_0)\right\}\\
&\quad +\int_{t_0}^{t_1}\Phi(t_1,t)\,\mathcal{B}_w(t)\,V(t)\,\mathcal{B}_w^T(t)\,\Phi^T(t_2,t)\,dt,\\
&\quad \tau_0=t_0,\ \tau_{n-1}=t_1,\ \tau_{m-1}=t_2\\
&= \Phi(t_1,t_0)\,Q_x(t_0)\,\Phi^T(t_2,t_0)\\
&\quad +\Phi(t_1,t_0)\lim_{\substack{m\to\infty\\ \Delta\tau\to 0}}\sum_{i=0}^{m-1}\left[\mathbb{E}\left\{\mathbf{x}(t_0)\,\mathbf{w}^T(\tau_i)\right\}\mathcal{B}_w^T(\tau_i)\,\Phi^T(t_2,\tau_i)\,\Delta\tau\right]\\
&\quad +\lim_{\substack{n\to\infty\\ \Delta\tau\to 0}}\sum_{i=0}^{n-1}\left[\Phi(t_1,\tau_i)\,\mathcal{B}_w(\tau_i)\,\mathbb{E}\left\{\mathbf{w}(\tau_i)\,\mathbf{x}^T(t_0)\right\}\Delta\tau\right]\Phi^T(t_2,t_0)\\
&\quad +\int_{t_0}^{\min(t_1,t_2)}\Phi(t_1,t)\,\mathcal{B}_w(t)\,V(t)\,\mathcal{B}_w^T(t)\,\Phi^T(t_2,t)\,dt\\
&= \Phi(t_1,t_0)\,Q_x(t_0)\,\Phi^T(t_2,t_0)\\
&\quad +\int_{t_0}^{\min(t_1,t_2)}\Phi(t_1,t)\,\mathcal{B}_w(t)\,V(t)\,\mathcal{B}_w^T(t)\,\Phi^T(t_2,t)\,dt
\end{aligned}
\tag{A.145}
$$

The covariance of the system state $Q_x(t) \coloneqq R_x(t,t)$ follows as

$$
Q_x(t) = \Phi(t,t_0)\,Q_x(t_0)\,\Phi^T(t,t_0)+\int_{t_0}^{t}\Phi(t,\tau)\,\mathcal{B}_w(\tau)\,V(\tau)\,\mathcal{B}_w^T(\tau)\,\Phi^T(t,\tau)\,d\tau \tag{A.146}
$$

Kwakernaak and Sivan [48] derives the covariance differential equation as follows

$$
\begin{aligned}
(\text{A.107}) \rightarrow \; \dot{Q}_x(t) =& \dot{\Phi}(t,t_0)\, Q_x(t_0)\, \Phi^T(t,t_0) + \Phi(t,t_0)\, Q_x(t_0)\, \dot{\Phi}^T(t,t_0) \\
&+ \int_{t_0}^{t} \frac{\partial}{\partial t}\left[\Phi(t,\tau)\, \mathcal{B}_w(\tau)\, V(\tau)\, \mathcal{B}_w^T(\tau)\, \Phi^T(t,\tau)\right] d\tau \\
&+ \Phi(t,t)\, \mathcal{B}_w(t)\, V(t)\, \mathcal{B}_w^T(t)\, \Phi^T(t,t) \\
=& \mathcal{A}(t)\, \Phi(t,t_0)\, Q_x(t_0)\, \Phi^T(t,t_0) + \Phi(t,t_0)\, Q_x(t_0)\, \Phi^T(t,t_0)\, \mathcal{A}^T(t) \\
&+ \mathcal{A}(t) \int_{t_0}^{t} \Phi(t,\tau)\, \mathcal{B}_w(\tau)\, V(\tau)\, \mathcal{B}_w^T(\tau)\, \Phi^T(t,\tau)\, d\tau \\
&+ \int_{t_0}^{t} \Phi(t,\tau)\, \mathcal{B}_w(\tau)\, V(\tau)\, \mathcal{B}_w^T(\tau)\, \Phi^T(t,\tau)\, d\tau \mathcal{A}^T(t) \\
&+ \mathcal{B}_w(t)\, V(t)\, \mathcal{B}_w^T(t) \\
=& \mathcal{A}(t)\, Q_x(t) + Q_x(t)\, \mathcal{A}^T(t) + \mathcal{B}_w(t)\, V(t)\, \mathcal{B}_w^T(t), \qquad (\text{A.147})
\end{aligned}
$$

and for convenience the Cholesky factors of $V(t) = F^T(t)\, F(t)$ are absorbed in terms $\mathcal{B}_w(t)$ and $\mathcal{B}_w^T(t)$,[13] resulting in

$$
\dot{Q}_x(t) = \mathcal{A}(t)\, Q_x(t) + Q_x(t)\, \mathcal{A}^T(t) + \mathcal{B}_w(t)\, \mathcal{B}_w^T(t) \qquad (\text{A.148})
$$

This result is referred to as the *Controllability Gramian Differential Equation* (CGDE).

A.2.7 Average output variance of an LTV system

In the stochastic setting, the linear time-varying system matrices of (A.127) are considered to be deterministic. The average output variance of the system output $z(t)$ of (A.127) is defined as

$$
\lim_{t_1 \to \infty} \frac{1}{t_1 - t_0} \mathbb{E}\left\{ \int_{t_0}^{t_1} \mathbf{z}^T(t)\, \mathbf{z}(t)\, dt \right\} \qquad (\text{A.149})
$$

13. $\mathcal{B}_w(t)$ is scaled such that $V(t) = I$

and derived in a similar manner to (A.145)-(A.148) with the use of the *trace* operator.

$$
\begin{aligned}
\mathbb{E}\left\{\int_{t_0}^{t_1}\mathbf{z}^T(t)\,\mathbf{z}(t)\,dt\right\} =& \mathbb{E}\left\{\int_{t_0}^{t_1}\operatorname{tr}\left(\mathbf{x}^T(t)\,\mathcal{C}_z(t)^T\,\mathcal{C}_z(t)\,\mathbf{x}(t)\right)dt\right\}\\
\text{(A.128)}\rightarrow \quad =& \int_{t_0}^{t_1}\operatorname{tr}\left(\mathbb{E}\left\{\mathbf{x}^T(t_0)\,\Phi^T(t,t_0)\,\mathcal{C}_z(t)^T\,\mathcal{C}_z(t)\,\Phi(t,t_0)\,\mathbf{x}(t_0)\,dt\right.\right.\\
&+2\mathbf{x}^T(t_0)\,\Phi^T(t,t_0)\,\mathcal{C}_z(t)^T\,\mathcal{C}_z(t)\int_{t_0}^{t}\Phi(t,\tau)\,\mathcal{B}_w(\tau)\,\mathbf{w}(\tau)\,d\tau\\
&+\int_{t_0}^{t}\mathbf{w}^T(\tau)\,\mathcal{B}_w^T(\tau)\,\Phi^T(t,\tau)\,d\tau\mathcal{C}_z(t)^T\\
&\left.\left.\cdot\mathcal{C}_z(t)\int_{t_0}^{t}\Phi(t,\tau)\,\mathcal{B}_w(\tau)\,\mathbf{w}(\tau)\,d\tau\right\}\right)dt\\
\text{(A.124)}\rightarrow \quad =& \int_{t_0}^{t_1}\operatorname{tr}\left(\mathbb{E}\left\{\mathbf{x}(t_0)\,\mathbf{x}^T(t_0)\right\}\Phi^T(t,t_0)\,\mathcal{C}_z(t)^T\,\mathcal{C}_z(t)\,\Phi(t,t_0)\right.\\
&+2\Phi^T(t,t_0)\,\mathcal{C}_z(t)^T\,\mathcal{C}_z(t)\int_{t_0}^{t}\Phi(t,\tau)\,\mathcal{B}_w(\tau)\,\mathbb{E}\left\{\mathbf{w}(\tau)\,\mathbf{x}^T(t_0)\right\}d\tau\\
&\left.+\int_{t_0}^{t}V(\tau)\,\mathcal{B}_w^T(\tau)\,\Phi^T(t,\tau)\,\mathcal{C}_z(t)^T\,\mathcal{C}_z(t)\,\Phi(t,\tau)\,\mathcal{B}_w(\tau)\,d\tau\right)dt\\
=& \operatorname{tr}\left(Q_x(t_0)\int_{t_0}^{t_1}\Phi^T(t,t_0)\,\mathcal{C}_z(t)^T\,\mathcal{C}_z(t)\,\Phi(t,t_0)\,dt\right.\\
&\left.+\int_{t_0}^{t_1}\int_{t_0}^{t}\mathcal{B}_w(\tau)\,V(\tau)\,\mathcal{B}_w^T(\tau)\,\Phi^T(t,\tau)\,\mathcal{C}_z(t)^T\,\mathcal{C}_z(t)\,\Phi(t,\tau)\,d\tau dt\right)\\
\text{(A.108)}\rightarrow \quad =& \operatorname{tr}\left(Q_x(t_0)\int_{t_0}^{t_1}\Phi^T(t,t_0)\,\mathcal{C}_z(t)^T\,\mathcal{C}_z(t)\,\Phi(t,t_0)\,dt\right)\\
&+\operatorname{tr}\left(\int_{t_0}^{t_1}\mathcal{B}_w(\tau)\,V(\tau)\,\mathcal{B}_w^T(\tau)\right.\\
&\left.\cdot\left(\int_{\tau}^{t_1}\Phi^T(t,\tau)\,\mathcal{C}_z(t)^T\,\mathcal{C}_z(t)\,\Phi(t,\tau)\,dt\right)d\tau\right)
\end{aligned}
\tag{A.150}
$$

Using the substitution

$$
P(t_1,t) \coloneqq \int_{t}^{t_1}\Phi^T(\tau,t)\,\mathcal{C}_z(\tau)^T\,\mathcal{C}_z(\tau)\,\Phi(\tau,t)\,d\tau \tag{A.151}
$$

and absorbing the Cholesky factors of $V(t) = F^T(t) F(t)$ in terms $\mathcal{B}_w(t)$ and $\mathcal{B}_w^T(t)$, as is done from (A.147) to (A.148), (A.150) simplifies to

$$\lim_{t_1\to\infty} \frac{1}{t_1 - t_0} \mathrm{tr} \left(Q_x(t_0) P(t_1, t_0) + \int_{t_0}^{t_1} \mathcal{B}_w^T(\tau) P(t_1, \tau) \mathcal{B}_w(\tau) d\tau \right) \tag{A.152}$$

where (A.151) is known as the *observability Gramian*. Given that $\mathrm{tr}(Q_x(t_0) \cdot P(t_1, t_0)) > 0$ and $\mathrm{tr}\left(\mathcal{B}_w^T(t) P(t_1, t) \mathcal{B}_w(t)\right) > 0$ and that $Q_x(t_0)$ and $\mathcal{B}_w(\tau)$ is finite, the second term in (A.152) is of infinite order larger than the first, and (A.152) may be simplified as

$$\lim_{t_1\to\infty} \frac{1}{t_1 - t_0} \mathbb{E} \left\{ \int_{t_0}^{t_1} \mathbf{z}^T(t) \mathbf{z}(t) dt \right\} = \lim_{t_1\to\infty} \frac{1}{t_1 - t_0} \mathrm{tr} \left(\int_{t_0}^{t_1} \mathcal{B}_w^T(\tau) P(t_1, \tau) \mathcal{B}_w(\tau) d\tau \right) \tag{A.153}$$

Differentiating (A.151) with respect to time, we obtain the *Observability Gramian Differential Equation* (OGDE) as

$$\begin{aligned}
-\frac{\partial P(t_1, t)}{\partial t} =& \frac{\partial}{\partial t} \int_{t_1}^{t} \Phi^T(\tau, t) \mathcal{C}_z^T(\tau) \mathcal{C}_z(\tau) \Phi(\tau, t) d\tau \\
\text{(A.107)} \rightarrow \quad =& \int_{t_1}^{t} \frac{\partial}{\partial t} \left[\Phi^T(\tau, t) \mathcal{C}_z^T(\tau) \mathcal{C}_z(\tau) \Phi(\tau, t) \right] d\tau \\
& + \Phi^T(t, t) \mathcal{C}_z(t)^T \mathcal{C}_z(t) \Phi(t, t) \\
=& \int_{t_1}^{t} \frac{\partial \Phi^T(\tau, t)}{\partial t} \mathcal{C}_z^T(\tau) \mathcal{C}_z(\tau) \Phi(\tau, t) d\tau \\
& + \int_{t_1}^{t} \Phi^T(\tau, t) \mathcal{C}_z^T(\tau) \mathcal{C}_z(\tau) \frac{\partial \Phi(\tau, t)}{\partial t} d\tau \\
& + \mathcal{C}_z(t)^T \mathcal{C}_z(t) \\
=& -\mathcal{A}^T(t) \int_{t_1}^{t} \Phi^T(\tau, t) \mathcal{C}_z^T(\tau) \mathcal{C}_z(\tau) \Phi(\tau, t) d\tau \\
& - \int_{t_1}^{t} \Phi^T(\tau, t) \mathcal{C}_z^T(\tau) \mathcal{C}_z(\tau) \Phi(\tau, t) d\tau \mathcal{A}(t) \\
& + \mathcal{C}_z^T(t) \mathcal{C}_z(t) \\
=& \mathcal{A}^T(t) P(t_1, t) + P(t_1, t) \mathcal{A}(t) + \mathcal{C}_z^T(t) \mathcal{C}_z(t)
\end{aligned} \tag{A.154}$$

This concludes the average output variance of an LTV system.

A.2.8 The $\mathcal{H}_2$-norm

Definition 2. [70, pp.163] Let T_{zw} denote a stable transfer function from $\mathbf{w} \in \mathbb{R}^{n_w \times 1}$ to $\mathbf{z} \in \mathbb{R}^{n_z \times 1}$. The $\mathcal{H}_2$-norm of T_{zw} is defined as

$$\|T_{zw}\|_{\mathcal{H}_2}^2 := \operatorname{tr} \int_{-\infty}^{\infty} T_{zw}^T(-j\omega)\, T_{zw}(j\omega)\, \frac{d\omega}{2\pi} \tag{A.155}$$

(A.155) may be directly calculated via *Cauchy's residual theorem* [73]. The use of the $\mathcal{H}_2$-norm in systems and control theory dates back to the 1960's, where Horowitz [40] relates the system transfer function from a white noise input to the spectrum of the output noise, and the spectrum area (infinite integral) to output noise power. It follows that the time-domain interpretation of the $\mathcal{H}_2$-norm for stable LTI systems subject to unit intensity white noise (see Appendix A.2.3 for white noise definition) input is

$$\|T_{zw}\|_{\mathcal{H}_2}^2 = \lim_{T\to\infty} \frac{1}{2T} \int_{T}^{T} \mathbb{E}\left\{\mathbf{z}^T(t)\,\mathbf{z}(t)\right\} dt = \lim_{t\to\infty} \mathbb{E}\left\{\mathbf{z}^T(t)\,\mathbf{z}(t)\right\} \tag{A.156}$$

Based on the work done by Kalman, also in the 1960's, the norm may be calculated very efficiently via Riccati equation solvers, using the system state-space realisation

$$T_{zw}: \begin{cases} \dot{\mathbf{x}}(t) = \mathcal{A}\mathbf{x}(t) + \mathcal{B}_w\mathbf{w}(t) \\ \mathbf{z}(t) = \mathcal{C}_z\mathbf{x}(t) + \mathcal{D}_{zw}\mathbf{w}(t) \end{cases} \tag{A.157}$$

For the system to have a finite $\mathcal{H}_2$-norm, it is requires that T_{zw} be strictly proper, *i.e.* $\mathcal{D}_{zw} = 0$. Then

$$\|T_{zw}\|_{\mathcal{H}_2}^2 = \operatorname{tr}\left(\mathcal{B}_w^T P \mathcal{B}_w\right), \quad \mathcal{A}^T P + P\mathcal{A} + \mathcal{C}_z^T\mathcal{C}_z = 0 \tag{A.158}$$

$$\|T_{zw}\|_{\mathcal{H}_2}^2 = \operatorname{tr}\left(\mathcal{C}_z Q \mathcal{C}_z^T\right), \quad \mathcal{A}Q + Q\mathcal{A}^T + \mathcal{B}_w\mathcal{B}_w^T = 0 \tag{A.159}$$

which have LMI equivalents, obtainable via Theorem 11 in Appendix A.2.14, given by

$$\|T_{zw}\|_{\mathcal{H}_2}^2 < \operatorname{tr}\left(\mathcal{B}_w^T P \mathcal{B}_w\right), \quad \mathcal{A}^T P + P\mathcal{A} + \mathcal{C}_z^T\mathcal{C}_z < 0, \quad P > 0 \tag{A.160}$$

$$\|T_{zw}\|_{\mathcal{H}_2}^2 < \operatorname{tr}\left(\mathcal{C}_z Q \mathcal{C}_z^T\right), \quad \mathcal{A}Q + Q\mathcal{A}^T + \mathcal{B}_w\mathcal{B}_w^T < 0, \quad Q > 0 \tag{A.161}$$

which may also be calculated very efficiently via SDP solvers.

Motivations for the use of the $\mathcal{H}_2$-norm as a system performance measure is [30, pp.230-231]:

1. $\|T_{zw}\|_{\mathcal{H}_2}^2$ is the steady-state power output of the system response to unit intensity white noise; the idealisation of system disturbance input as white noise is a common modelling tool (see Section 2.5 for an example); [68] output power has many useful interpretations relating to system performance, such as product quality, temperature, power efficiency and amplitude risk-bounds

when the variable has a Gaussian distribution; Q in (A.159) and (A.161) is the state-covariance matrix, describing the power distribution through the whole system; the power of various outputs may be calculated simply by selecting new $\mathcal{C}_z$ and recalculating $\text{tr}\left(\mathcal{C}_z Q \mathcal{C}_z^T\right)$ in (A.159) or (A.161), avoiding the re-calculation of the Riccati equation or the SDP as is required in (A.158) and (A.160).

2. For scalar inputs, $\|T_{zw}\|_{\mathcal{H}_2}^2$ is the energy output of the system impulse response; this quantity can be used to measure the transient response of an output in response to known initial conditions (which may be generated by an impulse); this quantity may be calculated for different initial conditions simply by selecting new $\mathcal{B}_w$ and recalculating $\text{tr}\left(\mathcal{B}_w^T P \mathcal{B}_w\right)$ in (A.158) or (A.160), avoiding recalculating the Riccati equation or SDP as is required in (A.159) and (A.161).

The amplitude of a *zero mean* Gaussian distributed stochastic process $\mathbf{z}(t)$ is closely related to its expected instantaneous power, and the relation is given by [64, pp.314]

$$\mathbb{P}\left\{\|\mathbf{z}(t)\|_2 \cap [0, 3\sigma_z(t)]\right\} = 0.9974 \tag{A.162}$$

where $\|\mathbf{z}(t)\|_2$ is the *Euclidean*-norm of $\mathbf{z}(t)$ and

$$\sigma_z^2(t) \coloneqq \mathbb{E}\left\{\mathbf{z}^T(t)\,\mathbf{z}(t)\right\} \tag{A.163}$$

its variance [14] (see Appendix A.2.5). The 3σ-bound is a useful indicator of amplitude levels in a stochastic system, when system variables have zero mean Gaussian distributions, which is the case when system *inputs* have zero-mean Gaussian distributions and the system is linear, *i.e.* the system admits super-position (see Appendix A.2.5). It follows that

$$\mathbb{P}\left\{\lim_{t\to\infty} \|\mathbf{z}(t)\|_2 \cap \left[0, 3\|T_{zw}\|_{\mathcal{H}_2}\right]\right\} = 0.9974 \tag{A.164}$$

i.e. statistically $\mathbf{z}(t)$ will satisfy $0 \leq \|\mathbf{z}(t)\|_2 \leq 3\|T_{zw}\|_{\mathcal{H}_2}$ 99.74% of the time, when the system has reached steady power levels, where $\lim_{t\to\infty}\|\mathbf{z}(t)\|_2$ is the steady-state Euclidean-norm of $\mathbf{z}(t)$. Now, given Q in (A.159) or (A.161), one may calculate various system amplitude levels with $3\sqrt{\text{tr}\left(\mathcal{C}_z Q \mathcal{C}_z^T\right)}$. For the case where the system inputs have arbitrary distributions and the system is non-linear, the reader is referred to the *central limit theorem* [64, 18].

We conclude the section by addressing the $\mathcal{H}_2$ performance over model *uncertainty* (LTI, LTV, non-linear), referred to as robust $\mathcal{H}_2$ performance in the literature [30, Ch.7]. Doyle [26] showed that the $\mathcal{H}_2$-optimal output-feedback regulator (LQG) possesses no stability margins, whereby arbitrarily small model uncertainty may cause the closed-loop system to become unstable, motivating the use of the *robust* $\mathcal{H}_2$ performance index, developed in Section 3.7. Much research has been done on the subject [30**?** , 75, 59, 52], and it is one of the main focuses of this thesis.

[30, Ch.7] provides a survey of different approaches to robust $\mathcal{H}_2$ performance.

14. *e.g.* the 3σ-bound for a zero mean Gaussian random variable with $\sigma_X^2 = 1$, given in Figure A.6, is $x = \pm 3$, where the area under the graph between $x = \pm 3$ is 99.74% of the total area.

A.2.9 Modal analysis of LTI model

Eigenvalues and eigenvectors are well known measures used to characterise the transient behaviour of LTI systems [70, 33].

Definition 3. System *transient behaviour* refers to the mechanics, of an *undisturbed system*, involved in the transition from an arbitrary state to its equilibrium.

The state-space representation of an LTI system is given by (A.157), and for the undisturbed case is given as

$$\dot{\mathbf{x}}(t) = \mathcal{A}\mathbf{x}(t) \tag{A.165}$$

[33, pp.161-203] The eigenvalue $\lambda \in \mathbb{C}^1$ and eigenvector $\mathbf{v} \in \mathbb{C}^{n_x \times 1}$ of state-matrix $\mathcal{A} \in \mathbb{R}^{n_x \times n_x}$ is defined as

$$\mathcal{A}\mathbf{v} = \lambda\mathbf{v}, \quad \mathbf{v} \neq \mathbf{0} \tag{A.166}$$

and is calculated as

$$\begin{aligned} (\text{A.166}) \iff & \quad ((\mathcal{A} - \lambda I)\,\mathbf{v} = \mathbf{0}, \quad \mathbf{v} \neq \mathbf{0}) \\ \implies & \quad \det(\mathcal{A} - \lambda I) = 0 \end{aligned} \tag{A.167}$$

The determinant results in an n_x-order polynomial in λ, which is factorised to give n_x solutions to λ, grouped on the diagonal of $\Lambda \coloneqq \text{diag}(\lambda_1, \lambda_2, ..., \lambda_{n_x})$. Each solution λ_i corresponds to an eigenvector $\mathbf{v}_i \neq \mathbf{0}$, which may be calculated via *Gaussian elimination*, and is grouped as $V \coloneqq [\mathbf{v}_1, \mathbf{v}_2, ..., \mathbf{v}_{n_x}]$.

Eigenvalues and eigenvectors have the following properties [70, pp.535-536]:

1. *uniqueness*: Eigenvalues are unique, whereas eigenvectors are invariant under complex scaling, *i.e.* $(\mathcal{A}\mathbf{v}_i = \lambda_i\mathbf{v}_i) \iff (\mathcal{A}(\gamma\mathbf{v}_i) = \lambda_i(\gamma\mathbf{v}_i),\ \gamma \in \mathbb{C}^1)$.
2. *appear in complex conjugate pairs*: If $\mathcal{A}$ is real, then eigenvalues and eigenvectors appear in complex conjugate pairs, *i.e.* $(\mathcal{A}\mathbf{v}_i = \lambda_i\mathbf{v}_i) \iff (\mathcal{A}\mathbf{v}_i^* = \lambda_i^*\mathbf{v}_i^*)$.
3. *realness*: If both $\mathcal{A}$ and λ_i are real, then $\mathbf{v}_i$ may be scaled to be real, *i.e.* $(\mathcal{A}\mathbf{v}_i = \lambda_i\mathbf{v}_i) \implies (\mathcal{A}\Re(\mathbf{v}_i) = \lambda_i\Re(\mathbf{v}_i))$
4. *relation to determinant*: The product of the eigenvalues of $\mathcal{A}$ is equal to the determinant of $\mathcal{A}$, *i.e.* $\det(\mathcal{A}) = \prod_i \lambda_i$
5. *relation to inverse*: The inverse $\mathcal{A}^{-1}$ exists if and only if all of the eigenvalues of $\mathcal{A}$ are non-zero, in which case $\mathcal{A}^{-1}$ has eigenvalues $1/\lambda_1, 1/\lambda_2, \ldots, 1/\lambda_{n_x}$.
6. *preservation under transposition*: $\mathcal{A}$ and $\mathcal{A}^T$ have the same eigenvalues, but may have different eigenvectors.
7. *preservation under similarity transformation*: $D^{-1}\mathcal{A}D$ and $\mathcal{A}$ have the same eigenvalues, but may have different eigenvectors, for any invertable matrix $D \in \mathbb{C}^{n_x \times n_x}$.
8. *diagonalisation*: If the eigenvectors of $\mathcal{A}$ are linearly independent, then $\mathcal{A}$ is diagonaliseable with the similarity transformation $\Lambda = V^{-1}\mathcal{A}V$.

9. *Gershgorin's theorem*: The eigenvalues of $\mathcal{A}$ lie in the union of n_x circles in the complex plane, each with centre a_{ii} and radius $r_i = \sum_{i \neq j} |a_{ij}|$, where

$$\mathcal{A} = \begin{bmatrix} a_{11} & a_{12} & \cdots & a_{1n} \\ a_{21} & a_{22} & \cdots & a_{2n} \\ \vdots & \vdots & \ddots & \vdots \\ a_{n1} & a_{n2} & \cdots & a_{nn} \end{bmatrix} \tag{A.168}$$

They also lie in the union of n_x circles, each with centre a_{ii} and radius $\acute{r}_i = \sum_{i \neq j} |a_{ji}|$.

(A.165) submit to first- or second-order solutions when initialised with $\frac{1}{2}(\mathbf{v}_i + \mathbf{v}_i^*)$, given as

$$\begin{aligned} \mathbf{x}(t) &= \frac{1}{2}\mathbf{v}_i e^{\lambda_i (t-t_0)} + \frac{1}{2}\mathbf{v}_i^* e^{\lambda_i^* (t-t_0)}, \quad \forall t \geq t_0 \\ &= \Re(\mathbf{v}_i)\, e^{\Re(\lambda_i)(t-t_0)} \cos\left(\Im(\lambda_i)(t-t_0)\right), \quad \forall t \geq t_0 \end{aligned} \tag{A.169}$$

These solutions form the most basic transient behaviour of the system, and are completely characterised by their exponential growth-rate $\Re(\lambda_i)$, damped frequency $\Im(\lambda_i)$ and direction $\Re(\mathbf{v}_i)$. Each trajectory converges if and only if the its exponential growth-rate $\Re(\lambda_i)$ is negative, and we define the exponential decay-rate as

$$\alpha_i \coloneqq -\Re(\lambda_i) \tag{A.170}$$

[16] presents necessary and sufficient LMI conditions for eigenvalues to reside within specified convex domains. The following theorem provides LMI conditions for the minimum exponential decay-rate, a disk eigenvalue region and a cone eigenvalue region. [15]

Theorem 8. *[16] (regional eigenvalue constraints) Given the matrix $\mathcal{A} \in \mathbb{R}^{n \times n}$ with eigenvalues $\lambda_1, \lambda_2, \ldots, \lambda_n$*

$$\begin{aligned} &\left(\{\lambda_1, \lambda_2, \ldots, \lambda_n\} \subset \left\{z \in \mathbb{C}^1 : z < -\mathfrak{a},\ \mathfrak{a} \in \mathbb{R}^1\right\}\right) \\ \iff &\left(\exists X_\mathfrak{a} > 0 : \mathcal{A}X_\mathfrak{a} + X_\mathfrak{a}\mathcal{A}^T + 2\mathfrak{a}X_\mathfrak{a} < 0,\ \frac{d}{dt}X_\mathfrak{a} = 0\right) \end{aligned} \tag{A.171}$$

$$\begin{aligned} &\left(\{\lambda_1, \lambda_2, \ldots, \lambda_n\} \subset \left\{z \in \mathbb{C}^1 : (z+\mathfrak{q})^H (z+\mathfrak{q}) < \mathfrak{r}^2,\ \{\mathfrak{q}, \mathfrak{r}\} \subset \mathbb{R}^1\right\}\right) \\ \iff &\left(\exists X_\ominus > 0 : \begin{bmatrix} -rX_\ominus & qX_\ominus + \mathcal{A}X_\ominus \\ qX_\ominus + X_\ominus\mathcal{A}^T & -rX_\ominus \end{bmatrix} < 0,\ \frac{d}{dt}X_\ominus = 0\right) \end{aligned} \tag{A.172}$$

15. The minimum exponential decay-rate eigenvalue region, disk eigenvalue region and cone eigenvalue region where the only regions whose corresponding LMI conditions remain linear when augmented for controller synthesis.

and

$$\left(\{\lambda_1, \lambda_2, \ldots, \lambda_n\} \subset \left\{z \in \mathbb{C}^1 : \tan(\mathfrak{c}) < \frac{|\Im(z)|}{-\Re(z)}\right\}\right) \iff$$
$$\left(\begin{array}{c} \exists X_{\mathfrak{c}} > 0 : \\ \left[\begin{array}{cc} \sin(\mathfrak{c})\left(\mathcal{A}X_{\mathfrak{c}} + X_{\mathfrak{c}}\mathcal{A}^T\right) & \cos(\mathfrak{c})\left(\mathcal{A}X_{\mathfrak{c}} - X_{\mathfrak{c}}\mathcal{A}^T\right) \\ \cos(\mathfrak{c})\left(-\mathcal{A}X_{\mathfrak{c}} + X_{\mathfrak{c}}\mathcal{A}^T\right) & \sin(\mathfrak{c})\left(\mathcal{A}X_{\mathfrak{c}} + X_{\mathfrak{c}}\mathcal{A}^T\right) \end{array}\right] < 0, \\ \frac{d}{dt}X_{\mathfrak{c}} = 0 \end{array}\right)$$

Proof: See [16].

Eigenvalue regions are the measure of the variety in LTI system transient behaviour, and is extended to the NLTV case in Section 3.7.

A.2.10 Description of uncertain time-varying non-linearity

Perhaps the simplest way to model a non-linear gain is with an upper- and lower-bound, called sector-bounds. The sector-bounds then serve to describe the class of all Non-Linear Time-Varying (NLTV), possibly uncertain, gains which fall within these bounds. In exchange for the simplicity of the sector-bound description, is conservatism, *i.e.* the sector-bounds describes a larger class of systems.

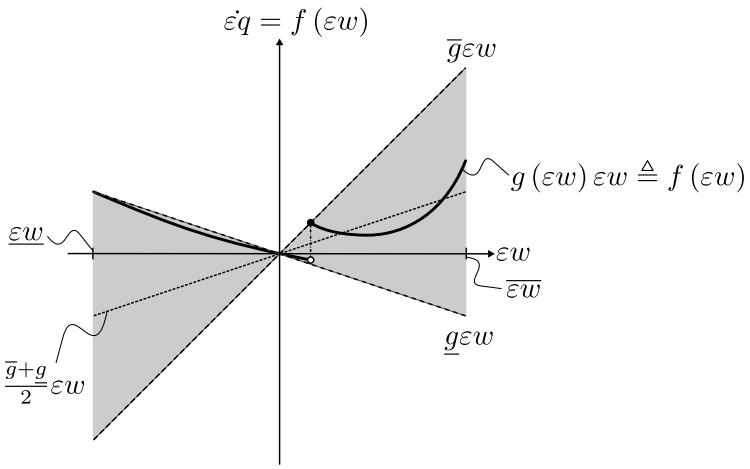

Figure A.7: Aircraft pitch-up non-linearity with sector-bounds.

The sector-bounds for aircraft pitch-up $\varepsilon\dot{q} = f(\varepsilon w)$ about trim (w_r, q_r) is illustrated in Figure A.7, and given by

$$\underline{g} < g(\varepsilon w) < \overline{g}\ \forall \varepsilon w \in [\underline{\varepsilon w}, \overline{\varepsilon w}],\ g(\varepsilon w)\,\varepsilon w := f(\varepsilon w) \tag{A.173}$$

where $\varepsilon q = q - q_r$ is the aircraft pitch perturbation from its reference q_r (see Appendix A.1.1 for notation), $\varepsilon w = w - w_r$ is the aircraft normal velocity perturbation from its reference w_r, $\underline{g}$ is the gain lower-bound and $\overline{g}$ is the gain upper-bound. It

follows that for any *finite*[16] scalar gain $g(\boldsymbol{\rho}) \in \left(\underline{g}, \overline{g}\right)$ for every $\boldsymbol{\rho} \in \mathfrak{D}_\rho$, there exists a scalar variation $\delta \in \boldsymbol{\Delta}$, such that

$$g(\boldsymbol{\rho}) = \left(\frac{\overline{g} - \underline{g}}{2}\right)\delta + \left(\frac{\overline{g} + \underline{g}}{2}\right) \tag{A.174}$$

where δ is commonly referred to as *parameter uncertainty* in the literature [**?** 75, 30, 70].

A finite *matrix* gain $G(\boldsymbol{\rho})$ may be represented in a similar manner

$$G(\Delta) := J + E\Delta H,\ \Delta \in \boldsymbol{\Delta} \tag{A.175}$$

where E, F and H assign appropriate offset and variation to the elements in $G(\boldsymbol{\rho})$, and, for illustration purposes, the uncertainty feedthrough D_{qp} is assumed to be zero. $D_{qp} \neq 0$ is typically used to express multiplication in the uncertainty elements, and also may results from state-space augmentation, *e.g.* loop-closure. Simultaneous variation of gain elements can be represented by $F\Delta H$ to reduce the size of the variation space as follows.

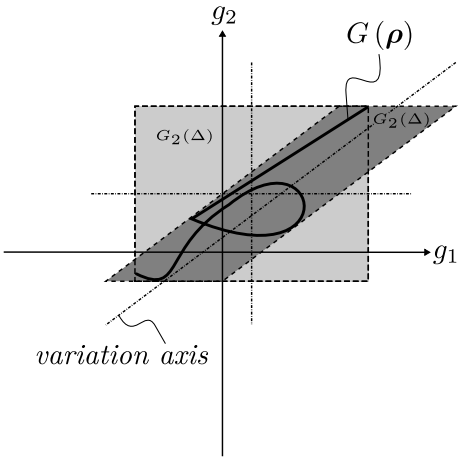

Figure A.8: 2D variation space illustrating joint variation.

Figure A.8 illustrates two variation spaces, each representing the finite non-linear matrix gain $G(\boldsymbol{\rho}) = \begin{bmatrix} g_1(\boldsymbol{\rho}) & g_2(\boldsymbol{\rho}) \end{bmatrix} \in \mathbb{R}^{1\times 2}$ for every $\boldsymbol{\rho} \in \mathfrak{D}_\rho$, of which the first uses independent element variation

$$\begin{aligned} G_1(\Delta) =& \frac{1}{2}\left(\begin{bmatrix} \overline{g_1} & \overline{g_2} \end{bmatrix} + \begin{bmatrix} \underline{g_1} & \underline{g_2} \end{bmatrix}\right) \\ &+ \begin{bmatrix} \frac{1}{2}\left(\overline{g_1} - \underline{g_1}\right) & \frac{1}{2}\left(\overline{g_2} - \underline{g_2}\right) \end{bmatrix} \begin{bmatrix} \delta_1 & 0 \\ 0 & \delta_2 \end{bmatrix} \begin{bmatrix} 1 & 0 \\ 0 & 1 \end{bmatrix} \end{aligned} \tag{A.176}$$

16. A non-linear function has finite gain if it passes through the origin. This is the case for aircraft perturbations, as I/O perturbations are zero about aircraft trim.

and the second uses joint element variation

$$G_2(\Delta) = \begin{bmatrix} j_1 & j_2 \end{bmatrix} + \begin{bmatrix} e_1 & e_2 \end{bmatrix} \begin{bmatrix} \delta_1 & 0 \\ 0 & \delta_2 \end{bmatrix} \begin{bmatrix} 1 & h \\ 1 & 0 \end{bmatrix} \tag{A.177}$$

both with minimal area description of $G(\boldsymbol{\rho})$ for fixed *variation axes* (see Figure A.8). The constant gain matrices J, E and H may be used to reduce the norm-bounded space, *i.e.* its area or volume, which leads us to the following theorem.

Theorem 9. *Suppose there exists two sets of expressions*

$$G_1(\boldsymbol{\Delta}) \tag{A.178}$$

and

$$G_2(\boldsymbol{\Delta}) \tag{A.179}$$

such that

$$G_2(\boldsymbol{\Delta}) \subseteq G_1(\boldsymbol{\Delta}) \tag{A.180}$$

Then,

$$G_1(\boldsymbol{\Delta}) \subseteq \boldsymbol{G} \implies G_2(\boldsymbol{\Delta}) \subseteq \boldsymbol{G} \tag{A.181}$$

but

$$G_2(\boldsymbol{\Delta}) \subseteq \boldsymbol{G} \not\Longrightarrow G_1(\boldsymbol{\Delta}) \subseteq \boldsymbol{G} \tag{A.182}$$

where $\boldsymbol{G}$ may be any set of expressions in $\boldsymbol{\rho}$.

Proof: The proof is deduced directly from the definition of subsets [51] and may easily be shown with a Venn diagram.

The significance of the theorem lies in the interpretation of $\boldsymbol{G}$. In accordance with Section 3.7, $\boldsymbol{G}$ represents a set of LMI conditions. Then, one may deduce from Theorem 9 that a norm-bounded gain $G_2(\boldsymbol{\Delta})$, whose expressions are included in a *larger* norm-bounded gain $G_1(\boldsymbol{\Delta})$, might satisfy a set of conditions which the larger one does not. It follows that $G_1(\boldsymbol{\Delta})$ might exclude controllers parametrised in Section 3.8 which are included by $G_2(\boldsymbol{\Delta})$, motivating the use of minimal norm-bounded space description.

The non-scalar norm-bounded variation Δ_k in (3.25), commonly referred to as *unstructured uncertainty*, is used to describes hyper-ellipsoidal joint variation, illustrated in Figure A.9 for 2D discrete gain $G(\boldsymbol{\rho}_i)$ representation and is given by

$$G_3(\Delta) = \begin{bmatrix} j_1 & j_2 \end{bmatrix} + \begin{bmatrix} e_1 & e_2 \end{bmatrix} \Delta_1 \begin{bmatrix} h_{11} & h_{12} \\ h_{21} & h_{22} \end{bmatrix} \tag{A.183}$$

where i denotes the index of the discrete dependency.

An algorithm is presented in Appendix B.1 used to calculate a minimal variation norm-bounded state-space representation from selected system I/O data.

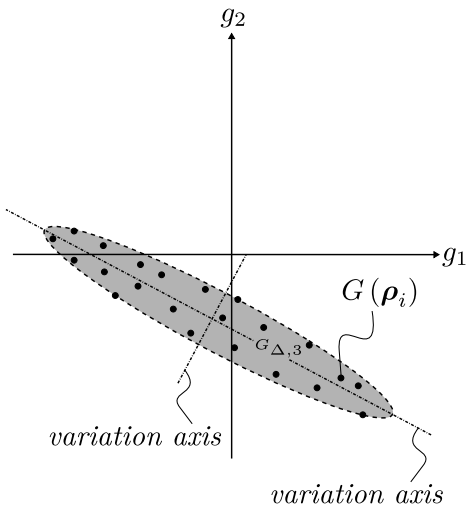

Figure A.9: 2D variation space illustrating ellipsoidal joint variation.

A.2.11 Padé approximations of a time-delay

A time-delay τ_d may be exactly represented by an infinite order transfer function, which follows from the *Taylor series* expansion of the *Laplace transform* of a time-delay [72, pp.111], given as

$$\begin{aligned}\mathcal{L}\{f(t-\tau_d)\} &= \mathcal{L}\{f(t)\star\uparrow(t-\tau_d)\}\\ &= \mathcal{L}\{f(t)\}\mathcal{L}\{\uparrow(t-\tau_d)\}\\ &= \mathcal{L}\{f(t)\}e^{-s\tau_d}\\ &= \mathcal{L}\{f(t)\}\left(\sum_{n=0}^{\infty}\frac{(-\tau_d)^n}{n!}s^n\right)\end{aligned} \tag{A.184}$$

where s^n is an n^{th} order differentiator operator, $\uparrow(t)$ the *Dirac delta* unit impulse and $f(t)$ represents the remainder of the system. Infinite order systems are difficult to analyse and are not numerically tractable. A common remedy is to use the Padé approximation of e^{-x}, given by [38, pp.572]

$$e^{-x} \approx R_{m,n}(x) = \frac{P_m(x)}{Q_n(x)} \tag{A.185}$$

where

$$P_m(x) := \sum_{k=0}^{m}\frac{(m+n-k)!m!}{(m+n)!k!(m-k)!}(-x)^k \tag{A.186}$$

$$Q_n(x) := \sum_{k=0}^{n}\frac{(m+n-k)!n!}{(m+n)!k!(n-k)!}(x)^k \tag{A.187}$$

and the order of the numerator and denominator may be chosen to achieve the desired accuracy. Thus, the Padé approximation of a time-delay has the form

$$e^{-s\tau_d} \approx \frac{a_0 + a_1(\tau_d s) + a_2(\tau_d s)^2 + \ldots + a_m(\tau_d s)^m}{b_0 + b_1(\tau_d s) + b_2(\tau_d s)^2 + \ldots + b_n(\tau_d s)^n} \tag{A.188}$$

The step and frequency response is plotted for $\tau_d = 1\,\text{sec}$ and various m and n in Figures A.10 and A.11 respectively. Table A.1 gives the corresponding transfer functions.

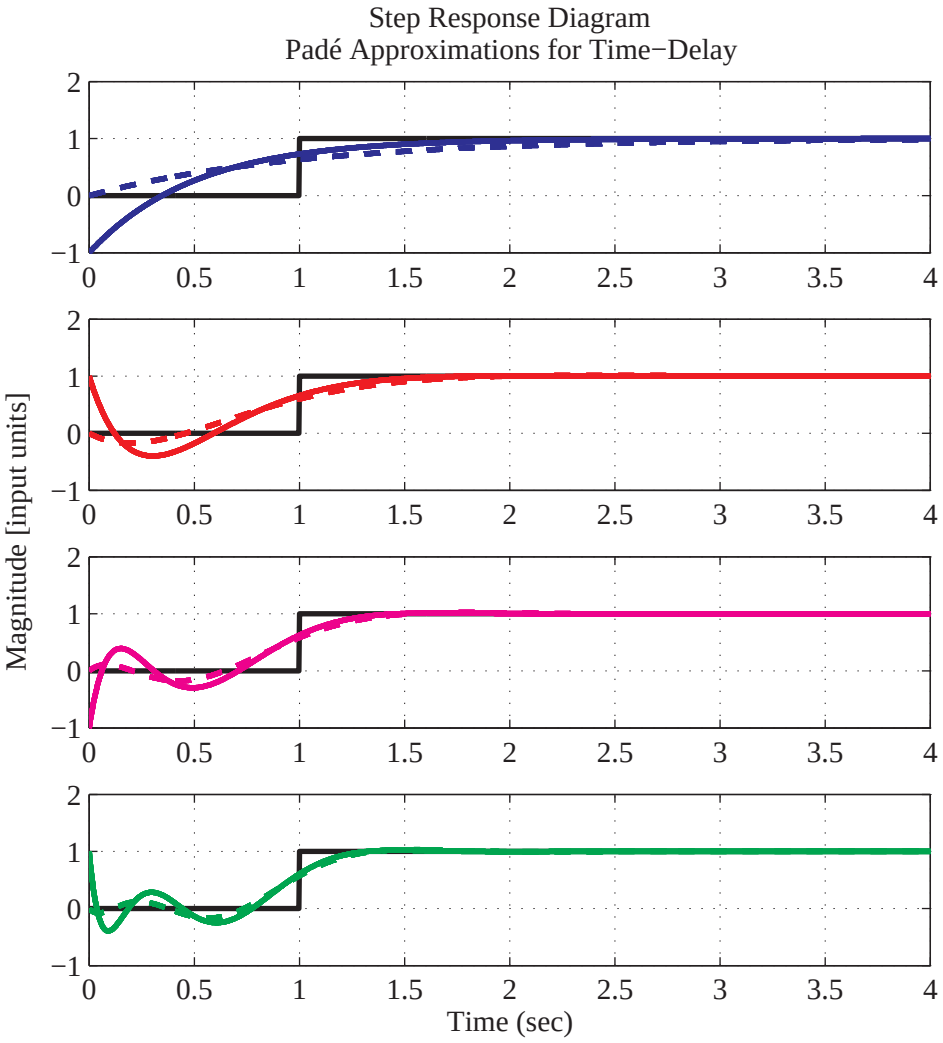

Figure A.10: Padé approximation step responses. Approximates: $m = n$ (solid); $m = n-1$ (dashed); $n = 1$ (blue); $n = 2$ (red); $n = 3$ (magenta); $n = 4$ (green).

A.2.12 LMI properties

LMI constraints have the following properties[12, pp.23,44]:

1. *preservation under addition:* If $F(\mathbf{x}) > 0$ and $G(\mathbf{x}) > 0$, then $F(\mathbf{x}) + G(\mathbf{x}) > 0$.
2. *preservation under positive scaling:* If $F(\mathbf{x}) > 0$ and a is a positive scalar, then $aF(\mathbf{x}) > 0$.

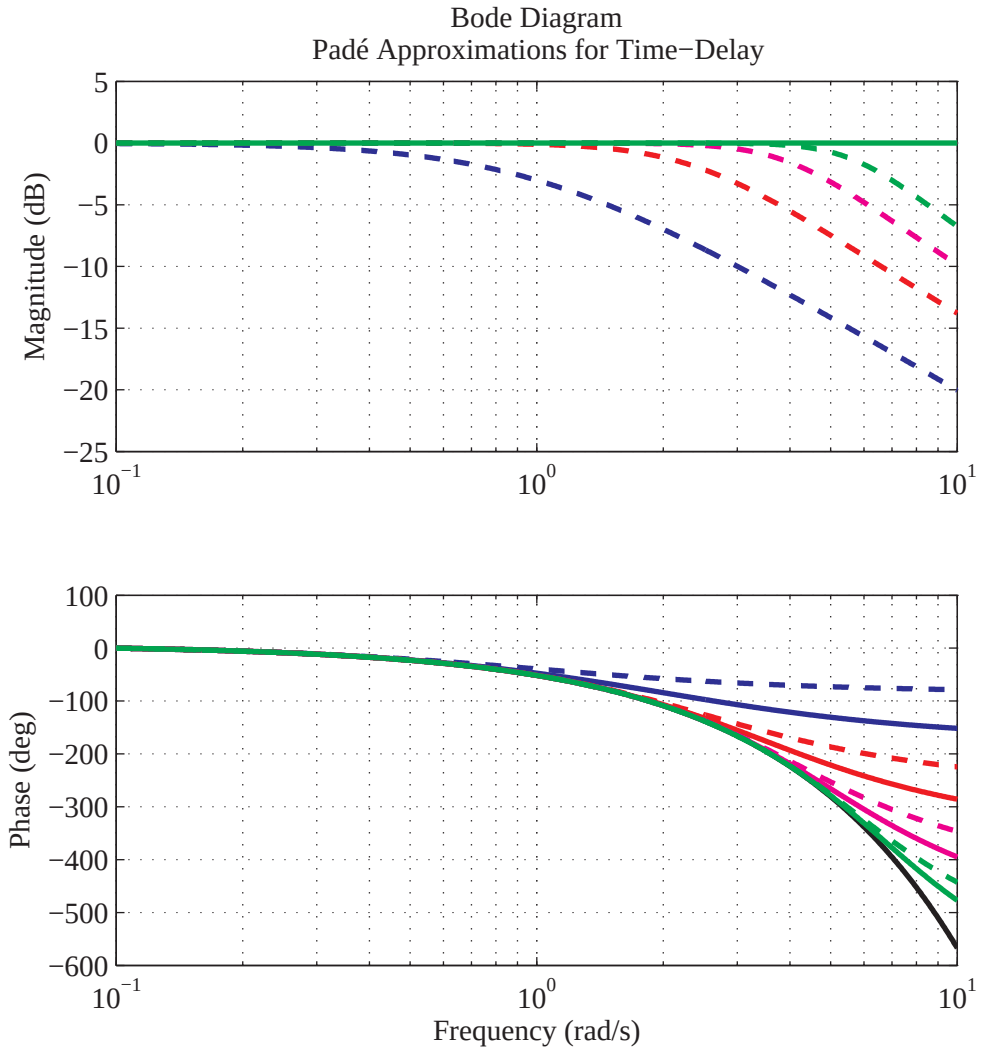

Figure A.11: Padé approximation frequency responses. Approximates: $m = n$ (solid); $m = n - 1$ (dashed); $n = 1$ (blue); $n = 2$ (red); $n = 3$ (magenta); $n = 4$ (green).

3. *preservation under congruent transformation*: If $F(\mathbf{x}) > 0$, and $T \in \mathbb{R}^{n \times n}$ has full rank, then $T^T F(\mathbf{x}) T > 0$.
4. *transitive:* If $F(\mathbf{x}) < G(\mathbf{x})$, *i.e.* $0 < G(\mathbf{x}) - F(\mathbf{x})$, and $G(\mathbf{x}) < H(\mathbf{x})$, then $F(\mathbf{x}) < H(\mathbf{x})$.
5. *antisymmetric:* $\{\mathbf{x} \in \mathbb{R}^{m \times 1} : F(\mathbf{x}) > 0,\ F(\mathbf{x}) < 0\} = \emptyset$.
6. *cascadable:* $\{\mathbf{x} \in \mathbb{R}^{m \times 1} : F(\mathbf{x}) > 0,\ G(\mathbf{x}) > 0\} = \{\mathbf{x} \in \mathbb{R}^{m \times 1} : \text{blkdiag}(F(\mathbf{x}), G(\mathbf{x})) > 0\}$, thus multiple LMI constraints may be cascaded into a single LMI constraint.
7. *preservation under diagonalisation*: If $F(\mathbf{x}) < G(\mathbf{x})$, then $\text{diag}(\text{diag}(F(\mathbf{x}))) < \text{diag}(\text{diag}(G(\mathbf{x})))$.
8. *convexity:* LMI constrained vector spaces are convex. A set $\mathcal{C}$ is convex if the line segment between any two points in $\mathcal{C}$ lies in $\mathcal{C}$, *i.e.* if for any $\{\mathbf{p}_1, \mathbf{p}_2\} \in \mathcal{C}$

n	$R_{n-1,n}(s\tau_d)$	$R_{n,n}(s\tau_d)$
1	$\frac{1}{1+s\tau_d}$	$\frac{2-s\tau_d}{2+s\tau_d}$
2	$\frac{6-2s\tau_d}{6+4s\tau_d+(s\tau_d)^2}$	$\frac{12-6s\tau_d+(s\tau_d)^2}{12+6s\tau_d+(s\tau_d)^2}$
3	$\frac{60-24s\tau_d+3(s\tau_d)^2}{160+36s\tau_d+9(s\tau_d)^2+(s\tau_d)^3}$	$\frac{120-60s\tau_d+12(s\tau_d)^2-(s\tau_d)^3}{120+60s\tau_d+12(s\tau_d)^2+(s\tau_d)^3}$
4	$\frac{840-360s\tau_d+60(s\tau_d)^2-(s\tau_d)^3}{840+480s\tau_d+120(s\tau_d)^2+16(s\tau_d)^3+(s\tau_d)^4}$	$\frac{1680-840s\tau_d+180(s\tau_d)^2-20(s\tau_d)^3+(s\tau_d)^4}{1680+840s\tau_d+180(s\tau_d)^2+20(s\tau_d)^3+(s\tau_d)^4}$

Table A.1: Padé approximation transfer functions.

and any $b \in [0,1]$, we have $b\mathbf{p}_1 + (1-b)\,\mathbf{p}_2 \in \mathcal{C}$.

9. *relation to eigenvalues*: $F(\mathbf{x}) > 0 \iff \mathrm{eig}_i(F(\mathbf{x})) > 0\ \forall i \in \{1,2,\ldots,n\}$
10. *preservation under the trace operator*: If $F(\mathbf{x}) < G(\mathbf{x})$, then $\mathrm{tr}(F(\mathbf{x})) < \mathrm{tr}(G(\mathbf{x}))$.

The first seven properties are inherent in the LMI scalar definition,

$$(F(\mathbf{x}) > 0) \iff \left(\mathbf{u}^T F(\mathbf{x})\,\mathbf{u} > 0\ \forall \mathbf{u} \in \mathbb{R}^{n_m \times 1} \neq 0\right) \tag{A.189}$$

property eight is inherent in the definition of convexity, while the last two properties may be derived using singular value decomposition and basic eigenvalue theory.

A.2.13 Proof of Theorem 1

Theorem 10. *[74] Suppose there exist time-invariant matrices* $\{S,N\} \subset \mathbb{R}^{q\times q}$, $\{E,F\} \subset \mathbb{R}^{m\times q}$, $R = R^T \in \mathbb{R}^{m\times m}$, $J = J^T \in \mathbb{R}^{q\times q}$ *and matrix expressions* $\{\Omega(\boldsymbol{\varrho}), \Lambda(\boldsymbol{\varrho})\} \subset \left\{M(\boldsymbol{\varrho}) \middle| M : \mathbb{R}^{n_\rho} \mapsto \mathbb{R}^{q\times q}\right\}$ *satisfying*

$$\begin{gathered}\Lambda(\boldsymbol{\varrho})\,\Lambda(\boldsymbol{\varrho})^T < I, \quad \Lambda(\boldsymbol{\varrho})\,S = S\Lambda(\boldsymbol{\varrho}), \\ I + \Omega(\boldsymbol{\varrho})\,\Lambda(\boldsymbol{\varrho})\,N = \Omega(\boldsymbol{\varrho})\end{gathered} \tag{A.190}$$

Then,

$$\begin{gathered}\left(\begin{bmatrix} R + ETE^T & F + ETN^T \\ \left(F + ETN^T\right)^T & -T + NTN^T + J \end{bmatrix} < 0\right) \\ \implies \left(R + E\Omega(\boldsymbol{\varrho})\,\Lambda(\boldsymbol{\varrho})\,F^T + F\left(E\Omega(\boldsymbol{\varrho})\,\Lambda(\boldsymbol{\varrho})\right)^T + E\Omega(\boldsymbol{\varrho})\,\Lambda(\boldsymbol{\varrho})\,J\left(E\Omega(\boldsymbol{\varrho})\,\Lambda\right)^T < 0\right)\end{gathered} \tag{A.191}$$

where

$$T := SS^T \tag{A.192}$$

Proof: According to Schur's complement, the sufficient condition in (A.191) *is equivalent to*

$$R + ETE^T + LH^{-1}L^T < 0, \quad H > 0 \tag{A.193}$$

where

$$L := F + ETN^T, \quad H := T - NTN^T - J \tag{A.194}$$

Then,

$$\begin{aligned}
&\{L.H.S.\ of\ (\text{A.193})\} - \{L.H.S.\ of\ (\text{A.191})\} \\
&\quad = \left[R + ETE^T + LH^{-1}L^T\right] - \\
&\qquad \left[R + E\Omega\left(\boldsymbol{\varrho}\right)\Lambda\left(\boldsymbol{\varrho}\right)\left(L - ETN^T\right)^T + \right. \\
&\qquad \left(L - ETN^T\right)\left(E\Omega\left(\boldsymbol{\varrho}\right)\Lambda\left(\boldsymbol{\varrho}\right)\right)^T + \\
&\qquad \left. E\Omega\left(\boldsymbol{\varrho}\right)\Lambda\left(\boldsymbol{\varrho}\right)J\left(E\Omega\left(\boldsymbol{\varrho}\right)\Lambda\left(\boldsymbol{\varrho}\right)\right)^T\right] \\
&\quad = \left(L - E\Omega\left(\boldsymbol{\varrho}\right)\Lambda\left(\boldsymbol{\varrho}\right)H\right)H^{-1}\left(L - E\Omega\left(\boldsymbol{\varrho}\right)\Lambda\left(\boldsymbol{\varrho}\right)H\right)^T + \\
&\qquad E\left(I + \Omega\left(\boldsymbol{\varrho}\right)\Lambda\left(\boldsymbol{\varrho}\right)N\right)T\left(I + \Omega\left(\boldsymbol{\varrho}\right)\Lambda\left(\boldsymbol{\varrho}\right)N\right)^T E^T - \\
&\qquad E\Omega\left(\boldsymbol{\varrho}\right)\Lambda\left(\boldsymbol{\varrho}\right)T\left(E\Omega\left(\boldsymbol{\varrho}\right)\Lambda\left(\boldsymbol{\varrho}\right)\right)^T \\
(\text{A.190}) \rightarrow \quad &= \left(L - E\Omega\left(\boldsymbol{\varrho}\right)\Lambda\left(\boldsymbol{\varrho}\right)H\right)H^{-1}\left(L - E\Omega\left(\boldsymbol{\varrho}\right)\Lambda\left(\boldsymbol{\varrho}\right)H\right)^T + \\
&\qquad E\Omega\left(\boldsymbol{\varrho}\right)T\Omega^T\left(\boldsymbol{\varrho}\right)E^T - E\Omega\left(\boldsymbol{\varrho}\right)S\Lambda\left(\boldsymbol{\varrho}\right)\Lambda^T\left(\boldsymbol{\varrho}\right)S^T\Omega^T\left(\boldsymbol{\varrho}\right)E^T \\
\left(\Lambda\left(\boldsymbol{\varrho}\right)\Lambda^T\left(\boldsymbol{\varrho}\right) \leq I\right) \rightarrow \quad &> \left(L - E\Omega\left(\boldsymbol{\varrho}\right)\Lambda\left(\boldsymbol{\varrho}\right)H\right)H^{-1}\left(L - E\Omega\left(\boldsymbol{\varrho}\right)\Lambda\left(\boldsymbol{\varrho}\right)H\right)^T \\
(H > 0) \rightarrow \quad &> 0
\end{aligned} \tag{A.195}$$

which concludes the proof.

The conservatism involved in Theorem (A.195) is quantified by $\left(L - E\Omega\left(\boldsymbol{\varrho}\right)\Lambda\left(\boldsymbol{\varrho}\right)H\right)H^{-1}\left(L - E\Omega\left(\boldsymbol{\varrho}\right)\Lambda\left(\boldsymbol{\varrho}\right)H\right)^T$.

A.2.14 Proof of Theorem 2

Theorem 11. *(Lyapunov variable upper bound) Suppose there exists a constant matrix* $W \in \mathbb{S}_{++}^n$ *and matrix expressions* $\{S\left(\boldsymbol{\varrho}\right), X\left(\boldsymbol{\varrho}\right)\} \subseteq \left\{M\left(\boldsymbol{\varrho}\right) \middle| M : \mathbb{R}^{n_{\boldsymbol{\varrho}} \times 1} \mapsto \mathbb{R}^{n \times n}, M\left(\boldsymbol{\varrho}\right) = M^T\left(\boldsymbol{\varrho}\right)\right\}$, $R\left(\boldsymbol{\varrho}\right) \in \left\{M\left(\boldsymbol{\varrho}\right) \middle| M : \mathbb{R}^{n_{\boldsymbol{\varrho}} \times 1} \mapsto \mathbb{R}^{n \times n}, M\left(\boldsymbol{\varrho}\right) > 0\right\}$, $F\left(\boldsymbol{\varrho}\right) \in \left\{M\left(\boldsymbol{\varrho}\right) \middle| M : \mathbb{R}^{n_{\boldsymbol{\varrho}} \times 1} \mapsto \mathbb{R}^{n \times n}\right\}$ *such that*

$$S\left(\boldsymbol{\varrho}\right) = F\left(\boldsymbol{\varrho}\right)X\left(\boldsymbol{\varrho}\right) + X\left(\boldsymbol{\varrho}\right)F^T\left(\boldsymbol{\varrho}\right) + R\left(\boldsymbol{\varrho}\right) \tag{A.196}$$

and

$$F\left(\boldsymbol{\varrho}\right)W + WF^T\left(\boldsymbol{\varrho}\right) + R\left(\boldsymbol{\varrho}\right) < 0 \tag{A.197}$$

Then

$$W > X\left(\boldsymbol{\varrho}\right) \tag{A.198}$$

Proof: Given (A.197) *and the transitive property of LMIs (see Section A.2.12)*

$$\begin{aligned}
F\left(\boldsymbol{\varrho}\right)W + WF^T\left(\boldsymbol{\varrho}\right) + R\left(\boldsymbol{\varrho}\right) &< 0 \\
\overset{R(\boldsymbol{\varrho})>0}{\Longrightarrow} \quad F\left(\boldsymbol{\varrho}\right)W + WF^T\left(\boldsymbol{\varrho}\right) &< 0
\end{aligned} \tag{A.199}$$

and we define the Lyapunov function

$$L(\boldsymbol{\varrho}) := F(\boldsymbol{\varrho})W + WF^T(\boldsymbol{\varrho}) < 0 \tag{A.200}$$

It follows from the scaling property of LMIs that W forms a family of solutions $\alpha W > 0$ to (A.200)*, where $\alpha \in \mathbb{S}^1_{++}$, i.e*

$$\begin{aligned} & F(\boldsymbol{\varrho})W + WF^T(\boldsymbol{\varrho}) < 0 \\ \iff \quad & \left(F(\boldsymbol{\varrho})(\alpha W) + (\alpha W)F^T(\boldsymbol{\varrho}) < 0,\ \alpha > 0\right) \end{aligned} \tag{A.201}$$

Adding the scaled Lyapunov term to A.196 gives

$$\begin{aligned} S(\boldsymbol{\varrho}) + \alpha L(\boldsymbol{\varrho}) &= F(\boldsymbol{\varrho})X(\boldsymbol{\varrho}) + X(\boldsymbol{\varrho})F^T(\boldsymbol{\varrho}) + R(\boldsymbol{\varrho}) \\ &\quad + \left(F(\boldsymbol{\varrho})(\alpha W) + (\alpha W)F^T(\boldsymbol{\varrho})\right) \\ &= F(\boldsymbol{\varrho})(X(\boldsymbol{\varrho}) + \alpha W) + (X(\boldsymbol{\varrho}) + \alpha W)F^T(\boldsymbol{\varrho}) + R(\boldsymbol{\varrho}) \\ &= F(\boldsymbol{\varrho})\acute{X}(\boldsymbol{\varrho}) + \acute{X}(\boldsymbol{\varrho})F^T(\boldsymbol{\varrho}) + R(\boldsymbol{\varrho}), \quad \acute{X}(\boldsymbol{\varrho}) := X(\boldsymbol{\varrho}) + \alpha W \end{aligned} \tag{A.202}$$

where

$$\alpha W > 0 \quad \iff \quad \left(\acute{X}(\boldsymbol{\varrho}) > X(\boldsymbol{\varrho})\right) \tag{A.203}$$

The singular value decomposition of $L(\boldsymbol{\varrho})$ is given in [70, pp.537-544] as

$$L(\boldsymbol{\varrho}) = U(\boldsymbol{\varrho})\Sigma(\boldsymbol{\varrho})V^T(\boldsymbol{\varrho}) \tag{A.204}$$

where $\Sigma(\boldsymbol{\varrho})$ is diagonal and $U(\boldsymbol{\varrho})$ and $V(\boldsymbol{\varrho})$ are orthonormal, i.e. $U^{-1}(\boldsymbol{\varrho}) = U^T(\boldsymbol{\varrho})$ and $V^{-1}(\boldsymbol{\varrho}) = V^T(\boldsymbol{\varrho})$. Given that $L(\boldsymbol{\varrho})$ is symmetric, $V(\boldsymbol{\varrho}) = U(\boldsymbol{\varrho})$ and $L(\boldsymbol{\varrho})$ is diagonalised with similarity transformation

$$U^{-1}(\boldsymbol{\varrho})L(\boldsymbol{\varrho})U(\boldsymbol{\varrho}) = \Sigma(\boldsymbol{\varrho}) \tag{A.205}$$

of which the negative definiteness of $L(\boldsymbol{\varrho})$ is preserved under congruent transformation, i.e.

$$\left(L(\boldsymbol{\varrho}) < 0\right) \quad \iff \quad \left(U^T(\boldsymbol{\varrho})L(\boldsymbol{\varrho})U(\boldsymbol{\varrho}) = \Sigma(\boldsymbol{\varrho}) < 0\right) \tag{A.206}$$

with eigenvalue relation

$$\left(\Sigma(\boldsymbol{\varrho}) < 0\right) \quad \iff \quad \left(\mathrm{eig}_i(\Sigma(\boldsymbol{\varrho})) < 0,\ \forall i = 1, 2, \ldots, n\right) \tag{A.207}$$

Eigenvalues are preserved under similarity transformation, thus

$$\mathrm{eig}\left(S(\boldsymbol{\varrho}) + \alpha L(\boldsymbol{\varrho})\right) = \mathrm{eig}\left(U^{-1}(\boldsymbol{\varrho})\left(S(\boldsymbol{\varrho}) + \alpha L(\boldsymbol{\varrho})\right)U(\boldsymbol{\varrho})\right) \tag{A.208}$$

$$= \mathrm{eig}\left(U^{-1}(\boldsymbol{\varrho})\left(S(\boldsymbol{\varrho}) + \alpha L(\boldsymbol{\varrho})\right)U(\boldsymbol{\varrho})\right) \tag{A.209}$$

$$= \mathrm{eig}\left(U^{-1}(\boldsymbol{\varrho})S(\boldsymbol{\varrho})U(\boldsymbol{\varrho}) + \alpha\Sigma(\boldsymbol{\varrho})\right) \tag{A.210}$$

and it follows from Gershgorin's theorem, given in Appendix A.2.9, that by increasing α*, the centres of the union of circles containing the eigenvalues may be moved to the left in the complex plane without affecting the radii. Thus, given* $U^{-1}(\boldsymbol{\varrho})\, S(\boldsymbol{\varrho})\, U(\boldsymbol{\varrho})$ *is finite*

$$\exists \alpha : S(\boldsymbol{\varrho}) + \alpha L(\boldsymbol{\varrho}) < 0 \tag{A.211}$$

and thus

$$\exists \alpha : F(\boldsymbol{\varrho})\, \acute{X}(\boldsymbol{\varrho}) + \acute{X}(\boldsymbol{\varrho})\, F^T(\boldsymbol{\varrho}) + R(\boldsymbol{\varrho}) < 0,\ \acute{X}(\boldsymbol{\varrho}) > X(\boldsymbol{\varrho}) \tag{A.212}$$

which concludes the first part of the proof.

Next, an upper-bound of $\acute{X}(\boldsymbol{\varrho})$ *which is invariant under* $\boldsymbol{\varrho}$*, is formulated by constraining the family of solutions*

$$\mathfrak{X}_V := \left\{ \acute{X}(\boldsymbol{\varrho}) \,\middle|\, \acute{X} : \mathbb{R}^{n_\varrho \times 1} \mapsto \mathbb{R}^{n \times n},\ F(\boldsymbol{\varrho})\, \acute{X}(\boldsymbol{\varrho}) + \acute{X}(\boldsymbol{\varrho})\, F^T(\boldsymbol{\varrho}) + R(\boldsymbol{\varrho}) < 0,\ \acute{X}(\boldsymbol{\varrho}) > 0 \right\} \tag{A.213}$$

with

$$\frac{\partial \acute{X}(\boldsymbol{\varrho})}{\partial \varrho_i} = 0\ \forall i = [1, 2, \ldots, n_\varrho] \tag{A.214}$$

i.e.

$$\begin{aligned} \mathfrak{X}_I : &= \mathfrak{X}_V \cap \mathbb{S}^n_{++} \\ &= \left\{ \overline{X} \in \mathbb{S}^n_{++} \,\middle|\, F(\boldsymbol{\varrho})\, \overline{X} + \overline{X} F^T(\boldsymbol{\varrho}) + R(\boldsymbol{\varrho}) < 0 \right\} \end{aligned} \tag{A.215}$$

and observing that any solution W *to* (A.197) *admits to*

$$W \in \mathfrak{X}_I \subseteq \mathfrak{X}_V \tag{A.216}$$

we have

$$W > X(\boldsymbol{\varrho}) \tag{A.217}$$

which concludes the proof.

The conservatism involved in Theorem 11, quantified by $W - X(\boldsymbol{\varrho})$, lies with the addition $\alpha L(\boldsymbol{\varrho})$ in (A.202) and the constraint $\frac{\partial \acute{X}(\boldsymbol{\varrho})}{\partial \boldsymbol{\varrho}} = 0$ in (A.214).

Appendix B

Algorithms

B.1 Norm-bounded state-space model calculation

Refer to Section 4.2.1.1.

Although the mechanics of atmospheric flight has well-known closed-form expressions (2.7) and (2.8), the functions describing aerodynamic forces are build from sample measurements and lack closed-form expressions. Thus, the norm-bounded state-space model cannot analytically be derived from the non-linear model finite gain $\mathbf{f}(\mathbf{x}, \boldsymbol{\rho})$, motivating the use of I/O sample pairs $\mathbf{y} = \mathbf{f}(\mathbf{x}, \boldsymbol{\rho})$ to construct the norm-bounded state-space model.

An algorithm is presented that calculates the norm-bounded state-space model representation of the IFR mechanics. LMI optimisation is used to find the sub-minimum norm-bounded space, motivated in Section A.2.10 by Theorem 9, via a sampled I/O based method. Gain component variation above a specified level is included with scalar norm-bounded variation δ_i, and is compared with other gain components to find joint variation in a predefined direction. The remaining variation is included with a non-scalar norm-bounded variation Δ_1 as a hyper-ellipsoid. The theoretical bases is formulated as follows.

Given a finite gain NLTV, possibly uncertain, system

$$\mathbf{y} = \mathbf{f}(\mathbf{x}, \boldsymbol{\rho}) = \begin{bmatrix} f_1(\mathbf{x}, \boldsymbol{\rho}) \\ f_2(\mathbf{x}, \boldsymbol{\rho}) \\ \vdots \\ f_{n_y}(\mathbf{x}, \boldsymbol{\rho}) \end{bmatrix}, \quad \mathbf{f}(\mathbf{0}, \boldsymbol{\rho}) = \mathbf{0},\ \mathbf{x} \in \mathfrak{E},\ \boldsymbol{\rho} \in \mathfrak{P} \tag{B.1}$$

and its norm-bounded state-space model representation

$$\mathbf{y} = F_\Delta \mathbf{x} = \left(F + B\Delta C^T\right)\mathbf{x}, \quad \Delta \in \boldsymbol{\Delta}^s \tag{B.2}$$

where $\mathbf{x} = [x_1, x_2, \ldots, x_{n_x}]^T \in \mathbb{R}^{n_x \times 1}$ is the system input, $\mathbf{y} = [y_1, y_2, \ldots, y_{n_y}]^T \in \mathbb{R}^{n_y \times 1}$ is the system output, $\boldsymbol{\rho} \in \mathbb{R}^{n_\rho \times 1}$ contains the remainding function dependencies and $\mathfrak{E}$ and $\mathfrak{P}$ defines the corresponding *variable domains*[1]. For (B.2) to

1. $\mathfrak{E}$ and $\mathfrak{P}$ are defined by the local flight envelope under consideration.

completely describe (4.13) it is required that

$$\exists \Delta \in \boldsymbol{\Delta}^{s} : F_{\Delta}\mathbf{x} = \mathbf{f}\left(\mathbf{x}, \boldsymbol{\rho}\right), \quad \forall \mathbf{x} \in \mathfrak{E}, \boldsymbol{\rho} \in \mathfrak{P} \tag{B.3}$$

Furthermore, (B.2) decomposed into its *joint variation form*

$$\begin{aligned}\mathbf{y} =& F\mathbf{x} + \begin{bmatrix} \mathbf{b}_1 & \mathbf{b}_2 & \cdots & \mathbf{b}_g & B_1 & B_2 & \cdots & B_q \end{bmatrix} \Delta \begin{bmatrix} \mathbf{c}_1^T \\ \mathbf{c}_2^T \\ \vdots \\ \mathbf{c}_g^T \\ C_1^T \\ C_2^T \\ \vdots \\ C_q^T \end{bmatrix} \mathbf{x} \\ =& \left(F + \sum_{i=1}^{g} \mathbf{b}_i \delta_i \mathbf{c}_i^T + \sum_{k=1}^{q} B_k \Delta_k C_k^T \right) \mathbf{x} \\ & \mathbf{b}_i \in \mathbb{R}^{n_y \times 1},\ B_k \in \mathbb{R}^{n_y \times n_{\Delta_k}},\ \mathbf{c}_i \in \mathbb{R}^{n_x \times 1},\ C_k \in \mathbb{R}^{n_x \times n_{\Delta_k}}\end{aligned} \tag{B.4}$$

Then, we transform the joint variation $\mathbf{b}_i \delta_i \mathbf{c}_i^T$ in (B.2) into its simplest form $\mathbf{e}_m \delta_i \mathbf{e}_k^T$, using invertable input and output scaling $\mathbf{x} = W_I \grave{\mathbf{x}}$ and $\grave{\mathbf{y}} = W_O \mathbf{y}$, *i.e.* $W_O \mathbf{b}_i \delta_i \mathbf{c}_i^T W_I = \mathbf{e}_m \delta_i \mathbf{e}_k^T$, where $\mathbf{e}_p$ is the p^{th} standard base vector, *i.e.* the p^{th} column of the identity matrix. Variation $\mathbf{e}_m \delta_i \mathbf{e}_k^T$ is dependent only on $\mathbf{e}_k^T \grave{\mathbf{x}}$, which we choose to represent a gain $\mathbf{e}_m g_i \left(\mathbf{e}_k^T \grave{\mathbf{x}} \right) \mathbf{e}_k^T$ which may vary arbitrarily within bounds $-1 < g_i \left(\mathbf{e}_k^T \grave{\mathbf{x}} \right) < 1$.[2] It follows from descaling that joint variation $\mathbf{b}_i \delta_i \mathbf{c}_i^T$ represents $W_O^{-1} \mathbf{e}_m g_i \left(\mathbf{e}_k^T W_I^{-1} \mathbf{x} \right) \mathbf{e}_k^T W_I^{-1} = \mathbf{b}_i g_i \left(\mathbf{c}_i^T \mathbf{x} \right) \mathbf{c}_i^T$ in $\mathbf{f}\left(\mathbf{x}, \boldsymbol{\rho}\right)$.

The method we use for calculating joint variation parameters $\mathbf{b}_i$ and $\mathbf{c}_i$, is based on the characterisation of (4.13) as a gain along *independently* varying inputs $x_p \mathbf{e}_p$, where x_p is the p^{th} component in $\mathbf{x}$, *i.e.* $x_p = \mathbf{e}_p^T \mathbf{x}$. It should be kept in mind that the size an numeric values of the parameters in (B.4) is dependent on the method presented and its parameters. The *gain* of (4.13) corresponding to input $x_p \mathbf{e}_p$ and the q^{th} output is given as

$$G_{qp}\left(x_p\right) := \frac{f_q\left(x_p \mathbf{e}_p, \boldsymbol{\rho}_0\right)}{x_p} = \left(F_{qp} + \mathbf{e}_q^T \sum_{i=1}^{g} \mathbf{b}_i g_i \left(\mathbf{c}_i^T x_p \mathbf{e}_p \right) \mathbf{c}_i^T \mathbf{e}_p + \frac{\check{f}_q\left(x_p \mathbf{e}_p, \boldsymbol{\rho}_0\right)}{x_p} \right) \tag{B.5}$$

where $\boldsymbol{\rho}$ is chosen as its nominal $\boldsymbol{\rho}_0$ and $\frac{\check{f}_q(x_p \mathbf{e}_p, \boldsymbol{\rho}_0)}{x_p}$ is the remainder. Two gains $G_{qp}\left(x_p\right)$ and $G_{mk}\left(x_k\right)$, with sufficiently large variation, are compared by solving the optimisation problem

$$\begin{aligned} \min_{\{s_I, s_O\} \subset \mathbb{R}^1} \quad & \overline{a} - \underline{a} \\ \text{s.t.} \quad & \underline{a} < G_{qp}\left(x_p\right)\big|_{x_p = v} + s_O G_{mk}\left(x_k\right)\big|_{x_k = s_I v} < \overline{a}, \quad \forall \mathbf{x} \in \mathfrak{E} \end{aligned} \tag{B.6}$$

2. $g_i \left(\mathbf{e}_k^T \grave{\mathbf{x}} \right)$ may be centred with F.

which aims to minimises the common variation in (B.5), say $g_j\left(\mathbf{c}_j^T\mathbf{x}\right)$ in

$$\begin{aligned}
&G_{qp}\left(x_p\right)|_{x_p=v}+s_O G_{mk}\left(x_k\right)|_{x_k=s_I v}\\
&=\left(F_{qp}+\mathbf{e}_q^T\sum_{i=1}^{g}\mathbf{b}_i g_i\left(\mathbf{c}_i^T v\mathbf{e}_p\right)\mathbf{c}_i^T\mathbf{e}_p+\frac{\check{f}_q\left(v\mathbf{e}_p,\boldsymbol{\rho}_0\right)}{v}\right)\\
&\quad+s_O\left(F_{mk}+\mathbf{e}_m^T\sum_{i=1}^{g}\mathbf{b}_i g_i\left(\mathbf{c}_i^T s_I v\mathbf{e}_k\right)\mathbf{c}_i^T\mathbf{e}_k+\frac{\check{f}_m\left(s_I v\mathbf{e}_k,\boldsymbol{\rho}_0\right)}{s_I v}\right)\\
&=\left(\check{F}_{qp}+s_O\check{F}_{mk}\right)\\
&\quad+\left(\mathbf{e}_q^T\mathbf{b}_j g_j\left(\mathbf{c}_j^T v\mathbf{e}_p\right)\mathbf{c}_j^T\mathbf{e}_p+s_O\mathbf{e}_m^T\mathbf{b}_j g_j\left(\mathbf{c}_j^T s_I v\mathbf{e}_k\right)\mathbf{c}_j^T\mathbf{e}_k\right)\\
&\quad+\sum_{\substack{i=1\\ i\neq j}}^{g}\left(\mathbf{e}_q^T\mathbf{b}_i g_i\left(\mathbf{c}_i^T v\mathbf{e}_p\right)\mathbf{c}_i^T\mathbf{e}_p+s_O\mathbf{e}_m^T\mathbf{b}_i g_i\left(\mathbf{c}_i^T s_I v\mathbf{e}_k\right)\mathbf{c}_i^T\mathbf{e}_k\right)\\
&\quad+\left(\frac{\check{f}_q\left(v\mathbf{e}_p,\boldsymbol{\rho}_0\right)}{v}+s_O\frac{\check{f}_m\left(s_I v\mathbf{e}_k,\boldsymbol{\rho}_0\right)}{s_I v}\right)
\end{aligned}\tag{B.7}$$

and is achieved when

$$\frac{\min\left(\overline{a}-\underline{a}\right)}{\underset{\mathbf{x}\in\mathfrak{E}}{\text{range}}\left(G_{qp}\left(x_q\right)\right)}<\epsilon_J$$

$$\underset{v\in\mathfrak{V}}{\text{range}}\left(v\right):=\min\left(\max_{v\in\mathfrak{V}}\left(v\right),-\min_{v\in\mathfrak{V}}\left(v\right)\right)>0\tag{B.8}$$

in which case

$$\left(\mathbf{e}_q^T\mathbf{b}_j g_j\left(\mathbf{c}_j^T v\mathbf{e}_p\right)\mathbf{c}_j^T\mathbf{e}_p+s_O\mathbf{e}_m^T\mathbf{b}_j g_j\left(\mathbf{c}_j^T s_I v\mathbf{e}_k\right)\mathbf{c}_j^T\mathbf{e}_k\right)\approx 0\tag{B.9}$$

thus

$$\mathbf{c}_j^T\mathbf{e}_p\approx s_I\mathbf{c}_j^T\mathbf{e}_k\tag{B.10}$$

$$\mathbf{e}_q^T\mathbf{b}_j\mathbf{c}_j^T\mathbf{e}_p\approx -s_O\mathbf{e}_m^T\mathbf{b}_j\mathbf{c}_j^T\mathbf{e}_k\tag{B.11}$$

Furthermore, we choose $\mathbf{c}_j^T\mathbf{e}_k=1$, accounted for by the scaling redundancy in g_j, and $\mathbf{e}_m^T\mathbf{b}_j$ may be calculated as

$$\mathbf{e}_m^T\mathbf{b}_j=\frac{1}{2}\underset{\mathbf{x}\in\mathfrak{E}}{\text{range}}\left(G_{mk}\left(x_k\right)\right)\tag{B.12}$$

Adding the calculated joint variation in the presence of coupled inputs is beneficial only if

$$\frac{\underset{\mathbf{x}\in\mathfrak{E}}{\text{range}}\left(\left.\frac{f_q(x_p\mathbf{e}_p+x_k\mathbf{e}_k)}{x_p}\right|\begin{array}{c}x_p=v\\ x_k=-\frac{\mathbf{c}_j^T\mathbf{e}_p}{\mathbf{c}_j^T\mathbf{e}_k}v\end{array}\right)}{\underset{\mathbf{x}\in\mathfrak{E}}{\text{range}}\left(G_{qp}\left(x_p\right)\right)}<\epsilon_J\tag{B.13}$$

where the input in the numerator is such that $\mathbf{c}_j^T\mathbf{x} = 0$ and thus $g_j\left(\mathbf{c}_j^T\mathbf{x}\right) = 0$.

To recast (B.6) as a solvable LMI optimisation problem, we discretise (4.13) with discrete input

$$x_p(l) = \overline{x}_p u(l) \tag{B.14}$$

where

$$\overline{x}_p = \min\left(\max_{\mathbf{x}\in\mathfrak{E}}(x_p), -\min_{\mathbf{x}\in\mathfrak{E}}(x_p)\right) > 0, \quad u(l) = -1 + 2\frac{l-1}{n_l - 1}, \quad l = 1, 2, \ldots, n_l \tag{B.15}$$

and in order to perform minimisation over input $v(l) = x_p(l)$, the input scaling is constrained to

$$s_I \in \left\{-\frac{\overline{x}_k}{\overline{x}_p}, \frac{\overline{x}_k}{\overline{x}_p}\right\} \tag{B.16}$$

It follows that (B.6) may be approximated by LMI optimisation problem

$$\begin{aligned} \min_{s_O\in\mathbb{R}^1, s_I\in\left\{-\frac{\overline{x}_k}{\overline{x}_p}, \frac{\overline{x}_k}{\overline{x}_p}\right\}} \quad & \overline{a} - \underline{a} \\ \text{s.t.} \quad & \underline{a} < G_{qp}(x_p(l)) + s_O G_{mk}(x_k(l))|_{x_k(l)=s_I x_p(l)} < \overline{a} \\ & l = 1, 2, \ldots, n_l \end{aligned} \tag{B.17}$$

Ellipsoidal gain variation is used to describe the remaining variation in (B.5) as

$$\check{\mathbf{y}} := \check{\mathbf{f}}(\mathbf{x}, \boldsymbol{\rho}) = B_1\Delta_1 C_1^T\mathbf{x}, \quad \forall\mathbf{x}\in\mathfrak{E}, \boldsymbol{\rho}\in\mathfrak{P} \tag{B.18}$$

where

$$n_{\Delta_1} := \max(n_x, n_y) \tag{B.19}$$

If $n_x = n_y$, then we may write

$$\begin{aligned} & & \check{\mathbf{y}} &= B_1\Delta_1 C_1^T\mathbf{x} \\ & \overset{B_1B_1^T>0}{\Longleftrightarrow} & B_1^{-1}\check{\mathbf{y}} &= \Delta_1 C_1^T\mathbf{x} \\ & \Longleftrightarrow & \check{\mathbf{y}}^T B_1^{-T}B_1^{-1}\check{\mathbf{y}} &= \mathbf{x}^T C_1\Delta_1^T\Delta_1 C_1^T\mathbf{x} \\ & \overset{C_1C_1^T>0}{\Longleftrightarrow} & \check{\mathbf{y}}^T B_1^{-T}B_1^{-1}\check{\mathbf{y}} &< \mathbf{x}^T C_1 C_1^T\mathbf{x} \\ & \Longleftrightarrow & 0 &< \begin{bmatrix} \mathbf{x}^T C_1 C_1^T\mathbf{x} & \check{\mathbf{y}}^T \\ \check{\mathbf{y}} & B_1B_1^T \end{bmatrix} \end{aligned} \tag{B.20}$$

The equivalence between the second and third line in B.20 is due to the input and output rotation redundancy in Δ_1. Using singular value decomposition (see [70, pp.537-544]), we show their equivalence as follows.

$$\begin{aligned} B_1^{-1}\check{\mathbf{y}} &= \Delta_1 C_1^T\mathbf{x} = \left(U_\Delta\Sigma_\Delta V_\Delta^T\right) C_1^T\mathbf{x} \\ \Longleftrightarrow \quad U_\Delta^T B_1^{-1}\check{\mathbf{y}} &= \Sigma_\Delta V_\Delta^T C_1^T\mathbf{x} \\ \Longleftrightarrow \quad \mathbf{e}_1^T U_\Delta^T B_1^{-1}\check{\mathbf{y}} &= \mathbf{e}_1^T\Sigma_\Delta V_\Delta^T C_1^T\mathbf{x} \end{aligned} \tag{B.21}$$

and by choosing U_Δ^T and V_Δ^T such that $U_\Delta^T B_1^{-1}\check{\mathbf{y}} = \mathbf{e}_1\mathbf{e}_1^T U_\Delta^T B_1^{-1}\check{\mathbf{y}}$ and $V_\Delta^T C_1^T\mathbf{x} = \mathbf{e}_1\mathbf{e}_1^T V_\Delta^T C_1^T\mathbf{x}$ it follows that

$$\begin{aligned}
U_\Delta^T B_1^{-1}\check{\mathbf{y}} &= \Sigma_\Delta V_\Delta^T C_1^T\mathbf{x} \\
\iff \left\|U_\Delta^T B_1^{-1}\check{\mathbf{y}}\right\|_2^2 &= \left\|\Sigma_\Delta V_\Delta^T C_1^T\mathbf{x}\right\|_2^2 \\
\iff \check{\mathbf{y}}^T B_1^{-T} U_\Delta U_\Delta^T B_1^{-1}\check{\mathbf{y}} &= \mathbf{x}^T C_1 V_\Delta \Sigma_\Delta^T \Sigma_\Delta V_\Delta^T C_1^T\mathbf{x} \\
\iff \check{\mathbf{y}}^T B_1^{-T} B_1^{-1}\check{\mathbf{y}} &= \mathbf{x}^T C_1 V_\Delta \Sigma_\Delta^T \Sigma_\Delta V_\Delta^T C_1^T\mathbf{x} \\
\iff \check{\mathbf{y}}^T B_1^{-T} B_1^{-1}\check{\mathbf{y}} &= \mathbf{x}^T C_1 V_\Delta \Sigma_\Delta^T \left(U_\Delta^T U_\Delta\right) \Sigma_\Delta V_\Delta^T C_1^T\mathbf{x} \\
\iff \check{\mathbf{y}}^T B_1^{-T} B_1^{-1}\check{\mathbf{y}} &= \mathbf{x}^T C_1 \Delta_1^T \Delta_1 C_1^T\mathbf{x} \qquad \text{(B.22)}
\end{aligned}$$

Thus, if $n_x = n_y$, $B_1 B_1^T > 0$ and $C_1 C_1^T > 0$, then

$$\check{\mathbf{y}} = B_1\Delta_1 C_1^T\mathbf{x} \iff \begin{bmatrix} \mathbf{x}^T C_1 C_1^T\mathbf{x} & \check{\mathbf{y}}^T \\ \check{\mathbf{y}} & B_1 B_1^T \end{bmatrix} > 0 \qquad \text{(B.23)}$$

We may calculate minimum variation hyper-ellipsoid parameters B_1 and C_1 by solving the optimisation problem

$$\begin{aligned}
\min_{\{W,V\}\subset\mathbb{S}_{++}^{n_x}} \quad & \operatorname{tr}(W) + \operatorname{tr}(V) \\
& \begin{bmatrix} \mathbf{x}^T V\mathbf{x} & \check{\mathbf{y}}^T \\ \check{\mathbf{y}} & W \end{bmatrix} > 0, \quad \forall \begin{bmatrix} \mathbf{x} \\ \check{\mathbf{y}} \end{bmatrix} \in \mathfrak{U} \qquad \text{(B.24)}
\end{aligned}$$

where

$$\mathfrak{U} := \left\{ \begin{bmatrix} \mathbf{x} \\ \check{\mathbf{y}} \end{bmatrix} \in \mathbb{R}^{(n_x+n_\rho)\times 1} \middle| \check{\mathbf{y}} = \check{\mathbf{f}}(\mathbf{x},\boldsymbol{\rho}), \mathbf{x}\in\mathfrak{E}, \boldsymbol{\rho}\in\mathfrak{P} \right\} \qquad \text{(B.25)}$$

$$W := B_1 B_1^T \qquad \text{(B.26)}$$

$$V := C_1 C_1^T \qquad \text{(B.27)}$$

and the objective

$$\operatorname{tr}(W) + \operatorname{tr}(V) = \operatorname{tr}(\Sigma_{B_1}\Sigma_{B_1}) + \operatorname{tr}(\Sigma_{C_1}\Sigma_{C_1}) \qquad \text{(B.28)}$$

minimises the quadratic sum of the input and output principle axes (see singular value decomposition [70, pp.537-544]). The case where $n_x \neq n_y$, we may augment the system as follows.

We define

$$n_{\Delta_1} := \max(n_x, n_y) \qquad \text{(B.29)}$$

and if $n_{\Delta_1} \geq n_x$, then

$$\begin{aligned}
\acute{\mathbf{y}} := \check{\mathbf{y}}, \quad \acute{B} := B_1, \quad \acute{C}^T := \begin{bmatrix} C_1^T & C_0^T \end{bmatrix}, \\
C_0 \in \mathbb{R}^{(n_{\Delta_1}-n_x)\times n_{\Delta_1}}, \quad \acute{\mathbf{x}} := \begin{bmatrix} \mathbf{x} \\ \mathbf{0}_{(n_{\Delta_1}-n_x)\times 1} \end{bmatrix} \qquad \text{(B.30)}
\end{aligned}$$

otherwise

$$\acute{\mathbf{y}} := \begin{bmatrix} \check{\mathbf{y}} \\ \mathbf{0}_{(n_{\Delta_1}-n_y)\times 1} \end{bmatrix}, \quad \acute{B} := \begin{bmatrix} B_1 \\ B_0 \end{bmatrix},$$
$$B_0 \in \mathbb{R}^{(n_{\Delta_1}-n_y)\times n_{\Delta_1}}, \quad \acute{C}^T := C_1^T, \quad \acute{\mathbf{x}} := \mathbf{x} \tag{B.31}$$

By constraining $\acute{B}\acute{B}^T > 0$ and $\acute{C}\acute{C}^T > 0$, (B.23) will hold for substitutes B.30 and B.31, and we may calculate minimum variation hyper-ellipsoid parameters B_1 and C_1 by solving B.24.

To recast B.24 as a solvable LMI optimisation problem, we constrain $\mathbf{x}$ and $\boldsymbol{\rho}$ to the finite sample sets

$$\begin{bmatrix} \mathbf{x} \\ \boldsymbol{\rho} \end{bmatrix} \in \mathfrak{S}, \quad |\mathfrak{S}| = n_s, \quad \mathfrak{S} \subset \left\{ \begin{bmatrix} \mathbf{x} \\ \boldsymbol{\rho} \end{bmatrix} \in \mathbb{R}^{(n_x+n_\rho)\times 1} \middle| \mathbf{x} \in \mathfrak{E}, \boldsymbol{\rho} \in \mathfrak{P} \right\} \tag{B.32}$$

We conclude the theoretical bases by constraining $B_1\Delta_1 C_1^T$ in B.24 to represent another ellipsoidal variation gain $\widetilde{B}_1\widetilde{\Delta}_1\widetilde{C}_1^T$, additional to the I/O pairs defined by $\mathfrak{S}$, and is achieved by using the $\mathcal{S}$-procedure [13, pp.24] and a method formulated in [45]. This extension serves to decouple B.24 over n_b *partitions* $\mathfrak{B}_i$ of $\mathfrak{S}$, *i.e.*

$$\bigcup_{i=1}^{n_b} \mathfrak{B}_i = \mathfrak{S}, \quad \mathfrak{B}_i \cap \mathfrak{B}_j = \emptyset \; \forall i \neq j \tag{B.33}$$

and a sub-minimum of B.24 may then be achieved by recursively including another subset and recalculating $\widetilde{B}_1\widetilde{\Delta}_1\widetilde{C}_1^T$ until $\mathfrak{S}$ included. [3]

Theorem 12. *[13, pp.24] ($\mathcal{S}$-procedure for quadratic forms and strict inequalities) Suppose there exist $\tau \in \mathbb{R}^1$, symmetric matrices $\{Q, P\} = \left\{Q^T, P^T\right\} \subset \mathbb{R}^{n_\zeta \times n_\zeta}$, $\zeta \in \mathbb{R}^{n_\zeta \times 1}$ and an arbitrary set $\mathfrak{Z} \subset \mathbb{R}^{n_\zeta \times 1}$ such that*

$$Q - \tau P > 0, \quad \tau \geq 0 \tag{B.34}$$

Then,

$$\zeta^T P \zeta > 0, \quad \forall \zeta \in \mathfrak{Z} \tag{B.35}$$

implies

$$\zeta^T Q \zeta > 0, \quad \forall \zeta \in \mathfrak{Z} \tag{B.36}$$

The converse holds, provided that

$$\exists \zeta \in \mathfrak{Z} : \zeta^T P \zeta > 0 \tag{B.37}$$

i.e.

$$Q - \tau P > 0, \quad \tau \geq 0$$
$$\overset{\exists \zeta \in \mathfrak{Z}: \zeta^T P \zeta > 0}{\Longleftrightarrow} \quad \left(\zeta^T P \zeta > 0 \; \forall \zeta \in \mathfrak{Z} \Longrightarrow \zeta^T Q \zeta > 0 \; \forall \zeta \in \mathfrak{Z}\right) \tag{B.38}$$

Proof: Refer to [13, pp.24,33-34].

3. The conservatism involved in recursively updating the ellipsoidal variation over the single calculation in B.24 is not included.

Now

$$\begin{aligned}(\text{B.20}) \rightarrow \quad \check{\mathbf{y}}^T B_1^{-T} B_1^{-1} \check{\mathbf{y}} &< \mathbf{x}^T C_1 C_1^T \mathbf{x} \\ \iff \quad 0 &< \begin{bmatrix} \mathbf{x} \\ \check{\mathbf{y}} \end{bmatrix}^T \begin{bmatrix} C_1 C_1^T & 0 \\ 0 & -B_1^{-T} B_1^{-1} \end{bmatrix} \begin{bmatrix} \mathbf{x} \\ \check{\mathbf{y}} \end{bmatrix}\end{aligned} \tag{B.39}$$

and following Lemma (12)

$$\begin{aligned}&\begin{bmatrix} C_1 C_1^T & 0 \\ 0 & -B_1^{-T} B_1^{-1} \end{bmatrix} - \tau \begin{bmatrix} \widetilde{C}_1 \widetilde{C}_1^T & 0 \\ 0 & -\widetilde{B}_1^{-T} \widetilde{B}_1^{-1} \end{bmatrix} > 0, \quad \tau \geq 0 \\ \iff \quad &\left(\begin{bmatrix} \mathbf{x} \\ \check{\mathbf{y}} \end{bmatrix}^T \begin{bmatrix} \widetilde{C}_1 \widetilde{C}_1^T & 0 \\ 0 & -\widetilde{B}_1^{-T} \widetilde{B}_1^{-1} \end{bmatrix} \begin{bmatrix} \mathbf{x} \\ \check{\mathbf{y}} \end{bmatrix} > 0, \, \forall \begin{bmatrix} \mathbf{x} \\ \check{\mathbf{y}} \end{bmatrix} \in \mathfrak{U} \right. \\ &\left. \implies \begin{bmatrix} \mathbf{x} \\ \check{\mathbf{y}} \end{bmatrix}^T \begin{bmatrix} C_1 C_1^T & 0 \\ 0 & -B_1^{-T} B_1^{-1} \end{bmatrix} \begin{bmatrix} \mathbf{x} \\ \check{\mathbf{y}} \end{bmatrix} > 0, \, \forall \begin{bmatrix} \mathbf{x} \\ \check{\mathbf{y}} \end{bmatrix} \in \mathfrak{U} \right)\end{aligned} \tag{B.40}$$

provided that

$$\exists \begin{bmatrix} \mathbf{x} \\ \check{\mathbf{y}} \end{bmatrix} \in \mathfrak{U} : \begin{bmatrix} \mathbf{x} \\ \check{\mathbf{y}} \end{bmatrix}^T \begin{bmatrix} \widetilde{C}_1 \widetilde{C}_1^T & 0 \\ 0 & -\widetilde{B}_1^{-T} \widetilde{B}_1^{-1} \end{bmatrix} \begin{bmatrix} \mathbf{x} \\ \check{\mathbf{y}} \end{bmatrix} > 0 \tag{B.41}$$

Thus, B.24 may be augmented as

$$\begin{aligned}\min_{\{W,V,R\} \subset \mathbb{S}_{++}^{n_x}, \tau \geq 0} \quad & \operatorname{tr}(W) + \operatorname{tr}(V) \\ & \mathbf{x}^T V \mathbf{x} - \check{\mathbf{y}}^T R \check{\mathbf{y}} > 0, \quad \forall \begin{bmatrix} \mathbf{x} \\ \check{\mathbf{y}} \end{bmatrix} \in \mathfrak{B}_i \\ & \begin{bmatrix} V & 0 \\ 0 & -R \end{bmatrix} - \tau \begin{bmatrix} \widetilde{C}_1 \widetilde{C}_1^T & 0 \\ 0 & -\widetilde{B}_1^{-T} \widetilde{B}_1^{-1} \end{bmatrix} > 0 \\ & \begin{bmatrix} W & 0 \\ 0 & R \end{bmatrix} > 0\end{aligned} \tag{B.42}$$

The algorithm proceeds as follows.

1. Initialisation:

   a. Choose parameters: grid resolution $\left(\frac{1}{2}n_l\right) \in \mathbb{Z}^1_{++}$; parameter variation threshold $\epsilon_P \in \mathbb{R}^1_{++}$; joint variation threshold $\epsilon_J \in \mathbb{R}^1_{++}$; joint variation confirmation sample set cardinality n_c; ellipsoidal variation sample set cardinality n_s; ellipsoidal variation sample set partition maximum cardinality n_b; *e.g.* $n_l = 50$, $\epsilon_P = 0.1$, $\epsilon_J = 0.4$, $n_c = 20$, $n_s = 1000$ and $n_b = 100$.

   b. Calculate the gridded gain $G \in \mathbb{R}^{n_y \times n_x \times n_l}$, linear gain $F \in \mathbb{R}^{n_y \times n_x}$ and remainder $R \in \mathbb{R}^{n_y \times n_x \times n_l}$ of $\mathbf{f}(\mathbf{x}, \boldsymbol{\rho})$ as

$$G_{qpl} = \frac{f_q\left(\overline{x}_p u\left(l\right)\mathbf{e}_p, \boldsymbol{\rho}_0\right)}{\overline{x}_p u\left(l\right)} \tag{B.43}$$

$$F_{qp} = \frac{1}{2}\left(\max_l\left(G_{qpl}\right) + \min_l\left(G_{qpl}\right)\right) \tag{B.44}$$

   and

$$R_{qpl} = G_{qpl} - F_{qp} \tag{B.45}$$

   for all $q = [1, n_y] \cap \mathbb{Z}$, $p = [1, n_x] \cap \mathbb{Z}$, $l = [1, n_l] \cap \mathbb{Z}$. Calculate parameter variation map $M \in \mathbb{B}^{n_y \times n_x}$ of G, where M_{qp} is true if and only if

$$\frac{\max_l\left(R_{qpl}\overline{x}_p\right)}{\max_i\left(\left|F_{qi}\right|\overline{x}_i\right)} > \epsilon_P \tag{B.46}$$

   where $\mathbb{B}$ is the boolean space.

   c. Set $B = \emptyset$, $\Delta = \emptyset$, $C = \emptyset$ and $g = 0$.

Description: Initialise algorithm parameters. Calculate G, which represents the gain of $\mathbf{f}(\mathbf{x}, \boldsymbol{\rho})$ along each input component, where the gridded input is aligned with the third dimension and $\boldsymbol{\rho}$ is fixed at its nominal. The maximum output variation of G is compared to the maximum nominal output, to determine which gain variations are sufficiently large to be included as parameter variation. [4]

4. ϵ_P and ϵ_J is chosen such that the structured uncertainty gain Δ maintains a computationally viable size for controller synthesis, *e.g.* if there is variation in all gain components and ϵ_P and ϵ_J are poorly chosen, the size of Δ may grow to be $n_y n_x \times n_y n_x$.

2. Include independent and joint parameter variation:
   Set counters $m = 1$, $k = 1$ and repeat{ [**outer loop**]

   a. If M_{mk}, then

      i. Reset in succession: $B = \begin{bmatrix} B & \max_l (R_{mkl})\, \mathbf{e}_m \end{bmatrix}$; $\Delta = \text{blkdiag}\,(\Delta, \delta_{g+1})$; $C = \begin{bmatrix} C & \mathbf{e}_k \end{bmatrix}$; $g = g + 1$.

      ii. Set counters: $q = m$; $p = k$. Repeat{ [**intermediate loop**]

         A. If M_{qp}, $(q == m)$ and $(p \neq k)$, then set counter $i = 1$ and repeat{ [**inner loop**]

            I. Set $s_I = \frac{\overline{x}_k}{\overline{x}_p}\,(3 - 2i)$. Solve

$$\begin{aligned} \min_{\{\overline{a},\underline{a}\}\subset\mathbb{R}^1} \quad & \overline{a} - \underline{a} \\ \text{s.t.} \quad & \underline{a} < \widetilde{R}_{qpl} < \overline{a}, \quad \forall l \in [1, n_l] \cap \mathbb{Z} \\ & \widetilde{R}_{qpl} := R_{qpl} - s_I R_{mkw} \\ & w := \begin{cases} l & \text{if } s_I > 0 \\ n_l + 1 - l & \text{if } s_I < 0 \end{cases} \end{aligned} \tag{B.47}$$

            II. If $\left(\frac{\overline{a} - \underline{a}}{2 \max_{l \in [1, n_l] \cap \mathbb{Z}} \left(R_{qpl} \right)} < \epsilon_J \right)$, then

a) Calculate $\boldsymbol{\varsigma} = \begin{bmatrix} \varsigma_1 & \varsigma_2 & \cdots & \varsigma_{n_c} \end{bmatrix}^T \in \mathbb{R}^{n_c \times 1}$

$$\begin{aligned} \hat{\mathbf{c}} &= \begin{bmatrix} C_{1g} & C_{2g} & \cdots & C_{n_x g} \end{bmatrix}^T + s_I \mathbf{e}_p \\ \mathbf{r}_j &= \operatorname{diag}\left(\begin{bmatrix} \alpha_1 \overline{x}_1 & \alpha_2 \overline{x}_2 & \cdots & \alpha_{n_x} \overline{x}_{n_x} \end{bmatrix}^T \right) (2\boldsymbol{\kappa}_j - \mathbf{1}_{n_x \times 1}) \in \mathbb{R}^{n_x \times 1} \\ \alpha_z &= \begin{cases} 1 & \text{if } \mathbf{e}_z^T \hat{\mathbf{c}} \neq 0 \\ 0 & \text{otherwise} \end{cases} \\ \mathbf{h}_j &= \mathbf{r}_j - \left(\frac{\hat{\mathbf{c}}^T \mathbf{r}_j}{\hat{\mathbf{c}}^T \hat{\mathbf{c}}} \right) \hat{\mathbf{c}} \\ \varsigma_j &= \frac{f_q(\mathbf{h}_j, \boldsymbol{\rho}_0)}{\mathbf{e}_p^T \mathbf{h}_j} \end{aligned} \tag{B.48}$$

where $\boldsymbol{\kappa}_j \in \mathbb{R}^{n_x \times 1}$ is the unit density random variable.

b) If $\left(\frac{\max_{j \in [1,n_c] \cap \mathbb{Z}}(\varsigma_j) - \min_{j \in [1,n_c] \cap \mathbb{Z}}(\varsigma_j)}{2 \max_{l \in [1,n_l] \cap \mathbb{Z}}(R_{qpl})} < \epsilon_J \right)$, then reset: $C_{pg} = s_I$; $R_{qpl} = \widetilde{R}_{qpl} - \frac{1}{2}(\overline{a} + \underline{a})$; $F_{qp} = F_{qp} + \frac{1}{2}(\overline{a} + \underline{a})$; counter $i = i + 1$.

III. If $C_{pg} \neq 0$, then recalculate M_{qp} with (B.46).

IV. Reset counter $i = i + 1$.

} [**inner loop**] until $i > 2$. Clear counter i.

B. If M_{qp}, $(q \neq m)$ and $(p == k)$, then

I. Solve

$$\begin{aligned} \min_{\{\overline{a}, \underline{a}, s_O\} \subset \mathbb{R}^1} \quad & \overline{a} - \underline{a} \\ \text{s.t.} \quad & \underline{a} < \widetilde{R}_{qpl} < \overline{a}, \quad \forall l \in [1, n_l] \cap \mathbb{Z} \\ & \widetilde{R}_{qpl} := R_{qpl} + s_O R_{mkl} \end{aligned} \tag{B.49}$$

II. If $\left(\frac{\overline{a}-\underline{a}}{2\max_{l\in[1,N]\cap\mathbb{Z}}\left(R_{qpl}\right)}<\epsilon_J\right)$, then

a) Calculate $\boldsymbol{\varsigma}=\begin{bmatrix}\varsigma_1 & \varsigma_2 & \cdots & \varsigma_{n_c}\end{bmatrix}^T\in\mathbb{R}^{n_c\times 1}$

$$\begin{aligned}
\hat{\mathbf{c}} &= \begin{bmatrix}C_{1g} & C_{2g} & \cdots & C_{n_xg}\end{bmatrix}^T\\
\mathbf{r}_j &= \operatorname{diag}\left(\begin{bmatrix}\alpha_1\overline{x}_1 & \alpha_2\overline{x}_2 & \cdots & \alpha_{n_x}\overline{x}_{n_x}\end{bmatrix}^T\right)\left(2\boldsymbol{\kappa}_j-\mathbf{1}_{n_x\times 1}\right)\in\mathbb{R}^{n_x\times 1}\\
\alpha_z &= \begin{cases}1 & \text{if } C_{zg}\neq 0\\ 0 & \text{otherwise}\end{cases}\\
\mathbf{h}_j &= \mathbf{r}_j-\left(\frac{\hat{\mathbf{c}}^T\mathbf{r}_j}{\hat{\mathbf{c}}^T\hat{\mathbf{c}}}\right)\hat{\mathbf{c}}\\
\varsigma_j &= \frac{f_q\left(\mathbf{h}_j,\boldsymbol{\rho}_0\right)}{\mathbf{e}_p^T\mathbf{h}_j}
\end{aligned}\tag{B.50}$$

where $\boldsymbol{\kappa}_j\in\mathbb{R}^{n_x\times 1}$ is the unit density random variable.

b) If $\left(\frac{\max_{j\in[1,n_c]\cap\mathbb{Z}}(\varsigma_j)-\min_{j\in[1,n_c]\cap\mathbb{Z}}(\varsigma_j)}{2\max_{l\in[1,n_l]\cap\mathbb{Z}}\left(R_{qpl}\right)}<\epsilon_J\right)$, then for all $i\in[1,n_x]\cap\mathbb{Z}$, $l\in[1,n_l]\cap\mathbb{Z}$ reset in succession: $B_{qg}=-s_OB_{mg}$; $R_{qil}=R_{qil}-C_{ig}R_{qpw}$, $i\neq p$, $w:=\begin{cases}l & \text{if } C_{ig}\geq 0\\ n_l+1-l & \text{if } C_{ig}<0\end{cases}$; $R_{qpl}=\widetilde{R}_{qpl}$; $F_{qi}=F_{qi}+\varepsilon F_{qi}$, $\varepsilon F_{qi}:=\frac{1}{2}\left(\max_{l\in[1,n_l]\cap\mathbb{Z}}\left(R_{qil}\right)+\min_{l\in[1,n_l]\cap\mathbb{Z}}\left(R_{qil}\right)\right)$; $R_{qil}=R_{qil}-\varepsilon F_{qi}$; M_{qi} with (B.46).

C. Reset counter $p=p+1$. If $p>n_x$, then reset counters $p=1$ and $q=q+1$.

} [**intermediate loop**] until $q>n_y$

iii. Reset $R_{mkl}=0$, $\forall l\in[1,n_l]\cap\mathbb{Z}$. Reset $M_{mk}=0$.

b. Reset counter $k=k+1$. If $k>n_x$, then reset counters $k=1$ and $m=m+1$.

} [**outer loop**] until $m > n_y$. Clear counters m, k, q and p.

Description: Find gain variation element R_{mk} with sufficiently large variation, quantified by B.46*, and include in F_Δ as $\max_l (R_{mkl})\, \mathbf{e}_m \delta_{g+1}(t)\, \mathbf{e}_k^T$. Then, find other sufficiently large gain variation elements R_{qp} with enough similarity to include as joint variation, quantified by* B.17 and B.13, and include with $\delta_{g+1}(t)$ as described by (B.10) and (B.11).

3. Include ellipsoidal variation:

   a. Generate n_s random I/O samples

$$\begin{aligned} \mathbf{x}_j &= \operatorname{diag}\left(\begin{bmatrix} \overline{x}_1 & \overline{x}_2 & \cdots & \overline{x}_{n_x} \end{bmatrix}^T \right) (2\acute{\boldsymbol{\kappa}}_j - \mathbf{1}_{n_x \times 1}) \in \mathbb{R}^{n_x \times 1} \\ \boldsymbol{\rho}_j &= \operatorname{diag}\left(\begin{bmatrix} \overline{\rho}_1 & \overline{\rho}_2 & \cdots & \overline{\rho}_{n_\rho} \end{bmatrix}^T \right) (2\grave{\boldsymbol{\kappa}}_j - \mathbf{1}_{n_\rho \times 1}) \in \mathbb{R}^{n_x \times 1} \\ \mathbf{y}_j &= \mathbf{f}\left(\mathbf{x}_j, \boldsymbol{\rho}_j \right) \end{aligned} \tag{B.51}$$

   where $j = 1, 2, \ldots, n_s$, $\acute{\boldsymbol{\kappa}}_j \in \mathbb{R}^{n_x \times 1}$ and $\grave{\boldsymbol{\kappa}}_j \in \mathbb{R}^{n_\rho \times 1}$ are the unit density random variables.

   b. Calculate minimum distance vector $\check{\mathbf{y}}_j$ outside $\left(F + \sum_{i=1}^{g} \mathbf{b}_i \delta_i \mathbf{c}_i^T \right) \mathbf{x}_j$

$$\begin{aligned} \min_{\begin{bmatrix} \delta_1 & \delta_2 & \cdots & \delta_g \end{bmatrix}^T \in \mathbb{R}^{g \times 1}} \quad & a \\ \text{s.t.} \quad & -1 < \delta_i < 1, \quad i = 1, 2, \ldots, g \\ & \begin{bmatrix} a & \check{\mathbf{y}}_j^T \\ \check{\mathbf{y}}_j & I_{n_y} \end{bmatrix} > 0 \\ & \check{\mathbf{y}}_j := \mathbf{y}_j - \left(F + \sum_{i=1}^{g} \mathbf{b}_i \delta_i \mathbf{c}_i^T \right) \mathbf{x}_j \end{aligned} \tag{B.52}$$

   c. Set $n_d = \max(n_x, n_y)$. If $n_d > n_x$, then reset $\mathbf{x}_j = \begin{bmatrix} \mathbf{x}_j^T & \mathbf{0}_{1 \times (n_d - n_x)} \end{bmatrix}^T$, otherwise if $n_d > n_y$, then reset $\check{\mathbf{y}}_j = \begin{bmatrix} \check{\mathbf{y}}_j^T & \mathbf{0}_{1 \times (n_d - n_y)} \end{bmatrix}^T$.

d. Set counter $i = 0$. Set $\widetilde{B}_1 = \mathbf{0}_{n_d \times n_d}$ and $\widetilde{C}_1 = \mathbf{0}_{n_d \times n_d}$. Repeat{ [**loop**]

i. Solve

$$\begin{aligned}
\min_{\{W,V,R\} \subset \mathbb{S}^{n_x}_{++}, \tau \geq 0} \quad & \operatorname{tr}(W) + \operatorname{tr}(V) \\
\text{s.t.} \quad & \operatorname{diag}\left(\operatorname{diag}\left(X_i^T V X_i - \check{Y}_i^T R \check{Y}_i\right)\right) > 0 \\
& \begin{bmatrix} V & 0 \\ 0 & -R \end{bmatrix} - \tau \begin{bmatrix} \widetilde{C}_1 \widetilde{C}_1^T & 0 \\ 0 & -\widetilde{B}_1^{-T} \widetilde{B}_1^{-1} \end{bmatrix} > 0 \\
& \begin{bmatrix} W & 0 \\ 0 & R \end{bmatrix} > 0 \\
& X_i := \begin{bmatrix} \mathbf{x}_{(1+n_b i)} & \mathbf{x}_{(2+n_b i)} & \cdots & \mathbf{x}_{(j+n_b i)} \end{bmatrix} \\
& \check{Y}_i := \begin{bmatrix} \check{\mathbf{y}}_{(1+n_b i)} & \check{\mathbf{y}}_{(2+n_b i)} & \cdots & \check{\mathbf{y}}_{(j+n_b i)} \end{bmatrix} \\
& j := \begin{cases} n_b & \text{if } n_s - n_b i \geq n_b \\ n_s - n_b i & \text{if } n_s - n_b i < n_b \end{cases}
\end{aligned}$$

ii. Recalculate $\widetilde{C}_1 = \operatorname{chol}(V)^T$ and $\widetilde{B}_1 = \operatorname{chol}(R)^{-1}$.

iii. Reset counter $i = i + 1$.

} [**loop**] until $n_s - n_b i \leq 0$. Clear counter i.

e. Reset: $B = \begin{bmatrix} B & \left(\begin{bmatrix} I & \mathbf{0}_{n_y \times (n_d - n_y)} \end{bmatrix} \widetilde{B}_1\right) \end{bmatrix}$; $\Delta = \operatorname{blkdiag}(\Delta, \Delta_1)$; $C = \begin{bmatrix} C & \left(\begin{bmatrix} I & \mathbf{0}_{n_x \times (n_d - n_x)} \end{bmatrix} \widetilde{C}_1\right) \end{bmatrix}$.

Description: n_s random I/O pairs are generated, for which $\check{\mathbf{y}}$, in (B.18)*, is calculated as the output component unaccounted for by the calculated parameter variation, with LMI optimisation problem* (B.52)*. Then, the ellipsoidal variation is iteratively calculated via LMI optimisation problem* (B.42)*.*

The algorithm is implemented with MATLAB, and given by Listing B.1 below followed by an example to illustrate its use. The implementation has the additional functionality of allowing multiple output column vectors, corresponding to multiple systems or operating points, for which a single norm-bounded state-space model is calculated. Furthermore, joint variation is approximated for a single output vector, before it is included for multiple output column vectors, and is done to reduce calculation time.

Listing B.1: Norm-bounded state-space model calculation

```
function [modelSnbu] = ehcIO2Snbu(IOevalCall,par,xMax)
% Input:-IOevalCall: character array defining system IO map, invoked by eval.m, used to calculate system output y for predefined input x,
%                    e.g. IOevalCall='y=functionName(x,par.element1,par.element2,...,par.elementN,sFlag,uFlag)'
%       -par: system IO map parameters (used in IOevalCall)
%       -xMax: maximum size of system input x
% Output modelSnbu.*    -A: system linear gain
%                       -b: parameter variation output matrix
%                       -c: parameter variation input matrix
%                       -B: unstructured variation output matrix
%                       -C: unstructured variation input matrix
%% ehcIO2Snbu.m parameters
eP=0.01;            % threshold factor of parameter variation relative to maximum linear output
eJ=0.9;             % threshold of joint parameter variation
iSys=1;             % system used to build joint variation map
tol=1e-8;           % threshold of finite gain system and for non-zero gain, i.e. finite if tol > y for x=0 and y(q)/x(p)=0 if <tol
nl=20;              % resolution of decoupled input used for F,b&c calculation, and to confirm joint variation
nc=10;              % confirmation sample set cardinality
ns=0;            % cardinality of set S used to calculate ellipsoidal/unstructured variation
nb=200;             % maximum cardinality of a partition of S
OPTS=sdpsettings; OPTS.solver='sdpt3'; OPTS.verbose=0;    % SDP solver options (suggest using sdpt3)
OPTS.cachesolvers=1; OPTS.shift=1e-8;
sFlag=0;            % parameter (structured) variation flag (used in IOevalCall)
uFlag=0;            % unstructured variation flag (used in IOevalCall)
%% system dimensions
x=zeros(size(xMax));
evalc(IOevalCall);
% test that IOevalCall specifies finite gain, i.e. y=0 for x=0
if max(abs(y)>tol)
    error(['|y|=',num2str(abs(y)),'> tol. y required to be zero (<tol) for x=0']);
end
nx=size(x,1);
ny=size(y,1);
nSys=size(y,2);             % number of systems (equals columns of y)
% calc. tIOpair used to estimate calc. time. Assume it takes approx 5 runs before tIOpair reaches steady-state
```

```
for i=1:5
    x=xMax.*(2.*rand(size(xMax))-1);
    tStartEval=cputime;
    evalc(IOevalCall);
    tIOpair=cputime-tStartEval;
end

%% I/O pairs for decoupled inputs
sFlag=1; uFlag=0;
% ensure that nl is even to exclude x=0 for gain calculation
nl=ceil(nl/(2*nSys))*2;
nc=ceil(nc/nSys);
% estimate decoupled I/O pairs calculation time and print to screen
disp(['Decoupled I/O pairs calculation time (est):',num2str(nx*nl*tIOpair
    ),' sec.']);
tStart=cputime;
E=eye(nx);
G=zeros(ny,nx,nl,nSys);
for p=1:nx
    for l=1:nl
        ul=-1+2*(l-1)/(nl-1);
        x=xMax*ul.*E(:,p);
        evalc(IOevalCall);   % y
        G(:,p,l,:)=y./x(p);
    end;
end; clear E ul p l x y;
disp(['Decoupled I/O pairs calculation time:',num2str(cputime-tStart),'
    sec.']); clear tStart;
%% calc. initial SNBU model G=F+R=F+[b,B]*blkdiag(d,D)*[c;C]'
F=(max(max(G,[],4),[],3)+min(min(G,[],4),[],3))./2;
R=zeros(size(G));
for l=1:nl
    for j=1:nSys
        R(:,:,l,j)=G(:,:,l,j)-F;
        R(:,:,l,j)=(1-(abs(R(:,:,l,j))<tol)).*R(:,:,l,j);   % remove
            small variation, i.e. <tol
    end
end

%% Parameter (structured) uncertainty Map MP (boolean)
MP=((max(max(R,[],4),[],3)*diag(xMax))>(eP.*max(abs(F)*diag(xMax),[],2)*
    ones(1,nx)));

%% Joint variation parameters map 'bB' and 'cB'
% Find joint variation in the iSys'th System and map using bB and cB (
    used to reduce computation time when nSys>1)
bB=zeros(ny,0);            % bB in {0,1} (boolean)
cU=zeros(nx,0);            % cU in {-1,0,1}

% sdp variables
aLower=sdpvar(1,1,'full');
aUpper=sdpvar(1,1,'full');
for m=1:ny
    for k=1:nx
        if MP(m,k)==1
            bB(m,(end+1))=1;
            cU(k,(end+1))=1;
```

```
87              % search for variations similar to G(m,k)
88              for q=m:ny
89                  for p=k:nx
90                      % similarity in same row, i.e. q==m
91                      if (MP(q,p)==1) && (q==m) && (p~=k)
92                          i=1;
93                          while i<=2
94                              sI=(xMax(k)/xMax(p))*(3-2*i); sO=-sI;
95                              R_qp(:,1)=R(q,p,:,iSys);
96                              R_mk(:,1)=flipdim(R(m,k,:,iSys),(1+2*(i-1)));
97                              rmd=R_qp+sO.*R_mk;
98                              LMI=[(aLower<rmd),(rmd<aUpper)];
99                              OBJ=aUpper-aLower;
100                             solvesdp(LMI,OBJ,OPTS);
101                             clear R_mk rmd LMI sO;
102                             if (double(OBJ)/(max(R_qp)-min(R_qp))) < eJ
103                                 % confirmation
104                                 E=eye(nx);
105                                 cHat=cU(:,end).*(xMax(k)./xMax)+sI*E(:,p)
                                        ;
106                                 varSigma=zeros(nc,1);
107                                 for j=1:nc
108                                     r_j=(cHat~=0).*xMax.*(2.*rand(nx,1)
                                            -1);
109                                     h_j=r_j-((cHat'*r_j)/(cHat'*cHat)).*
                                            cHat;
110                                     x=h_j;
111                                     evalc(IOevalCall);   % y
112                                     varSigma(j)=y(q,iSys)/x(p);
113                                 end; clear E cHat j r_j h_j x y;
114                                 if ((max(varSigma)-min(varSigma))/(max(
                                        R_qp)-min(R_qp))) < eJ
115                                     cU(p,end)=1-2*(sI<0);
116                                     i=i+1;
117                                 end; clear varSigma sI;
118                             end; clear OBJ R_qp;
119                             i=i+1;
120                         end; clear i;
121
122                     % similarity in same column, i.e. p==k
123                     elseif (MP(q,p)==1) && (q~=m) && (p==k)
124                         R_qp(:,1)=R(q,p,:,iSys);
125                         R_mk(:,1)=R(m,k,:,iSys);
126                         sO=sdpvar(1,1,'symmetric');
127                         rmd=R_qp+sO.*R_mk;
128                         LMI=[(aLower<rmd),(rmd<aUpper)];
129                         OBJ=aUpper-aLower;
130                         solvesdp(LMI,OBJ,OPTS);
131                         clear R_mk sO rmd LMI;
132                         if (double(OBJ)/(max(R_qp)-min(R_qp))) < eJ
133                             % confirmation
134                             cHat=cU(:,end).*(xMax(k)./xMax);
135                             varSigma=zeros(nc,1);
136                             for j=1:nc
137                                 r_j=(cHat~=0).*xMax.*(2.*rand(nx,1)-1);
138                                 h_j=r_j-((cHat'*r_j)/(cHat'*cHat)).*cHat;
139                                 x=h_j;
```

```
                                evalc(IOevalCall);   % y
                                varSigma(j)=y(q,iSys)/x(p);
                            end; clear j r_j h_j x y;
                            if ((max(varSigma)-min(varSigma))/(max(R_qp)-
                                min(R_qp))) < eJ
                                bB(q,end)=1;
                            end; clear varSigma;
                        end; clear OBJ R_qp;

                    end;   % end to 'if (MP(q,p)==1) && (q==m) && (p~=k)'
                end;    % end to 'for p=k:nx'
            end;    % end to 'for q=m:ny'
        end;    % end to 'if MP(m,k)==1'
    end;    % end to 'for k=1:nx'
end; clear m k q p; % end to 'for m=1:ny'
cB=abs(cU); clear cU;

%% parameter variation
b=zeros(ny,0);
c=zeros(nx,0);
for m=1:ny
    for k=1:nx
        if MP(m,k)==1
            b(m,(end+1))=(max(max(R(m,k,:,:),[],4),[],3)-min(min(R(m,k
                ,:,:),[],4),[],3))./2;
            c(k,(end+1))=1;
            % search for variations similar to G(m,k)
            iJ=ehcIndexLogic2Dec(((bB(m,:)~=0).*(cB(k,:)~=0))');    %
                converts Logic index to decimal, e.g. ehcIndexLogic2Dec
                ([1;0;0;1;1])=[1;4;5]
            for q=m:ny
                for p=k:nx
                    % similarity in same row, i.e. q==m
                    if (MP(q,p)==1) && (q==m) && (p~=k) && max(abs(cB(p,
                        iJ)))
                        i=1;
                        while i<=2
                            sI=(xMax(k)/xMax(p))*(3-2*i); sO=-sI;
                            R_qp(:,1)=reshape(R(q,p,:,:),[],1);
                            R_mk(:,1)=reshape(flipdim(R(m,k,:,:),(1+2*(i
                                -1))),[],1);
                            rmd=R_qp+sO.*R_mk;
                            LMI=[(aLower<rmd),(rmd<aUpper)];
                            OBJ=aUpper-aLower;
                            solvesdp(LMI,OBJ,OPTS);
                            clear R_mk LMI;
                            if (double(OBJ)/(max(R_qp)-min(R_qp))) < eJ
                                % confirmation
                                E=eye(nx);
                                cHat=c(:,end)+sI*E(:,p);
                                varSigma=zeros(nc,nSys);
                                for j=1:nc
                                    r_j=(cHat~=0).*xMax.*(2.*rand(nx,1)
                                        -1);
                                    h_j=r_j-((cHat'*r_j)/(cHat'*cHat)).*
                                        cHat;
                                    x=h_j;
```

```
189                                 evalc(IOevalCall);   % y
190                                 varSigma(j,:)=y(q,:)./x(p);
191                             end; clear E cHat j r_j h_j x y;
192                             if ((max(max(varSigma))-min(min(varSigma)
                                    ))/(max(R_qp)-min(R_qp))) < eJ
193                                 c(p,end)=sI;
194                                 % reset variation R and linear gain F
195                                 R(q,p,:,:)=R(q,p,:,:)+sO.*flipdim(R(m
                                        ,k,:,:),(1+2*(i-1)));
196                                 eF_qp=(max(max(R(q,p,:,:)))+min(min(R
                                        (q,p,:,:)))))./2;
197                                 F(q,p)=F(q,p)+eF_qp;
198                                 R(q,p,:,:)=R(q,p,:,:)-eF_qp.*ones
                                        (1,1,nl,nSys);
199                                 MP=((max(max(R,[],4),[],3)*diag(xMax)
                                        )>(eP.*max(abs(F)*diag(xMax)
                                        ,[],2)*ones(1,nx)));
200                                 i=i+1;
201                             end; clear varSigma sI sO;
202                         end; clear OBJ R_qp;
203                         i=i+1;
204                     end; clear i;
205
206                 % similarity in same column, i.e. p==k
207                 elseif (MP(q,p)==1) && (q~=m) && (p==k) && max(bB(q,
                        iJ)~=0)
208                     R_qp(:,1)=reshape(R(q,p,:,:),[],1);
209                     R_mk(:,1)=reshape(R(m,k,:,:),[],1);
210                     sO=sdpvar(1,1,'symmetric');
211                     rmd=R_qp+sO.*R_mk;
212                     LMI=[(aLower<rmd),(rmd<aUpper)];
213                     OBJ=aUpper-aLower;
214                     solvesdp(LMI,OBJ,OPTS);
215                     clear R_mk rmd LMI;
216                     if (double(OBJ)/(max(R_qp)-min(R_qp))) < eJ
217                         % confirmation
218                         cHat=c(:,end);
219                         varSigma=zeros(nc,nSys);
220                         for j=1:nc
221                             r_j=(cHat~=0).*xMax.*(2.*rand(nx,1)-1);
222                             h_j=r_j-((cHat'*r_j)/(cHat'*cHat)).*cHat;
223                             x=h_j;
224                             evalc(IOevalCall);   % y
225                             varSigma(j,:)=y(q,:)./x(p);
226                         end; clear j r_j h_j x y;
227                         if ((max(max(varSigma))-min(min(varSigma)))/(
                                max(R_qp)-min(R_qp))) < eJ
228                             b(q,end)=-sO*b(m,end);
229
230                             % reset variation R and linear gain F
231                             for i=1:nx
232                                 if c(i,end)~=0
233                                     R(q,i,:,:)=R(q,i,:,:)-c(i,end).*
                                            flipdim((-double(sO).*R(m,k
                                            ,:,:)),(1+2*(c(i,end)<0)));
234                                     eF_qi=(max(max(R(q,i,:,:)))+min(
                                            min(R(q,i,:,:)))))./2;
```

```
                                        F(q,i)=F(q,i)+eF_qi;
                                        R(q,i,:,:)=R(q,i,:,:)-eF_qi.*ones
                                            (1,1,nl,nSys);
                                    end
                                end; clear i sO eF_qi
                                MP=((max(max(R,[],4),[],3)*diag(xMax))>(
                                    eP.*max(abs(F)*diag(xMax),[],2)*ones
                                    (1,nx)));
                            end; clear varSigma;
                        end; clear OBJ R_qp;
                    end;    % end to 'if (MP(q,p)==1) && (q==m) && (p~=k)
                         && max(abs(cB(p,iJ)))'
                end;    % end to 'for p=k:nx'
            end;    % end to 'for q=m:ny'
            R(m,k,:,:)=R(m,k,:,:)-R(m,k,:,:);
            % recalculate parameter map
            MP=((max(max(R,[],4),[],3)*diag(xMax))>(eP.*max(abs(F)*diag(
                xMax),[],2)*ones(1,nx)));
        end;    % end to 'MP(m,k)==1'
    end;    % end to 'for k=1:nx'
end; clear m k q p;     % end to 'for m=1:ny'

%% test that sufficiently large parameter variations are included with b
    and c
MP=((max(max(R,[],4),[],3)*diag(xMax))>(eP.*max(abs(F)*diag(xMax),[],2)*
    ones(1,nx)));
if sum(sum(MP))~=0
    error('All sufficient parameter variation not included with b and c.'
        );
end

%% I/O pairs for coupled inputs (for unstructured variation calculation)
if ns~=0
sFlag=0; uFlag=1;
% estimate calculation time
disp(['Coupled I/O pairs calculation time (est):',num2str(ns*(tIOpair/
    nSys)),' sec.']);
tStart=cputime;
nP=ceil(ns/nSys);
xRand=(xMax*ones(1,nP)).*(2.*rand(nx,nP)-1);
ySave=zeros(ny,nP,nSys);
for i=1:nP
    x=xRand(:,i);
    evalc(IOevalCall);
    ySave(:,i,:)=y;
end; clear i nP;
disp(['Coupled I/O pairs calculation time:',num2str(cputime-tStart),' sec
    .']); clear tStart;
% re-organise I/O pairs
X=zeros(nx,ns);
Y=zeros(ny,ns);
rmd=ns-(ceil(ns/nSys)-1)*nSys;
for i=1:ceil(ns/nSys);
    iStart=1+nSys*(i-1);
    iEnd=nSys*i-(i==ceil(ns/nSys))*(nSys-rmd);
    X(:,iStart:iEnd)=xRand(:,i)*ones(1,(iEnd-iStart+1));
    Y(:,iStart:iEnd)=ySave(:,i,1:(iEnd-iStart+1));
```

```
end;

%% calc. minimum components of y outside (F+b*d(t)*c), i.e. yD:=y-(F+b*d*c)x: min norm((yD),2)^2
tStart=cputime;
YD=zeros(size(Y));
% SDP variables
delta=diag(sdpvar(size(b,2),1,'full'));
aux=sdpvar(1,1,'full');
for i=1:ns
    YD_i=(Y(:,i)-(F+b*delta*c')*X(:,i));
    LMI=[aux,YD_i';...
         YD_i,eye(ny)]>0;
    LMI=[LMI,(delta>-eye(size(b,2))),(delta<eye(size(b,2)))];
    OBJ=aux;
    if i==5; tStart5=cputime; end;
    solvesdp(LMI,OBJ,OPTS);
    % estimate calculation time
    if i==5; disp(['Unstructured variation ouput components calculation time (est):',num2str(ns*(cputime-tStart5)),' sec.']); clear tStart5; end;
    YD(:,i)=double(YD_i);
    clear YD_i LMI OBJ;
end; clear i aux delta;
disp(['Unstructured variation ouput components calculation time:',num2str(cputime-tStart),' sec.']); clear tStart;

%% unstructured variation calc. via LMI optimization
tStart=cputime;
% augment I/O to have equal dimensions by appending zeros (required by method)
if ny>nx; X=[X;zeros((ny-nx),ns)]; elseif ny<nx; YD=[YD;zeros((nx-ny),ns)]; end;
nD=max([nx,ny]);
% SDP variables
V=sdpvar(nD,nD,'symmetric');            % V:=C*C'
R=sdpvar(nD,nD,'symmetric');            % R:=inv(B')*inv(B)
tau=sdpvar(1,1,'full');                 % S-procedure variable
Wupper=sdpvar(nD,nD,'symmetric');       % used as auxilary variable. W:=B*B'=inv(R); Wupper>inv(R).
trUpper=sdpvar(1,1,'full');
rmd=ns-(ceil(ns/nb)-1)*nb;
for i=1:ceil(ns/nb)
    iStart=1+nb*(i-1);
    iEnd=nb*i-(i==ceil(ns/nb))*(nb-rmd);
    X_i=X(:,iStart:iEnd);
    Y_i=YD(:,iStart:iEnd);
    LMI=[(V>0),(V>eye(nD)),(R>0),(blkdiag(Wupper,R)>0),(diag(Y_i'*R*Y_i)<diag(X_i'*V*X_i))]; % ,(trUpper>trace(Wupper)),(trUpper>trace(V))
    if i>1
       LMI=[LMI,(blkdiag(V,-R)-tau.*blkdiag(double(V),-double(R))>0),(tau>0)];
    end
    OBJ=trace(Wupper)+trace(V); %trUpper;
    if i==5; tStart5=cputime; end;
    solvesdp(LMI,OBJ,OPTS);
    if i==5; disp(['Unstructured variation calculation time (est):',
```

```
        num2str((ns/nb)*(cputime-tStart5)),' sec.']); clear tStart5; end;
330 end
331 C=chol(double(V))'; maxC=max(max(abs(C(1:nx,:)))); C=C./maxC;
332 B=chol(eye(nD)/double(R))'.*maxC;
333 disp(['Unstructured variation calculation time:',num2str(cputime-tStart),
    ' sec.']);
334 else
335     B=zeros(ny,0);
336     C=zeros(nx,0);
337 end
338
339 %% output
340 modelSnbu.A=F;
341 modelSnbu.b=b;
342 modelSnbu.c=c;
343 modelSnbu.B=B(1:ny,:);
344 modelSnbu.C=C(1:nx,:);
```

Listing B.2: Logic index to decimal index conversion.

```
1  function DEC = ehcIndexLogic2Dec(LOGIC)
2  % convert logic index to decimal indexing, e.g. ehcIndexLogic2Dec
       ([1;0;0;1;0])=[1;4]
3  sizeLOGIC=size(LOGIC); nLOGIC=sizeLOGIC(1); sumLOGIC=sum(LOGIC);
4  if (sizeLOGIC(2) ~= 1) || (sum((LOGIC==0)+(LOGIC==1))~=nLOGIC)
5      disp('Function ehcIndexLogic2Dec.m defined for input type logic
           column vector. Function return 0.');
6      DEC=0; return;
7  end
8  SUB1=[1:nLOGIC]'.*LOGIC;
9
10 SUB2=zeros(sumLOGIC,1);
11 i=1; j=1;
12 while (j<=sumLOGIC)
13     if LOGIC(i)==1
14         SUB2(j)=SUB1(i);
15         j=j+1;
16     end
17     i=i+1;
18 end
19 DEC=SUB2;
20 end
```

Example 2. Norm-bounded state-space model calculation of A330 flight mechanics via the algorithm in Listing B.1:

We are given the MATLAB function `flightMechanicsA330`$= \mathbf{f}_M$ defined as

$$\mathbf{f}_M := \Big\{ \mathbf{f}_M : \mathbb{R}^{10\times 1} \times \mathbb{R}^{6\times 1} \times \mathbb{R}^{8\times 1} \times \mathbb{R}^1 \times \mathbb{R}^1 \mapsto \mathbb{R}^{10\times 1},\ \dot{\mathbf{m}} = \mathbf{f}_M\left(\mathbf{m}, \mathbf{g}_A, \boldsymbol{\delta}, m_A, cg_A\right), \\ (2.7)\text{-}(2.18) \Big\} \tag{B.53}$$

`nT` trim points compactly written as `T` defined as

$$\mathtt{T} := \left[\begin{bmatrix} \mathbf{m} \\ \mathbf{g}_A \\ \boldsymbol{\delta} \\ m_A \\ cg_A \\ \dot{\mathbf{m}} \end{bmatrix}_{r,1} \quad \begin{bmatrix} \mathbf{m} \\ \mathbf{g}_A \\ \boldsymbol{\delta} \\ m_A \\ cg_A \\ \dot{\mathbf{m}} \end{bmatrix}_{r,2} \quad \cdots \quad \begin{bmatrix} \mathbf{m} \\ \mathbf{g}_A \\ \boldsymbol{\delta} \\ m_A \\ cg_A \\ \dot{\mathbf{m}} \end{bmatrix}_{r,\mathtt{nT}} \right] \tag{B.54}$$

such that

$$\max \left| \mathbf{f}_M \left(\mathbf{m}_{r,i}, \mathbf{g}_{Ar,i}, \boldsymbol{\delta}_{r,i}, m_{Ar,i}, cg_{Ar,i} \right) - \dot{\mathbf{m}}_{r,i} \right| < \mathtt{tol} \quad \forall i \in [1, 2, \ldots, \mathtt{nT}] \tag{B.55}$$

and `xMax` defined as

$$\mathtt{xMax} := \begin{bmatrix} \min \left(\max_{\varepsilon \mathbf{m} \in \mathfrak{D}_x} \left(\varepsilon \mathbf{m} \right), -\min_{\varepsilon \mathbf{m} \in \mathfrak{D}_x} \left(\varepsilon \mathbf{m} \right) \right) \\ \min \left(\max_{\varepsilon \mathbf{g} \in \mathfrak{D}_g} \left(\varepsilon \mathbf{g}_A \right), -\min_{\varepsilon \mathbf{g} \in \mathfrak{D}_g} \left(\varepsilon \mathbf{g}_A \right) \right) \\ \min \left(\max_{\varepsilon \boldsymbol{\delta} \in \mathfrak{D}_u} \left(\varepsilon \boldsymbol{\delta} \right), -\min_{\varepsilon \boldsymbol{\delta} \in \mathfrak{D}_u} \left(\varepsilon \boldsymbol{\delta} \right) \right) \end{bmatrix} \tag{B.56}$$

where (2.7)-(2.18) incorporate aerodynamic coefficient and moment of inertia data provided by Airbus and `tol` is set in line 15 of Listing **??** as the finite-gain tolerance. The norm-bounded state-space representation of $\mathbf{f}_M$ is calculated as

Listing B.3: A330 norm-bounded state-space model calculation example.

```
1  IOEval='[';
2  par.T=T;
3  for i=1:nT
4      index=num2str(i);
5      IOEval=[IOEval,'flightMechanicsA330(par.T(1:10,',index,')+x(1:10),par
           .T(11:16,',index,')+x(11:16),par.T(17:24,',index,')+x(17:24),par.
           T(25,',index,'),par.T(26,',index,'))-T(par.T(27:36,',index,')'];
6  if i~=nT; IOEval=[IOEval,','];
7  end
8  IOEval=[IOEval,']'];
9  varGain=ehcIO2Snbu(IOEval,par,xMax);
10 ix=1:10; ig=11:16; iu=17:24;
11 ssA330.A=varGain.A(ix,ix);
12 ssA330.Bg=varGain.A(ix,ig);
13 ssA330.Bu=varGain.A(ix,iu);
14 ssA330.Bp=[varGain.b,varGain.B];
15 ssA330.Cq=[varGain.c(:,ix);varGain.C(:,ix)];
16 ssA330.Dqg=[varGain.c(:,ig);varGain.C(:,ig)];
17 ssA330.Dqu=[varGain.c(:,iu);varGain.C(:,iu)];
18 ssA330.nd=size(varGain.b,2);
19 ssA330.nD=size(varGain.B,2);
```

The calculated state-space model `ssA330` represents the NLTV perturbation mechanics of the A330 at all trim points defined by (B.54).

B.2 Gain-scheduler

Refer to Section 4.1 and Figure 4.1.

Gain-scheduling is a popular approach used to extend the reach of a single linear controller over an entire operating envelope. A gain-scheduling controller calculates controller gains for its present operating point with controller gain values designed for surrounding operating points via some interpolation scheme. The algorithm presented finds a small simplex in the operating envelope containing the present operating point, with operating points corresponding to designed controllers as its corners, and linearly interpolating between its corners, and is implemented on-line. By using simplexes, continuity of the calculated gain is maintained as long as the operating point varies continuously. The theoretical bases is formulated as follows.

Any vector $\mathbf{v} \in \mathbb{R}^{n\times 1}$ may be described as a *unique* combination of n linearly independent vectors $\mathbf{v}_i \in \mathbb{R}^{n\times 1}$ $i = 1, 2, \ldots, n$, *i.e.*

$$\begin{aligned} \mathbf{v} &= a_1\mathbf{v}_1 + a_2\mathbf{v}_2 + \ldots + a_n\mathbf{v}_n = V\mathbf{a},\ \mathrm{rank}\,(V) = n \\ V &\coloneqq \begin{bmatrix} \mathbf{v}_1 & \mathbf{v}_2 & \cdots & \mathbf{v}_n \end{bmatrix},\ \mathbf{a} \coloneqq \begin{bmatrix} a_1 & a_2 & \cdots & a_n \end{bmatrix}^T \end{aligned} \tag{B.57}$$

where $\mathbf{a}$ is unique. Equivalently, any absolute point $\mathbf{x} \in \mathbb{R}^{n\times 1}$ may be described as a *unique* combination of n linearly independent vectors $\mathbf{v}_i \in \mathbb{R}^{n\times 1}$ $i = 1, 2, \ldots, n$ and the offset $\mathbf{x}_0 \coloneqq \mathbf{x} - \mathbf{v}$, *i.e.*

$$\mathbf{x} = \mathbf{v} + \mathbf{x}_0 = V\mathbf{a} + \mathbf{x}_0,\ \mathrm{rank}\,(V) = n \tag{B.58}$$

where each vector may be replaced by the subtraction of two points, given as

$$\begin{aligned} \mathbf{x} &= a_1(\mathbf{x}_1 - \mathbf{x}_0) + a_2(\mathbf{x}_2 - \mathbf{x}_0) + \ldots + a_n(\mathbf{x}_n - \mathbf{x}_0) + \mathbf{x}_0, \\ &\mathrm{rank}\left(\begin{bmatrix} (\mathbf{x}_1 - \mathbf{x}_0) & (\mathbf{x}_2 - \mathbf{x}_0) & \cdots & (\mathbf{x}_n - \mathbf{x}_0) \end{bmatrix}\right) = n \end{aligned} \tag{B.59}$$

Any set of $n+1$ points $\mathcal{S} \coloneqq \{\mathbf{x}_0, \mathbf{x}_1, \ldots, \mathbf{x}_n\}$ in $\mathbb{R}^{n\times 1}$, corresponding to n linearly independent vectors when subtracted, may geometrically be interpreted as an n-simplex by taking its interior $\mathrm{poly}\,(\mathcal{S})$, *e.g.* 1-simplex is a line, 2-simplex is a triangle, 3-triangle is a tetrahedron, and is the minimum number of points required to describe a volume in n-dimensional space.

Now, suppose that a gain $G(\mathbf{x})$ is linear in $\mathbf{x}$, then

$$\begin{aligned} G(\mathbf{x}) &= a_1(G_1 - G_0) + a_2(G_2 - G_0) + \ldots + a_n(G_n - G_0) + G_0, \\ G_i &\coloneqq G(\mathbf{x}_i),\ i = 0, 1, \ldots, n \end{aligned} \tag{B.60}$$

If $G(\mathbf{x})$ is non-linear, however, the simplex corners $\mathbf{x}_i$, $i = 0, 1, \ldots, n$ have to be sufficiently close to $\mathbf{x}$, and $G(\mathbf{x})$ has to be continuous for $G(\mathbf{x})$ to be accurately approximated by (B.60). This may be proven by considering the Taylor series expansion of $G(\mathbf{x})$. Furthermore, if $G(\mathbf{x})$ is non-linear and $\mathbf{a}$ is not unique, *i.e.* more than $n+1$ points are used to describe $\mathbf{x}$, then the linear approximation (B.60) of $G(\mathbf{x})$ is also not unique, causing complications in the calculation of $G(\mathbf{x})$ when required to be continuous over time. This motivates the use of simplexes to approximate $G(\mathbf{x})$.

The gain-scheduling scheme presented approximates a non-linear gain $G(\mathbf{x})$ with (B.60) by using the n-simplex $\mathcal{S} \coloneqq \{\mathbf{x}_0, \mathbf{x}_1, \ldots \mathbf{x}_n\}$ in a finite set of operating points

$\mathcal{P} = \{\mathbf{p}_1, \mathbf{p}_2, \ldots, \mathbf{p}_p\} \subset \mathbb{R}^{n\times 1}$, $p \geq n+1$ whose corners are closest to $\mathbf{x}$ and also contains $\mathbf{x}$. By constraining $\mathbf{x}$ to be in poly $(\mathcal{S})$, continuity may be maintained as $\mathbf{x}$ progresses over the operating envelope simply by replacing the elements in $\mathcal{S}$ that are not involved in the calculation of $G(\mathbf{x})$ as $\mathbf{x}$ exits poly $(\mathcal{S})$, *e.g.* as $\mathbf{x}$ crosses one of the simplex surfaces described by n of the $n+1$ points, the remaining point does not form part of the calculation of $G(\mathbf{x})$ and may be replaced with an element in $\mathcal{P}$ without causing discontinuity in $G(\mathbf{x})$.

The simplex set $\mathcal{S}$ is initialised with a projection based method which has a polynomial time complexity. The projection method used may not find the smallest simplex in $\mathcal{P}$ containing $\mathbf{x}$, but avoids having to consider all possible combinations in $\mathcal{P}$. The closest point to $\mathbf{x}$ in $\mathcal{P}$ is included in $\mathcal{S}$ as $\mathbf{x}_0$, after which next closest points are only included if it increases the rank of the vectors described by the already included points in $\mathcal{S}$ *and* when combined with the already included points in $\mathcal{S}$ contains they contain the orthogonal projection of $\mathbf{x}$ (see algorithm).

Furthermore, elements in $\mathcal{S}$ is replaced as $\mathbf{x}$ exits the simplex $\mathcal{S}$ with an evolutionary method. Elements in $\mathcal{S}$ is replaced one at a time, by considering one crossed surface at a time, whereby the n points in $\mathcal{S}$ that represents a crossed surface remains in $\mathcal{S}$ and the remaining point replaced by a new point in $\mathcal{P}$ closest to the ball centre of the crossed surface such that the new simplex neighbours the previous. The ball centre of a simplex is defined as the centre of the largest sphere contained in the simplex.

Two theorems in convex theory are required to select and replace the elements in $\mathcal{S}$, and are given as follows.

Theorem 13. *[56]* $\mathbf{x} \in \mathbb{R}^{n\times 1}$ *is contained in the n-simplex* poly $(\mathcal{S})$ *if and only if* $a_i \geq 0$, $i = 1, 2, \ldots, n$ *and* $\sum_{i=1}^{n} a_i \leq 1$ *in* (B.59).

Theorem 14. *[56] The ball centre* ball $(\mathcal{S})$ *of the n-simplex* poly $(\mathcal{S})$ *is uniquely calculated as*

$$\text{ball}(\mathcal{S}) = \mathbf{x}_0 + \left(\frac{1}{(\mathbf{1}_{1\times n} V^{-1} V^{-T} \mathbf{1}_{n\times 1})^{\frac{1}{2}} + \text{trace}\,(V^{-1}V^{-T})^{\frac{1}{2}}}\right) V \text{diag}\left(V^{-1}V^{-T}\right)^{\frac{1}{2}} \tag{B.61}$$

The algorithm calculating $G(\mathbf{x})$ from a finite set of point $\mathcal{P}$ with corresponding gains $\Gamma := \{G(\mathbf{x}) : \mathbf{x} \in \mathcal{P}\}$ proceeds as follows.

1. Initialise simplex S:

   a. Arrange the finite set of operating points in $\mathcal{P}$ according to Euclidean distance from $\mathbf{x}$ in ascending order and store as the columns of C, *i.e.*

   $$(C\mathbf{e}_i - \mathbf{x})^T (C\mathbf{e}_i - \mathbf{x}) \leq (C\mathbf{e}_{i+1} - \mathbf{x})^T (C\mathbf{e}_{i+1} - \mathbf{x}) \ \forall i = 1, 2, \ldots, m-1 \tag{B.62}$$

   and

   $$C\mathbf{e}_i \in \mathcal{P} \ \forall i = 1, 2, \ldots, m \tag{B.63}$$

   where $\mathbf{e}_i$ is the i^{th} column of the identity matrix.

   b. Set $S = C\mathbf{e}_1$, n equal to the row-size of $\mathbf{x}$ and p equal to the cardinality of $\mathcal{P}$.

   c. Set counters $i = 2$, $n_S = 1$ and repeat{ [**loop**]

      i. Set $\mathbf{c} = C\mathbf{e}_i$ and create temporary matrix $T = S - \mathbf{c}\mathbf{1}_{1\times n_S}$.

      ii. Calculate the singular value decomposition of T as

      $$T = U\Sigma V^T \tag{B.64}$$

      iii. If $\left[\begin{array}{cc} I_{n_S} & 0_{n_S\times(n_S-n)} \end{array}\right] U^T T$ has full rank and contains $\left[\begin{array}{cc} I_{n_S} & 0_{n_S\times(n_S-n)} \end{array}\right] U^T (\mathbf{x} - \mathbf{c})$ according to Theorem 13, then reset $S = \left[\begin{array}{cc} S & \mathbf{c} \end{array}\right]$ and $n_S = n_S + 1$.

      iv. Reset counter $i = i + 1$. Clear temporary matrix T.

   } [**loop**] until $n_S = n + 1$ or $i > p$. Clear counter i.

   d. If $i > p$ and $n_S \neq n + 1$ then exit algorithm with an error message 'S could not be initialised with the projection based algorithm'.

Description: Initialise n-simplex set $\mathcal{S}$ with projection based method.

2. Recursive on-line recalculations: Repeat{ [**outer loop**]

   a. Recalculate S:

      i. If $\mathbf{x}$ is not contained in S according to Theorem 13, then set counter $i = 1$ and repeat{ [**inner loop**]

         A. Create temporary matrix $T = SE_i$, where E_i is the identity matrix with its i^{th} column removed.

         B. Create temporary vector $\mathbf{t}_0 = T\mathbf{e}_1$ and recalculate $T = TE_1 - \mathbf{t}_0$.

         C. Calculate the singular value decomposition of T as

$$T = U\Sigma V^T \tag{B.65}$$

         D. If $\left(\mathbf{e}_n^T U^T \left(S\mathbf{e}_i - \mathbf{t}_0\right)\right)\left(\mathbf{e}_n^T U^T \left(\mathbf{x} - \mathbf{t}_0\right)\right) < 0$, then [5]

            I. Set $\mathbf{v} = U\left(-\mathbf{e}_n^T U^T \left(S\mathbf{e}_i - \mathbf{t}_0\right)\mathbf{e}_n\right)$. [6]

            II. Reset (normalise) $\mathbf{v} = \frac{1}{\|\mathbf{v}\|_2}\mathbf{v}$.

            III. Set $\widehat{\mathbf{x}} = U\begin{bmatrix} \text{ball}\left(\begin{bmatrix} E_n^T U^T T & \mathbf{0}_{(n-1)\times 1} \\ 0 & \end{bmatrix}\right) \end{bmatrix} + \mathbf{t}_0 + \epsilon\mathbf{v}$, where ϵ is a small scalar of order 100 or more smaller than the shortest distance between operating points in $\mathcal{P}$. [7]

            IV. Set $S = \begin{bmatrix} \mathbf{c} & SE_i \end{bmatrix}$, where $\mathbf{c}$ is the closest point to $\widehat{\mathbf{x}}$ such that $\begin{bmatrix} \mathbf{c} & SE_i \end{bmatrix}$ contains $\widehat{\mathbf{x}}$ according to Theorem 13.

         E. Reset counter $i = i + 1$. Clear temporary matrix T and temporary vector $\mathbf{t}_0$.

         } [**outer loop**] until $\mathbf{x}$ is contained in S or $i > n + 1$.

      ii. If $i > n + 1$ and $\mathbf{x}$ is *not* contained in S, then exit algorithm with an error message 'S could not be recalculated with the evolutionary algorithm'.

5. If $\mathbf{x}$ and the temporary removed point $S\mathbf{e}_i$ is on opposite sides of the surface described by the remaining points SE_i, then $\mathbf{x}$ crossed that surface.
6. $\mathbf{v}$ is the vector orthogonal to the surface described by SE_i pointing outward of simplex S.
7. Calculate the ball centre of the surface described by the remaining points SE_i and calculate $\widehat{\mathbf{x}}$ which is just outside the simplex S in the direction $\mathbf{v}$.

Description: If $\mathbf{x}$ *is not contained in* $\mathcal{S}$*, replace elements in* $\mathcal{S}$ *one at a time by evolving through neighbouring simplexes in the direction of* $\mathbf{x}$*.*

b. Recalculation of $G(\mathbf{x})$:

   i. Calculate $\mathbf{a}$ according to (B.57).

   ii. Find gains corresponding to the operating points in S and calculate gain $G(\mathbf{x})$ with (B.60).

} [**outer loop**] indefinitely.

The gain-scheduler is implemented with MATLAB SIMULINK R2008b, whose block diagram is given by Figure B.1. The implementation of the gain-scheduling algorithm in SIMULINK is largely determined by the static variable size limitation of EMBEDDED MATLAB FUNCTION blocks and the single input limitation of MATLAB FUNCTION blocks, and are given by Listings B.4-B.7, where `p`$:= \mathbf{x}$, `N` $:= n$, `gridP` $:= \begin{bmatrix} \mathbf{p}_1 & \mathbf{p}_2 & \cdots & \mathbf{p}_m \end{bmatrix}$, `nGrid` $:= m$, `G`$:= G(\mathbf{x})$, `gridG` $:=$ `cat(3,`$G(\mathbf{p}_1), G(\mathbf{p}_2), \ldots, G(\mathbf{p}_m)$`)`, `cat.m`[8] is used to concatenate the gains along the third matrix dimension[9] and `Q` is used to concatenated variables for single variable block inputs.

Furthermore, `gridP` and `gridG` are augmented with `ehcGainScheduleGrid.m` in Listing B.8 prior to simulation. The augmentation involves extrapolating the the operating points to correspond to a hyper-rectangular operating envelope, to which end the gain-scheduler input block `ehcSimplicialComplexIn.m`, given by Listing B.4, simply projects the present operating point `p` onto the outer surfaces of a hyper-rectangle if `p` is outside operating envelope. The hyper-rectangular operating envelope avoids any complications of projecting `p` onto a non-rectangular polytope whilst maintaining continuity in the calculated gain.

Listing B.4: ehcSimplicialComplexIn.m

```
function R=ehcSimplicialComplexIn(Q)
% description: remove dimensions whose corresponding grid
%              values have zero range,
%              i.e. minimum description for gain-scheduling
% Q=[p,gridP]
% R=[swigp,swigGridP] i.e. Q with reduced dimension

% extract input
p=Q(:,1);
gridP=Q(:,2:end);

% constrain parameter to grid
pMin=min(gridP,[],2);
pMax=max(gridP,[],2);
p=p+(-p+pMax).*(p>pMax)+(-p+pMin).*(p<pMin);

iStatLogic=min((gridP==gridP(:,1)*ones(1,size(gridP,2))),[],2);
swigp=p(~iStatLogic);
swigGridP=gridP(~iStatLogic,:);

R=[swigp,swigGridP];
if isempty(R)
    R=[0,0];
end

end
```

8. `cat.m` is a standard MATLAB function.
9. The first and second matrix dimensions are along the matrix rows and columns respectively.

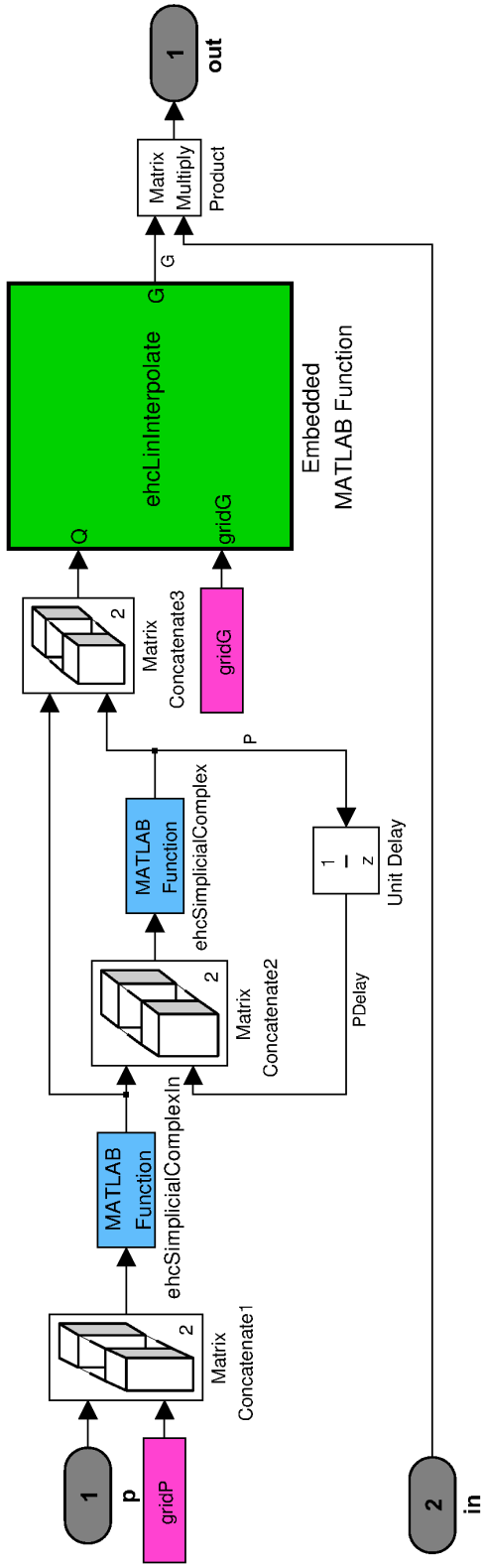

Figure B.1: Gain-scheduler SIMULINK block diagram.

Listing B.5: ehcSimplicialComplex.m

```
function P = ehcSimplicialComplex(Q)
% abrv.:-Gain (G)
%       -present operating point (p) in real [Nx1] space
%       -grid of operating points (gridP)   in real [N x nGrid] space
%       -simplex of previous gain-scheduling calculation (PDelay) in real
     [N x (N+1)] space
% This block supports the Embedded MATLAB subset.
% See the help menu for details.
% Input:  Q=[p,gridP,PDelay]
% Output: P (Simplex)

if min(size(Q)==[1,3])
    P=0;
else

    % extract input
    N=size(Q,1);
    p=Q(:,1);
    gridP=Q(:,2:(end-(size(p,1)+1)));
    nGrid=size(gridP,2);
    PDelay=Q(:,(end+1-(size(p,1)+1)):end);

    E=eye(N);
    if max(max(abs(PDelay)))==0
        % initialise P

        % Closest Grid Parameter
        [notUsed1,iCGP]=sort(sum(((gridP-p*ones(1,nGrid)).^2),1));
        P=[gridP(:,iCGP(1)),zeros(N,N)];
        nP=1; k=2;
        while (k<=nGrid) && (nP<(N+1))
            % candidate grid parameter
            c=gridP(:,iCGP(k));
            swigP=P-c*ones(1,(N+1));
            [U,notUsed2,notUsed3] = svd(swigP(:,1:nP));
            % include candidate if conditions are satisfied
            if rank(swigP(:,1:nP))==nP
                b = ehcSimplex([(E(1:nP,:)*U'*swigP(:,1:nP)),zeros(nP,1)
                    ],(E(1:nP,:)*U'*(p-c)));
                if b
                    P(:,(nP+1))=c;
                    nP=nP+1;
                end
            end
            k=k+1;
        end
        if nP~=(N+1)
            error('P could not be initialised.');
        end
    else
        P=PDelay;
        % recalculate P if p is not in polytope P
        [b,iP,pEvolve]=ehcSimplex(P,p);
        Prmd=[P(:,1:(iP-1)),P(:,(iP+1):end)];
        % Closest Grid Parameter
        if ~b
```

```
55              [notUsed6,iCGP]=sort(sum(((gridP-pEvolve*ones(1,nGrid)).^2)
                    ,1));
56          end
57          k=1;
58          while (k<=nGrid) && ~b
59              if rank(Prmd-gridP(:,iCGP(k))*ones(1,N))==N
60                  [b,notUsed7,notUsed8]=ehcSimplex([Prmd,gridP(:,iCGP(k))],
                        pEvolve);
61                  if b
62                      P=[Prmd,gridP(:,iCGP(k))];
63                      [b,iP,pEvolve]=ehcSimplex(P,p);
64                      if ~b
65                          Prmd=[P(:,1:(iP-1)),P(:,(iP+1):end)];
66                          [notUsed9,iCGP]=sort(sum(((gridP-pEvolve*ones(1,
                                nGrid)).^2),1));
67                      end;
68                      k=0;
69                  end
70              end
71              k=k+1;
72          end
73      end
74  end
```

Listing B.6: ehcSimplex.m

```
1  function [varargout] = ehcSimplex(X,varargin) %#eml
2  % based on: 'Ball centers of special polytopes'
3  %            by Katta G. Murty
4  % description: calculate either ball center c of N-simplex
5  %              described by N+1 points defined by columns of X
6  %              or boolean b and index iX
7  % abrv.      -N-simplex (X)
8  %            -operating point (p)
9  %            -boolean (b)
10 %            -ball centre (x)
11 %            -index of column in X not involved in the crossing of a
       simplex surface (iX)
12 % inputs: X (N-simplex) in Nx(N+1) real space
13 %         varargin: p
14 % output: varargout {x,b,iX}
15
16 l=1e3*eps;
17
18 N=size(X,2)-1;
19 if rank(X)~=N
20     error('S not full rank (not surface).');
21 end
22 B=X(:,1:N)-X(:,(N+1))*ones(1,N);
23
24 if isempty(varargin)
25     % calc. N-simplex ball center x
26     gamma=sqrt(sum((eye(N)/B).^2,2));
27     gammaNp1=norm((ones(1,N)*(eye(N)/B)),2);
28     x=X(:,(N+1))+(1/(sum(gamma)+gammaNp1)).*B*gamma;
29     varargout{1}=x;
```

```
else
    % check whether p is N-simplex. If not calc. column index iX
    %   of X which should be omitted when calc. neigbouring
    %   N-simplex which might contain p, along with pEvolve, the point
    %   just outside the N-simplex, nearest to ball centre of (N-1)-
        simplex
    %   [X(:,1:(iX-1)),X(:,(iX+1):end)]
    p=varargin{:};
    beta=B\(p-X(:,(N+1)));
    if min(beta>=0) && (sum(beta)<=1)
        b=true;
        iX=[];
        pEvolve=[];
    else
        b=false;
        E=eye(N);
        k=1; iX=[]; v=[];
        while (k<=(N+1)) && isempty(iX)
            Xrmd=[X(:,1:(k-1)),X(:,(k+1):end)];
            swigXrmd=Xrmd(:,1:(end-1))-Xrmd(:,end);
            [U,S,V]=svd(swigXrmd);
            if (prod(E(end,:)*U'*[(X(:,k)-Xrmd(:,end)),(p-Xrmd(:,end))]))
                <0
                iX=k;
                % calc. vector v orthagonal to Xrmd, in direction outside
                     of X from Xrmd
                v=U*(-(E(end,:)*U'*(X(:,k)-Xrmd(:,end))).*E(:,end));
                v=v./norm(v,2);
                xrmd = U*[ehcSimplex([(E(1:(N-1),:)*U'*swigXrmd),zeros((N
                    -1),1)]);0]+Xrmd(:,end);
                pEvolve=xrmd+l.*v;
            end
            k=k+1;
        end
        if isempty(iX)
            error('iX could not be found.');
        end
    end
    varargout{1}=b;
    varargout{2}=iX;
    varargout{3}=pEvolve;
end



end
```

Listing B.7: ehcLinInterpolate.m

```
function G = ehcLinInterpolate(Q,gridG)
% This block supports the Embedded MATLAB subset.
% See the help menu for details.
% Q=[p,gridP,P]

if min(size(Q)==[1,3])
    G=gridG(:,:,1);
```

```
else
    % calculate G via linear interpolation
    % p=P(:,1)+(P(:,2:end)-P(:,1)*ones(1,N))*a. Thus, a=(P(:,2:end)-P
        (:,1)*ones(1,N))\(p-P(:,1)).

    % extract input
    N=size(Q,1);
    p=Q(:,1);
    gridP=Q(:,2:(end-(N+1)));
    nGrid=size(gridP,2);
    P=Q(:,(end-N):end);
    % calc. beta: p=P(:,end)+(P(:,1:(end-1))-P(:,end)*ones(1,size(P(:,1:(
        end-1)),2)))*beta
    B=P(:,1:(end-1))-P(:,end)*ones(1,(size(P(:,1:(end-1)),2)));
    beta=(B\(p-P(:,end)));
    [notUsed10,iPNp1]=max(min((P(:,(end))*ones(1,nGrid)==gridP),[],1));
    G=gridG(:,:,iPNp1);
    for j=1:N
        [notUsed11,iPj]=max(min((P(:,j)*ones(1,nGrid)==gridP),[],1));
        G=G+beta(j).*(gridG(:,:,iPj)-gridG(:,:,iPNp1));
    end
end;
```

Listing B.8: ehcGainScheduleGrid.m

```
function [gridG,gridP] = ehcGainScheduleGrid(multiG,multiP)
% inputs:   multiG and multiP are incomplete gain scheduling data, where
%           multiP(:,j) is the j'th parameter corresponding to gain
    multiG(:,:,j)
% outputs:  gridG and gridP are organised gain scheduling data, completed
%           over hyper-rectangular grid, where gridP(:,j) is the j'th
    parameter
%           corresponding to gain gridG(:,:,j)

% calculate gridP
nP=size(multiP,1);
N=size(multiP,2);
for i=1:nP
    gridPi=sort(multiP(i,:));
    gridPi(ehcIndexLogic2Dec(max(tril(((ones(N,1)*gridPi)==(ones(N,1)*
        gridPi)'),-1),[],2)))=[];   % remove repeating parameters
    if i==1
        gridP=gridPi;
    else
        multiI=[];
        multi1=[];
        for j=1:length(gridPi)
            multiI=[multiI,eye(size(gridP,2))];
            multi1=blkdiag(multi1,ones(1,size(gridP,2)));
        end
        gridP=[gridP*multiI;gridPi*multi1];
    end
end

% calculate gridG
nGrid=size(gridP,2);
```

```
gridG=zeros(size(multiG,1),size(multiG,2),nGrid);
for j=1:nGrid
    Pj=gridP(:,j);
    [isEq,iEq]=max(min(((Pj*ones(1,N))==multiP),[],1));
    if isEq
        gridG(:,:,j)=multiG(:,:,iEq);

    % estimate gridG(:,:,j)
    else
        % calculate Close Parameter (CP) according to Euclidean norm
        [eucCP,iCP]=sort(sum(((multiP-Pj*ones(1,N)).^2),1));
        dPj=Pj-multiP(:,iCP(1));
        dPjBase=multiP(:,iCP(2))-multiP(:,iCP(1));
        idPjBase=iCP(2);
        k=3;
        while (k<=N) && max(abs(dPjBase*pinv(dPjBase)*dPj-dPj)>eps)
            % test if (multiP(:,iCP(k))-multiP(:,iCP(1))) should be
                included in base
            A=dPjBase;
            B=(multiP(:,iCP(k))-multiP(:,iCP(1)))*ones(1,size(dPjBase,2))
                ;
            theta=acos(sum(A.*B,1)./sqrt(sum(A.*A,1).*sum(B.*B,1)));
            if (pi*abs(theta/pi-floor(theta/pi)))>eps
                dPjBase=[dPjBase,(multiP(:,iCP(k))-multiP(:,iCP(1)))];
                idPjBase=[idPjBase,iCP(k)];
            end
            k=k+1;
        end
        if max(abs(dPjBase*pinv(dPjBase)*dPj-dPj)>eps)
            error('Grid parameter cannot be described by combination of
                multiP.');
        end
        gridG(:,:,j)=multiG(:,iCP(1));
        c=pinv(dPjBase)*dPj;
        for k=1:length(idPjBase)
            gridG(:,:,j)=gridG(:,:,j)+(multiG(:,:,idPjBase(k))-multiG(:,
                iCP(1))).*c(k);
        end
    end
end

end
```

Appendix C

Literature Study

Table C.1 lists the LMI control techniques considered for AIFR according to published papers, matching them with the various system components of IFR, and are discussed as follows.

ID	Method	Ref.	$\mathcal{H}_2$	Δ	NL	time-delay	VC/AC	η	SF	OF
1	SWLQG	[39]	✓	✓				✓		✓
2	Mixed $\mathcal{H}_2/\mathcal{H}_\infty$	[67]	✓	✓				✓		✓
3	CCLQG	[42]	✓				✓	✓		✓
4	Robust $\mathcal{H}_2$	[75]	✓	✓				✓	✓	
5	Generalised PCS	[58][59]	✓	✓	✓					✓
6	$\mathcal{L}_2/\mathcal{H}_2$ LPV	[21]	✓		✓		✓		✓	

Table C.1: LMI control techniques considered for AIFR.

1. Grocott [39, pp.38-45] derives additional LQG weights, called sensitivity weights, to desensitise LQG control against model uncertainty (Δ). Sensitivity Weighted LQG (SWLQG) neglects the change of high frequency dynamics due to parameter variation and removes the parameter variation from the feedback loop, and in doing so parameter variations are modelled as input disturbances. An implementation of SWLQG on an adaptation of the American Control Conference (ACC) benchmark problem in [34], *i.e.* a mass-spring system subject to white noise disturbance (η) and time-invariant uncertainty in all 4 masses and all 3 springs constants, reveals that the sensitivity weights successfully desensitises the closed-loop system against parameter variations while the $\mathcal{H}_2$ index is optimised for the relative position regulation of the two centre masses, although there are no guarantees for the stability and performance of the closed-loop system with parameter variations. SWLQG, as with LQG, optimises a scalar $\mathcal{H}_2$ performance index, and does not include Variance-Constraints (VC), *i.e.* *multiple* scalar $\mathcal{H}_2$ performance indexes. Section 7.2 gives insight in achieving variance-constraints via LQG using set theory and LMI formulations of $\mathcal{H}_2$ control.

2. Scherer et al. [67] derive bounds on the output variance, the system $\mathcal{H}_\infty$-norm and closed-loop pole-regions, of LTI models subject to white noise disturbance. It is shown that the feasibility of each individual system bound is equivalent to the feasibility of certain LMIs, and that the bounds hold simultaneously when *Lyapunov's shaping paradigm* is applied. Their solution to the $\mathcal{H}_2$-norm takes the form of the Observability Gramian Lyapunov Inequality (OGLI), *i.e.* $\mathcal{A}^T P + P\mathcal{A} + \mathcal{C}_z^T \mathcal{C}_z < 0$. The feasibility of the LMIs are also presented as an LMI optimisation problem, which solves Output-Feedback (OF) controller matrix variables for a specified closed-loop $\mathcal{H}_\infty$-norm and regional pole constraints, while minimising the $\mathcal{H}_2$-norm. Output-feedback is achieved via a congruent transformation, which eliminates bilinear terms and adds an additional *full-rank*-constraint to the LMIs. The non-linear rank-constraint is omitted from the LMI optimisation and confirmed following the optimisation. By omitting the rank-constraint, controller variables are optimised over a convex space containing bilinear output-feedback space, [1] to which end the optimum may fall outside the bilinear space, resulting in no solution. A remedy is suggested for rank deficiency, but tends to be insufficient for large systems, such as the IFR system. The technique demonstrates the versatility and generic property of LMI-based techniques.
   Mixed $\mathcal{H}_2/\mathcal{H}_\infty$ techniques provide means to synthesise controllers that are robustly stable and achieve a minimum $\mathcal{H}_2$-norm for the *nominal* system, although it lacks robust performance indexes, present in techniques 4-6. Furthermore, Popov [65] demonstrates the conservatism involved when applying *Lyapunov's paradigm* by implementing mixed $\mathcal{H}_2/\mathcal{H}_\infty$ control on a mass-spring system, with time-invariant uncertainty in both masses and the spring constant, which results in a *maximum performance degradation in the order of 50%.*
3. Huang et al. [42] show that the feasibility of covariance-constraints for LTI models subject to white noise disturbance, is equivalent to the feasibility of certain LMIs. Covariance-constraints are achieved by formulating an upper-bound on the system state-covariance matrix via the Controllability Gramian Lyapunov Inequality (CGLI), *i.e.* $\mathcal{A}^T Q + Q\mathcal{A}^T + \mathcal{B}_w^T \mathcal{B}_w < 0$, and directly including constraints on covariances with inequality bounds. The feasibility of the covariance-constraints is also presented as an LMI optimisation problem, which solves output-feedback controller matrix variables for specified closed-loop covariance-constraints while minimising an $\mathcal{H}_2$ performance bound, resulting in a Covariance-Constrained LQG (CCLQG) controller. However, their output-feedback formulation does not include a necessary rank constraint discussed in [67] (technique 2), which must be confirmed following the LMI optimisation. The technique does not include robustness against uncertainty or Non-Linearity (NL) *per se*, but LMI formulations are versatile in that multiple objectives may be added to a formulation [67].
4. Takaba and Katayama [75] derive an upper-bound on the worst-case immediate output variance, for LTI descriptor-system models subject to white noise disturbance and Linear Time-Varying (LTV) norm-bounded structured uncer-

1. The bilinear space is a subset of the convex space.

tainty. It is shown that the feasibility of the bound is equivalent to the feasibility of certain LMIs. The derivation is based on formulating an upper-bound on the system state-covariance matrix via the generalised CGLI. [2] The feasibility of the bound is also presented as an LMI optimisation problem, which solves the State-Feedback (SF) gain corresponding to the minimum bound.

5. Nampradit and Banjerdpongchai [58] derive an upper-bound on the worst-case average impulse-based $\mathcal{H}_2$ performance, for LTI state-space models subject to non-linear memoryless sector- and slope-bounded uncertainty. It is shown that the feasibility of the bound is equivalent to the feasibility of certain LMIs, and takes the form of the generalised OGLI. The bound is formulated as a BMI optimisation problem in terms of output-feedback controller matrix variables and presents a scheme for solving the controller matrices via linearisation, achieving a sub-minimal bound.
   How et al. [41] successfully design and implement Popov type control on a developmental model of the Middeck Active Control Experiment (MACE), demonstrating its applicability to high-order systems [3] with multiple real parametric uncertainties. Although, impulse-based $\mathcal{H}_2$ is not equivalent to the white noise disturbance $\mathcal{H}_2$ index in the non-linear framework, which makes the inclusion of the Dryden turbulence model infeasible.
6. Delibasi et al. [21] derive upper-bounds on both the worst-case average output variance and the worst-case system $\mathcal{L}_2$-gain, for Linear Parameter Varying (LPV) models subject to $\mathcal{L}_2$-bounded disturbances and Actuator-Constraints (AC). It is shown that the feasibility of the simultaneous system bounds is equivalent to the feasibility of certain LMIs, which takes the form of the generalised CGLI. The feasibility of the bounds is also presented as an LMI optimisation problem, which solves a Non-Linear Parameter-Varying (NLPV) state-feedback controller corresponding to the minimum output variance bound, for given system $\mathcal{L}_2$-gain upper-bound and a given degree of controller complexity. The NPV controller uses on-line knowledge of the varying parameters, for which no error margin is included.
   LPV techniques specify system matrices as a polytopic space (see [47]), and are generally less conservative than techniques which specify system matrices in terms of norm-bounds, such as technique 4, but requires approximately 2^n times the variables to formulate, which makes it computationally much more expensive.

None of the control techniques listed in Table C.1 provides a framework that includes all the system components of IFR. However, the generic property of LMI-based control techniques and the modelling techniques presented in this thesis, give means to extend technique 4 to include all the system components of IFR. Table C.2 lists the extensions.

2. Described as CGLI that are *generalised* to hold for time-varying systems.
3. A 59-order model is used for their design.

Component	Extension	Ref.
NL	Represent NL as time-varying uncertainty	Appendix A.2.10
time-delay	Represent with Padé approximation	Appendix A.2.11
VC	Bound symmetrically scaled state-covariance /controllability Gramian	[42]
OF	Linearisation or Genetic Algorithms or via the separation principle	[31],[20], [59], [65]
AC	Augment system with actuator dynamics and include via VC	Section 4.2.1.3

Table C.2: IFR system component extensions.

Appendix D

Receiver dedicated AIFR

State-feedback

The partially coupled AIFR state-feedback gain is synthesised with LMI optimisation problem (4.109) and IFR models

$$\begin{bmatrix} \dot{\mathbf{x}} \\ \mathbf{z} \\ \mathbf{y} \\ \mathbf{q} \end{bmatrix}_H = \begin{bmatrix} A & B_w & B_u & B_p \\ C_z & D_{zw} & D_{zu} & D_{zp} \\ C_y & D_{yw} & D_{yu} & D_{yp} \\ C_q & D_{qw} & D_{qu} & D_{qp} \end{bmatrix}_H \begin{bmatrix} \mathbf{x} \\ \mathbf{w} \\ \mathbf{u} \\ \mathbf{p} \end{bmatrix}_H \tag{D.1}$$
$$\mathbf{p}_H = \Delta_H \mathbf{q}_H, \quad \Delta_H \in \boldsymbol{\Delta}$$
$$\mathbf{z}_H \in \mathfrak{D}_{z_H}$$

for tanker hold, and

$$\begin{bmatrix} \dot{\mathbf{x}} \\ \mathbf{z} \\ \mathbf{y} \\ \mathbf{q} \end{bmatrix}_D = \begin{bmatrix} A & B_w & B_u & B_p \\ C_z & D_{zw} & D_{zu} & D_{zp} \\ C_y & D_{yw} & D_{yu} & D_{yp} \\ C_q & D_{qw} & D_{qu} & D_{qp} \end{bmatrix}_D \begin{bmatrix} \mathbf{x} \\ \mathbf{w} \\ \mathbf{u} \\ \mathbf{p} \end{bmatrix}_D \tag{D.2}$$
$$\mathbf{p}_D = \Delta_D \mathbf{q}_D, \quad \Delta_D \in \boldsymbol{\Delta}$$
$$\mathbf{z}_D \in \mathfrak{D}_{z_D}$$

for receiver dedicated AIFR, obtained with the following augmentations.

1. Isolate tanker: The tanker is isolated in (4.108) by applying *ad hoc* singular transformation

$$\begin{bmatrix} \dot{\mathbf{x}} \\ \mathbf{z} \\ \mathbf{y} \\ \mathbf{q} \end{bmatrix}_H =$$
$$\begin{bmatrix} T_{x_H} & 0 & 0 & 0 \\ 0 & T_{z_H} & 0 & 0 \\ 0 & 0 & T_{y_H} & 0 \\ 0 & 0 & 0 & I \end{bmatrix} \begin{bmatrix} A & B_w & B_u & B_p \\ C_z & D_{zw} & D_{zu} & D_{zp} \\ C_y & D_{yw} & D_{yu} & D_{yp} \\ C_q & D_{qw} & D_{qu} & D_{qp} \end{bmatrix}_C \begin{bmatrix} T_{x_H} & 0 & 0 & 0 \\ 0 & I & 0 & 0 \\ 0 & 0 & T_{u_H} & 0 \\ 0 & 0 & 0 & I \end{bmatrix}^T \begin{bmatrix} \mathbf{x} \\ \mathbf{w} \\ \mathbf{u} \\ \mathbf{p} \end{bmatrix}_H$$
$$\mathbf{p}_H = \Delta_H \mathbf{q}_H, \quad \Delta_H \in \boldsymbol{\Delta}$$
$$\mathbf{z}_H \in \mathfrak{D}_{z_H} \tag{D.3}$$

where

$$\Delta_H = \Delta_C,\ \mathfrak{D}_{z_H} = \{T_{z_H}\mathbf{x} : \mathbf{x} \in \mathfrak{D}_{z_C}\}$$
$$T_{x_H} \coloneqq \text{blkdiag}\left(\begin{bmatrix} I_{17} & 0_{17\times 20}\end{bmatrix}, \begin{bmatrix} I_6 & 0_{6\times 6}\end{bmatrix}, \begin{bmatrix} I_3 & 0_{3\times 4}\end{bmatrix}, \begin{bmatrix} I_4 & 0_{4\times 4}\end{bmatrix}\right)$$
$$T_{z_H} \coloneqq \begin{bmatrix} I_{25} & 0_{25\times 29}\end{bmatrix}$$
$$T_{y_H} \coloneqq \text{blkdiag}\left(\begin{bmatrix} I_{24} & 0_{24\times 28}\end{bmatrix}, \begin{bmatrix} I_3 & 0_{3\times 4}\end{bmatrix}, \begin{bmatrix} I_4 & 0_{4\times 4}\end{bmatrix}\right)$$
$$T_{u_H} \coloneqq \begin{bmatrix} I_8 & 0_{8\times 8}\end{bmatrix} \tag{D.4}$$

2. Apply tanker feedback: Similar to (3.103), augmentation of (4.108) with the tanker hold state-feedback gain K_H synthesised for (D.3) is given by

$$\begin{bmatrix}\dot{\mathbf{x}}\\ \mathbf{z}\\ \mathbf{y}\\ \mathbf{q}\end{bmatrix}_Y = \begin{bmatrix} \left(A_C + B_{u,C}T_{u_H}^T K_H T_{x_H}\right) & B_{w,C} & B_{u,C} & B_{p,C}\\ \left(C_{z,C} + D_{zu,C}T_{u_H}^T K_H T_{x_H}\right) & D_{zw,C} & D_{zu,C} & D_{zp,C}\\ \left(C_{y,C} + D_{yu,C}T_{u_H}^T K_H T_{x_H}\right) & D_{yw,C} & D_{yu,C} & D_{yp,C}\\ \left(C_{q,C} + D_{qu,C}T_{u_H}^T K_H T_{x_H}\right) & D_{qw,C} & D_{qu,C} & D_{qp,C}\end{bmatrix}\begin{bmatrix}\mathbf{x}\\ \mathbf{w}\\ \mathbf{u}\\ \mathbf{p}\end{bmatrix}_Y$$
$$\mathbf{p}_Y = \Delta_Y \mathbf{q}_Y, \quad \Delta_Y \in \mathbf{\Delta}$$
$$\mathbf{z}_Y \in \mathfrak{D}_{z_Y} \tag{D.5}$$

where

$$\Delta_Y = \Delta_C,\ \mathfrak{D}_{z_Y} = \mathfrak{D}_{z_C} \tag{D.6}$$

3. Remove tanker control input and performance output:

$$\begin{bmatrix}\dot{\mathbf{x}}\\ \mathbf{z}\\ \mathbf{y}\\ \mathbf{q}\end{bmatrix}_D =$$
$$\begin{bmatrix} I & 0 & 0 & 0\\ 0 & T_{z_D} & 0 & 0\\ 0 & 0 & I & 0\\ 0 & 0 & 0 & I\end{bmatrix}\begin{bmatrix} A & B_w & B_u & B_p\\ C_z & D_{zw} & D_{zu} & D_{zp}\\ C_y & D_{yw} & D_{yu} & D_{yp}\\ C_q & D_{qw} & D_{qu} & D_{qp}\end{bmatrix}_Y\begin{bmatrix} I & 0 & 0 & 0\\ 0 & I & 0 & 0\\ 0 & 0 & T_{u_D} & 0\\ 0 & 0 & 0 & I\end{bmatrix}^T\begin{bmatrix}\mathbf{x}\\ \mathbf{w}\\ \mathbf{u}\\ \mathbf{p}\end{bmatrix}_D$$
$$\mathbf{p}_D = \Delta_D \mathbf{q}_D, \quad \Delta_D \in \mathbf{\Delta}$$
$$\mathbf{z}_D \in \mathfrak{D}_{z_D} \tag{D.7}$$

where

$$\Delta_D = \Delta_Y,\ \mathfrak{D}_{z_D} = \{T_{z_D}\mathbf{x} : \mathbf{x} \in \mathfrak{D}_{z_C}\}$$
$$T_{u_D} \coloneqq \begin{bmatrix} 0_{8\times 8} & I_8\end{bmatrix}$$
$$T_{z_D} \coloneqq \begin{bmatrix} 0_{29\times 25} & I_{29}\end{bmatrix} \tag{D.8}$$

A decoupled turbulence estimator gain $L_{\mathcal{E},H}$ is synthesised with LMI optimisation problem (4.129) for the tanker hold model (D.1) and (4.125), where

$$\begin{aligned} T_{x_{\mathcal{E},H}} &= \begin{bmatrix} 0_{17\times 6} \\ I_6 \\ 0_{7\times 6} \end{bmatrix} \\ T_{x_{r,H}} &= \begin{bmatrix} I_{17} & 0_{17\times 7} \\ 0_{6\times 17} & 0_{6\times 7} \\ 0_{7\times 17} & I_7 \end{bmatrix} \\ R_{x_{\mathcal{E},H}} &= \begin{bmatrix} 0_{6\times 17} & I_6 & 0_{6\times 7} \end{bmatrix} \\ N_{y_{r,H}} &= \text{blkdiag}\left(\begin{bmatrix} I_{17} & 0_{17\times 7} \end{bmatrix}, I_7\right) \\ R_{y_{\mathcal{E},H}} &= \begin{bmatrix} 0_{6\times 18} & I_6 & 0_{6\times 7} \end{bmatrix} \end{aligned} \tag{D.9}$$

in (4.114) and tanker hold state-feedback gain K_H, synthesised with tanker hold model (D.1) in Section 4.3.2, is used as K in (4.125).

A coupled turbulence estimator gain $L_{\mathcal{E},D}$ is synthesised with LMI optimisation problem (4.129) for the receiver dedicated AIFR model (D.2) and (4.125), where

$$T_{x_{\mathcal{E},D}} = T_{x_{\mathcal{E},C}},\ T_{x_{r,D}} = T_{x_{r,C}},\ R_{x_{\mathcal{E},D}} = R_{x_{\mathcal{E},C}},\ N_{y_{r,D}} = N_{y_{r,C}},\ R_{y_{\mathcal{E},D}} = R_{y_{\mathcal{E},C}} \tag{D.10}$$

in (4.114) and receiver dedicated AIFR state-feedback gain K_D, synthesised with receiver dedicated AIFR model (D.2) in Section 4.3.2, is used as K in (4.125). $\mathbf{x}_H$ is uncontrollable in $\mathbf{x}_D$ due to the absence of $\mathbf{u}_H$ in $\mathbf{u}_D$. Thus, following the same logic as in the AIFR robust eigenvalue region design in Section 4.2.2.2, the eigenvalues of the tanker-hold model is required to be contained in the eigenvalue region specified for the receiver dedicated state-feedback synthesis.

Table D.1 summarises the decoupled controller synthesis and LTI analysis results for the nominal flight-case (4.134), corresponding to the results in Section 4.3.5, whose synthesis parameters are the same as the synthesis parameters of controller no.8 in Table 4.9.

Table D.1: IFR decoupled controller synthesis and LTI analysis results for the nominal flight-case (4.134).

	Tanker state-feedback synthesis			Receiver state-feedback synthesis			LTI analysis					
	$(\mathfrak{a},\mathfrak{r},\mathfrak{q},\mathfrak{c})_H =$ $(0, 2.225\,\text{rad/s}, 2.275\,\text{rad/s}, \frac{\pi}{2}\,\text{rad})$ $\mathfrak{s}_H = 0.05\,\text{rad}$			$(\mathfrak{a},\mathfrak{r},\mathfrak{q},\mathfrak{c})_D =$ $(0, 2.48\,\text{rad/s}, 2.52\,\text{rad/s}, \frac{\pi}{2}\,\text{rad})$ $\mathfrak{s}_D = 0.05\,\text{rad}$			$\mathfrak{s}_H, \mathfrak{s}_D, \mathfrak{s}_\Theta = 0$					
ID	$\iota_{H,SF}$ (rad)	∇ $(\times 10^{-6}\,\text{rad})$	t_{cpu} (s)	$\iota_{D,SF}$ (rad)	∇ $(\times 10^{-6}\,\text{rad})$	t_{cpu} (s)	$\iota_{H,SF}$ (rad)	$\iota_{D,SF}$ (rad)	$\iota_{\Theta,SF}$ (rad)	ι_Θ (rad)	DM_Θ (ms)	FM_Θ (rad/s)
16	1.01	0.975	485	0.196	581	11200	1.72	1.21	1.07	1.05	139	7

Appendix E

Numerical data for the A330 and control laws

All data is presented in SI units.

A straight and level flight case of the Airbus A330 is documented in the tables and equations below. Steady-state flight is defined by the flight-point

$$\left(h_r, \vartheta_{cas,r}, m_A, cg_A, \phi_r, \dot{h}_r\right) = (20'000\,\text{ft}, 265\,\text{kts}, 171.5\,\text{tons}, 29\,\%\text{RC}, 0, 0) \quad \text{(E.1)}$$

with trimmed variables calculated with the technique presented in Appendix A.1.6 and given in Tables E.1 and E.2.

Trimmed motion variables	
symbols	values
u_r	$182\,\text{m/s}$
v_r	0
w_r	$13.6\,\text{m/s}$
p_r	0
q_r	0
r_r	0
ϕ_r	0
θ_r	$7.45 \times 10^{-2}\,\text{rad}$
ψ_r	0
h_r	$6.10 \times 10^{3}\,\text{m}$

Table E.1: A330 trimmed motion variables.

Trimmed control surface and thrust	
symbols	values
$\delta_{p,r}$	0
$\delta_{h,r}$	3.00×10^{-2} rad
$\delta_{e,r}$	-1.31×10^{-1} rad
$\delta_{r,r}$	0
$\delta_{s_p,r}$	-2.98×10^{-1} rad
$\delta_{s_s,r}$	-2.98×10^{-1} rad
$\delta_{t_p,r}$	4.15×10^{-2} N/kg.m.s^{-2}
$\delta_{t_s,r}$	4.15×10^{-2} N/kg.m.s^{-2}

Table E.2: A330 trimmed control surface and thrust.

The A330 perturbation about the trim is represented by the norm-bounded state-space model

$$\begin{bmatrix} \varepsilon\dot{\mathbf{m}} \\ \mathbf{q}_{m,A} \end{bmatrix} = G_{m,A} \begin{bmatrix} \varepsilon\mathbf{m} \\ \mathbf{g}_{m,A} \\ \varepsilon\boldsymbol{\delta} \\ \mathbf{p}_{m,A} \end{bmatrix} = \begin{bmatrix} A & B_g & B_u & B_p \\ C_q & D_{qg} & D_{qu} & D_{qp} \end{bmatrix}_{m,A} \begin{bmatrix} \varepsilon\mathbf{m} \\ \mathbf{g}_{m,A} \\ \varepsilon\boldsymbol{\delta} \\ \mathbf{p}_{m,A} \end{bmatrix} \tag{E.2}$$

$$\mathbf{p}_{m,A} = \Delta_{m,A}\mathbf{q}_{m,A}, \quad \Delta_{m,A} \in \boldsymbol{\Delta}$$

as defined in Section 4.2.1.2. Aircraft 6DOF EOM (2.7)-(2.18) incorporate moment of inertia and aerodynamic coefficient data provided by Airbus, with 10% and 0% uncertainty in the data respectively, and is used by the algorithm presented Appendix B.1 to calculate $G_{m,A}$ over variable domain listed in Table 4.1, where the algorithm parameters are listed in Table E.3. The resulting system matrix $G_{m,A}$ is given by (E.3)-(E.13).

Parameters		
symbol	description	value
n_l	grid resolution	20
ϵ_P	parameter variation threshold	0.01
ϵ_J	joint variation threshold	0.9
n_c	joint variation confirmation sample set cardinality	10
n_s	ellipsoidal variation sample set cardinality	500
n_b	ellipsoidal variation sample set partition maximum cardinality	500

Table E.3: Norm-bounded state-space model calculation parameters of Listing **??**.

$$A_{m,A} =$$

$$\begin{bmatrix}
-7.78 \times 10^{-3} & 6.51 \times 10^{-18} & 8.62 \times 10^{-2} & 4.85 \times 10^{-27} & -1.35 \times 10^{1} & 5.65 \times 10^{-27} & 4.85 \times 10^{-27} & -9.78 & 7.27 \times 10^{-27} & 1.75 \times 10^{-5} \\
0 & -1.20 \times 10^{-1} & 0 & 1.31 \times 10^{1} & 0 & -1.81 \times 10^{2} & 9.78 & 0 & 0 & 0 \\
-4.69 \times 10^{-2} & 0 & -6.44 \times 10^{-1} & 1.05 \times 10^{-26} & 1.81 \times 10^{2} & 1.21 \times 10^{-26} & 0 & -7.30 \times 10^{-1} & 1.62 \times 10^{-26} & 9.31 \times 10^{-4} \\
0 & -2.97 \times 10^{-2} & 0 & -1.84 & 0 & 3.61 \times 10^{-1} & 0 & 0 & 0 & 0 \\
1.43 \times 10^{-4} & 0 & -3.72 \times 10^{-3} & 0 & -4.68 \times 10^{-1} & 0 & -2.63 \times 10^{-27} & -3.23 \times 10^{-27} & -3.64 \times 10^{-27} & -3.50 \times 10^{-6} \\
0 & 4.00 \times 10^{-3} & 0 & -1.76 \times 10^{-1} & 0 & -2.45 \times 10^{-1} & 0 & 0 & 0 & 0 \\
0 & 0 & 0 & 1.00 & 0 & 7.46 \times 10^{-2} & 0 & 0 & 0 & 0 \\
0 & 0 & 0 & 0 & 1.00 & 0 & 0 & 0 & 0 & 0 \\
0 & 0 & 0 & 0 & 0 & 1.00 & 0 & 0 & 0 & 0 \\
7.44 \times 10^{-2} & -3.94 \times 10^{-30} & -9.97 \times 10^{-1} & -6.56 \times 10^{-28} & -1.11 \times 10^{-27} & -7.07 \times 10^{-28} & 0 & 1.83 \times 10^{2} & -9.09 \times 10^{-28} & -3.35 \times 10^{-30}
\end{bmatrix} \tag{E.3}$$

$$B_{g,m,A} =$$

$$\begin{bmatrix}
1.46 \times 10^{-3} & 6.51 \times 10^{-18} & -8.65 \times 10^{-2} & 4.04 \times 10^{-27} & -1.15 \times 10^{-1} & 4.04 \times 10^{-27} \\
0 & 1.20 \times 10^{-1} & 0 & 5.29 \times 10^{-1} & 0 & -1.50 \\
9.38 \times 10^{-2} & 0 & 6.38 \times 10^{-1} & 8.08 \times 10^{-27} & 1.61 & 8.08 \times 10^{-27} \\
0 & 2.97 \times 10^{-2} & 0 & 1.84 & 0 & -3.59 \times 10^{-1} \\
2.78 \times 10^{-5} & 0 & 3.73 \times 10^{-3} & -2.22 \times 10^{-27} & 4.68 \times 10^{-1} & -2.22 \times 10^{-27} \\
0 & -4.00 \times 10^{-3} & 0 & 1.76 \times 10^{-1} & 0 & 2.44 \times 10^{-1} \\
0 & 0 & 0 & 0 & 0 & 0 \\
0 & 0 & 0 & 0 & 0 & 0 \\
0 & 0 & 0 & 0 & 0 & 0 \\
-3.55 \times 10^{-30} & -3.94 \times 10^{-30} & -4.34 \times 10^{-30} & -5.05 \times 10^{-28} & -5.05 \times 10^{-28} & -5.05 \times 10^{-28}
\end{bmatrix} \tag{E.4}$$

$$B_{u,m,A} =$$

$$\begin{bmatrix}
9.59 \times 10^{-28} & 9.57 \times 10^{-1} & 4.16 \times 10^{-1} & 2.02 \times 10^{-27} & 1.14 & 1.14 & 9.81 & 9.81 \\
-9.98 \times 10^{-1} & 0 & 0 & 4.74 & 2.05 \times 10^{-1} & -2.05 \times 10^{-1} & 0 & 0 \\
2.02 \times 10^{-27} & -1.33 \times 10^{1} & -5.52 & 4.44 \times 10^{-27} & -6.53 & -6.53 & 1.37 \times 10^{-26} & 1.37 \times 10^{-26} \\
-1.47 & 0 & 0 & 2.31 \times 10^{-1} & 1.63 & -1.63 & 4.71 \times 10^{-2} & -4.71 \times 10^{-2} \\
-5.05 \times 10^{-28} & -3.11 & -1.16 & -1.11 \times 10^{-27} & -1.05 \times 10^{-1} & -1.05 \times 10^{-1} & 9.55 \times 10^{-2} & 9.55 \times 10^{-2} \\
-2.67 \times 10^{-2} & 0 & 0 & -7.77 \times 10^{-1} & 1.39 \times 10^{-1} & -1.39 \times 10^{-1} & 5.07 \times 10^{-1} & -5.07 \times 10^{-1} \\
0 & 0 & 0 & 0 & 0 & 0 & 0 & 0 \\
0 & 0 & 0 & 0 & 0 & 0 & 0 & 0 \\
0 & 0 & 0 & 0 & 0 & 0 & 0 & 0 \\
-1.26 \times 10^{-28} & -1.62 \times 10^{-26} & -8.20 \times 10^{-29} & -2.52 \times 10^{-28} & -1.20 \times 10^{-28} & -1.20 \times 10^{-28} & -8.08 \times 10^{-28} & -8.08 \times 10^{-28}
\end{bmatrix} \tag{E.5}$$

$$B_{p,m,A}\begin{bmatrix} I_{10} \\ 0_{29\times 10} \end{bmatrix} =$$

$$\begin{bmatrix}
6.35\times10^{-3} & 1.99\times10^{-2} & 6.45\times10^{-2} & 1.49\times10^{-1} & 6.35\times10^{-3} & 5.94\times10^{-3} & 0 & 0 & 0 & 0 \\
0 & 0 & 0 & 0 & 0 & 0 & 0 & 0 & 0 & 0 \\
0 & 2.25\times10^{-2} & 0 & 0 & 0 & 0 & 2.06\times10^{-2} & 8.66\times10^{-1} & 0 & 0 \\
0 & 0 & 0 & 0 & 0 & 0 & 0 & 0 & 9.34\times10^{-2} & 1.41\times10^{-1} \\
0 & 1.72\times10^{-3} & 0 & 0 & 0 & 0 & 2.06\times10^{-3} & 0 & 0 & 0 \\
0 & 0 & 0 & 0 & 0 & 0 & 0 & 0 & 0 & 0 \\
0 & 0 & 0 & 0 & 0 & 0 & 0 & 0 & 0 & 0 \\
0 & 0 & 0 & 0 & 0 & 0 & 0 & 0 & 0 & 0 \\
0 & 0 & 0 & 0 & 0 & 0 & 0 & 0 & 0 & 0 \\
0 & 0 & 0 & 0 & 0 & 0 & 0 & 0 & 0 & 0
\end{bmatrix} \tag{E.6}$$

$$B_{p,m,A}\begin{bmatrix} 0_{10\times 10} \\ I_{10} \\ 0_{19\times 10} \end{bmatrix} =$$

$$\begin{bmatrix}
0 & 0 & 0 & 0 & 0 & 2.64\times10^{-1} & 0 & 0 & 0 & 0 \\
0 & 0 & 0 & 0 & 0 & -1.98\times10^{-2} & 2.58\times10^{-1} & 0 & 0 & 0 \\
0 & 0 & 0 & 0 & 0 & -2.65\times10^{-1} & 1.52\times10^{-2} & 5.26\times10^{-1} & 0 & 0 \\
9.39\times10^{-2} & 0 & 0 & 0 & 0 & 5.08\times10^{-3} & -1.68\times10^{-3} & 1.94\times10^{-3} & 7.50\times10^{-2} & 0 \\
0 & 1.64\times10^{-3} & 8.64\times10^{-4} & 2.28\times10^{-1} & 0 & 3.41\times10^{-4} & 5.92\times10^{-4} & -2.05\times10^{-3} & -2.03\times10^{-4} & 1.30\times10^{-2} \\
0 & 0 & 0 & 0 & 2.17\times10^{-2} & 2.09\times10^{-4} & -3.50\times10^{-3} & -2.90\times10^{-4} & 3.40\times10^{-3} & -3.53\times10^{-4} \\
0 & 0 & 0 & 0 & 0 & 3.74\times10^{-5} & 1.88\times10^{-5} & 3.25\times10^{-5} & -3.23\times10^{-5} & 1.08\times10^{-4} \\
0 & 0 & 0 & 0 & 0 & 6.55\times10^{-5} & 6.62\times10^{-5} & 7.16\times10^{-5} & -2.30\times10^{-5} & 1.10\times10^{-5} \\
0 & 0 & 0 & 0 & 0 & -4.77\times10^{-5} & -2.22\times10^{-5} & -5.92\times10^{-5} & -3.81\times10^{-5} & 9.47\times10^{-5} \\
0 & 0 & 0 & 0 & 0 & 1.56\times10^{-2} & -5.80\times10^{-3} & -1.48\times10^{-2} & -1.72\times10^{-2} & -7.49\times10^{-3}
\end{bmatrix} \tag{E.7}$$

$$B_{p,m,A}\begin{bmatrix} 0_{20\times 10} \\ I_{10} \\ 0_{9\times 10} \end{bmatrix} = \begin{bmatrix}
0 & 0 & 0 & 0 & 0 & 0 & 0 & 0 & 0 & 0 \\
0 & 0 & 0 & 0 & 0 & 0 & 0 & 0 & 0 & 0 \\
0 & 0 & 0 & 0 & 0 & 0 & 0 & 0 & 0 & 0 \\
0 & 0 & 0 & 0 & 0 & 0 & 0 & 0 & 0 & 0 \\
0 & 0 & 0 & 0 & 0 & 0 & 0 & 0 & 0 & 0 \\
1.14\times10^{-2} & 0 & 0 & 0 & 0 & 0 & 0 & 0 & 0 & 0 \\
-1.58\times10^{-6} & 1.06\times10^{-3} & 0 & 0 & 0 & 0 & 0 & 0 & 0 & 0 \\
1.34\times10^{-4} & -1.47\times10^{-4} & 1.44\times10^{-3} & 0 & 0 & 0 & 0 & 0 & 0 & 0 \\
-4.74\times10^{-5} & 6.72\times10^{-5} & 5.98\times10^{-5} & 8.62\times10^{-4} & 0 & 0 & 0 & 0 & 0 & 0 \\
1.78\times10^{-2} & -1.50\times10^{-2} & -2.19\times10^{-2} & 2.52\times10^{-2} & 2.15\times10^{-1} & 0 & 0 & 0 & 0 & 0
\end{bmatrix} \tag{E.8}$$

$$B_{p,m,A}\begin{bmatrix} 0_{29\times 9} \\ I_9 \end{bmatrix} = 0 \tag{E.9}$$

$$C_{q,m,A} =$$

$$\begin{bmatrix}
0 & 1.00 & -9.29\times10^{-1} & 0 & 0 & 0 & 0 & 0 & 0 & 0 \\
0 & 0 & 1.00 & 0 & 0 & 0 & 0 & 0 & 0 & 0 \\
0 & 0 & 0 & 0 & 0 & 0 & 0 & 0 & 0 & 0 \\
0 & 0 & 0 & 0 & 0 & 0 & 0 & 0 & 0 & 0 \\
0 & 0 & 0 & 0 & 0 & 0 & 0 & 0 & 0 & 0 \\
0 & 0 & 0 & 0 & 0 & 0 & 0 & 0 & 0 & 0 \\
0 & 0 & 1.00 & 0 & 0 & 0 & 0 & 0 & 0 & 0 \\
0 & 0 & 0 & 0 & 0 & 0 & 0 & 0 & 0 & 0 \\
0 & 0 & 0 & 0 & 0 & 0 & 0 & 0 & 0 & 0 \\
0 & 0 & 0 & 0 & 0 & 0 & 0 & 0 & 0 & 0 \\
0 & 0 & 0 & 0 & 0 & 0 & 0 & 0 & 0 & 0 \\
0 & 1.00 & 0 & 0 & 0 & 0 & 0 & 0 & 0 & 0 \\
0 & 0 & 1.00 & 0 & 0 & 0 & 0 & 0 & 0 & 0 \\
0 & 0 & 0 & 0 & 0 & 0 & 0 & 0 & 0 & 0 \\
0 & 0 & 0 & 0 & 0 & 0 & 0 & 0 & 0 & 0 \\
8.48\times10^{-1} & -2.17\times10^{-3} & -1.04\times10^{-3} & 3.09\times10^{-6} & 9.61\times10^{-7} & -2.39\times10^{-6} & -2.63\times10^{-7} & 1.41\times10^{-6} & 6.61\times10^{-7} & -5.76\times10^{-3} \\
0 & 9.23\times10^{-1} & 9.13\times10^{-3} & 5.35\times10^{-5} & -1.62\times10^{-5} & 4.13\times10^{-7} & -6.55\times10^{-5} & 2.93\times10^{-5} & -5.72\times10^{-5} & -9.17\times10^{-3} \\
0 & 0 & 9.44\times10^{-1} & -3.40\times10^{-5} & -2.11\times10^{-5} & 1.80\times10^{-4} & -4.88\times10^{-5} & -5.33\times10^{-5} & -1.13\times10^{-4} & 1.01\times10^{-1} \\
0 & 0 & 0 & 8.48\times10^{-1} & 2.17\times10^{-8} & 4.49\times10^{-8} & -4.10\times10^{-8} & 9.04\times10^{-8} & -2.49\times10^{-8} & -1.40\times10^{-4} \\
0 & 0 & 0 & 0 & 8.48\times10^{-1} & -4.39\times10^{-8} & -3.83\times10^{-8} & 7.96\times10^{-9} & 1.95\times10^{-8} & -3.85\times10^{-5} \\
0 & 0 & 0 & 0 & 0 & 8.48\times10^{-1} & 6.65\times10^{-9} & -7.22\times10^{-8} & -1.13\times10^{-7} & 1.60\times10^{-4} \\
0 & 0 & 0 & 0 & 0 & 0 & 8.48\times10^{-1} & 3.65\times10^{-8} & 6.16\times10^{-8} & 8.38\times10^{-6} \\
0 & 0 & 0 & 0 & 0 & 0 & 0 & 8.48\times10^{-1} & 8.86\times10^{-9} & -1.04\times10^{-4} \\
0 & 0 & 0 & 0 & 0 & 0 & 0 & 0 & 8.48\times10^{-1} & -2.91\times10^{-5} \\
0 & 0 & 0 & 0 & 0 & 0 & 0 & 0 & 0 & 1.00 \\
0 & 0 & 0 & 0 & 0 & 0 & 0 & 0 & 0 & 0 \\
0 & 0 & 0 & 0 & 0 & 0 & 0 & 0 & 0 & 0 \\
0 & 0 & 0 & 0 & 0 & 0 & 0 & 0 & 0 & 0 \\
0 & 0 & 0 & 0 & 0 & 0 & 0 & 0 & 0 & 0 \\
0 & 0 & 0 & 0 & 0 & 0 & 0 & 0 & 0 & 0 \\
0 & 0 & 0 & 0 & 0 & 0 & 0 & 0 & 0 & 0 \\
0 & 0 & 0 & 0 & 0 & 0 & 0 & 0 & 0 & 0 \\
0 & 0 & 0 & 0 & 0 & 0 & 0 & 0 & 0 & 0 \\
0 & 0 & 0 & 0 & 0 & 0 & 0 & 0 & 0 & 0 \\
0 & 0 & 0 & 0 & 0 & 0 & 0 & 0 & 0 & 0 \\
0 & 0 & 0 & 0 & 0 & 0 & 0 & 0 & 0 & 0 \\
0 & 0 & 0 & 0 & 0 & 0 & 0 & 0 & 0 & 0 \\
0 & 0 & 0 & 0 & 0 & 0 & 0 & 0 & 0 & 0 \\
0 & 0 & 0 & 0 & 0 & 0 & 0 & 0 & 0 & 0
\end{bmatrix} \quad \text{(E.10)}$$

$$D_{qg,m,A} =$$

$$\begin{bmatrix}
0 & 0 & 0 & 0 & 0 & 0 \\
0 & 0 & -1.02 & 0 & 0 & 0 \\
0 & 0 & 0 & 0 & 0 & 0 \\
0 & 0 & 0 & 0 & 0 & 0 \\
0 & 1.00 & 0 & 0 & 0 & 0 \\
0 & 0 & 1.00 & 0 & 0 & 0 \\
0 & 0 & -1.02 & 0 & 0 & 0 \\
0 & 0 & 0 & 0 & 0 & 0 \\
0 & 0 & 0 & 0 & 0 & 0 \\
0 & 0 & 0 & 0 & 0 & 0 \\
0 & 0 & 0 & 0 & 0 & 0 \\
0 & -9.56 \times 10^{-1} & 0 & 0 & 0 & 0 \\
0 & 0 & -1.02 & 0 & 0 & 0 \\
0 & 0 & 0 & 0 & 0 & 0 \\
0 & 0 & 0 & 0 & 0 & 0 \\
-9.73 \times 10^{-4} & 9.46 \times 10^{-5} & -9.04 \times 10^{-5} & 2.17 \times 10^{-6} & 1.13 \times 10^{-6} & -5.67 \times 10^{-7} \\
-1.49 \times 10^{-2} & -1.34 \times 10^{-2} & 7.72 \times 10^{-2} & -2.45 \times 10^{-5} & -1.72 \times 10^{-5} & 6.68 \times 10^{-5} \\
8.56 \times 10^{-3} & 8.96 \times 10^{-3} & 1.61 \times 10^{-2} & 4.07 \times 10^{-5} & 2.11 \times 10^{-5} & 8.14 \times 10^{-5} \\
-2.89 \times 10^{-5} & -1.33 \times 10^{-4} & 4.64 \times 10^{-5} & -7.60 \times 10^{-8} & -8.63 \times 10^{-8} & 1.22 \times 10^{-7} \\
-3.71 \times 10^{-5} & 1.27 \times 10^{-5} & 9.07 \times 10^{-6} & 2.75 \times 10^{-8} & 3.32 \times 10^{-9} & 3.15 \times 10^{-9} \\
1.01 \times 10^{-4} & -8.21 \times 10^{-5} & 3.66 \times 10^{-5} & -1.03 \times 10^{-7} & -7.31 \times 10^{-8} & 1.59 \times 10^{-7} \\
9.28 \times 10^{-5} & 7.70 \times 10^{-6} & -7.85 \times 10^{-5} & -1.26 \times 10^{-8} & -3.58 \times 10^{-8} & -6.21 \times 10^{-8} \\
-4.62 \times 10^{-5} & -4.06 \times 10^{-5} & -1.36 \times 10^{-6} & -1.22 \times 10^{-9} & -3.31 \times 10^{-8} & 6.73 \times 10^{-9} \\
-3.93 \times 10^{-6} & 4.93 \times 10^{-6} & -6.30 \times 10^{-5} & -2.15 \times 10^{-8} & 1.51 \times 10^{-8} & -8.64 \times 10^{-8} \\
6.75 \times 10^{-2} & 3.24 \times 10^{-3} & 1.22 \times 10^{-2} & -5.11 \times 10^{-5} & 6.22 \times 10^{-5} & 2.07 \times 10^{-6} \\
3.50 \times 10^{-5} & -1.62 \times 10^{-4} & -2.78 \times 10^{-4} & 3.58 \times 10^{-9} & -6.91 \times 10^{-8} & -4.09 \times 10^{-7} \\
1.21 \times 10^{-6} & 1.11 \times 10^{-6} & 6.81 \times 10^{-7} & 1.55 \times 10^{-10} & -3.86 \times 10^{-10} & 2.26 \times 10^{-9} \\
-1.52 \times 10^{-3} & -9.29 \times 10^{-4} & -8.75 \times 10^{-4} & 8.54 \times 10^{-7} & -2.82 \times 10^{-7} & -8.94 \times 10^{-7} \\
2.55 \times 10^{-4} & 3.12 \times 10^{-4} & 3.71 \times 10^{-5} & -2.67 \times 10^{-7} & -3.94 \times 10^{-9} & -5.56 \times 10^{-8} \\
-3.30 \times 10^{-4} & 2.04 \times 10^{-4} & -1.63 \times 10^{-4} & 5.22 \times 10^{-7} & 7.69 \times 10^{-8} & -2.33 \times 10^{-7} \\
-1.72 \times 10^{-4} & 5.39 \times 10^{-6} & -8.13 \times 10^{-4} & 4.55 \times 10^{-7} & 2.60 \times 10^{-7} & -7.02 \times 10^{-7} \\
-4.41 \times 10^{-5} & -1.51 \times 10^{-5} & 2.53 \times 10^{-5} & 1.25 \times 10^{-8} & 7.51 \times 10^{-9} & 6.52 \times 10^{-8} \\
-9.66 \times 10^{-6} & -3.48 \times 10^{-5} & -6.09 \times 10^{-5} & 4.33 \times 10^{-9} & -1.65 \times 10^{-8} & -4.60 \times 10^{-8} \\
9.27 \times 10^{-1} & 1.60 \times 10^{-2} & 8.25 \times 10^{-4} & -1.05 \times 10^{-4} & -5.32 \times 10^{-5} & 2.30 \times 10^{-5} \\
0 & 9.21 \times 10^{-1} & 1.63 \times 10^{-2} & 4.49 \times 10^{-5} & 6.26 \times 10^{-5} & -4.04 \times 10^{-5} \\
0 & 0 & 9.14 \times 10^{-1} & -4.95 \times 10^{-5} & 1.47 \times 10^{-6} & 1.07 \times 10^{-4} \\
0 & 0 & 0 & 8.48 \times 10^{-1} & 7.64 \times 10^{-8} & -6.29 \times 10^{-8} \\
0 & 0 & 0 & 0 & 8.48 \times 10^{-1} & -3.11 \times 10^{-8} \\
0 & 0 & 0 & 0 & 0 & 8.48 \times 10^{-1}
\end{bmatrix} \tag{E.11}$$

$$D_{qu,m,A} =$$

$$\begin{bmatrix}
0 & 0 & 0 & 0 & 0 & 0 & 0 & 0 \\
0 & 0 & 0 & 0 & 0 & 0 & 0 & 0 \\
0 & 0 & 1.00 & 0 & 0 & 0 & 0 & 0 \\
0 & 0 & 0 & 0 & 1.00 & 1.00 & 0 & 0 \\
0 & 0 & 0 & 0 & 0 & 0 & 0 & 0 \\
0 & 0 & 0 & 0 & 0 & 0 & 0 & 0 \\
0 & 0 & 0 & 0 & 0 & 0 & 0 & 0 \\
0 & 0 & 1.00 & 0 & 0 & 0 & 0 & 0 \\
1.00 & 0 & 0 & 0 & -1.01 & 0 & 0 & 0 \\
0 & 0 & 0 & 0 & 1.00 & -1.00 & 0 & 0 \\
0 & 0 & 0 & 0 & 0 & 1.00 & 0 & 0 \\
0 & 0 & 0 & 0 & 0 & 0 & 0 & 0 \\
0 & 0 & 0 & 0 & 0 & 0 & 0 & 0 \\
0 & 0 & 1.00 & 0 & 0 & 0 & 0 & 0 \\
0 & 0 & 0 & 1.00 & 0 & 0 & 0 & 0 \\
3.80 \times 10^{-6} & 8.83 \times 10^{-8} & 2.60 \times 10^{-5} & -5.90 \times 10^{-7} & 1.01 \times 10^{-5} & 1.58 \times 10^{-5} & 4.42 \times 10^{-8} & -8.58 \times 10^{-7} \\
-7.17 \times 10^{-5} & 2.18 \times 10^{-7} & -5.94 \times 10^{-4} & -3.15 \times 10^{-5} & -1.42 \times 10^{-4} & -5.54 \times 10^{-4} & 4.30 \times 10^{-5} & -3.98 \times 10^{-5} \\
-4.63 \times 10^{-4} & 1.49 \times 10^{-6} & -6.56 \times 10^{-4} & -1.26 \times 10^{-4} & -2.69 \times 10^{-4} & -2.54 \times 10^{-4} & 1.07 \times 10^{-4} & 3.68 \times 10^{-6} \\
1.42 \times 10^{-7} & 6.10 \times 10^{-10} & 5.36 \times 10^{-7} & -2.99 \times 10^{-7} & -1.76 \times 10^{-9} & -1.03 \times 10^{-7} & 2.82 \times 10^{-8} & -2.89 \times 10^{-8} \\
-9.53 \times 10^{-8} & 4.38 \times 10^{-10} & 1.81 \times 10^{-7} & 1.61 \times 10^{-8} & 7.92 \times 10^{-8} & 7.38 \times 10^{-8} & 7.94 \times 10^{-9} & -1.88 \times 10^{-8} \\
-4.27 \times 10^{-7} & 5.10 \times 10^{-10} & -1.01 \times 10^{-6} & -1.24 \times 10^{-7} & -7.75 \times 10^{-7} & -6.18 \times 10^{-7} & 8.30 \times 10^{-8} & 8.51 \times 10^{-9} \\
2.60 \times 10^{-7} & 4.69 \times 10^{-10} & -1.53 \times 10^{-7} & 1.66 \times 10^{-7} & 1.13 \times 10^{-7} & 1.70 \times 10^{-7} & -6.48 \times 10^{-8} & 1.59 \times 10^{-8} \\
1.10 \times 10^{-7} & 1.75 \times 10^{-10} & 7.03 \times 10^{-7} & -1.43 \times 10^{-7} & 2.58 \times 10^{-7} & 1.21 \times 10^{-7} & 1.17 \times 10^{-8} & -7.87 \times 10^{-9} \\
4.05 \times 10^{-7} & -1.65 \times 10^{-9} & 5.85 \times 10^{-7} & 1.05 \times 10^{-7} & 2.49 \times 10^{-7} & 3.82 \times 10^{-7} & -7.42 \times 10^{-8} & 1.88 \times 10^{-8} \\
-6.62 \times 10^{-5} & -2.67 \times 10^{-6} & -1.05 \times 10^{-3} & 8.76 \times 10^{-5} & -4.96 \times 10^{-4} & -2.84 \times 10^{-4} & 8.94 \times 10^{-6} & 3.55 \times 10^{-5} \\
8.48 \times 10^{-1} & -2.72 \times 10^{-10} & 3.18 \times 10^{-6} & 1.90 \times 10^{-7} & 1.53 \times 10^{-9} & 1.74 \times 10^{-6} & -3.41 \times 10^{-7} & 2.85 \times 10^{-8} \\
0 & 8.48 \times 10^{-1} & -2.13 \times 10^{-8} & 2.90 \times 10^{-9} & -2.06 \times 10^{-9} & -4.50 \times 10^{-9} & -1.18 \times 10^{-10} & -1.73 \times 10^{-9} \\
0 & 0 & 8.48 \times 10^{-1} & -3.57 \times 10^{-6} & 4.77 \times 10^{-6} & 6.95 \times 10^{-6} & -2.45 \times 10^{-7} & 5.61 \times 10^{-7} \\
0 & 0 & 0 & 8.48 \times 10^{-1} & 2.58 \times 10^{-8} & -4.28 \times 10^{-7} & -1.89 \times 10^{-7} & -2.69 \times 10^{-8} \\
0 & 0 & 0 & 0 & 8.48 \times 10^{-1} & 1.58 \times 10^{-6} & -4.64 \times 10^{-8} & -5.08 \times 10^{-8} \\
0 & 0 & 0 & 0 & 0 & 8.48 \times 10^{-1} & -2.72 \times 10^{-7} & 2.53 \times 10^{-7} \\
0 & 0 & 0 & 0 & 0 & 0 & 8.48 \times 10^{-1} & 6.90 \times 10^{-9} \\
0 & 0 & 0 & 0 & 0 & 0 & 0 & 8.48 \times 10^{-1} \\
0 & 0 & 0 & 0 & 0 & 0 & 0 & 0 \\
0 & 0 & 0 & 0 & 0 & 0 & 0 & 0 \\
0 & 0 & 0 & 0 & 0 & 0 & 0 & 0 \\
0 & 0 & 0 & 0 & 0 & 0 & 0 & 0 \\
0 & 0 & 0 & 0 & 0 & 0 & 0 & 0 \\
0 & 0 & 0 & 0 & 0 & 0 & 0 & 0
\end{bmatrix} \tag{E.12}$$

$$D_{qp,A} = 0, \quad \Delta_A = \text{blkdiag}\left(\delta_1, \delta_2, \ldots, \delta_{15}, \Delta_1\right), \quad \text{size}\left(\Delta_1\right) = 24 \times 24 \tag{E.13}$$

Furthermore, the state-feedback gain and predictor estimator feedback gain is given by (E.14)-(E.20) for coupled controller no.8 in Table 4.9 and by (E.21)-(E.31) for no.16 in Table D.1.

$$K_C \begin{bmatrix} I_{10} \\ 0_{50\times 10} \end{bmatrix} =$$

$$\begin{bmatrix}
-3.34\times10^{-3} & 3.35\times10^{-2} & 8.43\times10^{-3} & 3.42\times10^{-1} & -4.90\times10^{-2} & 1.37 & 3.66\times10^{-1} & -2.02 & -1.37\times10^{-3} & 6.62\times10^{-1} \\
5.68\times10^{-4} & 5.15\times10^{-6} & -5.54\times10^{-5} & 7.74\times10^{-5} & 2.42\times10^{-2} & 8.40\times10^{-4} & 4.89\times10^{-5} & 5.59\times10^{-2} & 1.82\times10^{-5} & -6.80\times10^{-6} \\
1.56\times10^{-2} & -3.09\times10^{-4} & 5.41\times10^{-3} & 1.54\times10^{-2} & 1.12 & 8.77\times10^{-2} & 2.36\times10^{-2} & -3.64\times10^{-1} & 2.53\times10^{-3} & -3.14\times10^{-3} \\
-1.90\times10^{-3} & -1.98\times10^{-3} & -1.49\times10^{-3} & -3.32\times10^{-2} & 1.68\times10^{-1} & 1.84\times10^{-1} & 3.45\times10^{-4} & 4.96\times10^{-1} & 6.70\times10^{-4} & 1.02\times10^{-2} \\
-2.55\times10^{-2} & 1.50\times10^{-2} & 1.80\times10^{-2} & -7.70\times10^{-2} & -8.89\times10^{-1} & -5.51\times10^{-1} & -1.95\times10^{-1} & -6.07 & -6.77\times10^{-3} & 4.27\times10^{-2} \\
-2.48\times10^{-2} & -1.42\times10^{-2} & 1.64\times10^{-2} & 6.29\times10^{-2} & -9.47\times10^{-1} & 5.03\times10^{-1} & 1.76\times10^{-1} & -5.73 & -6.93\times10^{-3} & -4.35\times10^{-2} \\
-5.32\times10^{-1} & -1.66\times10^{-2} & -1.82\times10^{-2} & -5.56\times10^{-2} & 2.88 & -1.69\times10^{-1} & -1.99\times10^{-2} & 3.62 & 1.65\times10^{-2} & 3.02\times10^{-2} \\
-5.32\times10^{-1} & 7.46\times10^{-3} & -2.62\times10^{-2} & 2.03\times10^{-2} & 2.67 & 4.95\times10^{-1} & 1.57\times10^{-2} & 5.27 & 1.71\times10^{-2} & -1.35\times10^{-2} \\
7.40\times10^{-3} & -2.42\times10^{-2} & -4.09\times10^{-3} & -1.64\times10^{-1} & -3.92\times10^{-1} & -1.76 & -2.26\times10^{-1} & 7.38\times10^{-1} & 1.01\times10^{-3} & 1.43\times10^{-1} \\
-3.39\times10^{-4} & -2.47\times10^{-5} & 4.45\times10^{-4} & -4.74\times10^{-4} & 3.03\times10^{-2} & -1.24\times10^{-3} & -5.80\times10^{-4} & -7.79\times10^{-2} & 5.75\times10^{-5} & 1.96\times10^{-4} \\
-1.88\times10^{-4} & -7.01\times10^{-4} & 1.63\times10^{-3} & -2.79\times10^{-2} & 1.57\times10^{-1} & -1.35\times10^{-1} & -3.89\times10^{-2} & -1.62\times10^{-1} & 2.88\times10^{-3} & 7.92\times10^{-3} \\
5.68\times10^{-3} & -9.09\times10^{-3} & 7.58\times10^{-4} & -7.47\times10^{-2} & -3.83\times10^{-1} & -5.00\times10^{-1} & -8.56\times10^{-2} & -5.20\times10^{-1} & -1.06\times10^{-3} & 3.85\times10^{-2} \\
2.26\times10^{-2} & 2.01\times10^{-2} & -2.16\times10^{-2} & -8.81\times10^{-2} & 2.73\times10^{-1} & -6.61\times10^{-1} & -2.43\times10^{-1} & 6.32 & -1.93\times10^{-3} & 5.95\times10^{-2} \\
1.84\times10^{-2} & -2.28\times10^{-2} & -1.76\times10^{-2} & 5.56\times10^{-2} & 6.56\times10^{-1} & 6.69\times10^{-1} & 2.12\times10^{-1} & 5.64 & -2.26\times10^{-3} & -5.33\times10^{-2} \\
5.01\times10^{-1} & 6.21\times10^{-2} & 2.93\times10^{-3} & -7.47\times10^{-2} & -2.81 & -5.68\times10^{-1} & -3.64\times10^{-1} & -4.42\times10^{-1} & -1.04\times10^{-2} & 1.55\times10^{-2} \\
4.96\times10^{-1} & -5.28\times10^{-2} & 2.68\times10^{-2} & 1.15\times10^{-1} & -2.37 & 3.55\times10^{-1} & 3.80\times10^{-1} & -5.68 & -9.31\times10^{-3} & -3.80\times10^{-2}
\end{bmatrix} \tag{E.14}$$

$$K_C \begin{bmatrix} 0_{10\times 10} \\ I_{10} \\ 0_{40\times 10} \end{bmatrix} =$$

$$\begin{bmatrix}
-6.29\times10^{-2} & -5.48\times10^{-3} & -6.50\times10^{-2} & 1.60\times10^{-1} & -1.89\times10^{-1} & 7.21\times10^{-2} & -4.46\times10^{-2} & 1.23\times10^{-3} & -4.31\times10^{-2} & -6.75\times10^{-3} \\
9.69\times10^{-1} & -4.98\times10^{-3} & -1.17\times10^{-5} & 1.40\times10^{-5} & -1.96\times10^{-6} & 1.88\times10^{-3} & 1.85\times10^{-3} & -6.12\times10^{-4} & -8.65\times10^{-7} & 2.24\times10^{-5} \\
-1.31 & 4.51\times10^{-1} & -7.93\times10^{-3} & -3.27\times10^{-2} & -4.12\times10^{-2} & 6.92\times10^{-2} & 5.54\times10^{-2} & -1.38\times10^{-2} & 3.40\times10^{-6} & -1.02\times10^{-2} \\
-6.25\times10^{-2} & -3.42\times10^{-2} & 8.67\times10^{-1} & 8.49\times10^{-4} & 1.01\times10^{-3} & 2.65\times10^{-2} & -4.25\times10^{-2} & 2.73\times10^{-3} & 2.58\times10^{-3} & 6.97\times10^{-4} \\
3.70\times10^{-1} & 1.24\times10^{-1} & 9.32\times10^{-2} & 7.95\times10^{-1} & 3.23\times10^{-2} & -1.37\times10^{-1} & 1.69\times10^{-2} & 2.20\times10^{-2} & -1.48\times10^{-2} & -1.06\times10^{-2} \\
4.05\times10^{-1} & 1.41\times10^{-1} & -9.37\times10^{-2} & 3.77\times10^{-2} & 7.99\times10^{-1} & 1.87\times10^{-2} & -1.47\times10^{-1} & 2.11\times10^{-2} & 1.38\times10^{-2} & -9.10\times10^{-3} \\
-1.43 & -5.53\times10^{-1} & -4.08\times10^{-3} & -1.92\times10^{-1} & -1.30\times10^{-1} & -4.25 & -1.29 & 5.06\times10^{-1} & 2.18\times10^{-2} & 2.28\times10^{-3} \\
-1.31 & -5.02\times10^{-1} & -6.51\times10^{-2} & -1.25\times10^{-1} & -1.72\times10^{-1} & -1.29 & -4.30 & 5.05\times10^{-1} & -8.13\times10^{-3} & 9.76\times10^{-3} \\
3.85\times10^{-1} & 1.45\times10^{-1} & 2.93\times10^{-1} & -1.74\times10^{-1} & 2.34\times10^{-1} & -2.24\times10^{-1} & 2.86\times10^{-1} & -4.74\times10^{-3} & 2.80\times10^{-2} & 3.54\times10^{-3} \\
-1.96\times10^{-2} & -8.69\times10^{-3} & 6.18\times10^{-5} & -1.74\times10^{-3} & -1.28\times10^{-3} & -3.69\times10^{-4} & -3.05\times10^{-4} & 3.90\times10^{-4} & 4.51\times10^{-5} & -5.83\times10^{-4} \\
-1.85\times10^{-1} & -5.38\times10^{-2} & 1.16\times10^{-2} & -2.84\times10^{-2} & -9.27\times10^{-3} & -1.45\times10^{-2} & 1.59\times10^{-2} & -1.29\times10^{-3} & 1.84\times10^{-3} & -4.95\times10^{-3} \\
1.81\times10^{-1} & 8.52\times10^{-2} & 5.87\times10^{-2} & -4.38\times10^{-2} & 5.00\times10^{-2} & -3.86\times10^{-2} & 7.44\times10^{-2} & -6.75\times10^{-3} & 1.11\times10^{-2} & 6.68\times10^{-4} \\
6.71\times10^{-2} & 2.31\times10^{-2} & 1.29\times10^{-1} & -3.26\times10^{-2} & 1.40\times10^{-1} & -1.75\times10^{-2} & 1.67\times10^{-1} & -2.72\times10^{-2} & -1.87\times10^{-2} & 2.49\times10^{-2} \\
-2.49\times10^{-1} & -9.90\times10^{-2} & -1.45\times10^{-1} & 1.10\times10^{-1} & -5.42\times10^{-2} & 1.59\times10^{-1} & -4.35\times10^{-2} & -2.44\times10^{-2} & 2.30\times10^{-2} & 2.10\times10^{-2} \\
1.41 & 5.66\times10^{-1} & 1.27\times10^{-1} & 1.38\times10^{-1} & 2.12\times10^{-1} & 1.22 & 1.31 & -5.20\times10^{-1} & -7.01\times10^{-2} & 5.08\times10^{-3} \\
1.13 & 4.44\times10^{-1} & -7.59\times10^{-2} & 1.91\times10^{-1} & 8.67\times10^{-2} & 1.33 & 1.28 & -5.14\times10^{-1} & 5.54\times10^{-2} & -2.01\times10^{-2}
\end{bmatrix} \tag{E.15}$$

$$K_C \begin{bmatrix} 0_{20\times 10} \\ I_{10} \\ 0_{30\times 10} \end{bmatrix} =$$

$$\begin{bmatrix}
-1.27\times10^{-1} & 1.85\times10^{-1} & -4.61\times10^{-1} & -4.94\times10^{-2} & 1.65 & 8.50 & 5.99\times10^{-2} & 3.30\times10^{-2} & -2.63\times10^{-2} & 2.22\times10^{-2} \\
-8.17\times10^{-6} & 1.13\times10^{-2} & -6.90\times10^{-4} & 2.65\times10^{-5} & 3.71\times10^{-3} & 3.16\times10^{-3} & 2.13\times10^{-5} & -4.89\times10^{-3} & -2.28\times10^{-3} & 3.18\times10^{-5} \\
-2.74\times10^{-3} & 6.81\times10^{-2} & 4.18\times10^{-2} & -1.62\times10^{-2} & 1.61 & -5.84\times10^{-4} & 1.61\times10^{-3} & -3.72\times10^{-2} & -6.58\times10^{-3} & -4.52\times10^{-3} \\
-4.63\times10^{-3} & -6.69\times10^{-2} & -2.37\times10^{-2} & -2.07\times10^{-2} & -2.96\times10^{-1} & -4.41\times10^{-1} & 2.57\times10^{-3} & 1.21\times10^{-3} & 1.32\times10^{-2} & 4.04\times10^{-3} \\
-5.92\times10^{-3} & 2.02\times10^{-2} & -3.10\times10^{-1} & 1.90\times10^{-1} & 2.33 & 2.63 & 1.33\times10^{-2} & 1.84\times10^{-1} & 3.80\times10^{-2} & 3.22\times10^{-2} \\
-8.00\times10^{-3} & 2.87\times10^{-2} & 3.17\times10^{-1} & -1.95\times10^{-1} & 2.05 & -2.57 & -9.95\times10^{-3} & 1.57\times10^{-1} & 3.04\times10^{-2} & -3.91\times10^{-2} \\
8.12\times10^{-2} & 1.57 & -1.57\times10^{-1} & -5.62\times10^{-2} & 1.00\times10^{1} & -3.41 & -2.22\times10^{-2} & -7.94\times10^{-1} & -3.03\times10^{-1} & 4.54\times10^{-2} \\
-1.12\times10^{-4} & 1.39 & -2.85\times10^{-1} & 6.66\times10^{-2} & 8.44 & 2.10 & 7.61\times10^{-3} & -7.44\times10^{-1} & -2.81\times10^{-1} & 2.61\times10^{-2} \\
2.53\times10^{-1} & -1.78\times10^{-1} & 2.26\times10^{-1} & 1.93\times10^{-1} & -1.04 & -6.29 & 7.28\times10^{-1} & 1.52\times10^{-1} & 6.28\times10^{-2} & 9.38\times10^{-2} \\
3.03\times10^{-4} & 2.01\times10^{-2} & -1.44\times10^{-3} & 4.76\times10^{-4} & 1.35\times10^{-1} & -6.04\times10^{-3} & -7.31\times10^{-5} & 9.67\times10^{-1} & -4.70\times10^{-3} & 2.41\times10^{-4} \\
1.80\times10^{-2} & 1.22 & -1.25\times10^{-1} & 3.30\times10^{-2} & 2.54 & -1.90\times10^{-1} & -6.57\times10^{-3} & -1.35 & 4.49\times10^{-1} & 1.89\times10^{-2} \\
2.30\times10^{-2} & 4.58\times10^{-2} & 3.45\times10^{-1} & 3.06\times10^{-2} & 6.80\times10^{-2} & -2.25 & -6.09\times10^{-3} & 2.68\times10^{-2} & -6.18\times10^{-3} & 8.71\times10^{-1} \\
-1.25\times10^{-2} & -2.38\times10^{-1} & -6.18\times10^{-1} & 2.24\times10^{-1} & -5.83 & 3.67 & 3.35\times10^{-2} & 5.05\times10^{-2} & -1.53\times10^{-2} & 8.31\times10^{-2} \\
2.89\times10^{-2} & -1.27\times10^{-2} & 4.36\times10^{-1} & -2.18\times10^{-1} & -4.73 & -4.12 & -3.69\times10^{-2} & -1.09\times10^{-1} & -8.17\times10^{-2} & -6.05\times10^{-2} \\
-1.55\times10^{-1} & -1.60 & -6.43\times10^{-1} & 5.35\times10^{-1} & -1.15\times10^{1} & 1.22\times10^{1} & 6.10\times10^{-2} & 8.01\times10^{-1} & 3.08\times10^{-1} & 1.02\times10^{-2} \\
6.25\times10^{-2} & -1.05 & 1.12 & -5.59\times10^{-1} & -6.21 & -1.08\times10^{1} & -4.21\times10^{-2} & 5.86\times10^{-1} & 2.24\times10^{-1} & -9.19\times10^{-2}
\end{bmatrix} \tag{E.16}$$

$$K_C \begin{bmatrix} 0_{30\times 10} \\ I_{10} \\ 0_{20\times 10} \end{bmatrix} =$$

$$\begin{bmatrix}
-5.09\times10^{-2} & 6.90\times10^{-2} & -7.88\times10^{-2} & 6.67\times10^{-2} & 7.95\times10^{-3} & 2.47\times10^{-2} & -7.45\times10^{-3} & 4.32\times10^{-4} & 9.76\times10^{-3} & 1.82\times10^{-3} \\
-6.78\times10^{-4} & -6.31\times10^{-4} & -1.54\times10^{-3} & -1.37\times10^{-3} & -6.40\times10^{-4} & 1.43\times10^{-5} & -2.68\times10^{-4} & -2.06\times10^{-5} & 3.16\times10^{-6} & -1.22\times10^{-4} \\
6.31\times10^{-3} & 8.17\times10^{-3} & -2.70\times10^{-2} & -2.94\times10^{-2} & -1.67\times10^{-2} & 2.37\times10^{-3} & -1.54\times10^{-2} & -5.89\times10^{-4} & 8.84\times10^{-5} & -1.36\times10^{-4} \\
-5.26\times10^{-3} & 2.67\times10^{-3} & 5.91\times10^{-3} & 1.47\times10^{-2} & -7.04\times10^{-4} & -1.23\times10^{-3} & -9.41\times10^{-4} & -2.36\times10^{-4} & -1.18\times10^{-3} & -6.52\times10^{-4} \\
2.14\times10^{-2} & 5.66\times10^{-2} & 6.19\times10^{-5} & 7.92\times10^{-2} & 2.60\times10^{-2} & -1.63\times10^{-2} & -6.22\times10^{-3} & 1.61\times10^{-3} & -1.71\times10^{-4} & 1.00\times10^{-2} \\
5.07\times10^{-2} & 2.03\times10^{-2} & 8.38\times10^{-2} & -5.97\times10^{-3} & 2.59\times10^{-2} & 1.39\times10^{-2} & -3.58\times10^{-3} & 1.58\times10^{-3} & 1.17\times10^{-4} & 9.65\times10^{-3} \\
8.16\times10^{-2} & 5.20\times10^{-2} & 1.34 & 1.37 & 5.05\times10^{-1} & 1.41\times10^{-2} & -5.92\times10^{-2} & -5.52\times10^{-3} & -1.73\times10^{-3} & -7.08\times10^{-3} \\
5.24\times10^{-2} & 7.33\times10^{-2} & 1.34 & 1.39 & 5.00\times10^{-1} & -1.03\times10^{-2} & -4.60\times10^{-2} & -5.70\times10^{-3} & 4.06\times10^{-4} & -8.09\times10^{-3} \\
2.28\times10^{-1} & -2.14\times10^{-1} & -5.90\times10^{-2} & -1.82\times10^{-2} & -7.99\times10^{-3} & 1.80\times10^{-2} & 1.55\times10^{-3} & -2.52\times10^{-7} & -3.70\times10^{-3} & -7.55\times10^{-4} \\
5.68\times10^{-4} & 4.95\times10^{-4} & 1.40\times10^{-3} & 1.75\times10^{-3} & 1.06\times10^{-4} & -3.58\times10^{-5} & -8.80\times10^{-4} & -5.17\times10^{-6} & -8.45\times10^{-6} & 4.41\times10^{-5} \\
-2.70\times10^{-2} & -3.46\times10^{-2} & 1.97\times10^{-2} & 3.50\times10^{-2} & 2.23\times10^{-3} & -3.06\times10^{-3} & -9.95\times10^{-3} & 1.31\times10^{-4} & -2.54\times10^{-4} & 1.21\times10^{-4} \\
2.59\times10^{-2} & -2.15\times10^{-2} & 2.99\times10^{-2} & -7.74\times10^{-2} & -2.27\times10^{-3} & -1.92\times10^{-3} & 4.66\times10^{-3} & 4.15\times10^{-4} & -1.39\times10^{-3} & 1.01\times10^{-3} \\
8.27\times10^{-1} & -5.81\times10^{-2} & -1.62\times10^{-1} & -1.15\times10^{-2} & -2.71\times10^{-2} & -2.10\times10^{-2} & 3.09\times10^{-2} & -1.29\times10^{-3} & -1.32\times10^{-4} & -8.79\times10^{-3} \\
-6.34\times10^{-2} & 8.21\times10^{-1} & 4.37\times10^{-3} & -1.28\times10^{-1} & -2.31\times10^{-2} & 1.96\times10^{-2} & 2.50\times10^{-2} & -1.31\times10^{-3} & -3.44\times10^{-4} & -8.18\times10^{-3} \\
-1.32\times10^{-1} & -1.12\times10^{-2} & -4.31 & -1.28 & -5.10\times10^{-1} & -6.01\times10^{-2} & 8.04\times10^{-2} & 4.92\times10^{-3} & 2.71\times10^{-3} & 7.81\times10^{-3} \\
1.19\times10^{-3} & -1.06\times10^{-1} & -1.27 & -4.38 & -4.73\times10^{-1} & 5.62\times10^{-2} & 3.62\times10^{-2} & 5.50\times10^{-3} & -1.55\times10^{-3} & 1.14\times10^{-2}
\end{bmatrix} \tag{E.17}$$

$$K_C \begin{bmatrix} 0_{40\times 10} \\ I_{10} \\ 0_{10\times 10} \end{bmatrix} =$$

$$\begin{bmatrix}
2.46\times10^{-1} & -4.28\times10^{-4} & -5.65\times10^{-3} & -1.60\times10^{-3} & -8.60\times10^{-2} & -1.17\times10^{-4} & -1.63\times10^{-4} & 2.46\times10^{-2} & -8.48\times10^{-5} & 4.46\times10^{-4} \\
1.32\times10^{-5} & -1.22\times10^{-5} & -2.35\times10^{-6} & -2.06\times10^{-5} & -2.77\times10^{-5} & -9.79\times10^{-6} & -2.90\times10^{-6} & 2.61\times10^{-5} & 7.36\times10^{-6} & -2.62\times10^{-5} \\
5.61\times10^{-3} & -2.83\times10^{-5} & -1.92\times10^{-4} & -9.14\times10^{-4} & -1.31\times10^{-3} & 3.19\times10^{-5} & -2.57\times10^{-5} & 8.35\times10^{-4} & 1.06\times10^{-5} & -8.57\times10^{-4} \\
-6.96\times10^{-5} & 2.09\times10^{-4} & 9.49\times10^{-5} & 5.02\times10^{-4} & -4.13\times10^{-3} & 4.22\times10^{-5} & -4.21\times10^{-5} & -9.52\times10^{-4} & 1.51\times10^{-5} & -9.68\times10^{-6} \\
-7.38\times10^{-2} & -1.19\times10^{-4} & -2.05\times10^{-4} & -7.93\times10^{-4} & -2.40\times10^{-2} & 8.03\times10^{-5} & 8.25\times10^{-5} & -5.54\times10^{-4} & -1.81\times10^{-4} & 1.19\times10^{-3} \\
7.54\times10^{-2} & -1.45\times10^{-4} & 1.70\times10^{-4} & -5.93\times10^{-4} & 2.07\times10^{-2} & 6.75\times10^{-5} & 6.50\times10^{-5} & 1.36\times10^{-4} & -2.00\times10^{-4} & 1.18\times10^{-3} \\
-4.10\times10^{-2} & -1.12\times10^{-4} & 2.21\times10^{-3} & -1.87\times10^{-2} & 2.17\times10^{-2} & -2.15\times10^{-3} & -2.37\times10^{-4} & -1.01\times10^{-2} & 1.26\times10^{-3} & 2.88\times10^{-2} \\
2.95\times10^{-2} & 7.73\times10^{-5} & -1.17\times10^{-3} & -1.80\times10^{-2} & -1.45\times10^{-2} & -2.22\times10^{-3} & -5.65\times10^{-4} & 8.63\times10^{-3} & 1.06\times10^{-3} & 2.83\times10^{-2} \\
-2.44\times10^{-1} & 2.99\times10^{-4} & 9.74\times10^{-3} & 7.95\times10^{-4} & 1.26\times10^{-1} & 2.37\times10^{-4} & 3.87\times10^{-4} & -1.38\times10^{-2} & 1.02\times10^{-4} & -4.33\times10^{-4} \\
-2.64\times10^{-4} & -2.42\times10^{-5} & 9.34\times10^{-6} & -1.27\times10^{-4} & 5.27\times10^{-5} & -2.47\times10^{-6} & -9.32\times10^{-7} & -1.83\times10^{-5} & 4.59\times10^{-6} & 1.19\times10^{-5} \\
-1.29\times10^{-2} & -1.43\times10^{-3} & 5.39\times10^{-4} & -4.61\times10^{-3} & 5.38\times10^{-3} & -3.99\times10^{-4} & -7.17\times10^{-5} & -1.75\times10^{-3} & 3.34\times10^{-4} & 3.87\times10^{-4} \\
-6.22\times10^{-2} & -2.76\times10^{-4} & 6.06\times10^{-4} & -5.49\times10^{-4} & 2.16\times10^{-2} & -4.05\times10^{-5} & 1.12\times10^{-4} & -5.21\times10^{-3} & -5.32\times10^{-5} & -1.26\times10^{-4} \\
-1.03\times10^{-1} & 9.58\times10^{-4} & -3.37\times10^{-4} & 8.21\times10^{-3} & -5.98\times10^{-2} & -4.60\times10^{-4} & -8.66\times10^{-5} & -1.32\times10^{-3} & 2.65\times10^{-4} & -1.01\times10^{-3} \\
9.74\times10^{-2} & 6.77\times10^{-4} & 8.74\times10^{-4} & 7.25\times10^{-3} & 6.03\times10^{-2} & -6.16\times10^{-4} & -1.19\times10^{-4} & 2.79\times10^{-4} & 4.01\times10^{-4} & -6.64\times10^{-4} \\
-4.30\times10^{-2} & 6.11\times10^{-4} & -4.68\times10^{-3} & 2.20\times10^{-2} & -8.42\times10^{-2} & 8.32\times10^{-4} & 2.59\times10^{-4} & 1.86\times10^{-2} & -1.87\times10^{-3} & -2.96\times10^{-2} \\
6.55\times10^{-2} & -5.63\times10^{-5} & 2.88\times10^{-3} & 1.89\times10^{-2} & 7.33\times10^{-2} & 8.97\times10^{-4} & 8.83\times10^{-4} & -1.86\times10^{-2} & -1.61\times10^{-3} & -2.71\times10^{-2}
\end{bmatrix} \tag{E.18}$$

$$K_C \begin{bmatrix} 0_{50\times 10} \\ I_{10} \end{bmatrix} =$$

$$\begin{bmatrix}
1.33\times10^{-3} & -5.70\times10^{-4} & 7.77\times10^{-4} & -8.96\times10^{-3} & 3.87\times10^{-4} & -1.70\times10^{-2} & -1.43\times10^{-3} & -3.28\times10^{-4} & -5.35\times10^{-4} & 1.35\times10^{-2} \\
4.15\times10^{-6} & -4.61\times10^{-5} & 2.77\times10^{-4} & 2.32\times10^{-6} & -2.59\times10^{-4} & 4.15\times10^{-5} & -2.29\times10^{-5} & 7.52\times10^{-8} & -2.93\times10^{-4} & -7.44\times10^{-5} \\
1.88\times10^{-4} & -8.59\times10^{-4} & -6.71\times10^{-4} & 1.38\times10^{-6} & -2.24\times10^{-3} & -9.21\times10^{-4} & -3.62\times10^{-4} & -1.35\times10^{-5} & -6.56\times10^{-4} & 7.60\times10^{-5} \\
-1.17\times10^{-4} & 1.67\times10^{-5} & -4.77\times10^{-4} & -5.59\times10^{-4} & -5.37\times10^{-4} & -2.95\times10^{-3} & 4.94\times10^{-4} & -4.09\times10^{-5} & 3.09\times10^{-4} & 4.84\times10^{-4} \\
-8.19\times10^{-4} & -1.42\times10^{-3} & 9.90\times10^{-4} & -3.20\times10^{-3} & 5.66\times10^{-3} & 1.84\times10^{-3} & 7.92\times10^{-4} & -1.77\times10^{-5} & 8.72\times10^{-3} & 3.39\times10^{-3} \\
1.22\times10^{-3} & -1.45\times10^{-3} & 1.10\times10^{-3} & 3.25\times10^{-3} & 5.55\times10^{-3} & 2.71\times10^{-3} & 8.46\times10^{-4} & -3.67\times10^{-5} & 8.60\times10^{-3} & 5.99\times10^{-4} \\
2.38\times10^{-4} & -3.67\times10^{-3} & -5.81\times10^{-3} & 4.53\times10^{-4} & -4.04\times10^{-2} & -1.44\times10^{-1} & -5.79\times10^{-3} & 1.80\times10^{-4} & -4.78\times10^{-2} & -9.39\times10^{-3} \\
-1.14\times10^{-4} & -2.61\times10^{-3} & -5.13\times10^{-3} & 8.02\times10^{-4} & -3.96\times10^{-2} & 1.38\times10^{-1} & -5.96\times10^{-3} & 1.89\times10^{-5} & -4.71\times10^{-2} & 1.74\times10^{-3} \\
5.19\times10^{-4} & 8.54\times10^{-4} & 1.21\times10^{-5} & -1.16\times10^{-3} & 4.12\times10^{-3} & 9.10\times10^{-3} & 9.70\times10^{-5} & -1.90\times10^{-3} & 3.96\times10^{-3} & -8.69\times10^{-3} \\
-3.37\times10^{-6} & -5.45\times10^{-5} & -8.52\times10^{-5} & -7.44\times10^{-7} & -1.71\times10^{-4} & 3.40\times10^{-6} & 3.95\times10^{-4} & 2.26\times10^{-7} & -1.53\times10^{-4} & -1.53\times10^{-5} \\
-5.12\times10^{-4} & 2.36\times10^{-4} & -1.67\times10^{-3} & 7.34\times10^{-6} & -6.56\times10^{-3} & -3.73\times10^{-4} & -1.42\times10^{-3} & 4.33\times10^{-5} & -1.41\times10^{-2} & -2.03\times10^{-3} \\
-1.68\times10^{-4} & 2.27\times10^{-4} & 8.34\times10^{-4} & -5.13\times10^{-5} & 1.53\times10^{-3} & 3.46\times10^{-3} & -6.19\times10^{-4} & 4.39\times10^{-5} & -2.71\times10^{-5} & -6.06\times10^{-3} \\
-1.16\times10^{-3} & 8.69\times10^{-5} & -2.38\times10^{-3} & -2.42\times10^{-4} & -1.02\times10^{-2} & 3.86\times10^{-4} & -1.36\times10^{-3} & -7.15\times10^{-4} & -1.06\times10^{-2} & 3.03\times10^{-3} \\
1.46\times10^{-3} & -8.79\times10^{-4} & -2.77\times10^{-3} & 3.00\times10^{-4} & -1.40\times10^{-2} & 2.54\times10^{-3} & -1.54\times10^{-3} & 7.31\times10^{-4} & -1.47\times10^{-2} & -1.46\times10^{-3} \\
-3.57\times10^{-3} & 7.54\times10^{-3} & 1.47\times10^{-2} & -4.21\times10^{-4} & 6.09\times10^{-2} & -3.00\times10^{-3} & 9.03\times10^{-3} & -2.80\times10^{-4} & 7.29\times10^{-2} & -1.33\times10^{-1} \\
3.37\times10^{-3} & 5.17\times10^{-3} & 1.42\times10^{-2} & -6.70\times10^{-4} & 6.24\times10^{-2} & 3.64\times10^{-3} & 8.76\times10^{-3} & 2.65\times10^{-6} & 7.27\times10^{-2} & 1.36\times10^{-1}
\end{bmatrix} \tag{E.19}$$

$$L_{\mathcal{E},C} = \begin{bmatrix} -1.05 \times 10^{3} & 1.88 \times 10^{-1} & -1.42 \times 10^{2} & 1.07 \times 10^{-1} & 1.16 \times 10^{1} & 9.63 \times 10^{-2} & 1.78 & -9.19 \times 10^{-2} \\ -1.48 & -9.44 \times 10^{1} & -1.95 \times 10^{-1} & -7.85 \times 10^{1} & 5.89 \times 10^{-1} & -1.50 \times 10^{-1} & 7.70 \times 10^{-2} & 6.13 \times 10^{-1} \\ 1.50 \times 10^{2} & -2.07 \times 10^{-2} & -2.14 & -4.75 \times 10^{-2} & -1.42 \times 10^{1} & -1.66 \times 10^{-2} & -1.90 & -3.92 \times 10^{-3} \\ -5.97 \times 10^{-3} & 1.08 & -7.78 \times 10^{-4} & -5.01 & -3.19 \times 10^{-3} & 5.01 \times 10^{-4} & -4.24 \times 10^{-4} & -3.76 \times 10^{-3} \\ -1.51 \times 10^{1} & -1.12 \times 10^{-1} & -1.74 & 2.47 \times 10^{-1} & -1.05 \times 10^{3} & -6.07 \times 10^{-2} & -1.42 \times 10^{2} & -1.84 \times 10^{-1} \\ -7.42 \times 10^{-1} & -6.46 \times 10^{-2} & -9.67 \times 10^{-2} & 3.85 \times 10^{-1} & 9.03 \times 10^{-1} & -9.43 \times 10^{1} & 1.17 \times 10^{-1} & -7.80 \times 10^{1} \\ -1.07 \times 10^{1} & 1.51 \times 10^{-2} & -1.45 & -1.00 \times 10^{-2} & 1.51 \times 10^{2} & 4.46 \times 10^{-2} & -2.11 & -9.43 \times 10^{-2} \\ 1.80 \times 10^{-3} & -1.30 \times 10^{-3} & 2.39 \times 10^{-4} & 2.17 \times 10^{-3} & 4.10 \times 10^{-3} & 1.08 & 5.69 \times 10^{-4} & -5.01 \end{bmatrix} \tag{E.20}$$

$$K_H \begin{bmatrix} I_{10} \\ 0_{18\times 10} \end{bmatrix} = \begin{bmatrix} -2.09 \times 10^{-4} & -3.67 \times 10^{-3} & 2.37 \times 10^{-5} & 5.41 \times 10^{-2} & -5.25 \times 10^{-2} & 3.74 \times 10^{-1} & 2.91 \times 10^{-2} & -5.58 \times 10^{-2} & -6.66 \times 10^{-6} & 8.18 \times 10^{-1} \\ 3.20 \times 10^{-5} & 5.11 \times 10^{-6} & -2.60 \times 10^{-5} & -2.17 \times 10^{-4} & 1.06 \times 10^{-2} & -1.44 \times 10^{-4} & -1.34 \times 10^{-4} & 1.87 \times 10^{-2} & 1.72 \times 10^{-5} & 2.63 \times 10^{-4} \\ 3.21 \times 10^{-4} & 5.62 \times 10^{-6} & -3.28 \times 10^{-3} & -7.55 \times 10^{-3} & 6.59 \times 10^{-1} & 2.89 \times 10^{-3} & -1.60 \times 10^{-2} & 1.15 & 1.24 \times 10^{-3} & 2.92 \times 10^{-3} \\ 9.36 \times 10^{-5} & -3.38 \times 10^{-4} & -1.14 \times 10^{-4} & 2.29 \times 10^{-3} & -1.15 \times 10^{-2} & 1.71 \times 10^{-1} & 3.20 \times 10^{-2} & 1.01 \times 10^{-2} & 1.15 \times 10^{-4} & -5.10 \times 10^{-3} \\ -1.08 \times 10^{-3} & 6.34 \times 10^{-4} & 1.72 \times 10^{-3} & -2.89 \times 10^{-2} & 1.63 \times 10^{-1} & -9.01 \times 10^{-3} & -4.94 \times 10^{-2} & -3.26 \times 10^{-1} & -5.00 \times 10^{-4} & 3.37 \times 10^{-2} \\ -8.86 \times 10^{-4} & -8.49 \times 10^{-4} & 1.70 \times 10^{-3} & 3.73 \times 10^{-2} & 1.97 \times 10^{-1} & 1.44 \times 10^{-2} & 5.99 \times 10^{-2} & -2.90 \times 10^{-1} & -4.78 \times 10^{-4} & -3.82 \times 10^{-2} \\ -5.17 \times 10^{-2} & 1.07 \times 10^{-4} & 2.19 \times 10^{-3} & -9.63 \times 10^{-3} & 6.32 \times 10^{-2} & -2.84 \times 10^{-2} & -7.06 \times 10^{-2} & -1.24 & -2.00 \times 10^{-3} & -1.36 \times 10^{-3} \\ -4.27 \times 10^{-2} & 1.78 \times 10^{-3} & 3.18 \times 10^{-3} & -3.61 \times 10^{-1} & -1.18 \times 10^{-2} & 2.48 \times 10^{-3} & -8.72 \times 10^{-1} & -1.42 & -2.33 \times 10^{-3} & 9.69 \times 10^{-2} \end{bmatrix} \tag{E.21}$$

$$K_H \begin{bmatrix} 0_{10\times 10} \\ I_{10} \\ 0_{8\times 10} \end{bmatrix} = \begin{bmatrix} 4.14 \times 10^{-2} & 1.74 \times 10^{-2} & -3.70 \times 10^{-2} & 2.31 \times 10^{-2} & -1.83 \times 10^{-2} & 2.40 \times 10^{-2} & -1.72 \times 10^{-2} & 1.16 \times 10^{-4} & 2.42 \times 10^{-3} & 1.90 \times 10^{-4} \\ 9.72 \times 10^{-1} & -2.69 \times 10^{-3} & -2.05 \times 10^{-5} & -4.99 \times 10^{-4} & 3.82 \times 10^{-5} & 4.17 \times 10^{-4} & 2.89 \times 10^{-4} & -1.43 \times 10^{-5} & -5.97 \times 10^{-6} & -4.81 \times 10^{-5} \\ -1.02 & 5.70 \times 10^{-1} & -7.89 \times 10^{-4} & -2.33 \times 10^{-2} & -1.76 \times 10^{-2} & 1.97 \times 10^{-2} & 2.22 \times 10^{-2} & -8.83 \times 10^{-4} & -6.94 \times 10^{-5} & -1.88 \times 10^{-3} \\ 1.03 \times 10^{-2} & 3.15 \times 10^{-3} & 8.96 \times 10^{-1} & 1.15 \times 10^{-2} & -8.82 \times 10^{-3} & 3.89 \times 10^{-2} & -2.33 \times 10^{-2} & 3.60 \times 10^{-5} & -8.78 \times 10^{-4} & 6.81 \times 10^{-5} \\ -1.62 \times 10^{-1} & -6.96 \times 10^{-2} & -4.97 \times 10^{-3} & 8.33 \times 10^{-1} & 1.84 \times 10^{-2} & -3.15 \times 10^{-3} & -4.04 \times 10^{-3} & 1.89 \times 10^{-4} & -8.33 \times 10^{-4} & 2.36 \times 10^{-3} \\ -1.88 \times 10^{-1} & -8.11 \times 10^{-2} & 6.00 \times 10^{-3} & 2.15 \times 10^{-2} & 8.27 \times 10^{-1} & 5.99 \times 10^{-4} & -7.89 \times 10^{-3} & 1.83 \times 10^{-4} & 9.56 \times 10^{-4} & 2.24 \times 10^{-3} \\ -7.22 \times 10^{-2} & -4.82 \times 10^{-2} & 1.09 \times 10^{-2} & -4.31 \times 10^{-2} & -4.03 \times 10^{-2} & -3.30 & 5.97 \times 10^{-2} & -5.29 \times 10^{-4} & -3.99 \times 10^{-4} & 1.36 \times 10^{-2} \\ -1.59 \times 10^{-2} & -2.01 \times 10^{-2} & -2.19 \times 10^{-2} & -1.47 \times 10^{-1} & 5.32 \times 10^{-2} & 4.30 \times 10^{-2} & -3.03 & -1.77 \times 10^{-4} & -3.50 \times 10^{-3} & 1.26 \times 10^{-2} \end{bmatrix} \tag{E.22}$$

$$K_H \begin{bmatrix} 0_{18\times 10} \\ I_{10} \end{bmatrix} =$$

$$\begin{bmatrix} 3.01\times10^{-2} & -5.80\times10^{-5} & 3.48\times10^{-5} & -2.01\times10^{-3} & -2.77\times10^{-4} & -1.88\times10^{-2} & 5.26\times10^{-4} & 1.53\times10^{-3} \\ -3.46\times10^{-4} & 1.68\times10^{-6} & -4.82\times10^{-7} & 1.86\times10^{-6} & 4.86\times10^{-4} & -1.99\times10^{-5} & -6.14\times10^{-5} & 1.50\times10^{-5} \\ -3.68\times10^{-3} & -4.92\times10^{-5} & -2.00\times10^{-5} & -1.08\times10^{-3} & -9.68\times10^{-4} & -1.68\times10^{-4} & -2.17\times10^{-3} & -2.91\times10^{-5} \\ 1.47\times10^{-2} & -8.42\times10^{-6} & -8.74\times10^{-5} & 2.67\times10^{-3} & -1.80\times10^{-4} & -2.02\times10^{-3} & 7.55\times10^{-5} & -2.23\times10^{-3} \\ -4.43\times10^{-2} & -9.30\times10^{-5} & -7.11\times10^{-5} & -5.26\times10^{-3} & -4.15\times10^{-4} & -5.61\times10^{-3} & -9.45\times10^{-3} & 1.08\times10^{-3} \\ 5.00\times10^{-2} & -6.83\times10^{-5} & -9.53\times10^{-5} & 5.67\times10^{-3} & -3.07\times10^{-4} & 6.21\times10^{-3} & -9.75\times10^{-3} & -9.94\times10^{-4} \\ 2.20\times10^{-3} & -3.04\times10^{-3} & 1.49\times10^{-5} & -1.87\times10^{-2} & -9.78\times10^{-4} & 6.49\times10^{-4} & 7.98\times10^{-3} & -1.21\times10^{-1} \\ -1.28\times10^{-1} & -2.53\times10^{-3} & 4.67\times10^{-5} & -7.03\times10^{-2} & 1.23\times10^{-4} & -8.87\times10^{-3} & 9.31\times10^{-3} & 1.26\times10^{-1} \end{bmatrix} \tag{E.23}$$

$$L_{\mathcal{E},H} \begin{bmatrix} 0_{18\times 10} \\ I_{10} \end{bmatrix} =$$

$$\begin{bmatrix} -1.06\times10^{3} & 2.59\times10^{-1} & -1.42\times10^{2} & 1.64\times10^{-2} \\ -1.98 & -9.45\times10^{1} & -2.60\times10^{-1} & -7.81\times10^{1} \\ 1.40\times10^{2} & -3.95\times10^{-2} & -3.51 & 4.46\times10^{-5} \\ -4.45\times10^{-3} & 1.08 & -5.85\times10^{-4} & -5.02 \end{bmatrix} \tag{E.24}$$

$$K_D \begin{bmatrix} I_{10} \\ 0_{50\times 10} \end{bmatrix} =$$

$$\begin{bmatrix} 1.11\times10^{-2} & -9.55\times10^{-2} & -4.64\times10^{-3} & -1.45\times10^{-1} & -6.14\times10^{-1} & -1.61 & 9.39\times10^{-2} & 6.10\times10^{-1} & -2.11\times10^{-3} & 7.24\times10^{-2} \\ -5.72\times10^{-4} & -3.60\times10^{-5} & 9.29\times10^{-4} & -6.79\times10^{-4} & 1.27\times10^{-2} & 2.83\times10^{-3} & -2.05\times10^{-3} & -2.28\times10^{-1} & -3.18\times10^{-5} & 2.23\times10^{-4} \\ -8.82\times10^{-4} & -2.40\times10^{-3} & 2.57\times10^{-2} & -7.32\times10^{-3} & -1.46\times10^{-2} & -5.02\times10^{-3} & -7.30\times10^{-3} & -6.60 & -1.60\times10^{-4} & 3.48\times10^{-3} \\ 2.01\times10^{-3} & -1.64\times10^{-2} & -8.03\times10^{-4} & -8.15\times10^{-3} & -3.62\times10^{-2} & 3.40\times10^{-1} & 9.69\times10^{-2} & 1.79\times10^{-1} & 9.15\times10^{-6} & -2.36\times10^{-3} \\ 5.56\times10^{-2} & -1.07\times10^{-2} & -4.02\times10^{-2} & -3.17\times10^{-2} & 1.03 & -1.70\times10^{-1} & -3.08\times10^{-2} & 1.22\times10^{1} & 2.39\times10^{-3} & 1.66\times10^{-2} \\ 4.48\times10^{-2} & 4.56\times10^{-3} & -3.61\times10^{-2} & -1.58\times10^{-3} & 1.43 & 2.28\times10^{-1} & -2.91\times10^{-2} & 1.15\times10^{1} & 3.34\times10^{-3} & -5.48\times10^{-3} \\ 4.98\times10^{-1} & 2.16\times10^{-1} & 6.52\times10^{-2} & -4.84\times10^{-2} & -2.84 & 1.96 & -9.98\times10^{-1} & -1.50\times10^{1} & -7.95\times10^{-3} & -3.54\times10^{-2} \\ 5.72\times10^{-1} & -2.05\times10^{-1} & 9.46\times10^{-2} & -2.13\times10^{-1} & -3.57 & -2.15 & 2.70\times10^{-1} & -2.22\times10^{1} & -1.83\times10^{-2} & 1.20\times10^{-1} \end{bmatrix} \tag{E.25}$$

$$K_D \begin{bmatrix} 0_{10\times 10} \\ I_{10} \\ 0_{40\times 10} \end{bmatrix} =$$

$$\begin{bmatrix} 3.65\times10^{-1} & 1.73\times10^{-1} & 1.49\times10^{-1} & -5.75\times10^{-2} & 1.14\times10^{-1} & -1.58\times10^{-1} & 2.14\times10^{-1} & -7.67\times10^{-3} & 1.04\times10^{-1} & 8.39\times10^{-3} \\ -1.67\times10^{-2} & -6.34\times10^{-3} & -1.90\times10^{-4} & -2.72\times10^{-3} & -2.23\times10^{-3} & -6.27\times10^{-4} & -9.11\times10^{-4} & 4.53\times10^{-4} & 1.63\times10^{-5} & -9.76\times10^{-4} \\ -1.50\times10^{-1} & -7.03\times10^{-2} & -4.13\times10^{-3} & -4.99\times10^{-2} & -4.52\times10^{-2} & 9.57\times10^{-3} & 1.18\times10^{-2} & -1.92\times10^{-3} & 3.05\times10^{-3} & -2.81\times10^{-2} \\ 3.70\times10^{-2} & 1.33\times10^{-2} & -7.73\times10^{-2} & 1.61\times10^{-2} & -1.17\times10^{-2} & 3.42\times10^{-2} & -3.69\times10^{-2} & -2.10\times10^{-3} & 1.58\times10^{-2} & 8.91\times10^{-4} \\ -3.24\times10^{-1} & -1.20\times10^{-1} & 1.26\times10^{-2} & 5.74\times10^{-2} & 9.05\times10^{-2} & 1.28\times10^{-1} & 1.71\times10^{-1} & -5.91\times10^{-2} & 1.29\times10^{-2} & 3.79\times10^{-2} \\ -5.88\times10^{-1} & -2.37\times10^{-1} & -3.16\times10^{-2} & 6.29\times10^{-2} & 4.35\times10^{-2} & 1.55\times10^{-1} & 1.05\times10^{-1} & -4.95\times10^{-2} & -5.63\times10^{-3} & 3.19\times10^{-2} \\ 1.33 & 4.48\times10^{-1} & -1.92\times10^{-2} & 7.08\times10^{-2} & 6.60\times10^{-2} & 1.59 & 1.22 & -5.40\times10^{-1} & -2.53\times10^{-1} & -5.22\times10^{-2} \\ 1.38 & 5.44\times10^{-1} & 4.66\times10^{-2} & -5.26\times10^{-2} & 1.46\times10^{-1} & 1.31 & 1.86 & -6.16\times10^{-1} & 2.44\times10^{-1} & -6.89\times10^{-2} \end{bmatrix} \tag{E.26}$$

$$K_D \begin{bmatrix} 0_{20\times 10} \\ I_{10} \\ 0_{30\times 10} \end{bmatrix} =$$

$$\begin{bmatrix}
3.72\times10^{-1} & -1.75\times10^{-1} & 1.61 & -3.47\times10^{-1} & -1.83 & -2.08\times10^{1} & 6.20\times10^{-1} & 1.28\times10^{-1} & 5.47\times10^{-2} & -5.79\times10^{-2} \\
-1.72\times10^{-4} & 2.78\times10^{-2} & 3.26\times10^{-3} & -4.35\times10^{-4} & 2.24\times10^{-1} & -5.35\times10^{-3} & -1.61\times10^{-5} & 9.64\times10^{-1} & -6.27\times10^{-3} & -4.52\times10^{-4} \\
3.60\times10^{-3} & 1.12 & 1.68\times10^{-2} & -2.56\times10^{-2} & 6.45 & -5.31\times10^{-1} & -2.04\times10^{-3} & -1.14 & 5.23\times10^{-1} & 1.13\times10^{-3} \\
8.19\times10^{-3} & -2.34\times10^{-2} & 6.35\times10^{-1} & -1.16\times10^{-1} & -2.21\times10^{-1} & -3.10 & -1.46\times10^{-2} & 1.36\times10^{-2} & 6.53\times10^{-3} & 8.26\times10^{-1} \\
3.27\times10^{-2} & -7.22\times10^{-1} & 7.45\times10^{-2} & -6.51\times10^{-2} & -9.42 & -2.36 & -1.30\times10^{-2} & 1.58\times10^{-1} & 5.60\times10^{-2} & 8.89\times10^{-3} \\
-2.27\times10^{-2} & -5.79\times10^{-1} & -5.20\times10^{-2} & 1.01\times10^{-2} & -8.05 & 1.15 & 7.32\times10^{-3} & 5.25\times10^{-2} & 1.16\times10^{-2} & -5.35\times10^{-3} \\
-4.37\times10^{-1} & 4.49\times10^{-1} & -2.44 & 1.84 & 2.29 & 4.65\times10^{1} & 1.84\times10^{-1} & -1.70\times10^{-1} & -5.70\times10^{-2} & 5.48\times10^{-2} \\
3.65\times10^{-1} & 8.27\times10^{-1} & 2.49 & -1.89 & 4.80 & -4.52\times10^{1} & -1.68\times10^{-1} & -3.35\times10^{-1} & -1.21\times10^{-1} & -6.48\times10^{-2}
\end{bmatrix} \tag{E.27}$$

$$K_D \begin{bmatrix} 0_{30\times 10} \\ I_{10} \\ 0_{20\times 10} \end{bmatrix} =$$

$$\begin{bmatrix}
3.58\times10^{-1} & -3.65\times10^{-1} & 1.55\times10^{-1} & -2.03\times10^{-1} & -5.10\times10^{-3} & 4.74\times10^{-2} & 6.60\times10^{-3} & 7.11\times10^{-5} & -3.44\times10^{-3} & -8.49\times10^{-4} \\
1.37\times10^{-3} & 1.23\times10^{-3} & 1.20\times10^{-3} & 8.24\times10^{-4} & 5.44\times10^{-4} & 1.19\times10^{-4} & -1.13\times10^{-3} & 1.92\times10^{-5} & -1.93\times10^{-5} & 2.19\times10^{-4} \\
1.97\times10^{-2} & 1.60\times10^{-2} & 8.33\times10^{-3} & 4.33\times10^{-3} & 3.09\times10^{-3} & 2.02\times10^{-3} & -3.21\times10^{-2} & 1.42\times10^{-3} & -4.87\times10^{-5} & 8.06\times10^{-3} \\
3.79\times10^{-2} & -3.92\times10^{-2} & 8.00\times10^{-2} & -8.83\times10^{-2} & -2.12\times10^{-3} & 1.43\times10^{-2} & 8.82\times10^{-4} & 1.81\times10^{-5} & -1.83\times10^{-3} & 3.88\times10^{-5} \\
8.61\times10^{-1} & -1.46\times10^{-1} & -1.58\times10^{-1} & -1.75\times10^{-1} & -5.64\times10^{-2} & 5.58\times10^{-3} & 4.22\times10^{-2} & -2.66\times10^{-3} & -3.09\times10^{-4} & -1.62\times10^{-2} \\
-1.39\times10^{-1} & 8.58\times10^{-1} & -1.46\times10^{-1} & -1.33\times10^{-1} & -4.94\times10^{-2} & -1.61\times10^{-3} & 3.59\times10^{-2} & -2.76\times10^{-3} & -2.44\times10^{-6} & -1.58\times10^{-2} \\
-2.38\times10^{-1} & 1.25\times10^{-1} & -4.73 & -1.25 & -4.18\times10^{-1} & -1.43\times10^{-1} & -1.91\times10^{-3} & 8.19\times10^{-3} & -1.02\times10^{-3} & 2.99\times10^{-2} \\
1.06\times10^{-1} & -2.27\times10^{-1} & -1.49 & -4.99 & -4.66\times10^{-1} & 1.40\times10^{-1} & -2.30\times10^{-2} & 8.58\times10^{-3} & -1.36\times10^{-3} & 3.42\times10^{-2}
\end{bmatrix} \tag{E.28}$$

$$K_D \begin{bmatrix} 0_{40\times 10} \\ I_{10} \\ 0_{10\times 10} \end{bmatrix} =$$

$$\begin{bmatrix}
-1.25\times10^{-1} & 2.19\times10^{-4} & 1.38\times10^{-2} & 9.98\times10^{-4} & 3.01\times10^{-1} & 4.50\times10^{-4} & 1.13\times10^{-3} & -3.74\times10^{-2} & 3.55\times10^{-4} & -2.22\times10^{-4} \\
-2.56\times10^{-4} & -4.35\times10^{-5} & -4.34\times10^{-6} & -1.84\times10^{-4} & 9.24\times10^{-5} & -1.15\times10^{-5} & -5.84\times10^{-7} & -2.38\times10^{-4} & -3.08\times10^{-6} & 3.25\times10^{-5} \\
-3.84\times10^{-3} & -1.46\times10^{-3} & 1.64\times10^{-4} & -5.79\times10^{-3} & 2.56\times10^{-3} & -1.68\times10^{-4} & 8.04\times10^{-5} & -3.54\times10^{-3} & 6.89\times10^{-5} & 3.99\times10^{-4} \\
1.74\times10^{-2} & 2.69\times10^{-5} & -2.14\times10^{-5} & 1.66\times10^{-4} & 4.11\times10^{-2} & -2.05\times10^{-5} & -8.85\times10^{-5} & -5.70\times10^{-4} & -7.09\times10^{-5} & -1.19\times10^{-4} \\
-2.45\times10^{-2} & 1.36\times10^{-3} & 1.06\times10^{-3} & 1.14\times10^{-2} & 1.66\times10^{-2} & -3.72\times10^{-4} & -2.11\times10^{-5} & -1.16\times10^{-2} & 1.88\times10^{-4} & -3.06\times10^{-3} \\
1.31\times10^{-2} & 1.22\times10^{-3} & -6.67\times10^{-4} & 1.06\times10^{-2} & -9.66\times10^{-3} & -5.33\times10^{-4} & -3.20\times10^{-4} & -2.07\times10^{-3} & 1.30\times10^{-4} & -2.64\times10^{-3} \\
4.98\times10^{-2} & -2.75\times10^{-3} & -1.62\times10^{-2} & 8.59\times10^{-3} & -2.59\times10^{-1} & -2.28\times10^{-3} & -2.73\times10^{-3} & 1.01\times10^{-1} & -1.21\times10^{-3} & -2.46\times10^{-2} \\
-1.67\times10^{-1} & -3.68\times10^{-3} & 1.50\times10^{-2} & 7.52\times10^{-3} & 2.38\times10^{-1} & -1.34\times10^{-3} & 3.82\times10^{-3} & -1.62\times10^{-1} & -1.76\times10^{-4} & -2.76\times10^{-2}
\end{bmatrix} \tag{E.29}$$

$$K_D \begin{bmatrix} 0_{50\times 10} \\ I_{10} \end{bmatrix} =$$

$$\begin{bmatrix} 2.89\times10^{-3} & 2.74\times10^{-4} & 2.59\times10^{-3} & 1.12\times10^{-2} & 6.86\times10^{-3} & 1.67\times10^{-2} & -7.03\times10^{-5} & -8.73\times10^{-4} & -3.81\times10^{-5} & -1.90\times10^{-2} \\ 1.35\times10^{-5} & -5.58\times10^{-5} & 7.34\times10^{-5} & -1.07\times10^{-4} & 7.90\times10^{-5} & 9.31\times10^{-5} & 4.40\times10^{-4} & 2.11\times10^{-7} & 7.53\times10^{-5} & 3.52\times10^{-5} \\ 5.12\times10^{-5} & -2.49\times10^{-3} & -5.74\times10^{-4} & 7.11\times10^{-4} & 5.42\times10^{-3} & 3.58\times10^{-4} & -6.82\times10^{-4} & -1.60\times10^{-5} & -3.61\times10^{-3} & -2.32\times10^{-4} \\ 9.59\times10^{-4} & 1.01\times10^{-4} & 1.30\times10^{-4} & -1.51\times10^{-3} & -2.24\times10^{-5} & 1.69\times10^{-3} & 2.13\times10^{-4} & -2.74\times10^{-5} & 3.76\times10^{-4} & -2.34\times10^{-3} \\ 2.19\times10^{-4} & 1.40\times10^{-3} & -1.56\times10^{-3} & 3.13\times10^{-3} & -2.24\times10^{-2} & 1.38\times10^{-3} & -3.04\times10^{-4} & -4.27\times10^{-4} & -8.14\times10^{-3} & -7.43\times10^{-4} \\ -2.83\times10^{-4} & 9.86\times10^{-4} & -2.60\times10^{-3} & -2.63\times10^{-5} & -2.61\times10^{-2} & -1.02\times10^{-3} & -3.77\times10^{-4} & 3.75\times10^{-4} & -8.74\times10^{-3} & 4.18\times10^{-7} \\ -9.24\times10^{-3} & 3.02\times10^{-3} & 5.29\times10^{-4} & -4.79\times10^{-2} & 5.98\times10^{-2} & -1.31\times10^{-2} & 5.19\times10^{-3} & -5.09\times10^{-4} & 3.86\times10^{-2} & -1.03\times10^{-1} \\ 9.68\times10^{-3} & 1.88\times10^{-3} & 9.23\times10^{-3} & 3.36\times10^{-2} & 7.97\times10^{-2} & 1.97\times10^{-2} & 2.89\times10^{-3} & 2.98\times10^{-4} & 3.66\times10^{-2} & 1.07\times10^{-1} \end{bmatrix} \tag{E.30}$$

$$L_{\mathcal{E},D} =$$

$$\begin{bmatrix} -1.05\times10^{3} & 1.92\times10^{-1} & -1.42\times10^{2} & 6.25\times10^{-2} & 1.09\times10^{1} & 9.32\times10^{-2} & 1.68 & -2.75\times10^{-2} \\ -1.41 & -9.44\times10^{1} & -1.86\times10^{-1} & -7.85\times10^{1} & 5.27\times10^{-1} & -2.57\times10^{-1} & 6.84\times10^{-2} & 9.51\times10^{-1} \\ 1.50\times10^{2} & -1.56\times10^{-2} & -2.14 & -6.03\times10^{-2} & -1.41\times10^{1} & -2.42\times10^{-2} & -1.89 & 8.72\times10^{-3} \\ -5.62\times10^{-3} & 1.08 & -7.28\times10^{-4} & -5.02 & -3.35\times10^{-3} & 2.30\times10^{-3} & -4.40\times10^{-4} & -9.21\times10^{-3} \\ -1.44\times10^{1} & -1.10\times10^{-1} & -1.64 & 2.65\times10^{-1} & -1.05\times10^{3} & -1.10\times10^{-2} & -1.42\times10^{2} & -3.79\times10^{-1} \\ -8.59\times10^{-1} & 4.09\times10^{-2} & -1.12\times10^{-1} & 5.36\times10^{-2} & 8.74\times10^{-1} & -9.45\times10^{1} & 1.08\times10^{-1} & -7.73\times10^{1} \\ -1.07\times10^{1} & 2.30\times10^{-2} & -1.44 & -3.80\times10^{-2} & 1.51\times10^{2} & 1.23\times10^{-1} & -2.13 & -3.50\times10^{-1} \\ 1.28\times10^{-3} & -3.11\times10^{-3} & 1.66\times10^{-4} & 7.64\times10^{-3} & 5.77\times10^{-3} & 1.08 & 8.57\times10^{-4} & -5.01 \end{bmatrix} \tag{E.31}$$

Bibliography

[1] MIL-F-8785C, 1980. Military Specification-Flying Qualities of Piloted Aircraft.

[2] MIL-HDBK-1797A, 1997. Military Specification-Flying Qualities of Piloted Aircraft.

[3] Riyanto T. Bambang, E. Shimemura, and K. Uchida. Variance constrained $\mathcal{H}_2/\mathcal{H}_\infty$ control. In *American Control Conference*, 1992.

[4] David Banjerdpongchai and Jonathan How. Parametric robust $\mathcal{H}_2$ control design using lmi synthesis. Technical report, Stanford University Stanford CA 94305, 1996.

[5] M. A. Bennington and K. D. Visser. Aerial refueling implications for commercial aviation. *Journal of Aircraft*, Vol. 42, No. 2:366–375, 2005.

[6] H.S. Black. Stabilized feedback amplifiers, 1934.

[7] A.W. Bloy and V. Trochalidis. The performance and longitudinal stability and control of large receiver aircraft during air to air refueling. *Aeronautical Journal*, 93:367–378, December 1989.

[8] A.W. Bloy and V. Trochalidis. The aerodynamic interference between tanker and receiver aircraft during air-to-air refueling. *Aeronautical Journal*, 94:165–171, May 1990.

[9] A.W. Bloy, P.J. Lamont, H.A. Abu-Assaf, and K.A.M. Ali. The lateral dynamic stability and control of a large receiver aircraft during air-to-air refueling. *Aeronautical Journal*, 90:237–243, June-July 1986.

[10] Hendrik W. Bode. *Network Analysis and Feedback Amplifier Design*. PhD thesis, Bell Telephone Laboratories, Inc., 1945.

[11] Stephen Boyd and Haitham Hindi. Analysis of linear systems with saturation using convex optimization. In *Proceedings of the* 37^{th} *conference on decision and control*, Tampa, Florida USA, 1998.

[12] Stephen Boyd and Lieven Vandenberghe. *Convex optimization*. Cambridge University Press, 2004.

[13] Stephen Boyd, Laurent El Ghaoui, Eric Feron, and Venkataramanan Balakrishnan. *Linear Matrix Inequalities in System and Control Theory*. Studies in Applied Mathematics Philadelphia, 1994.

[14] G. Campa, M. L. Fravolini, A. Ficola, M. R. Napolitano, B. Seanor, and M. G. Perhinschi. Autonomous aerial refueling for uavs using a combined gps-machine vision guidance. In *AIAA Guidance Navigation and Control Conference 2004*, Aug 16-19 2004.

[15] Bo Chen, Xinming Dong, Yuejian Xu, and Qinying Lin. Disturbance analysis and flight control law design for aerial refueling. In *Proceedings of the 2007 IEEE International Conference on Mechanics and Automation*, China, Aug 5-8 2007.

[16] Mahmoud Chilali and Pascal Gahinet. $\mathcal{H}_\infty$ design with pole placement constraints: An lmi approach. *IEEE Transactions on Automatic Control*, Vol. 41, No. 3:358–367, March 1996.

[17] Emmanuel Cortet. Requirements for an automatic aar function. Technical report, Airbus France S.A.S., April 2008.

[18] Harold Cramer. *Mathematical methods of statistics*. Asia publishing house, 1946.

[19] Mohammed Dahleh, Munther A. Dahleh, and George Verghese. Lectures on dynamic systems and control. Dynamic Systems & Control Lecture Notes.

[20] Maurìcio C. de Oliveira and José C. Geromel. Numerical comparison of output feedback design methods. In *Proceedings of the American Control Conference*, Albuquerque, New Mexico, June 1997.

[21] Akin Delibasi, Ibrahim B. Kucukdemiral, and Galip Cansever. $\mathcal{L}_2$, $\mathcal{H}_2$ guaranteed-cost control of lpv system with saturating actuators. In *Mediterranean Conference on Control and Automation*, 2008.

[22] Ryan P. Dibley, Michael J. Allen, and Nassib Nabaa. Autonomous airborne refueling demonstration phase 1 flight-test results. In *AIAA-2007-6639 Atmospheric Flight Mechanics Conference and Exhibit*, 2007.

[23] Atilla Dogan and Shinya Sato. Flight control and simulation for aerial refueling. In *AIAA Guidance, Navigation, and Control Conference and Exhibit*, Aug 2005.

[24] Atilla Dogan and Jayme Waishek. Derivation of the dynamics equations of receiver aircraft in aerial refueling. *Journal of guidance, control and dynamics*, 32 No. 2:585–597, 2009.

[25] Peter Dorato. A historical review of robust control, April 1987.

[26] John C. Doyle. Guaranteed margins for lqg regulators. *IEEE Transactions on Automatic Control*, AC-23:756–757, 1978.

[27] H. L. Dryden, Theodore Von Kármán, L. Bers, C. C. Lin, W. Prager, G. E. Hay, A. Weinstein, W. Z. Chien, M. Herzberger, S. A. Schelkunoff, W. Feller, and W. C. Randels. Quarterly of applied mathematics, 1943.

[28] Hugh L. Dryden. *A review of the statistical theory of turbulence.* Interscience Publishers, Inc., New York, 1961.

[29] L. El Ghaoui and V. Balakrishnan. Synthesis of fixed-structure controllers via numerical optimization. In *Decision and Control, 1994., Proceedings of the 33rd IEEE Conference on*, volume 3, pages 2678 –2683 vol.3, dec 1994. doi: 10.1109/CDC.1994.411398.

[30] L. El Ghaoui and Silviu lulian Niculescu. *Advances in Linear Matrix Inequality Methods in Control.* SIAM: Society for Industrial and Applied Mathematics Philadelphia, 2000.

[31] L. El Ghaoui, F. Oustry, and M. AitRami. A cone complementarity linearization algorithm for static output-feedback and related problems. *Automatic Control, IEEE Transactions on*, 42(8):1171 –1176, aug 1997. ISSN 0018-9286. doi: 10.1109/9.618250.

[32] Bernard Etkin. *Dynamics of atmospheric flight.* Wiley, 1972. ISBN 9780471246206. URL `http://books.google.com/books?id=iWamAAAAIAAJ`.

[33] Bernard Etkin and Lloyd Duff Reid. *Dynamics of Flight: Stability and Control.* John Wiley & Sons, Inc., third edition, 1996.

[34] A. Farag and H. H. Werner. K-s-ϕ iteration for robust $\mathcal{H}_2$ controller synthesis. In *Proceedings of the 6th European Control Conference*, 2003.

[35] Gene F. Franklin, J. David Powell, and Michael L. Workman. *Digital control of dynamic systems.* Addison-Wesley, 3rd edition, 1998.

[36] Jérôme Gauvain. Definition of an autonomous air-to-air refueling mode for the a330 mrtt during receiver's phase. Technical report, Airbus, 2006.

[37] J. Duncan Glover and Mulukutla S. Sarma. *Power systems: Analysis and design.* Brooks/Cole, third edition, 2002.

[38] Gene H. Golub and Charles F. Loan. *Matrix Computations.* The John Hopkins University Press, Baltimore and London, third edition, 1996.

[39] Simon C. O. Grocott. Comparison of control techniques for robust $\mathcal{H}_2$ performance on uncertain structural systems. Master's thesis, Massachusetts Institute of Technology, 1994.

[40] M. Horowitz. *Synthesis of Feedback Systems.* New York: Academic, 1963.

[41] Jonathan P. How, Steven R. Hall, and Wassim M. Haddad. Robust controllers for the middeck active control experiment using popov controller synthesis. *IEEE transactions on control systems technology*, 2:73–87, 1994.

[42] Xin Huang, Liqian Zhang, and Biao Huang. Stochastic lq control with generalized covariance constraints. *Dynamics of Continuous, Discrete and Impulsive Systems Series B: Applications and Algorithms*, 11:141–152, 2004.

[43] Tetsuya Iwasaki. Robust performance analysis for systems with structured uncertainty. *International Journal of Robust and Nonlinear Control*, 6:85–99, 1996.

[44] Dale L. Johnson. *Terrestrial environment (climatic) criteria handbook for use in aerospace vehicle developement.* NASA, 2000. URL `http://www.everyspec.com`.

[45] Matt Kraning, Arezou Keshavarz, and Lei Zhao. Bubble clustering: Set covering via union of ellipses. Technical report, Stanford University, 2009.

[46] Steven Kriel. *Receptacle Control for Autonomous Aerial Refuelling of a Large Receiver Aircraft.* PhD thesis, Stellenbosch University, 2013.

[47] Abhishek Kumar. Convex modeling techniques for aircraft control. Master's thesis, Virginia Polytechnic Institute and State University, 2000.

[48] H. Kwakernaak and R. Sivan. *Linear Optimal Control Systems.* Wiley Interscience, New York, 1972.

[49] Dina Shona Laila. *Design and analysis of nonlinear sampled-data control systems.* PhD thesis, University of Melbourne, 2003.

[50] L. Li and F. Paganini. Lmi relaxation to riccati equations in structured $\mathcal{H}_2$ control. *International Journal of Control*, 80:527–539, 2007.

[51] Seymour Lipschutz. *Schaum's Outlines: Set theory and related topics.* McGraw-Hill, second edition, 1998.

[52] C Livadas. Optimal $\mathcal{H}_2$/popov controller design using linear matrix inequalities. Master's thesis, Massachusetts Institute of Technology, 1996.

[53] W. Mao. *Effect of mass variation on the dynamics of receiver aircraft during aerial refueling.* University of California, Davis, 2008. ISBN 9780549671756. URL `http://books.google.co.za/books?id=b-VBKGJPf3YC`.

[54] W. Mao and F. O. Eke. A survey of the dynamics and control of aircraft during aerial refueling. *Nonlinear Dynamics and Systems Theory*, 8(4):375–388, 2008.

[55] J. L. Meriam and L. G. Kraige. *Engineering mechanics: Dynamcis.* Wiley, 5th edition, 2003.

[56] Katta G. Murty. Ball centers of special polytopes. Technical report, University of Michigan, Department of Industrial and Operations Engineering, 2009.

[57] P.M. Mäkilä, T. Westerlund, and H.T. Toivonen. Constrained linear quadratic gaussian control. In *Decision and Control, 21st IEEE Conference*, volume 21, pages 312–317, 1982.

[58] Thapana Nampradit and David Banjerdpongchai. Performance analysis of lur'e system with multiple slope restrictions using convex optimization. In *Proceedings of the 4th Asian Control Conference*, pages pp. 1097–1102, Singapore, September 2002.

[59] Thapana Nampradit and David Banjerdpongchai. A homotopy lmi approach to design robust $\mathcal{H}_2$ controller for lur'e systems with multiple slope restrictions. Technical report, Department of Electrical Engineering Chulalongkorn University Bangkok 10330, Thailand, 2003.

[60] G. D. Nastrom and K. S. Gage. A climatology of atmospheric wavenumber spectra of wind and temperature observed by commercial aircraft. *J. Atmos. Sci.*, 42(9):950–960, 1984.

[61] H. Nyquist. Regeneration theory, 1932.

[62] M. Pachter, C.H. Houpis, and D.W. Trosen. Design of an air-to-air automatic refueling flight control system using quantitative feedback theory. *International Journal of Robust and Nonlinear Control*, 7:561–580, 1997.

[63] I. K. Peddle. Advance automation 833 notes: Introductory course to aircraft dynamics, April 2012.

[64] Peyton Z. Peebles. *Probability, Random Variables and Random Signal Principles*. Irwin/McGraw-Hill, Blacksburg, Virginia, fourth edition, 2001.

[65] A. Popov. Less conservative mixed $\mathcal{H}_2/\mathcal{H}_{\text{inf}}$ controller design using multiobjective optimization. Technical report, Technical University Hamburg-Harburg Institute of Control Engineering, 2005.

[66] Anton Johan Runhaar. Autonomous airborne refueling: relative state estimation. Master's thesis, Stellenbosch University, 2011.

[67] Carsten Scherer, Pascal Gahinet, and Mahmoud Chilali. Multiobjective output-feedback control via lmi optimization. *IEEE Transactions on Automatic Control*, 42:896–911, 1997.

[68] Joseph P. Shunta. *Achieving World Class Manufacturing through Process Control*. Prentice Hall PTR, Upper Saddle River, NJ, USA, 1st edition, 1997. ISBN 0133090302.

[69] R. Skelton and M. Delorenzo. Space structure control design by variance assignment. *Journal of Guidance, Control and Dynamics*, 8:454–462, 1985.

[70] S. Skogestad and I. Postlethwaite. *Multivariable feedback control: analysis and design*. John Wiley, 2005. ISBN 9780470011676. URL `http://books.google.com/books?id=3dxSAAAAMAAJ`.

[71] Richard K. Smith. *Seventy-Five Years of Inflight Refueling: Highlights 1923-1998*. Air Force History and Museums Program, 1998.

[72] Murray R. Spiegel and John Lui. *Mathematical handbook of formulas and tables*. Schaum's outlines. McGraw-Hill, 2 edition, 1999.

[73] James Stewart. *Calculus*. Thomson Brooks/Cole, 5 edition, 2003.

[74] Kiyotsugu Takaba. Robust $\mathcal{H}_2$ control of descriptor system with time-varying uncertainty. *International Journal of Cotnrol*, 71:559–579, 1998.

[75] Kiyotsugu Takaba and Tohru Katayama. Robust $\mathcal{H}_2$ control of descriptor system with time-varying uncertainty. In *Proceedings of the American Control Conference*, pages 2421–2426, Philadelphia, Pennsylvania, 1998.

[76] Monish D. Tandale, Roshawn Bowers, and John Valasek. Trajectory tracking controller for vision-based probe and drogue autonomous aerial refueling. *Journal of Guidance, Control and Dynamics*, 29:846–857, July-Aug 2006.

[77] K. C. Toh, R. H. Tutuncu, and M. J. Todd. *On th implementation and usage of SDPT3 - a Matlab software package for semidefinite-quadratic-linear programming, version 4.0*, 17 July 2006.

[78] Murat Toydas. Fuel savings opportunities from air refueling. Master's thesis, Air Force Institute of Technology, 2010.

[79] Jeremy G. VanAntwerp and Richard D. Braatz. A tutorial on linear and bilinear matrix inequalities. *Journal of Process Control*, 10:363–385, 2000.

[80] J. Waishek. *Derivation of the dynamics equations for receiver aircraft in aerial refueling*. The University of Texas at Arlington. Aerospace Engineering, 2007. ISBN 9780549337287. URL `http://books.google.co.za/books?id=uZshNUGZDVUC`.

[81] Jiang Wang, Vijay V. Patel, Chengyu Cao, and Naira Hovakimyan. $\mathcal{L}_1$ adaptive neural network controller for autonomous aerial refueling with guaranteed transient performance. In *AIAA Guidance, Navigation, and Control Conference and Exhibit*, 2006.

[82] G. Zhu, M. A. Rotea, and R. E. Skelton. A convergent algorithm for the output covariance constraint control problem. *SIAM Journal on Control and Optimisation*, 35:341–361, 1997.

[83] Peter H. Zipfel. *Modeling and simulation of aerospace vehicle dynamics*. American Institute of Aeronautics and Astronautics, Blacksburg, Virginia, second edition, 2007.